MEDIDA DE pH EN RANGO COMPLETO MEDIANTE MATRICES SENSORAS ÓPTICAS Y TÉCNICAS DE INTELIGENCIA ARTIFICIAL

Tesis Doctoral

Sonia Capel Cuevas

Universidad de Granada
2012

UNIVERSIDAD DE GRANADA

Departamento de Química Analítica

"Profesor Fermín Capitán García"

Grupo de investigación FQM-118

"Espectrometría en Fase Sólida"

PROGRAMA OFICIAL DE DOCTORADO EN QUÍMICA

TESIS DOCTORAL

MEDIDA DE pH EN RANGO COMPLETO MEDIANTE MATRICES SENSORAS ÓPTICAS Y TÉCNICAS DE INTELIGENCIA ARTIFICIAL

presentada por

SONIA CAPEL CUEVAS

para optar a la mención de

DOCTOR INTERNACIONAL EN QUÍMICA

~ GRANADA, 2012 ~

Editor: Editorial de la Universidad de Granada
Autor: Sonia Capel Cuevas
D.L.: GR 578-2013
ISBN: 978-84-9028-395-0

MEDIDA DE pH EN RANGO COMPLETO MEDIANTE MATRICES SENSORAS ÓPTICAS Y TÉCNICAS DE INTELIGENCIA ARTIFICIAL

por

SONIA CAPEL CUEVAS

DEPARTAMENTO DE QUÍMICA ANALÍTICA

UNIVERSIDAD DE GRANADA

MEMORIA presentada para aspirar al Grado de Doctor en Química por la Universidad de Granada

Fdo. Sonia Capel Cuevas

Licenciada en Química

Fdo. Dr. D. Luis Fermín Capitán Vallvey

Catedrático del Departamento de Química Analítica de la Universidad de Granada.

VISADA en Granada,
a 19 de septiembre de 2012

Fdo. Dr. D. Ignacio de Orbe Payá

Profesor Titular del Departamento de Química Analítica de la Universidad de Granada

Fdo. Dr. Dña. María del Carmen Pegalajar Jiménez

Profesora Titular del Departamento de Ciencias de la Computación e Inteligencia Artificial de la Universidad de Granada

La doctoranda Sonia Capel Cuevas y los directores de la tesis Luis Fermín Capitán Vallvey, Ignacio de Orbe Payá y María del Carmen Pegalajar Jiménez garantizamos, al firmar esta tesis doctoral, que el trabajo ha sido realizado por la doctoranda bajo la dirección de los directores de la tesis y hasta donde nuestro conocimiento alcanza, en la realización del trabajo se han respetado los derechos de los autores a ser citados, cuando se han utilizado sus resultados o publicaciones.

Granada, a 19 de septiembre de 2012

Directores de la tesis

Doctorando

Fdo.: Luis Fermín Capitán Vallvey

Fdo.: Sonia Capel Cuevas

Fdo.: Ignacio de Orbe Payá

Fdo.: María del Carmen Pegalajar Jiménez

A mis padres, hermanos y abuelos

A mi ángel de la guarda

AGRADECIMIENTOS

A mis padres, quienes a pesar de todos los errores que he cometido a lo largo de mi vida, siempre han estado a mi lado para apoyarme, ayudarme a levantarme y animarme a seguir luchando.

A mi hermana Angy… mi todo. De mayor quiero ser como ella. A mi hermano Ismael, con el que me gustaría poder pasar más tiempo.

A mis abuelos Manoli, Francisco y Dolores, a quien añoro muchísimo.

A Faty, Miri, Vane, Tomás, Pablo y Keko, mis AMIGOS. Hemos echado los dientes juntos y lo que nos queda… ¡Qué cantidad de buenos y malos momentos hemos compartido! Agradezco su incondicional amistad.

A mi "piedrólogo" favorito, Iñaki, al que perdono por ser del Bilbao. Sólo le falta creerse la gran persona que es.

A mis directores de tesis. A Luis Fermín, a quien tengo que agradecer los conocimientos que me ha inculcado a lo largo de estos años, así como su continua disponibilidad y dedicación; sin su ayuda, nada de esto hubiera sido posible. A Ignacio, quien siempre está dispuesto a escucharte, ya sea para contarle una anécdota divertida como un problema; gracias por su bendita paciencia. A Mari Carmen, por animarme constantemente a seguir adelante y ayudarme a adentrarme en un campo totalmente desconocido para mí.

Al gremio de becarios y/o currantes del departamento de Química Analítica, con quienes he compartido tantas horas de esfuerzo, risas y, como no, desesperación cuando no se obtienen buenos resultados tras un experimento o un equipo deja de funcionar. A Estefanía, María Porcel, María Luisa, Anabel, Ismael, Inma Suárez, María, Manuel (que gentilmente ha diseñado la portada), Noemí, Samuel, Barto, Julio, Inma. A "nuestro" Julio, siempre dispuesto a ayudarte, pese a tener que anteponer lo demás a lo suyo y "vivir" en el departamento.

A todo el personal del departamento, en especial a D. Alberto Navalón.

Ai miei colleghi del grupo di Sensori della Università "Tor Vergata" di Roma. A Francesca, per l' aiuto e la pazienza. A Rosa, per l'incoraggiamento e di essere così gentile. A Alex, che sai come farti sorridere. A Grabrielle "zotico", il mio collega di Sistemi Sensoriali; grazie a lui le lezioni e il lavoro erano divertenti. A Alberto "tossico", Francesco "il gatto", Yuva, Ivan, Andrea, Massimo (grazie a lui

io sono ‘mmmmbuta), Eugenio, Marco (Santonico, Valdoni, Miranda), Sergio, Luca, Usman. Grazie ai professori Di Natale e D’Amico per avermi permesso di lavorare e di imparare. Grazie a tutti per l'ospitalità e per essere così gentile.

A mi ángel de la guarda, que me regaló sus alas.

En general, a todo aquel que me ha ayudado y aconsejado a lo largo de los primeros años de mi carrera investigadora.

ABSTRACT

This PhD dissertation examines the feasibility of measuring the pH of aqueous solutions in the full-range (0-14) by means of colour acquisition. The purposes of this discussion are threefold: 1) to prepare and characterize optical sensor arrays containing a set of immobilized acid-base indicators and measure them by scanning the hue coordinate H of the HSV colour space; 2) to evaluate the abilities of different artificial intelligence techniques to extract pH information considering the prediction errors and the computational requirement needed; and 3) to design and evaluate a portable and programmable instrument for optical pH determination.

Different colorimetric acid-base indicators were tested for membrane preparation fulfilling the conditions of: 1) no leaching; 2) change in tonal coordinate H by reaction; and 3) covering the full range with overlapping between the pH responses. An array containing 11 different sensing elements was characterized both spectrophotometrically and scanometrically.

Artificial intelligence techniques such as artificial neural networks, genetic algorithms and expert systems were applied to model data. Artificial neural networks are approximation models able to fit complex non-linear functions for prediction/approximation purposes, but also to provide how the predicted value is calculated. As they are black boxes, it is difficult to know their internal behaviour, and the rules that make the network work cannot be explained. To solve this limitation, the understanding capabilities of expert systems to know how an output value is predicted regarding the input data were also tested, using a set of cause-effect rules such as "*If* something happens, *then* conclude something/do an action/do a computation". This PhD also explores the use of genetic algorithms to solve the optimization problem of minimising: 1) the number of sensing elements required; 2) the pH prediction error of the neural network; and 3) the neural network complexity.

A programmable portable instrument based on the optimized sensor arrays was then developed. The optimal neural network obtained using multi-objective genetic optimization techniques was implemented in the microcontroller, maximising accuracy in real sample applications.

RIASSUNTO

Questo dottorato di ricerca esamina la possibilità di misurare il pH delle soluzioni acquose su tutto il range (0-14) per mezzo della acquisizione dell'informazione di colore. Gli scopi di questa discussione sono tre: 1) la preparazione e caratterizzazione di matrici di sensori ottici che contengono un set di indicatori acido-base immobilizzati e la misura con uno scanner della coordinata H dello spazio di colore HSV, 2) valutare la capabilità di alcuni tecniche di intelligenza artificiale per ottenere informazioni di pH se consideriamo gli errori di previsione e il tempo computazionale richiesto, e 3) disegnare e utilizzare uno strumento portatile programmabile per la determinazione ottica del pH.

Per la preparazione delle membrane, è stato selezionato un set di indicatori acido-base, tra quelli che soddisfano le seguenti condizioni: 1) che non si disciolga, 2) deve cambiare la coordinata tonale attraverso la reazione, e 3) coprire l'intero intervallo di pH con sovrapposizione tra le risposte degli elementi. Una matrice di 11 diversi elementi sensori è stata caratterizzata con uno spettrofotometro e uno scanner convenzionale.

Per modelare i dati, alcune tecniche di intelligenza artificiale come reti neurali artificiale, algoritmi genetici e sistemi esperti sono stati applicati. Le reti neurali artificiale sono modelli capace di adattare le funzioni non lineare complesse con gli scopi di previsione/approssimazione e di spiegare come calcolare il valore previsto. Questi sono "scatole nere", in modo che è difficile conoscere il loro comportamento interno e non possono essere spiegate le regole che consentono il funzionamento delle reti. Per risolvere questa limitazione, la capacità di comprensione di sistemi esperti per conoscere come un valore di output è previsto dai dati di input sono stata testata utilizzando un set di regole di causa-effetto come "*Se* succede qualcosa *allora* concludere qualcosa/ fare un'azione / fare un calcolo". Inoltre, in questo dottorato di ricerca studiamo l'uso di algoritmi genetici per risolvere il problema di ottimizzare la minimizzazione: 1) del numero di elementi sensori necessari, 2) dell'errore di previsione di pH della rete neurale, e 3) della complessità della rete neurale.

Quindi, si è sviluppato uno strumento portatile programmabile basato su matrici di sensori ottimizzati. La rete neurale ottima ottenuta utilizzando una

tecnica di ottimizzazione genetica multiobiettivo si è implementata nel microcontrollore per massimizzare la precisione nella misura di campioni reali.

RESUMEN

Esta tesis doctoral analiza la viabilidad de la medida del pH de disoluciones acuosas en el rango completo (0-14) mediante la medida de color. Los propósitos de esta tesis son tres: 1) preparar y caracterizar matrices sensoras ópticas que contengan un conjunto de indicadores ácido-base inmovilizados y medir mediante escaneo la coordenada tonal H del espacio de color HSV, 2) evaluar las capacidades de diferentes técnicas de inteligencia artificial para extraer la información del pH considerando los errores de predicción y los requerimientos computacionales necesitados, y 3) diseñar y evaluar un instrumento portátil programable para la determinación del pH.

Se probaron diferentes indicadores ácido-base colorimétricos para la preparación de las membranas que cumplieran las siguientes condiciones: 1) no lixiviación, 2) cambio en la coordenada tonal H mediante reacción, y 3) cubrir el rango completo mediante solapamiento entre sus respuestas frente al pH. Se caracterizó una matriz compuesta por 11 elementos sensores diferentes, tanto espectrofotométricamente como mediante el uso de un escáner.

Para modelar los datos, se aplicaron técnicas de inteligencia artificial tales como redes neuronales artificiales, algoritmos genéticos y sistemas expertos. Las redes neuronales artificiales son modelos de aproximación capaces de ajustar funciones no-lineales complejas con propósitos de predicción/aproximación y también de indicar cómo se calcula el valor predicho. Ya que son "cajas negras", es difícil conocer su funcionamiento interno, y las reglas que hacen funcionar a la red no pueden ser explicadas. Para solventar esta limitación, se evaluó la capacidad de los sistemas expertos para entender cómo se predice un valor de salida a partir de los datos de entrada, utilizando para ello un conjunto de reglas causa-efecto tales como "*Si* algo ocurre *entonces* concluir algo/hacer una acción/hacer un cálculo". En esta tesis doctoral también se estudia el uso de algoritmos genéticos para solucionar el problema de optimización de minimizar: 1) el número de elementos sensores requeridos, 2) el error de predicción de pH asociado a las redes neuronales, y 3) la complejidad de la red neuronal.

Posteriormente, se desarrolló un instrumento portátil programable basado en las matrices sensoras diseñadas. La red neuronal óptima obtenida empleando técnicas de optimización multiobjetivo se implementó en el microcontrolador, maximizando la precisión en el análisis de muestras reales.

ÍNDICE

ACRÓNIMOS

ADALINE	Adaptative Linear Element
AI	Artificial Intelligence
AMP	Adenosine Monophosphate
ANN	Artificial Neural Networks
API	Atmospheric Pressure Ionization
ART	Adaptative Resonance Theory
ATP	Adenosine Triphosphate
AZO	Aluminium-doped Zinc Oxide
BAM	Bi-directional Associative Memories
BPP	Bits per Pixel
BBPA	Bis(1-butylpenthyl) adipate
BCP	Bromocresol purple
BFGS	Broyden-Fletcher-Goldfarb-Shanno
BNN	Biological Neural Networks
BSB	Brain State in a Box
CA	Cellulose Acetate
CAS	Chemical Abstracts Service
CCD	Charge-coupled device
CL	Chemiluminescence
CMOS	Complementary Metal Oxide Semiconductor
CMYK	Cyan Magenta Yellow Key
CPU	Central Processing Unit
CRT	Cathode Ray Tube
CrTBPP	Chrome (III) 5,10,15,20-tetrakis(4-tert-butylphenyl)-porphyrin
CrTPP	Chrome (III) tetraphenylporphyrin
CSPT	Computer Screen Photo-assisted Technique

CTAB	Hexadecyltrimethylammonium bromide
DAD	Diode Array Detector
DBP	Dibutyl phthalate
DDQ	2,3-dicloro-5,6-diciano-1,4-benzoquinona
DENDRAL	Dendritic Algorithm
DLR	Dual Lifetime Referencing
DOP	Dioctyl phthalate
DOS	Dioctyl sebacate
ECL	Electrochemiluminescence
EDTA	Ethylenediaminetetraacetic acid
EG	Ethylene glycol
ES	Expert System
ESCA	Expert Systems for Chemical Analysis
ESPIRIT	European Strategic Program for Research and Development in Information Technology
FAAS	Flame Atomic Absorbtion Spectroscopy
FIA	Flow Injection Analysis
GA	Genetic Algorithm
GC	Gas Chromatography
GIF	Graphics Interchange Format
GPS	General Problem Solver
GRG	Generalized Reduced Gradient
GTP	Guanosine Triphosphate
HCA	Hierarchical Clustering Analysis
HEMC	Hydroxyethyl methyl cellulose
HPLC	High-Performance Liquid Chromatography

HSL	Hue Saturation Lightness
HSV	Hue Saturation Value
IR	Infrared
ITO	Indium-doped Tin Oxide
ISE	Ion Selective Electrode
ISFET	Ion Sensitive Field Effect Transitor
JPEG	Join Photograph Expert Group
KAS	Knowledge Adquisition System
KBS	Knowledge Based Systems
KES	Kansei Engineering System
K-NN	K-Nearest Neighbour
LCA	Life-cycle Assessment
LCD	Liquid Crystal Display
LED	Light-Emitting Diode
LIBS	Laser Induced Breakdown Spectroscopy
LIF	Laser Induced Fluorescence
LM	Levenberg-Marquardt
LMS	Least Mean Square
LOD	Limit of Detection
MADALINE	Multiple ADALINE
MILP	Mixed Integer Linear Programming
MIPs	Molecularly Imprinted Polymers
MLP	Multilayer Perceptron
MnTPP	Manganese (III) tetraphenylporphyrin
MOGA	Multiobjective Optimization Genetic Algorithm
MOSFET	Metal-Oxide-Semiconductor Field-Effect Transistor

MoTPP	Molybdenum(V) tetraphenylporphyrin
Mo(TPP)Br	Molybdenum (V) tetraphenylporphyrin bromide
MS	Mass Spectrometry
MSE	Mean Square Error
NaTFPB	Sodium tetrakis[3,5-bis(trifluoromethyl)phenyl]borate
NB	Nile blue
NC-TPP	N-confused tetraphenylporphyrins
NIR	Near Infrared
NMR	Nuclear Magnetic Resonance
NPGA	Niched Pareto Genetic Algorithm
NPOE	o-Nitrophenyl octyl ether
NSGA	Non-dominated Sorting Genetic Algorithm
NSGA II	Non dominated Sorting Genetic Algorithm II
PAHs	Polycyclic Aromatic Hydrocarbons
PAN	1-(2-piridilazo)-2-naftol
PAR	4-(2-piridilazo)resorcinol
PC	Personal Computer
PCA	Principal Component Analysis
PCR	Principal Component Regression
PDP	Parallel Distributed Processing
PEG-PS	Polyethylene glycol-polystyrene
Píxel	Picture Element
PLD	Pulsed Laser Deposition
PLS	Partial Least Squares
PNG	Portable Network Graphics
POCT	Point of Care Testing

PPI	Pixels per Inch
PPMA	Poly(methyl methacrylate)
PS	Polystirene
PTR	Proton Transfer Reaction
PVC	Polyvinyl Chloride
PVDF	Polyvinylidene Fluoride
QCM	Quartz Crystal Microbalance
RGB	Red Green Blue
ROIs	Regions of Interest
SERS	Surface Enhanced Raman Spectroscopy
SFS	Spectral Fluorescence Signature
SIA	Sequential Injection Analysis
SnTBPP	Tin (IV) 5,10,15,20-tetrakis(4-tert-butylphenyl)-porphyrin
SnTPP	Tin (IV) tetraphenylporphyrin
Sp	Pooled standard deviation
SSM	Separate Solutions Method
TBP	Tributyl phosphate
TCPB	Potassium tetrakis (4-chlorophenyl)borate
TDLAS	Tunable Diode Laser Absorption Spectroscopy
TDMAC	Tridodecylmethylammonium chloride
THF	Tetrahydrofuran
TIFF	Tagged Image File Format
VOCs	Volatile Organic Compounds
ZnTBPP	Zinc (II) 5,10,15,20-tetrakis(4-tert-butylphenyl)-porphyrin
ZnTPP	Zinc (II) tetraphenylporphyrin

OBJETIVOS DE LA TESIS

Esta tesis doctoral se centra en el desarrollo de una matriz óptica para determinación de pH en el rango completo (0-14), empleando para ello técnicas de inteligencia artificial. Los diversos elementos sensores que compondrán la matriz serán caracterizados mediante instrumentación de sobremesa (espectrofotómetro y escáner), para posteriormente ser implementados en instrumentación portátil de fácil uso y bajo coste. Se ensayarán diversas técnicas para el tratamiento de datos: métodos tradicionales de ajuste, redes neuronales artificiales, algoritmos genéticos multiobjetivo y sistemas expertos.

Para lograr el objetivo general se plantean un conjunto de objetivos específicos, con la finalidad de desarrollar diferentes aspectos del mismo:

1. Preparación y caracterización de membranas sensoras ópticas para pH elaboradas a partir de diferentes indicadores ácido-base, sales lipofílicas, plastificantes y matrices poliméricas.

2. Selección y optimización de la composición de las membranas para que no se produzca lixiviación, cambie el valor de su coordenada tonal mediante reacción y sus respuestas cubran el rango completo de pH.

3. Caracterización de los diferentes indicadores ácido-base empleados según su estructura química.

4. Tratamiento de los datos experimentales mediante técnicas de inteligencia artificial. Comparación de resultados.

5. Diseño de instrumentación portátil para medida de pH basada en la matriz desarrollada, con capacidad de independencia para llevar a cabo la medida *in situ.*

CAPÍTULO 1

Introducción

"Nothing happens unless first a dream".

Carl Sandburg

El análisis simultáneo de muestras complejas es uno de los retos más complejos que se pueden presentar en Química Analítica. De las diversas aproximaciones usadas para sistemas multanalito, los sensores son una de las más prometedoras. Un tipo de sensores de gran interés son los de un solo uso, también conocidos como sensores desechables o *one-shot sensors*, por las ventajas que presentan de corto tiempo de análisis, facilidad de uso, bajo precio, resultados *in situ*, sin necesidad de personal experto, almacenamiento, conservación y transporte de muestras y ausencia de residuos, siendo un ejemplo, en consecuencia, de metodología respetuosa con el medioambiente o verde. Este tipo de sensores se define como dispositivos analíticos autocontenidos, pues todos los reactivos necesarios están incorporados y responden al analito mediante una reacción (bio)química[1].

En este sentido, una de las cuestiones que suscita mayor interés en este campo de los sensores químicos son los sistemas multianalito. La aproximación convencional se basa en disponer de un sensor distinto para cada analito de interés, lo que exige preparar un conjunto de receptores específicos para cada uno de los analitos diana presentes en el problema a través del diseño y síntesis de receptores específicos usando conceptos tipo llave-cerradura[2]. Los inconvenientes de este enfoque se refieren a la dificultad para lograr una buena selectividad para analitos similares y al número de sensores necesarios, que crece linealmente con el número de analitos buscados. Por ello, ha surgido un paradigma alternativo de sensado basado en una imitación de la estructura y las propiedades de sistemas sensoriales biológicos, en concreto de los sistemas del gusto y olfato de los mamíferos. De esta manera, han surgido los conceptos de nariz y lengua electrónicas, que se han mostrado muy eficaces para tareas de reconocimiento, esto es, para clasificación, identificación y discriminación, abriendo las puertas a una correlación objetiva con los sentidos humanos gusto y olfato[3].

---

[1] L.F. Capitán-Vallvey. *Encyclopedia of Sensors*. Eds. C.A. Grimes, E.C. Dickey, M.V. Pishko, 1st ed., The Pennsylvania State University, Pennsylvania, USA (2005) 55-93

[2] J.J. Lavigne, E.V. Anslyn. *Sensing A Paradigm Shift in the Field of Molecular Recognition: From Selective to Differential Receptors*. Angew. Chem. Int. Ed., 40(17) (2001) 3118-3130

[3] A.K. Deisingh, D.C. Stone, M. Thompson. *Applications of electronic noses and tongues in food analysis*. Intern. J. Food Sci. Tech., 39(6) (2004) 587-604

En el caso del olfato, la discriminación (> 10.000 sustancias) se atribuye a un gran número de receptores poco selectivos, de alta reactividad cruzada, en combinación con un procesado de señales en los sistemas nerviosos central y periférico. Para el sentido del gusto, el número de receptores –al menos en humanos– es menor y con los cinco tipos existentes (dulce, salado, amargo, ácido y umami) se pueden describir y evaluar cuantitativamente el sabor de los alimentos[4], tanto referido a la sensación de sabores básicos como a la impresión global producida por un alimento junto con el olfato y las somatosensaciones[5]. En resumen, el resultado es la fabricación de una imagen interna del objeto (alimento, bebida) sensado.

La idea inicial de nariz electrónica surgió en 1982 con el trabajo de Persaud y Dodd en la revista científica *Nature*[6] y pocos años después se extendió como una consecuencia natural, apareciendo el concepto de lengua electrónica para las medidas en gases y en líquidos, respectivamente. En general, ambos conceptos suponen el uso de un conjunto, que denominaremos matriz, de sensores no específicos o de baja selectividad que producen señales analíticamente útiles para el análisis de muestras multicomponentes que son tratadas posteriormente mediante procedimientos matemáticos avanzados de procesamiento de señal por reconocimiento de patrones y/o análisis multivariado (redes neuronales, análisis por componentes principales u otros)[7]. Con el uso de estos procedimientos es posible la identificación de sustancias empleando sensores no selectivos, además de poderse detectar un gran número de especies con un pequeño conjunto de sensores. El nombre de estos dispositivos analíticos puede ser diferente, así *artificial nose, mechanical nose, odour sensor, taste sensor, taste system* y *taste chip*[8], denominaciones que frecuentemente están sujetas a controversia y son usadas según ámbitos geográficos. Se ha preferido,

[4] Y.G. Vlasov, A.V. Legin, A.M. Rudnitskaya. *Multisensor systems of the electronic tongue type as novel opportunities in design and applications of chemical sensors*. Rus. Chem. Rev., 75 (2006) 125-132

[5] F. Winquist, C. Krantz-Rulcker, I. Lundstrom. *Electronic Tongues and Combinations of Artificial Senses*. Sensors Update, 11(1) (2003) 279-306

[6] K. Persaud, G. Dodd. *Analysis of Discrimination Mechanisms in the Mammalian Olfactory System Using a Model Nose*. Nature, 299 (1982) 352-355

[7] Y. Vlasov, A. Legin, A. Rudnitskaya, C. Di Natale, A. D'Amico. *Non-specific sensor arrays ("electronic tongue") for chemical analysis of liquids*. Pure Appl. Chem., 77(11) (2005) 1965-1983

[8] P. Ciosek, W. Wroblewski. *Sensor arrays for liquid sensing – electronic tongue systems*. Analyst, 132(10) (2007) 963-978

no obstante, mantener las denominaciones de lengua y nariz electrónica a lo largo de esta memoria de tesis doctoral.

Una de las características de mayor interés de estos dispositivos es que han permitido abordar problemas analíticos irresolubles con las aproximaciones tradicionales, como son las descripciones cualitativas de productos naturales (buen café, vino o té), lo que no es fácilmente rastreable con la simple inspección de constituyentes.

La eficiencia de estos sistemas se puede lograr aumentando la cantidad de información químicamente ortogonal generada por el conjunto. Este objetivo se puede conseguir de varias formas: 1) aumentando el número de sensores en la matriz con materiales de diferente sensibilidad y que usen el mismo principio de transducción; 2) midiendo diversas propiedades físicas de cada sensor individual usando diferentes transductores; o bien 3) modulando las condiciones de operación de cada sensor individual[9].

De cualquiera de estas maneras, la matriz de sensores que constituyen tanto narices como lenguas electrónicas produce señales que no son necesariamente específicas de ninguna especie en concreto, sino que el patrón de señales originado se correlaciona con ciertas características o cualidades de la muestra. Esto es, suministran información cualitativa sobre la muestra analizada, siendo éste el enfoque más utilizado en ambos dispositivos electrónicos. La aplicación industrial de la clasificación mediante lenguas y narices electrónicas aumenta continuamente como una parte de la monitorización de procesos industriales, especialmente en industrias agroalimentarias[3].

Un segundo uso de estos dispositivos es para determinaciones cuantitativas, pues algunos analitos que originan señales solapadas o interferencias se pueden cuantificar directamente usando un conjunto de sensores que caractericen la respuesta cruzada junto con la adecuada calibración multivariada[5]. Esta posibilidad es especialmente importante para la detección de sustancias nocivas o peligrosas y en análisis en el ámbito biosanitario. En resumen, los objetivos de estos dispositivos en análisis cualitativo son la

[9] J. Mitrovics, H. Ulmer, U. Weimar, W. Goepel. *Modular sensor system for gas sensing and odor monitoring: Te MOSES concept*. Acc. Chem. Res., 31 (1998) 307-315

discriminación, la clasificación y la identificación, y en análisis cuantitativo, la determinación multicomponente.

Se han utilizado diferentes principios para la preparación de matrices de sensores, tanto para narices como para lenguas electrónicas. Para narices electrónicas, los sistemas más usados son: sensores catalíticos de óxido de estaño, sensores de polímeros conductores, sensores de onda acústica, sensores de microbalanza de cristal de cuarzo (QCM), sensores basados en transistores de efecto de campo de metal-óxido-semiconductor (MOSFET), sistemas basados en espectrometría de movilidad iónica así como en técnicas de espectrometría de masas como ionización a presión atmosférica (API) o con reacción de transferencia de protones (PTR) y, por último, técnicas ópticas principalmente fluorescencia en conjunción con fibra óptica[3,10].

En el caso de lenguas electrónicas, los sensores electroquímicos son los más comunes, así potenciométricos, amperométricos y voltamétricos, aunque también se han descrito sistemas basados en sensores ópticos y en biosensores[8,11]. Sin embargo, la mayoría de estos sistemas se basan en sensores potenciométricos, especialmente en electrodos selectivos de iones (ISE). La principal desventaja de las medidas potenciométricas es la influencia de la temperatura, la cual debe de ser minimizada mediante el control de la misma o con previa atemperación.

Las aplicaciones de estos dispositivos son muy amplias, existiendo muy pocos instrumentos comerciales[8,11]. En concreto, existen diez compañías en todo el mundo que comercializan lenguas electrónicas: Atsugi (Japón), Alpha MOS (Francia), McScience (Corea del Sur), Food Valley Netherlands (Holanda), CMP (Holanda), Erie Foods International (EE.UU.), Nerac Inc. (EE.UU.), Millipore Corp. (EE.UU.), TNO Food & Nutrition Research (Holanda) y Lianyungang Mupro Fi Plant Lianyungang (China).

Los tipos de sensores utilizados son electrodos potenciométricos, de tipo ISFET e ISE, respectivamente, con un número de sensores que oscila entre entre

[10] T.C. Pearce, S.S. Schiffman, H.T. Nagle, J.W. Gardner. *Handbook of Machine Olfaction - Electronic Nose Technology*. John Wiley & Sons (2003) pp. 624

[11] A. Legin, A. Rudnitskaya, Y. Vlasov. *Electronic tongues: new analytical perspective for chemical sensors*. Compr. Anal. Chem., 39 (2003) 437-486

7 y 8. El Taste Sensing System de Intelligent Sensor Technology Co. (Anritsu/Atsugi, Japón) está construido como un electrodo multicanal en un brazo robótico. Se mueve de un recipiente de muestras a una disolución de limpieza y vuelta a las muestras. La recalibración es necesaria después de algunos ciclos de medida. Otro sistema comercial –ASTREE (Alpha MOS, Francia)– está dedicado principalmente a la industria farmacéutica para la estimación de la acidez de sustancias biológicas, la investigación de los efectos enmascarantes de diversos aditivos saborizantes y la estabilidad de las fórmulas elaboradas. Por último, el Multiarray Chemical Sensor (McScience, Inc., Corea del Sur) se basa en membranas de polivinil cloruro (PVC) y poliuretano que responden a H^+, Na^+, K^+, Ca^{2+}, NH_4^+, NO_3^-, Cl^- y está dedicado al análisis cuantitativo de diferentes sabores y al reconocimiento de cerveza y té. En todos estos equipos el procedimiento para la obtención de resultados se basa en análisis de componentes principales (PCA). Los equipos son relativamente complejos tanto en su uso como en su mantenimiento y sólo utilizables en condiciones controladas de laboratorio. Solamente el último equipo se ha desarrollado en una versión portátil. Como ejemplos de interés se pueden citar algunos en la industria agroalimentaria, donde se han usado para la identificación de bebidas alcohólicas, aceites de oliva, quesos, productos cárnicos o aguas[3], o en agricultura, para desarrollar estrategias de fertirrigación[12], para la evaluación de madurez de frutas[13] o para la evaluación de la frescura de pescados[14].

En definitiva, la principal ventaja de los sistemas de tipo lengua electrónica es la posibilidad de ajustar el modo de operación a la aplicación deseada. Esto significa que, después de una calibración apropiada, tales dispositivos pueden realizar funciones como: a) análisis cuantitativo multianalito (análisis detallado de un vino); b) discriminación; c) clasificación (tipo de vino); d) reconocimiento (madurez de frutos) y e) simulación de paneles de cata humanos.

---

[12] M. Gutierrez, S. Alegret, R. Caceres, J. Casadesus, O. Marfa, M. Del Valle. *Application of a potentiometric electronic tongue to fertigation strategy in greenhouse cultivation*. Comp. Elec. Agr., 57 (2007) 12-22

[13] M.Y.M. Sim, M.N. Ahmad, A.Y.M. Shakaff, C.P. Jul, C.C. Cheen. *A Disposable Sensor For Assessing Artocarpus heterophyllus L. (Jackfruit) Maturity*. Sensors, 3(12) (2003) 555-564

[14] C. Di Natale, G. Ólafsdóttir. *Electronic nose and electronic tongue*. Fishery Products: Quality, safety and authenticity. John Wiley & Sons Ltd. (2009) Cap. 6, 105-26 pp. 496

Para narices electrónicas, la cantidad de dispositivos de laboratorio y comerciales es mucho mayor que en el caso de lenguas. Las aproximaciones experimentales más interesantes que se han descrito son:

1) Las basadas en un conjunto de fibras ópticas, con la fase sensora situada en el extremo distal, recogiendo la imagen mediante una cámara tipo CCD que luego es tratada con diferentes técnicas matemáticas. Al objeto de aumentar la dimensionalidad de la información se mide habitualmente fluorescencia (intensidad, tiempo de vida, longitud de onda y forma del espectro) e incluso la evolución de señal con el tiempo. Como fase sensora se ha usado un indicador solvatocrómico –usualmente rojo Nilo– adsorbido en diferentes polímeros de polaridad variada originando distintas pautas temporales por cambios en la polaridad microambiental y por el hinchamiento del polímero al exponerse a compuestos orgánicos volátiles (VOCs). Para la incorporación de estas fases sensoras en el conjunto (matriz) de fibras ópticas se han usado diferentes procedimientos: a) por simple recubrimiento[15], b) por fotopolimerización[16,17] y c) por grabado de un conjunto de micropocillos en el extremo de la fibra donde se sitúan las fases sensoras incorporadas en microesferas[18-20]. El principal problema de las matrices con fase sensora depositada es su incapacidad para transferir el entrenamiento de una matriz a otra debido a la falta de reproducibilidad en la preparación[21]. Con la incorporación de partículas de alúmina se logra un considerable aumento de la sensibilidad[19]; sin embargo, es con el empleo de microesferas cromatográficas de diferente composición con lo que se mejoran tanto la precisión como la estabilidad temporal. Esto es debido tanto a la alta homogeneidad del material

[15] T.A. Dickinson, J. White, J.S. Kauer, D.R. Walt. *A chemical-detecting system based on a cross-reactive optical sensor array*. Nature, 382 (1996) 697-700

[16] J. White, J.S. Kauer, T.A. Dickinson, D.R. Walt. *Rapid analyte recognition in a device based on optical sensors and the olfactory system.* Anal. Chem., 68 (1996) 2191-2202

[17] S.R. Johnson, J.M. Sutter, H.L. Engelhardt, P.C. Jurs, J. White, J.S. Kauer, T.A. Dickinson, D.R. Walt. *Identification of Multiple Analytes Using an Optical Sensor Array and Pattern Recognition Neural Networks*. Anal. Chem., 69 (1997) 4641-4648

[18] T.A. Dickinson, K.L. Michael, J.S. Kauer, D.R. Walt. *Convergent, self-encoded bead sensor arrays in the design of an artificial nose*. Anal. Chem., 71, (1999) 2192-2198

[19] D.R. Walt, T. Dickinson, J. White, J. Kauer, S. Johnson, H. Engelhardt, J. Sutter, P. Jurs. *Optical sensor arrays for odor recognition*. Biosens. Bioelectron., 13 (1998) 697-699

[20] K.J. Albert, D.R. Walt, D.S. Gill, T.C. Pearce. *Optical multibead arrays for simple and complex odour discrimination*. Anal. Chem., 73 (2001) 2501-2508

[21] D.R. Walt. *Imaging optical sensor arrays*. Current opinion in chemical biology, 6(5) (2002) 689-695

como al empleo de un gran número de sensores redundantes que permiten usar promediado de señales[22]. Esta tecnología se ha utilizado en situaciones donde es necesario discriminar la presencia de determinados compuestos a muy bajo nivel y de forma rápida, así para compuestos nitroaromáticos procedentes de la descomposición de explosivos en minas terrestres enterradas[23,24]. Se ha mejorado la detección en el caso de vapores de 2,4-dinitrotolueno combinando sensores no específicos como los arriba indicados, basados en polaridad, con sensores semiselectivos, así un polímero fluorescente de tipo pentipticeno que actúa como un interruptor molecular[25]. Con este tipo de detección, junto con técnicas de reconocimiento de pautas, se ha desarrollado una instrumentación portátil para uso en campo[25].

2) Dispositivos basados en un conjunto de membranas diferentes (matriz), por ejemplo, de 25 o 36, dispuestas sobre un soporte, las cuales cambian de color tras exponerse al gas o vapor y cuya imagen se recoge con un escáner convencional. A las señales generadas, habitualmente las coordenadas RGB de cada membrana, se les aplica reconocimiento de pautas y/o análisis multivariado (HCA o PCA)[26,27]. En esta estrategia, y a diferencia de la anterior, se usa una mayor variedad de reactivos que tratan de explorar diferencias en carga, polaridad, carácter ácido-base y carácter donor-aceptor de los analitos[26]. Cada analito genera un patrón de colores característico que permite su identificación, ya que se exploran a la vez diversas propiedades. En general, los sustratos usados son hidrófobos, así cromatoplacas de gel de sílice hidrófobo, polímeros como nylon o fluoruro de polivinilideno (PVDF), aunque también papel[28] y los potenciales analitos son más numerosos que con la primera aproximación

[22] S.E. Stitzel, L.J. Cowen, K.J. Albert, D.R. Walt. *Array-to-Array Transfer of an Artificial Nose Classifier*. Anal. Chem., 73 (2001) 5266-5271

[23] G.A. Bakken, G.W. Kauffman, P.C. Jurs, K.J. Albert, S.S. Stitzel. *Pattern Recognition Analysis of Optical Sensor Array Data to Detect Nitroaromatic Compound Vapors*. Sens. Actuators B, 79 (2001) 1-10

[24] K.J. Albert, D.R. Walt. *High-speed fluorescence detection of explosives-like vapors*. Anal. Chem., 72(9) (2000) 1947-1955

[25] K.J. Albert, M.L. Myrick, S.B. Brown, D.L. James, F.P. Milanovich, D.R. Walt. *Field-deployable sniffer for 2,4-dinitrotoluene detection*. Environ. Sci. Technol., 35(15) (2001) 3193-3200

[26] M.C. Janzen, J.B. Ponder, D.P. Bailey, C.K. Ingison, K.S. Suslick. *Colorimetric Sensor Arrays for Volatile Organic Compounds*. Anal. Chem., 78(11) (2006) 3591-3600

[27] N.A. Rakow, K.S. Suslick. *A colorimetric sensor array for odour visualization*. Nature, 406 (2000) 710-713

[28] K.S. Suslick, N.A. Rakow, A. Sen. *Colorimetric sensor arrays for molecular recognition*. Tetrahedron, 60 (2004) 11133-11138

descrita, fibra óptica (aminas, alcoholes, arenos, éteres, fosfinas, tioéteres, tioles, cetonas, hidrocarburos halogenados)[26], aunque gases inorgánicos como CO, PH_3, H_2S o NH_3 también pueden ser detectados. De esta manera, se puede identificar, e incluso cuantificar en ocasiones, grupos de entre dos y cuatro gases y/o vapores[29]. Una aplicación de interés es la distinción entre aminas; se han estudiado 12 diferentes, a través de la inclusión de fases sensoras que discriminan por tamaño y forma[30]. Adicionalmente, este concepto se ha aplicado a la diferenciación entre productos alimentarios como las cervezas[28]. El grupo de investigación del Dr. Suslick en la Universidad de Illinois (EE.UU.), que ha desarrollado este tipo de nariz electrónica, las ha comercializado a través de la empresa ChemSensing, Inc.

3) Hay otras aproximaciones, aunque de menor interés y utilidad limitada. Akrajas *et al.*[31] propusieron usar membranas tipo Langmuir-Blodgett conteniendo cuatro tipos de metaloporfirinas, situadas en un sistema de flujo midiendo la radiación reflejada tras reaccionar con los VOCs problema (dos alcoholes y dos cetonas) cuando son iluminados sucesivamente con cuatro diodos emisores de luz (LEDs) de diferente color. Tanaka *et al.*[32], por su parte, propusieron el empleo de los conocidos tubos indicadores de gases para monitorizar malos olores en ambientes habitados mediante la medida con un escáner cuando el gas pasa a través del tubo, utilizando la velocidad de reacción a través de la velocidad de cambio de color, como parámetro analítico.

Como antes se ha indicado, la mayoría de las lenguas electrónicas se basan en medidas de tipo electroquímico y en mucha menor extensión en medidas de tipo óptico. Si atendemos a las lenguas electrónicas de tipo óptico, se han descrito diversas aproximaciones:

1) Uso de fibra óptica con un conjunto de reactivos fluorescentes, así reactivos para pH, O_2 y CO_2, unidos de forma covalente o entrapados en el extremo distal de una misma fibra de forma que la señal transmitida por la

[29] C. Potera. *Smelling in color: a rainbow of possibilities*. Environ. Health Persp., 109(3) (2001) A129-A131

[30] N.A. Rakow, A. Sen, M.C. Janzen, J.B. Ponder, K.S. Suslick. *Molecular Recognition and Discrimination of Amines with a Colorimetric Array*. Angew. Chem. Int. Ed., 44 (2005) 4528-4532

[31] A.U. Akrajas, M. Mat Salleh, M. Yahaya. *Enriching the selectivity of metalloporphyrins chemical sensors by means of optical technique*. Sens. Actuators B, 85(3) (2002) 191-196

[32] Y. Tanaka, T. Nakamoto, T. Moriizumi. *Study of highly sensitive smell sensing system using gas detector tube combined with optical sensor*. Sens. Actuators B, 119(1) (2006) 84-88

misma genere una huella característica[33]; también pueden ser reactivos depositados en diferentes fibras ópticas[34] o bien incorporados en microesferas situadas en micropocillos grabados en el extremo de la fibra[35] y cuyas señales son posteriormente deconvolucionadas usando algoritmos multivariados.

2) Empleo de matrices de microesferas poliméricas con la superficie modificada químicamente para permitir la unión covalente de receptores (reactivos convencionales, enzimas, anticuerpos). Estas microesferas, que de alguna manera se asemejan a las papilas gustativas, se sitúan en pocillos micromecanizados fabricados en estructuras de silicio. Se han utilizado diversos procedimientos para poner en contacto la muestra con el dispositivo. En un primer diseño, una matriz de 3x3 se pone en contacto con el problema mediante un conjunto de tubos y, tras el equilibrado, se recoge la imagen mediante una cámara CCD[36]. Un ulterior refinamiento sitúa las microesferas dentro de micropocillos piramidales excavados en obleas de silicio, que pueden ser más de 100, los cuales sirven de microrreactores y cámaras de análisis, mejorando el contacto con la muestra mediante una célula de flujo e incluyendo una tarjeta de vídeo para medir la evolución de la señal con el tiempo[37]. Este diseño experimental se ha usado con diversos tipos de sistemas de reconocimiento para abordar distintos problemas: a) reactivos unidos covalentemente a microesferas de polietilenglicol-poliestireno (PEG-PS), como fluoresceína (para pH), o-cresolftaleín complexona (Ca(II), pH) alizarín complexona (Ce(III), Ca(II), pH) y ésteres borónicos (fructosa, pH)[36]; b) receptores diferenciales fijados sobre microesferas, así de tipo guanidinio sobre esferas de tentagel con transducción óptica por desplazamiento de indicadores para reconocimiento de los nucleótidos adenosín trifosfato (ATP), adenosín monofosfato (AMP) y guanosín trifosfato

---

[33] B.G. Healey, D.R. Walt. *Fast temporal response fiber-optic chemical sensors based on the photodeposition of micrometer-scale polymer arrays*. Anal. Chem., 69 (1997) 2213-2216

[34] K.L. Michael, L.C. Taylor, S.L. Schultz, F. Szurdoki, D.R. Walt. *Making Sensors out of disarray: optical sensor microarrays*. Proc. SPIE, B.L. Fearey, Ed., 3270 (1998) 34-41

[35] D.R. Walt. *Techview: molecular biology. Bead-based Fiber-Optic Arrays*. Science, 287(5452) (2000) 451-452

[36] J.J. Lavigne, S. Savoy, M.B. Clevenger, J.E. Ritchie, B. McDoniel, S.J. Yoo, E.V. Anslyn, J.T. McDevitt, J.B. Shear, D. Neikirk. *Solution-Based Analysis of Multiple Analytes by a Sensor Array: Toward the Development of an Electronic Tongue*. J. Am. Chem. Soc., 120 (1998) 6429-6430

[37] A.P. Goodey, J.J. Lavigne, S.M. Savoy, M.D. Rodriguez, T. Curey, A. Tsao, G. Simmons, J. Wright, S.J. Yoo, Y. Sohn, E.V. Anslyn, J.B. Shear, D.P. Neikirk, J.T. McDevitt. *Development of multianalyte sensor arrays composed of chemically derivatized polymeric microspheres localized in micromachined cavities*. J. Am. Chem. Soc., 123 (2001) 2559-2570

(GTP) usando PCA[38] o de receptores con grupos péptido y ácido borónico y transducción con rojo de bromopirogalol que forma un éster cíclico reversible con los grupos borónicos del receptor para el reconocimiento de proteínas y glicoproteínas mediante PCA[39]; c) microesferas multicapas con un reactivo que cambia de color en el interior y grupos enlazantes no coloreados en la superficie (llamadas microesferas con capas cromatográficas y de detección integradas), como alizarín complexona en el interior y unidades de ácido etilendiaminotetraacético (EDTA) y acetato en la superficie para reconocer Zn(II), Ni(II) y Pb(II) utilizando la variación de señales RGB con el tiempo y algoritmos de reconocimiento de pautas[40]; d) uso de matrices de membranas poliméricas conteniendo *quantum dots*, suspendidos en cavidades en obleas de silicio, con reactivos enlazados que cambian su color por interacción con los analitos, los cuales se miden por espectrofotometría o fluorimetría convencional[41].

3) Se han empleado polímeros de impronta molecular (MIPs) para discriminar entre aminas aromáticas usando la variación de la absorbancia de los propios analitos retenidos en el MIP tras la interacción junto con análisis discriminante lineal[42]. La restricción que supone que los propios analitos generen la señal se solventó en un estudio posterior usando la técnica de desplazamiento de un colorante[43].

4) Se han descrito diferentes aproximaciones a una lengua óptica utilizando un conjunto de receptores, aunque midiendo la respuesta óptica en disolución, usualmente disponiendo los reactivos en micropocillos y midiendo habitualmente la absorbancia a una o varias longitudes de onda. Un ejemplo es

---

[38] S.C. McCleskey, M.J. Griffin, S.E. Schneider, J.T. McDevitt, E.V. Anslyn. *Differential Receptors Create Patterns Diagnostic for ATP and GTP*. J. Am. Chem. Soc., 125 (2003) 1114-1115

[39] A.T. Wright, M.J. Griffin, Z. Zhong, S.C. McCleskey, E.V. Anslyn, J.T. McDevitt. *Differential Receptors Create Patterns That Distinguish Various Proteins*. Angew. Chem. Int. Ed., 44 (2005) 6375-6378

[40] A.P. Goodey, J.T. McDevitt. *Multishell microspheres with integrated chromatographic and detection layers for use in array sensors*. J. Am. Chem. Soc., 125 (2003) 2870-2871

[41] H. Hogan. *Suspended and Placed over Microcavities, Quantum Dots Become Brighter*. Photon. Spectra, 11 (2007) 98

[42] N.T. Greene, S.L. Morgan, K.D. Shimizu. *Molecularly imprinted polymer sensor arrays*. Chem. Comm., (2004) 1172-1173

[43] N.T. Greene, K.D. Shimizu. *Colorimetric molecularly imprinted polymer sensor array using dye displacement*. J. Am. Chem. Soc., 127 (2005) 5695-5700

la propuesta presentada por Rangin *et al.*[44] y modificada posteriormente por West *et al.*[45] para la identificación de bacterias gram negativas basada en la secuencia específica de glicolípidos que poseen. Para ello, se utiliza un conjunto de liposomas preparados a partir de diferentes polidiacetilenos derivados con aminoácidos. Los cambios de color de azul a púrpura del conjunto de diferentes liposomas con una bacteria dada proporciona una huella dactilar discernible. Otro ejemplo es la propuesta de Lee *et al.*[46] para la discriminación de 23 carbohidratos, basada en la reacción de éstos con un ácido borónico. La diferente constante de estabilidad de los esteres cíclicos resultantes hace que el pH de la disolución varíe según el carbohidrato presente, lo que se pone de manifiesto usando un conjunto de indicadores de pH.

En otras ocasiones, la información óptica de pocillos de microplacas se ha obtenido mediante una cámara CCD. Así, se ha descrito una matriz para la detección de proteínas usando tetrafenilporfirinas derivadas en la periferia con aminoácidos y péptidos originando receptores que difieren en carga, tamaño, hidrofobicidad y simetría, y que permiten la transducción fluorescente a través de variación o atenuación de fluorescencia[47]. Otro ejemplo es el empleo de una matriz de diferentes oligonucleótidos con zonas de reconocimiento basadas en intersecciones de tres vías funcionalizadas con un fluoróforo, capaces de interaccionar con diferentes moléculas y usados para discriminar cocaína y diversos esteroides[48].

A diferencia de estos anteriores ejemplos, los reactivos de reconocimiento se pueden fijar en la propia microplaca. Así, se han inmovilizado diversos indicadores fluorescentes en PEG para la detección de Ca(II), Na(I), Mg(II), Hg(II), SO_4^{2-} y Cl^- utilizando la técnica de medida *Dual Lifetime Referencing*

---

[44] M. Rangin, A. Basu. *Lipopolysaccharide identification with functionalized polydiacetylene liposome sensors*. J. Am. Chem. Soc., 126 (2004) 5038-5039

[45] M.R. West, T.W. Hanks, R.T. Watson. *Polydiacetylene-Based Liposomes: An "Optical Tongue" for Bacteria Detection and Identification*. J. Chem. Educ., 86(3) (2009) 373-375

[46] J.W. Lee, J.S. Lee, Y.T. Chang. *Colorimetric identification of carbohydrates by a pH indicator/pH change inducer ensemble*. Angew. Chem. Int. Ed., 45(39) (2006) 6485-6487

[47] L. Baldini, A.J. Wilson, J. Hong, A.D. Hamilton. *Pattern-based detection of different proteins using an array of fluorescent protein surface receptors*. J. Am. Chem. Soc., 126(18) (2004) 5656-5657

[48] M.N. Stojanovic, E.G. Green, S. Semova, D.B. Nikic, D.W. Landry. *Cross-reactive arrays based on three-way junctions*. J. Am. Chem. Soc., 125(20) (2003) 6085-6089

(DLR) con cámara CCD, aunque trabajando en escala de grises[49]. En un trabajo posterior se refinó el procedimiento para la determinación de mezclas de Ca(II), Cu(II), Ni(II), Cd(II) y Zn(II), mejorando el sistema instrumental para la medida de fluorescencia con la cámara CCD y usando redes neuronales y máquinas de soporte vectorial para el tratamiento de datos[50].

5) Sistemas basados en matrices de membranas colorimétricas diferentes, dispuestas bidimensionalmente sobre un soporte plano de sílice hidrofóbica. Éstos cambian de color tras la reacción, recogiéndose la imagen con un escáner. Las coordenadas RGB de cada membrana se emplean para la clasificación por HCA, habiéndose propuesto para el reconocimiento de compuestos orgánicos en agua[51]. Se han sugerido algunos otros sistemas de este tipo, así para especiación Fe(II)/Fe(III) con los reactivos dispuestos sobre papel de filtro[52].

En el grupo de investigación en el que se ha realizado esta tesis doctoral se han desarrollado lenguas ópticas desechables para iones alcalinos basadas en soportes transparentes que contienen una pareja de membranas que trabajan mediante química ionóforo-cromoionóforo y que posee cada membrana ionóforos diferentes y no selectivos para iones alcalinos. La imagen del sensor tras reacción con el problema se obtiene mediante un escáner y la señal analitica usada es la coordenada cromática H. Se han utilizado dos aproximaciones diferentes para el cálculo de concentraciones. En una de ellas se modela la respuesta de cada una de las membranas sensoras y se predicen las concentraciones usando el método de clasificación de *k-vecinos más próximos* (K-NN)[53], mientras que en la otra, las señales se procesan mediante redes neuronales artificiales multicapa[54].

---

[49] T. Mayr, G. Liebsch, I. Klimant, O.S. Wolfbeis. *Multi-ion imaging using fluorescent sensors in a microtiterplate array format*. Analyst, 127(2) (2002) 201-203

[50] T. Mayr, C. Igel, G. Liebsch, I. Klimant, O.S. Wolfbeis. *Cross-Reactive Metal Ion Sensor Array in a Microtiterplate Format*. Anal. Chem., 75 (2003) 4389-4396

[51] C. Zhang, K.S. Suslick. *A Colorimetric Sensor Array for Organics in Water*. J. Am. Chem. Soc., 127(33) (2005) 11548-11549

[52] A. Abbaspour, M.A. Mehrgardi, A. Noori, M.A. Kamyabi, A. Khalafi-Nezhad, M.N. Soltani Rad. *Speciation of iron(II), iron(III) and full-range pH monitoring using paptode: a simple colorimetric method as an appropriate alternative for optodes*. Sens. Actuators B, 113(2) (2006) 857-865

[53] M.M. Erenas, O. Piñeiro, M.C. Pegalajar, M.P. Cuellar, I. de Orbe-Payá, L.F. Capitán-Vallvey. *Surface Fit Approach with a Disposable Optical Tongue for Alkaline Ion Analysis*. Anal. Chim. Acta, 694 (2011) 128-135

[54] M.M. Erenas, M.C. Pegalajar, M.P. Cuellar, I. de Orbe-Payá, L.F. Capitán-Vallvey. *Disposable Optical Tongue for Alkaline Ion Analysis*. Sens. Actuators B, 156 (2011) 976-982

6) Estrategia muy diferente es la usada por Edelman *et al.*[55] para la estimación de la astringencia en vinos basada en la interacción de polifenoles con proteínas ricas en prolina inmovilizadas en la célula de un sistema de flujo monitorizado mediante espectroscopía infrarroja (IR).

Recapitulando, existen un gran número de aproximaciones al análisis multianalito utilizando tanto narices como lenguas electrónicas, de las que pocas son de tipo óptico, como se ve por el breve resumen anterior. Salvo muy contadas excepciones, los diferentes dispositivos ópticos simplemente se han estudiado para demostrar las posibilidades de uso sin que se hayan aplicado en la práctica[4].

La mayoría de las diferentes aproximaciones ópticas utilizadas tanto para lenguas como para narices, se basan en la medida de color usando diferentes espacios de color obtenidos a partir de la imagen generada por dispositivos fotosensibles, cámaras CCD y escáneres principalmente. Con mucho, el espacio más utilizado es el RGB, prácticamente el único, siendo estas coordenadas las que son procesadas por el sistema de reconocimiento de pautas y/o análisis multivariado.

Los requerimientos básicos para los sistemas tipo lengua óptica referidos a la matriz de sensores, clave del sistema, son que los sensores presenten baja selectividad, o lo que es lo mismo, alta sensibilidad cruzada y que tengan unas características analíticas reproducibles[4]. Por otra parte, se busca que los sensores sean cada vez más sensibles y más robustos, lo cual es contradictorio a partir de cierto punto, pues una mayor sensibilidad del sensor se traduce en una menor robustez[26]. Una solución es el empleo de sensores desechables y, por tanto, no integrados en el dispositivo. Requerimientos adicionales se refieren a costo y portabilidad.

Uno de los problemas que presentan muchos de los sistemas descritos es la falta de precisión de las medidas debida a la variabilidad en la preparación de los sensores, así como a la variabilidad lote a lote, lo que incrementa el error de las predicciones. Algunas de las alternativas propuestas, como las microesferas situadas en un chip de silicio micromecanizado[37], conducen a sistemas de

[55] A. Edelmann, B. Lendl. *Toward the optical tongue: flow-through sensing of tannin-protein interactions based on FTIR spectroscopy*. J. Am. Chem. Soc., 124(49) (2002) 14741-14747

buenas prestaciones, aunque complejos experimentalmente y de alto precio. La segunda alternativa más usada es la comercializada por la empresa ChemSensing, Inc.[51], aunque más para narices que para lenguas ópticas. La forma de preparación de estas matrices por deposición de microvolúmenes de una disolución de los reactivos sobre una cromatoplaca presenta cierta variabilidad, que se traduce en dificultades para la cuantificación de analitos.

La reciente y escasa instrumentación comercial en lenguas electrónicas, mencionada anteriormente, tiene como denominador común la necesidad de realizar la medida en condiciones controladas de laboratorio por personal experto, en muchos casos, con complejos sistemas de inserción y extracción de muestras. Esta característica es común a la mayoría de las técnicas instrumentales durante la fase inicial de desarrollo y ya ha sido mejorada por otras técnicas analíticas más asentadas, permitiendo el diseño y fabricación de equipos portátiles concebidos para trabajar "sobre el terreno" y por personal no experto en la materia. El diseño y la fabricación de tales sistemas requiere de la colaboración del conocimiento de varias ramas de la ciencia y la tecnología: tecnologías de sensores y de instrumentación electrónica, técnicas de inteligencia artificial y herramientas quimiométricas.

La alternativa que se utiliza en esta tesis doctoral es el empleo de espacios de color diferentes del RGB, en concreto del espacio orientado hacia el tono, HSV, cuya principal característica es que representa la información cognitiva del color en un único parámetro, la coordenada H (tono), no siendo necesarias las tres coordenadas para definir el mismo, como ocurre en RGB. Se emplea el espacio de color HSV a pesar de no ser el habitualmente utilizado para el intercambio de datos exactos de color, como son el CIElab y similares, porque no se busca la reproducción exacta de un color, sino un parámetro robusto que de forma simple indique el tono. Esta coordenada H se puede considerar como una señal cualitativa independiente de la concentración y del camino óptico, esto es, no le afectan las diferencias en espesor o la falta de homogeneidad de las membranas o de concentración de reactivos entre lotes de sensores, factores que reducen la precisión de las medidas. Estudios previos de nuestro grupo de investigación han demostrado que el empleo de la coordenada H en sensores

bitonales que originen un cambio de color por reacción, origina una sustancial mejora de precisión[56].

La propuesta que se presenta en esta tesis doctoral utiliza conceptos y metodologías desarrolladas en el estudio de lenguas ópticas aunque con una finalidad diferente: la determinación de la concentración protónica de disoluciones acuosas en rango completo, es decir, de pH 0 a 14. Este problema no se puede abordar mediante indicadores ácido-base convencionales, ya que sólo responden en el entorno de una o dos unidades de pH. La preparación de matrices (lenguas ópticas) desechables de indicadores ácido-base obtenidas por deposición sobre soportes transparentes, junto con la medida de color de los diferentes sensores mediante diferentes técnicas de imagen y su posterior procesamiento, permitirá el cálculo de pH. Por último, se pretenderá el diseño de una instrumentación portátil que pueda permitir la medida de la matriz, el cálculo de la coordenada H y el procesamiento en el propio microcontrolador del equipo. Uno de los criterios de diseño prioritario, al mismo nivel que la fiabilidad y la precisión, será el fácil manejo, de manera que pueda ser usado por cualquier persona fuera de laboratorio, y que esta tecnología comience a transferirse al mayor número de sectores y personas de nuestro entorno como ayuda en diversos ámbitos de su vida cotidiana, tanto personal como laboral.

En esta memoria de doctorado se aborda el problema de la medida óptica de pH en rango completo de forma sucesiva y utilizando diversos modelos de inteligencia artificial hasta llegar a su integración en instrumentación portátil. En los sucesivos capítulos se van mostrando las estrategias y metodologías experimentales y de cálculo utilizadas, así como los resultados alcanzados en forma de publicaciones obtenidas. Por ello, cada capítulo lleva su propia introducción que centra y justifica los recursos utilizados.

---

[56] K. Cantrell, M.M. Erenas, I. Orbe-Paya, L.F. Capitán-Vallvey. *Use of the hue parameter of the hue, saturation, value color space as a quantitative analytical parameter for bitonal optical sensors*. Anal. Chem., 82(2) (2010) 531-542

CAPÍTULO 2

Metodología experimental y técnicas de inteligencia artificial

"If you cannot measure something, you cannot really understand it.".

Lord Kelvin

1. INTRODUCCIÓN

En este capítulo se presenta la metodología seguida para la preparación de los diversos sensores desarrollados durante esta tesis doctoral, así como las diferentes estrategias empleadas para la obtención de las imágenes de dichos sensores y el cálculo de las coordenadas cromáticas que se han usado como parámetros analíticos. Por último, se señalan las diferentes técnicas y recursos de inteligencia artificial utilizadas a lo largo de la memoria para analizar datos, optimizar redes neuronales artificiales, extraer información analítica de los datos de color y caracterizar y validar los métodos analíticos resultantes.

2. METODOLOGÍA DE PREPARACIÓN DE LOS ELEMENTOS SENSORES

Para la fabricación de membranas sensoras se han descrito diversas metodologías experimentales. Por la sencillez de preparación y los buenos resultados que proporciona, se ha optado por la de evaporación controlada de disoluciones conteniendo los componentes necesarios en un disolvente orgánico de alta tensión de vapor. Esta forma general de trabajo se ha utilizado de dos maneras diferentes. En el caso de la preparación de elementos sensores individuales se usó un sistema centrífugo para asegurar un espesor de membrana reproducible, mientras que para las matrices de sensores se utilizaron placas de micropocillos en los que se depositaron volúmenes conocidos de las diferentes disoluciones, cuya evaporación permitió la preparación de las membranas sensoras.

Para ello, el primer paso fue la selección de los reactivos de reconocimiento y los diferentes materiales constituyentes de las membranas, tras lo cual se optimizaron las concentraciones y proporciones de cada uno de ellos para elaborar las disoluciones (denominadas en adelante cócteles). Ulteriormente se prepararon las membranas a partir de estos cócteles.

2.1. Preparación de membranas y matrices ópticas

La preparación de las membranas sensoras individuales se llevó a cabo por centrifugación utilizando un sistema rotatorio de velocidad variable (figura

II.1).

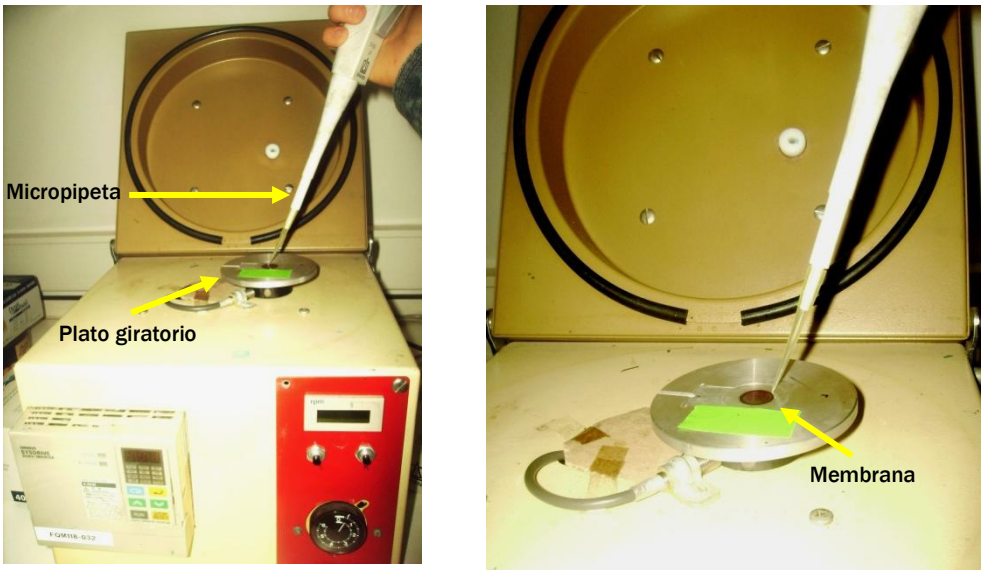

Figura II.1. Sistema rotatorio de velocidad variable para la preparación de las membranas

Este dispositivo consta de un motor que hace girar un plato que presenta una muesca superficial donde se encaja el soporte de la membrana sensora y que tiene las mismas dimensiones que ésta. Como soporte de las membranas se ha utilizado, a excepción del estudio presentado en el capítulo 9, una lámina de poliéster orientado biaxialmente tipo Mylar, tanto de 0,25 como de 0,5 mm de espesor, debido a las buenas características mecánicas y ópticas que presenta. Con ayuda de una micropipeta se deposita el volumen requerido de cóctel, habitualmente 20 µL, en la lámina de poliéster que se encuentra girando a una velocidad de 170 rpm. De esta forma, el cóctel depositado se expande de manera homogénea sobre el poliéster debido a la acción de la fuerza centrífuga. A continuación, se deja reposar la lámina en un recipiente cerrado que contiene el mismo disolvente para que el secado se realice lentamente.

Los sensores de pH se basan en que un indicador ácido-base, inmovilizado por medio de algún procedimiento en un soporte, presenta diferente color según se encuentre en forma ácida o en forma básica, de tal modo que, conociendo su constante de acidez en las condiciones de trabajo y la relación de concentraciones de forma ácida y básica en el equilibrio, o bien la relación de

propiedades relacionadas con esas concentraciones, se puede determinar el pH de la disolución mediante la ecuación de Henderson-Hasselbalch (ecuación II.2).

$$HA + H_2O \leftrightarrow A^- + H_3O^+ \qquad \text{(II.1)}$$

$$K = \frac{[A^-][H_3O^+]}{[HA]} \qquad pH = pK + \log\frac{[A^-]}{[HA]} \qquad \text{(II.2)}$$

La limitación de estos sensores ópticos se debe a su estrecho rango dinámico, que habitualmente es de ± 1 unidades de pH, aproximadamente. En consecuencia, para cada intervalo se necesita una membrana diferente, conteniendo un indicador ácido-base de pK_a adecuado. Como alternativa, se estudia en esta tesis doctoral el uso de una matriz de sensores ópticos que permita cubrir todo el rango de pH.

Las matrices desarrolladas para la determinación de pH se prepararon utilizando placas desechables de diseño propio conteniendo 12 micropocillos y de una capacidad aproximada de 1,2 µL cada uno. Dichas placas constan de dos láminas, la de fondo constituida por un soporte de Mylar de 50 mm × 40 mm, sobre la que se fija una película de PVC adhesiva, de 30,6 µm de espesor, que presenta 12 orificios de 5 mm de diámetro cada uno dispuestos en tres columnas y cuatro filas de acuerdo con las dimensiones señaladas, en milímetros, en la figura II.2. La película de PVC adhesiva es transparente cuando la medida se realiza mediante el uso de un escáner, siendo negra si se utiliza el instrumento portátil desarrollado, al objeto de reducir, en este segundo caso, la dispersión de la luz y prevenir el *cross talking* (transferencia de información de un elemento sensor a otro que se encuentra próximo debido a causas diversas).

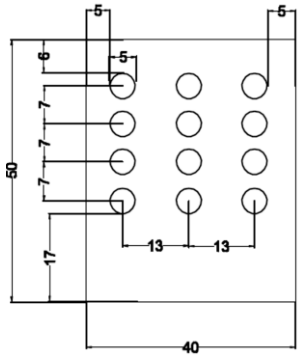

Figura II.2. Esquema de la matriz de elementos sensores

Para elaborar de modo reproducible los micropocillos con los que se preparan las placas desechables en las que se depositan los cócteles se utilizó un dispositivo de diseño propio. Es un taladro que consta de 12 punzones alineados en la misma disposición que los micropocillos, con una separación entre la placa móvil y la placa sacabocados del espesor de la lámina de PVC a agujerear y tres placas diferentes para realizar la perforación y extracción de la lámina (figura II.3).

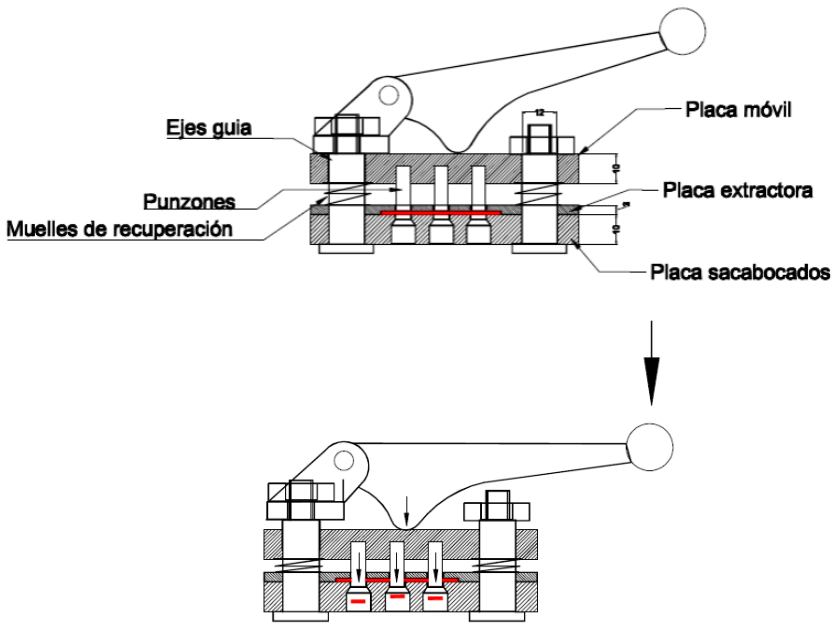

Figura II.3. Esquema del taladro usado para la fabricación de la matriz de elementos sensores

La selección y optimización de la matriz sensora se realizó a través de la preparación de más de 200 cócteles diferentes conteniendo diversos tipos y cantidades de polímeros, plastificantes, sales lipofílicas, humectantes (en caso necesario) e indicadores ácido-base.

Como indicadores ácido-base se estudió un conjunto considerando, tanto su carácter ácido o básico, como los cambios de color que experimentan al variar el pH y el número de estos cambios. Los indicadores estudiados fueron: alizarina, amarillo Sunset, 1-amino-4-hidroxiantraquinona, azul bromotimol, azul indigotina, azul Nilo lipofilizado, azul timol, 1,4-dihidroxiantraquinona, 1,5-dihidroxiantraquinona, 2,6-dihidroxiantraquinona, naranja xilenol, 1-(2-piridilazo)-2-naftol (PAN), 4-(2-piridilazo)resorcinol (PAR), púrpura bromocresol, púrpura m-cresol, purpurina, rojo cresol, rojo congo, rojo fenol, rojo metilo, rojo neutro, rojo Nilo, rojo sicomet P, sudan I y violeta cristal.

Los polímeros empleados para la preparación de la membrana que inmoviliza el indicador ácido-base fueron: acetato de celulosa, hidroxietilmetilcelulosa (HEMC), poliuretano D4, cloruro de polivinilo de alto peso molecular (PVC) y poliestireno (PS). Como plastificantes se ensayaron: bis(1-butilpentil)adipato (BBPA), dibutil ftalato (DBP), dioctil sebacato (DOS), dioctil ftalato (DOP), o-nitrofeniloctiléter (NPOE) y tributil fosfato (TBP). Las sales lipofílicas probadas fueron: Aliquat 336, bromuro de hexadeciltrimetilamonio (CTAB), cloruro de tridodecilmetilamonio (TDMAC), tetrakis(3,5-bis(trifluorometil)fenil)borato sódico (NaTFPB) y tetrakis(4-clorofenil)borato potásico (TCFB); y, por último, se usó etilenglicol (EG) como agente humectante.

A diferencia del caso anterior, las matrices de sensores no se prepararon por centrifugación, sino mediante deposición directa de 8 µl de cada uno de los cócteles preparados dentro de cada micropocillo de la placa y posterior evaporación del disolvente. A continuación se muestra un ejemplo de cada una de los dos tipos de placas de micropocillos utilizadas en esta tesis doctoral (figura II.4).

(a) (b)

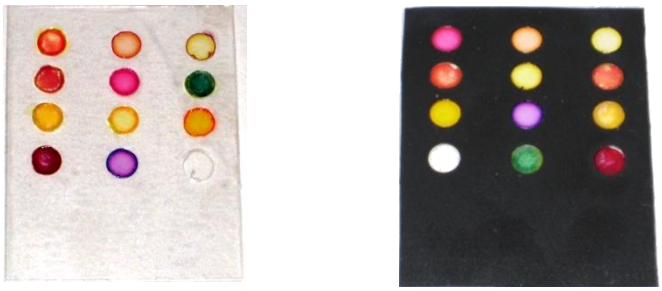

Figura II.4. Placas de micropocillos utilizadas para la determinación de pH (a) para la medida con escáner; b) para la medida con el instrumento portátil

2.2. Preparación de membranas y matrices ópticas y potenciométricas

En el último capítulo de esta tesis doctoral, se desarrolla una lengua electrónica basada en un mecanismo de transducción óptica y en otro potenciométrico para discriminación de sabores en disolución, utilizándose un tipo distinto de membranas y de soportes respecto a los capítulos anteriores.

En primer lugar, se preparó un conjunto de membranas individuales basadas en complejos metálicos de tetraporfirinas. Los complejos estudiados fueron: tetrafenilporfirina de zinc (ZnTPP), 5,10,15,20-tetrakis(4-butilfenil)porfirina de zinc(II) (ZnTBPP), tetrafenilporfirina de estaño(IV) (SnTPP), 5,10,15,20-tetrakis(4-butilfenil) porfirina de estaño(IV) (SnTBPP), tetrafenilporfirina de manganeso(III) (MnTPP), tetrafenilporfirina de molibdeno(V) (MoTPP), bromuro de tetrafenilporfirina de molibdeno(V) (Mo(TPP)Br), tetrafenilporfirina de cromo(III) (CrTPP) y 5,10,15,20-tetrakis(4-butilfenil)porfirina de Cr(III) (CrTBPP). Además, los cócteles contenían PVC, DOS y, en ocasiones, púrpura bromocresol (BCP) o azul Nilo (NB) como colorantes. Las membranas se prepararon mediante deposición y evaporación directa sobre la lámina soporte de las diferentes disoluciones en THF. Para ello, se utilizaron dos soportes diferentes. El primero de zafiro sobre el que se había depositado previamente una capa de óxido de zinc dopado con aluminio (AZO) mediante la técnica de deposición con láser pulsado (PLD). El segundo soporte fue de óxido de indio dopado con estaño (ITO). Ambos soportes son transparentes y conductores, de dimensiones 1 x 1 cm y con una resistividad comprendida entre 150 y 250 Ω. La irregularidad de las

membranas se debió a que los soportes no contenían micropocillos, sino que toda su superficie era plana.

Una vez caracterizadas las membranas individualmente mediante la medida de las señales ópticas y potentiométricas, se desarrolló un matriz para la medida conjunta de éstas. Las membranas se prepararon, como en el caso anterior, mediante deposición y evaporación directa sobre la lámina de las diferentes disoluciones de metaloporfirinas en THF. En la figura II.5 se observa una fotografía de una matriz preparada sobre un soporte de tipo AZO e insertada en el dispositivo para su posterior medida óptica.

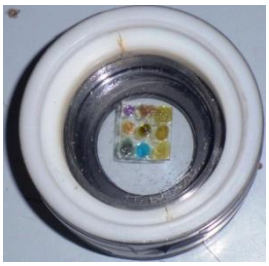

Figura II.5. Fotografía de una matriz para discriminación de sabores

3. TÉCNICAS DE MEDIDA

Durante esta tesis doctoral se han utilizado diferentes técnicas de medida, las primeras basadas en la medida de color a partir de dispositivos de imagen y utilizando los espacios de color RGB y HSV; por otra parte, también se ha utilizado, si bien minoritariamente, la medida de absorbancia en el rango visible de los elementos sensores.

3.1. Medida de color

El color es una percepción visual que se genera en el cerebro al interpretar las señales nerviosas enviadas por la retina ocular como consecuencia de la radiación electromagnética en la zona del visible que le llega. Por otra parte, no pertenece intrínsecamente a los objetos a los que asociamos un color, sino que es una propiedad de la luz que vemos después de reflejarse en ellos o de ser

transmitida por los mismos[57].

Aunque un color puede ser descrito de forma precisa midiendo la distribución de energía espectral de la luz que origina (energía por unidad de área y longitud de onda de una iluminación dada), esto conlleva un alto grado de redundancia debido a que la retina del ojo es sensible al color en tres zonas amplias de longitudes de onda, correspondientes aproximadamente a luz roja, verde y azul. Las señales eléctricas de estas células de la retina (conos) junto con las de las células sensibles a intensidad (bastones) se combinan en el cerebro dando lugar a las diferentes sensaciones de color: claridad, tono, saturación, forma, tamaño, textura, localización u otras, y se denominan atributos psicológicos del color.

Pese a su subjetividad y a que depende de cómo es percibido por el observador, el color se puede especificar numéricamente a partir de las leyes experimentales consecuentes de la generalización empírica conocida como generalización tricromática[58]. A partir de medidas físicas de potencia radiante y utilizando diversos tipos de detectores, es posible llegar a definir un color. Los dispositivos más habituales son térmicos y fotónicos, estando en este último caso basados en los efectos fotoeléctrico externo (fotoemisión) o fotoeléctrico interno (fotoconductividad y fotovoltaico), siendo muy frecuentes los dispositivos de carga acoplada CCD y los dispositivos CMOS.

La forma de especificar, crear y visualizar colores es mediante los denominados espacios de color[59]. Un espacio de color es la combinación de un modelo de color y de una apropiada representación gráfica de este modelo. Un modelo de color es un modelo matemático abstracto que describe los colores como secuencias de números, habitualmente tres o cuatro valores dependiendo del modelo, así RGB o CMYK (figura II.7). Los espacios de color se pueden clasificar en cuatro grupos que se relacionan mediante diferentes tipos de transformaciones: a) triestímulo lineales (CIE XYZ, RGB), b) cromáticos xy (CIE xyY), c) perceptualmente uniformes (CIE L*u*v*; CIE L*a*b*, R'G'B' no lineal) y

[57] E. Hita Villaverde. *El mundo del color*. 1st ed., Editorial Universidad de Granada, Granada (2001)

[58] G. Wyszecki, W.S. Stiles. *Color Science: Concepts and Methods, Quantitative Data and Formulae*. 2nd ed., Juhn Wiley & Sons Inc., New York (1982) pp. 968

[59] M. Melgosa, M.M. Pérez, A. Yebra, R. Huertas, E. Hita. *Algunas reflexiones y recientes recomendaciones internacionales sobre evaluación de diferencias de color*. Óptica Pura y Aplicada, 34 (2001) 1-10

d) orientados al tono (HSL, HSV)[58].

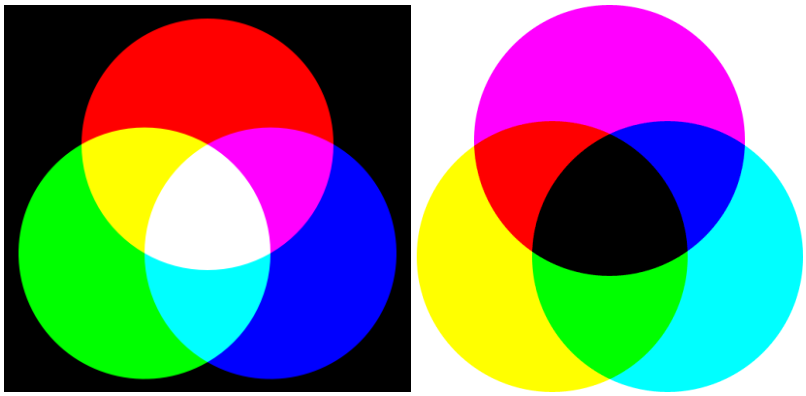

Figura II.7. Comparación entre los espacios de color RGB (mezcla de colores aditivos) y CMYK (mezcla de colores sustractivos)

En Química Analítica se ha utilizado la información procedente de diferentes dispositivos de imagen con propósitos cuantitativos; así, escáneres manuales[60] o de sobremesa trabajando tanto por reflexión[61] como por transmisión[62], dispositivos CCD[63], vídeo cámaras[64], cámaras fotográficas digitales[65] y analizadores digitales de color[66-68].

De todos los espacios de color antes citados, los más utilizados bajo el

[60] M. Kompany-Zareh, M. Mansourian, F. Ravaee. *Simple method for colorimetric spot-test quantitative analysis of Fe(III) using a computer controlled hand-scanner*. Anal. Chim. Acta, 471 (2002) 97-104

[61] J. Gabrielson, M. Hart, A. Jarelov, I. Kuhn, D. McKenzie, R. Mollby. *Evaluation of redox indicators and the use of digital scanners and spectrophotometer for quantification of microbial growth in microplates*. J. Microbiol. Methods, 50 (2002) 63-73

[62] A. Lapresta-Fernandez, L.F. Capitan-Vallvey. *Scanometric potassium determination with ionophore-based disposable sensors*. Sens. Actuators B, B134 (2008) 694-701

[63] J.J. Lavigne, S. Savoy, M.B. Clevenger, J.E. Ritchie, B. McDoniel, S.J. Yoo, E.V. Anslyn, J.T. McDevitt, J.B. Shear, D.J. Neikirk. *Solution-Based Analysis of Multiple Analytes by a Sensor Array: Toward the Development of an "Electronic Tongue"*. Am. Chem. Soc., 120 (1998) 6429-6430

[64] K. Tohda, M. Gratzl. *Micro-miniature autonomous optical sensor array for monitoring ions and metabolites 1: design, fabrication, and data analysis*. Anal. Sci., 22 (2006) 383-88

[65] V.V. Apyari, S.G. Dmitrienko. *Using a digital camera and computer data processing for the determination of organic substances with diazotized polyurethane foams*. J. Anal. Chem., 63 (2008) 530-537

[66] E. Hirayama, T. Sugiyama, H. Hisamoto, K. Suzuki. *Visual and Colorimetric Lithium Ion Sensing Based on Digital Color Analysis*. Anal. Chem., 72 (2000) 465-474

[67] K. Suzuki, E. Hirayama, T. Sugiyama, K. Yasuda, H. Okabe, D. Citterio. *Ionophore-Based Lithium Ion Film Optode Realizing Multiple Color Variations Utilizing Digital Color Analysis*. Anal. Chem., 74 (2002) 5766-5773

[68] Y. Suzuki, K. Suzuki. *Optical sensors for ions and protein based on digital color analysis*. Springer Ser. Chem. Sens. Biosens., 3 (2005) 343-365

punto de vista del análisis químico son los espacios triestímulo (RGB) y los de cromaticidad xy. El problema de estos espacios es que los colores se definen como mezcla de colores básicos y con frecuencia se utiliza un solo canal de los tres, con la consiguiente pérdida de información que ello supone, o bien varios de ellos a la vez, principalmente como cocientes de coordenadas. Por tanto, hay que decidir si o bien emplear un procedimiento en el que sean necesarias las tres coordenadas colorimétricas para así definir correctamente el color que adquiere el sistema analítico, lo que hace que el procedimiento sea más complejo, o bien utilizar un solo canal, con la pérdida de información que ello conlleva, aunque el procedimiento sea más sencillo. Esta pérdida de información se traduce a su vez en una disminución de la robustez de la señal.

Para resolver estas cuestiones se ha propuesto por este grupo de investigación el uso analítico del espacio de color HSV (Hue, Saturation, Value) y, en concreto, de su coordenada H[69]. Este espacio HSV define los colores como una combinación de tres parámetros: tono (H), saturación (S) y brillo (V). Por tanto, en este espacio el tono de un color viene definido por el parámetro H, mientras que las otras dos coordenadas añaden aspectos tales como intensidad en el caso de la saturación y claridad u oscuridad en el del brillo. De esta forma, es posible definir el tono del sensor mediante una sola coordenada y no tres como ocurre en las coordenadas RGB, resultando un parámetro analítico muy robusto.

Las ecuaciones II.3-II.5 permiten realizar el cálculo de H, S y V, respectivamente[70]. A partir de los valores RGB de cada píxel de la imagen se calcula la coordenada H y, a partir de todos los píxeles que existen en la imagen de cada elemento sensor, la moda del conjunto de datos de H obtenidos, que es utilizada como valor representativo.

---

[69] K. Cantrell, M.M. Erenas, I. Orbe-Paya, L.F. Capitan-Vallvey. *Use of the Hue Parameter of the Hue, Saturation, Value Color Space As a Quantitative Analytical Parameter for Bitonal Optical Sensors*. Anal. Chem. 82(2) (2010) 531-542

[70] A.R. Smith. Color gamut transform pairs. Proceedings of the 5th Annual Conference on Computer Graphics and Interactive Techniques, (1978) 12-19

$$H = \begin{cases} \dfrac{G - B}{máx_{canal} - mín_{canal}} + 0 \Big/ 6; & si\ máx = R \\ \dfrac{B - R}{máx_{canal} - mín_{canal}} + 2 \Big/ 6; & si\ máx = G \\ \dfrac{R - G}{máx_{canal} - mín_{canal}} + 4 \Big/ 6; & si\ máx = B \end{cases} \quad \text{(II.3)}$$

$$S = \frac{máx_{canal} - mín_{canal}}{máx_{canal}} \quad \text{(II.4)}$$

$$V = máx_{canal} \quad \text{(II.5)}$$

Debido a la naturaleza circular del parámetro H, frecuentemente es representado como un círculo cuyos valores posibles se sitúan entre 0 y 360º, representado ambos el mismo tono (figura II.8). Al objeto de simplificar todo el cálculo utilizando H, los valores angulares se normalizan entre 0 y 1.

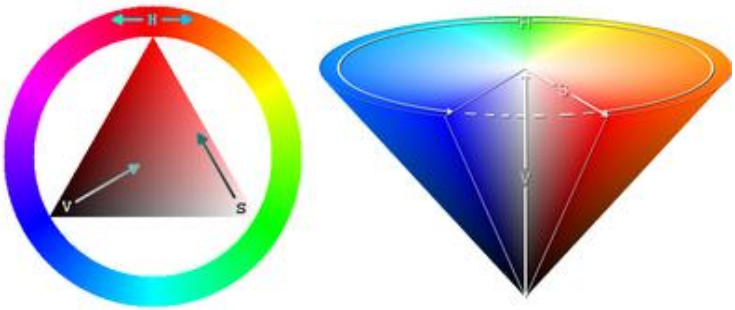

Figura II.8. Representación del espacio de color HSV

En un estudio previo realizado[69] se demostró que el parámetro analítico H, al contrario de lo que ocurre con los canales RGB, presenta una considerable insensibilidad frente a variaciones tanto del dispositivo de medida como de condiciones de iluminación o espesor, concentración de colorante o cromóforo o modo de fabricación de la membrana. No sólo presenta ventajas frente a otras coordenadas de color, sino que además, debido a la alta precisión que se obtiene con este parámetro, es posible su uso de forma directa sin necesidad de normalización de la señal entre un valor máximo (máxima concentración de analito) y uno mínimo (ausencia de analito) mediante el empleo del parámetro 1 -

α, como es habitual en este tipo de sensores[69].

3.2. Escáner óptico

La medida de la matriz sensora para pH se llevó a cabo utilizando un escáner óptico de sobremesa o plano, modelo Microtek ScanMaker i900 (figura II.9). Para la medida por reflexión dispone de una superficie plana de vidrio sobre la que se sitúa el elemento a escanear y bajo la cual se desplaza el elemento móvil donde se ubica la fuente de luz y el sensor, mientras que para medida por transmisión posee unos espejos, estando ahora localizada la fuente de luz encima del objeto a escanear. En cualquier caso, el sensor óptico convierte la luz en carga eléctrica, que con la ayuda de un software de conversión analógico/digital transforma la señal eléctrica generada en una señal electrónica en forma de una imagen de mapa de bits.

Figura II.9. Escáner modelo Microtek ScanMaker i900

La calidad de un escáner y, en consecuencia, de las imágenes digitales que genera, viene determinada por tres aspectos: 1) profundidad del color, medida en bits por píxel (BPP), que se refiere a la cantidad de bits de información necesarios para representar el color de un píxel; 2) resolución, que es la cantidad de píxeles que contiene una imagen y se mide en píxels por pulgada (PPI); y 3) rango de densidad, entendida como la capacidad de un escáner para recoger el rango completo de densidades de la imagen de partida o para distinguir variaciones, así como la linealidad de la diferenciación.

Como resultado del escaneo se obtiene una imagen RGB no comprimida que puede comprimirse y preprocesarse previamente a ser transferida al ordenador con algún firmware embebido en el periférico. Los formatos más habituales de las imágenes escaneadas son JPEG, TIFF, mapa de bits o PNG, dependiendo del uso que se vaya a dar a dicha imagen. En este caso se ha utilizado el formato TIFF, correspondiente a una imagen de alta resolución, recogiendo, además de los datos de la imagen propiamente dicha, información sobre las características de la imagen, lo que es útil para su tratamiento posterior.

Todas las imágenes fueron procesadas utilizando Matlab® r2007b v.7.5 (figura II.10). Tras la separación de cada archivo de imagen en sus correspondientes tres valores RGB, el primer paso, referido a la máscara, fue determinar qué píxeles formaban parte de las membranas y cuáles no. En este paso, cada canal se normalizó de forma independiente, generando unos valores de R, G y B en el rango de 0 a 1. Tras la normalización, se determinó la diferencia entre los canales que producían los valores máximos y mínimos para cada píxel de cada imagen. Estas diferencias fueron comparadas con la diferencia máxima observada en la imagen completa multiplicada por una fracción umbral, donde los píxeles con mayores diferencias se interpretaron como coloreados y los píxeles con menores diferencias como fondo. El valor usado como fracción umbral en todos los casos fue 0,3, ya que valores superiores dan lugar a una máscara más selectiva que interpreta más píxeles como fondo que coloreados. El ajuste de este valor sólo es necesario cuando las membranas sensoras son muy delgadas (la disminución del umbral incluye los píxeles blancos también) o cuando el balance de blancos no ha sido corregido adecuadamente (el aumento del umbral excluye los píxeles que no forman parte del material sensor que aparecen coloreados). Tras clasificar cada píxel como coloreado o no coloreado, se dividió la imagen en pequeñas subimágenes con forma rectangular, una por cada membrana, localizando las filas y columnas de la imagen que no contenían píxeles coloreados. Se consideraron las subimágenes que contenían un número suficiente de píxeles coloreados (16.000 o más), repitiendo el proceso dos veces más. Debido a que las membranas son circulares y los cortes fueron verticales y horizontales, las subimágenes cortadas tenían esquinas con píxeles no coloreados. Estos píxeles se usaron en el siguiente paso para reequilibrar los

canales de color entre sí y así controlar la apariencia del blanco en la imagen.

Tras la aplicación de la máscara y el recorte, se escalaron los canales RGB para cada subimagen entre 0 y 1, utilizando dos métodos diferentes. En el primer método, cada canal se divide por su máximo valor posible, 255 para una profundidad de color de 8 bits por píxel (color indexado) o 65.535 (color de alta resolución o HiColor) para 16 bits. En el segundo método se utilizan diferentes valores para cada canal, lo que afecta al balance de blancos de la imagen. Aquí, se dividió cada canal por el máximo valor observado para cada caso en el espacio de blancos de las esquinas de cada uno de los rectángulos. Tras estos pasos, los valores RGB escalados fueron la base de todos los cálculos posteriores considerados.

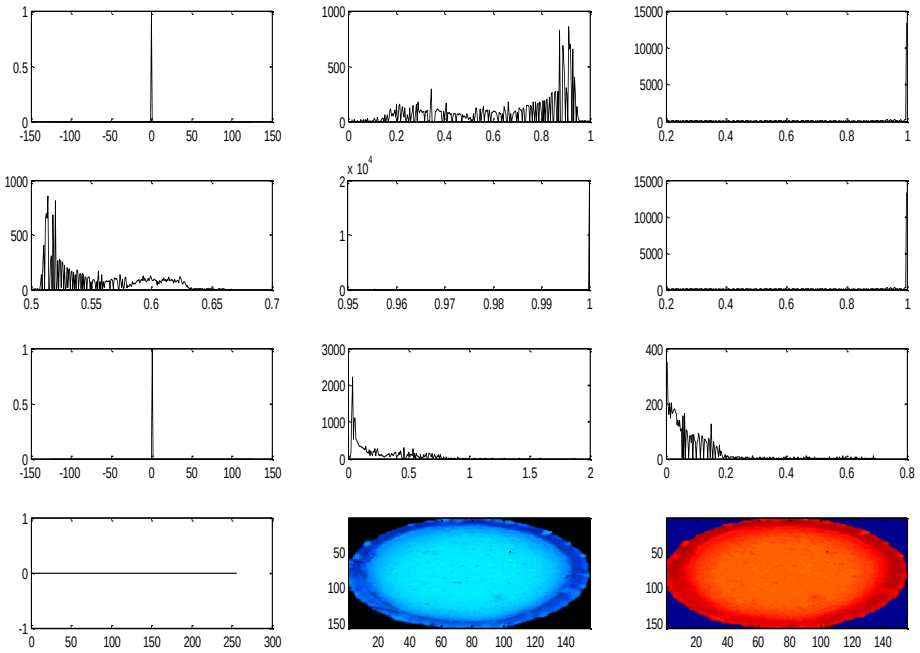

Figura II.10. Procesado de una membrana utilizando Matlab® r2007b v.7.5

3.3. Instrumento portátil

En el caso del instrumento portátil desarrollado, la información de color de la matriz se adquirió por medio de una fuente de luz programable y un conjunto de detectores de color sensibles a las regiones espectrales roja, verde y azul, permitiendo la medida simultánea de las coordenadas RGB

correspondientes a cada elemento sensor y calculando a partir de éstas los valores de H, S y V. Se seleccionó el microcontrolador modelo PIC18F4550 por su integración de un módulo USB, que permite la fácil comunicación con el ordenador.

En primer lugar se realizó un estudio de la influencia del iluminante en la medida (figura II.11), desarrollando una aplicación que permitía definir el iluminante de la pantalla. Se irradiaron los diferentes elementos sensores de la matriz con iluminantes estándar definidos de acuerdo con sus coordenadas cromáticas. Debido a que la iluminación definida como color blanco por la pantalla presentaba un exceso de componente azul, se probaron diferentes combinaciones de los componentes para obtener una fuente de luz similar al iluminante estándar D65. El mejor resultado de este proceso de optimización, al que se denominó "blanco modificado", fue el utilizado para realizar el estudio.

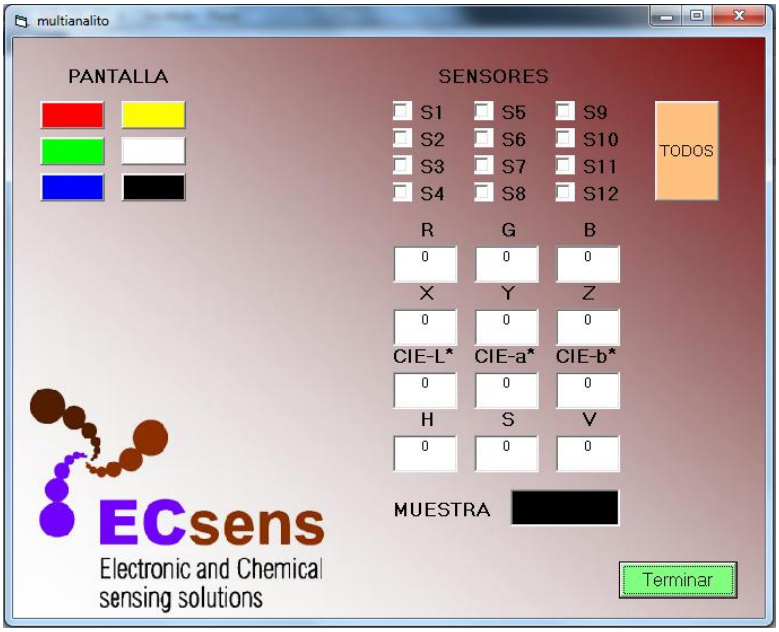

Figura II.11. Aplicación desarrollada para el estudio de la influencia del iluminante

Posteriormente se optimizó el tiempo de medida, así como el diámetro de los círculos iluminantes (figura II.12). El tiempo de integración, es decir, el intervalo de tiempo durante el cual la matriz de fotodiodos genera una fotocorriente para la adquisición de radiación óptica, se estudió entre 10 µs y 100

s. Se midió la respuesta de la matriz sensora en función del tiempo de integración en las condiciones de iluminación seleccionadas previamente, concluyéndose que el tiempo más corto con sensibilidad y velocidad de respuesta óptimas era 200 ms.

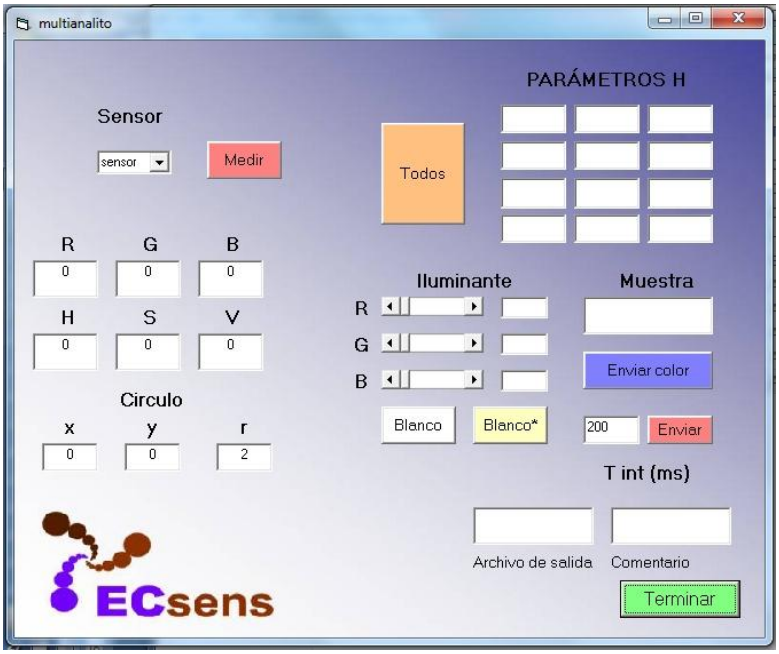

Figura II.12. Aplicación diseñada para la optimización del tiempo de medida y la posición y el radio de los círculos iluminantes

Respecto al estudio de la influencia del diámetro de los círculos iluminantes y considerando que el diámetro de los elementos sensores era de 5 mm, se demostró que no se producía ninguna variación significativa en el cálculo de H en el rango de 5,75 a 10,25 mm, con una desviación estándar relativa inferior al 5%. Finalmente, se seleccionó como valor óptimo de este parámetro 6,35 mm.

Tras la optimización de los anteriores parámetros se diseñó una nueva aplicación para el ordenador que, a partir de los valores de H correspondientes a los diversos elementos sensores, generaba un valor de pH y lo comparaba con el obtenido utilizando un método potenciométrico, considerado como valor de pH de referencia o real (figura II.13).

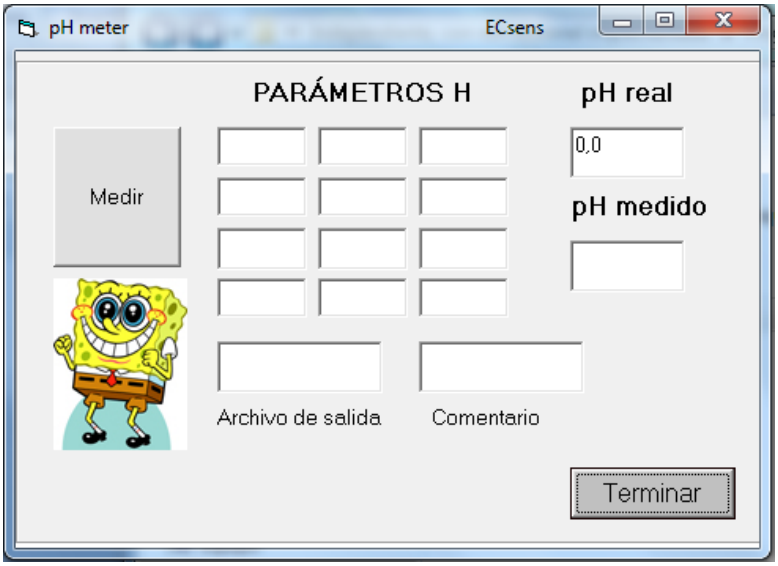

Figura II.13. Aplicación diseñada para la medida con el instrumento portátil conectado a un procesador de datos externo

Tras el primer estudio realizado, en el cual los datos se transferían al ordenador para realizar la predicción de pH, se modificó el instrumento portátil para su uso *in situ* sin necesidad de conexión a un procesador de datos externo. Para ello, se aplicó un algoritmo multiobjetivo que generó un conjunto de redes neuronales artificiales (ANN). Una vez seleccionada la ANN óptima para la predicción del pH e implementada en la memoria del microcontrolador del instrumento portátil, se determinó el pH de un amplio conjunto de muestras alimentarias, biológicas y de productos de uso doméstico, comparando los resultados con los obtenidos utilizando el escáner convencional empleado anteriormente y un potenciómetro (figura II.14).

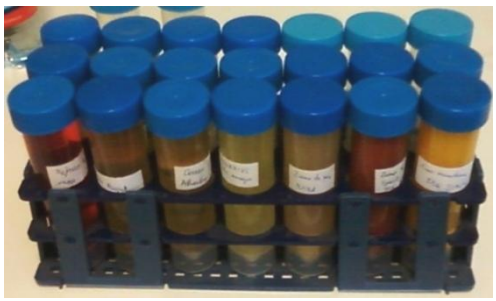

Figura II.14. Algunas de las muestras alimentarias, biológicas y de productos de uso doméstico medidas con el instrumento portátil

3.4. Computer Screen Photo-Assisted Technique (CSPT)

La CSPT se basa en una interfaz óptico-sensora propuesta por Lundström y Filippini[71] en 2003, que permite llevar a cabo la caracterización analítica de la absorción en el rango visible de diversos tipos de muestras. Esta técnica requiere periféricos computacionales fáciles de obtener, de bajo coste y extensa difusión. El hardware básico consta de una pantalla de ordenador, ya sea un tubo de rayos catódicos (CRT) o una pantalla de cristal líquido (LCD), que es utilizada como fuente de luz policromática programable, y una cámara web, que se emplea como detector de tres bandas (figura II.15).

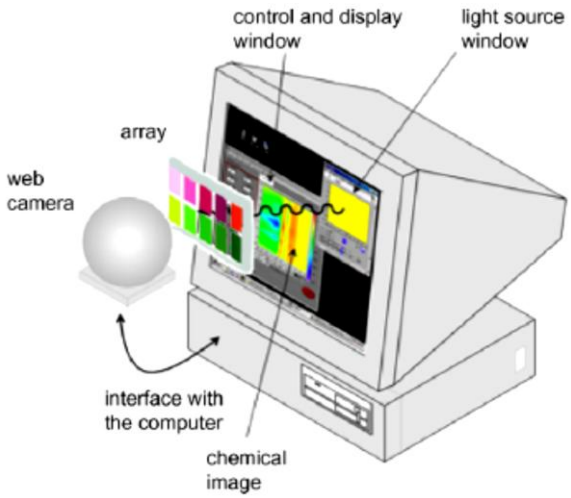

Figura II.15. Esquema de una plataforma CSPT

Las pantallas de ordenador son capaces de visualizar áreas confinadas con forma, color e intensidad arbitrarios, que pueden ser analizadas bi-dimensionalmente con una resolución de 200 µm definida por el *pixel pitch* (distancia entre dos puntos contiguos del mismo color)[72]. En lo que respecta a las medidas CSPT, las principales diferencias entre estos dos tipos de pantallas son la naturaleza del pulso de las pantallas CRT y la luz polarizada linealmente emitida por las pantallas LCD[73].

---

[71] D Filippini, S.P.S. Svensson, I. Lundström. *Computer screen as a programmable light source for visible absorption characterization of (bio)chemical assays*. Chemical Communications, 2 (2003) 240-241

[72] D. Filippini, A. Alimelli, C. Di Natale, R. Paolesse, A. D'Amico, I. Lundström. *Chemical Sensing with Familiar Devices*. Angew. Chemie, 118 (2006) 3884-3887

[73] E.F. Schubert, J. Kyu Kim. *Solid-state light sources getting smart*. Science, 308 (2005) 1274-1278

La luz emitida por una pantalla de ordenador no es monocromática, sino la combinación de tres fuentes primarias policromáticas. La radiancia espectral de estas fuentes primarias conlleva la percepción humana de los colores rojo, verde y azul. Cualquier otro color puede ser generado mediante combinación lineal de los colores primarios de acuerdo con la ecuación II.6[74]:

$$c_i(\lambda) = r_i R(\lambda) + g_i G(\lambda) + b_i B(\lambda) \qquad \text{(II.6)}$$

donde R(λ), G(λ) y B(λ) son las radiancias espectrales de los colores primarios; r_i, g_i y b_i son números comprendidos en el intervalo [0-1], que representan la modulación particular de las primarias para un color dado deseado; y λ, la longitud de onda, está limitada al rango visible (390-800 nm). Los sistemas de color convencionales presentan una resolución de 8 bits (valores entre 0-255) para cada canal de color, dando un total de 2^{24} colores, que pueden ser visualizados en la pantalla.

Durante una medida CSPT se ilumina la muestra mediante la emisión de una secuencia de colores en una zona determinada de la pantalla. La luz emergente es adquirida por la cámara, que trabaja a una velocidad de captura de 1 fotografía/s. El resultado es un archivo de vídeo digital (formato .avi) de la matriz expuesta a los diferentes colores iluminantes. El vídeo es posteriormente descompuesto en fotografías individuales, extrayéndose la información de las regiones de interés (ROIs) seleccionadas en la imagen. Las ROIs son indicadas con círculos en la figura II.16 y se localizan tanto en las membranas sensoras como en el área de fondo.

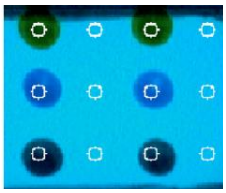

Figura II.16. Imagen adquirida con la cámara de las capas sensoras bajo una iluminación azulada

[74] R. Jackson, L. Mac Donald, K. Freeman. *Computer generated color*. Wiley (1994)

Los valores digitales de cada nivel de color (rojo, verde y azul) de los píxeles contenidos en las ROIs son promediadas, generando las variaciones de intensidad de cada canal de color de la pantalla. Como resultado se obtiene una firma espectral o huella dactilar distintiva de la muestra. Ésta contiene también la señal correspondiente al fondo, que se le debe restar para evaluar la absorción de cada membrana (figura II.17).

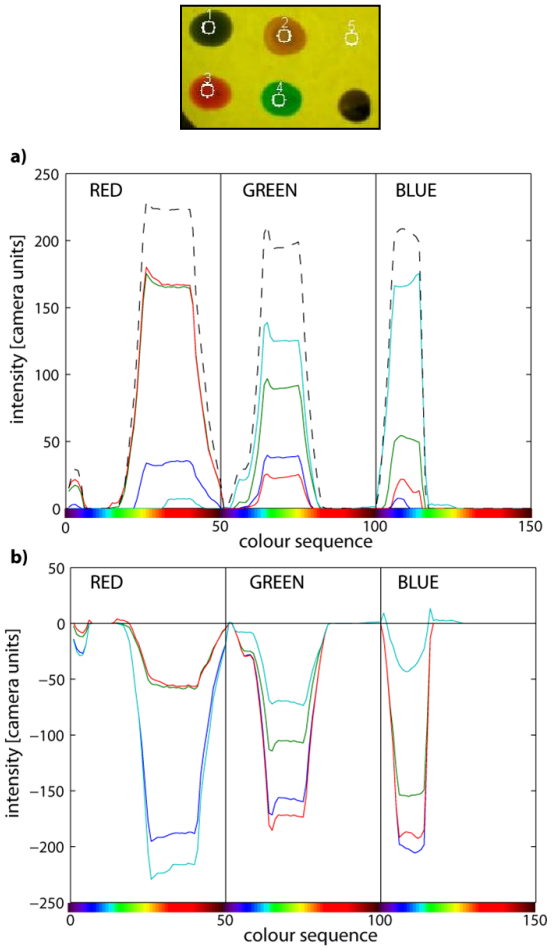

Figura II.17. a) Huellas dactilares CSPT de membranas sensoras obtenidas con una secuencia de iluminación de 50 colores. La línea negra discontinua representa la fuente de luz de referencia (fondo, círculo 5); b) Diferencia entre la intensidad de la huella dactilar y de fondo

En las medidas CSPT, dependiendo de la transmitancia de la sustancia evaluada, se agrupan los diferentes iluminantes en el espacio de color, pudiendo ser la información redundante y así reducir la diversidad espectral de la huella

dactilar. Obviamente, secuencias de color de mayor duración sufren cambios más intensos, al objeto de incorporar una mejor definición de los colores. Así, las secuencias de iluminación pueden ser optimizadas para cada caso particular considerando la transmitancia de la sustancia. Sin embargo, es también evidente que ciertas sustancias estarán siempre representadas por una mayor variación dentro del espacio de color. Cuanto mayor sea ésta, mayor será la posibilidad de encontrar una secuencia de iluminación que permita diferenciar todas sus características, creando una huella dactilar distintiva. En resumen, considerando la transmitancia de sustancias que presentan mínimos en la zona media del espectro visible, la CSPT permite obtener más características espectrales que en el caso de sustancias que absorban en regiones extremas del espectro. Estas condiciones son más adecuadas para las sustancias afectadas por luz verde, amarilla y naranja que por luz azul o roja, lo que puede asociarse a la contribución restringida en las señales procedentes de los diversos canales. Así, sustancias que absorben luz en el rojo lejano (o azul) sólo influyen en la señal roja (o azul) de la cámara web, mientras que una sustancia que absorbe verde, amarillo o naranja reúne contribuciones distintivas procedentes de todos los canales, enriqueciendo así la huella dactilar[75].

Normalmente la mayoría de las aplicaciones se llevan a cabo utilizando una secuencia de 50 colores que cambian gradualmente de color azul a rojo (figura II.18), produciendo una secuencia de color que se asemeja a la percepción humana del espectro visible. Sin embargo, para determinados indicadores seleccionados, se puede definir una secuencia más corta y dirigida, que permite adquirir imágenes de forma continua de las características espectrales de la sustancia.

[75] D. Filippini, I. Lundström. *Preferential color substances and optimized illuminations for computer screen photo-assisted classification*. Anal. Chim. Acta, 557 (2006) 393-398

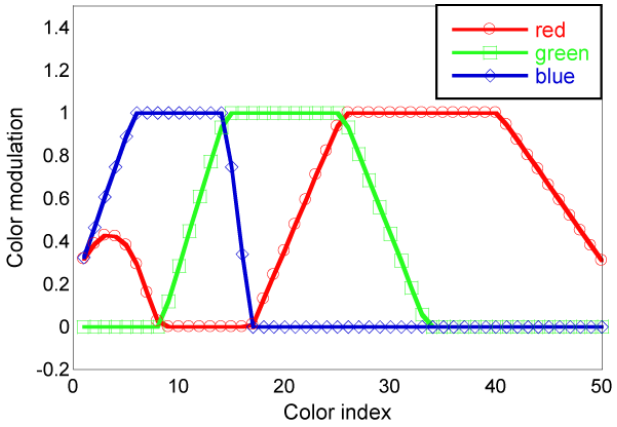

Figura II.18. Modulación del peso de la coordenadas r, g, b siguiendo la ecuación II.6

Para una descripción matemática de las características CSPT, debe considerarse el total de elementos que están implicados en la medida. Las radiancias espectrales de la pantalla están dadas por la ecuación II.7 y son especificadas por los tripletes (r_i, g_i, b_i). El siguiente paso consiste en la caracterización de la muestra en sí misma mediante su espectro de transmitancia. Para cada color que se visualiza en la pantalla se emite una radiancia espectral compuesta y modulada específicamente mediante la transmitancia de la sustancia ensayada T(λ)[76]. La luz emergente pasa a través de los filtros de la cámara [$F_R(\lambda)$, $F_G(\lambda)$ y $F_B(\lambda)$], incidiendo en el detector, que origina una respuesta espectral definida D(λ). Para sustancias no emisoras caracterizadas por una cierta transmitancia espectral y para cada color c_i visualizado en la pantalla, las intensidades de medida de la cámara web vienen dadas por:

$$\begin{aligned} Ir_i &= \int_\lambda c_i(\lambda)\cdot F_r(\lambda)\cdot T(\lambda)\cdot D(\lambda)\,d\lambda \\ Ig_i &= \int_\lambda c_i(\lambda)\cdot F_g(\lambda)\cdot T(\lambda)\cdot D(\lambda)d\lambda \\ Ib_i &= \int_\lambda c_i(\lambda)\cdot F_b(\lambda)\cdot T(\lambda)\cdot D(\lambda)d\lambda \end{aligned} \qquad \text{(II.7)}$$

[76] D. Filippini, I. Lundström. *Spectroscopic information retained in screen photo-assisted techniques*. Anal. Chim. Acta, 521 (2004) 237-244

Introduciendo la expresión analítica para c_i y reordenando, se obtiene:

$$\begin{bmatrix} Ir_i \\ Ig_i \\ Ib_i \end{bmatrix} = \begin{bmatrix} r_R & r_G & r_B \\ g_R & g_G & g_B \\ b_R & b_G & b_B \end{bmatrix} \begin{bmatrix} r_i \\ g_i \\ b_i \end{bmatrix} = S \begin{bmatrix} r_i \\ g_i \\ b_i \end{bmatrix} \qquad \text{(II.8)}$$

donde los términos de la matriz de la sustancia S son funciones de T(λ). Cada color iluminante produce tres ecuaciones de intensidad, y si proceden de tres fuentes de luz diferentes, se pueden obtener hasta nueve espectros T(λ) de cualquier sustancia particular.

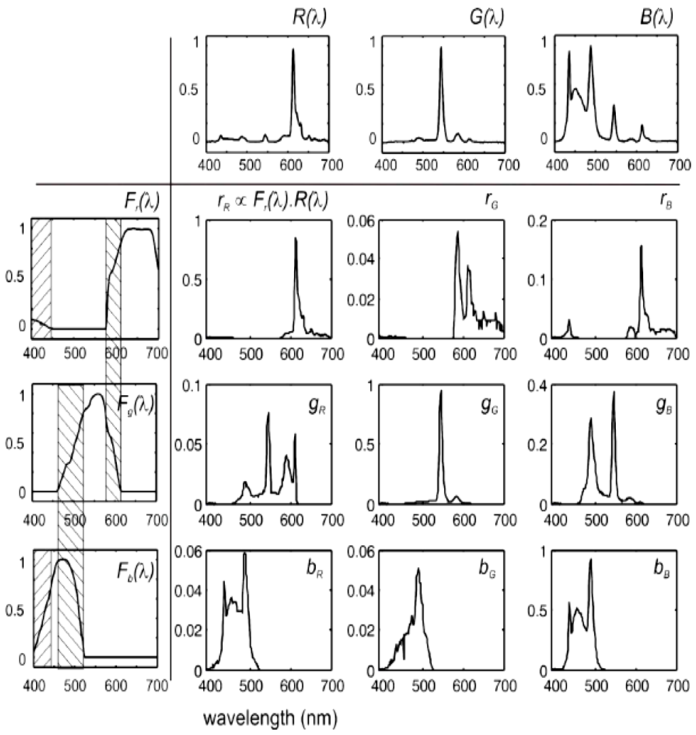

Figura II.19. Gráficas espectrales formadas mediante las combinaciones de las radiancias espectrales de la pantalla LCD y los tres filtros de la cámara para una transmitancia de la muestra T(λ)=1

La figura II.19 muestra las nueve combinaciones diferentes radiancia-filtro primarias obtenidas a partir de una pantalla LCD y una cámara web habitual

basada en un CCD[77].

Algunas veces puede resultar útil considerar una cantidad relacionada con la absorbancia espectral, pero que, a diferencia del caso anterior, depende del color iluminante y no de la longitud de onda. Se conoce como absorbancia CSPT y se define como sigue:

$$A(\text{color}) = -\log \frac{R_{muestra}(\text{color}) + G_{muestra}(\text{color}) + B_{muestra}(\text{color})}{R_{bg}(\text{color}) + G_{bg}(\text{color}) + B_{bg}(\text{color})} \qquad \text{(II.9)}$$

donde $R_{muestra}$, $G_{muestra}$ y $B_{muestra}$ son las intensidades registradas en las regiones espectrales, y R_{bg}, G_{bg} y B_{bg} son las intensidades en las regiones del fondo que corresponden a la fuente de luz de referencia.

Una característica interesante de la plataforma de medida CSPT es que, al estar basada en la adquisición de imágenes de una membrana sensora, el área sensible es descompuesta en un conjunto de sensores individuales, por ejemplo, píxeles individuales, cuyo número está limitado en última instancia por la resolución de la cámara. Así, se pueden analizar simultáneamente hasta varios miles de sensores virtualmente independientes, ya sean membranas en forma de gotas o distribuidas uniformemente en toda la superficie del soporte, facilitando la preparación de matrices de indicadores químicos. Las señales procedentes de las membranas sensoras podrían ser analizadas individualmente o podría calcularse un valor medio de píxeles pertenecientes a la ROI. La figura II.20 ilustra esquemáticamente este proceso e identifica pixeles individuales en la imagen, cuya variación de color durante una medida CSPT se considera la señal del sensor.

[77] D. Filippini, I. Lundström. *Spectral characteristics of computer screen photoassisted classification*. J. Appl. Physics, 99(11) (2006) 114518- 114518-8

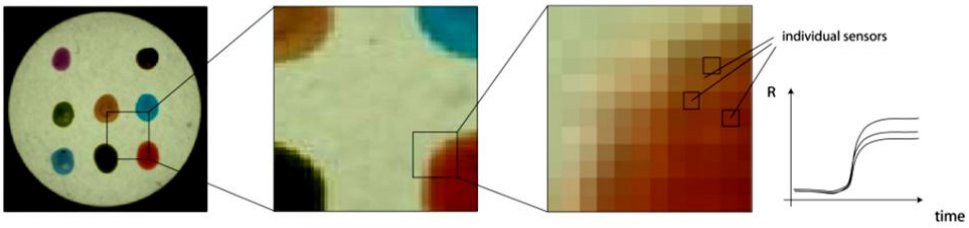

Figura II.20. Representación esquemática de la descomposición de la membrana sensora en sensores independientes (píxeles)

Como se ha comentado anteriormente, durante una medida CSPT la pantalla de ordenador ilumina la muestra mediante la secuencia de colores programada y las imágenes se adquieren simultáneamente mediante una cámara web. Por cada fotografía se genera un conjunto de tres matrices que contiene la intensidad de los píxeles individuales para cada filtro de la cámara. Se pueden representar las imágenes de cada matriz en un mapa codificado de color, como se muestra en la figura II.21, para la secuencia de colores iluminantes primarios rojo [255 0 0], verde [0 255 0] y azul [0 0 255]. De esta forma, es posible apreciar la intensidad de color en el fondo que representa la fuente de luz y la diferente absorción de luz llevada a cabo por las diversas membranas de cromóforos en cada banda. Normalmente, los colores primarios son capaces de captar suficiente información como para caracterizar las membranas sensoras, ya que cada otro color es el resultado de una combinación lineal de estos primarios. Considerando el caso de la secuencia RGB ilustrada en la figura II.21, cabe mencionar que tres de estas señales son consideradas incoherentes (color-filtro cámara: rojo-verde, rojo-azul y verde-azul), debido a que corresponden a una detección de más baja longitud de onda que la fuente iluminante. Estas señales originadas a partir de la superposición parcial de los filtros de la cámara, e incluso si contienen información parcial sobre la absorción, normalmente no son consideradas en el análisis, ya que la relación entre la señal y el ruido es pobre. El canal de la cámara correspondiente al color iluminante (color-filtro cámara: rojo-rojo, verde-verde y azul-azul) aporta información sobre la absorción, mientras que los canales de la cámara correspondientes a longitudes de onda más largas que el iluminante (color-filtro cámara: verde-rojo, azul-verde y azul-rojo) contienen información sobre la emisión. Por lo tanto, a partir de una secuencia de colores RGB, se extrapolan seis matrices bidimensionales significativas, pero si la

membrana sensora medida no es luminiscente, tres de estas contribuciones se originan también mediante superposición del filtro de la cámara, y no son consideradas, obteniéndose sólo tres matrices útiles.

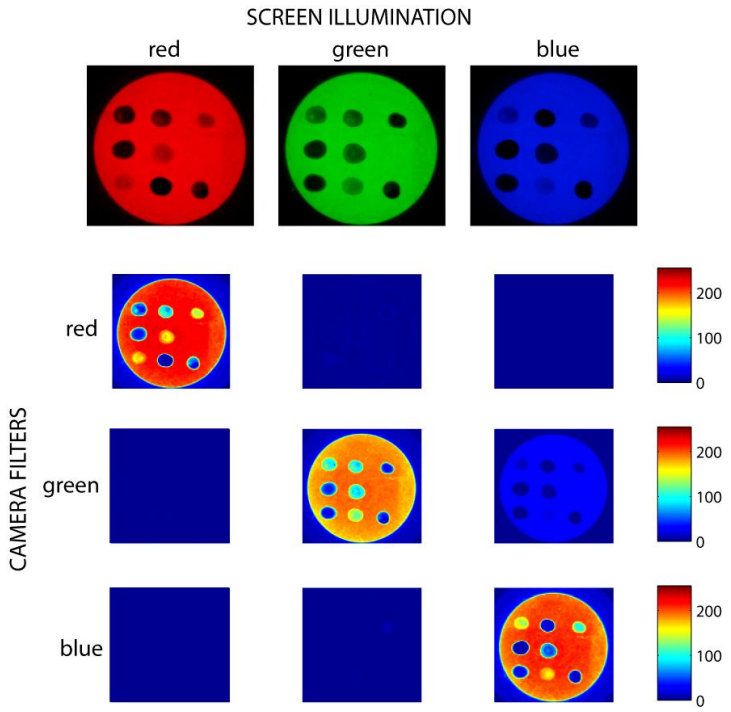

Figura II.21. Ejemplo de la imagen tomada de una matriz de membranas sensoras con una secuencia de colores rojo, verde y azul con el CSPT. Cada imagen puede ser descompuesta en tres componentes correspondientes a las tres regiones espectrales de los filtros de la cámara

Para reducir la gran cantidad de datos que proceden de las medidas CSPT temporales y evitar el complejo tratamiento de las matrices tridimensionales, se opera con una selección de ROIs que identifican el área útil de la imagen. La intensidad media de todos los píxeles contenidos en estas zonas es evaluada y normalmente referenciada con respecto a la primera fotografía. De este modo, cada medida aporta un número de señales correspondientes al número de ROIs para cada canal de la cámara y es posible representar y comparar las medidas.

4. CARACTERIZACIÓN DE LOS ELEMENTOS SENSORES

4.1. Caracterización de membranas y matrices ópticas

Las membranas depositadas en la matriz sensora para pH fueron caracterizadas individualmente mediante la medida de su variación de absorbancia con un espectrofotómetro y, posteriormente, de forma conjunta dispuestas como una matriz utilizando un escáner, como se ha indicado anteriormente. El pH se midió entre 0 y 14 cada 0,1 o 0,2 unidades y realizando 12 réplicas de cada matriz conteniendo 11 membranas. Para realizar las medidas, se sumergieron las matrices sensoras en una disolución acuosa y se añadieron diferentes volúmenes de hidróxido sódico o bien de ácido clorhídrico de concentraciones adecuadas para variar el pH. Tras esperar 5 minutos para la equilibración con la disolución, se registró el valor del pH mediante el uso de un pH-metro adecuadamente calibrado (figura II.22) y se escanearon las matrices. Las imágenes obtenidas se trataron como posteriormente se indica.

Figura II.22. Montaje realizado para la caracterización de las membranas sensoras de pH

Para el desarrollo del instrumento portátil, se estudió la respuesta de la matriz sensora de forma similar a la seguida con el escáner. Tras cada adición de

diferentes volúmenes de hidróxido sódico o de ácido clorhídrico y agitación, se dejó equilibrar la matriz durante 5 minutos y se insertó en el instrumento para su medida. Las medidas se mostraron en la pantalla del instrumento y se almacenaron en su memoria EEPROM.

4.2. Caracterización de membranas y matrices ópticas y potenciométricas

En primer lugar, se realizó la caracterización potenciométrica de las membranas utilizando los dos tipos de soportes previamente descritos, AZO e ITO. Se estudió su variación de potencial en presencia y ausencia de las membranas, preparadas a partir de los cócteles compuestos por una tetrafenilporfirina, PVC y DOS (en algunos casos, también NB o BCP) en THF mediante deposición sobre dicho soportes. Para ello, se sumergieron en agua destilada y se evaluaron las variaciones frente a disoluciones de diferente concentración de amoníaco, glutamato monosódico, etanol y ácido acético, al adicionar diferentes volúmenes de éstos. Con objeto de estudiar la influencia de la luz sobre los valores de potencial de las membranas preparadas, se midió el potencial primero en oscuridad y posteriormente iluminando las membranas tanto con un LED blanco como con una lámpara UV comercial (modelo VL-4L, 4 W: 365 nm) (figuras II.23a y II.23b).

(a) (b)

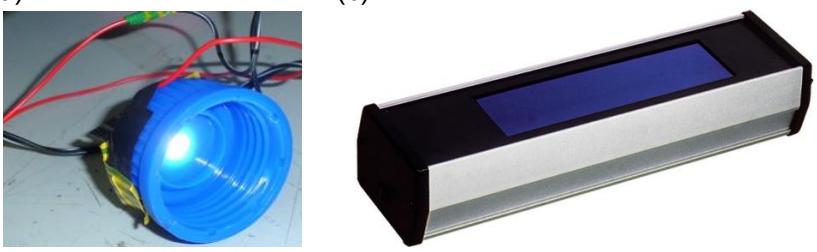

Figura II.23. Dispositivos utilizados para el estudio potenciométrico de las membranas. a: Iluminante LED; b: lámpara UV

La figura II.24 muestra el montaje experimental utilizado para llevar a cabo el estudio potenciométrico. Cada membrana depositada sobre los soportes se puso en contacto con el potenciómetro mediante una pinza de cocodrilo que la

sujetaba y posteriormente se sumergió en la disolución de medida. Con un multímetro de 3 canales se controlaron las variaciones de pH y de conductividad eléctrica de las disoluciones.

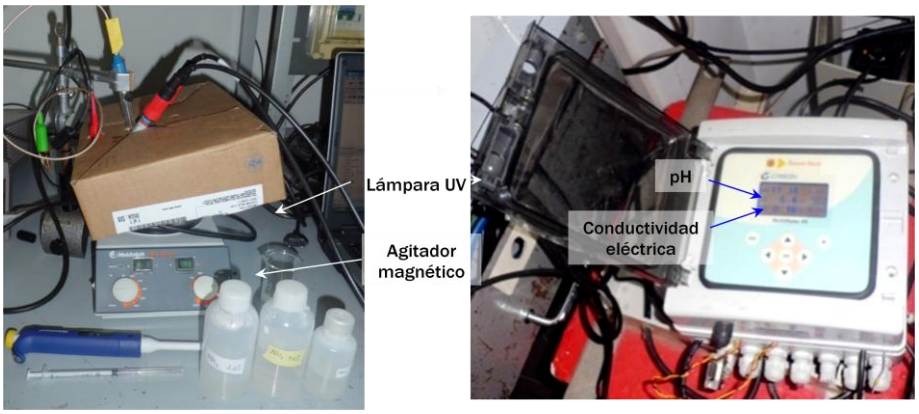

Figura II.24. Montaje experimental para el estudio potenciométrico de las membranas individuales

Para realizar la medida de las membranas con la plataforma CSPT, se situaron éstas en una placa Petri ubicada sobre una pantalla de ordenador y donde las disoluciones a analizar se introdujeron con una pipeta o una jeringa. Durante cada medida CSPT se iluminó la muestra desde abajo con la pantalla de ordenador y las imágenes se adquirieron mediante una cámara web situada en la parte superior con la secuencia de 50 colores definida en la figura II.18. Otra forma de medida empleada (figura II.25), consistió en tomar imágenes de cada matriz para la secuencia de colores iluminantes primarios, rojo [255 0 0], verde [0 255 0] y azul [0 0 255]. El conjunto se cubrió en todas las ocasiones con un paño negro para evitar interferencias de la luz ambiente.

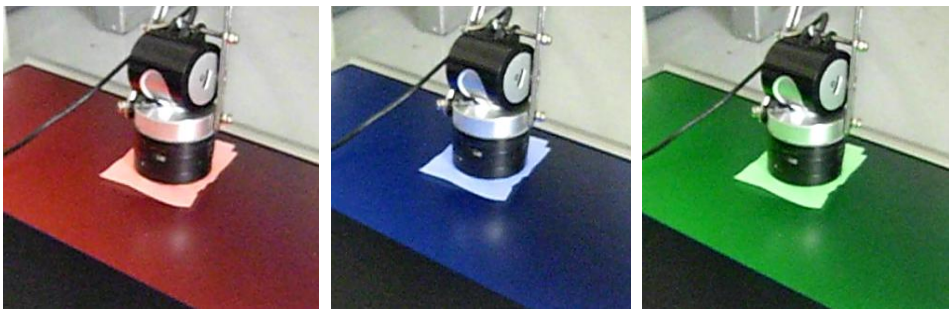

Figura II.25. Iluminación de la matriz utilizando las tres fuentes primarias

La recogida de las imágenes se efectuó con una aplicación desarrollada en el programa Matlab® (v.7.6, MathWorks, 2008, Inc., Natick, MA, USA), que entre otras opciones permitía definir la posición y el radio de las ROIs, captar fotografías instantáneas en el formato deseado y generar archivos de vídeo digital de la matriz expuesta a la secuencia de 50 colores o a los 3 iluminantes primarios (figura II.26). Los vídeos fueron posteriormente descompuestos en fotografías individuales, extrayéndose la información RGB de las ROIs.

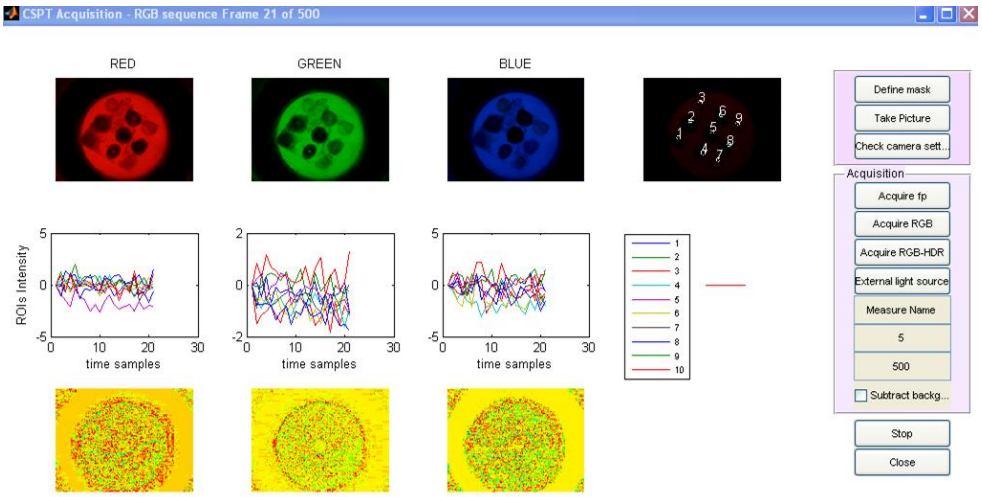

Figura II.26. Aplicación utilizada para obtener la información colorimétrica de la matriz

4.3. Caracterización de membranas mediante absorbancia

Además de en el caso de las membranas individuales que posteriormente se depositaron para formar la matriz sensora de pH, durante el estudio de nuevos ionóforos para calcio se llevó a cabo la caracterización espectrofotométrica de las membranas mediante la medida de su absorbancia (ver capítulo 8). Para realizar la medida de la señal analítica se introdujeron las diversas membranas preparadas de la forma que se ha indicado anteriormente en una cubeta de flujo de diseño propio (figura II.27), que se situó en el compartimento de medida de un espectrofotómetro DAD (figura II.28).

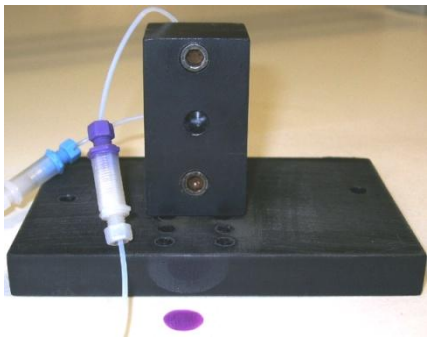

Figura II.27. Cubeta de flujo

Figura II.28. Bomba peristáltica, espectrofotómetro y disoluciones medidas

Las diferentes disoluciones a medir se hicieron pasar a través de la cubeta durante 2 minutos mediante una bomba peristáltica. Tras la equilibración de cada membrana (1 minuto), se midió su absorbancia a 660 nm. En la figura II.29 se muestra cómo varía el espectro de una de las membranas estudiadas en función de la concentración de analito.

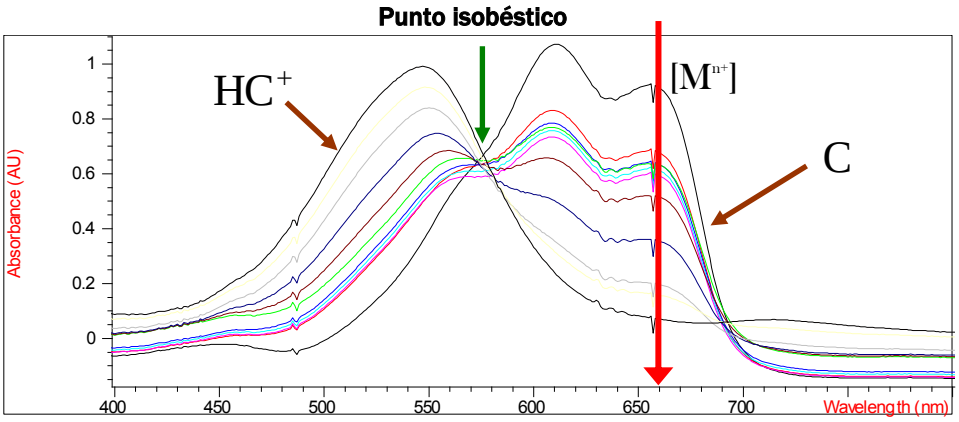

Figura II.29. Espectros de absorción de las formas desprotonada y protonada del cromoionóforo. La forma desprotonada presenta un máximo de absorción a 540 nm, mientras que la forma protonada tiene los máximos a 610 y 660 nm

Se representaron las funciones sigmoidales correspondientes a los datos experimentales obtenidos y, con la ayuda del software informático Mathematica 5.0, se compararon éstos con las curvas teóricas correspondientes a cada caso

(ver capítulo 8). A modo de ejemplo, en la figura II.30 puede verse la variación de $1-\alpha_{ef}$ frente a la concentración de los diversos iones estudiados utilizando una membrana preparada a partir del cóctel V, mientras que la figura II.31 recoge la comparativa entre los valores medidos y la curva teórica asociada a la medida de Ca^{2+} con una membrana procedente del cóctel II.

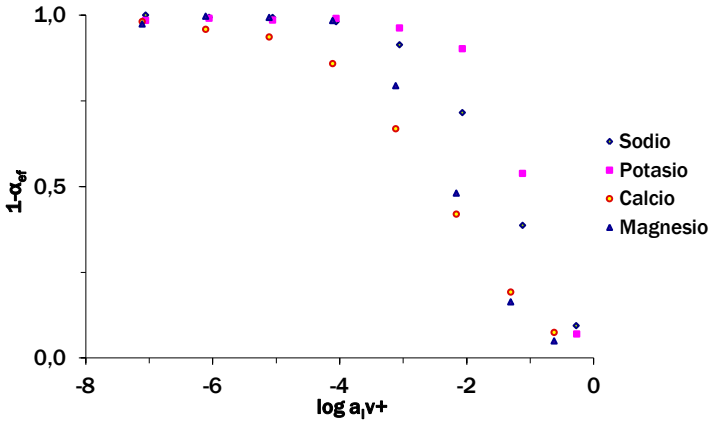

Figura II.30. Ejemplo de representación $1-\alpha_{ef}$ Vs log a_i^{v+} considerando los valores medios experimentales correspondientes a la variación de cada ion

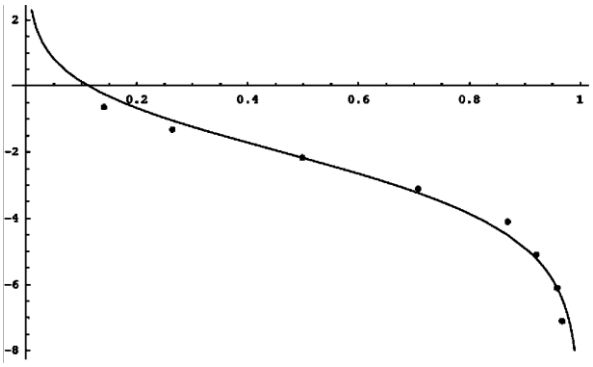

Figura II.31 Ejemplo de ajuste entre la curvas teórica y los puntos experimentales medios correspondientes a la medida de Ca^{2+}

5. TÉCNICAS DE INTELIGENCIA ARTIFICIAL

No existe una definición unánimamente aceptada sobre el término inteligencia artificial (AI), pese a la extensa difusión de la dada por Munakata[78] en 1998. Algunas definiciones hacen referencia a la capacidad de un ordenador para operar de forma similar a como el pensamiento humano ejecuta sus procesos de aprendizaje y reconocimiento.

Existen dos aproximaciones fundamentales dentro del amplio espectro de la AI. La AI simbólica se caracteriza por un alto nivel de abstracción y una visión macroscópica. A esta categoría pertenecen la psicología clásica, los sistemas basados en el conocimiento, el aprendizaje simbólico de las máquinas, las técnicas de búsqueda y el procesamiento del lenguaje natural. La segunda aproximación se caracteriza por un bajo nivel de abstracción y modelos biológicos microscópicos, como son las neuronas en las redes neuronales artificiales (ANN) y los cromosomas en los algoritmos genéticos (GA).

Con el rápido avance de los sistemas computacionales y la creación de grandes bases de datos han emergido nuevas técnicas de AI adscritas a los sistemas expertos (ES), como *Data Mining*, considerada una etapa previa en la generación de conocimiento.

En la actualidad la AI se está aplicando en numerosas líneas de investigación científicas, destacando, entre otras: robótica, visión artificial, técnicas de aprendizaje y gestión del conocimiento.

A continuación se describen las técnicas de IA que han sido aplicadas en esta memoria de doctorado: redes neuronales artificiales, algoritmos genéticos y sistemas expertos. Estas técnicas pueden combinarse para obtener una solución más adecuada del problema en estudio.

5.1. Redes neuronales artificiales

El cerebro es capaz de procesar a alta velocidad gran cantidad de información procedente de los sentidos, combinarla o compararla con la información almacenada y dar respuestas adecuadas, incluso en situaciones

[78] T. Munakata. *Fundamentals of the New Artificial Intelligence: beyond Traditional Paradigms*. Springer, (1998) 1-5

desconocidas. Pero lo más destacable en el desarrollo de tales habilidades es su capacidad de aprendizaje para representar la información necesaria sin poseer instrucciones explícitas para ello.

Aunque todavía se plantean dudas acerca de cómo el cerebro aprende a procesar la información, se han desarrollado modelos que tratan de mimetizar tales habilidades, denominados ANN o modelos de computación conexionista (otras denominaciones son computación neuronal y procesamiento distribuido paralelo). La elaboración de estos modelos supone, en primer lugar, la deducción de las características esenciales de las neuronas y sus conexiones; y en segundo lugar, la implementación del modelo en un ordenador, de forma que puedan ser simuladas. En definitiva, las ANN son un modelo artificial simplificado del cerebro humano, capaz de adquirir conocimiento a través de la experiencia. Una ANN es "*un nuevo sistema para el tratamiento de la información, cuya unidad básica de procesamiento está inspirada en la célula fundamental del sistema nervioso humano: la neurona*" (figura II.32).

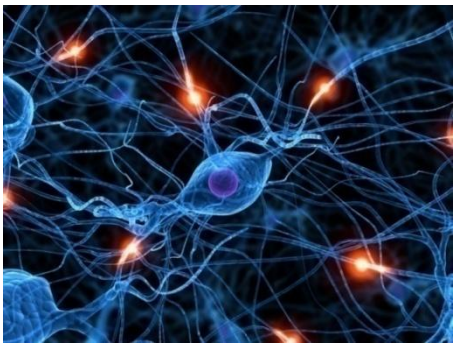

Figura II.32. Ilustración de una red neuronal

5.1.1. Analogía entre las redes neuronales biológicas y artificiales

a) Redes neuronales biológicas (BNN)

El cerebro humano se compone de decenas de billones de neuronas interconectadas entre sí formando circuitos o redes que desarrollan funciones específicas. Una neurona típica recoge señales procedentes de otras neuronas a través de un conjunto de dendritas, emitiendo impulsos eléctricos a lo largo del

axón, que se escinde en multitud de ramificaciones (figura II.33).

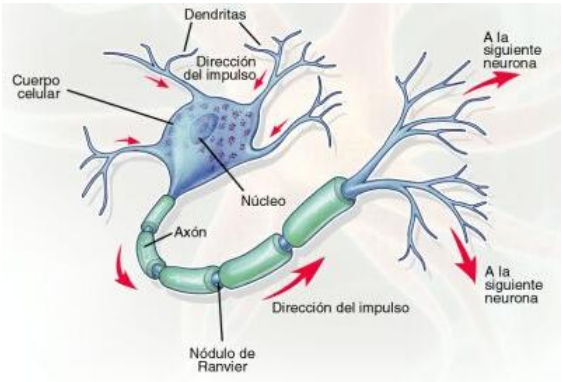

Figura II.33. Estructura básica de una neurona

Las extremidades de estas ramificaciones llegan hasta las dendritas de otras neuronas y establecen sinapsis, que conllevan la transformación del impulso eléctrico en un mensaje neuroquímico mediante la liberación de neurotransmisores. El efecto de los neurotransmisores sobre la neurona receptora puede ser excitatorio o inhibitorio y es variable (la intensidad del efecto depende de numerosos factores); las señales recibidas se combinan y, en función de la estimulación total recibida, la neurona adquiere un cierto grado de activación, que se traduce en la generación de breves impulsos nerviosos con una determinada frecuencia o tasa de disparo y su propagación a lo largo del axón hacia las neuronas con las cuales está enlazada.

De esta manera, la información se transmite de unas neuronas a otras y es procesada a través de las conexiones sinápticas y de las propias neuronas. El aprendizaje de las BNN se produce mediante la variación de la efectividad de las sinapsis, cambiando así la influencia que unas neuronas ejercen sobre otras. De aquí se deduce que la arquitectura, el tipo y la efectividad de las conexiones en un momento dado representan, en cierto modo, la memoria o el estado de su conocimiento. Se estima que el cerebro humano contiene más de 10^{11} neuronas y 10^{14} sinapsis.

b) Redes neuronales artificiales

Las ANN emulan las características esenciales de la estructura neuronal

del cerebro biológico (tabla II.1).

Tabla II.1. Comparación entre BNN y ANN

Redes Neuronales Biológicas	*Redes Neuronales Artificiales*
Neuronas	Unidades de proceso
Conexiones sinápticas	Conexiones ponderadas
Efectividad de las sinapsis	Peso de las conexiones
Efecto excitatorio o inhibitorio de una conexión	Signo del peso de una conexión
Efecto combinado de las sinapsis	Función de propagación o de red
Activación -> Tasa de disparo	Función de activación -> Salida

Constan de una serie de unidades de proceso, también llamadas neuronas artificiales, relacionadas mediante unas conexiones ponderadas. Cada unidad recibe señales a través de una serie de vías de entrada y responde a ese estímulo enviando una señal, que puede ser binaria (0,1) o real dentro de un intervalo continuo, a todas aquellas con las que a su vez tenga una conexión de salida. Por tanto, se componen de un núcleo de cálculo, un vector de conexiones de entrada y una salida (figura II.34).

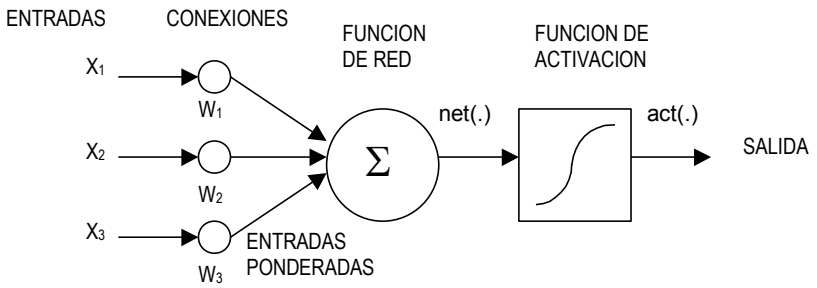

Figura II.34. Unidad de proceso típica de una ANN

- *Función de propagación o de red.* Calcula el valor de base o entrada total a la unidad, generalmente como una simple suma ponderada de todas las entradas recibidas, es decir, de las entradas multiplicadas por el peso o valor de las conexiones. Equivale a la combinación de las señales excitatorias e inhibitorias de las neuronas biológicas.

- *Función de activación.* Es la característica principal de las neuronas, ya que define el comportamiento de las mismas. Se usan diferentes tipos de funciones, desde simples funciones de umbral a funciones no lineales. Permite calcular el nivel o estado de activación de la neurona en función de la entrada total.
- *Conexiones ponderadas.* El peso de la conexión equivale a la efectividad de la sinapsis. La existencia de conexiones determina si es posible que una unidad influya sobre otra; el valor de los pesos y el signo de los mismos definen el tipo (excitatorio/inhibitorio) y la intensidad de la influencia.
- *Salida.* Calcula la salida de la neurona en función de la activación de la misma, aunque normalmente no se aplica más que la función identidad y se toma como salida el valor de activación. Corresponde a la tasa de disparo en las neuronas biológicas.

Por tanto, una ANN está formada por un conjunto de neuronas interconectadas y dispuestas en forma de capas, las cuales están compuestas a su vez por un cierto número de neuronas cada una. Aunque inicialmente se desarrollaron ANN de una sola capa, lo más usual es disponer de tres o más capas (redes multicapa)[79]. Así, los parámetros fundamentales de la ANN son: el número de capas, el número de neuronas por capa, el grado de conectividad y el tipo de conexiones entre neuronas.

Las ANN se pueden clasificar atendiendo a dos criterios:

a) Tipos de conexiones entre las neuronas

- *Redes neuronales por capas (en cascada o feed-forward).* Están compuestas por capas de neuronas y cada capa recibe señales de las capas previas (figura II.35), siendo el Perceptrón multicapa el más común. Este tipo de red se caracteriza porque las neuronas se agrupan en diferentes niveles (capa de entrada, capas ocultas y capas de salida). Las neuronas se encargan de recibir información bruta del exterior, almacenarla o realizar un sencillo pre-procesamiento y trasmitirla a las siguientes capas. Las capas intermedias u ocultas extraen, procesan y

[79] P.D. Wassermann. *Neural computing: Theory and Practice.* VNR. New York (1989)

memorizan la información, mientras que la última capa actúa como salida de la red, proporcionando la respuesta para cada uno de los patrones de entrada. Usualmente este tipo de red se utiliza en problemas de reconocimiento o clasificación de patrones.

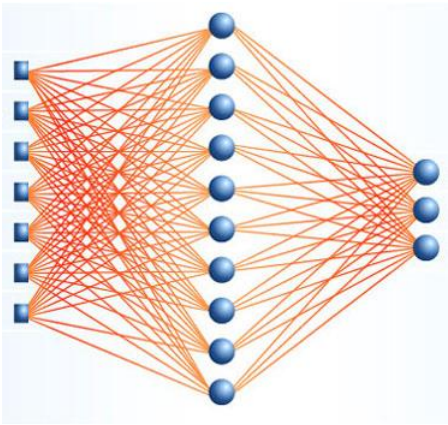

Figura II.35. Modelo de red en cascada de 3 capas

Las conexiones entre capas suelen ser totales, pero en el caso de ser parciales, se conectan generalmente siguiendo algún patrón aleatorio o pseudo-aleatorio (por ejemplo, mediante algoritmos genéticos).

- *Redes neuronales recurrentes (feed-back).* Cada neurona se conecta a todas las neuronas de la red, incluso consigo misma, de modo que la información puede retonar siguiendo un bucle. Se caracteriza por su dinámica, siendo la red es estable cuando su estado permanece igual tras varias iteraciones. Las redes de Hopfield ilustran son un ejemplo.
- *Redes neuronales conectadas lateralmente.* Las neuronas se disponen en los nodos de un retículo de aproximadamente 1 o 2 dimensiones. La red más común es la Kohonen.

b) Tipo de entrenamiento

- *Redes con aprendizaje supervisado.* Un agente externo (supervisor o maestro) comprueba la salida de la red, y en el caso de que ésta no coincida con la deseada, se modificarán los pesos de las conexiones.
- *Redes con aprendizaje no supervisado.* No requieren influencia externa

para ajustar los pesos de las conexiones entre neuronas. La red no recibe ninguna información por parte del entorno que le indique si la salida generada es o no correcta, así que existen varias posibilidades en cuanto a la interpretación de la salida de estas redes.

Adicionalmente, existen *ANN híbridas* que involucran ambos tipos de aprendizaje; así, los pesos se ajustan mediante aprendizaje supervisado y el resto se obtiene por medio de un aprendizaje no supervisado.

5.2. Algoritmos genéticos

Los algoritmos genéticos son el resultado de los recientes avances de la computación evolutiva. Simulan la mecánica de la selección natural y de la genética, buscando la solución óptima de un problema complejo y economizar el tiempo.

Los principios de la naturaleza en los cuales están inspirados son muy simples. De acuerdo con la teoría de Darwin[80], el principio de selección privilegia a los individuos más aptos con mayor longevidad y, por tanto, con mayor probabilidad de reproducción. Los individuos con más descendientes tienen más oportunidades de transmitir sus códigos genéticos, constituyendo éstos la identidad de cada individuo y estando representados en los cromosomas[81].

Los mecanismos que conducen esta evolución no son totalmente conocidos, pero sí algunas de sus características[80]:

- La evolución es un proceso que opera sobre los cromosomas.
- La selección natural es el enlace entre los cromosomas y la actuación de sus estructuras decodificadas.
- El proceso de reproducción es el punto en el cual la evolución interviene.
- La evolución biológica no tiene memoria.

La computación evolutiva está compuesta por modelos de evolución

[80] C. Darwin. On *the Origin of Species by Means of Natural Selection or the Preservations of Favored Races in the Struggle for Life*. London: John Murray (1859)

[81] M.A. Cavalcanti. *Algoritmos Genéticos: Principios e Aplicacoes.* ICA: Núcleo de Pesquisa em Inteligência Computacional Aplicada. Dpto de Engenharia Elétrica. Pontifícia Universidade Católica do Río de Janeiro (Brasil) (2000) 2-7

basados en poblaciones cuyos elementos representan soluciones a problemas. La simulación de este proceso en un ordenador resulta ser una técnica de optimización probabilística, que con frecuencia mejora a otros métodos clásicos en problemas difíciles.

Los GA son algoritmos de optimización de búsqueda y aprendizaje inspirados en los procesos de evolución natural y evolución genética (figura II.36).

Figura II.36. Componentes de un GA

A continuación se muestra la estructura del procedimiento de un GA clásico:

```
Inicio (1)
        t = 0;
        inicializar P(t);
        evaluar P(t);
        Mientras (no se cumpla la condición de parada) hacer Inicio (2)
                t = t + 1
                seleccionar P(t) desde P(t-1)
                recombinar P(t)
                mutación P(t)
                evaluar P(t)
        Final(2)
Final(1)
```

Los pasos para construir un GA son los siguientes:

a) *Representación.* Se debe disponer de un mecanismo para codificar un individuo como un genotipo. Una vez elegida una representación, debe considerarse cómo los genotipos (codificación) serán evaluados y qué operadores genéticos habrá que utilizar.

b) *Inicialización.* Debe ser uniforme sobre el espacio de búsqueda (cadena binaria: 0 ó 1 con probabilidad 0,5 si se utiliza una codificación binaria, y representación real uniforme sobre un intervalo dado si se utiliza codificación real). La población se debe elegir a partir de los resultados de una heurística previa.

c) *Correspondencia entre genotipo y fenotipo.* El genotipo es un conjunto de parámetros codificados en el cromosoma, mientras que el fenotipo es la estructura decodificada, solución potencial al problema. Algunas veces la obtención del fenotipo a partir del genotipo es un proceso obvio, pero en otras ocasiones el genotipo puede ser un conjunto de parámetros para algún algoritmo, el cual trabaja sobre los datos de un problema para obtener un fenotipo.

d) *Evaluación de un individuo.* Este es el paso más costoso para una aplicación real. Puede ser una subrutina, un simulador, o cualquier proceso externo (por ejemplo, experimentos en un robot). Se pueden utilizar funciones aproximadas para reducir el costo de evaluación. Cuando hay restricciones, éstas se pueden introducir en el costo como penalización y cuando existen múltiples objetivos se busca una solución de compromiso.

e) *Operador de mutación.* Puede haber uno o más operadores de mutación para la representación. Algunos aspectos importantes a tener en cuenta son: se debe permitir alcanzar cualquier parte del espacio de búsqueda, el tamaño de la mutación debe ser controlado y debe producir cromosomas válidos.

f) *Operador de cruce.* Al igual que el caso anterior, puede haber uno o más operadores de cruce para la representación. Algunos aspectos importantes a tener en cuenta son: los hijos deberían heredar algunas

características de cada padre (si éste no es el caso, entonces se trata de un operador de mutación), se debe diseñar de acuerdo a la representación escogida en el problema y la recombinación debe producir cromosomas válidos.

g) *Estrategia de selección.* Se debe garantizar que los mejores individuos tengan una mayor posibilidad de ser padres (reproducirse), pero se debe dar una oportunidad a los individuos de peores características, ya que pueden incluir material genético útil en el proceso de reproducción. Esta idea define la presión selectiva, que determina en qué grado la reproducción está dirigida por los mejores individuos.

   En el caso de la selección proporcional los mejores individuos tienen más probabilidad de ser seleccionados, pero presenta una serie de desventajas: peligro de convergencia prematura porque los mejores individuos dominan la población muy rápidamente y baja la presión selectiva cuando los valores de la función objetivo están muy cercanos. Como solución se plantea el escalado del *fitness*, ajustándolo a un rango (por ejemplo de 0 a 1) o normalizándolo (suma de los *fitness* igual a 1). En la selección por torneo se seleccionan k individuos aleatoriamente, sin reemplazamiento, y se elige el mejor, siendo k el tamaño del torneo. En la selección basada en orden, los individuos se ordenan por su valor de función objetivo de mejor a peor. La posición ocupada en la lista se llama orden del cromosoma. En lugar del valor de la función objetivo se utiliza el orden del cromosoma para ordenar entre un máximo y un mínimo.

h) *Estrategia de reemplazamiento.* La presión selectiva se ve también afectada por la forma en que los cromosomas de la población son reemplazados por los nuevos descendientes. Se pueden utilizar métodos de reemplazamiento aleatorios o determinísticos, pudiendo optar por no reemplazar al mejor cromosoma de la población: elitismo.

i) *Criterio de parada.* La parada tiene lugar cuando se alcanza el óptimo. Considerando los recursos limitados de CPU, debe fijarse el máximo número de evaluaciones. También se considera el límite que establece el usuario si después de algunas iteraciones no hay mejora.

   Respecto a la utilización de un GA, debe considerarse lo siguiente:

- Nunca sacar conclusiones de una única ejecución (usar medidas estadísticas tales como medias o medianas y determinar qué número de ejecuciones independientes sea suficiente).
- No ajustar/chequear la actuación de un algoritmo sobre ejemplos simples si se desea trabajar con casos reales.
- Desde el punto de vista de las aplicaciones se plantea un doble enfoque y diferente diseño: encontrar una solución muy buena al menos una vez y, al menos, una solución muy buena en cada ejecución.

5.2.1. Algoritmos genéticos de optimización multiobjetivo

Los problemas de optimización pueden ser de tipo simple o multiobjetivo, según el número de objetivos que haya que resolver. La optimización simple pretende obtener el mejor diseño o decisión, que suele ser un máximo o un mínimo global, según el caso. En cambio, en la optimización multiobjetivo se genera un conjunto de soluciones, aunque puede no existir una solución que sea la mejor considerando todos los objetivos.

Un problema multiobjetivo consiste en maximimar o minimizar, simultáneamente, un conjunto de funciones:

$$\text{Máx o Mín } z = f(x) = (f_1(x), f_2(x), \ldots, f_n(x)) \qquad \text{(II.10)}$$

Se dice que un vector a domina a otro b (se nota como a <= b) si, y sólo si (suponiendo maximización):

$$\forall i \in \{1,2,\ldots,n\} \mid f_i(a) \geq f_i(b) \ \wedge \exists j \in \{1,2,\ldots,n\} \mid f_j(a) > f_j(b) \qquad \text{(II.11)}$$

Es decir, una solución domina a otra si es mejor o igual en todos los objetivos y al menos mejor en uno de ellos.

Todos los vectores de decisión que no son dominados por ningún otro vector se llaman Pareto-optimales o no-dominados. No suele existir una única solución optimal, sino que existe un conjunto (a veces infinito) de soluciones no-dominadas que forma la frontera de Pareto. Por ejemplo, la figura II.37 muestra

gráficamente cómo identificar la frontera de Pareto para [Max Q(x), Max T(x)]

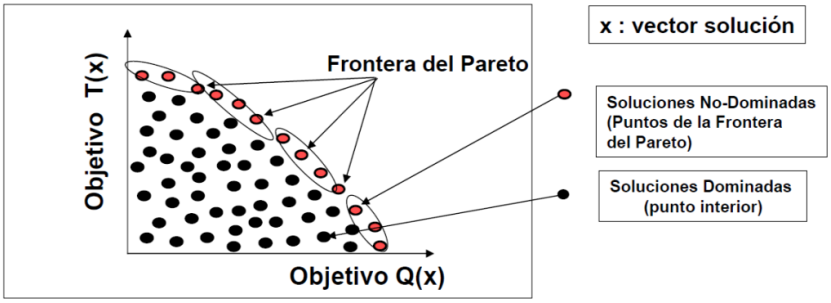

Figura II.37. Identificación de la frontera de Pareto para [Max Q(x), Max T(x)]

Para resolver este problema necesitamos: un método de búsqueda basado en los múltiples objetivos, una política de equilibrio entre los objetivos y un orden para este proceso de optimización. Se pueden considerar dos posibilidades: a) agregación + búsqueda y b) búsqueda + agregación/decisión (figura II.38). Se puede considerar una tercera posibilidad híbrida, combinando una zona amplia en el espacio de búsqueda y en una zona más pequeña o restringida de este espacio.

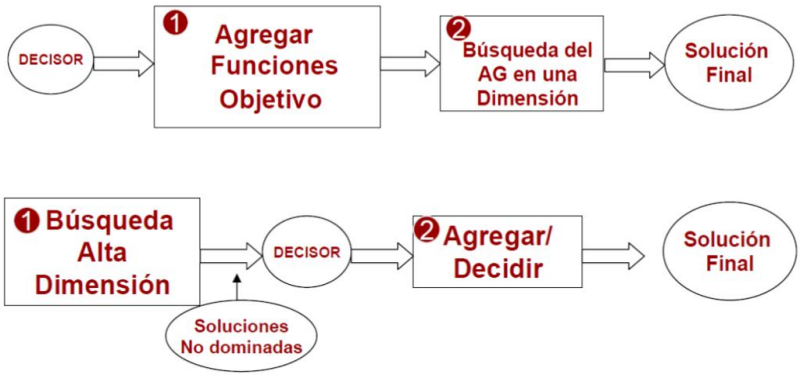

Figura II.38. Esquema genérico de problemas multiobjetivo

En los problemas multiobjetivo se evoluciona una población de soluciones al problema. Para ello se aplican mecanismos que mantengan diversidad en la población con el fin de conseguir un conjunto de soluciones no dominadas lo más grande posible. De acuerdo a las tipologías a) y b) se distinguen dos tipos de modelos evolutivos: los que utilizan pesos para la agregación de los objetivos y

los que generan poblaciones de soluciones no dominadas.

En cuanto a los modelos evolutivos que usan pesos, la agregación de los objetivos conduce a la obtención de un único punto de equilibrio en la frontera[82,83] (figura II.39).

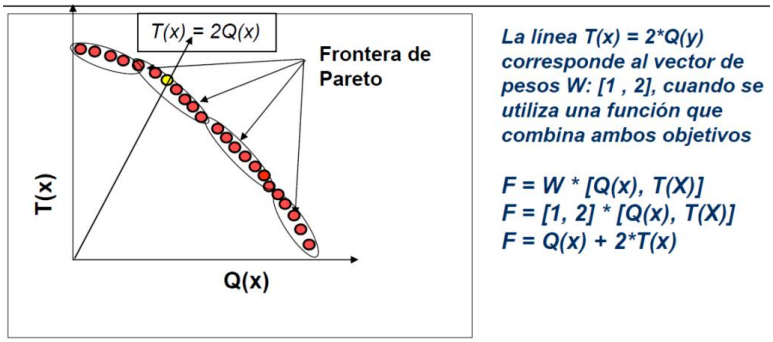

Figura II.39. Ejemplo de modelo evolutivo basado en pesos

Dentro de la primera generación de algoritmos evolutivos multiobjetivo basados en soluciones no-dominadas se distinguen tres clases: *multiobjective optimization GA* (MOGA), *niched Pareto GA* (NPGA) y *non-dominated sorting GA* (NSGA).

En MOGA[84] se generan poblaciones de soluciones no-dominadas. A cada individuo de la población se le asigna un rango. En el proceso de selección, este rango, que se asigna según un criterio de no dominancia, será utilizado para ordenar la población.

- Si x_i es no dominado, entonces rango (x_i) = 1.
- En otro caso, rango (x_i) = 1 + (número de individuos que lo dominan).

Una vez calculado el rango de los individuos de la población se siguen los siguientes pasos:

---

[82] P. Hajela, C.-Y. Lin. *Genetic search strategies in multicriterionoptimal design*. Struct. Optimization, 4 (1992) 99-107

[83] H. Ishibuchi, T. Murata, M. Gen. *Performance evaluation of fuzzy rule-based classification systems obtained by multi-objective genetic algorithms*. Comput. Ind. Eng., 35(3-4) (1998) 575-578

[84] C.M. Fonseca, P.J. Fleming. *Genetic algorithms for multiobjective optimization: Formulation, discussion and generalization*. S. Forrest (Ed.), Proc. 5th Int. Conf. on Genetic Algorithms, Morgan Kaufmann (1993) 416-423

- La población se ordena de menor a mayor de acuerdo al rango que se le ha asignado a cada individuo.
- Se asigna el valor de adaptación para cada individuo por interpolación desde el mejor (rango 1) hasta el peor.
- Se promedia la adaptación de los individuos con el mismo rango, para que tengan el mismo valor de adaptación.

Nuevas versiones utilizan técnicas de proporción de nichos (*sharing*) sobre los objetivos.

El algoritmo multiobjetivo NPGA[85] se basa en la combinación de la selección de torneo y el concepto de dominancia de Pareto. Dados dos individuos que compiten, se selecciona un subconjunto aleatorio de la población de tamaño t_{dom}. Si un individuo es dominado por cualquier miembro del conjunto y el otro no, entonces este último se considera el ganador del torneo. Si ambos individuos son dominados, el resultado del torneo se decide por el método de proporción. El individuo con menos cromosomas en su nicho es el seleccionado. La técnica de *sharing* se aplica a nivel de objetivos.

El algoritmo NSGA[86] se basa en una ordenación de la población según el criterio de no dominancia mediante fronteras de no dominancia (distinto de MOGA) y en el uso de una técnica de *sharing* aplicada sobre los valores de las variables de decisión de cada individuo (método de proporción continua y selección por torneo en implementaciones recientes). Actúa extrayendo frentes de individuos progresivamente, a los que se les asigna un valor de adaptación menor que el del frente anterior.

- En el primer frente se toman los individuos no dominados, a los que se les asigna un valor hipotético alto como valor de adaptación.
- Estos individuos se penalizan según un criterio de proporción en el fenotipo (*sharing* en las variables) con $\alpha = 2$.
- Los individuos anteriores son ignorados temporalmente para procesar el resto de la población de igual forma, identificando el segundo conjunto de

[85] J. Horn, N. Nafpliotis. *Multiobjective Optimization Using the Niched Pareto Genetic Algorithms*. IlliGAL Report 93005, University of Illinois, Urbana, Champaign (1993)

[86] N. Srinivas, K. Deb. *Multiobjetive Optimization Using Nondominated Sorting in Genetic Algorithms*. Evol. Comput., 2 (1995) 221-248

individuos no dominados (entre los dominados). A este segundo conjunto de individuos se le asigna un valor hipotético más pequeño que el mínimo valor alcanzado por el conjunto anterior tras la aplicación del método de proporción.

- El proceso continua hasta que toda la población se clasifica en frentes.

El modelo multiobjetivo *Non dominated Sorting Genetic Algorithm II* (NSGA II) fue propuesto por Deb[87] en 2000. Es una versión mejorada del NSGA que utiliza un nuevo operador, llamado operador de *crowding*. NSGA II emplea un esquema de selección más en el cual la población de padres se compara con la población de hijos. NSGA-II además de contar con el uso de elitismo, es mucho más eficiente (computacionalmente) que NSGA y es un algoritmo altamente competitivo en la convergencia al Pareto.

5.3. Sistemas expertos

En la literatura existente se pueden encontrar muchas definiciones de los sistemas expertos (ES). Por ejemplo, Stevens[88] dio en 1984 la definición siguiente:

"Los ES son máquinas que piensan y razonan como un experto lo haría en una cierta especialidad o campo. Por ejemplo, un ES en diagnóstico médico requeriría, como datos, los síntomas del paciente, los resultados de análisis clínicos y otros hechos relevantes y, utilizando éstos, buscaría en una base de datos la información necesaria para poder identificar la correspondiente enfermedad. [...] *Un ES real, no sólo realiza las funciones tradicionales de manejar grandes cantidades de datos, sino que también trata esos datos de forma tal que el resultado sea inteligible y tenga significado para responder a preguntas incluso no completamente especificadas".*

Aunque la anterior es una definición razonable, desde entonces surgieron muchas otras definiciones, debido al rápido desarrollo de la tecnología[89,90]:

---

[87] K. Deb, A. Pratap, S. Agarwal, T. Meyarivan. *A Fast and Elitist Multiobjective Genetic Algorithm: NSGA-II*. IEEE T. Evolut. Comput., 6(2) (2002) 182-197

[88] L. Stevens. *Artificial Intelligence. The Search for the Perfect Machine*. Hayden Book Company, Hasbrouck Heights, N.J. (1984) pp. 40

"Un ES puede definirse como un sistema informático (hardware y software) que simula a los expertos humanos en un área de especialización dada".

Consecuentemente, debe ser capaz de procesar y memorizar información, aprender y razonar en situaciones deterministas e inciertas, comunicar con los humanos y/u otros ES y tomar decisiones apropiadas justificando por qué. Por tanto, actúan como un consultor que puede proporcionar ayuda (o en algunos casos, sustituir completamente) a los expertos humanos con un grado razonable de fiabilidad.

Antes de desarrollar o adquirir un ES debe realizarse un análisis de factibilidad y de coste-beneficio. Las razones más importantes para utilizar estos sistemas son las siguientes:

- Con su ayuda, personal con poca experiencia puede resolver problemas que requieren el conocimiento de un experto.
- El conocimiento de varios expertos humanos puede combinarse, dando lugar a ES más fiables.
- Pueden responder a preguntas y resolver problemas de manera mucho más rápida que un experto humano. Por ello, son muy valiosos en casos en los que el tiempo de respuesta es crítico.
- Suministran respuestas rápidas y fiables en situaciones en las que los expertos humanos no pueden debido a la complejidad del problema.
- Pueden ser utilizados para realizar operaciones monótonas o aburridas.
- El ahorro mediante su uso puede ser grande.

5.3.1. Tipos de sistemas expertos

Los problemas con los que pueden tratar los ES pueden clasificarse en dos tipos: problemas esencialmente deterministas y problemas esencialmente estocásticos.

Los problemas de tipo determinista pueden ser formulados usando un conjunto de reglas que relacionen varios objetos bien definidos. Los ES que tratan problemas deterministas son conocidos como sistemas basados en reglas,

[89] E. Castillo, E. Alvarez. *Expert Systems: Uncertainty and Learning*. Computational Mechanics Publications and Elsevier Applied Science, London, U.K. (1991) pp. 31

[90] J. Durkin. *Expert Systems: Design and Development*. Maxwell Macmillan, New York (1994) pp. 800

porque sacan sus conclusiones basándose en un conjunto de reglas y utilizando un mecanismo de razonamiento lógico.

En situaciones inciertas es necesario introducir algunos medios para tratar la incertidumbre. Por ejemplo, algunos ES usan la misma estructura de los sistemas basados en reglas, pero introducen una medida asociada a la incertidumbre de las reglas y a la de sus premisas. Los ES que utilizan la probabilidad como medida de incertidumbre se conocen como sistemas probabilísticos y la estrategia de razonamiento que usan es el razonamiento probabilístico o inferencia probabilística. Algunas referencias para introducirse en este tipo de sistemas son las siguientes[89-95].

5.3.2. Sistemas expertos basados en reglas

Una introducción general a los ES basados en reglas puede encontrarse, por ejemplo, en[89-91,96,97]. El libro de Pedersen[98] muestra un enfoque práctico e incluye varios algoritmos. Los componentes principales de un ES basado en reglas son los siguientes (figura II.40):

---

[91] D.A. Waterman. *A Guide to Expert Systems*. Addison Wesley Publishing Company, 1st edition, MA. (1985) pp. 419

[92] J. Pearl. *Probabilistic Reasoning in Intelligent Systems: Networks of Plausible Inference*. Morgan Kaufmann Publishers, San Mateo, CA. (1988) pp. 552

[93] P. Jackson. *Introduction to Expert Systems.* Addison-Wesley, Reading, 2nd edition. MA. (1990) pp. 526

[94] R.E. Neapolitan. *Probabilistic Reasoning in Expert Systems: Theory and Algorithms*. Wiley-Interscience, New York (1990) pp. 433

[95] F.V. Jensen. *An Introduction to Bayesian Networks*. CRC Press, 1st edition, New York (1996) pp. 178

[96] F. Hayes-Roth, *Rule-Based Systems.* Communications of the ACM, 28(9) (1985) 921-932

[97] O.N. García, Y.T. Chien, *Knowledge-Based Systems: Fundamentals and Tools*. IEEE Computer Society Press, Los Alamitos, CA. (1991) pp. 495

[98] K. Pedersen, *Expert Systems Programming: Practical Techniques for Rule-Based Expert Systems*. John Wiley and Sons, New York (1989) pp. 298

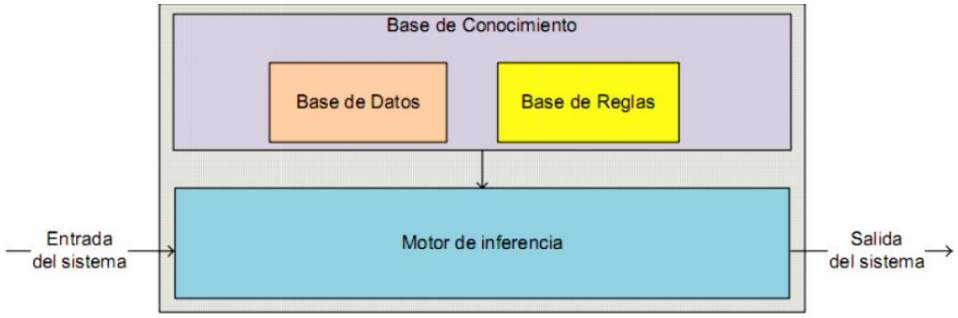

Figura II.40. Esquema básico de un ES basado en reglas

- *Base de conocimiento*. Contiene el conocimiento y las experiencias de los expertos en un determinado dominio representado por medio de símbolos. Dentro de ella se puede distinguir el conocimiento declarativo (hechos) y procedimental (reglas).
- *Base de datos, memoria de trabajo o modelo situacional*. Es una memoria auxiliar que contiene la información relacionada con el problema que se va a resolver, es decir, los datos iniciales y los datos intermedios que corresponden al estado del sistema a lo largo del proceso.
- *Motor de inferencia o estructura de control*. Se encarga de realizar los procesos de inferencia entre la información contenida en la base de datos o memoria de trabajo y la base de conocimiento, con el fin de obtener las conclusiones que sean necesarias.
- *Interfaz de usuario o subsistema de consulta*. Permite la comunicación entre el usuario y el motor de inferencia. Adicionalmente, permite introducir la información que necesita el sistema y comunica las respuestas de éste al usuario.
- *Modelo de justificación o subsistema de explicación*. Explica los pasos realizados por el motor de inferencia para llegar a las conclusiones esperadas, indicando también por qué se utilizan ciertas reglas y por qué se planteó determinada pregunta en el diálogo con el usuario.
- *Subsistema de adquisición del conocimiento*. Es una interfaz que facilita la introducción del conocimiento en la base de datos y de los mecanismos de inferencia. También se encarga de comprobar la veracidad y coherencia de los hechos y las reglas que se introducen en la base de conocimiento.

5.3.3. La base de conocimiento

Los datos están formados por los hechos conocidos en una situación particular. Este elemento es dinámico, de modo que cambia de una aplicación a otra y se almacena en la memoria de trabajo. Sin embargo, en situaciones deterministas, las relaciones entre un conjunto de objetos pueden ser representadas mediante un conjunto de reglas, siendo en ese caso la información almacenada de naturaleza permanente y estática, salvo que se incorporen al ES elementos de aprendizaje.

"Una regla es una afirmación lógica que relaciona dos o más objetos e incluye dos partes, la premisa y la conclusión. Cada una de estas partes consiste en una expresión lógica con una o más afirmaciones objeto-valor conectadas mediante los operadores lógicos y, o, o no".

La premisa de la regla es la expresión lógica entre las palabras clave *si* y *entonces*, mientras que la conclusión de la regla es la expresión lógica tras la palabra clave *entonces*. Consecuentemente, una regla se escribe normalmente como "*si* premisa, *entonces* conclusión". En general, la premisa y la conclusión de una regla pueden contener afirmaciones múltiples objeto-valor.

Algunos sistemas imponen ciertas restricciones a las reglas, debido a que éstas son fáciles de programar en un ordenador o a que las restricciones no dan lugar a una pérdida de generalidad, puesto que pueden ser reemplazadas (sustitución de reglas). Por tanto, el conjunto de reglas especificado inicialmente por el experto humano puede requerir una sustitución posterior por un conjunto de reglas equivalente para satisfacer estas restricciones.

La tabla II.2 recoge ejemplos de sustitución de reglas. Nótese que cada regla de la primera columna puede ser sustituida por el correspondiente conjunto de reglas de la segunda columna y que todas las reglas de ésta satisfacen las condiciones anteriores. En los seis primeros ejemplos las sustituciones se aplican a la premisa y en los cuatro últimos, a la conclusión.

Tabla II.2. Ejemplos de sustitución de reglas. Las reglas en la primera columna son equivalentes a las reglas de la segunda columna

Regla	Reglas equivalentes
Si A o B, entonces C	Si A, entonces C Si B, entonces C
Si $\overline{A \text{ o } B}$, entonces C	Si $\bar{A}$ y $\bar{B}$, entonces C
Si $\overline{A \text{ y } B}$, entonces C	Si $\bar{A}$, entonces C Si $\bar{B}$, entonces C
Si $(A$ o $B)$ y C, entonces D	Si A y C, entonces D Si B y C, entonces D
Si $\overline{A \text{ o } B}$ y C, entonces D	Si $\bar{A}$ y $\bar{B}$ y C, entonces C y D
Si $\overline{A \text{ y } B}$ y C, entonces D	Si $\bar{A}$ y C, entonces D Si $\bar{B}$ y C, entonces D
Si A, entonces B y C	Si A, entonces B Si A, entonces C
Si A, entonces B o C	Si A y $\bar{B}$, entonces C Si A y $\bar{C}$, entonces B
Si A, entonces $\overline{B \text{ y } C}$	Si A y B, entonces $\bar{C}$ Si A y C, entonces $\bar{B}$
Si A, entonces $\overline{B \text{ o } C}$	Si A, entonces $\bar{B}$ Si A, entonces $\bar{C}$

Como ejemplo adicional, la tabla II.3 muestra que la regla 2 ("Si $\overline{A o B}$, entonces *C*") puede ser reemplazada por la regla: "Si $\bar{A}$ y $\bar{B}$, entonces C", donde $\bar{A}$ significa *no* A. Esta tabla se denomina tabla de verdad. Los símbolos C y F se utilizan para cierto y falso, respectivamente.

Tabla II.3. Ejemplo de tabla de verdad

A	B	$\bar{A}$	$\bar{B}$	$\overline{A \text{ o } B}$	$\bar{A}$ y $\bar{B}$
C	C	F	F	F	F
C	F	F	C	F	F
F	C	C	F	F	F
F	F	C	C	C	C

5.3.4. El motor de inferencia

Tal como se ha mencionado anteriormente, hay dos tipos de elementos: los datos (hechos o evidencia) y el conocimiento (el conjunto de reglas almacenado en la base de conocimiento). El motor de inferencia usa ambos para obtener nuevas conclusiones o hechos. Por ejemplo, si la premisa de una regla es cierta, entonces la conclusión de la regla debe ser también cierta. Los datos iniciales se incrementan incorporando las nuevas conclusiones. Por ello, tanto los hechos iniciales o datos de partida como las conclusiones derivadas de ellos forman parte de los hechos o datos de que se dispone en un instante dado.

Las conclusiones pueden clasificarse en dos tipos: simples y compuestas. Las primeras son las que resultan de una regla simple, mientras que las conclusiones compuestas son las que resultan de más de una regla. Para obtener conclusiones, los expertos utilizan diferentes tipos de reglas y estrategias de inferencia y control[89-91,99].

En resumen, los ES pueden englobar una serie de características fundamentales para cumplir con el objetivo de ofrecer asesoramiento o tomar una decisión inteligente sobre una función de un proceso, como indicó Sánchez Tomás en 1995[100].

---

[99] S.C. Shapiro. *Encyclopedia of Artificial Intelligence*. John Wiley and Sons, New York (1987) pp. 1219

[100] A. Sánchez Tomás. *Aplicación de los sistemas expertos en contabilidad*. Dpto. de Contabilidad, Universidad de Valencia (1995)

CAPÍTULO 3

Matriz sensora para medida de pH basada en técnicas de imagen y modelos de ajuste

"Ma a me pare che quelle scienze sieno vane e piene di errori le quali non sono nate dall'esperienza, madre di ogni certezza".

Leonardo Da Vinci

1. INTRODUCCIÓN

De los diferentes tipos de sensores químicos, los sensores de pH han recibido especial atención debido a la importancia de la medida de este parámetro en innumerables aplicaciones prácticas y de investigación. La técnica de referencia para la medida de pH es la potenciometría, debido a las ventajas que presenta, entre las que se pueden citar: simplicidad, rapidez, precisión, reversibilidad y bajo coste. Sin embargo, los sensores ópticos presentan algunas ventajas tales como: insensibilidad a interferencias eléctricas, seguridad eléctrica, ausencia de elemento de referencia, posibilidad de formato desechable y autoclavable y posibilidad de medir pH extremos con buenas características.

Los sensores ópticos de pH se basan en indicadores de pH de muy diverso tipo, desde moléculas discretas a polímeros, inmovilizados de manera que al ponerse en contacto con la disolución problema cambien sus propiedades ópticas. A continuación, se revisa el estado actual de los sensores ópticos de pH.

1.1. Métodos de inmovilización

La inmovilización de indicadores de pH sobre o en un sustrato sólido es la clave del desarrollo de este tipo de sensores y puede llevarse a cabo principalmente mediante cuatro métodos: cambio iónico, adsorción, enlace covalente y entrapamiento.

La retención mediante cambio iónico se ha realizado con cambiadores de iones comerciales (Amberlite XAD1180, IRA400, IRA401 y Dowex-1)[101-104], cambiadores iónicos entrapando el indicador en un copolímero orgánico[105], o con

[101] A. Dybko, R.S. Romaniuk, J. Maciejewski, Z. Brzózka. *Fibre-optic pH-sensor*. Int. J. Optoelectron., 7(3) (1991) 443-448

[102] G. Vishnoi, T.C. Goel, P.K.C. Phillai. *A pH-optrode for the complete working range* Proc. SPIE Int. Soc. Opt. Eng., 3538 (1999) 319-325

[103] A. Dybko, J.Maciejewski, R.S. Romaniuk, W. Wróblewski. *Colourimetric sensor based on two optical fibre couplers*. Proc. SPIE, 2085 (1993) 131-136

[104] S. Zhang, S. Tanaka, Y.A.B.D. Wickramasinghe, P. Rolfe. *Fibre-optical sensor based on fluorescent indicator for monitoring physiological pH values*. Med. Biol. Eng. Comput., 33(2) (1995) 152-156

[105] N. Takai, T. Hirai, I. Sakuma, Y. Fukui, A. Kaneko, T. Fujie. *Development of an optical-fiber sensor using a functional membrane*. Sens. Actuators B, 13(1-3) (1993) 427-428

materiales como poliestireno sulfonado[106] o sílice conteniendo polielectrolitos[107]. En el caso de la adsorción mediante interacciones hidrofóbicas se han utilizado las resinas Amberlita XAD2 y XAD4[108-111] y polímeros de siloxano cíclico hidrofóbico entrecruzado con óxido de polietileno hidrofílico[112,113].

La celulosa ha sido ampliamente usada como soporte debido a su alta permeabilidad al agua y a determinados iones y a que puede emplearse tanto a pH ácido como básico. Algunos indicadores de pH pueden unirse covalentemente[114-120] o quedar entrapados[121-124] en la celulosa. En el caso de la

[106] S. Igarashi, K. Kuwae, T. Yotsuyanagi. *Optical pH Sensor of Electrostatically Immobilized Porphyrin on the Surface of Sulfonated-Polystyrene*. Anal. Sci., 10(5) (1994) 821-822

[107] Y. Shi, C.J. Seliskar. *Optically Transparent Polyelectrolyte-Silica Composite Materials: Preparation, Characterization, and Application in Optical Chemical Sensing*. Chem. Mater., 9(3) (1997) 821-829

[108] G. Serra, A. Schirone, R. Boniforti. *Fiber-optic pH sensor for seawater monitoring using a single dye*. Anal. Chim. Acta, 232 (1990) 337-344

[109] S. Motellier, M.H. Michels, B. Dureault, P. Toulhoat. *Fibre optic pH sensor foin situ applications*. Sens. Actuators B, 11 (1993) 467-473

[110] S. Motellier, M.H. Noire, H. Pitsch, B. Dureault. *pH determination of clay interstitial water using a fiber-optic sensor*. Sens. Actuators B, B29(1-3) (1995) 345-352

[111] B. Kuswandi, R. Narayanasway. *Polymeric encapsulated membrane for optrodes*. Fresenius J. Anal. Chem., 364(6) (1999) 605-607

[112] J.M. Price, W. Xu, J.N. Demas, B.A. DeGraff. *Polymer-Supported pH Sensors Based on Hydrophobically Bound Luminescent Ruthenium(II) Complexes*. Anal. Chem., 70(2) (1998) 265-270

[113] W. Xu, J. Mehlmann, J. Rice, J.E. Collins, C.L. Fraser, J.N. Demas, B.A. DeGraff, M. Bassetti. *pH sensors based on luminescent ruthenium(II) α-diimine complexes with diethylaminomethyl sensing groups*. Proc. SPIE, 3534 (1999) 456-465

[114] O.S. Wolfbeis, N.V. Rodriguez, T. Werner. *LED-compatible fluorosensor for measurement of near-neutral pH values*. Mikrochim. Acta, 108(3-6) (1992) 133-141

[115] Y. Kostov, S. Tzonkov, L. Yotova, M. Krysteva. *Membranes for optical pH sensors*. Anal. Chim. Acta, 280 (1993) 15-19

[116] T. Werner, O.S. Wolfbeis. *Optical sensor for the pH 10-13 range using a new support material*. Fresenius J. Anal. Chem., 346 (1993) 564-568

[117] G.J. Mohr, O.S. Wolfbeis. *Optical sensors for a wide pH range based on azo dyes immobilized on a novel support*. Anal. Chim. Acta, 292(1-2) (1994) 41-48

[118] A. Safavi, M. Pakniat. *Dipicrylamine-modified triacetylcellulose membrane for optical pH and potassium ion measurement*. Anal. Chim. Acta, 335 (1996) 227-233

[119] A. Safavi, H. Abdollahi. *Optical sensor for high pH values*. Anal. Chim. Acta, 367 (1998) 167-173

[120] A.A. Ensafi, A. Kazemzadeh. *Optical pH sensor based on chemical modification of polymer film*. Microchem. J.. 63(3) (1999) 381-388

[121] Y.V. Kostov. *Immobilized bromophenol blue as sensing element in optical pH sensor*. Sens. Actuators B, B8(1) (1992) 99-101

[122] T.J. Cardwell, R.W. Cattrall, L.W. Deady, M. Dorkos, G.R. O'Connell. *A fast-response membrane-based pH indicator optode*. Talanta, 40 (1993) 765-768

[123] W. Wroblewski, E. Roznicka, A. Dybko, Z. Brzozka. *Cellulose based bulk pH optomembranes*. Sens. Actuators B, B48(1-3) (1998) 471-475

inmovilización a través de enlace covalente, en primer lugar la triacetilcelulosa es hidrolizada para aumentar su porosidad. Las membranas de celulosa hidrolizada son tratadas con diversos reactivos y posteriormente lavadas con agua destilada. El enlace covalente con el indicador se produce mediante inmersión en una disolución de éste. En cuanto al entrapamiento físico, se suelen añadir algunos reactivos para mejorar las propiedades de las membranas sensoras; entre otros: (1) agentes de coagulación como el cloroformo, que reduce el tiempo de respuesta por medio de la reducción del espesor e incremento de la porosidad[121], (2) plastificantes como el dietilftalato, para mejorar la transparencia[122], (3) agentes humectantes como el etilenglicol, que reduce la hidrofobicidad[123] y (4) reactivos controladores del equilibrio iónico como el tetrafenilborato sódico, que incrementan la respuesta del sensor al mantener la electroneutralidad en la membrana durante los cambios de pH[122,123].

Por otra parte, Walt *et al.* fabricaron sensores de pH de fibra óptica utilizando un procedimiento de inmovilización fotoquímica[125-131]. Kopelman *et al.* adaptaron el método para la fabricación de sensores con tamaño inferior a la micra por fotopolimerización sobre puntas de fibra óptica nanofabricadas[132-134],

---

[124] A. Dybko, W. Wroblewsi, J. Maciejewski, R. Romaniuk, Z. Brzozka. *Efficient reagent immobilization procedure for ion-sensitive optomembranes*. Sens. Actuators B, B39(1-3) (1997) 207-211

[125] S.M. Barnard, D.R. Walt. *A Fiber Optic Chemical Sensor with Discrete Sensing Sites*. Nature, 353 (1991) 338-340

[126] K.S. Bronk, D.R. Walt. *Fabrication of patterned sensor arrays with aryl azides on a polymer-coated imaging optical fiber bundle*. Anal. Chem., 66(20) (1994) 3519-3520

[127] P. Pantano, D.R. Walt. *Analytical applications of optical imaging fibers*. Anal. Chem., 67(15) (1995) 481A-487A

[128] J.A. Ferguson, B.G. Healey, K.S. Bronk, S.M. Barnard, D.R. Walt. *Simultaneous monitoring of pH, CO2 and O2 using an optical imaging fiber*. Anal. Chim. Acta, 340(1-3) (1997) 123-131

[129] B.G. Healey, D.R. Walt. *Fast temporal response fiber-optic chemical sensors based on the photodeposition of micrometer-scale polymer arrays*. Anal. Chem., 69(11) (1997) 2213-2216

[130] K.S. Bronk, K.L. Michael, P. Pantano, D.R. Walt. *Combined imaging and chemical sensing using a single optical imaging fiber*. Anal. Chem., 67(17) (1995) 2750-2757

[131] A. Panova, P. Pantano, D.R. Walt. *In situ fluorescence imaging of localized corrosion with a pH-sensitive imaging fiber*. Anal. Chem., 69(8) (1997) 1635-1641

[132] W. Tan, Z.-Y. Shi, R. Kopelman. *Development of submicron chemical fiber optic sensors*. Anal. Chem., 64(23) (1992) 2985-2990

[133] W. Tan, Z. Shi, S. Smith, D. Birnbaum, R. Kopelman. *Submicrometer intracellular chemical optical fiber sensors*. Science, 258(5083) (1992) 778-781

[134] A. Song, S. Parus, R. Kopelman. *High-performance fiber-optic pH microsensors for practical physiological measurements using a dual-emission sensitive dye*. Anal. Chem., 69(5) (1997) 863-867

mientras que Millar *et al.*[135] utilizaron la polimerización electroquímica para inmovilizar tiofeno sustituido con fluoresceína sobre vidrio recubierto con platino. Por su parte, Luo *et al.*[136] fabricaron un sensor óptico de pH mediante inmovilización covalente de rojo cresol sobre el copolímero formado por acetato de polivinilo (PVA) reticulado transparente y acrilamida, actuando el par Fe^{2+}/H_2O_2 como iniciador. Cajlakovic[137] utilizó el copolímero formado por el PVA y el gel de sílice como sustrato sensor óptico de pH para la inmovilización de la fluoresceína.

Para la unión covalente de indicadores de pH también se han empleado fibras de poliestireno clorosulfonado[138] y microesferas de poliacrilamida[139], mientras que para el entrapamiento se han empleado poli(metilmetacrilato) (PMMA)[140,141], gel de agarosa[142], hidrogel de poliuretano[143,144] y PVC[145]. Desde su primer uso en 1990[146], los materiales de tipo sol-gel han sido también

[135] D. Millar, M. Uttamlal, R. Henderson, A. Keeper. *Electrochemical immobilization of a pH sensitive fluorescein derivative: synthesis and characterization of a fluorescein-derivatized polythiophene*. Chem. Commun., 4 (1998) 477-478

[136] F.-L. Luo, T.-L. Chen. *Preparation of high hydrophilic optical chemical pH sensitive membranes via covalent immobilization method and its performance*. Fenxi Huaxue, 38(11) (2010) 1609-1614

[137] M. Cajlakovic, A. Lobnik, T. Werner. *Stability of new optical pH sensing material based on cross-linked poly(vinyl alcohol) copolymer*. Anal. Chim. Acta, 455 (2002) 207-213

[138] B.S. Rao, J.B. Puschett, K. Matyjaszewski. *Preparation of pH sensors by covalent linkage of dye molecules to the surface of polystyrene optical fibers*. J. Appl. Polym. Sci., 43(5) (1991) 925-928

[139] D. Cui, Q. Cao, J. Han, J. Cai, Y. Li, Z. Zhu. *Optical-fiber pH sensor*. Sens. Actuators B, 12(1) (1993) 29-32

[140] C. Egami, K. Takeda, M. Isai, M. Ogita. *Evanescent-wave spectroscopic fiber optic pH sensor*. Opt. Commun., 122(4-6) (1996) 122-126

[141] C. Egami, Y. Suzuki, O. Sugihara, H. Fujimura, N. Okamoto. *Wide range pH fiber sensor with congo-red- and methyl-red-doped poly (methyl methacrylate) cladding*. Jpn. J. Appl. Phys., 36(5A) (1997) 2902-2905

[142] T. Hao, X. Xing, C.-C. Liu. *A pH sensor constructed with two types of optical fibers: the configuration and the initial results*. Sens. Actuators B, B10(2) (1993) 155-159

[143] T. Werner, C. Huber, S. Heinl, M. Kollmannsberger, J. Daub, O.S. Wolfbeis. *Novel optical pH-sensor based on a boradiaza-indacene derivative*. Fresenius J. Anal. Chem., 359(2) (1997) 150-154

[144] S. Draxler, M.E. Lippitsch. *Effect of polymer matrixes in lifetime based sensing*. Proc. SPIE, 2388 (1995) 363-368

[145] D.B. Papkovsky, G.V. Ponomarev, O.S. Wolfbeis. *Protonation of porphyrins in liquid PVC membranes: Effects of anionic additives and application to pH-sensing*. J. Photochem. Photobiol. A Chem., 104 (1997) 151-158

[146] R. Zusman, C. Rottoman, M. Ottolenghi, D. Avnir. *Doped sol-gel glasses as chemical sensors*. J. Non-Cryst. Solids, 122(1) (1990) 107-109

ampliamente utilizados como sustratos para este tipo de sensores[147,148]. Pueden ser preparados a temperatura ambiente mediante hidrólisis, condensación o policondensación de un precursor alcóxido (por ejemplo, tetrametoxisilano para la preparación de sílice gel-sol[149], ya que es un material poroso que permite entrapar indicadores de pH). Comparado con los polímeros orgánicos, el vidrio sol-gel es un sustrato sólido inorgánico que ofrece numerosas ventajas: (1) alta estabilidad química, fotoquímica y térmica, así como resistencia mecánica, (2) transparencia óptica, (3) compatibilidad con varios tipos de indicadores y (4) posibilidad de deposición directa sobre cristal y fibras de sílice[148]. Sin embargo, también presenta algunos problemas como su lenta respuesta y la lixiviación del reactivo.

1.2. Métodos espectroscópicos

La mayoría de los sensores de pH ópticos están basados en métodos de absorción y fluorescencia. La absorción de radiación es un método simple y fácil de usar, pero no muy sensible, por lo que requiere una alta concentración de indicador de pH y/o una capa sensora delgada. Los sensores de fibra óptica basados en métodos de absorción son difícilmente miniaturizables, especialmente en modo transmisión, en el cual un elemento sensor se ubica entre dos fibras[142]. Por eso, normalmente se mide en modo reflexión para solventar este problema[110]. Sin embargo, los métodos fluorescentes son más sensibles y pueden ser utilizados para sensores de pequeño tamaño y/o baja concentración de indicador[132,133,134,150,151].

---

147 O.S. Wolfbeis, R. Reisfeld, I. Oehme. *Sol-gels and chemical sensors*. Struct. Bonding, 85 (1996) 51-98

148 J. Lin, C.W. Brown. *Sol-gel glass as a matrix for chemical and biochemical sensing*. Trends Anal. Chem., 16(4) (1997) 200-211

149 C.J. Brinker, G.W. Scherer. *Sol-gel Science: the Physics and Chemistry of Sol-gel Processing*. Academic Press, New York, 1990

150 W. Shi, S. He, M. Wei, D.G. Evans, X. Duan. *Optical pH Sensor with Rapid Response Based on a Fluorescein-Intercalated Layered Double Hydroxide*. Adv. Funct. Mater., 20 (2010) 3856-3863

151 W. Jin, J. Jiang, X. Wang, X. Zhu, G. Wang, Y. Song, C. Bai. *Continuous intra-arterial blood pH monitoring in rabbits with acid–base disorders*. Resp. Physiol. Neurobi., 177 (2011) 183–188

Chen[152] construyó un sensor de pH basado en un sistema de dos LEDs: un LED (λ máxima 465 nm) usado para excitar el indicador fluorescente de pH, la 6-carboxifluoresceína (CF) y el otro LED (λ máxima 660 nm) para suministrar una señal de referencia. Las dos señales, fluorescencia y referencia, fueron capturadas utilizando una cámara comercial. Por otra parte, se diseñaron sensores ópticos fluorescentes proporcionales[153-155]. Badugu[153] desarrolló un sensor de pH fluorescente utilizando alilo hidroxiquinolina copolimerizada con dimetacrilato de polietilenglicol. Se observó un decrecimiento en el espectro de emisión del sensor para una excitación a 360 nm y un incremento para 420 nm con el aumento del pH; la relación de emisión para una excitación 420:360 nm mostró un cambio máximo entre pH 5 y 8, con un pK_a aparente de 6,40.

La mayoría de los sensores ópticos de pH se basan en indicadores de pH inmovilizados sobre o en los sustratos sólidos, y se fabrican en forma de membranas o finas capas depositadas sobres soportes sólidos transparentes. Sin embargo, algunos sensores presentan características menos comunes en términos de principios, diseño o aplicaciones.

1.2.1. Sensores de pH basados en polímeros conductores

Ciertos polímeros conductores cambian de color en función del pH, como es el caso de la polianilina[156,157], polianilinas sustituidas[158,159,160] y el polipirrol[161],

---

[152] H.-X. Chena, X.-D. Wanga, X.-H. Songa, T.-Y. Zhoua, Y.-Q. Jianga, X. Chen. *Colorimetric optical pH sensor production using a dual-color system*. Sens. Actuators B, 146 (2010) 278–282

[153] R. Badugu, Y. Kostov, G. Rao, L. Tolosa. *Development and application of an excitation ratiometric optical pH sensor for bioprocess monitoring*. Biotechnol. Prog., 24 (2008) 1393-1401

[154] A. Sohanghpurwala, G. Rao, Y. Kostov. *Optical Replacement of pH Electrode*. IEEE Sens. J., 9(3) (2009) 219-220

[155] S. Vuppu, Y. Kostov, G. Rao. *Economical wireless optical ratiometric pH sensor*. Meas. Sci. Technol., 20 (2009) 1-7

[156] Z. Ge, C.W. Brown, L. Sun, S.C. Yang. *Fiber-optic pH sensor based on evanescent wave absorption spectroscopy*. Anal. Chem., 65(17) (1993) 2335-2338

[157] U.W. Grummt, A. Pron, M. Zagorska, S. Lefrant. *Polyaniline based optical pH sensor*. Anal. Chim. Acta, 357(3) (1997) 253-259

[158] M.D.P.T. Sotomayor, M.A. de Paoli, W.A.D. Oliveira. *Fiber-optic pH sensor based on poly(o-methoxyaniline)*. Anal. Chim. Acta, 353 (1997) 275-280

[159] E. Pringsheim, E. Terpetschnig, O.S. Wolfbeis. *Optical sensing of pH using thin films of substituted polyanilines*. Anal. Chim. Acta, 357(3) (1997) 247-252

[160] P.T. Sotomayor, I.M. Raimundo Jr., A.J.G. Zarbin, J.J.R. Rohwedder, G. Oliveira Neto, O.L. Alves. *Construction and evaluation of an optical pH sensor based on polyaniline-porous Vycor glass nanocomposite*. Sens. Actuators B, 74 (2001) 157-162

que han sido usados en sensores basados en su absorción tanto en las regiones del visible como del infrarrojo cercano. Estos sensores ofrecen diversas ventajas: (1) fácil fabricación, ya que los polímeros son reactivos sensores intrínsecos, (2) amplio rango dinámico lineal, debido a que estos polímeros son básicamente polielectrolitos con valores de pK_a múltiples y (3) medida en la región de infrarrojo cercano, donde son menores la interferencia espectral y el grado de dispersión de luz comparados con las regiones UV y visible. Sin embargo, también presentan algunos inconvenientes tales como: (1) largo tiempo de respuesta debido a la lenta difusión en polímeros, (2) interferencia de otros iones, agentes reductores y oxidantes y (3) necesidad de pre/reacondicionamiento antes de cada medida (por ejemplo, en 0,1 M HCl), para evitar la histéresis debida al cambio conformacional en cadenas de polímeros que tiene lugar con los cambios de pH[157,161].

1.2.2. Sensores de pH basados en micropartículas y nanoesferas

Walt *et al.*[162] prepararon micropartículas sensoras de pH usando partículas de vidrio porosas de aminopropilo de tamaño comprendido entre 37 y 74 µm. Para determinar el pH, las partículas sensoras se difunden sobre un sustrato de muestra, detectándose la señal fluorescente[162].

Kopelman *et al.* fabricaron sensores nanoesféricos llamados *Probes Encapsulated By Biologically Localized Embedding* (PEBBLEs)[163,164]. Estos sensores fueron preparados en una microemulsión mediante entrapamiento de indicadores de pH fluorescentes en microesferas de poliacrilamida (20-200 nm de diámetro). Son biocompatibles, con insignificantes efectos biológicos, pudiendo ser inyectados en células individuales para la medida del pH intracelular a partir de imágenes de microscopía de fluorescencia.

---

[161] S. De Marcos, O.S. Wolfbeis. *Optical sensing of pH based on polypyrrole films*. Anal. Chim. Acta, 334(1-2) (1996) 149-153

[162] K.L. Michael, L.C. Taylor, D.R. Walt. *A far-field-viewing sensor for making analytical measurements in remote locations*. Anal. Chem. 71(14) (1999) 2766-2773

[163] H.A. Clark, M. Hoyer, M.A. Phibert, R. Kopelman. *Optical nanosensors for chemical analysis inside single living cells. 1. Fabrication, characterization, and methods for intracellular delivery of PEBBLE sensors*. Anal. Chem., 71(21) (1999) 4831-4836

[164] H.A. Clark, R. Kopelman, R. Tjalkens, M.A. Philbert. *Optical Nanosensors for Chemical Analysis inside Single Living Cells. 2. Sensors for pH and Calcium and the Intracellular Application of PEBBLE Sensors*. Anal. Chem., 71(21) (1999) 4837-4843

1.2.3. Sensores de pH con amplio rango dinámico y respuesta lineal

Los sensores ópticos de pH basados en el uso de indicadores de pH tienen dos limitaciones principales: 1) estrecho rango dinámico y 2) respuesta no lineal. No obstante, se puede ampliar el rango dinámico empleando matrices de sensores con diferentes indicadores de pH que presenten distintos valores de pK_a[165,166], seleccionados de entre los numerosos indicadores de pH descritos. Además, se han sintetizado nuevos indicadores al objeto de cubrir el rango completo de pH[117,167,168]. Otro enfoque es ampliar el rango dinámico de un único sensor de pH mediante co-inmovilización de varios indicadores de pH[169-173] o usar un indicador poliprótico que presente diferentes formas coloreadas[113,174]. Sin embargo, dichos sensores de pH de amplio rango frecuentemente son de respuesta no lineal. Se han descrito algunos sensores de pH con una respuesta amplia y lineal[171,172,175], lo cual es deseable porque permite una calibración más sencilla y una sensibilidad y precisión constantes en la medida de pH en este rango. Lin y Liu investigaron el método para producir una respuesta lineal en un

---

165 S. Capel-Cuevas, M.P. Cuéllar, I. de Orbe-Payá, M.C. Pegalajar, L.F. Capitán-Vallvey. *Full-range optical pH sensor based on imaging techniques*. Anal. Chim. Acta, 681 (2010) 71-81

166 A. Safavi, M. Bagheri. *Novel optical pH sensor for high and low pH values*. Sens. Actuators B, 90 (2003) 143-150

167 E. Bakker, M. Lerkus, T. Rosatzin, B. Rusterholz, W. Simon. *Synthesis and characterization of neutral hydrogen ion-selective chromoionophores for use in bulk optodes*. Anal. Chim. Acta, 278(2) (1993) 211-225

168 P. Hashemi, R.A. Zarjani, M.M. Abolghasemi, A. Olin. *Agarose film coated glass slides for preparation of pH optical sensors*. Sens. Actuators B, 121 (2007) 396-400

169 J.Y. Ding, M.R. Shahriari, G.H. Sigel Jr. *Fiber optic pH sensors prepared by sol-gel immobilization technique*. Electron. Lett., 27(17) (1991) 1560-1562

170 T.M. Butler, B.D. MacCraith, C.M. McDonagh. *Development of an extended range fiber optic pH sensor using evanescent wave absorption of sol-gel entrapped pH indicators*. Proc. SPIE, 2508 (1995) 168-178

171 B.D. Gupta, S. Sharma. *A long-range fiber optic pH sensor prepared by dye doped sol-gel immobilization technique*. Opt. Commun., 154(5-6) (1998) 282-284

172 G. Vishnoi, T.C. Goel, P.K.C. Pillai. *A pH-optrode for the complete working range*. Proc. SPIE, 3538 (1999) 319-325

173 S. Rouhani, S. Salimi, K. Haghbeen. *Development of optical pH sensors based on derivatives of hydroxyazobenzene, and the extended linear dynamic range using mixture of dyes*. Dyes Pigments, 77 (2008) 363-368

174 S.G. Schulman, S. Chen, F. Bai, M.J.P. Leiner, L. Lewis, O.S. Wolfbeis. *Dependence of the fluorescence of immobilized 1-hydroxypyrene-3,6,8-trisulfonate on solution pH: extension of the range of applicability of a pH fluorosensor*. Anal. Chim. Acta, 304(2) (1995) 165-170

175 Z. Liu, F. Luo, T. Chen. *Phenolphthalein immobilized membrane for an optical pH sensor*. Anal. Chim. Acta, 510 (2004) 189–194

amplio rango usando una mezcla de indicadores de pH[176]. En este método, se consideran requisitos de los indicadores de pH tales como la diferencia entre las constantes de acidez de los indicadores usados (ΔpKa), así como sus colores, siendo la relación entre las concentraciones de indicador optimizada por medio de computación. El método se utilizó para desarrollar un sensor de pH en vidrio sol-gel por entrapamiento de tres indicadores de pH (verde de bromocresol, púrpura de bromocresol y rojo de fenol) que presenta una respuesta lineal en un rango de 3,5 unidades de pH: de 6,3 a 9,8[176].

1.2.4. Sensores de pH basados en fibra óptica

Los sensores de pH ópticos de tamaño inferior a la micra fueron desarrollados por primera vez en 1992 por Kopelman *et al.*[132,133], siendo capaces de medir en un pequeño volumen de muestra y con tiempos de respuesta de milisegundos. Sensores similares fueron diseñados por McCulloch[177] y Plaschke[178]. Para la medida de este parámetro, Samuel *et al*.[179] fabricaron microsensores utilizando puntas de micropipeta rellenas con vidrio sol-gel dopado, mientras que Narang *et al.*[180] prepararon fibras ópticas incluyendo materiales sol-gel dopados.

Walt *et al.*[127] desarrollaron tanto sensores de pH como de CO_2 y O_2. Los haces de fibras ópticas constan de miles de fibras individuales juntas y distribuidas de forma coherente, de modo que se puede obtener una imagen. Por ejemplo, un haz de fibras ópticas de 350 µm de diámetro puede contener hasta 6000 fibras individuales de 3-4 µm de diámetro. Si se controla la iluminación, una matriz de sensores de pH o sensores multianalito (por ejemplo, pH, CO_2 y O_2) puede formarse en el extremo distal de un único haz de fibras[125-129] mediante

---

[176] J. Lin, D. Liu. *An optical pH sensor with a linear response over a broad range*. Anal. Chim. Acta, 408(1-2) (2000) 49-55

[177] S. McCulloch, D. Uttamchandani. *Development of a fiber optic micro-optrode for intracellular pH measurements*. IEEE Proc. Optoelectron., 144(3) (1997) 162-167

[178] M. Plaschke, M. Geyer, J. Reichert, H.J. Ache. *Submicron fiber-optic sensors for calcium-ions and pH with internal calibration*. SPIE, 3105 (1997) 31-37

[179] J. Samuel, A. Strinkovski, S. Shalom, K. Lieberman, M. Ottolenghi, D. Avnir, A. Lewis. *Miniaturization of organically doped sol-gel materials: a microns-size fluorescent pH sensor*. Mat. Lett. 21(5-6) (1994) 431-434

[180] U. Narang, R. Gvishi, F.V. Bright, P.N. Prasad. *Sol-gel-derived micron scale optical fibers for chemical sensing*. J. Sol-Gel Sci. Technol., 6(1) (1996) 113-119

polimerización. Alternativamente, el extremo distal de este tipo de fibras puede ser recubierto mediante centrifugación con una capa sensora y el sensor fabricado, por lo tanto, puede utilizarse para visualizar una muestra y medir simultáneamente el pH con alta resolución espacial[130,131,162,181].

Los sensores de pH de fibra óptica distribuida suelen responder mediante campo evanescente o en modo de reflexión total atenuada, y se fabrican por recubrimiento con una capa sensora de pH de secciones de fibra óptica sin el revestimiento[182-185]. La técnica de medida puede ser la reflectometría óptica de dominio de tiempo[182,183] o fluorescencia de tiempo resuelto[184,185].

Los sensores ópticos para pH son particularmente útiles para la medida en rangos muy ácidos o muy básicos, por ejemplo, pH de 10 a 14, donde los electrodos de vidrio presentan problemas de "error alcalino" y deterioro químico, y pH<1, donde también se producen problemas. Varios grupos de investigadores han empleado la celulosa y el vidrio sol-gel para el desarrollo de sensores que solventen estos problemas. Entre los basados en enlaces covalente sobre celulosa se incluyen: (1) colorante Merck N8 para pH entre 10 y 13[116], (2) amarillo tiazol para pH entre 12,0 y 13,5[119], (3) amarillo alizarina GG para pH entre 9,5 y 13[120], (4) dipicrilamina para pH entre 0,0 y 3,2[118] y (5) mezcla de azul Victoria y dipicrilamina para valores de pH entre 0,56 y 7,12, y entre 7,12 y 12,63[166]. Entre los basados en entrapamiento en vidrio sol-gel se incluyen: (1) púrpura de bromocresol en sílice sol-gel para alta acidez ($[H^+]=10^{-11}$ M)[186,187], (2) cromoxano de cianina R en sílice sol-gel para HNO_3 en el rango de concentración

[181] K.L. Michael, D.W. Walt. *Combined imaging and chemical sensing of fertilization-induced acid release from single sea urchin eggs*. Anal. Biochem. 273(2) (1999) 168-178

[182] E.A. Mendoza, J. Sorenson, A. Iossi, Z. Sun, D. Robinson, R.A. Lieberman. *Demonstration of self-referenced fiber optic moisture and pH sensors using optical time domain reflectometry*. SPIE, 2836 (1996) 242-249

[183] P.A. Wallace, M. Uttamlal, N. Elliot, A.S. Holmes-Smith, M. Campbell. *Quasi-distributed optical fiber fluorosensor for pH measurement*. Proc. SPIE, 3483 (1998) 128-131

[184] C.A. Browne, D.H. Tarrant, M.S. Olteanu, J.W. Mullens, E.L. Chronister. *Intrinsic Sol-Gel Clad Fiber-Optic Sensors with Time-Resolved Detection*. Anal. Chem., 68(14) (1996) 2289-2295

[185] P.A. Wallace, M. Campbell, Y. Yang, A.S. Holmes-Smith, M. Uttamlal. *A distributed optical fiber fluorosensor for pH measurement*. J. Lumin, 72-74 (1997) 1017-1019

[186] L.R. Allain, K. Sorasaenee, Z. Xue. *Doped Thin-Film Sensors via a Sol-Gel Process for High-Acidity Determination*. Anal. Chem., 69(15) (1997) 3076-3080

[187] L.R. Allain, Z. Xue, M.J. Roberts. *A portable sol-gel sensor system for in-situ high acidity measurements*. J. Process Anal. Chem., 3(3-4) (1998) 98-103

de 1 a 10 M[188], (3) azul Nilo en sílice sol-gel dopada con 30% de Zr para pH 11-13[189] y (4) amarillo tiazol GGM en sol-gel SiO_2/ZrO_2 ($[OH^-]$= 1-10 M)[190].

También se han desarrollado numerosos sensores ópticos para gases tales como CO_2, NH_3 y NO basados en sensores de pH. En el caso del CO_2 se han usado dos métodos. En el método basado en el principio del electrodo de Severinghaus, se inmoviliza en el extremo de una fibra óptica un indicador de pH en tampón hidrógenocarbonato sensible a variaciones de CO_2, usando una membrana permeable al gas. La difusión del gas en el tampón a través de la membrana provoca un cambio en el pH y, por lo tanto, en la respuesta del indicador de pH[191,192]. En los sensores de membrana seca para CO_2, el par iónico formado entre un indicador de pH y un agente de transferencia de fase tal como hidróxido de tetraoctilamonio, es entrapado en una capa de material hidrófobo como silicona, que es permeable al CO_2 pero no a protones, siendo las moléculas de agua de hidratación del par iónico las responsables de la respuesta al gas[193,194]. Para NH_3 se han desarrollado sensores similares basados en este procedimiento[195,196], mientras que para la medida de NO en sangre se utilizó un sensor basado en xerogel[197].

---

[188] M.H. Noire, C. Bouzon, L. Couston, J. Gontier, P. Marty, D. Pouyat. *Optical sensing of high acidity using a sol-gel entrapped indicator*. Sens. Actuators B, B51(1-3) (1998) 214-219

[189] R. Blue, G. Stewart. *Optical pH sensor for the alkaline region*. Electron. Lett., 33(6) (1997) 526-528

[190] L.R. Allain, Z. Xue. *Optical Sensors for the Determination of Concentrated Hydroxide*. Anal. Chem., 72(5) (2000) 1078-1083

[191] J.W. Parker, O. Laksin, C. Yu, M.-L. Lau, S. Klima, R. Fisher, I. Scott, B.W. Atwater. *Fiber-optic sensors for pH and carbon dioxide using a self-referencing dye*. Anal. Chem., 65(17) (1993) 2329-2334

[192] M.B. Tabacco, M. Uttamlal, M. McAllister, D.R. Walt. *An Autonomous Sensor and Telemetry System for Low-Level pCO_2 Measurements in Seawater*. Anal. Chem., 71(7) (1999) 154-161

[193] A. Mills, Q. Chang, N. McMurray. *Equilibrium studies on colorimetric plastic film sensors for carbon dioxide*. Anal. Chem., 64(13) (1992) 1383-1389

[194] B.H. Weigl, O.S. Wolfbeis. *New hydrophobic materials for optical carbon dioxide sensors based on ion pairing*. Anal. Chim. Acta, 302(2-3) (1995) 249-254

[195] T. Werner, I. Klimant, O.S. Wolfbeis. *Ammonia-sensitive polymer matrix employing immobilized indicator ion pairs*. Analyst, 120(6) (1995) 1627-1631

[196] M. Trinkel, W. Trettnak, F. Reininger, R. Benes, P. O'Leary, O.S. Wolfbeis. *Study of the performance of an optochemical sensor for ammonia*. Anal. Chim. Acta, 320(1-2) (1996) 235-243

[197] K.P. Dobmeier, G.W. Charville, M.H. Schoenfisch. *Nitric Oxide-Releasing Xerogel-Based Fiber-Optic pH Sensors*. Anal. Chem., 78 (2006) 7461-7466

La mayoría de los sensores ópticos para pH se basan en el uso de indicadores ácido-base y en espectroscopia de absorción o de fluorescencia para su medida. Otros métodos espectroscópicos, por ejemplo, espectroscopia Raman[198], se utilizan raramente para el sensado de este parámetro. Algunos sensores de pH están basados en el cambio de alguna propiedad diferente del reactivo inmovilizado. Así, Niwa *et al.*[199] desarrollaron un sensor de fibra óptica basado en el cambio del índice de refracción de la capa de revestimiento de poli(ácido metacrílico), resultado de un cambio conformacional del polímero entre el estado cristalino rígido y fluido con el pH. Zamarreño[200], por su parte, diseñó en 2010 un sensor de fibra óptica cubierta por ITO y este, a su vez, por una capa polimérica sensora de pH. El pH del medio externo modifica el espesor del recubrimiento polimérico y, por lo tanto, el índice de refracción efectivo. Seitz *et al.* propusieron un sensor de basado en el hinchamiento del poliestireno aminado; el polímero se expande conforme se protonan los grupos amina, lo cual viene acompañado por un aumento en la transparencia del polímero y una disminución en la intensidad de luz que se refleja[201,202]. Por su parte, Flannery *et al.*[203] fabricaron sensores de fibra óptica depositando membranas tipo Langmuir-Blodgett conteniendo un colorante tipo merocianina sobre fibras ópticas pulidas. En ellas, el acoplamiento evanescente entre la fibra y la membrana depende del cambio en la absorción y en el índice de refracción tras la protonación del colorante, siendo el pH determinado mediante la medición de la longitud de onda resonante (desplazamiento de 18,8 nm/unidad de pH) o intensidad de luz. Egamic *et al.* también utilizaron el cambio de longitud de onda del espectro de absorción con el pH para la medida de éste con sensores de fibra óptica basados

---

198 K.I. Mullen, D. Wang, L.G. Crane, K.T. Carron. *Determination of pH with surface-enhanced Raman fiber optic probes*. Anal. Chem., 64(8) (1992) 930-936

199 M. Niwa, T. Yamamoto, N. Higashi. *pH-responsive plastic optical fibers modified with polyion-complexed multibilayers containing a poly(methacrylic acid) segment*. J. Chem. Soc. Chem. Commun., 6 (1991) 444-445

200 C.R. Zamarreño, M. Hernáez, I. Del Villar, C. Fernandez-Valdivielso, F.J. Arregui, I.R. Matias. *Optical fiber pH sensor fabrication by means of indium tin oxide coated optical fiber refractometers*. Phys. Status Solidi C. 7(11–12) (2010) 2705-2707

201 Z. Shakhsher, W.R. Seitz, K.D. Legg. *Single fiber-optic pH sensor based on changes in reflection accompanying polymer swelling*. Anal. Chem., 66(10) (1994) 1731-1735

202 L. Zhang, M.E. Langmuir, M. Bai, W.R. Seitz. *A sensor for pH based on an optical reflective device coupled to the swelling of an aminated polystyrene membrane*. Talanta, 44(9) (1997) 1691-1698

203 D. Flannery, S.W. James, R.P. Tatam, G.J. Ashwell. *pH sensor using Langmuir-Blodgett overlays on polished optical fibers*. Opt. Lett., 22(8) (1997) 567-569

en campo evanescente empleando revestimiento con PMMA dopado con rojo de metilo y rojo Congo[140,141]. Deboux *et al.*[204] desarrollaron un sensor de fibra óptica basado en la adsorción del colorante azul de metileno, en la superficie ionizada del núcleo de una fibra de sílice, en el rango de pH de 3-9, mientras que Yulianti *et al*.[205] han propuesto este año un sensor de pH basado en una fibra tipo rejilla de Bragg recubierta con hidrogel sensible al pH. La detección se realiza a través de la medida de los cambios de longitud de onda resultantes de la tensión inducida en la fibra debido a la expansión mecánica del hidrogel.

La siguiente gráfica (figura III.1) muestra la evolución temporal del número de publicaciones relacionadas con la determinación óptica de pH mediante diversos tipos de sensores.

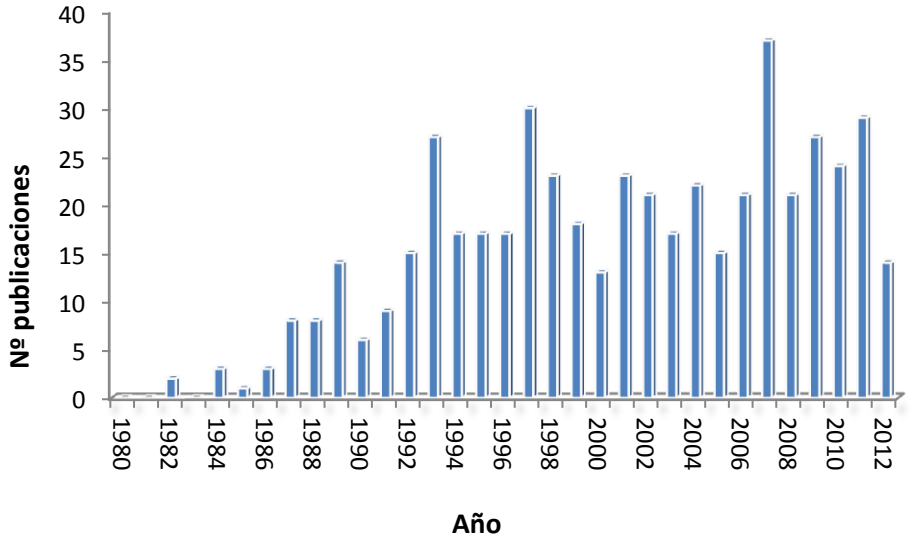

Figura III.1. Evolución temporal del nº de publicaciones sobre sensores ópticos para determinación de pH (Database: CAplus)

[204] B.J.-C. Deboux, E. Lewis, P.J. Scully, R. Edwards. *A novel technique for optical fiber pH sensing based on methylene blue adsorption*. J. Lightwave Technol., 13(17) (1995) 1407-1414

[205] I. Yulianti, A.S.M. Supa'at, S.M. Idrus, O. Kurdi, M.R.S. Anwar. *Sensitivity improvement of a fibre Bragg grating pH sensor with elastomeric coating*. Meas. Sci. Technol., 23 (2012) 1-7

2. OBJETIVOS

El objetivo general del trabajo que se desarrolla en este capítulo es:

- Desarrollo de una matriz sensora óptica para medida de pH en rango completo (0-14) de disoluciones acuosas a partir de los valores de coordenadas cromáticas H obtenidos mediante técnicas de imagen a partir de los elementos sensores de la matriz.

Los objetivos particulares a alcanzar son:

- Caracterizar los diferentes indicadores ácido-base empleados según su estructura química y las reacciones que experimentan en las membranas cuando se ponen en contacto con las disoluciones de medida.

- Modelar los datos de absorbancia obtenidos mediante un espectrofotómetro y los de coordenadas H derivados del uso de un escáner convencional trabajando en modo transmisión. Calcular el valor de la constante de equilibrio K_e de los indicadores inmovilizados a partir del parámetro experimental α y realizarse una estimación de este mismo parámetro a partir de los valores de H.

- Aplicación de diversas estrategias de cálculo para correlacionar los datos experimentales de coordenadas H con la variación del pH.

- Comparar los modelos de ajuste considerando los errores cuadráticos medios y los requerimientos de memoria computacional y tiempo de análisis.

- Comparar los valores de pH predichos a partir de los diferentes modelos de ajuste empleados con aquellos obtenidos utilizando el procedimiento potenciométrico estándar como método de referencia.

PUBLICACIÓN I:

Analytica Chimica Acta, 681 (2010) 71–81
DOI: 10.1016/j.aca.2010.09.033

Full-range optical pH sensor based on imaging techniques

S. Capel-Cuevas[a], M.P. Cuéllar[b], I. de Orbe-Payá[a], M.C. Pegalajar[b], L.F. Capitán-Vallvey[a,*]

ECSens. [a]Department of Analytical Chemistry, Faculty of Sciences, Avda. Fuentenueva s/n.
[b]Department of Computer Science and Artificial Intelligence,
E.T.S. Ingenierías Informática y de Telecomunicación,
C/ Periodista Daniel Saucedo Aranda s/n.
University of Granada, E-18071, Granada, Spain

Abstract

A new colour-based disposable sensor array for a full pH range (0-14) is described. The pH sensing elements are a set of different pH indicators immobilized in plasticized polymeric membranes working by ion-exchange or co-extraction. The colour changes of the 11 elements of the optical array are obtained from a commercial scanner using the hue or H component of the hue, saturation, value (HSV) colour space, which provides a robust and precise parameter, as the analytical parameter. Three different approaches for pH prediction from the hue H of the array of sensing elements previously equilibrated with an unknown solution were studied: linear model, sigmoid competition model and sigmoid surface model providing mean square errors (MSE) of 0.1115, 0.0751 and 0.2663, respectively, in the full-range studied (0-14). The performance of the optical disposable sensor was tested for pH measurement, validating the results against a potentiometric reference procedure. The proposed method is quick, inexpensive, selective and sensitive and produces results similar to other more complex optical approaches for broad pH sensing.

Keywords: Full-range optical pH sensor; H coordinate; HSV colour space.

* Corresponding author; e-mail: lcapitan@ugr.es

1. Introduction

pH measurement by potentiometry is the standard technique because of its simplicity, speed, precision, reversibility and inexpensiveness, but in some applications, optical sensors offer some advantages, mainly insensitivity to electrical interferences, electrical safety, lack of the need for a reference element, presentation as low-cost disposable, autoclavable, precalibrated sensor patches and better characteristics when measuring extreme pH values, low ionic strength solutions or in the presence of organic matter.

Optical pH sensors are mainly based on reversible changes in the indicator's structure induced by pH and translated into changes in spectroscopic phenomena such as absorption, reflectance, luminescence, and energy transfer. Notwithstanding, some optical sensors not based on acid-base indicators exist, such as that based on changes in the ionization of uncladded silica optic fibre by pH traced by methylene blue adsorption via evanescent field [1] and the pH-dependent polymer swelling of functionalized polymer microspheres dispersed in a hydrogel membrane that change the membrane turbidity [2].

Unlike potentiometric pH determination, in which the pH depends linearly on the activity of hydrogen ions, pH in optical sensors is a function of the concentration of the acid and basic forms of the indicator [3]. Thus, calibration functions in pH sensors come from mass-action law relationships between pH and radiation intensity, referring here only to absorption-based sensors, or experimental functions obtained by complete calibration in the case of pH-dependent interactions between indicator and matrix [4], and using in all cases: (a) single-intensity measurements both absolute [5], relative [6] or normalized signals [7] or (b) multiple intensity measurements as the intensity ratio at two or more wavelengths [8].

The immobilization of the indicating molecule is a key issue in determining the analytical and operational characteristics of pH sensors in any of the dispositions used: probe (optic fibre), flow or disposable format. Different types of immobilization techniques for pH indicating dyes have been used [9],

including: (a) dye entrapment in different materials such as cellulose acetate [10,11], sol-gel [12], PVC [7], methacrylic-acrylic copolymers [13] and different composites like SiO_2/ZrO_2-organic polymer (styrene/methyl methacrylate copolymer or Nafion) [14], (b) retention of dye by ion-exchange materials such as Amberlite XAD-2 resin [15] or Dowex I-X10 resin [16], in some instances including the ion-exchanger containing dyes in polymeric encapsulated membranes using PVC [17], (c) adsorption of the dye on materials such as non-ionic styrene/divinylbenzene copolymer [18], polyester/lycra blends textile [19], cellulose [20], cellulose acetate [21], or polymer track membranes combining retention in surface and bulk [22], (d) covalent binding of dye by different synthetic strategies to form microparticles or membranes, in some cases formed on glass fibre, using different polymers such as polyacrylamide [8,23], triacetylcellulose [24], cellulose acetate [25,26], agarose [27] or polyamide [28], among others, (e) polymerization of monomers to prepare both membrane and dye, as with aniline [29] or pyrrole [30].

Typically, the change in the measured signal with pH results in a narrow sigmoidal shape dependence according to the Henderson-Hasselbalch equation. Thus, the dynamic working range for pH optical sensors is limited to a few pH units (2-3) [13] and even shorter if the linear relationship in the middle of the sigmoidal response is used. This short range is one of the main drawbacks of these optical sensors for pH, along with their non-linear response, which requires different sensing membranes to cover the whole pH range.

Different strategies have been devised to extend the working range of pH optical sensors. The working range of membranes containing only one indicator can be broadened using polyprotic acids as indicators; for instance, membranes containing neutral red show a pH range from pH 2.0 to 8.5 [31]. Additionally, in some instances the adsorption of indicators leads to broader ranges than in solution due to multilayered adsorption; for instance, the immobilization of phenol red on Amberlite XAD-2 doubles the range with respect to aqueous solution [32]. Alternatively, the reflectance spectra of immobilised bromophenol blue on Amberlite XAD 7 was used to model the pH between 2.0 and 12.0 by means of a back-propagation artificial neural network (ANN) technique [33]. An interesting approach is to include the dynamic optical response of a pH flow

sensor as analytical signal which allows an increase in the measurement range up to 10 pH units with only one indicator [34].

Some conductive polymers change their absorption properties, both in the visible and near-IR regions, as a function of pH, as is the case of polyaniline [29,35,36], substituted polyanilines [37], polypyrrole [30] or copolymers such as poly(*o*-methoxyaniline) doped with *p*-toluene sulfonic acid [38] or the copolymer of 3-aminophenylboronic acid with aniline [39]. That broad pH range (4-8 pH units) is based on the presence of different polymeric species of variable chain lengths and composed of different structural moieties that exhibit different pK_a values.

Another approach to broaden the dynamic range is to prepare a single pH sensor, typically in optical fibre format, by co-immobilizing multiple pH indicators. The immobilization of two spectroscopically compatible indicators with complementary pH responses is used for: (1) selected pH zones far away each other, for instance very low and high pH values [40] or (2) for ample pH ranges by means of one or several linear stretches [27] or multivariate calibration (ANN) [41]. In other cases, the number of immobilized indicators is higher, typically 3; to acquire more information and offer a simple linear calibration over a broad pH range (8-12 pH units) [42-44], although the immobilization of a universal indicator mixture containing five indicators for the same purpose was reported [45].

A final strategy consists of the preparation of arrays of sensing membranes containing complementary pH indicators acquiring the analytical information by imaging techniques. In this way, commercial multi-colour pH paper strips have been measured with a conventional scanner [20]; alternatively, arrays of five pH membranes in a triacetylcellulose support measured with a CCD colour camera have been described [46]. In both cases, the average RGB values of each sensing area image are used for calibration with multi-linear mathematical models.

The above review of optical pH sensors based only on absorption, reflection or colour measurement shows that the most of the proposed sensors use probe or flow formats and very rarely are in a disposable format. In this paper, we study a disposable optical array for a broad pH range made up of a set of transparent membranes containing immobilized pH indicators with a complementary pH response. The imaging of the array after reaction by means of

a scanner working by transmission mode makes it possible to calculate the *H* (hue) value of the hue, saturation, value (*HSV*) colour space used as a robust and precise analytical parameter [47] along with different multivariate calibration strategies to obtain very precise results over the whole pH range.

2. Experimental

2.1. Reagents and materials

The chemicals used for preparing the pH-sensitive films were high molecular weight polyvinyl chloride (PVC), *o*-nitrophenyloctylether (NPOE), dioctyl sebacate (DOS), bis(1-butylpentyl)adipate (BBPA), tributyl phosphate (TBP), potassium tetrakis (4-chlorophenyl)borate (TCPB), tridodecylmethylammonium chloride (TDMAC), aliquat 336, cellulose acetate (CA), ethylenglycol and tetrahydrofuran (THF) all purchased from Sigma (Sigma-Aldrich Química S.A., Madrid, Spain). As acid-base indicators: 1-amino-4-hydroxyanthraquinone, sodium 3,3-[(1,1-biphenyl)-4,4-diyl(azo)] bis(4-aminonaphtalenesulfonate), *N*-[4-[bis[4-(dimethylamino)phenyl]methylene]-2,5-cyclohexadien-1-ylidene]-*N*-methylmethanaminium chloride (crystal violet), 2-(1,3-dihydro-3-oxo-2H-indol-2-ylidene)-1,2-dihydro-3H-indol-3-one (indigotin blue), 2-[2-[4-(dimethylamino)phenyl]diazenyl]benzoic acid (methyl red), 4,4'-(1,1-dioxide-3H-2,1-benzoxathiol-3-ylidene)bis[2-bromo-3-methyl-6-(1-methylethyl)phenol (bromothymol blue), 4,4'-(1,1-dioxide-3H-2,1-benzoxathiol-3-ylidene)bis[2-bromo-6-methylphenol (bromcresol purple), *N,N'*-[(1,1-dioxide-3H-2,1-benzoxathiol-3-ylidene)bis[(6-hydroxy-5-methyl-3,1 -phenylene)methylene]]bis[*N*-(carboxymethyl)-glycine (xylenol orange), 4,4'-(1,1-dioxide-3H-2,1-benzoxathiol-3-ylidene)bis-phenol (phenol red), 4,4'-(1,1-dioxide-3H-2,1-benzoxathiol-3-ylidene)bis[5-methyl-2-(1-methylethyl)phenol] (thymol blue), 4,4'-(1,1-dioxide-3H-2,1-benzoxathiol-3-ylidene)bis[3-methylphenol] (m-cresol purple), N8,N8,3-trimethyl-2,8-phenazinediamine hydrochloride (neutral red) and 1-phenylazo-2-naphthol (sudan I), 1-(2-pyridylazo)-2-naphthol (PAN) from Sigma, (1,2-benzo-7-(diethylamino)-3-(octadecanoylimino) phenoxazine (liphophilized Nile blue), 9-(diethylamino)-5H-benzo[a]phenoxazin-5-one (Nile red), 1,2,4-trihydroxy-9,10-anthracenedione (purpurin) and 4-(2-pyridylazo)resorcinol (PAR) from Fluka (Fluka, Madrid, Spain),

4,4'-(1,1-dioxide-3H-2,1-benzoxathiol-3-ylidene)bis[2-methylphenol] (cresol red) from Panreac (Panreac, Barcelona, Spain), 1,2-dihydroxy-9,10-anthracenedione (alizarine) from TCI (TCI Europe, Belgium), calcium 3-hydroxy-4-[2-(4-methyl-2-sulfophenyl)diazenyl]-2-naphthalenecarboxylate from BASF (BASF, Ludwigshafen, Germany), 1,4-dihydroxyanthraquinone and 1,5-dihydroxyanthraquinone from ICN (ICN K&K Laboratories, Plainview, NY, USA), 2,6-dihydroxyanthraquinone from EGA (EGA Chemie, Steinheim, Germany) were used. Sheets of Mylar-type polyester (Goodfellow, Cambridge, UK) were used as support. HCl and NaOH were supplied by Sigma. All reagents were of analytical reagent grade and were used without any further purification. All solutions were prepared in reverse-osmosis type quality water (Milli-RO 12 plus Milli-Q station from Millipore, conductivity 18.2 Mohm/cm).

2.2. Instruments and Software

A Microtek ScanMaker i700 scanner (Microtek, CA, USA) was used to acquire images of the membranes. Absorbance measurements of the membranes for comparative purposes were performed by a Hewlett Packard diode array spectrophotometer (model 8453; Nortwalk, CT, USA) equipped with a home-made membrane cell holder.

The software used to manage the scanner was Silver Fast Ai provided by Microteck. The images were processed with a set of scripts and functions developed by us in Matlab r2007b (The MathWorks, Inc, Natick, MA, USA). The acquisition and manipulation of the spectral data were carried out using the Chemstation software package supplied by HP for absorbance measurements. Statistical calculations were performed with Statgraphics software package (Manugistics Inc. and Statistical Graphics Corporation, USA, 1992), and Microsoft Excel (Microsoft Corp., Redmond, WA, USA) was used for general calculations.

Other apparatus consist of a laboratory-made spin-on device and a Crison pH-meter (Crison Instruments, Barcelona, Spain, model Basic 20) with a combined double junction glass electrode, calibrated against two standard buffer solutions (pH 4.0 and 7.0), was used for pH measurements.

2.3. Preparation of sensing membranes

The multimembrane pH sensor was prepared on a 50 mm x 40 mm Mylar support covered by an adhesive and transparent PVC layer with 12 holes of 5 mm of diameter each (1.2 µL volume) disposed in 3 columns and 4 rows (figure 3.1). The membranes were cast by carefully placing in each hole 8 µL of the corresponding cocktail, whose surface tension and quick evaporation makes it possible to prepare the sensing membrane. The different cocktails for pH sensing were prepared by dissolution in 1 mL of freshly distilled THF in all cases for the different chemicals needed according to the following composition. Cocktail 1: 2.10 mg of m-cresol purple, 9.40 mg of TDMAC, 19.60 mg of DOS, 23.10 mg of CA and 15.80 mg of ethylene glycol. Cocktail 2: 0.50 mg of purpurin, 2.90 mg of TDMAC, 23.45 mg of NPOE and 8.15 mg of PVC. Cocktail 3: 0.50 mg of alizarin, 3.60 mg of TDMAC, 23.45 mg of NPOE and 7.45 mg of PVC. Cocktail 4: 1.10 mg of thymol blue, 4.05 mg of TDMAC, 9.80 mg of DOS, 12.95 mg of CA and 7.15 mg of ethylene glycol. Cocktail 5: 1.00 mg of sicomet red P, 4.00 mg of Aliquat 336, 47.00 mg of NPOE and 19.00 mg of PVC. Cocktail 6: 2.10 mg of bromothymol blue, 2.80 mg of TDMAC, 19.60 mg of DOS, 25.90 mg of CA and 19.60 mg of ethylene glycol. Cocktail 7: 1.00 mg of phenol red, 4.85 mg of TDMAC, 18.20 mg of BBPA, 21.00 mg of CA and 24.95 mg of ethylene glycol. Cocktail 8: 0.50 mg of cresol red, 1.59 mg of Aliquat 336, 23.45 mg of NPOE and 9.46 mg of PVC. Cocktail 9: 1.00 mg of PAN, 7.00 mg of TDMAC, 45.50 mg of NPOE and 16.52 mg of PVC. Cocktail 10: 3.50 mg of thymol blue, 12.88 mg of TDMAC, 19.60 mg of DOS, 23.10 mg of CA and 10.92 mg of ethylene glycol. Cocktail 11: 0.50 mg of liphophilized Nile blue, 1.27 mg of TCPB, 23.45 mg of TBP and 9.77 mg of PVC.

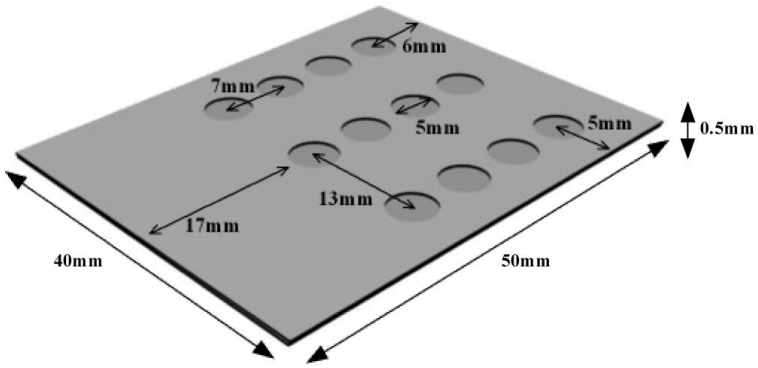

Figure 3.1. Multimembrane pH sensor support

Additionally, individual membranes (12 mm in diameter and around 5 µm thick each) were prepared on a Mylar polyester substrate (14 mm x 40 mm x 0.5 mm) for their spectrophotometric characterization using 20 µL of above cocktails using a spin-coating technique.

2.4. Response evaluation

The response of the multimembrane pH sensor was evaluated by adding volumes of 1.0 M, 0.1 M or 0.01 M HCl or NaOH with a microburette to an aqueous solution containing the multimembrane sensor hanging from a support with a clamp. After each addition and magnetic stirring, the pH of the solution was measured using a pH-meter. The multimembrane sensor was equilibrated for 5 min, then was pulled out and inserted into a holder, obtaining the image with a transmission flatbed scanner. The resolution and colour depth were set to 300 dpi for higher resolution without membrane degradation and 48-to-24 bits of colour, respectively.

To evaluate and compare the response of the membranes, the same experimental setup indicated above was used, measuring individual pH membranes with a DAD spectrophotometer.

2.5. Image acquisition and treatment

The obtained images were stored in uncompressed TIFF (True Image File Format) format to avoid loss of information using 24 bits per pixel. The scanner was calibrated before using by means an IT8 calibration target which is designed to measure the performance of input devices and generate ICC (International Colour Consortium) profiles.

All images were processed using Matlab. After the image files were opened and read into memory as separate RGB channels, the first step, referred to here as masking, was to determine which pixels are parts of the coloured membrane and which are not. In the first step of this process each channel was normalized independently of each other.

The resulting values for R, G, and B ranged from 0 to 1. After normalization the difference between the channels that produce the maximum and minimum values was then determined for each pixel in the image. These differences were then compared to the maximum observed difference in the entire image multiplied by some threshold fraction, where pixels with greater differences were interpreted as coloured and pixels with smaller differences were interpreted as grey background, coming from the Mylar substrate and scanner lid. A typical value for the threshold fraction was 0.3, where larger values result in a more selective mask that interprets more pixels as being grey rather than coloured. After each pixel was sorted into a coloured or non-coloured category, the image was then divided into smaller sub-images, one for each membrane in the image. This process searched the image for entire rows and columns that did not contain coloured pixels. In this way the image was cut into smaller rectangles that contain coloured pixels. Sub-images that contained the coloured pixels (typically some 1,600) were retained, and the process was repeated twice more so that there was a single membrane per rectangle. Because the membranes are circular and the cuts were vertical and horizontal, the cut images have corners that contained non-coloured pixels. These pixels could be used in a subsequent step to rebalance the colour channels relative to each other to control the appearance of white in the image [47].

The calculation of H, S, and V coordinates from RGB values is given in equations 3.1, 3.2 and 3.3, respectively [48]. From R, G and B values of each pixel, the H coordinate is calculated and the mode of the set of H data obtained from all pixels of a sensing element is used as the representative value. Because of the circular nature of H (it is often reported as an angle that varies between 0 and 360º and represented as a colour wheel where 0º is located at the top of the wheel), the values are bounded between 0 and 1, with both 0 and 1 representing the same hue. However, in this work we allow H to be from -360º to 360º (the normalized values are therefore between -1 and 1) in order to avoid discontinuities in H evolution with pH if it passes through the origin.

$$H = \begin{cases} \left(\dfrac{G-B}{\max_{channel}-\min_{channel}}+0\right)/6; & \text{if } \max = R \\ \left(\dfrac{B-R}{\max_{channel}-\min_{channel}}+2\right)/6; & \text{if } \max = G \\ \left(\dfrac{R-G}{\max_{channel}-\min_{channel}}+4\right)/6; & \text{if } \max = B \end{cases} \quad (3.1)$$

$$S = \frac{\max_{channel}-\min_{channel}}{\max_{channel}} \quad (3.2)$$

$$V = \max_{channel} \quad (3.3)$$

3. Rationale

This section describes three approaches for the prediction of pH from the hue values (H) of n optical sensing elements in a multimembrane. The hue from each optical sensor is obtained from a multimembrane scanned in transmission mode: the resulting scanned image is processed by the colour feature extraction method previously developed [47,49] and the hue is computed with the equations 3.1-3.3.

The two preliminary approaches assume that the response hue $H^{S,R}(x)$ of a sensing element *S* may be modelled with a sigmoid-shape function in a pH range *R*. This function depends on 5 parameters $Z_i^{S,R}$, i=1, ..., 5 (equation 3.4), which are optimized in the calibration data using a non-linear programming method according to an error criterion (equation 3.5). In equation 3.5, the values (pH_k^S, H_k^S) are the data from the calibration data set.

$$H^{S,R}(pH) = Z_1^{S,R} + \frac{Z_2^{S,R}}{(1+e^{-Z_3^{S,R}pH+Z_4^{S,R}})^{Z_5^{S,R}}} \quad (3.4)$$

$$[Z_i^{S,R}] = \min_{[Z_i^{S,R}]}\left(\sum_k (H^{S,R}(pH_k^S) - H_k^S)^2\right) \quad (3.5)$$

The first approach (Sigmoid surface fit model) builds a discrete surface with *n+1* dimensions $(h_1, h_2, h_3, ..., h_n, H_k^{S,R}(x))$, in the pH range from 0 to 14 with

a precision between pH points of 0.01. The first *n* dimensions are matched with the hue of each sensing element for the corresponding pH point, and the last one contains the parameters of the function $H_k^{S,R}(x)$ that provides the best accuracy in that point. The pH prediction is carried out using the *Nearest Neighbour* classification method [50], considering the Euclidean distance (equation 3.6). Given a vector of *n* hue values from the sensing elements in a multimembrane, $h=(h_1, h_2, h_3, ..., h_n)$, it is searched the surface point $k\ (h_1^k, h_2^k, ..., h_n^k, H_k^{S,R}(x)^k)$ whose distance to *h* is minimum. The pH is predicted with the function $H^{-1S,R}(h_S)$, where the values *S* and *R* are obtained from the dimension *n+1* of the selected point of the surface.

$$<S,R>=<S,R>^k : k = \min_k \{\sqrt{\sum_{j=1}^{n} (h_j^k - h_j)^2}\} \qquad (3.6)$$

This approach may consume a high amount of computer memory depending on the precision to be achieved by the surface. This amount may be calculated according to equation 3.7, where *K* is the number of bytes used to represent a real value, *M* is the number of approximations $Z_i^{S,R}$ required to model the sensing elements with i=1...5, *n* is the number of sensing elements considered in the approach, Prec is the precision of the surface, and $[min_{pH}, max_{pH}]$ is the covered pH range.

$$Memory = K \cdot (5 \cdot M + (n+1) \cdot (max_{pH} - min_{pH}) \cdot Prec) \qquad (3.7)$$

In order to solve this limitation, the second approach, called Sigmoid function competition model, arises as a simplification of the previous Sigmoid-shape surface fit approach in order to reduce the memory resources consumption to $Memory=K\cdot(5\cdot M)$, although it is required an increase of the computer processing time during the prediction stage. This model encompasses just the set of all functions $H^{S,R}(x)$ optimized. During the pH prediction stage for an input hue vector $(h_1, h_2, h_3, ..., h_n)$, all inverse functions are used to propose a pH prediction value $pH^{S,R} = H^{-1S,R}(h_S)$. The set of all proposed values $\{pH^{S,R}\}$ are then used to recalculate an approximation of the original input hues vector $(h_1^{S,R}, h_2^{S,R}, h_3^{S,R}, ...,$

$h_n^{S,R}$), with the functions $H^{S',R'}(pH^{S,R})$. The value $pH^{S,R}$ that fulfils the best input vector approximation, considering the Euclidean distance between the input hue vector and the hues recalculation, is determined as the response pH and returned by the model. In this approach, the amount of computer memory used is low so that it could be suitable to be implemented in electronic devices with memory limitations. Additionally, one or more sensing elements may be removed from the prediction model without any need for recalibration, although the precision could be lower in these cases. However, both of these approaches are based on the need that the function $H^{S,R}(x)$ fit the calibration data suitably. Unfortunately, this is not always true due to local optima solutions regarding the parameters $Z_i^{S,R}$, obtained from the non-linear optimization methods.

In order to overcome these limitations the third prediction model, called linear surface fit approach, provides a pH prediction based on linear approximations of pH in respect of a sensor hue. As done in the first model, a (n+1)-dimension surface is built from the calibration data (pH_i^S, H_i^S), which must be large enough for each sensing element so that a linear approximation between two points (pH_i^S, H_i^S) and (pH_{i+1}^S, H_{i+1}^S) does not provide a high error. For the calibration of the model, firstly it is made a linear approximation of H in respect of pH for each sensing element and consecutive points in the calibration data, as equations 3.8, 3.9 and 3.10 states:

$$H'^S = a_i^S pH' + b_i^S \tag{3.8}$$

$$a_i^S = \frac{H_{i+1}^S - H_i^S}{pH_{i+1}^S - pH_i^S} \tag{3.9}$$

$$b_i^S = H_i^S - a_i^S pH_i^S \tag{3.10}$$

After that, the surface is built to cover the desired pH range [*0, 14*] with a pH precision of *Prec*. Each point in the surface is a (n+1)-dimension vector $(h_1, h_2, \ldots, h_n, pH)$ where h_i is the hue that should provide the i-th sensing element in the multimembrane, and *pH* the pH resulting from the formula in equation 3.8. The computer memory resources required in this model may be computed according to equation 3.11.

$$Memory = K \cdot (n+1) \cdot (max_{pH} - min_{pH}) \cdot Prec) \quad (3.11)$$

This value is reduced being compared with the first approach, and higher than the memory used in the second case. In addition, the computer processing time equals the first approach and is lower than the second one.

The prediction of pH is carried out in a similar way to the first model: a vector of hues $h=(h_1, h_2, ..., h_n)$ is provided. Then, the surface point of minimum Euclidean distance to h is searched with the *Nearest Neighbour* classification method. Then, the $(n+1)$-th component of this point is the predicted pH. The main advantage of this strategy is that the precision in the prediction does not depend on the results of the non-linear optimization method and the sensing elements modelling. However, a high amount of calibration data is needed to achieve a suitable accuracy. From a computational point of view, the amount of computer memory for this approach is similar to the first approach, although the computational time for calibration is low.

4. Results and Discussion

The RGB space is an additive representation of colour in which all the colours can be represented as a combination of red, green and blue primaries. The colour space used here, HSV, is an alternate representation of colour derived from the red, green, and blue intensity values of the RGB space. A pixel in this colour space is defined by its Hue (H), Saturation (S), and Value (V) coordinates. In broad terms, H is a numerical representation of the colour, S gives the degree to which a single channel dominates, and V represents the brightness. We have demonstrated previously that the H value is stable, simple to calculate, and easily obtained from commercial devices, maintaining a superior precision with variations in indicator concentration, membrane thickness, detector spectral responsivity, and illumination [47]. In contrast to other approaches that make use of the RGB colour space to achieve the pH prediction [46], our proposal to use the parameter H provides the additional advantage of the degression of the parameter space from three dependent variables to only one.

The calibration data were obtained separately for each sensing element from the multimembrane, covering the pH range from 0 to 14 to know their active hue and pH ranges that are useful for prediction. The information obtained from some sensing elements provides more than one active range, and also may overlap other sensing elements' information. This overlapping is useful to manage noisy data during the hue value acquisition. In the following sections, we describe the membrane selection and characterization procedures, the calibration models and the results obtained.

4.1. pH-sensitive membrane selection

The goal of this study was to prepare a multimembrane pH sensor covering the full pH range [0, 14] based on colour measurement using imaging techniques and HSV colour space. A set of pH membranes was selected containing colorimetric acid-base indicators with the conditions of: 1) no leaching in the whole pH range studied; 2) change in tonal colour coordinate by reaction and 3) covering the full pH range by overlapping between responses of different membranes.

24 different acid-base indicators were studied (alizarin, 1-amino-4-hydroxyanthraquinone, bromcresol purple, bromothymol blue, congo red, m-cresol purple, cresol red, crystal violet, 1,4-dihydroxyanthraquinone, 1,5-dihydroxyanthraquinone, 2,6-dihydroxyanthraquinone, indigotin blue, liphophilized Nile blue, methyl red, neutral red, Nile red, PAN, PAR, phenol red, purpurin, sicomet red P, sudan I, thymol blue and xylenol orange) preparing 200 different cocktails containing different types and amounts of membrane polymer, plasticizer, humectant, if necessary, lipophilic salt in addition to an acid-base indicator.

The selection criteria for pH membranes used were both high variation in H coordinate by reaction and non-redundant information from different sensing elements, so that the entire pH range was covered. Sometimes to displace the pH response of a membrane, we used the same acid-base indicator but changing the plasticizer, membrane polymer, lipophilic salt and/or lipophilic salt/indicator ratio.

As a result, 11 different membranes (table 3.1) were selected as candidates for the multimembrane pH sensor containing 10 different pH indicators, because two membranes were prepared containing the same components including thymol blue, but with a different lipophilic salt/indicator ratio.

Table 3.1. pH membranes selected

Indicator	Membrane Number	Type	pH Range	K_e	Membrane colours	
					Acid	Base
m-Cresol purple	1	H_2I	0.0-1.5	$4.9 \cdot 10^{0}$	amaranth (0.964)	canary yellow (0.151)
m-Cresol purple	1	HI^-	8.5-10.5	$2.8 \cdot 10^{-9}$	mustard (0.129)	blue (0.679)
Purpurin	2	H_3I	2.0-5.0	$2.0 \cdot 10^{-3}$	amber (0.132)	magenta (0.848)
Purpurin	2	H_2I^-	5.5-7.5	$9.4 \cdot 10^{-7}$	magenta (0.841)	medium red-violet (0.893)
Purpurin	2	HI^{2-}	8.0-11.5	$7.3 \cdot 10^{-10}$	purple (0.806)	deep pink (0.909)
Alizarin	3	HI	4.0-7.0	$2.2 \cdot 10^{-5}$	maize (0.149)	blue (0.649)
Thymol blue	4	H_2I	0.6-2.0	$3.7 \cdot 10^{0}$	magenta (0.796)	canary yellow (0.147)
Thymol blue	4	HI^-	7.5-9.5	$1.3 \cdot 10^{-8}$	yellow (0.168)	celestial blue (0.576)
Sicomet red P	5	HI^{2-}	4.5-6.5	$7.1 \cdot 10^{-5}$	persian rose (0.879)	amber (0.122)
Bromothymol blue	6	HI	5.0-8.0	$7.1 \cdot 10^{-6}$	pear (0.186)	pine green (0.497)
Phenol red	7	HI	7.0-9.3	$1.2 \cdot 10^{-8}$	old gold (0.135)	violet (0.779)
Cresol red	8	HI	8.6-10.6	$4.3 \cdot 10^{-9}$	yellow (0.134)	violet (0.644)
PAN	9	HI	7.5-10.0	$3.4 \cdot 10^{-9}$	lemon (0.145)	red (0.062)
Thymol blue	10	H_2I	0.0-1.6	$1.5 \cdot 10^{0}$	fuchsia (0.913)	golden yellow (0.132)
Thymol blue	10	HI^-	9.5-11.2	$3.7 \cdot 10^{-9}$	yellow (0.165)	blue (0.663)
Liphophilized Nile blue	11	HI^+	10.5-12.0	$1.30 \cdot 10^{-10}$	celestial blue (0.572)	magenta (0.796)

* Although alizarin is a diprotic acid, only one change is observed in the pH range studied

Then, the compositions of the different membranes were optimized in terms of leaching minimization (lipophilic salt, plasticizer, and membrane polymer), colour intensity (acid-base indicator) and response time (plasticizer, membrane polymer, humectant and cocktail volume). Optimum compositions are indicated in the Experimental section and the usual lipophilic salt/indicator ratio was 3:1 except for bromothymol blue (1.5:1) and sicomet red P (4:1).

4.2. Membranes characterization and modellization of their behaviour

In order to characterize the 11 pH membranes selected, we considered the response mechanisms involved. The acid-base indicators studied belong to neutral, cationic and anionic types and their reaction in membranes phase involve both ion-exchange and co-extraction mechanisms.

In the case of cationic acids (liphophilized Nile blue), an ion-exchange equilibrium occurs between protons and alkaline ions as shown in equation 3.12 where the bars indicate species in the membrane phase.

$$X^+ + \overline{HI^+} + R \quad \leftarrow^{K_e} \rightarrow \quad \dot{I} + H^+ + \overline{XR} \tag{3.12}$$

This equilibrium is characterized by a constant K_e that includes acidity constant, distribution constant between aqueous and membrane phases of different species, and dissociation constants for the different ion-pairs involved.

The proton/alkaline ion activities ratio in aqueous phase is related to the equilibrium constant K_e through a sigmoidal response function (equation 3.13) that includes the degree of protonation α, and the analytical concentrations of indicator C_I and lipophilic salt C_R, respectively.

$$K_e = \frac{\alpha \cdot (C_R - (1-\alpha) \cdot C_I) \cdot a_{H^+}}{(1-\alpha) \cdot a_{X^+}} \tag{3.13}$$

The second mechanism assumes the presence of a neutral acid-base indicator in the membrane (alizarine, PAN, phenol red, bromothymol blue, cresol red), giving the co-extraction equilibrium shown in the equation 3.14.

$$\overline{HI} + \overline{XR} \xleftrightarrow{K_e} \overline{IR} + X^- + H^+ \qquad (3.14)$$

As in the previous case, the equilibrium constant K_e is related to the proton activity and the degree of protonation α through the next response function:

$$K_e = \frac{\alpha \cdot C_I \cdot a_{X^-} \cdot a_{H^+}}{(1-\alpha) \cdot C_I \cdot (C_R - \alpha \cdot C_I)} \qquad (3.15)$$

Some of the neutral indicators studied are formally polyprotic acids (alizarine, PAN) but behave like monoprotic in the pH range studied when included in the membrane. Additionally, other indicators are diprotic (m-cresol purple and thymol blue) and even triprotic (purpurin), but as the analytical parameter used, the H coordinate, only offers information on the position of the equilibrium between the majoritary species present and the sigmoid curves are sufficiently separated, the corresponding K_e values were calculated as independent equilibria.

In the group of anionic indicators, two cases can be considered: monobasic and dibasic. In the first (m-cresol purple, thymol blue), the following co-extraction equilibrium holds (equation 3.16), which gives rise to the response function in equation 3.17.

$$\overline{HIR} + \overline{XR} \xleftrightarrow{K_e} \overline{IR_2} + X^- + H^+ \qquad (3.16)$$

$$K_e = \frac{\alpha \cdot C_I \cdot a_{X^-} \cdot a_{H^+}}{(1-\alpha) \cdot C_I \cdot (C_R - (1-\alpha) \cdot C_I - 2 \cdot \alpha \cdot C_I)} \qquad (3.17)$$

In the case of dibasic acid (sicomet red P, purpurin) the equilibrium is shown in equation 3.18 and the equilibrium constant K_e is described in equation 3.19.

$$\overline{HIR_2} + \overline{XR} \xleftrightarrow{K_e} \overline{IR_3} + X^- + H^+ \qquad (3.18)$$

$$K_e = \frac{\alpha \cdot C_I \cdot a_{X^-} \cdot a_{H^+}}{(1-\alpha) \cdot C_I \cdot (C_R - 2(1-\alpha) \cdot C_I - 3 \cdot \alpha \cdot C_I)} \quad (3.19)$$

The experimental parameter 1 - α, the degree of protonation, is defined as:

$$1 - \alpha = \frac{X - X_I}{X_{HI} - X_I} \quad (3.20)$$

with X being the analytical signal measured, which can be absorbance [51], fluorescence [52], reflectance [53], transflectance [54], refractive index [55], and even one RGB channel [49], for a given quantity of analyte X; and X_{HI} and X_I the values of the parameter at the fully protonated and deprotonated indicator, respectively.

To check the correctness of above models, 4 membranes containing one indicator of each type (liphophilized Nile blue, alizarine, thymol blue and sicomet red P) were studied through absorbance measurement. Figure 3.2 shows, as an example, a good fit to model in the case of alizarin and table 3.2 presents the calculated K_e values for the 4 indicators studied.

Since the experimental parameter used was the tonal coordinate H coming from the scanned image of the multimembrane, we studied its ability to estimate the degree of protonation 1 - α through the H, H_{HI} and H_I values. Table 3.2 shows the K_e values calculated from H and their close similarity to the value calculated from the absorbance.

Table 3.2. K_e value for selected membranes of different sensing mechanisms calculated from absorbance and H values.

Type	Indicator	K_e (Absorbance)	r^{2a}	K_e (H coordinate)	r^{2a}
HI^+	Liphophilized Nile blue	$1.44 \cdot 10^{-10}$	0.9997	$1.30 \cdot 10^{-10}$	0.9999
HI	Alizarin	$2.21 \cdot 10^{-5}$	0.9999	$2.25 \cdot 10^{-5}$	0.9999
HI^2	Sicomet red P	$4.87 \cdot 10^{-5}$	0.9995	$7.15 \cdot 10^{-5}$	0.9997
H_2I	Thymol blue[b]	$1.89 \cdot 10^{1}$	0.9988	$0.15 \cdot 10^{1}$	0.9976
HI	Thymol blue[b]	$3.47 \cdot 10^{-9}$	0.9979	$3.69 \cdot 10^{-9}$	0.9996

a: Correlation coefficient; b: prepared from cocktail 10.

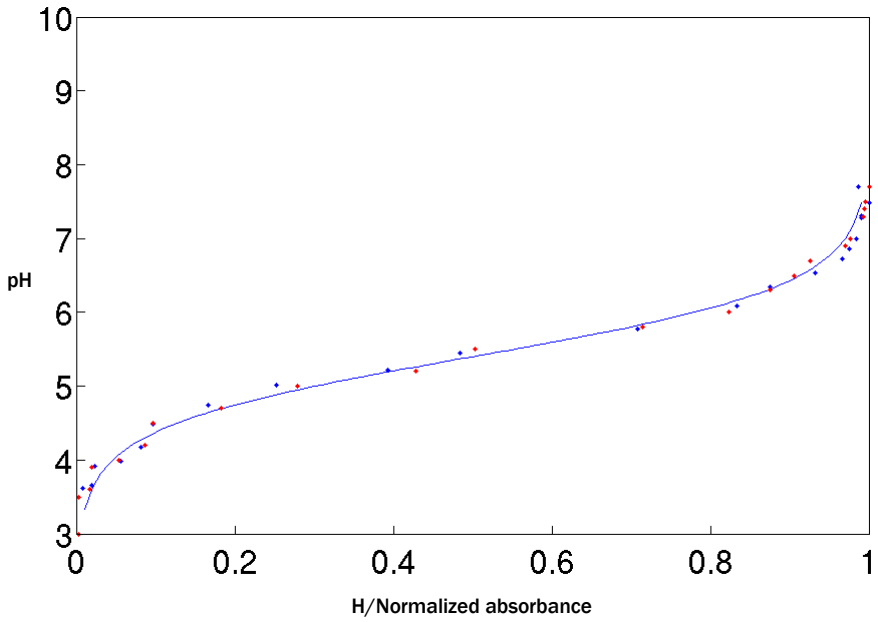

Figure 3.2. Theoretical model for alizarin-based membrane (membrane 3). Experimental data from absorbance (red dots); experimental data from H (blue dots)

4.3. Experimental pH array calibration

In this proof of concept study, the 11 pH membranes selected and characterized above were arranged on a support containing 12 microwells (4 rows x 3 columns) 1.2 µL each by casting a volume of each cocktail in the corresponding microwell.

The analytical parameter selected for the pH sensor array was the H coordinate and not the degree of protonation 1 - α obtained from the H value and indicated above. This is because the 1 - α calculation must measure the signals from the fully protonated and deprotonated species in addition to the signal coming from the sample or standard. The use of just H avoids the use of calibrants for the protonated and deprotonated forms of the indicator in each membrane.

The experiments for calibration purposes between pH from 0 to 14 were performed using 12 replicate sensors each containing the 11 pH membranes indicated above. The H variation was obtained for each 0.1-0.2 pH unit by adding HCl or NaOH solution to an aqueous solution with the array inside and after

equilibration imaging with the scanner. The experimental results for each membrane (figure 3.3) show the usual sigmoidal shape.

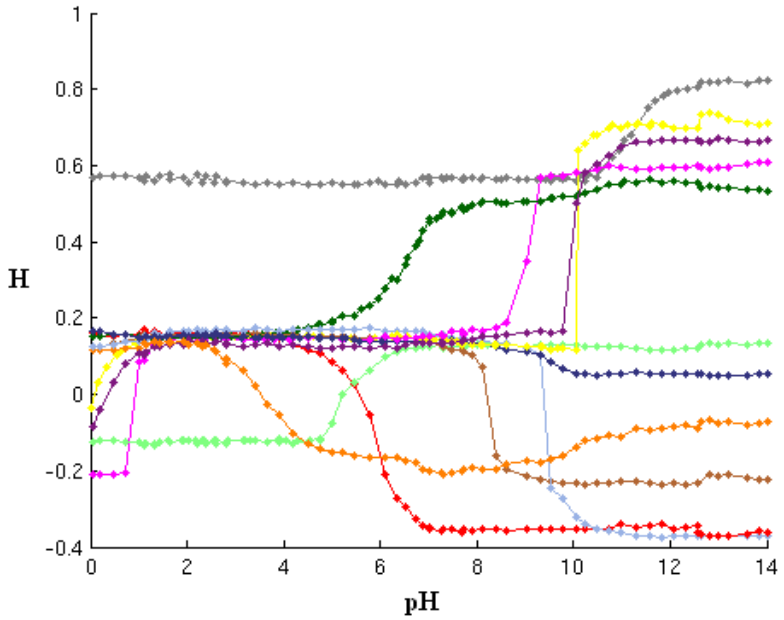

Figure 3.3. Calibration data measured for each sensing element in a pH range from 0 to 14. Colour code used (membranes from 1 to 11, see table 3.1): yellow, orange, red, pink, light green, dark green, brown, light blue, dark blue, purple, and grey

4.4. Calibration models

There were defined 26 hue function approximations $H^{S,R}(x)$ from the calibration data shown in figure 3.3. The next step in the construction of the sigmoid approaches is the computation of the parameters $Z_i^{S,R}$. Table 3.3 describes these parameters after optimization with the non-linear programming method.

Table 3.3. Calculated parameters $Z_i^{S,R}$ optimized for the functions $H^{S,R}(x)$ using the sigmoid surface-based approach

Sensor (S)	Partition (R) and covered pH range	$Z_1^{S,R}$	$Z_2^{S,R}$	$Z_3^{S,R}$	$Z_4^{S,R}$	$Z_5^{S,R}$
1	1 [0.00-5.87]	0.2582	-0.1063	2.3848	0.1161	-1.3493
	2 [5.45-7.74]	0.1366	0.5664	13.9156	134.7675	185.1905
	3 [7.00- 12.57]	0.6972	464.8211	2.4752	29.1406	85.3417
	4 [12.34-14.00]	0.3134	0.3825	1.0089	8.4515	-9.3502
2	1 [0.05-1.94]	0.1364	-0.0205	-5.6243	-8.1815	8.7823
	2 [1.10-5.77]	-0.1663	0.3046	-2.3616	-8.3187	0.8574
	3 [5.77-12.82]	-0.2046	0.0459	-2.8489	-21.5036	9.5773
	4 [12.31-14.00]	-0.2019	0.1301	1.1218	10.1015	2.694
3	1 [0.05-12.57]	0.1601	-0.512	4.2687	26.5196	0.3882
	2 [7.00-14.00]	-0.7462	0.8663	-0.0351	0.6573	0.5811
4	1 [0.05-5.77]	0.1462	-0.3575	-53.0117	-40.1471	0.1168
	2 [5.77-12.82]	0.5903	-0.435	-5.0581	-49.284	21.4606
	3 [12.57-14.00]	-0.2121	0.6225	-0.8825	0.1444	-0.0223
5	1 [0.05-12.57]	0.1278	-0.252	-7.3304	-36.3205	0.2672
	2 [12.34-14.00]	-0.3424	0.4771	2.0102	18.2191	18.9593
6	1 [0.05-9.05]	0.1519	0.3513	3.1839	21.9285	0.3922
	2 [8.97-12.21]	0.5605	-0.0662	-1.2971	-15.469	7.5289
	3 [12.07-14.00]	0.4867	0.5137	-0.5323	-1.4828	0.4034
7	1 [0.05-12.57]	-0.2297	0.3802	-4.6638	-41.2953	12.8058
	2 [12.34-14.00]	-0.2169	-4.5964	-0.5347	-6.2822	6.9204
8	1 [0.05-14.00]	0.1573	-0.5206	7.5403	66.3753	98.238
9	1 [0.05-14.00]	0.1516	-0.0999	2.6202	25.7429	0.3342
10	1 [0.05-5.77]	0.1312	-1.3803	-0.9779	-1.2592	7.1164
	2 [5.01-14.00]	0.1384	0.5217	6.0375	55.4742	82.9794
11	1 [0.05-12.35]	0.5626	0.2649	1.9717	18.3225	31.4555
	2 [12.35-14.00]	0.0926	0.7304	1.8662	16.5213	17.0935

After the calibration of the parameters $Z_i^{S,R}$, the functions $H^{S,R}(x)$ are well defined and provide an approximation of the hue for a given pH in a concrete pH range. At this point, the sigmoid function competition model has been calibrated. However, to finish the construction of the sigmoid-shape surface-based model it is necessary to build the response surface. Figure 3.4 shows the first 11 dimensions of the surface with respect to pH.

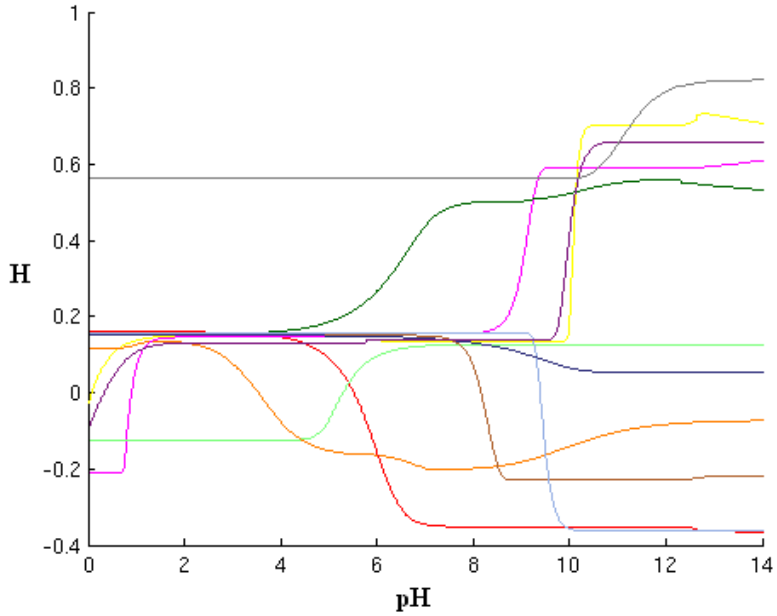

Figure 3.4. Distribution of sensing element hues across the 12 dimensions of the surface created with the Sigmoid-shape surface-based model in the pH calibration range from 0 to 14. Same colour code as in figure 3.3

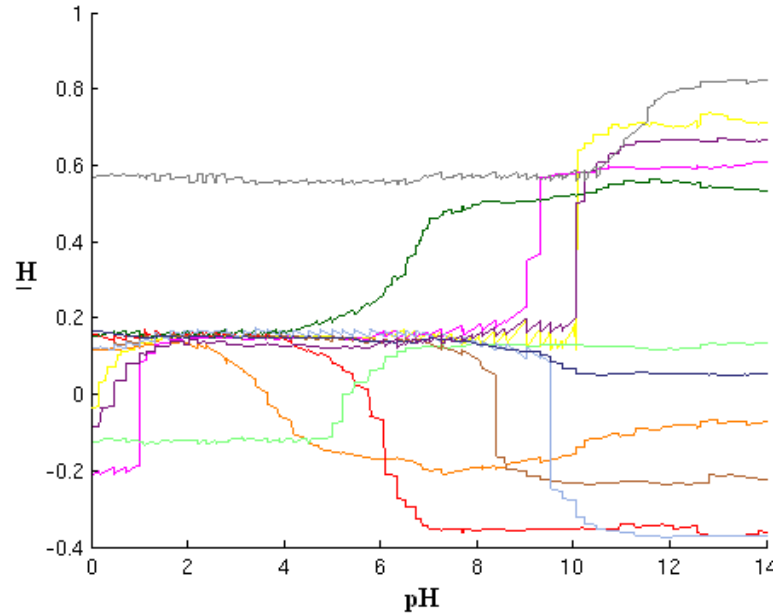

Figure 3.5. Representation of the 12-dimension surface obtained after calibration of the linear surface-based approach. The X-axis is the pH from 0 to 14, and the Y-axis is the value of a sensing element hue. Each line in the figure represents the evolution of a sensing element hue across the pH range. Same colour code as in figure 3.3

The pH prediction model using the linear surface-based approach was constructed with (11+1) dimensions and a precision of *Prec=0.01* in the pH range from 0 to 14. Thus, the discrete surface contains 1401 points of 12 dimensions, where the first 11 are matched with the corresponding sensing element's hue and dimension 12 contains the pH to be predicted, from 0 to 14 in steps of 0.01 for each surface point. After calibration using linear approximations with pairs of consecutive calibration data in each membrane, the surface obtained is depicted in figure 3.5.

4.5. Model validation and test

A set of 70 multimembrane pH sensors, with three replicates, was used to validate the prediction capabilities of the different calibration models against solutions equally spaced and covering the full pH range (validation set).

Additionally, the procedure was applied to 13 real water samples (tap and river water from Granada, Spain) to test the models (test set) with three replicates again, with the pH adjusted with acid and base, sampling the full pH range from 0 to 14. Samples 6 and 7 were taken from the Genil and Monachil rivers and were measured without acid or base addition.

After reaction with samples of the validation and test sets, the arrays were scanned and the hues of all the sensing elements were saved in order to build the validation and test data sets. Each prediction approach was applied over the hue data obtained from the previous procedure in order to provide a pH prediction. We applied a Kolmogorov-Smirnov normality test with a standard 80% confidence level in the real and predicted pH data, in order to learn if the mean and standard deviations are significant statistical estimators that could be used in our study. All data distributions passed the test. Table 3.4 describes the mean absolute error in pH units, MSE and the pooled standard deviation (Sp) of the models in the study data sets.

Table 3.4. Error measurements obtained in pH units in the validation and test data sets for the three approaches studied: mean absolute error, mean squared error, pooled standard deviation

Data Set	Estimator	Linear surface-based approach	Sigmoid surface-based approach	Sigmoid function competition approach
Validation	Mean absolute error*	0.1105	0.1950	0.1298
	Sp*	0.0825	0.1929	0.1054
	MSE	0.0226	0.1245	0.0546
Test	Mean absolute error*	0.1776	0.3168	0.2076
	Sp*	0.1055	0.2310	0.0929
	MSE	0.1115	0.2663	0.0751

Sp.: pooled standard deviation of the mean absolute error.

* In pH units.

According to the results in table 3.4, the models that provide the best results are the linear surface-based and the sigmoid function competition approaches, since they have the lowest MSE, mean absolute error and pooled standard deviation in the real water samples. The sigmoid surface-based model presents the highest MSE and mean absolute error.

Comparing the mean absolute error obtained from the models, the Linear surface-based approach is able to return a prediction with 0.1105 mean absolute error in pH units in the validation set with a pooled standard deviation of 0.0825, and 0.1776 mean absolute error in real water samples. On the other hand, the best MSE in real water samples is obtained with the sigmoid function competition approach. This discordance between the mean absolute error and the MSE between these two prediction models is explained by the existence of a pH prediction error higher than the unit for one test pH value predicted by the linear surface-based approach (see table 3.5). When this error is squared in order to calculate the MSE, the value of this estimator increases significantly. However, the average absolute error in pH units remains lower in the linear surface-based approach, due to the high accuracy in the other pH values of the test data set. The calculation of the pooled standard deviation is also influenced by the pH prediction values with high error, so that the value Sp is higher for the linear

surface-based approach than for the sigmoid function competition model. This analysis suggests that the latter method has better robustness.

In order to test the prediction performance of the approaches, we applied a Student's t-test with a confidence level of 95%, to check if the data distributions resulting from the predicted values in the test set differ significantly from the real data. The probability values obtained were 0.9481 (linear model), 0.9997 (sigmoid surface model) and 0.9373 (sigmoid competition model), respectively. With these results, we may conclude that all the models are able to predict pH suitably since there are no significant differences between the real and predicted pH data. Finally, a Pearson correlation test was applied to verify if the real and predicted pH values match correctly and therefore that the prediction made is right. The results of the R^2 correlation coefficient obtained from the test data suggest a high correlation between the real and predicted pH values, with R^2 of 0.9974 (linear model), 0.9928 (sigmoid surface model) and 0.9979 (sigmoid competition model), which shows that there is no matrix effect in the water sample tested. These results are supported by the regression lines between the real and predicted pH data for each model in the test data, plotted in figure 3.6.

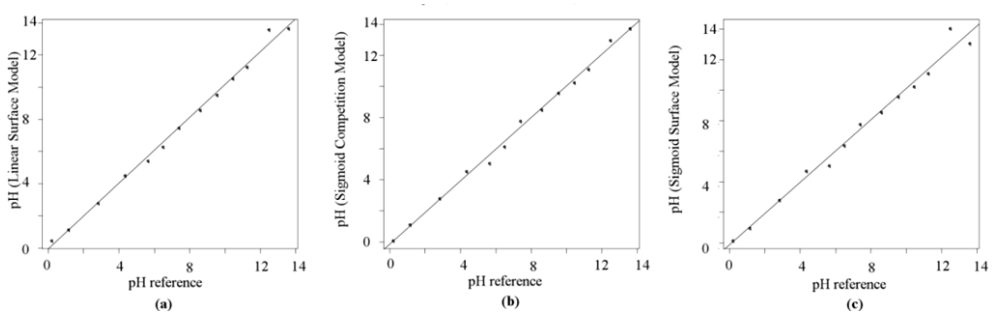

Figure 3.6. Correlation between the reference pH (X-axis) and the predicted pH by the models (Y-axis): a) linear model; b) sigmoid competition model; c) sigmoid surface model

4.6. Analysis of performance in acid and basic pH ranges

Another aspect of interest when the pH is predicted in both acid and basic ranges is to know if the precision in the prediction is different in both ranges, therefore providing a better prediction for either acid or basic pH values. We

studied the balance of error in the pH ranges [0, 7) and (7, 14] in the validation data set. All the 70 data in the validation data were separated into two different sets with 35 experiments for basic pH and 35 experiments for acid pH. The pH predicted by the approaches was used to compute the absolute error between all the predicted values and the real ones obtained from the pontentiometric procedure. A Kolmogorov-Smirnov test concluded that both error distributions do not follow a normal probability distribution, so we applied a non-parametric Kruskal-Wallis test with a 95% confidence level to learn if there were significant differences between the absolute error in acid and basic ranges. The resulting probability values of the test were 0.4614 (linear model), 0.9090 (sigmoid surface model) and 0.9318 (sigmoid competition model). These results suggest that there are no significant statistical differences between the absolute error in basic and acid ranges. Furthermore, from this information we may extract some conclusions about the robustness of the methods in both basic and acid ranges. The least robust is the linear surface approach, since it has the lowest p-value, while the most robust is the sigmoid function competition approach. The sigmoid function competition approach also provides high robustness being compared with the linear model, although its accuracy measured in absolute error is low, as shown in table 3.4.

4.7. Comparison of performance of the prediction approaches

In this section, we test the performance of the approaches for pH prediction statistically. Our aim is to know if a model produces better pH predictions than the other approaches. The study was carried out using a Student's t-test with a 95% confidence level to check if the pH prediction data distributions differ significantly from each other. The test was applied in the test data set, obtaining the probability values of 0.9728 (linear model vs. sigmoid surface model), 0.9445 (linear model vs. sigmoid competition model) and 0.9719 (sigmoid surface model vs. sigmoid competition). Since the test provides probability values over 0.05 in all the cases studied, we conclude that there are no significant statistical differences between the three models and we may assume that they are equivalent for the pH prediction considering the

performance of the approaches although the model that provides the best results in MSE is the sigmoid function competition.

Additionally, we also measured the pH of each solution of the test data set made up of tap and river water samples using a standard potentiometric procedure as a reference method to compare the results. Table 3.5 shows the pH prediction values obtained using the three proposed models compared to the results found by potentiometry as a reference method. This table includes the mean values from the determinations of each sample and the absolute error.

Table 3.5. Determination of pH using the proposed sensor array in tap and river water samples using a potentiometric procedure as reference method

Sample	Potentiometric reference method		Linear surface-based approach		Sigmoid surface-based approach		Sigmoid function competition approach	
	pH prediction	Absolute error	pH prediction	Absolute error	pH prediction	Absolute error	pH prediction	Absolute error
1	0.196	0.004	0.480	0.280	0.165	0.034	0.110	0.089
2	1.149	0.001	1.160	0,010	0.987	0,162	1,142	0.007
3	2.662	0.168	2.810	0.020	2.821	0.008	2.821	0.008
4	4.350	0.001	4.530	0.180	4.727	0.377	4.562	0.212
5	5.747	0.097	5.440	0.210	5.080	0.569	5.080	0.569
6	6.510	0.010	6.310	0.190	6.398	0.101	6.151	0.348
7	7.400	0.000	7.490	0.090	7.792	0.392	7.794	0.394
8	8.630	0.030	8.600	0.000	8.579	0.020	8.522	0.077
9	9.554	0.004	9.540	0.010	9.599	0.049	9.598	0.048
10	10.451	0.001	10.560	0.110	10.261	0.188	10.265	0.184
11	11.239	0.011	11.280	0.030	11.126	0.123	11.126	0.123
12	12.489	0.001	13.600	1.110	14.068	1.578	12.983	0.493
13	13.593	0.007	13.670	0.070	13.090	0.598	13.742	0.142

To finish the analysis in this section, we compared the absolute error data distributions resulting from the predictions in table 5 to compare the proposed models with the standard potentiometric procedure. A Student's t-test with a 95%

confidence level was applied over the absolute error data distributions provided by the pH-meter and models. We obtained the probability value of 0.089 for the comparison with the linear surface-based approach, 0.028 for the comparison with the sigmoid surface-based approach, and 0.004 for the comparison with the sigmoid function competition model. These results conclude that there are no significant statistical differences in the error between the glass electrode potentiometry and the linear surface-based approach, while the potentiometric procedure performs better than the remaining methods.

In summary, the previous analyses make it possible to conclude that the model able to provide the best accuracy is the linear surface-based approach. However, the most robust method is the sigmoid function competition approach, since the pooled standard deviation of the absolute error prediction is the lowest in this model. This result may be verified with the errors from the pH prediction values in table 3.5 for both models.

4.8. Comparison with other optical approaches for pH

To conclude this study, we compare the proposed approach with the existing literature. Considering the use of RGB colour space coordinates for pH prediction in a wide range, the paper by Safavi *et al.* [46] provides the performance of three different approaches to optimize an objective multilinear function to predict the pH from RGB data coming from a set of triacetylcellulose membranes containing 5 different indicators. The MSE provided is 0.03 using Neural Networks, 0.04 with Generalized Reduced Gradient (GRG) and 0.05 with Partial Least Squares algorithms. Abbaspour *et al.* [20] also use the GRG technique to optimize a non-linear function that makes a pH approximation from RGB values obtained by means of a scanner from commercial multi-colour pH paper strips, providing an MSE of 0.029. We would like to remark that the approaches based on RGB colour space use three different dependent parameters to achieve a suitable prediction (Red, Green and Blue colour components). In this way, our approach has an added value since we only need a single parameter (the hue from the HSV space) and therefore the optimization parameter space is simplified.

Other authors have approached the problem considering spectral data. With the absorbance spectra of a sensor containing a mixture of two indicators immobilized on a membrane and covering a range of pH from 0 to 14, network inputs for neural networks using Principal Component Analysis can be acquired [40]. The results of this approach also provide an MSE of 0.03 and 0.04 depending on the network structure. Lin *et al.* [44] use the reflectance spectra of a membrane containing a mixture of three indicators immobilized in sol-gel and neural networks with a mean error between 0.02 and 0.054 in a pH range from 2 to 12. The use of conductive polymers such as polyaniline [29] bounds the prediction error in ranges of 0.1 and 0.2 for pH from 4 to 9, and in the case of poly(*o*-methoxyaniline) doped with *p*-toluene sulfonic acid [38] provides a pH precision of 0.01 in the range 5.5-11.0. The use of a pH flow sensor containing only one indicator but including the dynamic optical response as analytical signal achieves an MSE of 0.02 using neural networks in the pH range from 0 to 12 [34]. Other relevant works with similar results may be found in references [27,31,36,41,43].

Most of the previous methods differ on the sensor design and construction, but share some points in common: the data acquisition and selection for the pH prediction is usually based on the absorbance spectra, although other works propose the use of reflectance spectra and the RGB colour space. Furthermore, the use of neural networks and linear/non-linear approximation formulae to model the pH with respect to the dependent parameters is very common, as are the algorithms used for the model calibration. With respect to our results, we have proposed models based on linear and non-linear approximations as a basis for building prediction surfaces depending on colour features of several sensing elements. The approaches shown in this work provide an MSE of 0.0751 (sigmoid function competition model), 0.1115 (linear surface fit model) and 0.2663 (sigmoid surface fit model) in the water samples analyzed.

5. Conclusions

An optical disposable sensor array has been developed using a set of immobilized colorimetric acid-base indicators for full-range pH determination implemented in a transparent multimembrane that works by ion-exchange or

coextraction and based on colour measurement from imaging techniques offering an easy-to-measure analytical signal.

Three approaches for pH prediction from the hue H of eleven optical sensing elements disposed in a multimembrane previously equilibrated with an unknown solution have been proposed. All the models have shown suitable prediction capabilities, and statistical tests concluded that there are no significant differences between all these models considering their prediction accuracy. Moreover, we provided computational aspects to be considered for the use of one of the three models depending on the hardware device that implements the approach: the linear model is easy to perform with a computer. The procedure for prediction in this approach is simple and efficient, so that it may be implemented in hardware where the microchip speed resources are low. However, the memory space required to build and maintain the surface was high if we tried to achieve great surface precision. Another limitation is the huge amount of calibration data necessary to obtain a suitable linear approximation. The second model, the sigmoid surface fit approach, is more difficult to build due to the optimization of the dependent parameters. Moreover, the memory requirements are similar in both approaches. Finally, the sigmoid function competition approach shares a disadvantage with the sigmoid surface fit model: the optimization of the approximation function may become trapped in local optima during the model calibration. The consumption of computational time is high due to the calculation of multiple pH predictions and the re-computation of the hue which should produce the predicted pH. However, it is easier to implement than the sigmoid surface-based model and its memory requirements are lower. To summarize, the selection of the model should not only consider the performance of the approach, but also the background aspects regarding the hardware where it will be implemented: if the electronic device has some memory limitations (as with, for example, mobile devices like cell phones), the sigmoid function competition approach might be a good choice since it consumes a smaller amount of memory. However, for real-time processing requirements, we would suggest using one of the other two approaches since the prediction time is lower.

Compared to the literature, these improvements may be due to the general model strategy: the use of hue H from HSV colour space has been shown to be suitable for modelling sensor behaviour. Furthermore, the use of 11 sensing

elements in the multimembrane whose response is usually overlapped leads to better model calibration and prediction accuracy. The development of small, hand-held, and battery-operated instruments that will include developed algorithms to work with captured imaging data coming from cheap sensing array is now being investigated.

Acknowledgements

We acknowledge financial support from the *Ministerio de Educación y Ciencia, Dirección General de Enseñanza Superior* (Spain) (Projects CTQ2009-14428-C02-01 and CTQ2009-14428-C02-02); and the *Junta de Andalucia* (Proyecto de Excelencia P06-FQM-01467 and P08-FQM-3535).

References

[1] B.J. Deboux, E. Lewis, P.J. Scully, R. Edwards. *A Novel Technique for Optical Fiber pH Sensing Based on Methylene Blue Adsorption*. J. Lightwave Technol., 13 (1995) 1407-1414.

[2] Z.M. Shakhsher, I. Odeh, S. Jabr, W. Rudolf Seitz. *An Optical Chemical Sensor Based on Swellable Dicarboxylate Functionalized Polymer Microspheres for pH Copper and Calcium Determination*. Microchim. Acta, 144 (2004) 147-153.

[3] J. Janata. *Do Optical Sensors Really Measure pH?* Anal. Chem., 59 (1987) 1351-1356.

[4] M.J.P. Leiner, P. Hartmann. *Theory and practice in optical pH sensing*. Sens. Actuators B, B11 (1993) 281-289.

[5] L.R. Allain, T.A. Canada, Z. Xue. *Optical Sensors and the Salt Effect: A Dual-Transducer Approach to Acidity Determination in a Salt-Containing Concentrated Strong Acid*. Anal. Chem., 73 (2001) 4592-4598.

[6] N.K. Sharma, B.D. Gupta. *Fabrication and Characterization of a Fiber-Optic pH Sensor for the pH Range 2 to 13*. Fiber Integr. Opt., 23 (2004) 327-335.

[7] M. Puyol, S. Miltsov, I. Salinas, J. Alonso. *Ketocyanine Dyes: H^+-Selective Ionophores for Use in Integrated Waveguides Absorbance Optodes*. Anal. Chem., 74 (2002) 570-576.

[8] J.I. Peterson, S.R. Goldstein, R.V. Fitzgerald, D.K. Buckhold. *Fiber Optic pH Probe for Physiological Use*. Anal. Chem., 52 (1980) 864-869.

[9] J. Lin. *Recent development and applications of optical and fiber-optic pH sensors*. TrAC-Trends Anal. Chem., 19(9) (2000) 541-552.

[10] T.J. Cardwell, R.W. Cattrall, L.W. Deady, M. Dorkos, G.R. O'Connell. A fast response membrane-based pH indicator optode. Talanta, 40 (1993) 765-768.

[11] A.A. Ensafi, A. Kazemzadeh. *Optical pH Sensor Based On Chemical Modification of Polymer Film*. Microchem. J., 63 (1999) 381-388.

[12] M. Garcia-Heras, C. Gil, N. Carmona, J. Faber, K. Kromka, M.A. Villegas. *Optical behaviour of pH detectors based on sol–gel technology*. Anal. Chim. Acta, 540 (2005) 147-152.

[13] L.Y. Heng, T.H. Fang, L.H. Chern, M. Ahmad. *Influence of Methacrylic-Acrylic Copolymer Composition on Plasticiser-free Optode Films for pH Sensors*. Sensors, 3 (2003) 83-90.

[14] L.R. Allain, Z. Xue. *Optical Sensors for the Determination of Concentrated Hydroxide*. Anal. Chem., 72 (2000) 1078-1083.

[15] R. Narayanaswamy, F. Sevilla III. *Reflectometric study of the acid-base equilibria of indicators immobilised on a styrene/divinylbenzene copolymer*. Anal. Chim. Acta, 189 (1986) 365-369.

[16] M.C. Moreno-Bondi, M. Jiménez, C. Pérez Conde, C. Cámara. *Analytical performance of an optical pH sensor for acid-base titration*. Anal. Chim. Acta, 230 (1990) 35-40.

[17] B. Kuswandi, R. Narayanaswamy. *Polymeric encapsulated membrane for optrodes*. Fresenius J. Anal. Chem., 364 (1999) 605-607.

[18] G.F. Kirkbright, R. Narayanaswamy, N.A. Welti. *Fibre-optic pH probe based on the use of an immobilised colorimetric indicator*. Analyst, 109 (1984) 1025-1028.

[19] D. Morris, S. Coyle, Y. Wu, K.T. Lau, G. Wallace, D. Diamond. *Bio-sensing textile based patch with integrated optical detection system for sweat monitoring*. Sens. Actuators B, 139 (2009) 231-236.

[20] A. Abbaspour, M.A. Mehrgardi, A. Noori, M.A. Kamyabi, A. Khalafi-Nezhad, M.N. Soltani Rad. *Speciation of iron(II), iron(III) and full-range pH monitoring using paptode: A simple colorimetric method as an appropriate alternative for optodes*. Sens. Actuators B, 113 (2006) 857-865.

[21] T.P. Jones, M.D. Porter. *Optical pH Sensor Based on the Chemical Modification of a Porous Polymer Film*. Anal. Chem., 60 (1988) 404-406.

[22] A. Dybko, W. Wroblewski, J. Maciejewski, R. Romaniuk, Z. Brzózka. *Efficient reagent immobilization procedure for ion-sensitive optomembranes*. Sens. Actuators B, 38-39 (1997) 207-211.

[23] C. Munkholm, D.R. Walt, F.P. Milanovich, S.M. Klainer. *Polymer Modification of Fiber Optic Chemical Sensors as a Method of Enhancing Fluorescence Signal for pH Measurement*. Anal. Chem., 58 (1986) 1427-1430.

[24] A. Safavi, M. Pakniat. *Dipicrylamine-modified triacetylcellulose membrane for optical pH and potassium ion measurement*. Anal. Chim. Acta, 335 (1996) 227-233.

[25] Y. Kostov, G. Rao. *Low-cost gated system for monitoring phosphorescence lifetimes*. Rev. Sci. Instrum., 74(9) (2003) 4129-4133.

[26] A. Holobar, B.H. Weigl, W. Trettnak, R. Benes, H. Lehmann, N.V. Rodriguez, A. Wollschlager, P. O'Leary, P. Raspor, O.S. Wolfbeis. *Experimental results on an optical pH measurement system for bioreactors*. Sens. Actuators B, B11(1-3) (1993) 425-430.

[27] P. Hashemi, R.A. Zarjani. *A wide range pH optical sensor with mixture of Neutral Red and Thionin immobilized on an agarose film coated glass slide*. Sens. Actuators B, 135 (2008) 112-115.

[28] T. Seung, C. Yang. *Synthesis of Congo Red linked with alkyl amide polymer and its optical ion-sensing property*. Pol. Bull., 42 (1999) 655-660.

[29] S. de Marcos, C. Asensio, I. Urunuela, F. Gallarta, J. Galban, J.R. Castillo. New approaches to polyaniline optical sensors: pH, acetic acid and ammonia determination. Quim. Anal., 19(1) (2000) 99-104.

[30] S. de Marcos, O.S. Wolfbeis. *Optical sensing of pH based on polypyrrole films*. Anal. Chim. Acta, 334 (1996) 149-153.

[31] P. Hashemi, R.A. Zarjani, M.M. Abolghasemi, A. Olin. *Agarose film coated glass slides for preparation of pH optical sensors*. Sens. Actuators B, 121 (2007) 396-400.

[32] M. Bacci, F. Baldini, A.M. Scheggi. *Spectrophotometric investigations on immobilized acid-base indicators*. Anal. Chim. Acta, 207 (1988) 343-348.

[33] F.B.M. Suah, M. Ahmad, M.N. Taib. *Optimisation of the range of an optical fibre pH sensor using feed-forward artificial neural network*. Sens. Actuators B, 90 (2003) 175-181.

[34] A. Safavi, A. Rostamzadeh, S. Maesum. *Wide range pH measurements using a single H^+-selective chromoionophore and a time-based flow method*. Talanta, 68 (2006) 1469-1473.

[35] U.W. Grummt, A. Pron, M. Zagorska, S. Lefrant. *Polyaniline based optical pH sensor*. Anal. Chim. Acta, 357 (1997) 253-259.

[36] Z. Ge, C.W. Brown, L. Sun, S.C. Yang. *Fiber-optic pH Sensor Based on Evanescent Wave Absorption Spectroscopy*. Anal. Chem., 65 (1993) 2335-2338.

[37] E. Primgsheim, E. Terpetchnig, O.S. Wolfbeis. *Optical sensing of pH using thin films of substituted polyanilines*. Anal. Chim. Acta, 357 (1997) 247-252.

[38] M. del P. Taboada Sotomayor, M.A. de Paoli, W.A. de Oliveira. *Fiber-optic pH sensor based on Poly(o-methoxyaniline)*. Anal. Chim. Acta, 353 (1997) 275-280.

[39] J-.Z. Tao, G-.R. Xu, S-.W. Yao, P. Liu, Y-.P. Zhang. *Optical response of copolymer of 3-aminophenylboronic acid with aniline film against pH*. Guangpu Shiyanshi, 25(6) (2008) 1053-1056.

[40] A. Safavi, M. Bagheri. *Novel optical pH sensor for high and low pH values*. Sens. Actuators B, 90 (2003) 143-150.

[41] M. Shamsipur, F. Abbasitabar, V. Zare-Shahabadi, M. Akhond. *Broad-Range Optical pH Sensor Based on Binary Mixed-Indicator Doped Sol-Gel Film and Application of Artificial Neural Network*. Anal. Lett., 41 (2008) 3113-3123.

42. G. Vishnoi, T.C. Goel, P.K.C. Pillai. *A pH-optrode for the complete working range*. Proc. SPIE-Int. Soc. Opt. Eng., 3538 (1999) 319-325.

[43] B.D. Gupta, S. Sharma. *A long-range fiber optic pH sensor prepared by dye doped sol-gel immobilization technique*. Opt. Commun., 154 (1998) 282-284.

[44] J. Lin, D. Liu. *An optical pH sensor with a linear response over a broad range*. Anal. Chim. Acta, 408 (2000) 49-55.

[45] F.J. Arregui, M. Otano, C. Fernandez-Valdivielso, I.R. Matias. *An experimental study about the utilization of Liquicoat® solutions for the fabrication of pH optical fiber sensors*. Sens. Actuators B, 87 (2002) 289-295.

[46] A. Safavi, N. Maleki, A. Rostamzadeh, S. Maesum. *CCD camera full range pH sensor array*. Talanta, 71 (2007) 498-501.

[47] K. Cantrell, M.M. Erenas, I. de Orbe-Payá, L.F. Capitán-Vallvey. *Use of the Hue Parameter of the Hue, Saturation, Value Color Space As a Quantitative Analytical Parameter for Bitonal Optical Sensors*. Anal. Chem., 82 (2010) 531-542.

[48] A.R. Smith. *Color gamut transform pairs*. Proceedings of the 5th Annual Conference on Computer Graphics and Interactive Techniques (1978) 12-19.

[49] A. Lapresta-Fernández, L.F. Capitán-Vallvey. *Scanometric potassium determination with ionophore-based disposable sensors*. Sens. Actuators B, 134 (2008) 694-701.

[50] D. Michie, D.J. Spiegelhalter, C.C. Taylor. *Machine Learning, Neural and Statistical Classification*. Ed. Ellis Horwood: Chichester, UK (1994) pp. 298.

[51] E. Bakker, P. Bühlmann, E. Pretsch. *Carrier-Based Ion-Selective Electrodes and Bulk Optodes. 1. General Characteristics*. Chem. Rev., 97 (1997) 3083-3132.

[52] A. Ceresa, Y. Quin, S. Peper, E. Bakker. *Mechanistic Insights into the Development of Optical Chloride Sensors Based on the [9]Mercuracarborand-3 Ionophore*. Anal. Chem., 75 (2003) 133-140.

[53] R.H. Ng, K.M. Sparks, B.E. Statland. *Colorimetric Determination of Potassium in Plasma and Serum by Reflectance Photometry with a Dry-Chemistry Reagent*. Clin. Chem., 38(7) (1992) 1371-1372.

[54] I. de Orbe-Payá, M. Erenas, L.F. Capitán-Vallvey. *Potassium disposable optical sensor based on transflectance and cromaticity measurements*. Sens. Actuators B, 127 (2007) 586-592.

[55] D. Freiner, R.E. Kunz, D. Citterio, U.E. Spichiger, M.T. Gale. *Integrated optical sensors based on refractometry of ion-selective membranes*. Sens. Actuators B, 29 (1995) 277-285.

3. CONCLUSIONES

El objetivo de este capítulo ha sido el desarrollo de una matriz sensora óptica para medida de pH en rango completo (0-14) basada en técnicas de imagen. Tras la aplicación de diversas estrategias de cálculo para correlacionar los datos experimentales de coordenadas H provenientes de las matrices sensoras con la variación del pH, se han encontrado buenos resultados usando tres modelos de ajuste de datos diferentes: superficies lineales, superficies sigmoidales y de competición de las funciones sigmoidales de las membranas.

Como principales conclusiones podemos resaltar las siguientes:

- Se ha desarrollado una matriz formada por once elementos sensores que, debido a sus distintos valores de pK_a, cambian su color en diferentes intervalos de pH, al objeto de cubrir el rango completo.

- Se han establecido cinco modelos químicos diferentes que explican el comportamiento de los diversos indicadores ácido-base empleados de acuerdo a su estructura química (neutra, catiónica o aniónica) y a las reacciones que tienen lugar en la membrana (mecanismos de intercambio iónico o de co-extracción).

- Se han modelado los datos de absorbancia y de coordenadas H de acuerdo con el modelo teórico, obteniéndose un buen ajuste de los datos. Pudo así calcularse el valor de K_e a partir del parámetro experimental α y realizarse una estimación de este mismo parámetro a partir de los valores de H. Los resultados son muy similares, lo que indica que este sistema basado en medida de color es comparable al estándar de absorbancia, confirmando así su validez.

- Tras la aplicación de los diferentes modelos de ajuste de datos (lineal, sigmoidal y de competición, respectivamente), se han obtenido los siguientes valores de MSE, en unidades de pH: 0,023, 0,125 y 0,055 en los datos de validación y 0,111, 0,266 y 0,075 en muestras de agua de

grifo y de los ríos Genil y Monachil de Granada.

- Respecto al conjunto de datos de test, se han comparado los valores de pH predichos utilizando cada uno de los modelos con aquellos medidos utilizando un procedimiento potenciométrico estándar como método de referencia.

- En cuanto a la comparación de los modelos entre sí, todos los modelos de ajuste han mostrado adecuadas capacidades de predicción y los test estadísticos han concluido que no existen diferencias significativas entre ellos.

  El modelo lineal puede ser implementado en un hardware con bajos requerimientos de velocidad del microchip, pero la memoria requerida para construir y mantener las superficies es elevada y se requiere un gran volumen de datos de calibración.

  El modelo de ajuste de superficies sigmoidales es más difícil de construir debido a la optimización de los parámetros de los que depende y los requerimientos de memoria son similares al caso anterior.

  El ajuste mediante la competición de las funciones sigmoidales es complejo y el consumo de tiempo computacional es alto debido al cálculo de numerosas prediciones de pH y a la re-computación de H, a partir de cuyos valores se predice el pH. Sin embargo, es más fácil de implementar que el modelo basado en superficies sigmoidales y los requerimientos de memoria son menores.

  Consecuentemente, si el dispositivo electrónico a diseñar posteriormente tiene algunas limitaciones de memoria, el tercer ajuste podría ser una buena elección. Pero para requerimientos como procesado a tiempo real, sería más adecuado usar cualquiera de los otros dos debido a que el tiempo de predicción es menor.

CAPÍTULO 4

Matriz sensora óptica para la medida de pH basada en redes neuronales artificiales

"Mientras los filósofos discuten si es posible o no la inteligencia artificial, los investigadores la construyen".

Carlo Frabetti

1. INTRODUCCIÓN

La base teórica de las redes neuronales biológicas (BNN), en la cual posteriormente se basaron las actuales redes neuronales artificiales (ANN), no fue establecida hasta 1878 por Bain[206] y, posteriormente, por James[207,208]. En sus trabajos partieron de que tanto los pensamientos como la actividad del cuerpo son el resultado de las interacciones entre las neuronas en el cerebro. Para Bain, cada actividad implicaba la activación de un determinado conjunto de neuronas; así, cuando las actividades se repiten, las conexiones entre las neuronas se refuerzan, y esta repetición conduce a la formación de la memoria. La comunidad científica, en general, se mostró escéptica ante esta teoría, ya que requería un excesivo número de conexiones neuronales en el cerebro. La teoría de James era similar a la de Bain; sin embargo, sugirió que los recuerdos y las acciones eran el resultado de las corrientes eléctricas que fluyen entre las neuronas en el cerebro.

En 1898, Sherrington[209] experimentó aplicando corrientes eléctricas a ratas para probar la teoría de James, pero en lugar de observar un incremento de la corriente eléctrica como supuso James, encontró que la intensidad disminuía con el tiempo. La importancia de este trabajo fue el descubrimiento del concepto de habituación.

Lashley[210] fue un psicólogo conductista estadounidense famoso por su contribución al estudio del aprendizaje y a la memoria. Su fracaso al intentar encontrar un único origen de la memoria en el cerebro (engrama) le hizo pensar que el recuerdo estaba ampliamente distribuido a través del córtex. Sin embargo, el origen de los modelos conexionistas proviene de la definición de neurona dada por McCulloch (neurofisiólogo) y Pitts[211] (matemático) en 1943, considerándola

---

[206] A. Bain. *Mind and body: the theories of their relation*. New York: D. Appleton and Company (1873) pp. 216

[207] W. James. *The Principles of Psychology*. New York: Henry Holt and Company, 1 (1890) pp. 711

[208] W. James. *The Principles of Psychology*. New York: Henry Holt and Company, 2 (1905) pp. 721

[209] C.S. Sherrington. *Experiments in Examination of the Peripheral Distribution of the Fibers of the Posterior Roots of Some Spinal Nerves.* Proceedings of the Royal Society of London, 190 (1898) 45-186

[210] K.S. Lashley. *Brain mechanisms and intelligence: a quantitative study of injuries to the brain.* Chicago, IL, US: University of Chicago Press (1929) pp. 207

[211] W.S. McCulloch, W.H. Pitts. *A logic calculus of ideas immanent in nervous activity*. Bulletin of Mathematical Biophysics, 5 (1943) 115-133

"un dispositivo binario con varias entradas y salidas". Los resultados de sus modelos fueron funciones lógicas elementales tales como "a o b" y "a y b".

El psicólogo Hebb[212] introdujo en 1949 dos ideas fundamentales que influyeron de manera decisiva en el campo de las ANN: que una percepción o un concepto se representa en el cerebro por un conjunto de neuronas activas simultáneamente y que la memoria se localiza en las conexiones entre las neuronas (sinápsis). Las hipótesis de Hebb presentaron de manera intuitiva el modo en que las neuronas memorizan información y se plasmaron en la regla de aprendizaje de Hebb (o regla del producto). Según ésta, las conexiones entre dos neuronas se refuerzan si ambas son activadas. Los trabajos de Hebb formaron las bases de la teoría de las ANN. Muchos de los algoritmos actuales proceden de estos conceptos y, a pesar de las críticas recibidas debido a la existencia de conexiones inhibitorias y no sólo excitatorias, siguen teniendo una gran influencia.

Farley y Clark[213] (1954) fueron los primeros en utilizar, para simular una ANN de tipo Hebb, las máquinas computacionales que posteriormente fueron llamadas calculadoras. Por otra parte, en 1955 IBM organizó un grupo de trabajo encabezado por Rochester para estudiar el reconocimiento de patrones y las teorías de información y de circuitos de intercambio. Junto a otros proyectos, el grupo simuló el comportamiento de ANN abstractas en ordenadores IBM 704[214].

En 1956, McCarthy, Minsky, Rochester y Shannon organizaron en Dartmouth la primera conferencia sobre inteligencia artificial. Se discutió el uso potencial de las computadoras para simular "*todos los aspectos del aprendizaje o cualquier otra característica de la inteligencia*" y se presentó la primera simulación de una ANN, aunque todavía se desconocía cómo interpretar los datos resultantes.

Tras dos años de trabajo, Rosenblatt publicó en 1959 los resultados de un ambicioso proyecto de investigación, el Perceptrón[215-217], un identificador de

---

[212] D.O. Hebb. *Organization of behavior: a neuropsychological theory*. New York: John Wiley & Sons, Inc., (1949) pp. 335

[213] B. Farley, W.A. Clark. *Simulation of self-organizing systems by digital computer*. IRE Transactions on Information Theory, 4(4) (1954) 76-84

[214] D. Crevier. *Ai: The tumultuous history of the search for artificial intelligence*. New York, NY: Basic Books, (1993) pp. 386

[215] F. Rosenblatt. *The Perceptron–a perceiving and recognizing automaton.* Cornell Aeronautical Laboratory, Ithaca, New York, Project Para No. 85-460-1 (1957)

patrones ópticos de salida binaria. Esta es la ANN más antigua, utilizándose hoy en día fundamentalmente en aplicaciones de reconocimiento de patrones. Este modelo es capaz de generalizar, es decir, después de haber aprendido una serie de patrones, puede reconocer otros similares, aunque no se le hayan presentado anteriormente. Sin embargo, tenía una serie de limitaciones asociadas: la incapacidad de aprendizaje en problemas de clasificación no separables linealmente y la disminución de precisión a medida que aumentaba el número de patrones que intentaba aprender.

Las capacidades del Perceptrón se extendieron al desarrollar la regla de aprendizaje delta, que permitía emplear señales continuas de entrada y salida, de modo que, bajo ciertas condiciones, el aprendizaje convergía hacia un estado finito (teorema de convergencia del Perceptrón). El primer modelo de Perceptrón, el Fotoperceptrón, era un dispositivo que respondía a señales ópticas, imitando así el funcionamiento del ojo humano (figura IV.1).

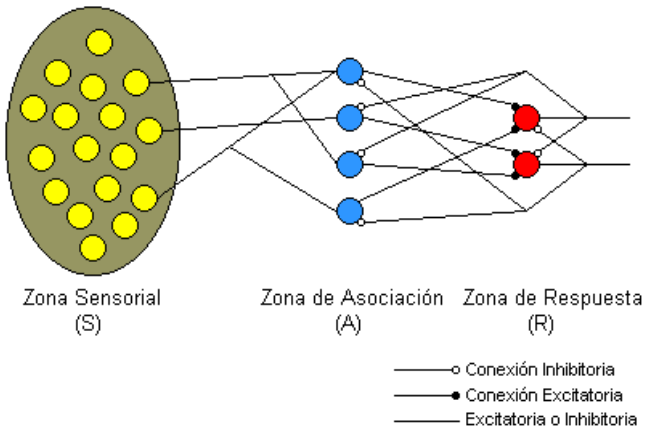

Figura IV.1. Modelo del Fotoperceptrón de Rosenblatt

Widrow[218] y Hoff publicaron en 1960 una teoría sobre la adaptación neuronal y unos modelos inspirados en ella, el *Adaline* (Adaptative Linear Element). Aunque originalmente el nombre correspondía a Adaptative Linear

[216] F. Rosenblatt. *The Perceptron: a probabilistic model for information storage and organization in the brain.* Psychological Review, 65(6) (1958) 386-408

[217] R. Rosenblatt. *Principles of neurodynamics: Perceptrons and the theory of brain mechanisms*. New York: Spartan Books (1962) pp. 616

[218] B. Widrow, M.E. Hoff. *Adaptive Switching Circuits*. IRE WESCON Convention Record, 4 (1960) 96-104

Neuron, al caer las ANN en decadencia se optó por la primera definición dada (figuras IV.2 y IV.3).

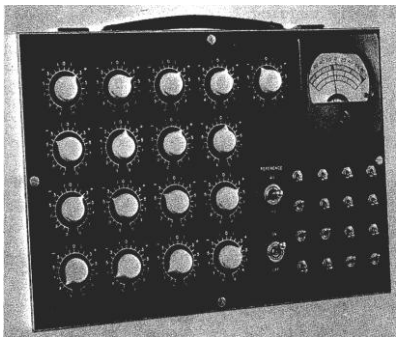

Figura IV.2. Primera máquina de clasificación de patrones adaptativa (Adaline)

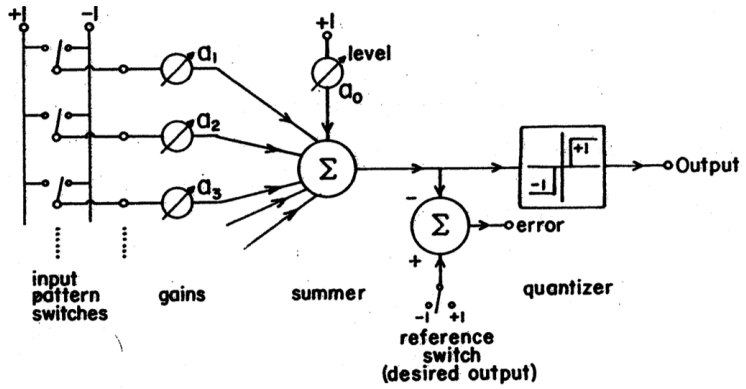

Figura IV.3. Esquema de Adaline

La diferencia entre Adaline y Perceptrón es que este último sólo tiene capacidad para clasificar, ya que utiliza una función umbral sobre la suma ponderada de las entradas, a diferencia de Adaline, que es capaz de estimar una salida real. Además, Adaline utiliza la denominada regla Delta de Widrow-Hoff o regla LMS, basada en la búsqueda del mínimo de una expresión del error entre la salida deseada y la salida lineal obtenida antes de aplicarle la función de activación escalón, evitando la gran cantidad de problemas del Perceptrón durante el entrenamiento, debido a que su función de error (o de coste) posee numerosos mínimos locales. Estas redes pueden procesar información analógica, tanto de entrada como de salida, usando una función de activación lineal o sigmoidal. Por otra parte, en el campo del procesamiento de señal se emplean

como filtros de ruido de señales transmisoras de información y como filtros adaptativos.

Madaline (Multiple Adaline) es una ANN de dos capas con un conjunto de Adalines en paralelo formando la capa de entrada y un elemento procesador que constituye la capa de salida. Se utiliza en problemas de predicción basados en múltiples entradas. Estos modelos fueron usados en numerosas aplicaciones y permitieron utilizar, por primera vez, una ANN en un problema real: filtros adaptativos para eliminar ecos en las líneas telefónicas.

Lernmatrix es el primer modelo matemático de memoria asociativa del que se tiene constancia y fue propuesto en 1961 por Steinbuch[219]. Por su parte, Grossberg desarrolló en 1967 la red Avalancha, que consistía en elementos discretos con actividad que variaba en el tiempo y satisfacía ecuaciones diferenciales continuas, para resolver actividades como reconocimiento del habla y aprendizaje de los brazos de un robot.

En 1969, Minsky y Papert[220] realizaron una seria crítica del Perceptrón, revelando su incapacidad para resolver problemas tales como el aprendizaje de funciones no-lineales, que son ampliamente empleadas en computación. Este trabajo creó serias dudas sobre las capacidades de los modelos conexionistas y frenó, hasta 1982, la investigación sobre ANN. A pesar de esto, Anderson, en 1977, desarrolló un modelo llamado Asociador Lineal, que consistía en unos elementos integradores lineales (neuronas) que sumaban sus entradas y cuyas conexiones eran reforzadas cada vez que eran activados.

Werbos difundió en 1974 la idea básica del algoritmo de aprendizaje de propagación hacia atrás (*backpropagation* o retropropagación), cuyo significado quedó definitivamente establecido en 1985. En esencia, una red de retropropagación es un Perceptrón con múltiples capas, con diferentes funciones de activación en las neuronas y con una regla de aprendizaje más robusta y confiable. Por otra parte, Anderson[221] diseñó en 1977 una potente extensión del Asociador Lineal, conocido como modelo BSB. Tres años más tarde,

---

[219] K. Steinbuch. *Die Lernmatrix*. Biological Cybernetics, 1(1) (1961) 36-45

[220] M.L. Minsky, S.A. Papert. *Perceptrons*. Cambridge, MA: MIT Press, 1969

[221] J.A. Anderson, J.W. Silverstein, S.A. Ritz, R.S. Jomnes. *Distinctive features, categorical perception and probability learning: some applications of a neural model*. Psychological Review, 84 (1977)

Fukushima[222] creó un modelo neuronal para el reconocimiento de patrones visuales.

Hopfield[223] elaboró un modelo de red consistente en unidades de proceso interconectadas que alcanzaban mínimos energéticos, aplicando los principios de estabilidad desarrollados por Grossberg. El modelo de Hopfield resultó muy ilustrativo sobre los mecanismos de almacenamiento y recuperación de la memoria, dando un nuevo impulso a la investigación en este campo con su libro "Computación neuronal de decisiones en problemas de optimización".

Grossberg[224] aportó importantes innovaciones con su modelo ART, y junto a Cohen, elaboró un importante teorema sobre la estabilidad de las redes recurrentes. Esta teoría consistía en una arquitectura de red que, a diferencia de todas las demás, simulaba otras habilidades del cerebro tales como la memoria a largo y corto plazo.

En 1984, Kohonen[225] continuó el trabajo de Anderson y desarrolló modelos de aprendizaje competitivo basados en el principio de inhibición lateral. Su principal aportación consistió en un procedimiento para conseguir que unidades físicamente adyacentes aprendieran a representar patrones de entrada similares.

Rumelhart, McClelland y Hinton[226-228] crearon el grupo PDP. El estudio asociado al algoritmo de aprendizaje de propagación hacia atrás (backpropagation) o algoritmo de retropropagación, solucionó los problemas planteados por Minsky y Papert y extendió enormemente el campo de aplicación de los modelos de computación conexionistas. Otros desarrollos destacables de

---

[222] K. Fukushima. *Neocognitron: a self-organizing neural network model for a mechanism of pattern recognition unaffected by shift in position.* Biol. Cybernetics, 36 (1980) 193-202

[223] J.L. Hoplfield. *Neural networks and physical systems with emergent collective computational abilities.* Proceedings of the National Academy of Science USA, 79 (1982) 2554-2558

[224] S. Grossberg. *Competitive learning: from interactive activation to adaptative resonance*. Cognitive Science, 11 (1987) 23-63

[225] T. Kohonen. *Self-organization and associative memory*. Series in Information Sciences, 8. Berlin: Springer-Verlag (1984)

[226] D.E. Rumelhart, G.E. Hinton, R.J. Williams. *Parallel distributed processing.* Learning internal representations by error propagation. Cambridge, MA: MIT Press (1986) 318-362

[227] D.E. Rumelhart, J.L. McClelland, Group, P.D.P. *Parallel distributed processing: Explorations in the microstructure of cognition.* Cambridge, MA: MIT Press (1986)

[228] J.L. McClelland, D.E. Rumelhart. *Explorations in Parallel Distributed Processing.* A Handbook of Models. Programs and Exercices. Cambridge, MA: MIT Press (1988)

esta década fueron la máquina de Boltzmann[229] y los modelos BAM[230].

A partir de entonces el panorama fue alentador con respecto al desarrollo y las aplicaciones de las ANN. Para discriminar el tipo de aplicación, Cajal *et al.*[231] clasificaron en 2001 las 2057 aplicaciones registradas en 43 áreas (figura IV.4) que abarcaban prácticamente cualquier disciplina de conocimiento.

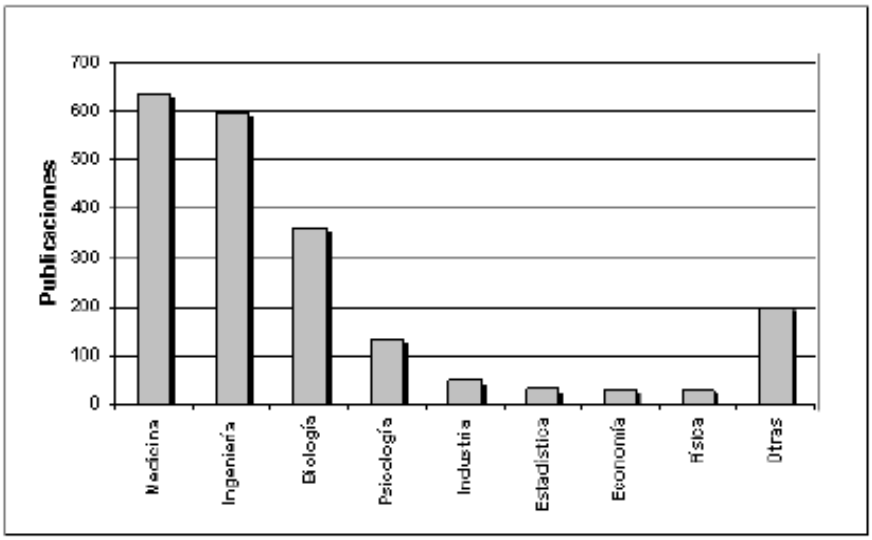

Figura IV.4. Áreas de aplicación más frecuentes de las ANN

En general, las aplicaciones estudiadas tenían por objeto el reconocimiento de patrones, tanto en la vertiente de clasificación como de estimación de variables continuas. La red neuronal más ampliamente utilizada fue Perceptrón multicapa (MLP) asociado al algoritmo de retropropagación orientado a la clasificación, que supuso aproximadamente el 80% de estos trabajos.

En la figura IV.4 se observa que el campo de aplicación mayoritario era la medicina, principalmente en el diagnóstico o la discriminación de pacientes con algún tipo de patología a partir de una serie de variables de entrada en la red,

[229] G.E. Hinton, T.J. Sejnowski. *Learning and relearning in Boltzman machines*. En Rumerlhart & McClelland (1986)

[230] B. Kosko. *Bi-directional associative memories*. IEEE T. Syst. Man Cyb., 18(1) (1988) 49-60

[231] B. Cajal, R. Jiménez, J.M. Losilla, J.J. Montaño, J.B. Navarro, A. Palmer, A. Pitarque, M. Portell, M.F. Rodrigo, J.C. Ruiz, J. Vives. *Las redes neuronales artificiales en psicología: un estudio bibliométrico.* Metodología de las ciencias del comportamiento, 3(1) (2001) 53-65

susceptibles de poder explicar el estado del sujeto. En este sentido, el trabajo de Baxt[232] de 1991 puede considerarse pionero, con la aplicación de una red MLP para la clasificación de pacientes con cardiopatías en función de un conjunto de variables explicativas. Otras áreas de aplicación mayoritarias eran la ingeniería, con importantes trabajos en el campo de la energía nuclear[233,234], y la biología, con la identificación de cadenas de ADN[235,236].

En la actualidad, son numerosos los trabajos que se realizan y publican cada año, las aplicaciones nuevas que surgen (sobre todo en el área de control) y las empresas que lanzan al mercado productos nuevos, tanto hardware como software (sobre todo para simulación).

1.1. Las ANN en Química Analítica

Entre 1960 y 1970 la escasa potencia de los ordenadores dificultaba la utilización de métodos de AI, tales como GA o ANN. Sin embargo, gradualmente aumentaron su velocidad, y el potencial de la inteligencia artificial dentro de los laboratorios científicos comenzó a ser reconocida y utilizada. El libro de Goldberg sobre algoritmos genéticos[237], libro influenciado por Holland[238], sugirió que las herramientas revolucionarias que los científicos computacionales estaban desarrollando alcanzarían otras ramas de la ciencia. Dos años antes del libro de Goldberg, una breve pero notable revisión de Bounds en la revista *Nature*, planteó de forma optimista el futuro de estos métodos[239], y Zupan y Gasteiger[240,241]

[232] W.G. Baxt. *Use of an artificial neural network for the diagnosis of myocardial infarction.* Ann. Intern. Med., 115(11) (1991) 843-848

[233] Z. Guo, R.E. Uhrig. *Sensitivity analysis and applications to nuclear power plant*. International Joint Conference on Neural Networks. Piscataway, NJ: IEEE (1992) 453-458

[234] A.G. Bahbah, A.A Girgis. *Input feature selection for real-time transient stability assessment for artificial neural network (ANN) using ANN sensitivity analysis*. Proceedings of the 21st International Conference on Power Industry Computer Applications. Piscataway, NJ: IEEE (1999) 295-300

[235] H. Ogura, H. Agata, M. Xie, T. Odaka, H. Furutani. *A study of learning splice sites of DNA sequences by neural networks.* Comput. Biol. Med., 27(1) (1997) 67-75

[236] W. Choe, O. Ersoy, M. Bina. *Neural network schemes for detecting rare events in human genomic DNA.* Bioinformatics, 16(12) (2000) 1062-1072

[237] D.E. Goldberg. *Genetic algorithms in search, optimization and machine learning*. Addison-Wesley, Reading, MA (1989)

[238] J.H. Holland. *Adaptation in natural and artificial systems*. University of Michigan Press, Ann Arbor (1975)

[239] D.G. Bounds. *New optimization methods from physics and biology*. Nature, 329 (1987) 215-219

argumentaron que la química era un campo de gran interés para el uso de las ANN. Un estudio del potencial de los métodos de inteligencia artificial dentro de la química[242] insinuó el rango de aplicaciones que iba a desarrollarse.

La evaluación de patrones e imágenes, desde micrografías electrónicas hasta espectros NMR, es una característica de las ANN. Un ejemplo típico de análisis es la evaluación de aceites de oliva[243] con vistas a evitar su adulteración. Técnicas como GC, MS, espectroscopia IR y NMR permiten demostrar la calidad de los productos. Este problema se ha abordado en numerosas publicaciones, como en la de Rezzi *et al.* [244].

En el área de la Química Analítica se han utilizado ANN con diferentes propósitos y uno de ellos es en el campo de los sensores. Así, en 2005 se pudo llevar a cabo la identificación de una amplia variedad de analitos de forma cualitativa[245], utilizando "narices electrónicas". Ozmen *et al.*[246] usaron una matriz de sensores basados en QCM conteniendo ftalocianinas para el establecimiento de la composición de una mezcla de gases, mientras que Dutta *et al.*[247] identificaron infecciones por *Staphyloccocus aureus* en hospitales.

Otras matrices de sensores[248] fueron estudiadas en 1995 mediante técnicas tales como PCA y PCR, pero surgieron dudas acerca de si estos modelos lineales eran completamente apropiados, ya que los datos que los sensores

---

[240] J. Zupan, J. Gasteiger. Neural networks-a new method for solving chemical problems or just a passing phase? Anal. Chim. Acta, 248 (1991) 1-30

[241] J. Zupan, J. Gasteiger. *Neural networks for chemists-an introduction*. VCH, Weinheim. (1993) 215-219

[242] H.M. Cartwright. *Applications of artificial intelligence in chemistry*. Oxford University Press, Oxford (1993)

[243] R. Goodacre, D.B. Kell, G. Bianchi. *Neural networks and olive oil*. Nature, 359 (1992) 594

[244] S. Rezzi, D.E. Axelson, K. Heberger, F. Reniero, C. Mariani, C. Guillou. *Classification of olive oils using high throughput flow ^{1}H NMR fingerprinting with principal component analysis, linear discriminant analysis and probabilistic neural networks*. Anal. Chim. Acta, 552 (2005) 13-24

[245] M. O'Farrell, E. Lewis, C. Flanagan, W. Lyons, N. Jackman. *Comparison of k-NN and neural network methods in the classification of spectral data from an optical fibre-based sensor system used for quality control in the food industry.* Sens. Actuators B, 111-112 (2005) 254-362

[246] A. Ozmen, F. Tekce, M.A. Ebeolgu, C. Tasaltin, Z.Z. Ozturk. *Finding the composition of gas mixtures by a phthalocyanine-coated QCM sensor array and an artificial neural network*. Sens. Actuators B, 115 (2006) 450-454

[247] R. Dutta, D. Morgan, N. Baker, J.W, Gardner, E.L. Hines. *Identification of Staphylococcus aureus infections in hospital environment: electronic nose based approach.* Sens. Actuators B, 109 (2005) 355-362

[248] D. Hodgins, D. Simmonds. *The electronic NOSE and its application to the manufacture of foods*. J. Autom. Chem., 17 (1995) 179-185

generaban eran parcialmente no lineales. Este inconveniente pudo ser solventado con éxito gracias al empleo de ANN[249,250].

Aplicaciones habituales en Química Analítica, tales como la determinación de iones metálicos en disolución, son también susceptibles de una aproximación mediante ANN, como indicaron Lubal *et al.*[251] en 2006 para la determinación analítica de molibdeno (VI) y volframio (VI).

En cuanto a los sensores ópticos para pH, se ha demostrado que mediante el uso de ANN es posible la extensión del rango de respuesta. Su aplicación ha permitido ampliar la respuesta de un optodo desde el inicial rango lineal estrecho (pH 5-7,25) hasta un amplio rango (pH 2,51-9,76)[252]. En otro estudio, se usó una multicapa de prealimentación (*feed-forward*) para modelar los datos de entrada-salida de un sensor de pH de fibra óptica usando datos de absorbancia de tres diferentes longitudes de onda. El modelo resultante fue ensayado con 70 disoluciones de pH entre 1,60 y 10,17, siendo el error de predicción medio de 0,2 unidades de pH[253].

Posteriormente, Safavi y Bagheri[254] describieron el desarrollo de un sensor óptico para pH basado en la inmovilización de una mezcla de dos indicadores de pH sobre una membrana de triacetilcelulosa. El sensor mostró un rango de utilidad para valores de pH tanto bajos como altos, donde los electrodos de vidrio muestran error ácido o básico, respectivamente. La aplicación de una ANN de retroalimentación permitió extender el rango de medida de ese optodo al rango completo.

---

[249] J. Auge, P. Hauptmann, J. Hartmann, S. Rosler, R. Lucklum. *Versatile microcontrolled gas sensor array system using the quartz microbalance principle and pattern recognition methods.* Sens. Actuators B, 26 (1995) 181-186

[250] W.L. Xing, X.W. He. *Crown ether-coated piezoelectric crystal sensor array for detection of organic vapour mixtures using several chemometric methods*. Analyst, 122 (1997) 587-592

[251] P. Lubal, H. Koprivova, O. Sedo, J. Havel, S. Lis, S. But. *Simultaneous determination of molybdenum (VI) and tungsten (VI) and its application in elemental analysis of polyoxometalates*. Talanta, 69 (2006) 800-806

[252] M.N. Taib, R. Andres, R. Narayanaswamy. *Extending the response range of an optical fibre pH sensor using an artificial neural network*. Anal. Chim. Acta, 330 (1996) 31-40

[253] M.N. Taib, R. Narayanaswamy. *Multichannel calibration technique for optical-fibre chemical sensor using artificial neural network*. Sens. Actuators B, 39 (1-3) (1997) 365-370

[254] A. Safavi, M. Bagheri. *Novel optical pH sensor for high and low pH values*. Sens. Actuators B, 90 (2003) 143-150

2. OBJETIVOS

El objetivo general del trabajo que se desarrolla en este capítulo es:

- El uso de calibración multivariante basada en ANN para predecir el pH en rango completo (0-14) de una disolución a partir de los valores de la coordenada cromática H procedentes de la imagen obtenida de una matriz sensora óptica compuesta por once elementos sensores.

Los objetivos particulares a alcanzar son:

- Selección de los indicadores ácido-base colorimétricos más adecuados para la preparación de las membranas sensoras considerando las siguientes condiciones: 1) que no sufran lixiviación; 2) que originen cambio en la coordenada H mediante reacción y 3) que cubran el rango completo de pH mediante solapamiento entre las respuestas.

- Utilización de un escáner que opere en modo transmisión para recoger la información de color de la matriz sensora tras reacción con el problema.

- Establecimiento del valor de la coordenada H del espacio de color HSV correspondiente a cada elemento sensor a partir de sus valores RGB medidos, y obtención del conjunto de datos de calibración del sistema.

- Determinación por el método de ensayo y error de la mejor ANN entrenada a partir de los datos de calibración del sistema.

- Validación del sistema de predicción de pH y medida en muestras de agua.

PUBLICACIÓN II:

Microchemical Journal, 97 (2011) 225-233
DOI: 10.1016/j.microc.2010.09.008

Full-range optical pH sensor array based on neural networks

S. Capel-Cuevas[a], M.P. Cuéllar[b], I. de Orbe-Payá[a], M.C. Pegalajar[b], L.F. Capitán-Vallvey[a,*]

[a]Department of Analytical Chemistry.
[b]Department of Computer Science and Artificial Intelligence.
University of Granada, E-18071 Granada, Spain

Abstract

A neural network multivariate calibration is used to predict the pH of a solution in the full-range (0-14) from hue (H) values coming from imaging an optical pH sensor array based on 11 sensing elements with immobilized pH indicators. Different colorimetric acid-base indicators were tested for membrane preparation fulfilling the following conditions: 1) no leaching; 2) change in tonal coordinate by reaction and 3) covering the full pH range with overlapping between their pH responses. The sensor array was imaged after equilibration with a solution using a scanner working in transmission mode. Using software developed by us, the H coordinate of the colour space HSV was calculated from the RGB coordinates of each element.

The neural network was trained with the calibration data set using the Levenberg-Marquardt training method. The network structure has 11 input neurons (each one matching the hue of a single element in the sensor array), 1 output (the pH approximation value) and 1 hidden layer with 10 hidden neurons. The network provides an MSE=0.0098 in the training data, MSE=0.0183 in the validation data and MSE=0.0426 in the test data coming from a set of real water samples. The resulting correlation coefficient R obtained in the Pearson correlation test is R=0.999.

Keywords: Full-range optical pH sensor array; Neural network; H coordinate; HSV colour space.

* Corresponding author; e-mail: lcapitan@ugr.es

1. Introduction

Optical pH sensors are principally based on reversible changes in the structure of an acid-base indicator induced by pH and translated into changes in spectroscopic phenomena such as absorption, reflectance, luminescence, and energy transfer.

The immobilization of the indicator molecule is a key issue in determining the analytical and operational characteristics of pH sensors in any of the usual dispositions, such as probe (optic fibre), flow or disposable format. Different types of immobilization techniques for pH indicating dyes have been used [1], including: a) dye entrapment in different materials such as cellulose acetate [2], sol-gel [3], PVC [4], methacrylic-acrylic copolymers [5] and different composites like SiO_2/ZrO_2-organic polymer [6]; b) retention of dye by ion-exchange materials such as Amberlite XAD-2 resin [7] or Dowex I-X10 resin [8], in some instances including the ion-exchanger containing dyes in polymeric encapsulated membranes using PVC [9]; c) adsorption of the dye on materials such as non-ionic styrene/divinylbenzene copolymer [10], polyester/lycra blends textile [11], cellulose [12], cellulose acetate [13], or polymer track membranes combining retention in surface and bulk [14]; d) covalent binding of dye by different synthetic strategies to form microparticles or membranes, in some cases formed on glass fibre, using different polymers such as polyacrylamide [15,16], triacetylcellulose [17,18], cellulose acetate [19,20], agarose [21] or polyamide [22], among others; e) polymerization of monomers to prepare both membrane and dye, as with aniline [23] or pyrrole [24].

Unlike potentiometric pH determination, in which the pH depends linearly on the activity of hydrogen ions, pH in optical sensors is a function of the concentration of the acid and basic forms of the indicator [25]. The change in the measured signal with pH results in a narrow sigmoidal shape dependence

according to the Henderson-Hasselbalch equation. The main drawbacks of optical pH sensors are accordingly, short dynamic working range (2-3 pH units) and non-linear response, which require different sensing membranes to cover the whole pH range.

Different strategies have been devised to stretch the working range of optical pH sensors. The working range of membranes containing only one indicator can be broadened using polyprotic acids as indicators; for instance, when using neutral red the working pH ranges from 2.0 to 8.5 [26]. Additionally, in some instances the adsorption [27] or chemical immobilization [18] of indicators leads to broader ranges than in solution. In other cases, the whole reflectance spectra of the immobilised indicator along with multivariate techniques were used to model the pH in a broad range [28]. An interesting approach includes the dynamic optical response of a flow sensor as the analytical signal, increasing the range up to 10 pH units with only one indicator [29].

Some conductive polymers change their visible and near-IR absorption properties as a function of pH, as is the case with polyaniline [23,30,31], substituted polyanilines [32], polypyrrole [24] or copolymers such as poly(*o*-methoxyaniline) doped with *p*-toluene sulfonic acid [33] and the copolymer of 3-aminophenylboronic acid with aniline [34].

Another approach to broaden the dynamic range is to prepare a single membrane, typically in optical fibre format, by co-immobilizing multiple pH indicators. The immobilization of two spectroscopically compatible indicators with complementary pH responses is used for selected pH zones far away each other, for instance for very low and high pH values [35]; or for ample pH ranges by means of one or several linear stretches [21] or multivariate calibration (ANN) [36]. In other cases, the number of immobilized indicators is higher, typically 3, to acquire more information and offer a simple linear calibration over a broad pH range (8-12 pH units) [37-39], although the immobilization of a universal indicator mixture containing 5 indicators for the same purpose has been reported [40].

A final strategy consists of using arrays of sensing membranes containing complementary pH indicators acquiring the analytical information by imaging techniques. In this way, commercial multi-colour pH paper strips have been measured with a conventional scanner [12]; alternatively, arrays of five pH

membranes in a triacetylcellulose support measured with a CCD colour camera have been described [41]. In both cases, the average RGB values of each sensing area image are used for calibration with multi-linear mathematical models.

As shown in the above review of optical pH sensors based on absorption, reflection or colour measurement, most of the sensors work using probe or flow formats and are very rarely found in disposable format. In this paper, a disposable optical sensor array is used to predict the pH of a solution in the full-range (0-14) from the hue (H) values of the HSV colour space using a scanner to image the optical array containing 11 sensing elements with immobilized pH indicators and using a neural network multivariate calibration.

2. Material and methods

2.1. Reagents

The chemicals used to prepare the pH sensitive films were potassium tetrakis (4-chlorophenyl)borate (TCPB, CAS No. 14680-77-4), tridodecylmethylammonium chloride (TDMAC, CAS No. 7173-54-8), aliquat 336 (CAS No. 5137-55-3), o-nitrophenyloctylether (NPOE, CAS No. 37682-29-4), dioctyl sebacate (DOS, CAS No. 122-62-3), bis(1-butylpentyl)adipate (BBPA, CAS No. 77916-77-9), tributyl phosphate (TBP, CAS No. 126-73-8), high molecular weight polyvinyl chloride (PVC, CAS No. 9002-86-2), cellulose acetate (CA, CAS No. 9004-35-7), ethylenglycol (EG, CAS No. 107-21-1) and tetrahydrofuran (THF, CAS No. 109-99-9) all purchased from Sigma (Sigma-Aldrich Química S.A., Madrid, Spain). 1-amino-4-hydroxyanthraquinone (CAS No. 116-85-8), congo red (CAS No. 573-58-0), crystal violet (CAS No. 548-62-9), indigotin blue (CAS No. 482-89-3), methyl red (CAS No. 493-52-7), bromothymol blue (CAS No. 76-59-5), bromcresol purple (CAS No. 115-40-2), xylenol orange (CAS No. 1611-35-4), phenol red (CAS No. 143-74-8), thymol blue (CAS No. 76-61-9), m-cresol purple (CAS No. 2303-01-7), neutral red (CAS No. 553-24-2) and PAN (CAS No. 85-85-8) from Sigma, liphophilized Nile blue (CAS No. 125829-24-5), nile red (CAS No. 7385-67-3), purpurin (CAS No. 81-54-9) and PAR (CAS No. 1141-59-9) from Fluka (Fluka, Madrid, Spain), cresol red (CAS No. 1733-12-6) from Panreac (Panreac,

Barcelona, Spain), alizarine (CAS No. 72-48-0) from TCI (TCI Europe, Belgium), sicomet red P (CAS No. 5281-04-9) from BASF (BASF, Ludwigshafen, Germany), 1,4-dihydroxyanthraquinone (CAS No. 81-64-1) and 1,5-dihydroxyanthraquinone (CAS No. 117-12-4) from ICN (ICN K&K Laboratories, Plainview, NY, USA), 2,6-dihydroxyanthraquinone (CAS No. 84-60-6) from EGA (EGA Chemie, Steinheim, Germany) were used as acid-base indicators. As support sheets Mylar-type polyester (Goodfellow, Cambridge, UK) were used. HCl and NaOH were supplied by Sigma. All reagents were of analytical reagent grade and were used without any further purification. All aqueous solutions were prepared in reverse-osmosis type quality water (Milli-RO 12 plus Milli-Q station from Millipore, conductivity 18.2 mS).

2.2. Instruments and Software

To acquire the images of the prepared sensor array, a Microtek ScanMaker i700 scanner (Microtek, CA, USA) was used. Absorbance measurements of the membranes for comparative purposes were performed by a Hewlett Packard diode array spectrophotometer (model 8453; Nortwalk, CT, USA) equipped with a homemade membrane cell holder.

The software used to manage the scanner was Silver Fast Ai provided by Microteck. The images were processed with a set of scripts and functions developed by us in Matlab r2007b (The MathWorks, Inc, Natick, MA, USA). The acquisition and manipulation of the spectral data were carried out using the Chemstation software package supplied by HP for absorbance measurements. Statistical calculations were performed with a Statgraphics software package (Manugistics Inc. and Statistical Graphics Corporation, USA, 1992), and Microsoft Excel (Microsoft Corp., Redmond, WA, USA) was used for general calculations.

A laboratory-made spin-on device was used to prepare individual membranes for their spectrophotometric characterization. A Crison pH-meter (Crison Instruments, Barcelona, Spain, model Basic 20) with a combined double junction glass electrode, calibrated against two standard buffer solutions (pH 4.0 and 7.0), was used for pH measurements.

2.3. Preparation of sensing membranes

The disposable sensor array was prepared on a 50 mm x 40 mm Mylar support covered by an adhesive and transparent PVC layer with 12 holes 5 mm diameter each (1.2 µL volume) arranged in 3 columns and 4 rows (figure 4.1). The membranes were cast by carefully placing in each hole 8 µL of the corresponding cocktail, whose surface tension and quick evaporation makes it possible to prepare the sensing membrane. The different cocktails for pH sensing were prepared by dissolution in 1 mL of freshly distilled THF in all cases for the different chemicals needed with the composition indicated in table 4.1.

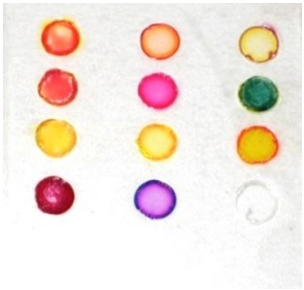

Figure 4.1. pH sensor array

Table 4.1. Composition of the membranes (% w/w) used for the pH sensor array preparation

Membrane	Indicator (%)	Lipophilic salt (%)	Plasticizer (%)	Membrane polymer (%)	Humectant (%)
1	m-Cresol purple (3.00)	TDMAC (13.47)	DOS (28.00)	CA (33.00)	EG (22.57)
2	Purpurin (1.43)	TDMAC (8.29)	NPOE (67.00)	PVC (23.29)	–
3	Alizarin (1.43)	TDMAC (10.29)	NPOE (67.00)	PVC (21.3)	–
4	Thymol blue (3.14)	TDMAC (11.57)	DOS (28.00)	CA (37.00)	EG (20.43)
5	Sicomet red P (1.41)	Aliquat 336 (5.63)	NPOE (66.20)	PVC (26.76)	–
6	Bromothymol blue (3.00)	TDMAC (4.00)	DOS (28.00)	CA (37.00)	EG (19.60)
7	Phenol red (1.43)	TDMAC (6.93)	BBPA (26.00)	CA (30.00)	EG (35.64)
8	Cresol red (1.43)	Aliquat 336 (4.54)	NPOE (67.00)	PVC (27.00)	–
9	PAN (1.43)	TDMAC (10.00)	NPOE (65.00)	PVC (23.60)	–
10	Thymol blue (5.00)	TDMAC (18.40)	DOS (28.00)	CA (33.00)	EG (15.60)
11	Liphophilized Nile blue (1.43)	TCPB (3.63)	TBP (67.00)	PVC (27.91)	–

Additionally, individual membranes (12 mm in diameter and around 5 µm thick each) were prepared on a Mylar polyester substrate (14 mm x 40 mm x 0.5 mm) for their spectrophotometric characterization by spin-coating using 20 µL of the above cocktails.

2.4. Response evaluation

The evolution of the sensor array was assessed by adding volumes of solutions of different HCl or NaOH concentrations (1.0 M, 0.1 M or 0.01 M), with the help of a microburette, to an aqueous solution with the sensor array dipped by hanging it from a support. After each addition and magnetic stirring up for 5 min, the pH of the solution was measured potentiometrically. Then, the sensor array was pulled out and inserted into a holder to obtain the image of the sensor array with a transmission flatbed scanner. The resolution and colour depth were set to 300 dpi for higher resolution without membrane degradation and 48-to-24 bits of colour, respectively.

To evaluate and compare the response of the membranes, the same experimental setup indicated above was used, measuring individual pH membranes with a DAD spectrophotometer.

2.5. Sensor array signal processing and hue acquisition

The first step in the pH prediction procedure was the acquisition of the hue H from the sensing elements of the sensor array. To obtain the H values, after equilibrating the sensor array with the acidic or basic solution that modified the sensing element colours, the whole sensor array was scanned storing the image in the PC in 24 bit TIFF format using the standard RGB colour space. The scanner was calibrated each day before use by means of an IT8 calibration target to measure the performance of the input devices and generate ICC (International Colour Consortium) profiles. We developed software in Matlab that uses the Image Processing Toolbox to extract the hue parameter H from each sensing element in the image scanned [42], according to the diagram in figure 4.2.

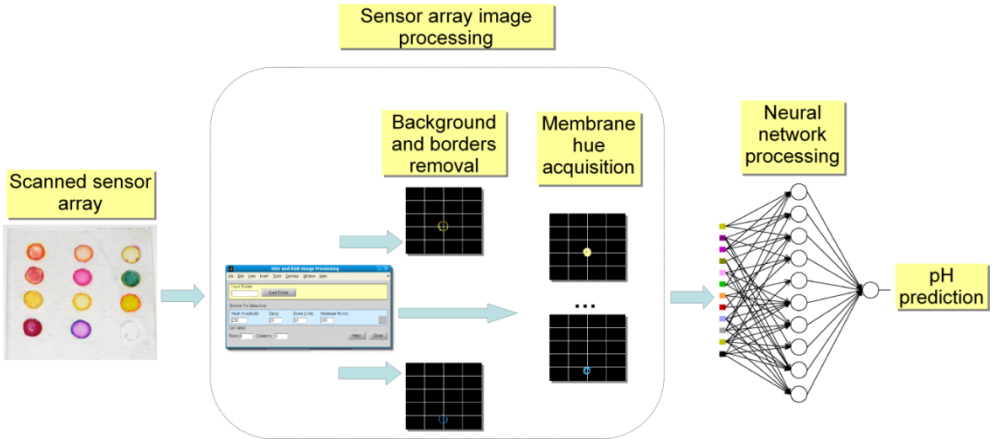

Figure 4.2. Procedure for hue acquisition from the sensing elements in the array

First, each sensing element was located in the image by checking the colour differences of the pixels with the background and using Canny's algorithm [43] for border detection. The pixels with the greatest differences were interpreted as coloured and the pixels with the smallest differences were interpreted as grey background, coming from the Mylar substrate and scanner lid. After that, the borders of the scanned sensing elements were discarded to prevent noise in the hue computation. The hue of the HSV colour space was calculated for the remaining pixels from each membrane using the colour space transformation equations [44], and finally the hue H returned by the software for each membrane was the mode of the hues calculated for all the pixels in the same membrane. This procedure provided the data sets needed for the experimental calibration and validation as described in the following sections.

Because of the circular nature of H, which is defined as an angle that varies between 0 and 360° and is typically represented as a colour wheel where 0° is located at the top of the wheel, the values were bounded between 0 and 1, with both 0 and 1 representing the same hue. However, in this work we allowed H to be from -360º to 360º (the normalized values are therefore between -1 and 1) to avoid discontinuities in the H evolution with the pH if it passed through the origin.

2.6. Neural networks

Neural networks [45] are bioinspired optimization models that have been widely used in classification, pattern recognition, function approximations and prediction problems, among others. The most popular neural network model is Multilayer Perceptron. It is composed of simple computing units called neurons which are interconnected and organized in layers, so that the output value of a neuron is used as the input for all the neurons at the next layer. The usual operation of a neuron is a sigmoid function applied over the weighted sum of its inputs in the intermediate layers, and a linear function in the last layer. The inputs to the neurons at the first layer must be the independent variables of the problem to be solved, while the output of the neurons at the last layer are the network response and an approximation of the dependent variables of the problem. This procedure is described in depth in equations 4.1 and 4.2, where $f_i^l(x_i^l)$ is the output value of the *i*-th neuron at layer *l*, w_{ij}^l is the weight for the connection from the the *j*-th neuron at layer *l-1* to the *i*-th neuron at layer *l*, N^l is the number of neurons at layer *l*, I_j^P is the value of the *j*-th independent variable in sample *P*, *L* is the number of layers in the network, and b_i^l is a bias value matched with the *i*-th neuron at layer *l*.

$$f_i^l(x_i^l) = \begin{cases} \dfrac{1}{1+e^{-x_i^l}};\ x_i^l;\ \ 1 \le l < L \\ x_i^l;\ \ l = L \end{cases} \tag{4.1}$$

$$x_i^l = \begin{cases} \displaystyle\sum_{j=1}^{N^{l-1}} (w_{ij}^l I_j^P) + b_i^l;\ \ l = 1 \\ \displaystyle\sum_{j=1}^{N^{l-1}} (w_{ij}^l f_j^{l-1}(x_j^{l-1})) + b_i^l;\ \ 1 < l \le L \end{cases} \tag{4.2}$$

The training of a neural network consists of the optimization of the weights of the neurons' inputs w_{ij}^l and the biases b_i^l so that the network is able to provide a suitable approximation of the dependent variables of the problem, according to an error measure. The most widely used error criterion is the minimization of the Mean Square Error (MSE) between the network outputs and their desired values, as described in equation 4.3 for a set of *M* samples, and the best known training algorithm is backpropagation. However, Quasi-Newton

optimization techniques such as BFGS and Levenberg-Marquardt [46] have been used to train neural networks over the last decade with promising results. In this work, we use the Levenberg-Marquardt non-linear training method due to its high performance for the problem being addressed.

$$MSE = \frac{1}{M} \sum_{P=1}^{M} \sum_{i=1}^{N} (D_i^P f_i^L(x_i^L))^2 \quad (4.3)$$

3. Results and Discussion

The RGB space is an additive representation of colour in which all the colours can be represented as a combination of red, green and blue primaries. The colour space used here, HSV, is an alternate representation of colour derived from the red, green, and blue intensity values of the RGB space. A pixel in this colour space is defined by its Hue (H), Saturation (S), and Value (V) coordinates. In broad terms, H is a numerical representation of the colour, S gives the degree to which a single channel dominates, and V represents the brightness. We have demonstrated previously that the H value is stable, simple to calculate, and easily obtained from commercial devices, maintaining a superior precision with variations in indicator concentration, membrane thickness, detector spectral responsivity, and illumination [47]. In contrast to other approaches that make use of the RGB colour space to achieve the pH prediction [29], our proposal to use the H parameter provides the additional advantage of the degression of the parameter space from three dependent variables to only one.

The calibration data were obtained separately for each sensing element from the array, covering the pH range from 0 to 14 to find out their active hue and the pH ranges that are useful for prediction. The information obtained from some sensing elements of the set provides more than one active range and also may overlap to other sensing elements' information. This overlapping is useful to manage noisy data during the hue value acquisition. In the following sections, we describe the membrane selection and characterization procedures, the calibration model and the results obtained.

3.1. pH-sensitive membrane selection

A set of pH sensing membranes was prepared containing colorimetric acid-base indicators selected according to the conditions of no leaching in the whole pH range studied, changing in the tonal colour coordinate by reaction and covering the full pH range by overlapping between responses of different membranes.

A set of 24 different acid-base indicators were studied, namely alizarin, 1-amino-4-hydroxyanthraquinone, bromcresol purple, bromothymol blue, congo red, m-cresol purple, cresol red, crystal violet, 1,4-dihydroxyanthraquinone, 1,5-dihydroxyanthraquinone, 2,6-dihydroxyanthraquinone, indigotin blue, liphophilized nile blue, methyl red, neutral red, nile red, PAN, PAR, phenol red, purpurin, sicomet red P, sudan I, thymol blue and xylenol orange, with which we prepared different cocktails containing different types and amounts of membrane polymers, plasticizers, humectants, if necessary, lipophilic salts in addition to the acid-base indicator.

The selection criteria for pH membranes used were both high variation in H coordinate by reaction and non-redundant information from different sensing elements, so that the entire pH range was covered. Sometimes, to modify the pH response of a membrane, we used the same acid-base indicator but changed the plasticizer, membrane polymer, lipophilic salt and/or lipophilic salt/indicator ratio.

The composition of the different membranes was optimized considering leaching minimization (lipophilic salt, plasticizer, and membrane polymer), colour intensity (acid-base indicator) and response time (plasticizer, membrane polymer, humectant and cocktail volume). Optimum compositions are indicated in the Experimental section, although the usual lipophilic salt/indicator ratio was 3:1 except for bromothymol blue (1.5:1) and sicomet red P (4:1).

As a result, 11 different membranes were selected as candidates for the pH sensor array containing 10 different pH indicators, because two membranes were prepared containing the same components including thymol blue, but with a different lipophilic salt/indicator ratio (table 4.1).

3.2. pH membrane characterization

In order to characterize the different pH membranes selected, the different response mechanisms involved were studied. The acid-base indicators selected belong to neutral, cationic and anionic types and the heterogeneous reaction with acids or bases in membranes phase involve both ion-exchange and co-extraction mechanisms.

All these equilibria are characterized by a constant K_e that includes acidity constant, the distribution constant between aqueous and membrane phases of different species, and dissociation constants for the different ion-pairs involved.

In the case of cationic acids (liphophilized Nile blue), ion-exchange equilibrium occurs between protons and, typically, alkaline ions as shown in equation 4.4 where the bars indicate species in the membrane phase.

$$X^+ + \overline{HI^+} + R \xleftrightarrow{K_e} \overline{I^-} + H^+ + \overline{XR} \qquad (4.4)$$

A second mechanism is based on co-extraction and occurs with membranes containing neutral acid-base indicators (alizarine, PAN, phenol red, bromothymol blue, cresol red) (equation 4.5).

$$\overline{HI} + \overline{XR} \xleftrightarrow{K_e} \overline{IR} + X^- + H^+ \qquad (4.5)$$

For anionic indicators two cases can be considered, monobasic and dibasic. In the first (m-cresol purple, thymol blue), the following co-extraction equilibrium holds (equation 4.6):

$$\overline{HIR} + \overline{XR} \xleftrightarrow{K_e} \overline{IR_2^-} + X^- + H^+ \qquad (4.6)$$

In the case of dibasic acid (sicomet red P, purpurin) the equilibrium (equation 4.7) is:

$$\overline{HIR_2^-} + \overline{XR} \xleftrightarrow{K_e} \overline{IR_3^{2-}} + X^- + H^+ \qquad (4.7)$$

Some of the neutral indicators studied are formally polyprotic acids (alizarine, PAN), but behave like monoprotics in the pH range studied when immobilized in the membrane. Additionally, other indicators are diprotic (m-cresol purple and thymol blue) and even triprotic (purpurin), but since the analytical parameter used, the H coordinate, only offers information on the position of the equilibrium between majoritary species present and the sigmoid curves are sufficiently separated, the corresponding K_e values were calculated as independent equilibria. Table 4.2 presents the calculated K_e values for the indicators studied.

Table 4.2. Evolution of colour and H coordinate of sensing elements with pH

Sensor	Indicator	Type	pH Range	K_e	Membrane colours (H coordinate)	
					Acid	Base
1	m-Cresol purple	H_2I	0.0-1.5	$4.9 \cdot 10^{0}$	amaranth (0.964)	canary yellow (0.151)
1	m-Cresol purple	HI^-	8.5-10.5	$2.8 \cdot 10^{-9}$	mustard (0.129)	blue (0.679)
2	Purpurin	H_3I	2.0-5.0	$2.0 \cdot 10^{-3}$	amber (0.132)	magenta (0.848)
2	Purpurin	H_2I^-	5.5-7.5	$9.4 \cdot 10^{-7}$	magenta (0.841)	medium red-violet (0.893)
2	Purpurin	HI^{2-}	8.0-11.5	$7.3 \cdot 10^{-10}$	purple (0.806)	deep pink (0.909)
3	Alizarin	HI	4.0-7.0	$1.4 \cdot 10^{-5}$	maize (0.149)	blue (0.649)
4	Thymol blue	H_2I	0.6-2.0	$3.7 \cdot 10^{0}$	magenta (0.796)	canary yellow (0.147)
4	Thymol blue	HI^-	7.5-9.5	$1.3 \cdot 10^{-8}$	yellow (0.168)	celestial blue (0.576)
5	Sicomet red P	HI^{2-}	4.5-6.5	$7.1 \cdot 10^{-5}$	persian rose (0.879)	amber (0.122)
6	Bromothymol blue	HI	5.0-8.0	$7.1 \cdot 10^{-6}$	pear (0.186)	pine green (0.497)
7	Phenol red	HI	7.0-9.3	$1.2 \cdot 10^{-8}$	old gold (0.135)	violet (0.779)
8	Cresol red	HI	8.6-10.6	$4.3 \cdot 10^{-9}$	yellow (0.134)	violet (0.644)
9	PAN	HI	7.5-10.0	$3.4 \cdot 10^{-9}$	lemon (0.145)	red (0.062)
10	Thymol blue	H_2I	0.0-1.6	$1.5 \cdot 10^{0}$	fuchsia (0.913)	golden yellow (0.132)
10	Thymol blue	HI^-	9.5-11.2	$3.7 \cdot 10^{-9}$	yellow (0.165)	blue (0.663)
11	Liphophilized nile blue	HI^+	10.5-12.0	$1.3 \cdot 10^{-10}$	celestial blue (0.572)	magenta (0.796)

* Although alizarin is a diprotic acid, only one change is observed in the full pH range.

The proton/alkaline ion activities ratio in the aqueous phase is related to the equilibrium constant K_e through a sigmoidal response function that includes the degree of protonation α, and the analytical concentrations of indicator C_I and lipophilic salt C_R, respectively, as seen in equation 4.8 for cationic indicators, equation 4.9 for neutral indicators and equations 4.10 and 4.11 for anionic monobasic and dibasic indicators, respectively.

$$K_e = \frac{\alpha \cdot (C_R - (1-\alpha) \cdot C_I) \cdot a_{H^+}}{(1-\alpha) \cdot a_{X^+}} \quad (4.8)$$

$$K_e = \frac{\alpha \cdot C_I \cdot a_{X^-} \cdot a_{H^+}}{(1-\alpha) \cdot C_I \cdot (C_R - \alpha \cdot C_I)} \quad (4.9)$$

$$K_e = \frac{\alpha \cdot C_I \cdot a_{X^-} \cdot a_{H^+}}{(1-\alpha) \cdot C_I \cdot (C_R - (1-\alpha) \cdot C_I - 2 \cdot \alpha \cdot C_I)} \quad (4.10)$$

$$K_e = \frac{\alpha \cdot C_I \cdot a_{X^-} \cdot a_{H^+}}{(1-\alpha) \cdot C_I \cdot (C_R - 2(1-\alpha) \cdot C_I - 3 \cdot \alpha \cdot C_I)} \quad (4.11)$$

The experimental parameter $1 - \alpha$, degree of protonation, is defined as:

$$1 - \alpha = \frac{X - X_I}{X_{HI} - X_I} \quad (4.12)$$

with X being the analytical signal measured, which can be absorbance [48], fluorescence [49], reflectance [50], transflectance [51], refractive index [52], and even one RGB channel [53], for a given quantity of analyte X; and X_{HI} and X_I the values of the parameter at the fully protonated and deprotonated indicator, respectively.

The correctness of the models indicated above was checked through a spectrophotometric study of individual membranes. Figure 4.3 shows the sigmoid curves $1 - \alpha$ vs. pH obtained from the absorbance and H coordinate displaying the ability of tonal coordinate H to estimate the degree of protonation $1 - \alpha$ through the H, H_{HI} and H_I values.

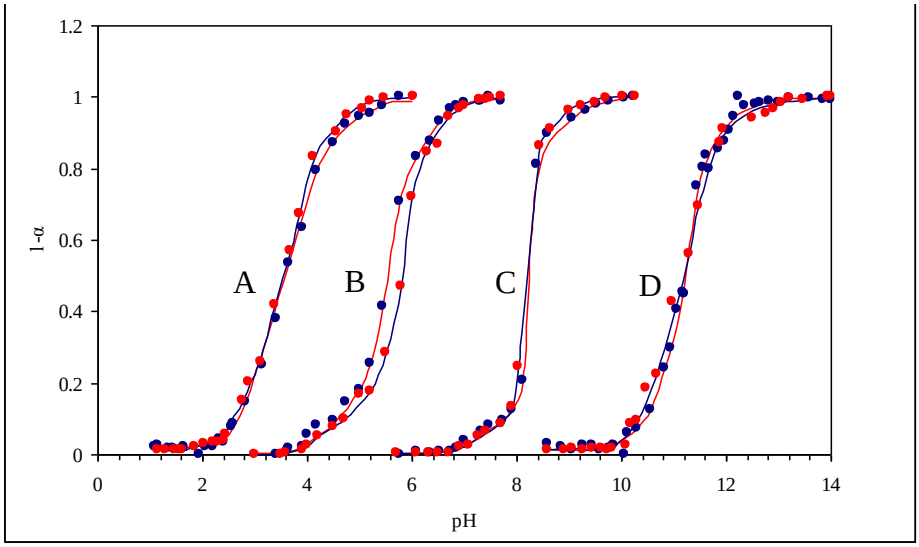

Figure 4.3. Sigmoid curves 1- α vs. pH obtained for selected membranes working by different sensing mechanisms. From absorbance (Ab): experimental data (red dots) and theoretical model (blue sigmoid curve); from H: experimental data (blue dots) and theoretical model (red sigmoid curve). A: purpurin, K_e (Ab) = $2.11 \cdot 10^{-3}$, r^2 = 0.9995; K_e (H) = $1.96 \cdot 10^{-3}$, r^2 = 0.9996; B: alizarin, K_e (Ab) = $2.21 \cdot 10^{-5}$, r^2 = 0.9999; K_e (H) = $2.25 \cdot 10^{-5}$, r^2 = 0.9999; C: phenol red, K_e (Ab) = $2.12 \cdot 10^{-7}$, r^2 = 0.9991; K_e (H) = $1.86 \cdot 10^{-7}$, r^2 = 0.9992; D: liphophilized nile blue, K_e (Ab) = $1.44 \cdot 10^{-10}$, r^2 = 0.9999; K_e (H) = $1.30 \cdot 10^{-10}$, r^2 = 0.9999

3.3. Experimental pH sensor array calibration

The 11 selected pH membranes were prepared on a support containing 12 microwells (4 rows x 3 columns) with 1.2 µL capacity each by casting a volume of each cocktail into the corresponding microwell. The analytical parameter used for the pH sensor array was the H coordinate. The use of H alone avoids the use of calibrants for the protonated and deprotonated forms of the indicator in each membrane.

The experiments for calibration purposes between pH from 0 to 14 were performed using 12 replicate sensor arrays each containing the 11 pH membranes indicated above. The H variation was obtained for each 0.1-0.2 pH unit by adding HCl or NaOH solution to an aqueous solution with the sensor array inside and imaging with the scanner after equilibration (figure 4.4).

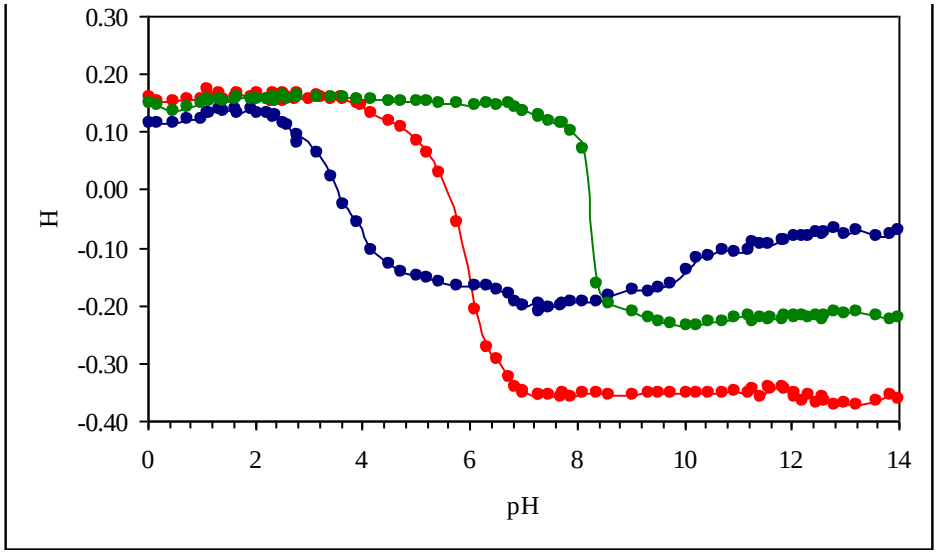

Figure 4.4. Calibration data measured for three membranes in a pH range from 0 to 14. Colour code used (membranes 2, 3 and 7, see table 1): blue, red and green, respectively

3.4. Neural network optimization

For the optimization of the neural network, we used a calibration data set containing 961 pairs of (H, pH) values measured in the laboratory for each of the 11 sensing elements, forming the sensor array in the pH range from 0 to 14. From this data set, a training data was built synthetically containing 1400 input/output patterns to train the neural network. Each pattern was a vector of 12 components containing 11 hue values obtained from the sensing elements and their corresponding pH value.

In order to test the performance of the approach, we used an additional independent data set for validation. The validation data contain 70 input/output patterns, each containing 11 hue values obtained from the sensing elements in the same sensor array equilibrated with solutions equally spaced covering the whole pH range from 0 to 14 and their corresponding pH value. After reaction, the sensor arrays were scanned and the hues of all the sensing elements were saved in order to build the validation data set. We also measured the pH of each solution using a standard potentiometric procedure to compare the results.

The optimal network topology was found by using the traditional *trial-and-*

error procedure with a network with between 3 and 15 hidden neurons and 1 or 2 hidden layers. The training was carried out by mean of a cross validation method with 70% of the calibration data for training and the remaining 30% for testing. We applied the cross validation 10 times to generate the training and test data, and 5 networks were trained for each training set generated.

The network was trained with the Levenberg–Marquardt optimization algorithm from the Neural Networks Toolbox in MatLab, running a maximum number of 1000 iterations as the primary stopping criterion, and reaching an MSE of 0.01 in the calibration data as the secondary stopping criterion. The structure of the optimized neural network used is a Multilayer Perceptron with three layers: the first contains 11 neurons matched with the sensing elements in the sensor array; the second layer has 10 neurons for the internal network processing, and the third has one neuron with a linear activation kernel to provide the predicted pH. Tables 4.3 and 4.4 describe the optimal weights and bias network values for our pH sensor.

Table 4.3. Weights and biases of the best network trained: Network weights from the inputs to the hidden layer are w_{NIj} while the weights between the hidden and the output layers are w_{O1NI}

Weights	N_1	N_2	N_3	N_4	N_5	N_6	N_7	N_8	N_9	N_{10}
I_1	-3.398	-0.9756	0.0552	-0.4804	0.8315	-1.2048	1.0812	6.2997	0.7482	-4.2301
I_2	0.5246	0.6446	4.0171	2.0260	-1.1082	-3.5618	0.1419	-4.8663	0.1131	3.3143
I_3	2.9543	1.2206	2.4926	0.9963	2.4047	-5.6451	-0.6704	-0.4021	0.5233	0.1339
I_4	-4.9603	1.0395	-3.2505	0.5742	1.3140	-1.4154	2.4775	-5.1401	1.2442	5.1215
I_5	-1.5060	1.0264	-4.2148	-0.9344	2.3646	6.3565	0.1095	-0.8114	0.4843	2.9208
I_6	-1.6458	-6.8661	-1.3545	-0.4530	-0.6665	1.3932	1.5763	-0.3582	0.1014	-8.7329
I_7	-1.1328	3.6097	1.1339	-0.8154	0.1257	-1.9989	-0.0629	2.1623	0.2897	4.4253
I_8	-4.4073	0.4776	1.1261	0.2366	0.7011	-2.4608	0.4257	1.9087	0.2541	0.3941
I_9	0.2693	1.3648	0.7438	0.4218	-2.2024	-3.4628	1.2980	-0.2485	0.6830	0.8079
I_{10}	-2.5854	0.6432	-0.7718	-0.4407	1.2491	-2.3395	0.8224	1.0421	0.3535	1.1851
I_{11}	3.4616	0.0561	-4.2769	-0.5023	6.6032	1.3076	2.6543	1.1432	1.1683	2.0873
O_1	-2.7523	-8.8232	-1.6169	-0.6801	2.1149	2.4803	-0.3126	4.6827	-0.4163	6.6849

Network inputs I_1-I_{11} , Hidden neurons N_1-N_{10}, output neuron O_1

Table 4.4. Bias value of the neurons at the hidden and output layers

N_1	N_2	N_3	N_4	N_5	N_6	N_7	N_8	N_9	N_{10}	O_1
-0,0752	3,3988	-3,1482	-1,7024	2,2654	-7,3640	3,4816	-0,2081	2,0970	2,8203	-0,1938

Hidden neurons N_1-N_{10}, output neuron O_1

3.5. Results for pH prediction

After the training process of the neural network, it provides an MSE of 0.0098 in the calibration data set and an MSE of 0.0183 in the validation data set. Since the values are low if we consider that the comparison range is from 0 to 14, these results suggest that the neural network performance is suitable. However, to support this assumption, we validated the approach with a statistical analysis.

First, we applied a Kolmogorov-Smirnov test to check if the validation data set and their neural network predictions may be assumed to be normal. The confidence level of the test was the standard 80%, providing the probability values of 0.59 (validation set) and 0.46 (prediction for the validation set). Therefore, all the data distributions passed the test and we may use Student's t-test to compare whether the distributions of the predicted data differ significantly from their real values. These tests were applied with a standard confidence level of 95%, and provided the probability values of 0.95 for the validation data. Since none of the probability values are under 0.05, we may assume that there are no significant differences between the real and predicted values in the data set.

To finish the analysis, we applied a Pearson correlation test to measure the quality of the predicted versus the real values. The result of the test provided a probability value under $2.22 \cdot 10^{-16}$ in the validation data set, and we therefore may conclude that there is a significant correlation between the real and predicted values. The correlation coefficient R^2 was calculated and the test provided the value 0.999. This fact ensures that there is a high positive correlation between the real and predicted data carried out by the neural networks, so that it may be assumed that the prediction model provides a suitable performance for the task of pH prediction. This is supported by figure 4.5, which contains the regression lines between the real and predicted data validation.

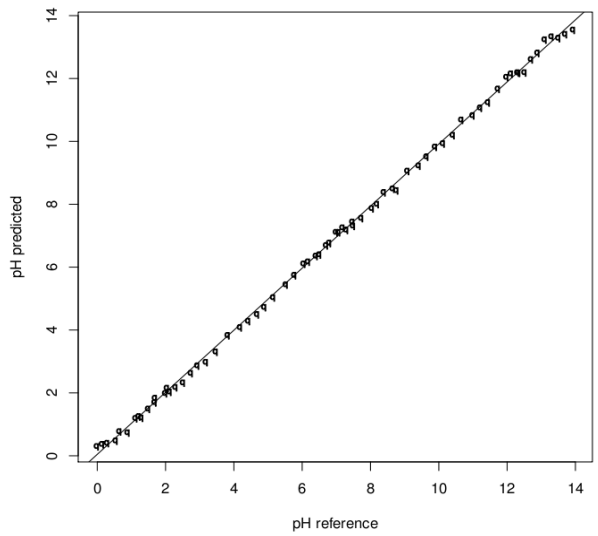

Figure 4.5. Regression line between the real and predicted values in the validation data set

3.6. Analysis of performance in acid and basic pH ranges

Our interest in this section is to check the performance of the predicted values in acid and basic pH ranges separately. First, the absolute error between the predicted and real values of each sample was calculated. After that, these errors were separated into two sets according to their acid or basic pH level. A Student's t-test with a 95% confidence level was applied over these prediction error distributions in acid and basic pH ranges, and returned the probability value of 0.08. Therefore, we may conclude that there are no significant differences in the neural network performance for the prediction of pH depending on the pH range of the sample.

3.7. Application to real samples

The feasibility of the described pH sensor array was checked by analyzing a set of natural water samples. The test data set contained 13 patterns with the same structure as the previous ones obtained from the analysis of a real water sample (tap water from Granada town) with the pH adjusted with the acid and base covering the full pH range from 0 to 14. After reaction, the sensor arrays

were scanned and the hues of all the sensing elements were saved in order to build the test data set. We also measured the pH of each solution using a standard potentiometric procedure to compare the results.

Table 4.5 shows the results obtained using the single use sensor array described here compared to the results found by glass electrode potentiometry used as a reference. This table also includes the mean values from 12 determinations of each sample and the absolute error. According to the results in the table, the average absolute error in the prediction performance is 0.177 with a standard deviation of 0.111.

Table 4.5. Determination of pH using the proposed sensor array in natural water samples using glass electrode potentiometry as reference method

Sample	Potentiometric reference method		Sensor array method	
	pH prediction	Absolute error	pH prediction	Absolute error
1	0.196	0.004	0.221	0.021
2	1.149	0.001	0.987	0.162
3	2.662	0.168	2.503	0.327
4	4.350	0.001	4.321	0.029
5	5.747	0.097	5.372	0.278
6	6.510	0.010	6.315	0.185
7	7.400	0.000	7.294	0.100
8	8.630	0.030	8.497	0.102
9	9.554	0.004	9.265	0.285
10	10.451	0.001	10.508	0.058
11	11.239	0.011	11.101	0.148
12	12.489	0.001	12.805	0.315
13	13.593	0.007	13.315	0.285

We also applied a Pearson correlation test to study the differences between the predictions obtained with the standard potentiometric procedure and the neural network approach. The resulting correlation coefficient R^2 was 0.999, thus ensuring a high statistical correlation between the results obtained with the potentiometric and optical sensor array procedures. To support these results, figure 4.6 shows the regression line between the predicted values using both the reference and proposed procedures.

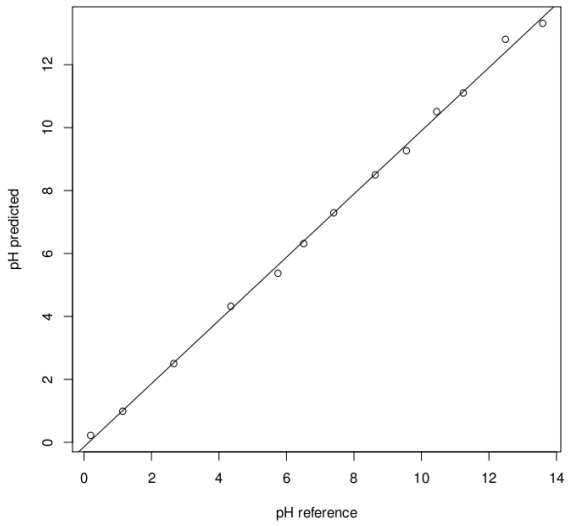

Figure 4.6. Regression line between the measured pH with the potentiometric method and the predicted pH with proposed method

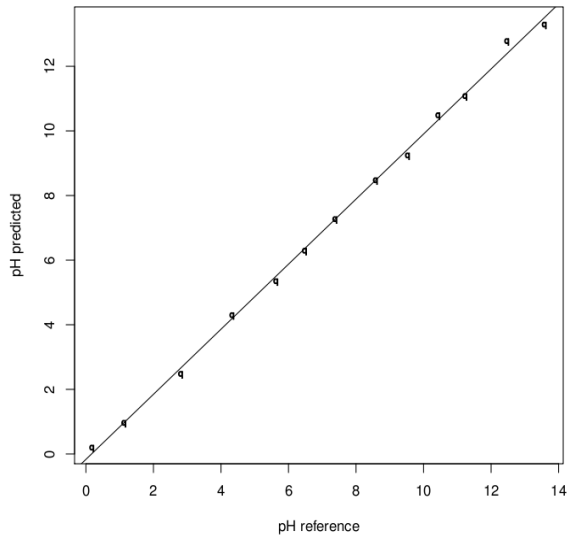

Figure 4.7. Regression line between the real and predicted values in the real water samples

The MSE in the test data set was 0.0426, which shows a good performance of the single-use optical procedure. As in the case of the validation data set, different tests were applied to check results. The Kolmogorov-Smirnov test, with a confidence level of 80%, provided the probability values of 0.99 for the test set and 0.99 for prediction in the test set. The Student's t-test (at 95%) gave a

probability value of 0.94, assuming there are no significant differences between the real and predicted values in the test data set. The Pearson correlation test provided a probability value under $2.22 \cdot 10^{-16}$, showing there is a significant correlation between the reference and predicted values. The good correlation coefficient R^2 calculated (0.999) ensures a high positive correlation between the real and predicted data (figure 4.7).

3.8. Comparison to other optical sensing approaches for pH prediction

We compared our approach to others existing in the literature. Works regarding optical sensors for pH prediction in the full range are not very common; instead, the most of the papers focus on the development of sensing membranes for small and mid-size ranges. However, Safavi *et al.* [35] demonstrated that the absorbance spectra of two indicators inmobilized on a membrane were efficient enough for pH prediction in the range 0-14. They used a Principal Component Analysis to extract the relevant features to achieve the prediction and neural networks as the prediction model. The performance of the system was able to provide an MSE between 0.03 and 0.04 depending on the network structure. Our approach provided similar results in real water samples, but the MSE in the validation is 0.018, a slight improvement over the previous performance. Moreover, the reduction of the complexity of the optimization parameter space achieved by the use of general colour spaces such as HSV, and the hue parameter from that space, gives an added value to our approach. Another proposal covering the full pH range was developed by us [54] in which linear and non-linear surface-based approximations were proposed to achieve the pH prediction from HSV colour space parameters, obtaining a minimum MSE of 0.07 in real water samples. In contrast, the proposed approach does not only improve the average performance of the prediction model, but also the computational drawbacks about memory requirements and processor speed are overcome with the use of neural networks.

Other interesting approaches for pH prediction using optical sensors [21,12] do not cover the full pH range, but their results are included in this section due to their interest and proximity to our approach. They use the three parameters of the RGB colour space as independent variables for the prediction, and propose

neural networks and non-linear functions optimized with techniques such as the Generalized Reduced Gradient as prediction models with MSE values of 0.03 (Neural Networks) [36] and 0.029 (GRG) [12]. In this study, the authors make a pH approximation from RGB values obtained by means of a scanner from commercial pH paper strips. The MSE obtained by us is similar, although it has the added value of considering the full pH range and simplifying the parameter space due to the use of the hue colour feature.

Other relevant papers, because of their impact in this research field and their proximity to our approach, are key references for our work. Lin *et al.* [39] published a method for achieving broad-range optical pH sensors with a linear response over a range of 4.5 pH units using a mixture of four indicators in solution and over 3.5 pH units by co-entrapping three indicators in sol–gel glass; with a standard deviation of 0.03 in both cases. Safavi *et al.* [41] provide the performance of three different approaches to optimize an objective multilinear function to predict the pH from RGB data coming from a set of triacetylcellulose membranes containing five entrapped indicators. The MSE values provided are 0.03 using Neural Networks, 0.04 with Generalized Reduced Gradient (GRG) and 0.05 with Partial Least Squares (PLS) algorithms.

As a general conclusion after the comparison, all the prediction models are able to provide a low MSE from 0.02 to 0.054 for pH prediction. However, the method designs differ significantly from one approach to another. Regarding the prediction models, it has been shown that neural networks are mathematical machines that are useful for the purpose of pH prediction. Their high accuracy, low complexity, noise tolerance and ease of design make these models a powerful method in contrast to other approximation models such as linear or non-linear functions.

Those methods that use the absorbance spectra have proved to provide fine prediction accuracy, although the instrumentation required to acquire the absorbance or reflectance spectra may make the prediction process difficult, especially if the goal is to develop a portable electronic device. On the other hand, the use of general colour spaces and their parameters partially overcomes this limitation. The RGB colour space has been used in a wide variety of papers using the Red, Green and Blue components as analytical parameters. This implies a

decrease in the model complexity since there is no need to analyze the whole absorbance spectra to find the best prediction parameters, but their main drawback is that ambient light conditions may alter the parameter acquisition and therefore the resulting prediction values. These models require that the data acquisition from the sensing elements be always done under the same light conditions to ensure an accurate prediction. Finally, the use of the HSV colour space provides an additional advantage in this way: the use of the hue feature reduces the parameter space from three dimensions to one, in contrast to the RGB colour space. Furthermore, properties such as ambient light independence [47] make this parameter useful for improving the robustness of the prediction models and a good alternative for the implementation of portable devices that could be used outdoors.

4. Conclusions

In this work we have addressed the problem of pH prediction using a disposable optical sensor array. We developed a sensor array containing sensing elements that change their colour in different pH intervals to cover the full pH range. The pH is predicted using neural networks depending on the hue parameter of the HSV colour space. With respect to the existing literature, our proposal has a key advantage: the hue has been proved to be a suitable parameter for this purpose. Other approaches that make use of the RGB colour space require three parameters for the prediction, while this work shows that the single hue parameter is sufficient to achieve a suitable pH approximation. Thus, the problem space is reduced and the prediction models become simpler in computer complexity terms, and this approach is able to reduce the number of parameters in previous works that make use of the RGB colour space from three to one. In contrast to methods that use the absorbance spectra to make the prediction, our approach requires lower data pre-processing since the hue is automatically extracted from the sensing elements and does not require any specific apparatus to acquire the sensor signal.

Regarding the prediction accuracy, neural networks have shown a suitable performance obtaining an MSE of 0.042 in real water samples for the full pH range. Statistical tests helped to corroborate the results obtained in this work, and

they concluded that there are no significant differences between the real pH values and the ones predicted by the approach, which corroborates its good prediction performance.

At this time, the development of small, hand-held, battery-operated instruments that will include developed algorithms to work with captured imaging data is being researched.

Acknowledgements

We acknowledge the financial support from the *Ministerio de Educación y Ciencia, Dirección General de Enseñanza Superior* (Spain) (Projects CTQ2009-14428-C02-01 and CTQ2009-14428-C02-02); and the *Junta de Andalucia* (Proyecto de Excelencia P06-FQM-01467 and P08-FQM-3535).

References

[1] J. Lin. *Recent development and applications of optical and fiber-optic pH sensors*. TrAC-Trends Anal.Chem., 19 (2000) 541-552.

[2] T.J. Cardwell, R.W. Cattrall, L.W. Deady, M. Dorkos, G.R. O'Connell. *A fast-response membrane-based pH indicator optode*. Talanta, 40 (1993) 765-768.

[3] M. Garcia-Heras, C. Gil, N. Carmona, J. Faber, K. Kromka, M.A. Villegas. *Optical behaviour of pH detectors based on sol-gel technology*. Anal. Chim. Acta, 540 (2005) 147-152.

[4] M. Puyol, S. Miltsov, I. Salinas, J. Alonso. *Ketocyanine Dyes: H^+-Selective Ionophores for Use in Integrated Waveguides Absorbance Optodes*. Anal. Chem., 74 (2002) 570-576.

[5] L.Y. Heng, T.H. Fang, L.H. Chern, M. Ahmad. *Influence of Methacrylic-Acrylic Copolymer Composition on Plasticiser-free Optode Films for pH Sensors*. Sensors, 3 (2003) 83-90.

[6] L.R. Allain, Z. Xue. *Optical Sensors for the Determination of Concentrated Hydroxide*. Anal. Chem., 72 (2000) 1078-1083.

[7] R. Narayanaswamy, F. Sevilla III. *Reflectometric study of thre acid-base equilibria of indicators immobilised on a styrene/divinylbenzene copolymer*. Anal. Chim. Acta, 189 (1986) 365-369.

[8] M.C. Moreno-Bondi, M. Jiménez, C. Pérez Conde, C. Cámara. *Analytical performance of an optical pH sensor for acid-base titration*. Anal. Chim. Acta 230 (1990) 35-40.

[9] B. Kuswandi, R. Narayanaswamy. *Polymeric encapsulated membrane for optrodes*. Fresenius J. Anal. Chem., 364 (1999) 605-607.

[10] G.F. Kirkbright, R. Narayanaswamy, N.A. Welti. *Fibre-Optic pH Probe Based on the Use of an Immobilised Colorimetric Indicator*. Analyst, 109 (1984) 1025-1028.

[11] D. Morris, S. Coyle, Y. Wu, K.T. Lau, G. Wallace, D. Diamond. *Bio-sensing textile based patch with integrated optical detection system for sweat monitoring*. Sens. Actuators B, 139 (2009) 231-236.

[12] A. Abbaspour, M.A. Mehrgardi, A. Noori, M.A. Kamyabi, A. Khalafi-Nezhad, M.N. Soltani Rad. *Speciation of iron(II), iron(III) and full-range pH monitoring using paptode: A simple colorimetric method as an appropriate alternative for optodes*. Sens. Actuators B, 113 (2006) 857-865.

[13] T.P. Jones, M.D. Porter. *Optical pH sensor based on the chemical modification of a porous polymer film*. Anal. Chem., 60 (1988) 404-406.

[14] A. Dybko, W. Wroblewski, J. Maciejewski, R. Romaniuk, Z. Brzózka. *Efficient Reagent Immobilization Procedure for Ion-Sensitive Optomembranes*. Sens. Actuators B, 39 (1997) 207-211.

[15] J.I. Peterson, S.R. Goldstein, R.V. Fitzgerald, D.K. Buckhold. *Fiber optic pH probe for physiological use*. Anal. Chem., 52 (1980) 864-869.

[16] C. Munkholm, D.R. Walt, F.P. Milanovich, S.M. Klainer. *Polymer Modification of Fiber Optic Chemical Sensors as a Method of Enhancing Fluorescence Signal for pH Measurement*. Anal.Chem., 58 (1986) 1427-1430.

[17] A. Safavi, M. Pakniat. Dipicrylamine-modified triacetylcellulose membrane for optical pH and potassium ion measurement. Anal. Chim. Acta, 335 (1996) 227-233.

[18] A.A. Ensafi, A. Kazemzadeh. *Optical pH Sensor Based On Chemical Modification of Polymer Film*. Microchem. J., 63 (1999) 381-388.

[19] Y. Kostov, G. Rao. *Low-cost gated system for monitoring phosphorescence lifetimes*. Rev. Sci. Instrum., 74 (2003) 4129-4133.

[20] A. Holobar, B.H. Weigl, W. Trettnak, R. Benes, H. Lehmann, N.V. Rodriguez, A. Wollschlager, P. O'Leary, P. Raspor, O.S. Wolfbeis. *Experimental results on an optical pH measurement system for bioreactors*. Sens. Actuators B, B11 (1993) 425-430.

[21] P. Hashemi, R.A. Zarjani. *A wide range pH optical sensor with mixture of Neutral Red and thionin immobilized on an agarose film coated glass slide*. Sens. Actuators B, 135 (2008) 112-115.

[22] T. Seung, C. Yang. *Synthesis of Congo Red linked with alkyl amide polymer and its optical ion-sensing property*. Pol. Bull., 42 (1999) 655-660.

[23] S. de Marcos, C. Asensio, I. Urunuela, F. Gallarta, J. Galban, J.R. Castillo. *New approaches to polyaniline optical sensors: pH, acetic acid and ammonia determination*. Quim. Anal., 19 (2000) 99-104.

[24] S. de Marcos, O.S. Wolfbeis. *Optical Sensing of pH Based on Polypyrrole Films*. Anal. Chim. Acta, 334 (1996) 149-153.

[25] J. Janata. *Do Optical Sensors Really Measure pH?* Anal. Chem., 59 (1987) 1351-1356.

[26] P. Hashemi, R.A. Zarjani, M.M. Abolghasemi, A. Olin. *Agarose film coated glass slides for preparation of pH optical sensors*. Sens. Actuators B, 121 (2007) 396-400.

[27] M. Bacci, F. Baldini, A.M. Scheggi. *Spectrophotometric investigations on immobilized acid-base indicators*. Anal. Chim. Acta, 207 (1988) 343-348.

[28] F.B.M. Suah, M. Ahmad, M.N. Taib. *Optimization of the range of an optical fiber pH sensor using feed-forward artificial neural network*. Sens. Actuators B, 90 (2003) 175-181.

[29] A. Safavi, A. Rostamzadeh, S. Maesum. *Wide range pH measurements using a single H^+-selective chromoionophore and a time-based flow method*. Talanta, 68 (2006) 1469-1473.

[30] U.W. Grummt, A. Pron, M. Zagorska, S. Lefrant. *Polyaniline based optical pH sensor*. Anal. Chim. Acta, 357 (1997) 253-259.

[31] Z. Ge, C.W. Brown, L. Sun, S.C. Yang. *Fiber-optic pH sensor based on evanescent wave absorption spectroscopy*. Anal. Chem., 65 (1993) 2335-2338.

[32] E. Primgsheim, E. Terpetchnig, O.S. Wolfbeis. *Optical Sensing pH of Using Thin Films of Subtituted Polyanilines*. Anal. Chim. Acta, 357 (1997) 247-252.

[33] M. del P. Taboada Sotomayor, M.A. de Paoli, W.A. de Oliveira. *Fiber Optic pH Sensor Based on Poly(o-Methoxyaniline)*. Anal. Chim. Acta, 353 (1997) 275-280.

[34] J.Z. Tao, G.R. Xu, S.W. Yao, P. Liu, Y.P. Zhang. *Optical response of copolymer of 3-aminophenylboronic acid with aniline film against pH*. Guangpu Shiyanshi, 25 (2008) 1053-1056.

[35] A. Safavi, M. Bagheri. *Novel optical pH sensor for high and low pH values*. Sens. Actuators B, 90 (2003) 143-150.

[36] M. Shamsipur, F. Abbasitabar, V. Zare-Shahabadi, M. Akhond. *Broad-Range Optical pH Sensor Based on Binary Mixed-Indicator Doped Sol-Gel Film and Application of Artificial Neural Network*. Anal. Lett., 41 (2008) 3113-3123.

[37] G. Vishnoi, T.C. Goel, P.K.C. Pillai. *A pH-optrode for the complete working range*. Proc. SPIE-Int. Soc. Opt. Eng., 3538 (1999) 319-325.

[38] B.D. Gupta, S. Sharma. *A long-range fiber optic pH sensor prepared by dye doped sol-gel immobilization technique*. Opt. Commun., 154 (1998) 282-284.

[39] J. Lin, D. Liu. *An optical pH sensor with a linear response over a broad range*. Anal. Chim. Acta, 408 (2000) 49-55.

[40] F.J. Arregui, M. Otano, C. Fernandez-Valdivielso, I.R. Matias. *An experimental study about the utilization of Liquicoat® solutions for the fabrication of pH optical fiber sensors*. Sens. Actuators B, 87 (2002) 289-295.

[41] A. Safavi, N. Maleki, A. Rostamzadeh, S. Maesum. *CCD camera full range pH sensor array*. Talanta, 71 (2007) 498-501.

[42] M.P. Cuéllar, M.M. Erenas, M.C. Pegalajar, I. de Orbe-Payá, L.F. Capitán-

Vallvey. *Automatic Colour feature extraction from disposable optical sensors*. Proc. International Workshop on Multivariate Image Analysis, Valencia, Spain (2009) 45.

[43] D.A. Forsyth, J. Ponce. *Computer Vision: A Modern Approach.* Prentice Hall: Upper Saddle River, NJ, US (2002).

[44] A.R. Smith. *Color gamut transform pairs*. Proceedings of the 5th Annual Conference on Computer Graphics and Interactive Techniques (1978) 12-19.

[45] S. Haykin. *Neural Networks: A comprehensive foundation.* Prentice Hall: Upper Saddle River, NJ, USA (1999).

[46] M.P. Cuéllar, M. Delgado, M.C. Pegalajar. *An application of non-linear programming to train recurrent neural networks in time series prediction problems*. Proc. International Conference on Enterprise and Information Systems (2005) 35-42.

[47] K. Cantrell, M.M. Erenas, I. de Orbe-Payá, L.F. Capitán-Vallvey. *Use of the Hue Parameter of the Hue, Saturation, Value Color Space As a Quantitative Analytical Parameter for Bitonal Optical Sensors*. Anal. Chem., 82 (2010) 531-542.

[48] E. Bakker, P. Bühlmann, E. Pretsch. *Carrier-based Ion-Selective Electrodes and Bulk Optodes. 1. General Characteristics*. Chem. Rev., 97 (1997) 3083-3132.

[49] A. Ceresa, Y. Quin, S. Peper, E. Bakker. *Mechanistic insights into the development of optical chloride sensor based on the mercuracarborand-3 ionophore*. Anal. Chem., 75 (2003) 133-140.

[50] R.H. Ng, K.M. Sparks, B.E. Statland. C*olorimetric determination of potassium in plasma and serum by reflectance photometry with a dry-chemistry reagent*. Clin. Chem., 38 (1992) 1371-1372.

[51] I. de Orbe-Payá, M. Erenas, L.F. Capitán-Vallvey. *Potassium disposable optical sensor based on transflectance measurements*. Sens. Actuators B, 127 (2007) 586-592.

[52] D. Freiner, R.E. Kunz, D. Citterio, U.E. Spichiger, M.T. Gale. *Integrated optical sensors based on refractometry of ion-selective membranes*. Sens. Actuators

B, 29 (1995) 277-285.

[53] A. Lapresta-Fernández, L.F. Capitán-Vallvey. *Scanometric potassium determination with ionophore-based disposable sensors*. Sens. Actuators B, 134 (2008) 694-701.

[54] S. Capel-Cuevas, I. de Orbe-Payá, M.P. Cuéllar, M.C. Pegalajar, L.F. Capitán-Vallvey. *Full-range optical pH sensor based on imaging techniques*. Proc. Europtrode X (2010) 110.

3. CONCLUSIONES

El objetivo de este capítulo ha sido el desarrollo de una matriz sensora óptica para medida de pH en rango completo basada en el uso de NNA.

Como principales conclusiones podemos resaltar las siguientes:

- La matriz sensora desarrollada contiene once elementos sensores que cambian su color en diferentes intervalos de pH, al objeto de cubrir el rango completo. El pH se predice empleando una ANN (seleccionada tras un proceso de ensayo y error) que depende del parámetro tonal (coordenada H) del espacio de color HSV. Otras aproximaciones encontradas en bibliografía que hacen uso del espacio de color RGB requieren tres parámetros para realizar la predicción, mientras que en este caso se ha demostrado que el parámetro tonal por sí solo permite lograr una aproximación adecuada del pH de la disolución. En consecuencia, el modelo de predicción se simplifica en términos de complejidad computacional al reducir el número de parámetros necesarios. Respecto a métodos que utilizan los espectros de absorción para realizar la predicción, esta aproximación requiere menor pre-procesamiento de los datos, ya que la coordenada H se determina de forma rápida mediante el uso de un escáner y un software sencillo, como el desarrollado por nosotros.

- La ANN fue entrenada a partir del conjunto de datos de calibración utilizando el algoritmo de entrenamiento Levenberg–Marquardt, debido a su elevado rendimiento para el problema considerado. La estructura de la ANN tiene once neuronas de entrada (cada una de ellas asociada a la coordenada H correspondiente a un elemento sensor de la matriz), una salida (el valor de pH aproximado) y una capa oculta con diez neuronas ocultas.

- La aplicación de la ANN ha mostrado un adecuado rendimiento de predicción, obteniéndose los siguientes valores de MSE, en unidades de

pH: 0,010 en los datos de calibración, 0,018 en los datos de validación y 0,042 en muestras de agua de grifo de Granada. Los test estadísticos han corroborado los resultados obtenidos en este trabajo, concluyéndose que no hay diferencias estadísticamente significativas entre los valores de pH reales y los predichos por el modelo.

CAPÍTULO 5

Minimización del número de elementos de una matriz de sensores para medida de pH

"I do not fear computers.
I fear the lack of them".
Isaac Asimov

1. INTRODUCCIÓN

Los primeros ejemplos de algoritmos genéticos aparecieron a finales de los años 50 y principios de los 60, programados en ordenadores por biólogos evolutivos que buscaban modelizar aspectos de la evolución natural. En 1962, investigadores tales como G.E.P. Box, G.J. Friedman, W.W. Bledsoe y H.J. Bremermann, desarrollaron independientemente algoritmos inspirados en la evolución para optimización de funciones y aprendizaje automático, aunque sus trabajos tuvieron poca repercusión. En 1965, apareció un desarrollo que tuvo más éxito con la introducción de la técnica de estrategia evolutiva por I. Rechenberg. Esta técnica no utilizaba ni una población de individuos ni un operador de cruce; un padre era mutado para producir un descendiente y se conservaba el mejor de los dos, convirtiéndose en el padre de la siguiente ronda de mutación[255]. Versiones posteriores introdujeron la idea de población.

El siguiente hito importante en este campo apareció en 1966, cuando L.J. Fogel, A.J. Owens y M.J. Walsh desarrollaron en EE.UU. una técnica denominada programación evolutiva. En este método, las soluciones candidatas para los problemas se representaban como máquinas de estado finito sencillas; al igual que en la estrategia evolutiva de Rechenberg, su algoritmo funcionaba mutando aleatoriamente una de estas máquinas simuladas y conservando la mejor de las dos[256,257]. Sin embargo, lo que todavía faltaba en estas dos metodologías era el reconocimiento de la importancia del operador de cruce.

En 1962, el trabajo de Holland[258] sobre sistemas adaptativos estableció las bases para desarrollos posteriores, y lo que es más importante, fue el primero en proponer explícitamente el operador de cruce y otros operadores de recombinación. Sin embargo, el trabajo fundamental en el campo de los algoritmos genéticos apareció en 1975 con la publicación del libro "*Adaptation in natural and artificial systems: an introductory analysis with applications to biology, control, and artificial intelligence*". Esta obra fue la primera en presentar

[255] R. Haupt, S.E. Haupt. *Practical Genetic Algorithms*. John Wiley & Sons (1998) pp. 252

[256] M. Mitchell. *An Introduction to Genetic Algorithms*. MIT Press (1996) pp. 209

[257] D. Goldberg. *Genetic Algorithms in Search, Optimization, and Machine Learning*. Addison-Wesley, Longman Publishing Co., Inc. Boston, MA, USA (1989) pp. 372

[258] J.H. Holland. *Adaptation in natural and artificial systems: an introductory analysis with applications to biology, control, and artificial intelligence*. University of Michigan Press (1975) pp. 183

sistemática y rigurosamente, el concepto de sistemas digitales adaptativos utilizando la mutación, la selección y el cruce, simulando el proceso de la evolución biológica como estrategia para resolver problemas. Además, intentó plantear los algoritmos genéticos sobre una base teórica firme introduciendo el concepto de esquema[256,255]. Ese mismo año Kenneth De Jong, en su tesis doctoral, estableció el potencial de los algoritmos genéticos demostrando que podían utilizarse adecuadamente en una gran variedad de funciones de prueba, incluyendo espacios de búsqueda con ruido, discontinuos y multimodales[257].

Estos trabajos fundacionales aumentaron el interés por la computación evolutiva. Durante los años 80, los algoritmos genéticos se aplicaron en una amplia variedad de áreas, desde problemas matemáticos abstractos como el "problema de la mochila" (*bin-packing*) y el coloreo de grafos, hasta asuntos más concretos de ingeniería como el control de flujo en una línea de ensamblaje, reconocimiento y clasificación de patrones y optimización estructural[257].

Al principio, estas aplicaciones eran principalmente teóricas. Sin embargo, al continuar avanzando en la investigación, los algoritmos genéticos se empezaron a utilizar en el sector comercial al cobrar importancia debido al crecimiento exponencial de la potencia de computación y el desarrollo de Internet. Hoy en día, la computación evolutiva es un campo floreciente, y los algoritmos genéticos están resolviendo problemas cotidianos de interés[255] en áreas de estudio tan diversas como la predicción en la Bolsa de Valores y la planificación de la cartera de valores, ingeniería aeroespacial, diseño de microchips, bioquímica y biología molecular y diseño de horarios en aeropuertos y líneas de montaje.

Existen numerosos artículos y libros sobre los algoritmos genéticos multi-objetivo, tales como los de Srinivas y Deb[259], Fonseca y Fleming[260], Zitzler y Thiele[261], Hanne[262], Coello[263] y Fleming y Purshouse[264]. En cuanto a su uso para

---

[259] N. Srinivas, K. Deb. *Multiobjective optimization using nondominated sorting in genetic algorithms*. Evol. Comput., 2(3) (1994) 221-248

[260] C. Fonseca, P. Fleming. *An overview of evolutionary algorithms in multiobjective optimization*. Evol. Comput., 3(1) (1995) 1-16

[261] E. Zitzler, L. Thiele. *Multiobjective evolutionary algorithms: a comparative case study and the Strength Pareto approach.* IEEE Trans. Evol. Comput., 3(4) (1999) 257-271

[262] T. Hanne. *Global multiobjective optimization using evolutionary algorithms*. J. Heuristics, 6(3) (2000) 347-360

la resolución de problemas específicos, se encuentran los de Beasley, Tang *et al.*[265] en 1996, Burnham y Mills[266] en 1997, Williams, Koza *et al.*[267] en 1999, Obayashi *et al.*[268], Hughes y Leyland[269], He y Mort[270] en 2000, Haas, Chryssolouris y Subramaniam[271], Sonander y Havelock[272], Crossley y Lang[273], Sasaki *et al.*[274] en 2001, Benini y Toffolo[275], Kewley y Embrechts[276], Sato *et al.*[277] en 2002, Koza *et al.*[278] en 2003.

1.1. Algoritmos genéticos multi-objetivo en Química

Los algoritmos genéticos multi-objetivo han sido poco aplicados hasta el momento en el campo de la Química Analítica. Sin embargo, son muy frecuentes

[263] C. Coello. *An updated survey of GA-based multiobjective optimization techniques*. ACM Computing Surveys, 32(2) (2000) 109-143

[264] P. Fleming, R.C. Purshouse. *Evolutionary algorithms in control systems engineering: a survey*. Control Eng. Pract., 10 (2002) 1.223-1.241

[265] K.S. Tang, K.F. Man, S. Kwong, Q. He. *Genetic algorithms and their applications*. IEEE Signal Proc. Mag., 13(6) (1996) 22-37

[266] O.C.L. Haas, K.J. Burnham, J.A. Mills. *On improving physical selectivity in the treatment of cancer: A systems modelling and optimisation approach*. Control Eng. Pract., 5(12) (1997) 1739-1745

[267] J. Koza, John, F. Bennett, D. Andre, M. Keane. *Genetic Programming III: Darwinian Invention and Problem Solving*. Morgan Kaufmann Publishers, 1999

[268] S. Obayashi, D. Sasaki, Y. Takeguchi, N. Hirose. *Multiobjective evolutionary computation for supersonic wing-shape optimization*. IEEE Trans. Evol. Comput., 4(2) (2000) 182-187

[269] E. Hughes, M. Leyland. *Using multiple genetic algorithms to generate radar point-scatterer models*. IEEE Trans. Evol. Comput., 4(2) (2000) 147-163

[270] L. He, N. Mort. *Hybrid genetic algorithms for telecommunications network back-up routeing*. BT Technol. J., 18(4) (2000) 42-50

[271] G. Chryssolouris, V. Subramaniam. *Dynamic scheduling of manufacturing job shops using genetic algorithms*. J. Intell. Manuf., 12(3) (2001) 281-293

[272] J.E. Beasley, J. Sonander, P. Havelock. *Scheduling aircraft landings at London Heathrow using a population heuristic*. J. Oper. Res. Soc., 52(5) (2001) 483-493

[273] E. Williams, W. Crossley, T. Lang. *Average and maximum revisit time trade studies for satellite constellations using a multiobjective genetic algorithm*. J. Astronaut. Sci., 49 (3) (2001) 385-400

[274] D. Sasaki, M. Morikawa, S. Obayashi, K. Nakahashi. *Aerodynamic shape optimization of supersonic wings by adaptive range multiobjective genetic algorithms*. Evolutionary Multi-Criterion Optimization: First International Conference, EMO 2001, Zurich, Switzerland (2001): Proceedings

[275] E. Benini, A. Toffolo. *Optimal design of horizontal-axis wind turbines using blade-element theory and evolutionary computation*. J. Sol. Energ. Eng., 124(4) (2002) 357-363

[276] R. Kewley, M. Embrechts. *Computational military tactical planning system*. IEEE Trans. Systems, Man Cyber., Part C - Appl. Rev., 32(2) (2002) 161-171

[277] S. Sato, K. Otori, A. Takizawa, H. Sakai, Y. Ando, H. Kawamura. *Applying genetic algorithms to the optimum design of a concert hall*. J. Sound Vib., 258(3) (2002) 517-526

[278] J. Koza, M. Keane, M. Streeter, W. Mydlowec, J. Yu, G. Lanza. *Genetic Programming IV: Routine Human-Competitive Machine Intelligence*. Kluwer Academic Publishers (2003)

en el ámbito de la ingeniería química, principalmente para el control medioambiental, y en la síntesis específica de diferentes tipos de moléculas, especialmente fármacos.

Es muy importante destacar el trabajo realizado por Cela *et al.*[279], quienes los aplicaron por primera vez en Química Analítica, y en concreto, en el campo de la cromatografía, con objeto de desarrollar una optimización automática de las separaciones con gradiente en HPLC en fase inversa. Esta aproximación permitió una definición fácil y directa de los objetivos del cromatógrafo en el proceso de optimización, proporcionando no sólo una única solución óptima parcial, sino un conjunto muy amplio dentro del frente de Pareto de soluciones no-dominadas. Consecuentemente, la optimización automática no requería el uso de funciones respuesta cromatográficas tales como las que habitualmente se emplean para evaluar la calidad de procedimientos cromatográficos. Para demostrar las ventajas prácticas y de procedimientos de trabajo utilizando esta nueva aproximación, se estudió la separación de 11 residuos de productos farmacéuticos de interés ambiental.

Durante los años 90, la amplia utilización de una nueva técnica de diseño de fármacos, la llamada química combinatoria, revolucionó la industria farmacéutica. Glen y Payne[280] describieron en 1995 el diseño automático de nuevas moléculas que presentaban una serie de propiedades concretas. El algoritmo genético permitió optimizar simultáneamente un gran número de objetivos, incluyendo el peso y el volumen molecular; el número de enlaces, centros quirales, átomos y enlaces rotables; la polarizabilidad; el momento dipolar, etc. Como resultado, la empresa Unilever[281] patentó y utilizó algoritmos genéticos para diseñar nuevos componentes antimicrobianos para su uso en productos de limpieza. Posteriormente, Gillet[282] describió el uso de un algoritmo genético multi-objetivo para el diseño basado en los productos de bibliotecas combinatorias, considerando características como la diversidad y el peso

[279] R. Cela, J.A. Martínez, C. González-Barreiro, M. Lores. *Multi-objective optimisation using evolutionary algorithms: its application to HPLC separations*. Chemomet. Intell. Lab., 69 (2003) 137-156

[280] R.C. Glen, A.W.R. Payne. *A genetic algorithm for the automated generation of molecules within constraints.* J. Comput. Aid. Mol. Des., 9 (1995) 181-202

[281] B. Lemley. *Machines that think.* Discover (2001) 75-79

[282] V. Gillet. *Reactant- and product-based approaches to the design of combinatorial libraries*. J. Comput. Aid. Mol. Des., 16 (2002) 371-380

molecular, la similitud estructural, el coste de los suministros, la toxicidad, la absorción, la distribución y el metabolismo.

En el campo de la ingeniería química, son muchos los trabajos desarrollados. Así por ejemplo, Lim *et al.*[283,284] llevaron a la práctica el concepto de optimización multi-objetivo para mantener el equilibrio entre economía y contaminación con el método de análisis adecuado. Sun *et al.*[285,286] demostraron la efectividad del método a partir de los resultados obtenidos en la optimización del proceso de síntesis de amoníaco llevado a cabo por las plantas. Pu, Hu y Wang[287,288] desarrollaron un modelo de optimización del ciclo de vida de la emisión contaminante de combustibles verdes de gasolina mezclados con etanol obtenido de mandioca. La optimización multi-objetivo de los procedimientos de control llevada a cabo por Logist *et al.*[289] en 2009 permitió el diseño de un reactor químico, equilibrando los costes de conversión y de energía, así como el rendimiento y la productividad. Investigadores como Guillen-Gosalbez[290,291] y Gebreslassiea[292,293] combinaron el impacto del ciclo de vida (LCA) con la optimización multi-objetivo para una planificación, incluyendo planteamientos medioambientales de los sistemas de producción de energía. Esta técnica

[283] Y.I. Lim, P. Floquet, X. Joulia. *Multiobjective optimization considering economics and environmental impact*. Récents Progrès en Génie des Procédés, 13(70) (1999) 63-70

[284] Y.I. Lim, P. Floquet, X. Joulia. *Efficient Implementation of the Normal Boundary Intersection (NBI) Method on Multiobjective Optimization Problems*. Ind. Eng. Chem. Res., 40(2) (2001) 648-655

[285] L. Sun, X. Fan, P. Yao. *Study on multi-objective fuzzy optimization algorithm for chemical process*. Comput. Aid. Chem. Eng., 15B (2003) 1370-1375

[286] L. Sun, H.H. Lou. *A strategy for multi-objective optimization under uncertainty in chemical process design*. Chinese J. Chem. Eng., 16(1) (2008) 39-42

[287] G. Pu, Z. Hu, C. Wang. *Multi-objectives optimization on life cycle pollutants emission of cassava-based ethanol blended gasoline fuels*. Huanjing Kexue, 25(5) (2004) 37-42

[288] Z. Hu, P. Tan, G. Pu. *Multi-objective optimization of cassava-based fuel ethanol used as an alternative automotive fuel in Guangxi, China.* Appl. Energ., 83(8) (2006) 819-840

[289] F. Logist, P.M.M. Van Erdeghem, J.F. Van Impe. *Efficient deterministic multiple objective optimal control of (bio)chemical processes*. Chem. Eng. Sci., 64(11) (2009) 2527-2538

[290] G. Guillen-Gosalbez, M. Turkay. *Life cycle assessment coupled with multi-objective optimization for environmentally conscious planning of energy production systems*. AIChE Annual Meeting, Conference Proceedings, Philadelphia, PA, United States, Nov. 16-21, 2008, 678/1-678/2

[291] G. Guillen-Gosalbez. *A novel MILP-based objective reduction method for multi-objective optimization: Application to environmental problems*. Comput. Chem. Eng., 35(8) (2011) 1469-1477

[292] B.H. Gebreslassiea, G.G. Guillen-Gosalbez, L. Jimenez, D. Boer. *Design of environmentally friendly absorption cooling systems via multi-objective optimization and life cycle assessment*. Comput. Aid. Chem. Eng., 26 (2009) 1099-1104

[293] B.H. Gebreslassie, M. Jimenez, G. Guillen-Gosalbez, L. Jimenez, D. Boer. *Multi-objective optimization of solar assisted absorption cooling system*. Comput. Aid. Chem. Eng., 28 (2010) 1033-1038

también permitió a Tian[294] en 2011 optimizar la producción de 1,3-butadieno a partir de acetonitrilo utilizando el líquido iónico [C_2MIM][PF_6] como aditivo para mejorar la resolución del proceso. Ese mismo año Kostin[295] presentó una formulación de programación lineal integrada mixta (MILP) multi-objetivo que consideraba simultáneamente la minimización del coste y del impacto ambiental en cadenas de suministro de bioetanol-azúcar. Kilkis[296] propuso el uso de esta técnica para optimizar la eficiencia energética en sistemas refrigerantes y edificios verdes, mientras que este año, Pozo *et al.*[297] han utilizado PCA para reducir las medidas medioambientales redundantes mediante una optimización multi-objetivo, al objeto de aplicarlo al diseño de cadenas de suministro químico. Por su parte, Salcedo *et al.*[298] han acoplado la optimización multi-objetivo de colectores solares y ciclos de Rankine con la desalinización mediante ósmosis inversa de plantas de agua de mar, considerando los aspectos ambientales y económicos.

---

[294] X. Tian, X. Zhang, S. Zeng, Y. Xu, Y. Yao, Y. Chen, L. Huang, Y. Zhao, S. Zhang. *Process Analysis and Multi-Objective Optimization of Ionic Liquid-Containing Acetonitrile Process to Produce 1,3-Butadiene Chemical*. Eng. Technol., 34(6) (2011) 927-936

[295] A. Kostin, F.D. Mele, G. Guillen-Gozalbez. *Multi-objective optimization of integrated bioethanol-sugar supply chains considering different LCA metrics simultaneously*. Comput. Aid. Chem. Eng., 29 (2011) 1276-1280

[296] S. Kilkis, B. Kilkis. *An analytical, multi-objective an optimization algorithm for energy efficiency in district cooling systems and green buildings*. ASHRAE Transactions, 117(1) (2011) a13/1-a13/8

[297] C. Pozo, R. Ruiz-Femenia, J. Caballero, G. Guillen-Gosalbez, L. Jimenez. *On the use of Principal Component Analysis for reducing the number of environmental objectives in multi-objective optimization: Application to the design of chemical supply chains*. Chem. Eng. Sci., 69(1) (2012) 146-158

[298] R. Salcedo, E. Antipova, D. Boer, L. Jimenez, G. Guillen-Gosalbez. *Multi-objective optimization of solar Rankine cycles coupled with reverse osmosis desalination considering economic and life cycle environmental concerns*. Desalination, 286 (2012) 358-371

2. OBJETIVOS

El objetivo general del trabajo desarrollado en este capítulo pretende:

- A partir de la matriz sensora óptica desarrollada en el capítulo anterior, compuesta inicialmente por once elementos sensores, llegar a establecer el número mínimo de elementos necesarios que proporcionen la mayor información de color y permitan llevar a cabo una adecuada predicción de pH, entre 0 y 14, reduciendo de esta manera el tamaño de la matriz sensora.

Los objetivos particulares a alcanzar son:

- Obtener la información de color de la matriz sensora inicial con once elementos tras su reacción con el problema usando un escáner que trabaje en modo transmisión.

- Cálculo del valor de la coordenada H del espacio de color HSV correspondiente a cada elemento sensor a partir de sus valores RGB medidos y obtención del conjunto de datos de calibración del sistema.

- Desarrollar un modelo híbrido formado por el algoritmo genético multi-objetivo NSGA-II y la técnica de optimización no lineal Levenberg-Marquardt, con el fin de optimizar tres aspectos: el número de elementos sensores utilizados para la predicción, el error de predicción de la red neuronal y la complejidad de dicha red. El resultado será un conjunto de redes neuronales artificiales generadas según el criterio de óptimos de Pareto.

- Validación de las soluciones recogidas en el frente de Pareto.

- Selección de la solución que mantenga un equilibrio adecuado entre los tres aspectos señalados, proporcionando un error de predicción de pH mínimo con el mínimo número de elementos sensores.

- Determinación del pH de muestras de agua, tanto de grifo como de río.

PUBLICACIÓN III:

New Journal of Chemistry, 35 (2011) 1042-1053
DOI: 10.1039/c0nj00951b

Minimization of sensing elements for full-range optical pH device formulation

M.P. Cuéllar[2], S. Capel-Cuevas[1], M.C. Pegalajar[2], I. de Orbe-Payá[1], L.F. Capitán-Vallvey[1,*]

[1]Department of Analytical Chemistry.
[2]Department of Computer Science and Artificial Intelligence.
University of Granada, E-18071 Granada, Spain

Abstract

The goal of this work is to find the minimum number of sensing elements that can be used to build a sensor array suitable for pH prediction for a full-range (0-14) optical pH sensor array based on hue (H) data from HSV color space. The hue of each element coming from the pH sensor array imaging is used as input data for a neural network that provides the pH prediction approximation as the output response. This problem may be considered a multicriteria optimization task with the dual objectives of error minimization between the network pH prediction and the reference pH in the calibration data, and of minimizing the network complexity and the number of network inputs. To that end, this work proposes a multi-objective optimization method applied to a collection of 11 sensing elements that returns a set of optimal networks considering the Pareto optimality criterion. A solution from the Pareto front was selected to achieve a minimum pH prediction error with the minimum number of sensing elements. After this analysis, it can be concluded that the use of a sensor array made up of 4 sensing elements offers a good pH prediction (Mean Square Error of 0.052) over the full-range working with 4 hidden neurons.

Keywords: Full-range optical pH sensor array; Sensing elements optimization; Neural network; HSV colour space; H coordinate.

* Corresponding author; e-mail: lcapitan@ugr.es

1. Introduction

Unlike potentiometric pH determination, in which the pH depends linearly on the activity of hydrogen ions, pH in optical sensors is a function of the concentration of the acid and basic forms of the indicator [1]. Optical sensors for pH are mainly based on reversible changes in the structure of chemicals induced by pH and translated into changes in spectroscopic phenomena such as absorption, reflectance, luminescence, and energy transfer (acid-base indicator) chemically or physically immobilized in or on a solid support, and placed as a thin layer or coating. The change in the measured signal with the pH typically results in narrow sigmoidal shape dependence according to the Henderson-Hasselbalch equation. This leads to the main drawbacks of optical pH sensors – their short dynamic working range (2-3 pH units) and non-linear response [2] – which require different sensing membranes to cover the whole pH range.

Different strategies have been devised to extend the working range of optical pH sensors. The working range of membranes containing only one indicator can be broadened using polyprotic acids as indicators [3], although in some instances the adsorption [4] or chemical immobilization [5] of the indicators leads to broader ranges than in solution. In other cases, the use of the whole reflectance spectra of an immobilized indicator [6] or the dynamic optical response of a flow sensor as analytical signal [7] increases the range with only one indicator. Alternatively, some conductive polymers change their visible and near-IR absorption properties as a function of pH in a broad range, as is the case with polyaniline [8] and polypyrrole [9]. Another approach to broaden the pH range is to co-immobilize multiple pH indicators (two [10,11], three [12] and even five indicators [13]).

A final strategy consists of using arrays of membranes containing complementary pH indicators acquiring the analytical information by imaging

techniques. In this way, commercial multi-color pH paper strips have been measured with a conventional scanner [14]; alternatively, arrays of five pH membranes in a triacetylcellulose support measured with a CCD color camera have been described [15]. In both cases, the average RGB values of each sensing area image are used for calibration with multivariate mathematical models. One drawback of this calibration process is the non-linear dynamics of the functions to approximate the pH with respect to the color parameters. Here, neural networks [16] have been proposed to solve this problem, although the limitations of their classic training methods, becoming trapped in local optima solutions [17], may make the model calibration processes difficult. Genetic algorithms [18] have proven to overcome these problems in some applications regarding sensor modeling, such as the generation of regional maps of α-chlorophyll concentration or total suspended matter from the ocean color [19], strain sensing using a Mach–Zehnder fiber interferometer [20,21], and strain and temperature sensing by fiber Bragg gratings [22-24]. One more recent training strategy for neural networks consists of the use of hybrid techniques that combine evolutionary algorithms with non-linear optimization methods to overcome local optima solutions [25-29].

In our approach, the hue color feature, obtained by means of imaging techniques from a sensor array, is used as input for a neural network that provides the pH of aqueous solutions applied, in this case, to water samples. The two steps required to prepare a full-range pH sensor array are the design and selection of the sensing elements to be included in the sensor array and the selection and calibration of a suitable pH prediction model. Typically, the researcher carries out both tasks manually. A set of candidate sensing elements are evaluated with respect to their analytical response and accuracy, and the best ones are included in the sensor array. Then, a multivariate prediction model is calibrated. This process is repeated until a suitable solution is found. At the same time, the prediction models are calibrated depending on parameters that must be optimized, so that the calibration process usually requires a large number of computer experiments, resulting in a difficult trial-and-error procedure.

In this work, a method to complete both tasks automatically and simultaneously by means of multi-objective optimization techniques [30-32] is proposed. The approach used in this paper considers two stages (figure 5.1): first,

a sensor array containing all of the candidate sensing elements is used as the input for a multi-objective optimization method. The hue color parameter from each sensing element is extracted to build the calibration data set. Then, the multi-objective algorithm provides a set of neural networks with maximum accuracy and the optimal sensing elements to be included in the sensor array. In a second stage, all the possible neural networks and corresponding sensor arrays containing a different number of sensing elements returned by the method are validated. The main advantage of this calibration strategy is that the neural network training is carried out simultaneously to automatically select the sensing elements within the multi-objective procedure. In addition, a hybridation of the Quasi-Newton Levenberg-Marquardt training algorithm within the NSGA-II multi-objective method is used to overcome local optima solutions and to achieve better neural network prediction accuracy [33].

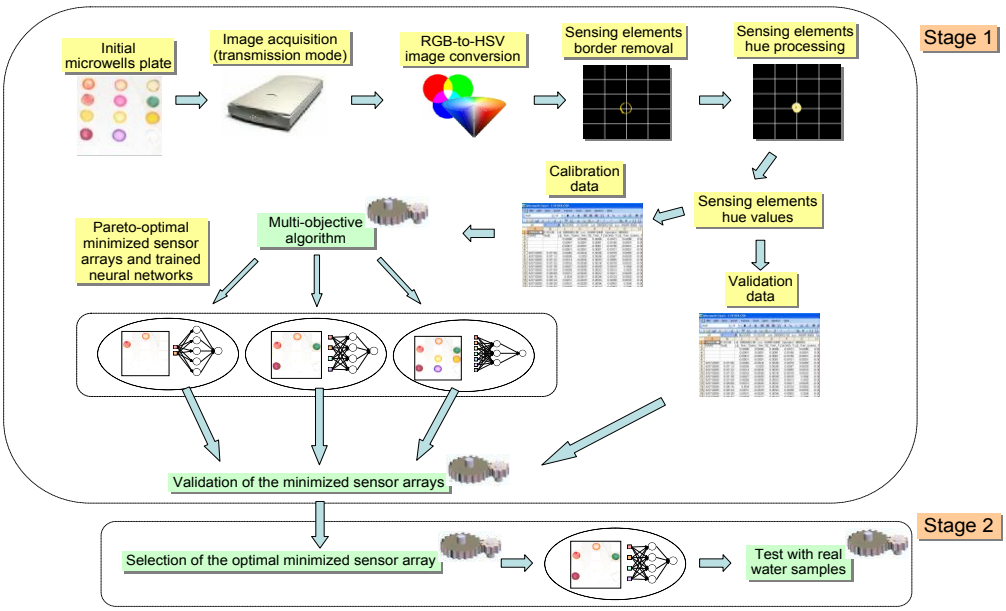

Figure 5.1. Scheme of the hue acquisition and processing from the candidate sensing elements in the microwells plate

Additional key points in our approach are the use of: a) the H from the HSV color space [34] as the analytical parameter to reduce the problem complexity in contrast to RGB-based proposals, b) a novel non-differentiable error optimization criterion for the neural network calibration, and c) the inclusion of

the results of the method to estimate the relevance of the candidate sensing elements for pH prediction.

To the best of our knowledge, there are no similar papers in the literature that solve these problems simultaneously, although some recent examples regarding sensor modeling management and multi-objective optimization include systems to detect and respond to contamination events in water distribution systems [35], an air quality monitoring system based on satellite remote sensing of the troposphere [36] and a pollution load modeling system [37].

2. Experimental

2.1. Reagents

The chemicals used to prepare the pH sensitive films were potassium tetrakis (4-chlorophenyl)borate (TCPB, CAS No. 14680-77-4), tridodecylmethylammonium chloride (TDMAC, CAS No. 7173-54-8), aliquat 336 (CAS No. 5137-55-3), onitrophenyloctylether (NPOE, CAS No. 37682-29-4), dioctyl sebacate (DOS, CAS No. 122-62-3), bis(1-butylpentyl)adipate (BBPA, CAS No. 77916-77-9), tributyl phosphate (TBP, CAS No. 126-73-8), high molecular weight polyvinyl chloride (PVC, CAS No. 9002-86-2), cellulose acetate (CA, CAS No. 9004-35-7), ethylenglycol (EG, CAS No. 107-21-1) and tetrahydrofuran (THF, CAS No. 109-99-9) all purchased from Sigma (Sigma-Aldrich Química S.A., Madrid, Spain). Bromothymol blue (CAS No. 76-59-5), phenol red (CAS No. 143-74-8), thymol blue (CAS No. 76-61-9), m-cresol purple (CAS No. 2303-01-7) and PAN (CAS No. 85-85-8) from Sigma, liphophilized Nile blue (CAS No. 125829-24-5) and purpurin (CAS No. 81-54-9) from Fluka (Fluka, Madrid, Spain), cresol red (CAS No. 1733-12-6) from Panreac (Panreac, Barcelona, Spain), alizarine (CAS No. 72-48-0) from TCI (TCI Europe, Belgium), and sicomet red P (CAS No. 5281-04-9) from BASF (BASF, Ludwigshafen, Germany) were used as acid-base indicators. As the support, sheets of Mylar-type polyester (Goodfellow, Cambridge, UK) were used. HCl and NaOH were supplied by Sigma. All reagents were of analytical reagent grade and were used without any further purification. All aqueous solutions were prepared in reverse-osmosis type quality water (Milli-RO 12 plus Milli-Q station from Millipore, conductivity 18.2 mS).

2.2. Instruments and Software

A Microtek ScanMaker i900 scanner (Microtek, Taiwan) was used to acquire images of the different sensing elements. The software used to manage the scanner was Silver Fast Ai provided by Microteck. The images were processed with a set of scripts and functions developed by us in Matlab r2007b (The MathWorks, Inc, Natick, MA, USA). Statistical calculations were performed with Statgraphics software package (Manugistics Inc. and Statistical Graphics Corporation, USA, 1992), and Microsoft Excel (Microsoft Corp., Redmond, WA, USA) was used for general calculations.

A laboratory-made spin-on device was used to prepare individual membranes for their spectrophotometric characterization. A Crison pH-meter (Crison Instruments, Barcelona, Spain, model Basic 20) with a combined double junction glass electrode, calibrated against two standard buffer solutions (pH 4.0 and 7.0), was used for pH measurements.

2.3. Preparation of sensing elements

Different pH microwell plates were prepared on 50 mm x 40 mm Mylar supports covered by an adhesive and transparent PVC layer with different numbers of microwells 5 mm in diameter each (from 2 to 11 microwells). The microwell plates were cast by placing 8 µL of corresponding cocktail in each hole and then placing them in a dryer with THF saturated atmosphere at room temperature to enable slow solvent evaporation (figure 5.1). The different cocktails for pH sensing were prepared by dissolution in 1 mL of distilled THF in all the cases for the different reagents needed.

A set of pH microwell plates was prepared according to the conditions of: a) no leaching, b) a change in the tonal color coordinate by the reaction, and finally c) covering the full pH range by overlapping the responses of the different membranes. The sensing elements selected were prepared from different cocktails containing different types and amounts of colorimetric acid-base indicators, polymers, plasticizers, lipophilic salts and, if necessary, humectant.

The selection criteria for the pH sensing elements used were both a high variation in the H coordinate by reaction and non-redundant information from different sensing elements, so that the entire pH range was covered. The composition of the different sensing elements was optimized considering leaching minimization (lipophilic salt, plasticizer, and membrane polymer), colour intensity (acid-base indicator) and response time (plasticizer, membrane polymer, humectant and cocktail volume). The usual lipophilic salt/indicator ratio was 3:1.

To modify the pH response of a sensing element, the same acid-base indicator was used but the plasticizer, membrane polymer, lipophilic salt and/or lipophilic salt/indicator ratio were changed. As a result, 11 different membranes that cover the whole pH range were selected as candidates for the pH sensor array. They only contained 10 different pH indicators due to that fact that two membranes were prepared containing the same components including thymol blue, but with a different lipophilic salt/indicator ratio [38].

2.4. Response evaluation

The response of each candidate sensing element was evaluated for each 0.1-0.2 pH unit from 0 to 14 by adding volumes of 1.0 M, 0.1 M or 0.01 M HCl or NaOH with the help of a microburette to an aqueous solution containing the 11 candidate membranes arranged in the microwell plate described above hanging from a support. After each addition of reagents and magnetic stirring, the solution pH was measured using a standard potentiometric procedure. Each pH microwell plate was equilibrated for 5 min; it was then pulled out and inserted into a holder to obtain the image of the sensing elements with a transmission flatbed scanner. The resolution and color depth were set to 300 dpi for high resolution without membrane degradation and 48 to 24 bits of color, respectively.

2.5. Microwell plate signal processing and hue acquisition

The first step in the pH prediction procedure was the hue acquisition from the candidate sensing elements arranged on the microwell plate. To do this, after the equilibration of the microwell plates containing the pH membranes with the acidic or basic solutions that produce changes in the sensing element colors, the whole microwell plate was scanned and stored in the PC in 24-bit TIFF format using the standard RGB color space. The scanner was calibrated before use by means of an IT8 calibration target to measure the performance of input devices and generate ICC (International Color Consortium) profiles.

To extract the hue parameter from each sensing element in the scanned image, software developed by us in Matlab [39] was used. First, each sensing element was located in the image by checking the color differences of the pixels with the background and with Canny's algorithm [40] for border detection. Pixels with significant differences were interpreted as colored and pixels with small differences were interpreted as grey background, coming from the Mylar substrate and scanner lid. Next, the borders of the scanned sensing elements were discarded to prevent noise in the hue computation. The H of the HSV color space was calculated for the remaining pixels of each sensing element using color space transformation equations [41], and finally the H value returned by the software for each sensing element was the mode of the hues calculated for all the pixels in the same membrane, since this parameter provides a low error during the image processing. This procedure provided us with the data sets necessary for the experimental calibration and validation as described in the following sections.

Because of the circular nature of H, which is defined as an angle that varies between 0 and 360º and represented as a color wheel where 0º is located at the top of the wheel, the values are bounded between 0 and 1, with both 0 and 1 representing the same hue. However, this work allows H to be from -360º to 360º, with the values therefore between -1 and 1, to avoid discontinuities in H evolution with the pH if it passes through the origin.

2.6. Multi-objective optimization of pH sensor array and neural networks

Multi-objective problems are expressed as the minimization/maximization of a vector of functions $F(x) = (f_1(x), f_2(x), ..., f_n(x))$ that depends on the set of variables $x=(x_1, x_2, ..., x_m)$. The objective is to find a solution or set of solutions $\{x^*\}$ whose evaluation in all the criteria in $F(x)$ provides an optimal value. However, if the criteria are opposed to each other, it is usually found that the optimal value in an objective function $f_i(x)$ also implies a non-optimal value for the remaining objectives. In order to overcome this situation, the *Pareto optimality criterion* is defined over the dominance of solutions. A solution x dominates another solution y, and it is written $x<y$ if, and only if:

$$x < y \leftrightarrow \forall i \in \{1,2,...,n\}\ f_i(x) \leq f_i(y) \wedge \exists j \in \{1,2,...,n\} : f_j(x) < f_j(y) \quad (5.1)$$

In brief, it is said that a solution x dominates the solution y if the solution y is not better than x in any of the criteria to be optimized, and also x is better than y in at least one of these objectives. If a solution x does not dominate y and also y does not dominate x, both are *non-dominated solutions*. The set of solutions that is not dominated by any other solution is assumed to be the optimal one under the Pareto optimality criterion. This set is also called the *Pareto front*.

The aim of this multi-objective approach is to automatically select the minimum number of a set of candidate sensing elements that can provide a maximum accuracy for pH prediction. In addition, an accurate Multi-layer Perceptron neural network [16] prediction model that uses the hue from the candidate sensing elements is provided. The use of neural networks as a prediction technique is motivated by the fact that other simpler models such as linear or non-linear regression have been tested [38] and a better performance was obtained with this technique. In terms of multi-objective optimization, the objectives are to minimize: a) the number of sensing elements to be included in the proposed sensor array; b) the pH prediction error of the neural network; and c) the neural network complexity, to avoid overtraining and to achieve a suitable problem generalization capability. These three objectives are formulated mathematically in equations 5.2-5.5, where x stands for the neural network and sensor array parameters to be optimized, $f_1(x)$ is the error minimization criterion,

$f_2(x)$ is the network complexity minimization objective, $f_3(x)$ is the minimization of the number of sensing elements used for the prediction and x^* is an optimal solution covering all the objectives. In equation 5.3, the constant S is the size of the calibration data set, pH_P is the pH value associated with the P-th sample in the calibration data and pH_P' is the network prediction for this value. Finally, values $N^1(x)$ and $N^0(x)$ in equations 5.4 and 5.5 are the number of neurons in the hidden and first network layers, respectively. The number of neurons at the first layer is also the number of sensing elements used for the prediction. The error optimization used in this work (equation 5.3) is the minimization of the maximum error provided by the network pH prediction in any sample of the calibration data set. In contrast to the classic error criterion of minimizing the Mean Square Error (MSE) [16], this approach provided the best experimental results with our problem.

$$x^* = min_x\{f(x)) = min_x\{(f_1(x), f_2(x), f_3(x))\} \quad (5.2)$$

$$f_1(x) = max_P\{|pH'_P pH_P|\}, 1 \leq P \leq S \quad (5.3)$$

$$f_2(x) = N^1(x) \quad (5.4)$$

$$f_3(x) = N^o(x) \quad (5.5)$$

We remark that the selection of the minimum number of sensing elements $f_3(x)$ complements the criterion of error minimization $f_1(x)$ so that the optimal sensing elements are obtained to achieve an accurate pH prediction. In brief, these two objectives guide the search in the multi-objective algorithm to find those sensing elements that provide the best information and the best network performance. This is the main advantage of our multi-objective proposal for the problem addressed. Multi-objective hybrid training of neural networks has been tested previously obtaining better results than manual training [39,43,44], with the advantage of low time consumption.

The criterion $f_2(x)$ to minimize the network complexity has two complementary goals. On one hand, networks with a large number of neurons are not desired for two reasons: a) may not be trained correctly due to limitations of the classic gradient-based training algorithms and could become trapped in local optima with low performance, and b) may learn training data features that cannot

be generalized to the test and validation data sets. This last situation is called over-fitting. On the other hand, small networks do not have a powerful computation capability and cannot learn the data correctly. In combination with the criterion $f_1(x)$, our multi-objective approach is able to provide networks with the minimum complexity necessary to achieve a high performance, always under the Pareto optimality criterion.

The selection of the neural network parameters to be optimized is a key aspect for the evaluation of the earlier objectives. According to the objectives described in equations 5.2-5.5, the network weights and biases must be optimized to minimize the pH prediction error, as well as the number of neurons at the hidden and input layers to optimize the number of sensing elements in the array and the network complexity, respectively. With these considerations, the network representation in this approach is as follows:

1. A matrix W of real numbers and size $(N^0+N^1)*(N^1+N^2)$ encoding the network weights, where N^0, N^1 and N^2 stand for the maximum number of inputs, neurons in the hidden layer, and network outputs, respectively. A component at column j and row i is the weight from neuron j to neuron i.

2. A vector B of real numbers and size (N^1+N^2) with the biases of the neurons in the hidden and output layers.

3. A vector *I* with binary values and size N^0 to encode the active and inactive membranes used for the prediction.

4. A vector *H* with binary values and size N^1 to encode the active and inactive hidden neurons. The components of this vector and the previous one have value 1 if the corresponding input/neuron is active, and value 0 otherwise.

Figure 5.2 shows an example of a neural network whose representation is given by equation 5.6. This network has a maximum number of 3 inputs, 5 hidden neurons and 1 output. The inputs 1 and 3, and the hidden neurons 2, 3, 4 are inactive. The same representation scheme may be used to model other network structures beyond multilayer perceptrons.

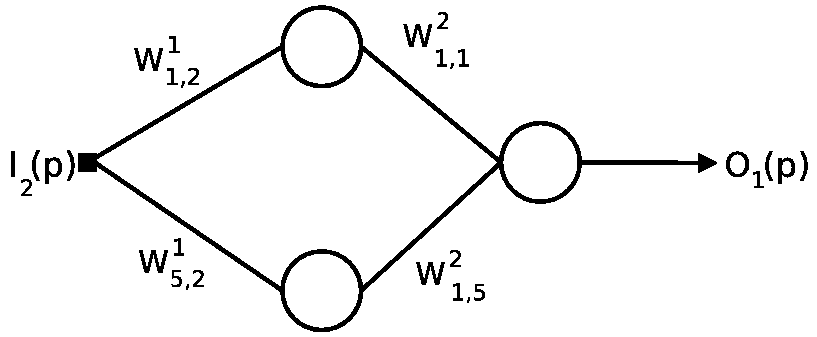

Figure 5.2. Network represented in equation 5.6

$$
W = \begin{matrix}
w^1_{1,1} & w^1_{1,2} & w^1_{1,3} & 0 & 0 & 0 & 0 & 0 \\
w^1_{2,1} & w^1_{2,2} & w^1_{2,3} & 0 & 0 & 0 & 0 & 0 \\
w^1_{3,1} & w^1_{3,2} & w^1_{3,3} & 0 & 0 & 0 & 0 & 0 \\
w^1_{4,1} & w^1_{4,2} & w^1_{4,3} & 0 & 0 & 0 & 0 & 0 \\
w^1_{5,1} & w^1_{5,2} & w^1_{5,3} & 0 & 0 & 0 & 0 & 0 \\
0 & 0 & 0 & w^2_{1,1} & w^2_{1,2} & w^2_{1,3} & w^2_{1,4} & w^2_{1,5}
\end{matrix} \quad (5.6)
$$

$$B = \begin{Bmatrix} b^1_1 & b^1_2 & b^1_3 & b^1_4 & b^1_5 & b^2_1 \end{Bmatrix}$$

$$I = \{0 \quad 1 \quad 0\}$$

$$H = \{1 \quad 0 \quad 0 \quad 0 \quad 1\}$$

An adaptation of the NSGA-II multi-objective genetic algorithm [42], hybridized with the Levenberg-Marquardt (LM) non-linear optimization method, is used to select the minimum number of sensing elements to be included in the sensor array and to optimize the neural network with the previous representation. This hybridation strategy has been previously tested in neural network optimization problems [25,28,29,43,44]. In particular, this work adapts an earlier approach that was developed for recurrent neural networks [33]. The crossover and mutation genetic operators developed have been adapted to the Multilayer Perceptron network model; however, their operation remains the same.

The proposed hybrid method returns a set of trained optimal networks and proposals for sensor arrays, in the sense of Pareto optimality. After that, the second step in the experimentation is the selection of the best solution obtained and its validation in real water samples.

3. Results and Discussion

3.1. Analytical parameters and experiment fundamentals

The HSV color space is an alternative representation of color derived from the red, green, and blue intensity values of the RGB space. A pixel in this color space is defined by its Hue (H), Saturation (S) and Value (V) coordinates. The main feature of the HSV color space is the representation of the cognitive color information in a single parameter, the hue component or H. It has been shown before that the H value is stable, simple to calculate, and easily obtained from commercial devices, maintaining a superior precision with variations in indicator concentration, sensor thickness, detector spectral responsivity and illumination [34]. Thus, the main reason to use H, that only considers hue variations of sensing elements and not intensity variations, connected to S and V coordinates, is to avoid problems such as dye leaching or lot-to-lot variations. The evolution of S and V components with pH for different membranes was studied, observing small variations except in some cases, and in general they do not contribute to improve the results. Furthermore, the use of the parameters S and V involve a more complex treatment and a high consumption of computational time. In contrast to other approaches that use the RGB color space to achieve the pH prediction [7], our proposal to use the parameter H provides the additional advantage of the degression of the parameter space from three dependent variables to only one.

The calibration data were obtained separately for each sensing element from the microwell plate, covering the pH range from 0 to 14 to discover the hue and pH ranges that are useful for prediction. The information obtained from some sensing elements provides more than one active range, and may also overlap to other sensing element information. This overlapping is useful for managing noisy data during the hue value acquisition as well as redundant data to improve the model's accuracy. The following sections show how the proposed calibration method is able to selectively remove the number of sensing elements to reduce the size of the array, also assuming an increase in the pH prediction error.

3.2. Experimental calibration of pH sensing elements

The 11 pH candidate sensing elements were prepared on the above-described support containing 12 microwells (4 rows x 3 columns) with 1.2 mL capacity each by casting a volume of each cocktail into the corresponding microwell. The analytical parameter used for the pH sensing elements was the H coordinate.

The experiments for calibration purposes for pH from 0 to 14 were performed using 12 replicate microwell plates, each containing the 11 pH membranes indicated above. The H variation was obtained for each 0.1-0.2 pH unit by adding various concentrations of HCl or NaOH solutions to an aqueous solution with the microwell plate hung from a support and, after equilibration, imaging the sensing elements with the scanner. The experimental results for each membrane (figure 5.3) show the usual sigmoidal shape.

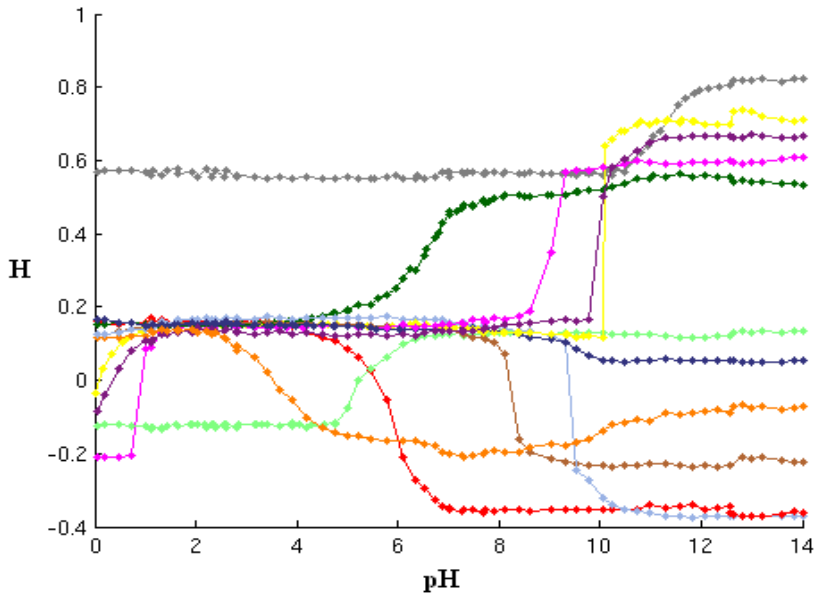

Figure 5.3. Calibration data measured for each sensing element in pH range from 0 to 14. Colour code used (membranes 1-11, see table 1): yellow, orange, red, pink, light green, dark green, brown, light blue, dark blue, purple, and grey

The acid-base indicators immobilized in the membranes belong to neutral, cationic and anionic types and the heterogeneous reaction with acids or bases in membrane phase involve both ion-exchange and co-extraction

mechanisms characterized by the equilibrium constant K_e. Table 5.1 shows the changes in color or colors for each membrane next to their H variation and the corresponding K_e values.

Table 5.1. Characteristics of pH candidate sensing elements

Membrane	Indicator	pH range	K_e	H coordinate	
				Acid	Base
1	m-Cresol purple	0.0-1.5	$4.9 \cdot 10^{0}$	0.964	0.151
		8.5-10.5	$2.8 \cdot 10^{-9}$	0.129	0.679
2	Purpurin	2.0-5.0	$2.0 \cdot 10^{-3}$	0.132	0.848
		5.5-7.5	$9.4 \cdot 10^{-7}$	0.841	0.893
		8.0-11.5	$7.3 \cdot 10^{-10}$	0.806	0.909
3	Alizarin	4.0-7.0	$1.4 \cdot 10^{-5}$	0.149	0.649
4	Thymol blue	0.6-2.0	$3.7 \cdot 10^{0}$	0.796	0.147
		7.5-9.5	$1.3 \cdot 10^{-8}$	0.168	0.576
5	Sicomet red P	4.5-6.5	$7.1 \cdot 10^{-5}$	0.879	0.122
6	Bromothymol blue	5.0-8.0	$7.1 \cdot 10^{-6}$	0.186	0.497
7	Phenol red	7.0-9.3	$1.2 \cdot 10^{-8}$	0.135	0.779
8	Cresol red	8.6-10.6	$4.3 \cdot 10^{-9}$	0.134	0.644
9	PAN	7.5-10.0	$3.4 \cdot 10^{-9}$	0.145	0.062
10	Thymol blue	0.0-1.6	$1.5 \cdot 10^{0}$	0.913	0.132
		9.5-11.2	$3.7 \cdot 10^{-9}$	0.165	0.663
11	Liphophilized Nile blue	10.5-12.0	$1.3 \cdot 10^{-10}$	0.572	0.796

3.3. Sensing elements minimization

3.3.1. Multi-objective optimization of sensor array

The hue response data in respect to the pH from the 11 candidate sensing elements were used to find the minimum number of membranes that can be selected to achieve an accurate pH prediction by a neural network. The experimental data set used was obtained from 961 pairs of values (Hue, pH) measured in the laboratory for each sensing membrane, equally distributed along the full pH range. These values were used to build the calibration data containing

1400 training samples with 12 dimensions: 11 hue values matched with the corresponding sensing elements, and the remaining one with the pH associated with these hues. Another additional data set was used to validate the network performance. The validation set contains 70 data samples with the hue of the 11 membranes and its corresponding pH measured with the pH-meter. The hybrid NSGA-II optimization algorithm was then executed with the following parameters:

- Bounds for the number of hidden neurons: 2 (minimum) and 11 (maximum).
- Bounds for the number of sensing membranes considered: 1 (minimum) and 11 (maximum).
- Bounds for network biases and weights: [-10, 10].
- Number of layers of the neural networks: 1 (input), 1 (hidden), 1 (output).
- Mutation probability: 0.2 (number of sensing membranes used), 0.2 (number of hidden neurons), 0.2 (network weights), 0.1 (mutation per gene).
- Population size: 100.
- Number of algorithm generations: 700.
- Number of local search iterations with Levenberg-Marquardt: 15.

The algorithm was executed 30 times to better explore the solution space and to obtain a wider Pareto front. Cross-validation was not applied since the training data set is large and covers the full pH range. The data space was uniformly sampled and the networks were able to learn the features of the entire space. Furthermore, over-fitting is controlled with the objective $f_2(x)$, so that the inclusion of the cross-validation technique into our approach does not provide significant improvements and, on the other hand, may slow the computer experimental time.

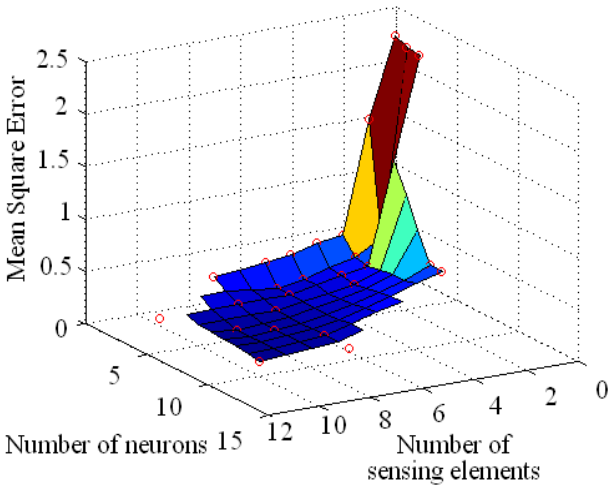

Figure. 5.4. Pareto front obtained: approximate surface covering the whole Pareto front

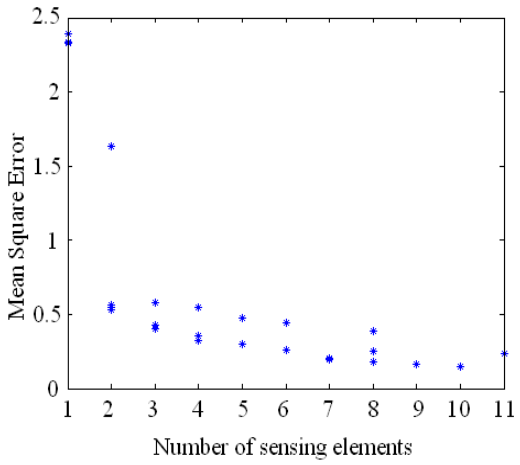

Figure. 5.5. Pareto front obtained: slice of the Pareto surface for the number of sensing elements and MSE

27 non-dominated solutions were found in the overall process, according to the criteria of minimization of the maximum network prediction error, minimum number of sensing elements used and minimum number of neurons in the neural network. These results are summarized in figures 5.4–5.7. Figure 5.4 shows the approximated Pareto surface, where the non-dominated solutions found have been highlighted with a circle. The remaining figures describe the Pareto front solution in 2-D, considering every pair of criteria to be optimized. An inverse relationship between the calibration error and the number of proposed

sensing elements to be used for pH prediction and the network complexity is observed, since the prediction error decreases when either the network complexity or the number of sensing elements used for the prediction increase (figures 5.5 and 5.7). Additionally, the high dispersion of the points in figure 5.6 suggests that there are no relevant dependencies or correlations between the network complexity and the number of selected sensing elements for the solutions obtained.

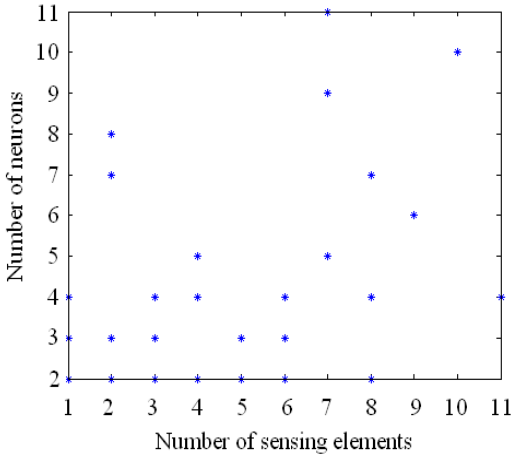

Figure 5.6. Pareto front obtained: slice of the Pareto surface for the number of sensing elements and neurons

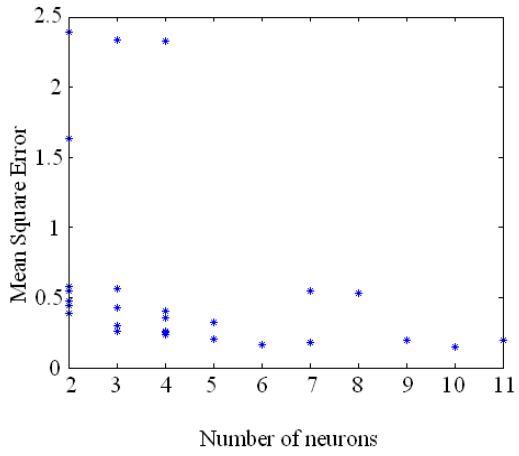

Figure. 5.7. Pareto front obtained: slice of the Pareto surface for the number of neurons and MSE

Table 5.2 describes the neural networks obtained in depth. The first column is an identification number for each network, and columns 2-4 contain the values of the optimized objectives. Finally, columns 5-6 show the MSE of each solution in the calibration and network validation data sets.

Table 5.2. Pareto front obtained with the hybrid NSGA-II algorithm

Solution	Maximum AE in calibration	Number of neurons	Sensing elements used	Calibration MSE	Validation MSE
1	0.179	5	2, 3, 4, 6, 9, 10, 11	0.003	0.091
2	0.576	2	2, 4, 5	0.046	0.071
3	0.192	7	1, 2, 3, 4, 6, 8, 9, 11	0.003	0.039
4	0.447	2	2, 4, 6, 9, 10, 11	0.021	0.097
5	0.302	3	2, 3, 4, 7, 10	0.015	0.058
6	0.261	3	2, 3, 4, 7, 9, 10	0.010	0.062
7	0.261	4	2, 3, 4, 7, 9, 10	0.010	0.062
8	0.324	5	2, 4, 7, 10	0.010	0.093
9	0.391	2	1, 2, 3, 4, 6, 7, 9, 11	0.012	0.281
10	0.232	4	2, 3, 4, 5, 6, 9, 10, 11	0.004	0.025
11	0.547	2	2, 3, 4, 11	0.036	0.062
12	0.566	3	2, 4	0.043	0.110
13	0.477	2	2, 4, 6, 10, 11	0.032	0.105
14	0.199	4	1, 2, 3, 4, 5, 6, 7, 8, 9, 10, 11	0.004	0.036
15	0.532	8	2, 4	0.016	45796.000
16	0.353	4	2, 4, 6, 10	0.012	0.065
17	0.126	11	1, 2, 4, 5, 7, 10, 11	0.001	0.058
18	0.128	9	1, 2, 4, 5, 7, 10, 11	0.001	0.058
19	0.547	7	2, 4	0.019	0.161
20	2.336	3	6	0.723	0.734
21	2.332	4	6	0.722	0.734
22	0.400	4	2, 4, 9	0.015	0.720
23	0.129	10	1, 2, 3, 4, 5, 7, 8, 9, 10, 11	0.001	0.173
24	2.388	2	6	0.754	0.776
25	0.186	6	2, 3, 4, 5, 6, 7, 8, 10, 11	0.002	0.115
26	1.635	2	4, 5	0.327	0.374
27	0.429	3	2, 3, 4	0.030	0.401

These values are included so that the average performance of the networks and their generalization capabilities can be measured. Considering the

minimum error criterion, solution 17 provided a maximum error in the calibration data of 0.126, using the maximum network complexity and 7 sensing elements. However, although the calibration error is small, the network complexity is too high and its generalization capabilities are not suitable. This may be checked against the MSE validation data, which is very high when compared with the MSE calibration. Considering the criterion of minimum network complexity, the networks with optimum value in this objective (solutions 2, 4, 9, 13, 24 and 26) provide a poor prediction performance, regardless of the number of sensing elements used. It is possible to conclude that the complexity of these networks is not sufficient to learn the calibration data correctly. Finally, focusing on the criterion to obtain the minimum number of sensing elements for the prediction, all the solutions obtained conclude that the membranes at position 6 provide the best option, although the prediction error is very high as well. In summary, the extreme optimal solutions are not suitable to solve the problem addressed, and other additional criterion must be taken into account to select the best approach. Therefore, intermediate solutions that provide non-optimal but suitable prediction performance, with low complexity and a different number of sensing elements required for the prediction were considered. The most interesting solution can be focused on solutions 3 for the following analysis due to its high generalization capabilities, and 16 and 19 because of the lower number of sensing elements used in respect to the other solutions. Although the MSE in the validation set increases with respect to solution 3 for these 16 and 19 solutions, the number of sensing elements used is drastically reduced to 4 and 2, respectively. Figure 5.8 presents the active regions of the sensing elements used in these networks to support the previous results and to study the selected sensing elements. The membranes in positions 2 and 4 are common to the three solutions. While membrane 2 provides a different hue response throughout the whole pH range, membrane 4 is used to distinguish between ranges where membrane 2 may provide the same hue value. The remaining membranes in the solutions contribute redundant information that is relevant to produce accurate pH prediction.

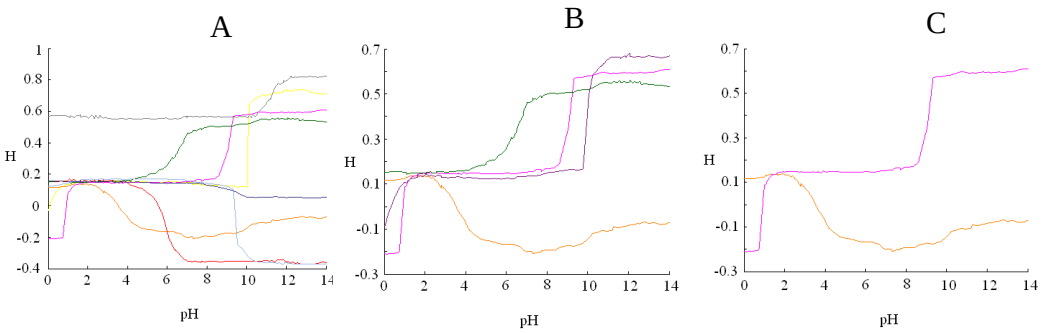

Figure 5.8. H evolution respect to pH of the sensing elements used by the selected solutions in the pH range 0-14. A: Solution 3; B: Solution 16; C: Solution 19

3.3.2. Performance of the selected neural networks

In this section, the selected neural networks (solutions 3, 16 and 19) provided by the multi-objective optimization method are studied considering their prediction performance in the validation data.

First, a Student's t-test with a 95% confidence level was applied over the reference and predicted pH values by each neural network for the validation data set, to check if the data distributions are significantly different. The probability values obtained were 0.95 for solution 3, 0.94 for solution 16, and 0.93 for solution 19; thus it can be assumed that there are no significant differences between the data. After that, a Pearson correlation test was applied to check if the predicted values fit the real pH data (from potentiometry), for the three networks. The probability value resulting from the test was lower than $2.2 \cdot 10^{-16}$ in all cases; thus the correlation between the data can be assumed. To support these results, the determination coefficient R^2 was calculated, obtaining the correlation values of 0.9989, 0.9985 and 0.9976 for the three solutions, respectively. Figure 5.9A also supports these results with the regression line between the real and the predicted pH values. To finalize the analysis, figure 5.10A describes the residuals of the predictions measured, in pH units. The minimum error is achieved by solution 3, which uses 8 sensing elements to achieve the pH prediction. In contrast, figure 5.10A shows that solutions 16 and 19 may provide unsuitable predictions due to the loss of information from the missing membranes, and this fact increases the prediction error.

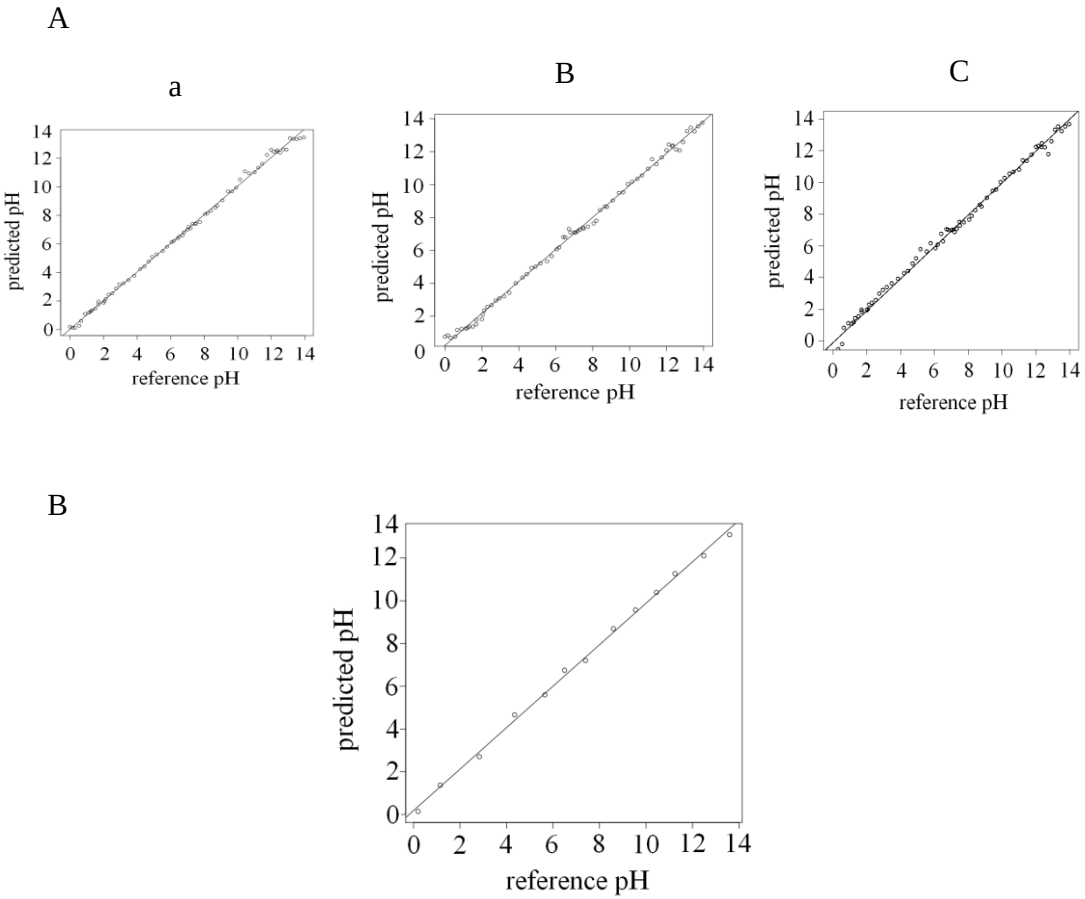

Figure 5.9. A: Regression lines for a) Solution 3; b) Solution 16; c) Solution 19, between the reference and predicted pH values in validation data set; B: Regression line between the reference and prediction pH values in real water samples using the proposed sensor array

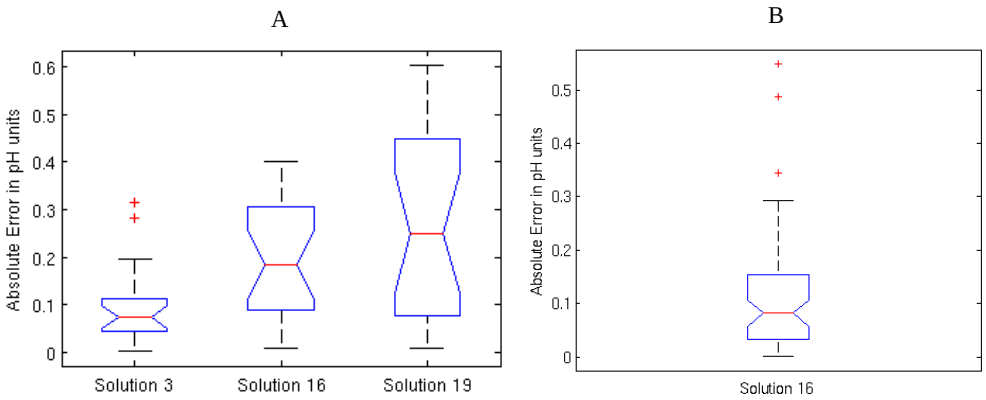

Figure 5.10. Box plot of the residuals for A: Solutions 3, 16 and 19 in validation data set; B: the proposed sensor array in real water samples

Finally, the performance of the selected solutions in both acid and basic pH ranges was tested, to find out whether there were statistical differences in the prediction error depending on the pH range. Table 5.3 shows the average of the absolute error (AE) of the solutions in both pH ranges (0, 7) and (7, 14), with the error standard deviation (SD). In order to check if there were significant differences between the prediction error in the selected pH ranges over the same network, an unpaired means t-test with a 95% confidence level was applied over the absolute error in both ranges for each solution. The probability values of 0.223, 0.139 and 0.152 for the three networks, respectively, were obtained. Thus, there are no significant differences for the prediction in both the acid and basic pH ranges for networks 3, 16 and 19.

Table 5.3. Average and standard deviation of absolute error of selected solutions in the working acid and basic pH ranges

Network	Acid Range		Basic Range	
	Average AE	SD	Average AE	SD
Solution 3	0.088	0.076	0.131	0.069
Solution 16	0.222	0.185	0.162	0.145
Solution 19	0.304	0.411	0.195	0.166

3.3.3. Selection of the sensing elements for the sensor array

This section discusses the selection of the sensing elements to minimize the initial candidate membranes, once the multi-objective algorithm has provided a set of minimized candidate sensor arrays and their corresponding trained neural networks have been validated. The relative frequency graph in figure 5.11 was built, to discover the selection frequency of each sensing element in the Pareto optimal solutions in table 5.2 and their relevance for an accurate pH prediction. The sensing elements that provide the best performance are included in more sensor arrays in the Pareto front than the other membranes that do not.

Three types of sensing elements can be distinguished according to their relevance: membranes 2 and 4 provide the most information for the prediction since their frequency is above 2/3 of the solutions in the Pareto front. On the

other hand, the membranes that are used in less than 1/3 of the solutions may be assumed to be the least relevant, as happens with membranes 1, 5, 8. The remaining sensing elements have a moderate relevance and they are used in between 1/3 and 2/3 of the solutions. Classifying them, the most relevant is the membrane at position 4, after that the membranes at positions 2, 10, and the membranes 3, 6 and 11 which share the same relevance. Finally, membranes 7, 9, 5, 1 and 8 are the least used and therefore the least relevant.

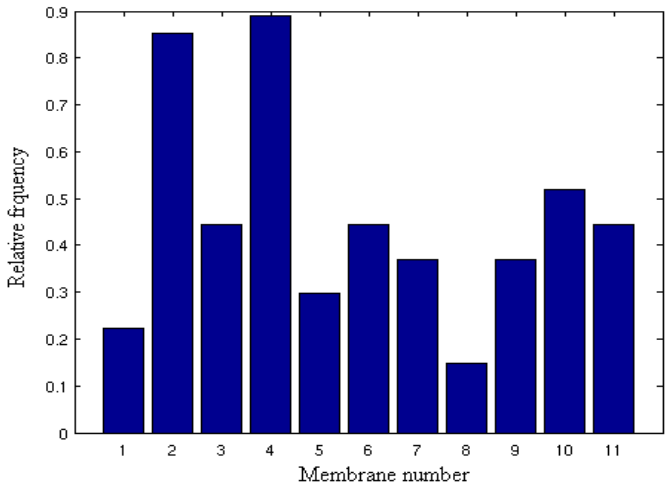

Figure 5.11. Relative frequency of the sensing elements used in the Pareto front solutions

According to the earlier analysis, the solution 16 (containing the sensing elements 2, 4, 6, 10) was selected, since is the minimized sensor array that provides the most accurate pH prediction. In addition, the neural network trained with the data from these membranes provides a MSE of 0.065 in the validation data set, while the MSE of the solution 19, which uses membranes 2 and 4 only, is 0.161. Solution 3 uses more sensing elements to provide a MSE of 0.039. Solution 16, then, provides a suitable balance between the number of sensing elements to be included in a minimized sensor array and the prediction accuracy and is thus proposed as the best choice. To support this choice, a t-test with a 95% confidence level was applied to check for any significant differences between the pH prediction error provided by solutions 3 and 16 in the validation data. A probability value of 0.99 was obtained, meaning that there are no

significant improvements in solution 3 and the use of the least number of sensing elements is sufficient to achieve a minimum prediction error.

3.4. Application to real water samples

In order to check the usefulness of the selected neural network 16, it was tested with real water samples (tap and river water from Granada, Spain) with the pH adjusted with acid and base, sampling the full pH range from 0 to 14. Samples 6 and 7 were taken from the Genil and Monachil rivers and were measured without any acid or base addition. The data set contained 13 data patterns with the hue of the sensing elements 2, 4, 6 and 10 in the minimized pH sensor array, and the water pH measured with the pH-meter as the reference method. A MSE of 0.052 and an absolute error, in pH units, of 0.176 was provided, with a standard deviation of 0.152.

The testing procedure followed was the same as for the validation data set. An unpaired means t-test with a 95% confidence level reported a probability value of 0.982, meaning that there are no significant differences between the predicted pH values and the real water pH measured with the pH-meter. After that, a Pearson correlation test was applied and the probability value $6.7 \cdot 10^{-16}$ was obtained, confirming the correlation. The determination coefficient R^2 calculated was 0.999, and figures 5.9B and 5.10B help to suggest a high positive correlation between the reference and predicted data.

The pH of each solution was measured using a standard potentiometric procedure to compare the results. Table 5.4 shows the results obtained using the single use sensor array described here and the network 16 compared to the results found by glass electrode potentiometry used as the reference method. This table includes the mean values from 12 determinations of each sample and the absolute error in pH units. According to the results in the table, the average absolute error in the prediction performance is 0.18 with a standard deviation of 0.15.

Table 5.4. pH determination in real water samples

Sample	Sensor array method		Potentiometric reference method	
	Predicted pH	AE	Measured pH	AE
1	0.14	0.060	0.196	0.004
2	1.40	0.219	1.149	0.001
3	2.70	0.126	2.830	0,001
4	4.70	0.311	4.350	0.001
5	5.60	0.051	5.647	0.003
6	6.75	0.250	6.510	0.010
7	7.20	0.198	7.400	0.001
8	8.69	0.093	8.630	0.030
9	9.57	0.018	9.554	0.004
10	10.39	0.059	10.451	0.001
11	11.27	0.020	11.240	0.011
12	12.10	0.380	12.489	0.001
13	13.10	0.505	13.593	0.007

3.5. Comparison with other optical approaches for pH

The operation of the multi-objective method developed here cannot be compared with any other work regarding optical sensors for pH prediction, because similar papers in the literature differ significantly both in methodology and goals from those used in this work. However, considering the prediction accuracy criterion alone, some comparative results with the performance of other methods can be provided.

Safavi and Bagheri [10] demonstrated that a sensor with two immobilized indicators can be used for this purpose by means of their absorbance spectra and Principal Component Analysis to reduce the dimensionality of the problem and the neural network as a prediction model. Depending on the network complexity, the MSE of the method varies between 0.03 and 0.04. Another proposal developed by us [38] for full pH range prediction based on a Sigmoid competition approach provided an MSE of 0.075 for tap and river water samples. Another relevant work based on optical sensors for pH prediction [14] uses the Generalized Reduced Gradient (GRG) to optimize a non-linear function that depends on RGB colour space parameters to achieve a MSE of 0.029. Other papers [12,15] find a similar performance in shorter pH ranges using reflectance spectra features as the analytical parameter.

With respect to previous works, our approach has the advantage of using the hue parameter H, which helps to reduce the dimensionality of the problem. For instance, the works based on RGB colour space use three analytical parameters for each indicator, while only the hue H is required in this work. In addition, comparing this proposal with the ones where the prediction model is based on reflectance spectra, this method has the advantage of low data pre-processing and a decrease in the data acquisition procedure.

The advantages of the proposed multi-objective optimization algorithm against traditional neural network training are considered. The best network structure obtained with the traditional trial-and-error procedure using the Levenberg-Marquardt training algorithm is made up of 11 input neurons, 10 hidden neurons and one output neuron for pH prediction provide an MSE of 0.043 [45].

4. Conclusions

In this work, a disposable sensor array for full-range pH determination has been developed using a set of immobilized colorimetric acid-base indicators in a transparent microwell plate that works by ion-exchange or coextraction mechanisms and based on color measurement from imaging techniques offering an easy-to-measure analytical signal. Neural networks are used for the prediction

model and the hue feature from the HSV color space provided by each sensing element is used as the analytical parameter.

The initial microwell plate made up of 11 sensing elements involves a more complex treatment and a high consumption of computational time, which could complicate the implementation of this optical procedure for pH in portable devices with low processing capacity. Consequently, the number of elements must be reduced, and our aim was not only to find the optimal sensing elements necessary to achieve a high prediction performance, but also to develop a prediction model with optimal network performance. To achieve these goals, a multi-objective hybrid genetic algorithm based on NSGA-II and the Levenberg-Marquardt non-linear optimization technique was developed.

Our approach has different advantages in both analysis and methodology. First, the use of the hue parameter helps to reduce the complexity of the analytical parameters which achieves a suitable prediction with respect to other approaches existing in the literature. It has also been shown that the optical sensor array developed is suitable to model the pH with respect to the hue analytical parameter. Regarding the calibration method developed for neural networks, three objectives were achieved simultaneously: obtaining the optimal network performance, the optimal structure and the minimum number of sensing elements needed to achieve high prediction accuracy. This methodology has also been compared with the classic trial-and-error procedure to train and find the optimal structure of neural networks. A non-differentiable error criterion that cannot be applied using traditional non-linear optimization methods to train neural networks was proposed. It has been shown that this could help to overcome local optima being included in hybrid genetic algorithms.

In conclusion, a prediction method based on a sensor array in which only 4 sensing elements and 4 hidden neurons are required to achieve a suitable prediction with an MSE of 0.052 in real water samples is proposed. At this time, the development of small, hand-held, battery-operated instruments that will include developed algorithms to work with captured imaging data is being researched.

Acknowledgements

We acknowledge financial support from the *Ministerio de Ciencia e Innovación, Dirección General de Investigación y Gestión del Plan Nacional de I+D+i* (Spain) (Projects CTQ2009-14428-C02-01 and CTQ2009-14428-C02-02); and the *Junta de Andalucía* (*Proyecto de Excelencia* P08-FQM-3535). These projects were partially supported by European Regional Development Funds (ERDF).

References

[1] J. Janata. *Do Optical Sensors Really Measure pH?* Anal. Chem., 59 (1987) 1351-1356.

[2] L.Y. Heng, T.H. Fang, H.L. Chern, M. Ahmad. *Influence of Methacrylic-Acrylic Copolymer Composition on Plasticiser-free Optode Films for pH Sensors*. Sensors, 3 (2003) 83-90.

[3] P. Hashemi, R.A. Zarjani, M.M. Abolghasemi, A. Olin. *Agarose film coated glass slides for preparation of pH optical sensors*. Sens. Actuators B, 121 (2007) 396-400.

[4] M. Bacci, F. Baldini, A.M. Scheggi. *Spectrophotometric investigations on immobilized acid-base indicators*. Anal. Chim. Acta, 207 (1988) 343-348.

[5] A.A. Ensafi, A. Kazemzadeh. *Optical pH Sensor Based On Chemical Modification of Polymer Film*. Microchem. J., 63 (1999) 381-388.

[6] F.B.M. Suah, M. Ahmad, M.N. Taib. *Optimization of the range of an optical fiber pH sensor using feed-forward artificial neural network*. Sens. Actuators B, 90 (2003) 175-181.

[7] A. Safavi, A. Rostamzadeh, S. Maesum. *Wide range pH measurements using a single H^+-selective chromoionophore and a time-based flow method*. Talanta, 68 (2006) 1469-1473.

[8] S. de Marcos, C. Asensio, I. Urunuela, F. Gallarta, J. Galban, J.R. Castillo. *New approaches to polyaniline optical sensors: pH, acetic acid and ammonia determination*. Quim. Anal., 19 (2000) 99-104.

[9] S. de Marcos, O.S. Wolfbeis. *Optical Sensing of pH Based on Polypyrrole Films*. Anal. Chim. Acta, 334 (1996) 149-153.

[10] A. Safavi, M. Bagheri. *Novel optical pH sensor for high and low pH values*. Sens. Actuators B, 90 (2003) 143-150.

[11] P. Hashemi, R.A. Zarjani. *A wide range pH optical sensor with mixture of Neutral Red and thionin immobilized on an agarose film coated glass slide*. Sens. Actuators B, 135 (2008) 112-115.

[12] J. Lin, D. Liu. *An optical pH sensor with a linear response over a broad range*. Anal. Chim. Acta, 408 (2000) 49-55.

[13] J. Arregui, M. Otano, C. Fernandez-Valdivielso, I.R. Matias. *An experimental study about the utilization of Liquicoat® solutions for the fabrication of pH optical fiber sensors*. Sens. Actuators B, 87 (2002) 289-295.

[14] A. Abbaspour, M.A. Mehrgardi, A. Noori, M.A. Kamyabi, A. Khalafi-Nezhad, M.N. Soltani Rad. *Speciation of iron(II), iron(III) and full-range pH monitoring using paptode: A simple colorimetric method as an appropriate alternative for optodes*. Sens. Actuators B, 113 (2006) 857-865.

[15] A. Safavi, N. Maleki, A. Rostamzadeh, S. Maesum. *CCD camera full range pH sensor array*. Talanta, 71 (2007) 498-501.

[16] S. Haykin. *Neural Networks: A comprehensive foundation*. Prentice Hall, Upper Saddle River, NJ, USA (1999).

[17] Y. Bengio, P. Simard, P. Frasconi. *Learning long-term dependencies with gradient descent is difficult*. IEEE T. Neural Networ., 5 (1994) 157-166.

[18] T. Bäck, D. Fogel, Z. Michalewicz. *Handbook of Evolutionary Computation*. Oxford Univ. Press, New York, USA (1997).

[19] C.H. Chang, C.C. Liu, C.G. Wen. *Integrating semianalytical and genetic algorithms to retrieve the constituents of water bodies from remote sensing of ocean color*. Opt. Express, 15 (2007) 252-265.

[20] S.K. Ghorai, D. Kumar, B.K. Hura. *Strain measurement in a Mach-Zehnder fiber interferometer using genetic algorithm*. Sens. Actuators A, 122 (2005) 215-221.

[21] A. Gill, K. Peters, M. Studer. *Genetic algorithm for the reconstruction of Bragg grating sensor strain profiles*. Meas. Sci. Technol., 15 (2004) 1877-1884.

[22] H.C. Cheng, J.F. Huang, Y.L. Lo. *Simultaneous strain and temperature distribution sensing using two fiber Bragg grating pairs and a genetic algorithm*. Opt. Fiber Technol., 12 (2006) 340-349.

[23] C.Z. Shi, C.C. Chan, W. Jin, Y. B. Liao, Y. Zhou, M.S. Demokan. *Improving the performance of a FBG sensor network using a genetic algorithm*. Sens. Actuators A, 107 (2003) 57-61.

[24] G. Cormier, R. Boudreau, S. Theriault. *Real-coded genetic algorithm for Bragg grating parameter synthesis*. J. Opt. Soc. Am. B, 18 (2001) 1771-1776.

[25] M. Delgado, M.C. Pegalajar, M.P. Cuéllar. *Memetic Evolutionary Training for Recurrent Neural Networks: An application to time-series prediction*. Expert Syst., 23 (2006) 99-117.

[26] K. Ku, M. Mak. *Exploring the effects of lamarckian and baldwinian learning in evolving recurrent neural networks*. Proc. of the IEEE International Conference on Evolutionary Computation (1997) 617-621.

[27] P. Moscato, C.C. Porras. *An introduction to memetic algorithms*. Metaheuristics, 2 (2003) 131-148.

[28] J.E. Fieldsend, S. Singh. *Pareto Evolutionary Neural Networks*. IEEE T. Neural Networ., 16 (2005) 338-354.

[29] M. Delgado, M.C. Pegalajar. *A multiobjective genetic algorithm for obtaining the optimal size of a recurrent neural network for grammatical inference*. Patt. Recog., 38 (2005) 1444-1456.

[30] C.A. Coello Coello. *An Updated Survey of GA-Based Multiobjective Optimization Techniques*. ACM Computing Surveys, New York, USA (2000) 109-143.

[31] C.A. Coello Coello, D.A. Van Veldhuizen, G.B. Lamont. *Evolutionary Algorithms for Solving Multi-Objective Problems*. Kluwer Academic Publishers, New York, USA (2002).

[32] Y. Jin. *Multi-objective machine learning*. Springer, New York, USA (2006).

[33] M. Delgado, M.P. Cuéllar, M.C. Pegalajar. *Multiobjective Hybrid optimization and training of Recurrent Neural Networks*. IEEE T. Syst. Man Cyb. B, 38 (2008) 1-25.

[34] K. Cantrell, M.M. Erenas, I. de Orbe-Payá, L.F. Capitan-Vallvey. *Use of the Hue Parameter of the Hue, Saturation, Value Color Space As a Quantitative Analytical Parameter for Bitonal Optical Sensors*. Anal. Chem., 82 (2010) 531-542.

[35] M. Guidorzi, M. Franchini, S. Alvisi. *A multi-objective approach for detecting and responding to accidental and intentional contamination events in water distribution systems*. Urban Water J., 6 (2009) 115-135.

[36] D.A. Sarigiannis, M. Saisana. *Multi-objective optimization of air quality monitoring*. Environ. Monit. Assess., 136 (2008) 87-99.

[37] V. Gamerith, D. Muschalla, P. Konemann, G. Gruber. *Pollution load modelling in sewer systems: an approach of combining long term online sensor data with multi-objective auto-calibration schemes*. Water Sci Technol., 59 (2009) 73-79.

[38] S. Capel-Cuevas, M.P. Cuéllar, I. de Orbe Payá, M.C. Pegalajar, LF. Capitán-Vallvey, Full-range optical pH sensor based on imaging techniques. Anal. Chim. Acta, 681 (2010) 71-81.

[39] M.P. Cuéllar, M.M. Erenas, M.C. Pegalajar, I. de Orbe-Payá, L.F. Capitán-Vallvey. *Automatic Colour feature extraction from disposable optical sensors*. Proc. International Workshop on Multivariate Image Analysis, Valencia, Spain (2009) 45.

[40] D.A. Forsyth, J. Ponce. *Computer Vision: A Modern Approach.* Prentice Hall, Upper Saddle River, NJ, USA (2002).

[41] A.R. Smith. *Color gamut transform pairs*. Proceedings of the 5th Annual Conference on Computer Graphics and Interactive Techniques (1978) 12-19.

[42] K. Deb, A. Pratap, A. Agarwaland, T. Meyarivan. *A fast and elitist multiobjective genetic algorithm: Nsga-II*. IEEE T. Evolut. Comput., 6 (2002) 182-197.

[43] R. Prudencio, T. Ludemir. *Neural network hybrid learning: Genetic algorithms and Levenberg-Marquardt*. Proc. 26th Annu. Conf. Gesellschaft for Classifikation, (2003) 617-621.

[44] H.A. Abbass. *A Memetic Pareto Evolutionary Approach to Artificial Neural Networks*. Australian Joint Conference on Artificial Intelligence. Lecture Notes in Artificial Intelligence. Springer, 2256 (2001) 1-12.

[45] S. Capel-Cuevas, M.P. Cuéllar, I. de Orbe-Payá, M.C. Pegalajar, L.F. Capitán-Vallvey. *Full-range optical pH sensor array based on neural networks*. Microchem. J,. 97 (2011) 225-233.

3. CONCLUSIONES

El objetivo de este capítulo ha sido minimizar el número de elementos necesarios que componen la matriz sensora óptica para la medida de pH en rango completo, partiendo de la matriz anteriormente desarrollada de once elementos sensores. Las conclusiones principales derivadas del estudio son las siguientes:

- Se ha medido la variación de color frente al pH de los once elementos sensores que componen la matriz sensora inicial, obteniéndose el conjunto de datos de calibración. Para ello, se ha utilizado un escáner convencional para recoger la imagen de la matriz y a partir de ella el parámetro tonal (coordenada H) del espacio de color HSV.

- Con el fin de reducir la complejidad del tratamiento y el alto consumo computacional asociados a la matriz inicial, se ha desarrollado un modelo híbrido entre el algoritmo genético multi-objetivo NSGA-II y la técnica de optimización no lineal Levenberg-Marquardt. El objetivo no era sólo establecer el número y tipo de elementos sensores necesarios para llevar a cabo una buena predicción, sino también el desarrollo de un modelo de predicción con un rendimiento de red óptimo. Esta metodología se ha comparado con el procedimiento clásico de ensayo y error para entrenar y encontrar la estructura óptima de la red neuronal.

- El método híbrido propuesto ha generado un conjunto de ANN óptimas de acuerdo con el criterio de optimización de Pareto. Se ha seleccionado la solución del frente de Pareto que mejor se ajusta a los tres objetivos perseguidos: máximo rendimiento, estructura de ANN óptima y mínimo número de elementos sensores necesarios para conseguir una alta precisión de predicción.

- La matriz sensora óptima finalmente seleccionada sólo requiere 4 elementos sensores y 4 neuronas ocultas para conseguir una predicción con un MSE de 0,052 en muestras de aguas de grifo y río. Además, el modelo presenta las características adecuadas para ser implementado

en pequeños dispositivos portátiles con baja capacidad de procesamiento, los cuales también incluirán los algoritmos desarrollados para analizar los datos de las imágenes tomadas *in situ*.

CAPÍTULO 6

Sistema experto para la predicción de pH con una matriz sensora óptica desechable

"Without context, analysis and understanding… all data is just noise".

Lucian Randolph

1. INTRODUCCIÓN

Los sistemas expertos (ES) surgieron a mediados de los años sesenta. En ese momento se consideraba que bastaban unas pocas leyes de razonamiento, junto con potentes ordenadores, para producir resultados destacables. En ese sentido, Newell, Shaw y Simon[299] desarrollaron un programa denominado General Problem Solver (GPS), que podía trabajar con criptoaritmética, con el problema de las torres de Hanoi y con problemas similares, aunque no podía resolver problemas reales tales como un diagnóstico médico. Consecuentemente, algunos investigadores cambiaron el enfoque del problema hacia dominios específicos intentando simular el razonamiento de un experto humano. De esta manera nacieron los ES.

El proyecto DENDRAL tuvo sus orígenes en 1965 de la mano de Feigenbaum y Lederberg, quienes plantearon la posibilidad de usar los ordenadores para modelar el pensamiento científico. Fue el primer ES utilizado para propósitos reales, al margen de la investigación computacional. Durante una década aproximadamente el sistema tuvo cierto éxito entre químicos y biólogos, ya que permitía identificar estructuras químicas moleculares a partir de sus datos espectroscópicos. Realmente no se considera el precursor de los KBS; este papel se asignó a otro proyecto llamado MYCIN[300], un sistema que permitía identificar las posibles enfermedades que los microorganismos podían causar en la sangre y recomendar una terapia adecuada para dicha enfermedad. Así surgió EMYCIN (*MYCIN Essential*), con el que se construyeron los sistemas SACON (utilizado para estructuras de ingeniería), PUFF (para estudiar la función pulmonar) y GUIDON (para elegir tratamientos terapéuticos). Además de MYCIN, para calcular la incertidumbre asociada a las conclusiones se propusieron otros ES basados en la lógica difusa[301,302] y la teoría de la evidencia de Shafer[303]. Aunque MYCIN se desarrolló con posterioridad a DENDRAL, es considerado el pionero de los ES

[299] A. Newell, J.C. Shaw, H.A. Simon. *Chess-Playing Programs and the Problem of Complexity.* IBM J. Res. Dev., IBM Corp. Riverton, New York, 2(4) (1958) 320-335

[300] B.G. Buchanan, E.H. Shortliffe. *Rule-Based Expert Systems: The MYCIN Experiments of the Stanford Heuristic Programming Project*. Addison-Wesley, Reading, MA. (1984) pp. 754

[301] L.A. Zadeh. *The Role of Fuzzy Logic in the Management of Uncertainty in Expert Systems.* Fuzzy Set. Syst., 11 (1983) 199-227

[302] J.J. Buckley, W. Siler, D. Tucker. *A Fuzzy Expert System.* Fuzzy Set. Syst., 20 (1986) 1-16

[303] G. Shafer. *A Mathematical Theory of Evidence*. Princeton University Press, Princeton, NJ. (1976) pp. 297

porque introdujo la separación entre la base de conocimiento y el motor de inferencia.

En esa época se desarrollaron también los sistemas HERSAY, que intentaba identificar la palabra hablada, y PROSPECTOR[304], que utilizaba el teorema de Bayes para la exploración mineralógica. De este último derivó el *shell* KAS. Actualmente el término *shell* se emplea para referirse a aquellos programas que proveen una interfaz de usuario para acceder a los servicios del sistema operativo. Estos pueden ser gráficos o de texto simple, dependiendo del tipo de interfaz que empleen. Los *shells* están diseñados para facilitar la forma en que se ejecutan los distintos programas disponibles en el ordenador.

A partir de 1980 numerosas empresas de alta tecnología desarrollaron SE para su comercialización, como CASHVALUE, para evaluar proyectos de inversión, y VATIA, para asesorar acerca del IVA. A finales de los 90 y en los años posteriores se desarrollaron numerosas aplicaciones de estos sistemas en muchos campos[305,306]. Durkin[90] examinó unos 2.500 sistemas expertos y los clasificó por criterios, tales como áreas de aplicación, tareas realizadas, etc. Como se observa en la figura VI.1, la economía, la industria y la medicina fueron los campos en los que se utilizaron mayoritariamente este tipo de sistemas.

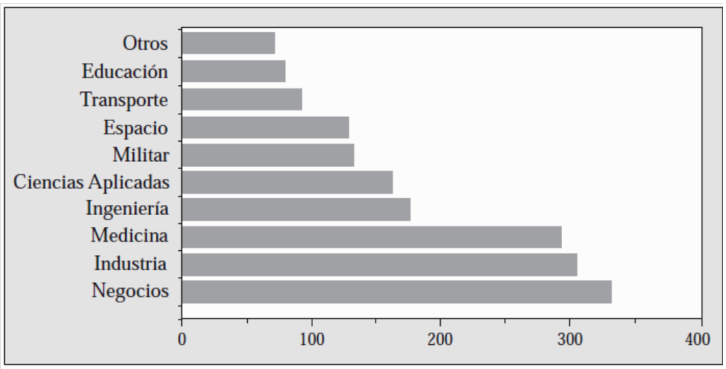

Figura VI.1. Campos de aplicación de los sistemas expertos[307]

[304] R.O. Duda, J.G. Gaschnig, P.E Hart. *Model Design in the Prospector Consultant System for Mineral Exploration.* Expert Systems in the Microelectronic Age. Edinburgh University Press, Edinburgh (1980) 153-167

[305] J. Quinlan. *Applications of Expert Systems.* Addison-Wesley, Reading, MA. Vol. 1 (1987) pp. 244

[306] J. Quinlan. *Applications of Expert Systems.* Addison-Wesley, Reading, MA. Vol. 2 (1989) pp. 408

[307] E. Castillo, J.M. Gutiérrez, A.S. Hadi, *Expert Systems and Probabilistic Network Models.* Springer-Verlag, New York, Inc. (1997) pp. 605

1.1. Los sistemas expertos en Química Analítica

La AI y, en particular, los ES, están desempeñando un papel importante en relación a la metodología e instrumentación analítica, y especialmente en análisis de alimentos. Algunos de estas aplicaciones son capaces incluso de seleccionar el procedimiento más adecuado disponible, diseñar un programa de trabajo y detectar y, en algunos casos reparar, funciones incorrectas.

Dentro del campo de la Química Analítica, la cromatografía es el área donde se ha aplicado mayoritariamente la tecnología de los ES. Se han descrito numerosas aplicaciones basadas en metodología analítica asistida por ordenador[308-340]. El proyecto ESCA comenzó en 1897 y fue subvencionado por el

[308] T. Hamoir, B. Bourguignon, D.L. Massart, H. Hindriks. *Model-Building for the Prediction of Initial Chromatographic Conditions in Pharmaceutical Analysis Using Reversed-Phase Liquid Chromatography.* J. Chromatogr., 633 (1993) 43-56

[309] B. Bourguignon, P. Vankeeberghen, D.L. Massart. *Crisebook, a Hypermedia Version of an Expert System for the Selection of Optimization Criteria in High Performance Liquid Chromatography.* J. Chromatogr., 592 (1992) 51-57

[310] G. Szepesi, K. Valko. *Prediction of Initial High Performance Liquid Chromatographic Conditions for Selectivity Optimization in Pharmaceutical Analysis by an Expert System Approach.* J. Chromatogr., 550 (1991) 87-100

[311] P.J. Schoenmakers, A. Bartha, H.A.H. Billiet. *Gradient Elution Methods for Predicting Isocratic Conditions*. J. Chromatogr., 550 (1991) 425-447

[312] J.A. van Leeuwen, B.G.M. Vandeginste, G. Kateman, M. Mulholland, A. Cleland. *An Expert System for the Choice of Factors for a Ruggedness Test in Liquid Chromatography.* Anal. Chim. Acta, 228 (1990) 145-153

[313] M. Mulholland, N. Dunand, A. Cleland, J.A. van Leeuwen, B.M.G. Vandeginste. *Expert System for Method Validation in Chromatography*. J. Chromatogr., 485 (1989) 283-296

[314] S.S. Williams, J.F. Karnicky, J.L. Excoffier, S.R. Abbott. *Expert System Program for Assistance in High Performance Liquid Chromatographic Method Development.* J. Chromatogr., 485 (1989) 267-281

[315] M. Desmet, G. Musch, A. Peeters, L. Buydens, D.L. Massart. *Expert System for the Selection of High Performance Liquid Chromatographic Methods for the Analysis of Drugs.* J. Chromatogr., 485 (1989) 237-253

[316] P.J. Schoenmakers, N. Dunand. *Explanations and Advices Provided by an Expert System for System Optimization in High Performance Liquid Chromatography.* J. Chromatogr., 485 (1989) 219-236

[317] P. Conti, T. Hamoir, M. DeSmet, H. Piryns, N. van den Driessche, F. Maris, H. Hindiks, P.J. Schoenmakers, D.L. Massart. *Integrating Expert Systems for High Performance Liquid Chromatographic Method Development.* Chemometr. Intell. Lab. Syst., 11 (1991) 27-35

[318] Y. Zhang, H. Zou, P. Lu. *Advances in Expert Systems for High Performance Liquid Chromatography*. J. Chromatogr., 515 (1990) 13-26

[319] R. Wehrens, L. Buydens, H. Hindriks, F. Maris. *Prediction of a Suitable Mobile Phase Composition in Reverse-phase High Performance Liquid Chromatography Using Fragmental Constants.* Chemometr. Intell. Lab. Syst., 25 (1994) 341-354

[320] R. Bach, J. Karnicky, S. Abbott. *Artificial Intelligence Application in Chemistry*. American Chemical Society: Washington, DC, ACS Symposium Series, 306(22) (1986) 278-296

[321] L. Buydens, P. Schoenmakers, F. Maris, H. Hindriks. *Expert Systems in Chromatography. Results from the ESCA project.* Anal. Chim. Acta, 272 (1993) 41-51

European Strategic Program for Research and Development in Information Technology (ESPRIT), dando lugar a la creación de un grupo internacional de expertos con el fin de demostrar la aplicabilidad de los ES en HPLC y

[322] M. Mulholland, N. Walker, F. Maris, H. Hindriks, L. Buydens, T. Blaffert, P.J. Schoenmakers. *Expert System for Repeatability Testing of High Performance Liquid Chromatographic Methods.* J. Chromatogr., 550 (1991) 257-266

[323] F. Maris, R. Hindriks, J. Vink, A. Peeters, N. van den Driessche, L. Massart. *Validation of an Expert System for the Selection of Initial High Performance Liquid Chromatographic Conditions for the Analysis of Basic Drugs.* J. Chromatogr., 506 (1990) 211-221

[324] L.M.C. Buydens, J.A. van Leeuwan, M. Mulholland, B.G.G. Vandeginste, G. Kateman. *An Expert System for the Validation of High Performance Liquid Chromatographic Methods.* Trends Anal. Chem., 9 (1990) 58-62

[325] J.A. van Leeuwan, L.M.C. Buydens, B.G.M. Vandeginste, G. Kateman. *Expert System for Precision Testing Validation of Liquid Chromatographic Methods.* Anal. Chim. Acta, 235 (1990) 27-40

[326] J.A. van Leeuwan, L.M.C. Buydens, B.G.M. Vandeginste, G. Kateman, P.J. Schoenmakers, M. Mulholland. *RES, an Expert System for the Setup and Interpretation of a Ruggedness Test in HPLC Method Validation. Part 2. The Rugdeness Expert System.* Chemometr. Intell. Lab. Syst., 11 (1991) 37-55

[327] J.A. van Leeuwan, L.C.M. Buydens, B.G.M. Vandeginste, G. Kateman, A. Cleland, M. Mulholland, C. Jasen, F.A. Maris, P.H. Hoogkamer, J.H.M. van den Berg. *RES, an Expert System for the Setup and Interpretation of a Ruggedness Test in HPLC Method Validation. Part 3. The Evaluation.* Chemometr. Intell. Lab. Syst., 11 (1991) 161-174

[328] M. Mulholland, P.R. Haddad, D.B. Hibbert. *Expert Systems for Ion Chromatographic Methods Using Dynamically Coate Ion-interaction Separation.* J. Chromatogr., 602 (1992) 9-14

[329] I. Ruisanchez, M.S. Larrechi, F.X. Rius, M. Esteban. *Computeraided Voltametric Method Development Employing a Knowledgebased Expert System.* Trends Anal. Chem. 111 (1992) 135-142

[330] M. Esteban, I. Ruisanchez, M.S. Larrechi, F.X. Rius. *Expert System for the Voltametric Determination of Trace Metals. 1. Determination of Copper, Zinc, Cadmium, Lead, and Indium.* Anal. Chim. Acta, 268 (1992) 95-105

[331] M. Esteban, I. Ruisanchez, M.S. Larrechi, F.X. Rius. *Expert System for the Voltametric Determination of Trace Metals. 2. Methods for Determining Nickle, Cobalt, and Thallium at Different Concentration Ratios.* Anal. Chim. Acta, 268 (1992) 107-114

[332] M. Esteban, C. Arino, I. Ruisanchez, M.S. Larrechi, F.X. Rius. *Expert System for the Voltametric Determination of Trace Metals. 3. Methods for Determining Mercury, Selenium and Vanadium*. Anal. Chim. Acta, 284 (1993) 435-443

[333] M. Esteban, C. Arino, I. Ruisanchez, M.S. Larrechi, F.X. Rius. *Expert System for the Voltametric Determination of Trace Metals. 4. Methods for Speciation of Chromium and Arsenic.* Anal. Chim. Acta, 285 (1994) 193-208

[334] M. Esteban, C. Arino, I. Ruisanchez, M.S. Larrechi, F.X. Rius. *Expert System for the Voltametric Determination of Trace Metals. 5. Methods for Determining Total Iron, Maganese(II), Aluminum and Titanium.* Anal. Chim. Acta, 285 (1994) 377-389

[335] L. Buydens, M. Detaevernier, D. Tombeur, D.L. Massart. *An Expert System for the Development of Analytical Procedures: UV Spectrophotometric Determination of Pharmaceutically Active Substance in Tablets.* Chemometr. Intell. Lab. Syst. 1 (1986) 99-108

[336] P.R. Martz, M. Heffron, O. Griffth. *Artificial Intelligence Application in Chemistry.* American Chemical Society: Washington, DC, ACS Symposium Series 306(23) (1986) 297

[337] C.P. Cheng, Y.C. Liang. *OPSAESsOrganic Pollutants Sampling and Analysis Expert System*. J. Chinese Chem. Soc., 41 (1994) 89-95

[338] L.M.L. Nollet. *Food Analysis by HPLC*. 2nd edition, Marcel Dekker, New York (2000)

[339] I. Molnar, L.R. Snyder, J.W. Dolan. *Reversed-phase gradient elution: How to get better results with less work.* LC-GC Int., 11 (1998) 374-387

[340] N. Gros, B. Gorenc. *Expert system for the ion-chromatographic determination of alkali and alkaline-earth metals in mineral waters.* J. Chromatogr. A, 697 (1995) 31

obteniéndose como resultado un conjunto de módulos sub-sistema[319,321-327]. Otro ejemplo fue la aplicación a la determinación voltamperométrica de trazas de un amplio rango de metales, utilizando KES para llevar a cabo el análisis electroquímico, tanto cualitativo como cuantitativo[329-334].

En cuanto a la aplicación de ES en el análisis de alimentos, se pueden distinguir dos grupos de aplicaciones bien definidas: a) la determinación de parámetros químicos y físico-químicos en muestras simples de alimentos y b) la monitorización de determinados analitos durante el proceso de producción del alimento. En general, el propósito de su implantación en laboratorios de análisis químico, tanto para control de calidad como para investigación, ha sido conseguir el mayor grado de automatización posible de un determinado proceso. Para ello, en primer lugar se desarrollan los sistemas expertos en laboratorios de investigación, y una vez han sido comprobados y validados, se incorporan a los laboratorios de control de calidad en industrias alimentarias, convirtiéndose tanto en sistemas de un solo usuario (centralizados) como multi-usuario (distribuidos).

En 1997, Chow *et al.*[341] desarrollaron un sistema inteligente automático de monitorización de amoníaco basado en un electrodo selectivo comercial de este analito usado en un sistema FIA. El sistema puede ser utilizado en conjunción con sensores de oxígeno disuelto y temperatura, llevándose a cabo la monitorización y el control de los diversos sensores para conseguir una calidad óptima de agua usada en acuicultura.

Matheson[342] propuso un sistema automático para reproducir las etapas de un método de análisis manual de grasa en productos lácteos (método gravimétrico estándar Röse Gottlieb). Para el análisis microbiológico de alimentos, Gordon[343] presentó en 1998 un ES organizado jerárquicamente usando factores epidemiológicos tales como la variedad de maíz, el estrés de la planta y la susceptibilidad a la infección, la localización geográfica y las condiciones de almacenamiento, además de los datos analíticos, para predecir la

[341] C.W. Chow, D.E. Davey, D.E. Mulcahy. *An intelligent sensor system for the determination of ammonia using flow injection analysis.* Lab. Autom. Inf. Manage., 33(1) (1997) 17-27

[342] A.R. Matheson, P. Otten. *Automation of the Rose Gottlieb method for fat determination in dairy products using an expert system.* Am. Lab., 31(6) (1999) 13-16, 18-19

[343] S.H. Gordon, B.C. Wheeler, R.B. Schudy, D.T. Wicklow, R.V.J. Greene. *Neural network pattern recognition of photoacoustic FTIR spectra and knowledge-based techniques for detection of mycotoxigenic fungi in food grains.* J. Food Prot., 61(2) (1998) 221-230

contaminación por *Aspergillus flavus* y otros hongos tóxicos que puede producirse en grano de cereal.

El aceite de oliva ha sido clasificado atendiendo a diferentes parámetros. En 1998 se analizaron mediante NMR[344] (600 MHz) 55 muestras de aceite de oliva virgen procedentes de cuatro regiones italianas y de diferentes variedades de aceituna, procediéndose a su clasificación mediante PCA. Sin embargo, previamente ya se había intentado diferenciar este producto de otro similar, distinguiendo entre aceite de oliva y otros aceites vegetales. El método SEXIA[345] se basó en un ES cuyas reglas se construyeron de forma independiente, de manera que cada propuesta está relacionada con un parámetro químico, una relación entre parámetros o una ecuación que permita distinguir entre categorías diferentes.

Una de las mayores contribuciones al análisis automático de alimentos fue el desarrollo de un sistema digestor de microondas[346]. Se ensayó en cinco tipos diferentes de alimentos y el resultado fue satisfactorio, a excepción de matrices ricas en grasa y azúcar, como el chocolate. Por su parte, Fischer[347] utilizó un sistema basado en el conocimiento para determinar las condiciones óptimas en la extracción con fluidos supercríticos de diversos ácidos grasos libres, como mirístico, palmítico, esteárico, oleico y linoleico procedentes de semillas de soja y algodón. Rius *et al.*[348] desarrollaron un ES para la determinación simultánea de calcio y magnesio en agua mediante SIA utilizando arsenazo III como reactivo cromogénico, mientras que Raptis *et al.*[349] evaluaron, en el año 2000, el aroma y el sabor de bebidas espirituosas griegas mediante redes neuronales y sistemas de lógica difusa.

---

[344] R. Sacchi, L. Mannina, P. Fiordiponti, P. Barone, L. Paolillo, M. Patumi, A. Segre. *Characterization of Italian extra virgin olive oils using ^1H NMR spectroscopy.* J. Agric. Food Chem., 46(10) (1998) 3947-3951

[345] M.V. Alonso, R. Aparicio. *Characterization of european virgin olive oil using fatty acids.* Grasas y Aceites, 44 (1993) 18-24

[346] M. Feinberg, C. Suard, R.J. Ireland. *Development of a fully automated open vessel focused microwave digestion system.* Chemometr. Intell. Lab. Syst., 22(1) (1994) 37-47

[347] M. Fischer, T.M. Jefferies. *Optimization of Supercritical Fluid Conditions for the Rapid Determination of Free Fatty Acids in Soy and Cottonseed Meals.* J. Agric. Food Chem. 43 (1995) 1259-1266

[348] A. Rius, M.P. Callao, F.X. Rius. *Self-configuration of sequential injection analytical systems.* Anal. Chim. Acta, 316(1) (1995) 27-37

[349] C.G. Raptis, C.I. Siettos, C.T. Kiranoudis, G.V. Bafas. *Classification of Aged Wine Distillates using Fuzzy and Neural Network Systems.* J. Food Eng., 46 (2000) 267-275

Ade-Hall[350] estudió sistemas de visión inteligentes para analizar en tiempo real productos alimentarios (ALINSPEC). Los objetivos específicos del proyecto eran desarrollar un software para procesar datos e imágenes y, especialmente, un ES para análisis de carne utilizando como técnicas analíticas la espectroscopia visible, IR y rayos X.

En 1998, Linko[351] realizó una revisión acerca de las aplicaciones de los ES en la industria alimentaria, distinguiendo entre sistemas de algoritmos convencionales empleados tradicionalmente en la industria y los utilizados en años posteriores, basados en bases de conocimiento y técnicas tales como lógica difusa. Señaló la importancia de conocer las propiedades fisicoquímicas y químicas de los materiales y procesos alimenticios, para así clasificarlos en bancos de datos.

Sin embargo, debe destacarse que casi todas las aplicaciones descritas anteriormente no están limitadas a sus respectivos casos. De hecho, pueden ser utilizadas para la construcción de sistemas de monitorización de laboratorios para diversas aplicaciones; por ejemplo, en plantas piloto y en la monitorización on-line de procesado de alimentos y en industrias químicas[352].

Peris *et al.*[353] fueron los pioneros en la aplicación de ES a la fermentación de la uva, diseñando un sistema basado en reglas que determinaba on-line, por métodos de inyección en flujo, algunos parámetros químicos fundamentales. Debe destacarse que trabajos previos ya habían demostrado que el empleo de FIA como herramienta de monitorización de ciertos analitos durante el proceso de fermentación alcohólica era apropiado[354,355] y constituía un sistema relativamente barato para lograr buenos resultados, de modo que no era

---

[350] A. Ade-Hall. *Intelligent vision system for real-time automatic inspection of alimentary products (ALINSPEC).* R&D Report, Campden & Chorleywood Food Research Association, 31(12978) (1996) pp. 79

[351] S. Linko. *Expert systems-0 what can they do for the food industry?* Trends Food Sci. Tech., 9 (1998) 3-12

[352] A. Hopgood. Intelligent Systems for Engineers and Scientists, 2nd Edition, CRC Press, Boca Raton (2000) pp. 467

[353] M. Peris, R. Ors, A. Bonastre, P. Gil, J. Serrano. *Advanced application of rule nets to the automation of chemical analysis systems*. Anal. Chim. Acta, 354(1-3) (1997) 249-253

[354] K. Schügerl, L. Brandes, T. Dullau, K. Holzhauer-Rieger, S. Hotop, U. Huebner, X. Wu, W. Zhou. *Fermentation monitoring and control by on-line flow injection and liquid chromatography*. Anal. Chim. Acta, 249(1) (1991) 87-100

[355] G.D. Christian, J. Ruzicka. *The second coming of flow-injection analysis.* Anal. Chim. Acta, 261(1-2) (1992) 11-21

necesario recurrir a instrumentación sofisticada y costosa.

Por otra parte, los ES pueden considerarse un ejemplo de cooperación entre químicos, ingenieros computacionales e ingenieros industriales. Este es el caso de la monitorización on-line del contenido de etanol durante el proceso de fermentación alcohólica[356], basada en la oxidación del etanol por la nicotinamida, y catalizada por la alcohol deshidrogenasa.

Bonastre *et al.*[357] propusieron un ES distribuido para la monitorización del proceso de fermentación de malta mediante la determinación por inyección en flujo de acidez total, azúcares reductores, etanol y pH. Su configuración se basó principalmente en el uso de nodos distribuidos conectados por medio de una red, siendo capaz de adaptarse por sí mismo a diferentes situaciones.

---

[356] M. Peris, R. Ors, A. Bonastre, P. Gil. *Application of rule nets to temporal reasoning in the monitoring of a chemical analysis process.* Lab. Autom. Inf. Manage., 33(1) (1997) 49-54

[357] A. Bonastre, R. Ors, M. Peris. *Monitoring of a wort fermentation process by means of a distributed expert system.* Chemometr. Intell. Lab. Syst., 50(2) (2000) 235-242

2. OBJETIVOS

El objetivo general del trabajo desarrollado en este capítulo es:

- Aplicación de un ES para la predicción de pH a partir de la matriz sensora previamente desarrollada y como alternativa a otras técnicas utilizadas en capítulos anteriores, al objeto de solventar las limitaciones de éstas como, por ejemplo, la poca expresividad del funcionamiento de las ANN.

  Como se expone en el capítulo 3, previamente se ha empleado el método de regresión multivariante, el cual presenta requerimientos elevados en términos de memoria y velocidad del microprocesador, por lo que no es adecuado para su implementación en dispositivos electrónicos portátiles con bajos recursos. Por otra parte, el trabajo que se recoge en el capítulo 4 está basado en una ANN, cuyo comportamiento no puede explicarse de manera trivial y se describe habitualmente como el de una caja negra, la cual ante una entrada produce una determinada salida sin ser fácilmente explicable el por qué.

  Los objetivos particulares a alcanzar son:

- Empleo de un escáner que opere en modo transmisión para recoger la información de color de la matriz sensora tras reaccionar con el problema.

- Diseñar un ES que a partir de un conjunto de reglas permita seleccionar la función sigmoidal que mejor prediga el pH, considerando la variación de las coordenadas H respecto al pH de los once elementos sensores que componen la matriz. La base de conocimiento se construirá a partir de los datos de calibración del sistema.

- El ES debe ser fácilmente interpretado por el usuario, y sus reglas modificadas de forma sencilla, sin necesidad de recalibración para posteriores avances o cambios en el sistema.

- Validación del sistema de predicción de pH y medida en muestras de aguas tanto de grifo como naturales.

PUBLICACIÓN IV:

IEEE Sensors Journal, 12(5) (2012) 1197-1206
DOI: 10.1109/JSEN.2011.2168815

An Expert System for full pH range prediction using a disposable optical sensor array

S. Capel-Cuevas[a], M.P. Cuéllar[b], M.C. Pegalajar[b], I. de Orbe-Payá[a],
L.F. Capitán-Vallvey[a,*]

[a]Department of Analytical Chemistry.
[b]Department of Computer Science and Artificial Intelligence.
University of Granada, E-18071 Granada, Spain

Abstract

The design of optical sensor arrays encompasses tasks such as the acquisition of sensor optical parameters, as for example color features, and the calibration of a multivariate method to model the array global behavior. Different techniques have been used to model the sensor array responses, such as multivariate regression or neural networks, although they show certain limitations. The former methods require either high amount of computer memory or speed so therefore they are not suitable for implementation in portable electronic devices with low resources, while the later is a black box whose operation cannot be easily modeled and explained for industrial development validation. This work addresses these problems and proposes an expert system to overcome the previous drawbacks. The approach makes an accurate pH prediction, and it comprises a balance between memory and microprocessor speed for its integration within embedded systems with low memory and chip resources. In addition, it is also able to provide a high expressive explanation of why such prediction was made, so that the industrial validation is easier than using other proposals such as neural networks.

Keywords: Expert systems; Optical sensor array; Full pH range determination; H coordinate.

* Corresponding author; e-mail: lcapitan@ugr.es

1. Introduction

Chemical imaging combines standard digital imaging with spectroscopic techniques to provide the spatial distribution of sample components [1]. Chemical imaging with sensors use sensor arrays to monitor chemical species with a number of distributed selective chemical sensors providing spatial resolution [2]. Focusing on optical pH detection, the literature offers different solutions using sensor arrays [3]-[9], fluorescent excitation-ratiometric pH sensing dyes [10], and further fluorescent and fiber-optic pH sensors [11].

Multivariate calibration techniques have been used in previous works to solve the problem of the sensor array response modeling. Focusing on pH determination by means of optical sensors, on one hand we find linear and nonlinear regressions [4,9]. If the number of sensing elements in the array is small, some researchers offer simple regression formulae to model the sensor response [4]. However, as the number of sensors increases, more complex techniques such as multidimensional surface fit approaches are required [9]. In these cases, the approaches have the drawback of high computer memory or processor speed requirements, which makes difficult their implementation in small hand-held devices with low processor resources. On the other hand, other approaches such as neural networks are used when the sensor response functions are difficult to approximate, due to non-linearities in the sensor array outputs or high dimensionality of the problem [12]. However, their validation for industrial developments is often hard since the interpretation and modeling of the network behavior cannot be easily explained and correctly justified.

In this work, we propose an alternative approach to solve the previous limitations, which is also statistically equivalent to previous calibration techniques in terms of approximation accuracy. We develop an expert system [13,14] architecture to model the sensor array responses. The system operation is

described in two stages: first, the model calibration comprises the approximation of a set of candidate pH prediction functions that depends on the input optical parameters acquired from the sensing elements in the array, and the generation of a knowledge base to select the best candidate functions to achieve an accurate pH prediction. To be more precise, the knowledge base contains production rules of the form "*If <Optical parameters have some value> Then <Use the pH prediction function X>*" with a reliability degree of each rule. On the other hand, during the system use, the optical parameter values are fetched from the array and a reasoner module uses these values to infer the best pH prediction functions with a reliability degree that can be used to obtain an accurate pH approximation value. Finally, a predictor module coordinates the output of each pH prediction function selected by the reasoner to provide the pH prediction value.

In contrast to previous approaches in the literature, our proposal has the advantages of smaller computer memory and speed requirements than using multivariate regression techniques. The efficiency measured in computing time has complexity *O(n)* [15], where *n* is the number of rules in the knowledge base. The required memory depends on the number of rules obtained after the calibration, which is usually smaller than the required for the maintenance of a multidimensional surface in the computer memory. In comparison to neural networks, the validation of the expert system for industrial developments is easier in our proposal since the knowledge base contains high expressive rules and the pH prediction functions are verifiable by means of classic functional analysis methods. Further improvements are the modularity of the system, which can be upgraded or modified by an expert engineer without need of recalibration by simply modifying the knowledge base manually or replacing the pH prediction functions to improve the prediction accuracy.

2. Experimental

2.1. Reagents and materials

The acid-base indicators used for preparing the pH sensitive films were: 1-amino-4-hydroxyanthraquinone, sodium 3,3-[(1,1-biphenyl)-4,4-diyl(azo)] bis(4-

aminonaphtalenesulfonate), N-[4-[bis[4-(dimethylamino)phenyl]methylene]-2,5-cyclo-hexadien-1-ylidene]-N-methylmethanaminium chloride (crystal violet), 2-(1,3-dihydro-3-oxo-2H-indol-2-ylidene)-1,2-dihy-dro-3H-indol-3-one (indigotin blue), 2-[2-[4-(dimethylami-no)phenyl]diazenyl]benzoic acid (methyl red), 4,4'-(1,1-dioxide-3H-2,1-benzoxathiol-3-ylidene)bis[2-bromo-3-methyl-6-(1-methylethyl)phenol (bromothymol blue), 4,4'-(1,1-dioxide-3H-2,1-benzoxathiol-3-ylidene)bis[2-bromo-6-methyl-phenol (bromcresol purple), N,N'-[(1,1-dioxide-3H-2,1-benzoxathiol-3-ylidene)bis[(6-hydroxy-5-methyl-3,1-phenylene)methylene]]bis[N-(carboxymethyl)-glycine (xylenol orange), 4,4'-(1,1-dioxide-3H-2,1-benzoxathiol-3-ylidene)bis-phenol (phenol red), 4,4'-(1,1-dioxide-3H-2,1-benzoxathiol-3-ylidene)bis[5-methyl-2-(1-methylethyl)phenol (thymol blue), 4,4'-(1,1-dioxide-3H-2,1-benzoxathiol-3-ylidene)bis[3-methylphenol] (m-cresol purple), N8,N8,3-trimethyl-2,8-phenazinediamine hydrochloride (neutral red) and 1-phenylazo-2-naphthol (sudan I), 1-(2-pyridylazo)-2-naphthol (PAN) from Sigma, (1,2-benzo-7-(diethylamino)-3-(octadecanoylimino) phenoxazine (liphophilized Nile blue), 9-(diethylamino)-5H-benzo[a]phenoxazin-5-one (Nile red), 1,2,4-trihydroxy-9,10-anthracenedione (purpurin) and 4-(2- pyridylazo)resorcinol (PAR) from Fluka (Fluka, Madrid, Spain), 4,4'-(1,1-dioxide-3H-2,1-benzoxathiol-3-ylidene)bis[2-methylphenol] (cresol red) from Panreac (Panreac, Barcelona, Spain), 1,2-dihydroxy-9,10-anthracenedione (alizarine) from TCI (TCI Europe, Belgium), calcium3-hydroxy-4-[2-(4-methyl-2-sulfophenyl)diazenyl]-2-naphthalenecarboxylate from BASF (BASF, Ludwigshafen, Germany), 1,4-dihydroxyanthraquinone and 1,5-dihydroxyanthraquinone from ICN (ICN K&K Laboratories, Plainview, NY, USA), 2,6-dihydroxyanthraquinone from EGA (EGA Chemie, Steinheim, Germany). The rest of reagent used were: high molecular weight polyvinyl chloride (PVC), *o*-nitrophenyloctylether (NPOE), dioctyl sebacate (DOS), bis(1-butylpentyl)adipate (BBPA), tributyl phosphate (TBP), potassium tetrakis (4-chlorophenyl)borate (TCPB), tridodecylmethylammonium chloride (TDMAC), aliquat 336, cellulose acetate (CA), ethylenglycol and tetrahydrofuran (THF) all purchased from Sigma (Sigma-Aldrich Química S.A., Madrid, Spain). HCl and NaOH were supplied by Sigma. All reagents were of analytical reagent grade and were used without any further purification. All aqueous solutions were prepared in reverse-osmosis type quality water (Milli-RO 12 plus Milli-Q station from Millipore, conductivity 18.2 mS).

2.2. Instruments and software

A Microtek ScanMaker i900 scanner (Microtek, Taiwan) was used to acquire images of the different sensing elements. The software used to manage the scanner was Silver Fast Ai provided by Microteck. The images were processed with a set of scripts and functions developed by us in Matlab r2007b (The MathWorks, Inc, Natick, MA, USA). Statistical calculations were performed with Statgraphics software package (Manugistics Inc. and Statistical Graphics Corporation, USA, 1992), and Microsoft Excel (Microsoft Corp., Redmond, WA, USA) was used for general calculations.

A Crison pH-meter (Crison Instruments, Barcelona, Spain, model Basic 20) with a combined double junction glass electrode, calibrated against two standard buffer solutions (pH 4.0 and 7.0), was used for pH measurements.

2.3. Preparation of the sensor array

A 50 mm x 40 mm Mylar support covered by an adhesive and transparent PVC layer with 12 microwells of 5 mm of diameter each (1.2 μL volume) disposed in 3 columns and 4 rows was necessary to prepare the pH sensor array. The sensor array was cast by placing 8 μL of the corresponding reagents, whose surface tension and quick evaporation makes it possible to prepare the sensing membrane, and then placing them in a dryer with THF saturated atmosphere at room temperature to enable slow solvent evaporation. The different cocktails were prepared by dissolution in 1 mL of distilled THF in all the cases for the different chemicals needed according to composition indicated in table 6.1. According to this table, the array contains 11 sensing elements so that the remaining hole in the prototype Mylar support was unused.

Table 6.1. Composition of the membranes (% w/w) used for the pH sensor array preparation

Sensing element	Indicator (%)	Lipophilic salt (%)	Membrane polymer (%)	Plasticizer (%)	Humectant (%)
1	Thymol blue (5.00)	TDMAC (18.40)	CA (33.00)	DOS (28.00)	EG (15.60)
2	m-Cresol purple (3.00)	TDMAC (13.47)	DOS (28.00)	CA (33.00)	EG (22.57)
3	Thymol blue (3.14)	TDMAC (11.57)	CA (37.00)	DOS (28.00)	EG (20.43)
4	Purpurin (1.43)	TDMAC (8.29)	NPOE (67.00)	PVC (23.29)	–
5	Alizarin (1.43)	TDMAC (10.29)	PVC (21.3)	NPOE (67.00)	–
6	Sicomet red P (1.41)	Aliquat 336 (5.63)	PVC (26.76)	NPOE (66.20)	–
7	Bromothymol blue (3.00)	TDMAC (4.00)	CA (37.00)	DOS (28.00)	EG (19.60)
8	Phenol red (1.43)	TDMAC (6.93)	CA (30.00)	BBPA (26.00)	EG (35.64)
9	PAN (1.43)	TDMAC (10.00)	PVC (23.60)	NPOE (65.00)	–
10	Cresol red (1.43)	Aliquat 336 (4.54)	PVC (27.00)	NPOE (67.00)	–
11	Liphophilized Nile blue (1.43)	TCPB (3.63)	PVC (27.91)	TBP (67.00)	–

2.4. Response evaluation

The sensor array was introduced in an aqueous solution and the responses of the different sensing elements were evaluated modifying the pH by adding volumes of 1.0 M, 0.1 M or 0.01 M HCl or NaOH solutions with a microburette. A standard potentiometer was used to measure the pH of the solution after each addition of reagents and magnetic stirring. Each pH sensor array was equilibrated for 5 min; then it was pulled out and inserted into a holder to obtain the image of the sensor array with a transmission flatbed scanner. The resolution and color depth were set to 300 dpi for high resolution without membrane degradation and 48 to 24 bits of color, respectively.

2.5. Sensor array analytical parameter and treatment

The analytical parameters to achieve the pH prediction are acquired by means of image feature extraction methods from the optical sensing elements in the sensor array. In this work, the obtained images were stored in 24 bits uncompressed TIFF (True Image File Format) format, using the standard RGB color space. The scanner was calibrated before use with an IT8 calibration target to measure the performance of input devices and generate ICC (International Color Consortium) profiles.

We use the hue (H) feature from the HSV color space as analytical parameter. This parameter was proposed previously [16] and it provides advantages in respect to other color space features such as RGB, as the robustness to ambient light changes and the parameter complexity reduction in respect to similar RGB approaches that require three parameters (Red, Green, Blue) [7,8].

In our experiments, the H value of each sensing is extracted from the scanned image of the array using software developed in previous works [17] and applying the Canny's algorithm [18]. Finally, the mode of the H values for each sensing element thought the RGB to HSV color space transformation equations [16] is obtained.

3. Expert System architecture for pH prediction

3.1. General architecture design

We have designed general system architecture to model the response of a sensor array using an expert system [13]. Figure 6.1 describes the system architecture and the interaction between these modules.

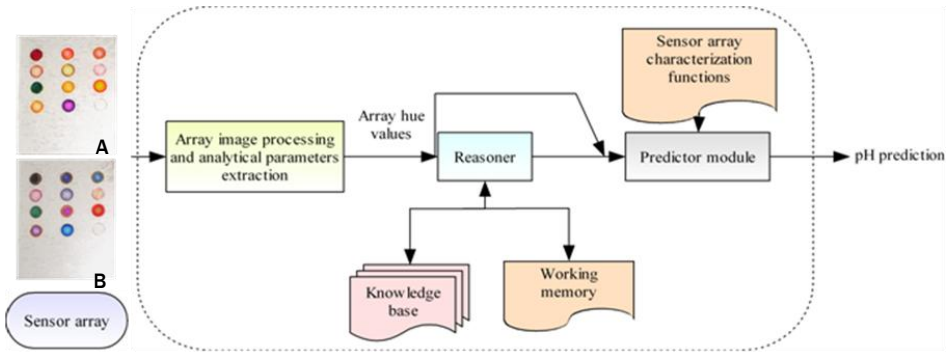

Figure 6.1. System design and interaction between modules. A: Initial sensor array B: Sensor array at pH=12.5

During the system use, the sensor array is input for the system, and each sensing element in the array is processed by imaging techniques to acquire the analytical parameters. In our experiments, we have used the Matlab r2007b image processing toolbox software to identify each sensing element in the 11 dimensional sensor array, and to extract the mode of their hue. After that, the sensing element H values extracted are used as input data for the reasoner module, which finds the rules in the knowledge base useful to find the best pH prediction functions by means of the reasoner. Then, this module returns a set of candidate pH prediction functions with a reliability degree, and the predictor integrates the results using a prediction function combination policy to provide the user with a pH approximation value from the H analytical parameters extracted. On the other hand, the calibration of the system requires only the characterization functions of the sensing elements in the array, and the generation of the knowledge base from a calibration data set.

3.2. Sensing elements characterization

The experiments for calibration between pH from 0 to 14 were performed using 12 replicate sensor arrays each containing the 11 pH membranes. The H variation was obtained each 0.1-0.2 pH unit by adding various concentrations of HCl or NaOH solutions to an aqueous solution with the array hung inside and, after equilibration, imaging the array with the scanner.

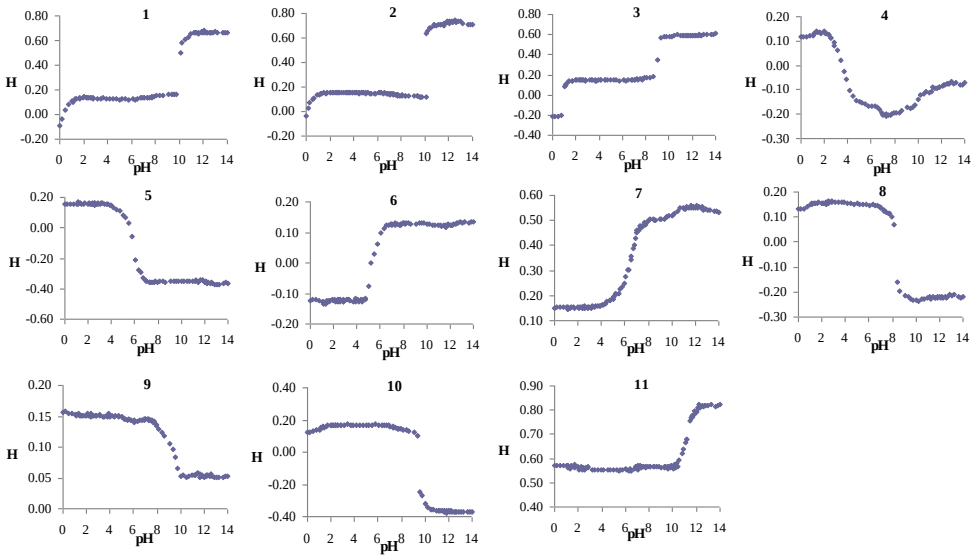

Figure 6.2. Calibration data measured for each sensing element in pH range from 0 to 14

According to the shape of the sensing elements response of figure 6.2, the hue provided from each sensing element in the array may be modeled with sigmoid-shape functions in a concrete pH range. Equation 6.1 describes the general sensing element characterization function, where z_i are parameters to be optimized for each prediction model, and x and H(x) stand for the pH and hue approximation values, respectively. The pH prediction function is obtained as its inverse.

$$H(x) = z_1 + \frac{z_2}{(1 + e^{z_3 x + z_4})^{z_5}} \tag{6.1}$$

A single sensing element may be modeled with one or more functions of this form, which may be overlapped. This is the reason that allows us to have more than one prediction function using the information from a single sensing element. After the sensor array data processing, we obtained 23 prediction functions from the 11 sensing elements. Table 6.2 describes the pH range and sensing element of each function, and the number of pairs of data pH/H measured in the laboratory for the function approximation.

Table 6.2. Number of sigmoid-shape functions to model each sensing element response, pH range of the functions, and number of calibration data used for their optimization

Sensing element	Function	pH range	Number of calibration data
1	1	[0.00, 5.77]	31
	2	[5.01, 14.00]	42
2	1	[0.00, 5.87]	44
	2	[5.87, 12.57]	51
	3	[12.31, 12.82]	4
	4	[12.82, 14.00]	7
3	1	[0.00, 5.77]	36
	2	[5.77, 14.00]	39
4	1	[0.00, 1.94]	12
	2	[1.10, 5.77]	26
	3	[5.45, 7.74]	14
	4	[7.00, 14.00]	26
5	1	[0.00, 12.57]	69
	2	[12.57, 14.00]	8
6	1	[0.00, 12.57]	80
	2	[12.57, 14.00]	8
7	1	[0.00, 9.05]	70
	2	[8.97, 12.57]	19
	3	[11.28, 14.00]	13
8	1	[0.48, 14.00]	67
9	1	[0.00, 14.00]	84
10	1	[0.00, 14.00]	69
11	1	[0.00, 14.00]	88

The calibration of the parameters z_i for each function was carried out using the Levenberg-Marquardt non-linear optimization method [19]. Finally, the calibrated parameters were stored into the sensor array characterization functions data base to be used by the predictor module for pH. The problem of pH determination is now stated as the selection of the function or functions that best can approximate the pH of the solution, based on the hue values acquired from the sensor array.

3.3. Sensor data discretization

In order to achieve high rule expressivity to ease the system validation and manipulation, the antecedent of the designed rules, i.e. the "if" area, are discretized in this work considering three possible states of a sensing element response: 1) *Inactive*, where its value is minimum, 2) *Active*, associated to the transition area, and 3) *Saturated*, associated to the area of a response whose value is maximum. With the discretization of the sensors state, the production rules of the knowledge base are of the form "*If sensing element S_1 is in state $E(S_1)$* and *sensing element S_2 is in state $E(S_2)$* and ... and *sensing element S_N is in state $E(S_N)$, then use the prediction function F_y from sensing element S_x with confidence level CL*", so that the interpretation of the system operation is eased for its validation and behavior tracking.

We say that a sensing element response is *active* if its H value is in a range where its variation ΔH is maximum in respect to the pH, i.e. the H value is between two threshold values [$\mu-\sigma$, $\mu+\sigma$]. On the other hand the sensing element would be *inactive* or *saturated* if its H value is under/over such range, respectively. To illustrate this idea, figure 6.3 shows an example of the calibration data used to model a sensing element (red dots), its characterization function in the pH range [0, 6] (blue line), and the description of the sensor states in the pH range.

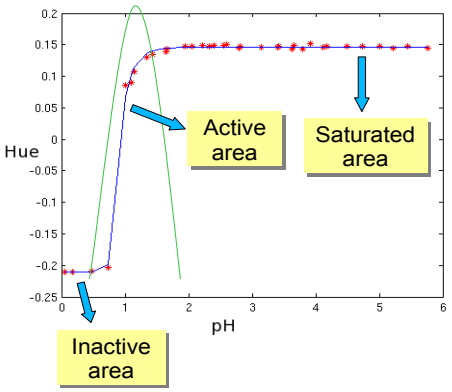

Figure 6.3. Description of the *active*, *inactive* and *saturated* sensing elements states. Red dots: sensing element response calibration data; blue line: response approximation function; green curve: Gaussian function to model the active area

Table 6.3. Number of sigmoid-shape functions to model each sensing elementresponse, and weight parameter used for the simulated annealing procedure

Sensing element	Function	*w* parameter
1	1	0.10
	2	0.30
2	1	0.05
	2	0.30
	3	0.07
	4	0.10
3	1	0.10
	2	0.30
4	1	0.01
	2	0.20
	3	0.30
	4	0.30
5	1	0.30
	2	0.07
6	1	0.10
	2	0.05
7	1	0.10
	2	0.10
	3	0.05
8	1	0.30
9	1	0.30
10	1	0.30
11	1	0.30

The problem of finding the *Active* area of a sensor response encompasses to find the widest H range [$\mu-\sigma$, $\mu+\sigma$] that provides the maximum accuracy for the pH prediction. Equation 6.2 shows these two criteria, to be minimized, where $E(\mu,\sigma)$ stands for the Mean Error of the points in the calibration data that belong to [$\mu-\sigma$, $\mu+\sigma$], and $P(\mu,\sigma)$ is the number of data discarded for their inclusion in the *active* state. The value *w* is a weight to penalize each point discarded, and it is a parameter for the function optimization. The value $E(\mu,\sigma)$ is used to maximize the active area prediction accuracy, while $P(\mu,\sigma)$ maximizes the sensor active area so that the full pH range is covered by all sensing elements in the array. $P(\mu,\sigma)$ is discrete, so that traditional optimization techniques cannot be applied since it is not differentiable. Instead, we used a Simulated Annealing [15] procedure with the weights *w* shown in table 6.3 to find the values μ and σ for each sensing element.

$$S^*(\mu,\sigma) = min\{S(\mu,\sigma)\} = min\{E(\mu,\sigma) + wP(\mu,\sigma)\} \quad (6.2)$$

3.4. Knowledge base generation

To build the knowledge base, we start from a calibration data table obtained by means of sampling each sensing element H value response in the pH range from 0 to 14 as shown in figure 6.2 and table 6.2.

The samples were taken with a precision of 0.01 pH units. After that, the H value of each sensing element in the table was discretized to the values *active*, *inactive* and *saturated*, following the criteria explained in the previous section. Thus, the resulting table has 1401 rows (calibration samples) and 12 columns. The first 11 columns describe the sensing element state of each sample, while the last one is the sensor characterization function that provides the best accuracy for the sample. Then, the table only contains discrete ordinal values and a simple Decision Tree extraction procedure such as ID3 [13,14] can be used to generate the knowledge base. We used the criterion of minimum information entropy to select the relevant sensors to be included in the tree. Figure 6.4 shows a synthesized example built to better illustrate how the rules are generated with ID3. We may observe that each tree branch is a rule, where the edges between nodes are matched with a sensing element, the intermediate nodes are the values of the sensing element state, and the leaf nodes is the sensor characterization function to be used for the pH value prediction.

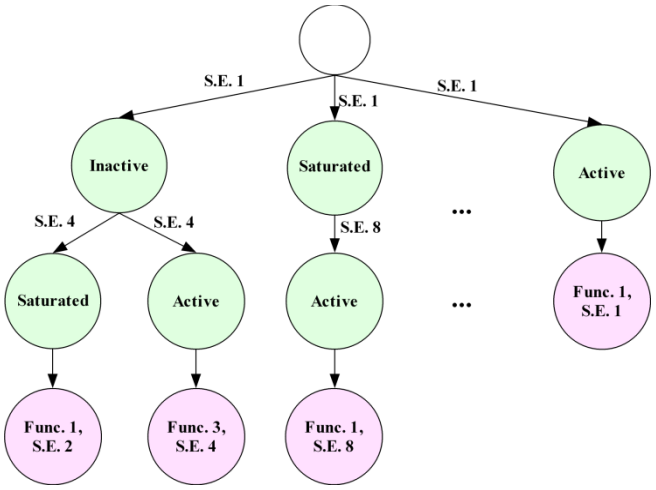

Figure 6.4. Example decision tree to generate the knowledge base

The tree in figure 6.4 describes four rules:

Rule 1: *If sensing element 1 is inactive and sensing element 4 is saturated then use the function 1 from sensing element 2.*

Rule 2: *If sensing element 1 is inactive and sensing element 4 is active then use the function 3 from sensing element 4.*

Rule 3: *If sensing element 1 is saturated and sensing element 8 is active then use the function 1 from sensing element 8.*

Rule 4: *If sensing element 1 is active then use the function 1 from sensing element 1.*

The confidence level *CL(r)* of each rule *r* is computed as the conditioned probability of the rule consequent in respect to the values of the rule premises in the calibration data. As an example, equation 6.3 shows how the confidence level of the previous rules is calculated.

$$\begin{aligned} CL(Rule1) &= P(function1, element2 \mid element1 = inactive and element4 = saturated) \\ CL(Rule2) &= P(function3, element4 \mid element1 = inactive and element4 = active) \\ CL(Rule3) &= P(function1, element8 \mid element1 = saturated and element8 = active) \\ CL(Rule4) &= P(function1, element1 \mid element1 = active) \end{aligned} \tag{6.3}$$

To generate the rules of the knowledge base, we followed the classic procedure described in [20]. 10 different decision trees were generated by mean of the removal of the attribute with the minimum entropy and applying ID3 iteratively. The rule extraction from these decision trees generated repeated and subsumed rules, which were removed in order to avoid unsuitable results during the reasoning stage as suggested in [20]. Finally, we obtained 487 rules to model the entire pH range and the sensing elements' responses, with an average size in the antecedents of 5.1 premises. This fact puts in manifest the simplicity of the rules in the system and the high speed of the rules evaluation by the reasoner.

3.5. Reasoning and prediction

The *reasoner module* receives the numeric H value from each sensing element in the array in the range [-1, 1], and its discrete value with label *active, inactive* or *saturated* according to the thresholds of each sensing element

previously calibrated. These labels are used to start the inference process to finally obtain a set of candidate pH prediction functions with their corresponding confidence level. In this work we have developed a fast and simple reasoner to achieve linear order efficiency [21], whose operation is detailed in the algorithm in table 6.4.

Table 6.4. Reasoning algorithm

```
Procedure Reasoner(S, ε)

Inputs:
        S- State of each sensing element
        ε- Minimum Confidence Level (CL) of a rule for its
consideration
Outputs:
        M- Set of prediction functions and their CL
Begin
        Initialize M=ø
        Put S in the working memory
        For each rule r in the Knowledge Base, do
                Put r in the working memory
                If (CL(r) < ε) Then
                        Discard r
                Else if (S contains A_r) Then
                  If M^C(r) is in the working memory then
      Update CL(M^C(r))
     Else
      Add M^C(r) to the working memory
      CL(M^C(r))=CL(r)
                   End-if-else
                End-if-else
        End-for
        Return {M}
End
```

In brief, the reasoner checks all the rules *r* in the knowledge base whose antecedent A_r is true for the sensing element states in *S*, and whose confidence level is over a threshold *ε*. The remaining rules are discarded for the inference process. The consequents of the selected rules $M^{C(r)}$ are added to the results to be returned. Finally, the confidence level $CL(M^{C(r)})$ of all the consequents $M^{C(r)}$ are updated iteratively each time it is found a rule *r* with such consequent according to equation 6.4.

$$CL(M^{C(r)}) = CL(M^{C(r)}) + CL(r)(1 - CL(M^{C(r)})) \quad (6.4)$$

The set of candidate prediction functions $M^{C(r)}$ returned by the *reasoner* are sent to the *predictor module* selects the calibration function with maximum confidence level $CL(M^{C(r)})$ and then calculates the pH with this function. Other possible prediction policy could be to use a weighted average of the pH predicted by some selected functions returned by the reasoner. We tested some variants of this approach in our experiments, but we finally discarded them due to the lower accuracy obtained in respect to the selected method.

4. Results and discussion

4.1. Analytical parameter

As an alternative representation of color derived from the RGB space, the HSV color space was chosen. The main feature of the HSV color space is the representation of the cognitive color information in a single parameter, the hue component or H. It has been shown before that the H value is stable, simple to calculate, and easily obtained from commercial devices, maintaining a superior precision with variations in indicator concentration, sensor thickness, detector spectral responsivity and illumination. Thus, the main reason to use H, that only considers hue variations of sensing elements and not intensity variations, connected to S and V coordinates, is to avoid problems such as dye leaching or lot-to-lot variations. The evolution of S and V components with pH for different sensing elements was studied (figure 6.5), observing small variations except in some cases, and in general they do not contribute to improve the results.

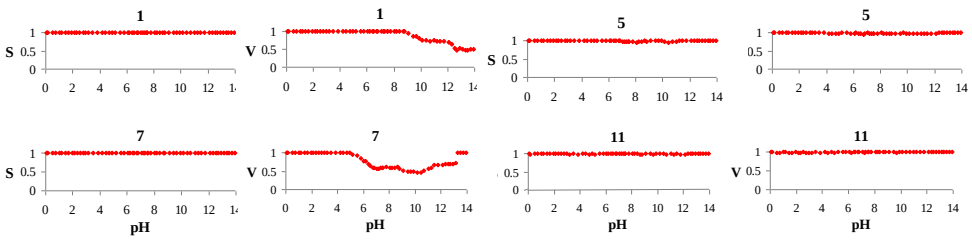

Figure 6.5. S and V evolution in respect to the pH for 4 sensing elements

On the other hand, the hue value from the sensing elements in the array is always acquired under the same environmental conditions of light and temperature in the scanner, so that no external sources can influence the data extraction in calibration, validation and test.

4.2. pH sensing elements selection

Sensor arrays were prepared containing colorimetric acid-base indicators selected according to the conditions of no leaching in the whole pH range studied, a change in the tonal color coordinate by the reaction and final covering the full pH range by overlapping between the responses of the different membranes.

Several colorimetric acid-base indicators were studied preparing different cocktails containing different types and amounts of polymers, plasticizers, lipophilic salts, and, if necessary, humectant. The composition of the different sensing elements was optimized considering leaching minimization (lipophilic salt, plasticizer, and membrane polymer), color intensity (acid-base indicator) and response time (plasticizer, membrane polymer, humectant and cocktail volume).

11 different membranes were selected to cover the whole pH range. The acid-base indicators immobilized in the membranes belong to neutral, cationic and anionic types and the heterogeneous reaction with acids or bases in membrane phase involve both ion-exchange and co-extraction mechanisms characterized by the equilibrium constant K_e [9].

4.3. Calibration, validation and test results

In this section we validate the approach over a validation data set containing 70 samples equally spaced covering the full pH range. In addition, the expert system is tested in 15 real water samples (tap and river water from Granada, Spain), with the pH adjusted with acid and base, also covering the pH range from 0 to 14. Samples 7 and 8 were taken from the Beiro and Monachil rivers and were measured without acid or base addition. A total number of 210 sensor arrays were used for the validation, to obtain three replicates of each sample, and 45 sensor arrays for the test. In respect to the results for pH

prediction, table 6.5 describes the average absolute error in the calibration, validation and test sets, its standard deviation and the Mean Square Error (MSE). We use the MSE measure for the later comparison with other techniques used for pH prediction using disposable optical sensors.

Table 6.5. Results obtained for pH prediction in the calibration, validation and test data sets

Data Set	Average Absolute Error (AE)	Standard Deviation of AE	Mean Square Error
Calibration	0.10	0.22	0.06
Validation	0.14	0.28	0.09
Test	0.15	0.26	0.08

A Student's t-test was applied with a confidence level of 95%. The tests returned a probability value of 0.95 and 0.96 for validation and test data set, respectively. These results suggest that there are no significant differences between the reference and predicted pH values in both data sets. Second, a Pearson correlation test was applied to check the pH prediction quality. The test results were under $2.2 \cdot 10^{-16}$ in the validation data set and $1.5 \cdot 10^{-14}$ in the water samples set, concluding in a correlation between the reference and predicted pH values. The determination coefficient R^2 was also calculated, and its value was 0.997 for the validation data and 0.998 for the test data. Figure 6.6 supports the results with the regression line between the real and predicted pH values for the validation data.

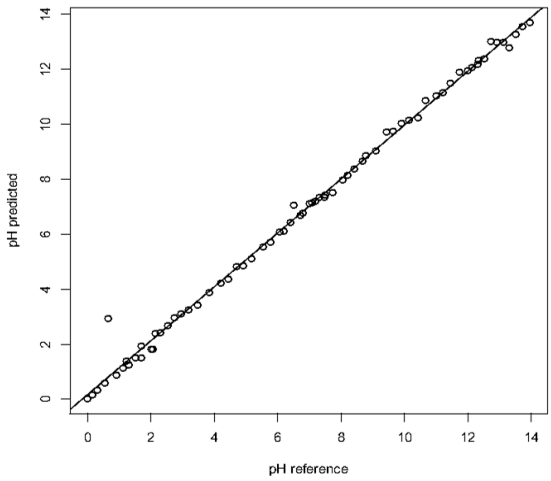

Figure 6.6. Regression line between the real and predictied pH values in the validation data set

In addition, we analyze the absolute error between the reference and predicted data with the box plots of figure 6.7 to support the previous conclusions. Considering the validation data set, we may observe the lowest error deviation in respect to the average absolute error. However, we also find outliers which provide an absolute error over 0.5. On the other hand, the average error in the test set is also low. However, in this case we did not find outliers, although the higher deviation of the error in respect to the mean value suggests that the precision is lower than the one obtained in the validation set.

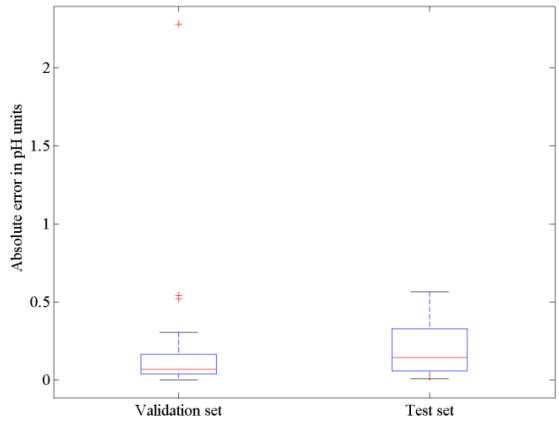

Figure 6.7. Box plots with the analysis of residuals for pH prediction values in the validation and in the test data sets

Additionally, we also measured the pH of each solution of the test data set using a standard potentiometric procedure as reference method to compare the results. Table 6.6 includes the mean values from the determinations of each sample and the absolute error. According to the results in the table, the average absolute error in the prediction performance is 0.157 with a standard deviation of 0.261.

We also applied a Pearson correlation test to study the differences between the predictions obtained with the standard potentiometric procedure and the expert system. The resulting correlation coefficient R^2 was 0.997, thus ensuring a high statistical correlation between the results.

Table 6.6. pH determination in real water samples

Sample	Expert system Predicted pH	Potentiometric reference method Measured pH	Absolute error
1	0.139	0.121	0.018
2	1.034	0.976	0.058
3	2.169	1.924	0.245
4	2.937	2.846	0.091
5	3.731	3.764	0.033
6	4.683	4.634	0.049
7	5.504	5.508	0.004
8	6.899	6.412	0.487
9	7.403	7.344	0.059
10	8.288	8.273	0.015
11	9.225	9.254	0.029
12	10.530	10.371	0.159
13	11.136	11.214	0.078
14	12.466	12.519	0.053
15	12.684	13.673	0.989

We also studied the robustness of the predicted values in the acid and basic pH ranges, to check if the accuracy differs significantly in both ranges. A Student's t-test with 95% of confidence level was applied over the absolute error

distributions in acid and basic ranges from 0 to 7 and from 7 to 14, in the validation data set. 35 pH samples were considered in each range. The probability value resulting from the test was 0.55, concluding that the prediction approach based on expert systems is robust since there are no significant differences in the error produced in either acid or basic range.

4.4. Comparison with other approaches in the literature

In this section, we compare the pH prediction results with previous approaches. There are two main techniques to model pH optical sensors in the literature. The first one uses linear and non-linear approximations of the sensor responses to finally predict the pH. The second one uses more complex non-linear function modeling techniques such as neural networks. Three approaches based on linear and sigmoid surface approximations to predict in the full pH range are presented [9]. The errors provided by these methods in real water samples are MSE of 0.11 (Linear surface fit approach), 0.27 (Sigmoid surface fit approach) and 0.07 (Sigmoid competition approach). These models suffer of some limitations: the Surface fit approaches require a high amount of computer memory to maintain the surfaces. On the other hand, the Sigmoid competition proposal is lower efficient in polynomial time and it consumes lower memory than the surface-based approaches.

The expert system developed in this work overcomes these limitations and provides and MSE of 0.08 in real water pH prediction. The only required memory is used to store the rules in the knowledge base, and the reasoner has an efficient linear time. Considering the design aspects, the expert system is preferable to the previous approaches since it consumes low computer resources and it would be more suitable for its implementation in portable devices. We compared the results of the prediction errors statistically with a Student's t-test with 95% of confidence level over the test data set, to know the real differences between the expert system and the described techniques. The result of the test was a 0.29 probability value in the comparison between the RBES and the Linear surface fit approach, 0.31 for the comparison with the Sigmoid surface fit approach, and 0.33 for the Sigmoid competition approach. None of these values

are under 0.05, so that we assume that there are no significant differences in the pH prediction using the expert system developed in this work or the approaches.

Second, we also tested the expert system performance with neural networks [12]. A Multilayer Perceptron [22] was trained with the calibration data to predict the pH in the full range. The network has 11 input neurons, one for each H value of a sensing element in the sensor array, 10 hidden neurons at the intermediate layer to process the input data, and one output neuron to provide the pH prediction. All the neurons at the first and hidden layers have sigmoid activations, while the neurons at the output layer has a linear activation and it provides the weighted sum of all neuron responses at the hidden layer. The network was trained with the Levenberg-Marquardt training algorithm for neural networks [19], with a stopping criterion of 1000 iterations left or to reach a MSE of 0.01 in calibration data. The MSE obtained by this network in the real water samples data set is 0.04. A Student's t-test was also used to compare the absolute errors of the pH prediction results between neural networks and the expert system, obtaining a probability value of 0.36. According to this value, neural networks and expert systems are the most similar approaches in respect to the pH prediction data distributions. However, the MSE is low using the neural network. Comparing the design aspects of both pH prediction approaches, we encounter that the neural network is a black box whose behavior is difficult to model and to predict by an industry engineer. They have been proven to be powerful tools to learn the calibration data and to predict the pH. In addition, their validation is hard for commercial applications. Moreover, a change in the number of sensing elements or pH range would require recalibrating the neural network model. In this sense, the expert system shows the advantage of being more expressive and easy to validate, since the rules in the knowledge base may be easily modified and understood by the user.

The works regarding optical sensors and full pH range prediction are not very usual in the literature. The papers usually focus in small and middle pH ranges and the development of accurate sensors and prediction models. However, the optical parameters used to model the sensors are wide. We find the use of the absorbance spectra and two indicators were used for full pH prediction in. In this case, the prediction model was a neural network trained with the parameters extracted from the spectra after a principal component analysis

procedure. The best accuracy provided by the model has a MSE of 0.03. Optical sensors for small and middle pH range were developed [4,23,24]. The best prediction model in this case is a non-linear function optimized with the generalized reduced gradient algorithm and using the RGB color space features as analytical parameters, providing an MSE of 0.03 [7]. Another interesting paper is [8], which uses a multi-linear function to predict the pH, using the RGB color space and five indicators in a middle pH range. The MSE of this approach is 0.05 with Partial Least Squares optimization algorithms and 0.04 with the generalized reduced gradient. The authors also tested the approach with neural networks, obtaining a MSE of 0.03.

5. Conclusions

We have described expert system for a full range pH prediction. The hue value from 11 elements in a colorimetric sensor array is used as analytical parameters to achieve the prediction. When the elements in the array were characterized, they showed a sigmoid-shape response of H in respect to the pH in different pH ranges. Thus, each sensing element was modeled with a set of sigmoid-shape functions operating in different pH ranges. The problem solved by the expert system is the selection of the sigmoid-shape function that can provide the best accuracy for the pH prediction with two requirements: a) to be computationally efficient so that the approach can be implemented in small hand-held electronic devices; and b) to be simple enough so that an industry validation could be done easily. In this way, the expert system developed contain rules with high expressivity that can be easily understood by an user, and these rules may be modified easily without need of recalibration for later developments or changes in the system. Our approach obtains a Mean Square Error of 0.08 in real water samples. Being compared with other techniques in the literature such as neural networks and linear or non-linear approximations, the expert system provides similar results with the advantages of high efficiency, simplicity and expressivity.

Acknowledgement

We acknowledge financial support from the Ministerio de Ciencia e Innovación, Dirección General de Investigación y Gestión del Plan Nacional de I+D+i (Spain) (Projects CTQ2009-14428-C02-01 and CTQ2009-14428-C02-02); and the Junta de Andalucía (Proyecto de Excelencia P08-FQM-3535). These projects were partially supported by European Regional Development Funds (ERDF).

References

[1] J. Workman, M. Koch, B. Lavine, R. Chrisman. *Process analytical chemistry*. Anal. Chem., 81(12) (2009) 4623-4643.

[2] W. Gopel. *Chemical imaging I, concepts and visions for electronic and bioelectronic noses*. Sens. Actuators B, 52 (1998) 125-142.

[3] M. del P. Taboada Sotomayor, M.A. de Paoli, W.A. de Oliveira. *Fiber-optic pH sensor based on poly(o-methoxyaniline)*. Anal. Chim. Acta, 353(2-3) (1997) 275-280.

[4] T. Seung, C. Yang. *Synthesis of Congo red linked with alkyl amide polymer and its optical ion-sensing property*. Pol. Bull., 42 (1999) 655-660.

[5] S. de Marcos, C. Asensio, I. Urunuela, F. Gallarta, J. Galban, J.R. Castillo. *New approaches to polyaniline optical sensors: pH, acetic acid and ammonia determination*. Quim. Anal., 19 (2000) 99-104.

[6] J. Lin, D. Liu. *An optical pH sensor with a linear response over a broad rang*. Anal. Chim. Acta, 408 (2000) 49-55.

[7] A. Abbaspour, M.A. Mehrgardi, A. Noori, M.A. Kamyabi, A. Khalafi-Nezhad, M.N. Soltani Rad. *Speciation of iron(II), iron(III) and full-range pH monitoring using paptode: A simple colorimetric method as an appropriate alternative for optodes*. Sens. Actuators B, 113 (2006) 857-865.

[8] A. Safavi, N. Maleki, A. Rostamzadeh, S. Maesum. *CCD camera full range pH sensor array*. Talanta, 71 (2007) 498-501.

[9] S. Capel-Cuevas, M.P. Cuéllar, I. de Orbe-Payá, M.C. Pegalajar, L.F. Capitán-Vallvey. *Full-range optical pH sensor based on imaging techniques*. Anal. Chim. Acta, 681 (2010) 71-81.

[10] A. Sohanghpurwala, G. Rao, Y. Kostov. *Optical Replacement of pH Electrode*. IEEE Sens. J., 9(3) (2009) 219-220.

[11] O. Korostynska, K. Arshak, E. Gill, A. Arshak. *Review Paper: Materials and Techniques for In Vivo pH Monitoring*. IEEE Sens. J., 8(1) (2008) 20-28.

[12] S. Capel-Cuevas, M.P. Cuéllar, M.C. Pegalajar, I. de Orbe-Payá, L.F. Capitán-Vallvey. *Full range optical pH sensor array based on neural networks.* Microchem. J., 97(2) (2010) 225-233.

[13] J.P. Ignizio. *Introduction to expert systems: The development and implementation of rule-based expert systems*. Mc Graw-Hill, New York (1991).

[14] P. Jackson. *Introduction to Expert Systems*. Pearson Education (1999).

[15] L. Ingber. *Simulated Annealing: Practice versus Theory*. Math. Comput. Modelling, 18 (1993) 29-57.

[16] K. Cantrell, M.M. Erenas, I. de Orbe-Payá, L.F. Capitán-Vallvey. *Use of the Hue parameter of the Hue, Saturation, Value color space as a quantitative analytical parameter for bitonal optical sensors*. Anal. Chem., 82 (2010) 531-542.

[17] M.P. Cuéllar, M.M. Erenas, M.C. Pegalajar, I. de Orbe-Payá, L.F. Capitán-Vallvey. *Automatic colour feature extraction from disposable optical sensors*. Proc. International Workshop on Multivariate Image Analysis, Valencia, Spain (2009) 45.

[18] D.A. Forsyth, J. Ponce. *Computer vision: a modern approach*. Prentice Hall, Upper Saddle River, NJ, USA (2002).

[19] M.P. Cuéllar, M. Delgado, M.C. Pegalajar. *An application of non-linear programming to train recurrent neural networks in time series prediction problems*. Proc. International Conference on Enterprise and Information Systems (2005) 35-42.

[20] A.J. González, D.D. Dankel. *The engineering of Knowledge-Based Systems*. Prentice Hall (1993).

[21] G. Brassard, P. Bratley. *Fundamentals of Algorithmics*. Prenticel Hall (2004).

[22] S. Haykin. *Neural Networks: a comprehensive foundation*. Prentice Hall: Upper Saddle River, NJ, USA (1999).

[23] C. Munkholm, D.R. Walt, F.P. Milanovich, S.M. Klainer. *Polymer modification of fiber optic chemical sensors as a method of enhancing fluorescence signal for pH measurement*. Anal Chem., 58 (1986) 1427-1430.

[24] J.I. Peterson, S.R. Goldstein, R.V. Fitzgerald, D.K. Buckhold. *Fiber optic pH probe for physiological use*. Anal. Chem., 52 (1980) 864-869.

3. CONCLUSIONES

En este capítulo se ha desarrollado un ES basado en reglas para la medida de pH en rango completo (de 0 a 14) utilizando la matriz sensora óptica previamente desarrollada. Las principales conclusiones que se derivan del estudio son las siguientes:

- Tras medir el pH de disoluciones acuosas entre 0 y 14 cada 0,1-0,2 unidades de pH, al objeto de obtener un conjunto de datos de calibración correspondientes a las variaciones de cada elemento sensor de la matriz, se han modelado las respuestas utilizando el algoritmo de optimización Levenberg–Marquardt.

- Los datos de calibración han sido clasificados considerando tres posibles estados de acuerdo con la respuesta de cada elemento (activo, inactivo y saturado) al objeto de discriminar unos respecto a otros. Las reglas consideradas son del tipo: *"Si el elemento sensor S_1 se encuentra en el estado $E(S_1)$ y el elemento sensor S_2 en el estado $E(S_2)$ y... el elemento sensor S_N en el estado $E(S_N)$, entonces utiliza la función de predicción F_y del elemento sensor S_x con nivel de confianza C_L",* de modo que la interpretación de las operaciones ha permitido llevar a cabo de forma sencilla la validación y el seguimiento del comportamiento del sistema.

- Se ha empleado un parámetro para establecer un peso para cada función sigmoidal, y posteriormente se ha aplicado la técnica de optimización Enfriamiento Simulado *(Simulated Annealing)* con el fin de encontrar el rango más estrecho de H, dentro del área activa de cada respuesta de los diversos elementos sensores, que proporciona la máxima precisión en la predicción del pH.

- Tras clasificar los valores de H, se ha aplicado el algoritmo ID3 para construir un árbol de decisión, a partir del cual se ha generado la base de conocimiento. Se ha utilizado un criterio de mínima entropía de información para seleccionar los elementos sensores a incluir en el árbol.

El módulo razonador ha recibido los valores de H de cada elemento sensor; una vez clasificados estos valores, se han usado para iniciar el proceso de inferencia, obteniéndose un conjunto de posibles funciones de predicción de pH con su correspondiente grado de confianza. Estas funciones han sido enviadas al módulo de predicción para que seleccionara la función con el mayor grado de confianza posible; el pH se ha calculado a partir de ésta.

- Los MSE (en unidades de pH) derivados de este estudio son los siguientes: 0,06 en los datos de calibración; 0,09 en los datos de validación y 0,08 en muestras de agua de grifo y de río. Comparado con otras técnicas como redes neuronales y ajustes lineales o no lineales, este ES proporciona resultados similares con alta eficiencia y mayor simplicidad.

CAPÍTULO 7

Desarrollo de un instrumento portátil para la determinación de pH basado en una matriz sensora óptica

"The greatest enemy of knowledge is not ignorance, it is the illusion of knowledge".

Stephen Hawking

1. INTRODUCCIÓN

La instrumentación portátil basada en sensores ópticos ha experimentado un considerable auge en la última década como consecuencia de la aparición de nuevas tecnologías[358]. Las condiciones requeridas por estos instrumentos son, esencialmente, pequeño tamaño y bajos coste de mantenimiento y consumo energético. Se han realizado grandes avances en cuanto a la reducción del tamaño y peso de los instrumentos, pero muchos de ellos todavía requieren estar conectados a un ordenador para el control, la recogida y el procesamiento de datos.

La viabilidad de los instrumentos basados en sensores ópticos depende no sólo de los principios de reconocimiento o transducción, sino también del sistema sensor en su totalidad: ajuste correcto para la transducción, capa sensora, electrónica de adquisición de datos y software de evaluación[359]. Además, para el diseño de un instrumento portátil[360] es necesario considerar las características de la muestra, incluyendo: volumen, interferentes, concentración del analito en estudio y propiedades físicas. Por último, deben considerarse las restricciones del usuario: tipo y calidad de la información necesitada, tiempo y frecuencia de medida, coste, consumibles, mantenimiento y requerimientos de energía.

Trabajando bajo condiciones instrumentales y operacionales bien definidas para analitos específicos y en ciertas matrices, la selectividad y la sensibilidad pueden ser suficientes para el análisis directo con un tratamiento mínimo, o incluso sin tratamiento previo de la muestra.

Se han realizado diferentes revisiones relacionadas con el tema, entre otras sobre instrumentación biomédica óptica de bajo coste[361], sobre sistemas

---

[358] L.F. Capitán-Vallvey, A.J. Palma. *Recent developments in handheld and portable optosensing-A review*. Anal. Chim. Acta, 696 (2011) 27-46

[359] G. Gauglitz. *Direct optical sensors: principles and selected applications*. Anal. Bioanal. Chem., 381 (2005) 141-155

[360] F.S. Ligler. *Perspective on optical biosensors and integrated sensor systems*. Anal. Chem., 81 (2009) 519-526

[361] Y. Kostov, G. Rao. *Low-cost optical instrumentation for biomedical measurement*. Rev. Sci. Instrument., 71 (12) (2000) 4361-4374

para diagnóstico inmediato (POCT)[362], sobre instrumentación de estado sólido basada en sensores de fibra óptica[363], sobre sensores químicos y micro-instrumentación[364], sobre instrumentación analítica portátil[365-368] y sobre métodos de lectura directa[369]. También existen trabajos relevantes publicados sobre el uso de diversos elementos optoelectrónicos en dispositivos analíticos[370-373], así como la obra de McMahon acerca de instrumentos miniaturizados y portátiles[374].

Los instrumentos pueden clasificarse considerando si el reconocimiento se lleva a cabo de forma directa o mediante reactivos. En nuestro caso, se ha diseñado un instrumento portátil basado en la segunda opción.

1.1. Instrumentos basados en reconocimiento directo

A continuación, se recogen algunos ejemplos de equipos portátiles para sensado óptico basados en propiedades intrínsecas del analito/s, clasificados de

[362] P. Von Lode. *Point-of-care immunotesting: approaching the analytical performance of central laboratory methods*. Clin. Biochem., 38(7) (2005) 591-606

[363] M.N. Taib, R. Narayanaswamy. *Solid-state Instruments for Optical Fibre Chemical Sensors*. Analyst, 120 (1995) 1617-1625

[364] R.W. Murray. *Chemical sensors and microinstrumentation. An overview*. ACS Symp. Ser., 403 (1989) 1-19

[365] H. Wei, Z. Guo, Z. Zhu, Y. Tan, Z. Du, R. Yang. *Sensitive detection of antibody against antigen F1 of Yersinia pestis by an antigen sandwich method using a portable fiber optic biosensor*. Sens. Actuators B, 127(2) (2007) 525-530

[366] E.B. Overton, H. P. Dharmasena, U. Ehrmann, K.R. Carney. *Trends and advances in portable analytical instrumentation*. Field Anal. Chem. Technol., 1(2) (1996) 87-92

[367] D.M. Wilson, S. Hoyt, J. Janata, K. Booksh, L. Obando. *Chemical sensors for portable, handheld field instruments*. IEEE Sens. J., 1 (2001) 256-274

[368] K. Ashley. *Analytical instrument performance criteria: field-portable spectroscopy*. Appl. Occup. Environ., 18(1) (2003) 10-15

[369] C.C. Coffey, T.A. Pearce. *Direct-reading methods for workplace air monitoring*. J. Chem. Health Saf., 17(3) (2010) 10-21

[370] P.K. Dasgupta, H.S. Bellamy, H. Liu, J.L. Lopez, E.L. Loree, K. Morris, K. Petersen, K.A. Mir. *Light emitting diode based flow-through optical absorption detectors*. Talanta, 40(1) (1993) 53-74

[371] M. O'Toole, D. Diamond. *Absorbance based light emitting diode optical sensors and sensing devices.* Sens., 8(4) (2008) No pp. given

[372] R.A. Yotter, D.M.Wilson. *A review of photodetectors for sensing light-emitting reporters in biological systems*. IEEE Sens. J., 3(3) (2003) 288-303

[373] J. Shinar, R. Shinar. *Organic light-emitting devices (OLEDs) and OLED-based chemical and biological sensors: an overview*. J. Phys. D: Appl. Phys., 41(13) (2008) 133001/1-133001/26

[374] G. McMahon. *Analytical Instrumentation. A Guide to Laboratory Portable and Miniaturized Instruments*, first ed., John Wiley & Sons, Chichester (2007)

acuerdo con el proceso que tiene lugar: absorción o emisión, tanto molecular como atómica en los que, en general, se requiere poca o ninguna preparación de muestra.

En cuanto a sistemas basados en absorción, los sensores de IR para gases (CO_2 y CH_4, entre otros, así como vapores orgánicos e inorgánicos) empezaron a comercializarse a principios de la década de los 80. Se desarrollaron instrumentos de tipo FTIR para determinaciones diversas, por ejemplo: contaminantes orgánicos volátiles en agua subterránea[375], gases volcánicos y de combustión industrial[376], hidrocarburos clorados en agua[377], BTEX en atmósferas industriales[378], escapes de gases industriales basada en TDLAS[379], y otros gases como CH_4, HF y H_2S[380-382]. También se ha caracterizado un instrumento IR portátil para CO_2 basado en una óptica de doble haz y en RNA[383].

El uso de la absorción NIR para sensado presenta el inconveniente de una baja sensibilidad; pese a ello, se han desarrollado diversos instrumentos portátiles con diferentes propósitos, así: automatización de procesos[384], medida del contenido de azúcar en manzanas[385], detección de gasolina adulterada[386],

---

[375] H. Steiner, M. Jakusch, M. Kraft, M. Karlowatz, T. Baumann, R. Niessner, W. Konz, A. Brandenburg, K. Michel, C. Boussard-Pledel, B. Bureau, J. Lucas, Y. Reichlin, A. Katzir, N. Fleischmann, K. Staubmann, R. Allabashi, J.M. Bayona, B. Mizaikoff. *In situ sensing of volatile organic compounds in groundwater: First field tests of a mid-infrared fiber-optic sensing system*. App. Spectros., 57(6) (2003) 607-613

[376] U. Willer, D. Scheel, I. Kostjucenko, C. Bohling, W. Schade, E. Faber. *Fiber-optic evanescent-field laser sensor for in-situ gas diagnostics*. Spectrochim. Acta A, 58A(11) (2002) 2427-2432

[377] B. Mizaikoff, M. Karlowatz, M. Kraft. *Mid-infrared sensors for marine monitoring*. Proc. SPIE Int. Soc. Opt. Eng., 4204 (2001) 263-273

[378] L.I.B. Silva, T.A.P. Rocha-Santos, A.C. Duarte. *Remote optical fibre microsensor for monitoring BTEX in confined industrial atmospheres*. Talanta, 78(2) (2009) 548-552

[379] C. McDonagh, C.S. Burke, B.D. MacCraith. *Optical Chemical Sensors*. Chem. Rev., 108(2 (2008) 400-422

[380] T. Iseki. *A portable remote methane detector using an InGaAsP DFB laser*. Environ. Geol., 46(8) (2004) 1064-1069

[381] T. Iseki, H. Tai, K. Kimura. *A portable remote methane sensor using a tunable diode laser*. Meas. Sci. Technol., 11(6) (2000) 594-602

[382] D. Li, C.A. Mills, J.M. Cooper. *Microsystems for optical gas sensing incorporating the solvatochromic dye Nile Red*. Sens. Actuators B, B92(1-2) (2003) 73-80

[383] G. Zhang, X. Wu. A *novel CO_2 gas analyzer based on IR absorption*. Opt. Lasers Eng., 42 (2004) 219-231

[384] J. Malinen, M. Kansakoski, R. Rikola, C.G. Eddison. *LED-based NIR spectrometer module for hand-held and process analyzer applications*. Sens. Actuators B, B51(1-3) (1998) 220-226

[385] T. Temma, K. Hanamatsu, F. Shinoki. *Development of a portable near infrared sugar-measuring instrument*. J. Near Infrared Spectrosc., 10(1) (2002) 77-83

[386] E.da N. Gaiao, S.R. Bezerra dos Santos, V. Bezerra dos Santos, E.C. Lima do Nascimento, R.S. Lima, M.C. Ugulino de Araujo. *An inexpensive, portable and microcontrolled near infrared LED-photometer for screening analysis of gasoline*. Talanta, 75(3) (2008) 792-796

identificación de plásticos[387], evaluación de medidores de alcohol en aliento[388] o autentificación de comprimidos[389], determinación de la concentración de nitrógeno en hojas de caña de azúcar[390], e incluso medida de la saturación de oxígeno en sangre para prevenir potenciales lesiones del cerebro [391].

El problema que presenta la amplia banda de absorción IR del agua es solventado mediante el uso de espectroscopia Raman, la cual, debido a la combinación de su capacidad para caracterizar sustancias mediante la huella dactilar de éstas, posibilidad de control remoto y no ser invasiva ni destructiva, es una técnica adecuada para especies mayoritarias. Sin embargo, presenta los inconvenientes de baja intensidad e interferencia de la fluorescencia cuando se trabaja a longitudes de onda de excitación UV cercano-visible. Durante la pasada década, se desarrollaron diversos instrumentos Raman portátiles de tipo compacto para aplicaciones en seguridad[392], análisis de mezclas de disolventes orgánicos[393], aplicaciones medioambientales y militares[394,395], monitorización continua de sulfato, carbonato, nitrato y diferentes minerales en fuentes hidrotermales en fondos marinos[396], identificación de explosivos[397-405] y

[387] M. Kumagai, H. Suyama, T. Sato, T. Amano, N. Ogawa. *Discrimination of plastics using a portable near infrared spectrometer*. J. Near Infrared Spectrosc., 10(4) (2002) 247-255

[388] G. Razatos, R. Luthi, S. Kerrigan. *Evaluation of a portable breath alcohol analyzer*. Forensic Sci. Int., 153(1) (2005) 17-21

[389] A.J. O'Neil, R.D. Jee, G. Lee, A. Charvill, A.C. Moffat. *Use of a portable near infrared spectrometer for the authentication of tablets and the detection of counterfeit versions*. J. Near Infrared Spectrosc., 16(3) (2008) 327-333

[390] E.M. Abdel-Rahman, F.B. Ahmed, M. van den Berg. *Imaging spectroscopy for estimating sugarcane leaf nitrogen concentration*. Proc. SPIE, 7104 (2008) 71040V/1- 71040V/12

[391] A. Bozkurt, A. Rosen, H. Rosen, B. Onaral. *A portable near infrared spectroscopy system for bedside monitoring of newborn brain*. Biomed. Eng. Online, 4(1) (2005) 29

[392] E.L. Izake. *Forensic and homeland security applications of modern portable Raman spectroscopy*. Forensic Sci. Int., 202(1-3) (2010) 1-8

[393] B.M. Cullum, J. Mobley, Z. Chi, D.L. Stokes, G.H. Miller, T. Vo-Dinh. *Development of a compact, handheld Raman instrument with no moving parts for use in field analysis*. Rev. Sci. Instrum., 71(4) (2000) 1602-1607

[394] M.B. Wabuyele, M.E. Martin, F. Yan, D.L. Stokes, J. Mobley, B.M. Cullum, A.L. Wintenberg, R. Lenarduzzi, T. Vo-Dinh. *Portable Raman integrated tunable sensor (RAMiTs) for environmental field monitoring*. Proc. SPIE Int. Soc. Opt. Eng., 5586 (2004) 60-67

[395] F. Yan, T. Vo-Dinh. *Surface-enhanced Raman scattering detection of chemical and biological agents using a portable Raman integrated tunable sensor*. Sens. Actuators B, B121(1) (2007) 61-66

[396] T.M. Battaglia, E.E. Dunn, M.D. Lilley, J. Holloway, B.K. Dable, B.J. Marquardt, K.S. Booksh. *Development of an in situ fiber optic Raman system to monitor hydrothermal vents*. Analyst, 129(7) (2004) 602-606

[397] D.S. Moore, R.J. Scharff. *Portable Raman explosives detection*. Anal. Bioanal. Chem., 393(6-7) (2009) 1571-1578

precursores de explosivos[406], detección de drogas de abuso en materiales de relevancia forense[407,408] y determinación directa de cianuro en muestras ambientales[409]. El análisis de trazas por Raman es llevado a cabo utilizando la técnica SERS, por lo que se han sugerido diferentes aproximaciones para integrar estas medidas en espectrofotómetros portátiles, como son: superficies de poliuretano cubiertas con nanopartículas de plata[410], nanoesferas cubiertas de películas de plata (AgFON) preparadas sobre vidrio[411,412], sustratos metálicos electroquímicos[413,414], películas de nanopartículas de plata preparadas sobre

[398] S.K. Sharma, A.K. Misra, B. Sharma. *Portable remote Raman system for monitoring hydrocarbon, gas hydrates and explosives in the environment*. Spectrochim. Acta A, 61A(10) (2005) 2404-2412

[399] D.S. Moore. *Instrumentation for trace detection of high explosives*. Rev. Sci. Instrum., 75 (2004) 2499-2512

[400] M.L. Lewis, I.R. Lewis, P.R. Griffiths. *Raman spectrometry of explosives with a no-moving-parts fiber coupled spectrometer: A comparison of excitation wavelength*. Vib. Spectrosc., 38(1-2) (2005) 17-28

[401] J.C. Carter, S.M. Angel, M. Lawrence-Snyder, J. Scaffidi, R.E. Whipple, J.G. Reynolds. *Standoff detection of high explosive materials at 50 meters in ambient light conditions using a small Raman instrument*. Appl. Spectrosc., 59(6) (2005) 769-775

[402] A. Pettersson, I. Johansson, S. Wallin, M. Nordberg, H. Oestmark. *Near Real-Time Standoff Detection of Explosives in a Realistic Outdoor Environment at 55 m Distance*. Propellants, Explos., Pyrotech., 34(4) (2009) 297-306

[403] S.D. Harvey, M.E. Vucelick, R.N. Lee, B.W. Wright. *Blind field test evaluation of Raman spectroscopy as a forensic tool*. Forensic Sci. Int., 125(1) (2002) 12-21

[404] S.D. Harvey, T.J. Peters, B.W. Wright. *Safety considerations for sample analysis using a near-infrared (785 nm) Raman laser source*. Appl. Spectrosc., 57 (2003) 580-587

[405] M. Gaft, L. Nagli. *UV gated Raman spectroscopy for standoff detection of explosives*. Opt. Mater., 30(11) (2008) 1739-1746

[406] M. Del Rio Anaya, G. Garcia-Torales, V. Rodriguez Betancourtt, R. Rodriguez Rojas, J. Flores Nunez, G. Garcia Torales, J.L. Flores Nunez, G. Gomez Rosas, E. Rosas. *Analysis of explosives' precursors by means of a portable Raman spectrometer*. Proc. SPIE, 7499 (2009) 749902/1 -749902/6

[407] E.M.A. Ali, H.G.M. Edwards, M.D. Hargreaves, I.J. Scowen. *In situ detection of cocaine hydrochloride in clothing impregnated with the drug using benchtop and portable Raman spectroscopy*. J. Raman Spectrosc., 41(9) (2010) 938-943

[408] M.D. Hargreaves, K. Page, T. Munshi, R. Tomsett, G. Lynch, H.G.M. Edwards. *Analysis of seized drugs using portable Raman spectroscopy in an airport environment - a proof of principle study*. J. Raman Spectrosc., 39(7) (2008) 873-880

[409] F. Yan, C.V.G. Reddy, Y. Zhang, T. Vo-Dinh. *A novel cyanide ion sensing approach based on Raman scattering for the detection of environmental cyanides*. Ecotoxicol. Environ. Saf., 73(6) (2010) 1490-1494

[410] H. Huo, C. Wang, H. Ren, M. Johnson, M. Shen. *Surface Enhanced Raman Scattering Sensing with Nanostructures Fabricated by Soft Nanolithography*. J. Macromol. Sci. Part A: Pure Appl. Chem., 46(12) (2009) 1182-1184

[411] C.L. Haynes, C.R. Yonzon, X. Zhang, R.P. Van Duyne. *Surface-enhanced Raman sensors: Early history and the development of sensors for quantitative biowarfare agent and glucose detection*. J. Raman Spectrosc., 36(6/7) (2005) 471-484

[412] X. Zhang, M.A. Young, O. Lyandres, R.P. Van Duyne. *Rapid detection of an anthrax biomarker by surface-enhanced Raman spectroscopy*. J. Am. Chem. Soc., 127(12) (2005) 4484-4489

[413] J.M. Sylvia, J.A. Janni, J.D. Klein, K.M. Spencer. *Surface-Enhanced Raman Detection of 2,4-Dinitrotoluene Impurity Vapor as a Marker To Locate Landmines*. Anal. Chem., 72(23) (2000) 5834-5840

superficies de vidrio[395], películas nanoesféricas de poliestireno cubiertas por oro[415] y suspensión de nanopartículas de oro[416].

El reconocimiento directo basado en la absorción de la radiación visible no es muy común, aunque se han diseñado algunos instrumentos portátiles con diferentes fines: evaluación de la interferencia de lipemia, hemólisis, y/o bilirrubinemia de forma directa en muestras de sangre[417], análisis de mezclas de colorantes en alimentos[418], análisis simultáneo de Cr(III) y Cr(VI) en muestras de agua[419], diferenciación entre licores, así como de tionina mediante una instrumentación que combina la emisión programada de una pantalla de ordenador con una cámara web como detector de imagen y el uso de coordenadas RGB para cuantificar[420,421].

La absorción UV se utiliza principalmente en análisis atmosférico y de higiene industrial, mediante diferentes instrumentos portátiles disponibles en el mercado para monitorizar gases tales como ozono, vapor de mercurio, óxidos de nitrógeno, dióxido de azufre y amoniaco[422,423].

En cuanto a los sistemas basados en emisión, la luminiscencia es una técnica adecuada para sensado debido a su selectividad y sensibilidad. No

---

[414] J.M. Sylvia, K.M. Spencer, J.A. Janni. *Sniffing landmines with Surface-Enhanced Raman Spectroscopy*. J. Process Anal. Chem., 6(4) (2001) 146-147

[415] F.A. Calzzani, Jr., R. Sileshi, A. Kassu, J.M. Taguenang, A. Chowdhury, A. Sharma, P.B. Ruffin, C. Brantley, E. Edwards. *Detection of residual traces of explosives by surface enhanced Raman scattering using gold coated substrates produced by nanospheres imprint technique*. Proc. SPIE, 6945 (2008) 694510/1-694510/9

[416] N.A. Hatab, G. Eres, P.B. Hatzinger, B. Gu. *Detection and analysis of cyclotrimethylenetrinitramine (RDX) in environmental samples by surface-enhanced Raman spectroscopy*. J. Raman Spectrosc., 41(10) (2010) 1131-1136

[417] L. Rovati, F. Docchio. *Determination of the concentrations of interferents in blood serum by use of a novel solid-state colorimeter*. Meas. Sci. Technol., 11(3) (2000) 185-192

[418] M.H. Sorouraddin, M. Saadati. *A simple fabrication of portable diffuse reflectometer for simultaneous analysis of common food dyes*. Sens. Actuators B, B145(1) (2010) 367-372

[419] J.J. Xin, Y.H. He, J. Hu, Y.X. Duan, X.D. Hou. *A Compact Spectrophotometer Using Liquid Core Waveguide and Handheld Charge Coupled Device: For Green Method and Ultrasensitive Speciation Analysis of Cr(III) and Cr(VI)*. Spectros. Lett., 42(6 & 7) (2009) 351-355

[420] G.R. Jones, A.G. Deakin, R.J. Brookes, J.W. Spencer. *A portable liquor monitoring system using a PC-based chromatic technique*. Meas. Sci. Technol., 20(7) (2009) 075305/ -075305/8

[421] K.M. Cantrell, J.D. Ingle Jr. *The SLIM spectrometer*. Anal. Chem., 75(1) (2003) 27-35

[422] P.C. Andersen, C.J. Williford, J.W. Birks. *Miniature Personal Ozone Monitor Based on UV Absorbance*. Anal. Chem., 82(29) (2010) 7924-7928

[423] J. Wang, P. Xie, A. Li, F. Si, K. Dou, W. Fang, F. Wu, Y. Jiang, M. Qin. *Measurement of ammonia by a portable UV-DOAS gas sensor based on multi-pass cell*. Proc. SPIE, 7853 (2010) 78533B/1-78533B/10

obstante, dado que el número de luminóforos intrínsecos es limitado, el uso de instrumentos portátiles basados en fluorescencia usando reconocimiento directo está limitado a casos específicos. Algunos ejemplos de aplicaciones son: identificación y cuantificación de drogas de abuso usando SFS[424], caracterización de PAHs en sedimentos acuáticos por espectroscopia LIF[425], identificación de compuestos orgánicos mediante los espectros de emisión de fragmentos moleculares (CH y CN)[426] y de trazas de nitrógeno en gases inertes (He, Ar)[427], e identificación y cuantificación de diferentes elementos en zonas contaminadas mediante espectroscopia LIBS[428].

1.2. Instrumentos basados en reconocimiento mediante reactivos

1.2.1. Sistemas basados en absorción

Los sistemas basados en las medidas de absorción o transmisión presentan una amplia aplicabilidad y versatilidad frente a un gran número de analitos, pese a su baja sensibilidad, relativamente alto tiempo de respuesta e interferencias debidas a la turbidez de muestras en el caso de absorción. Los instrumentos más comunes, basados en dispositivos de química seca aparecieron a principios de los 70, principalmente para análisis clínico de sangre. Palma *et al.*[429-431] presentaron un instrumento para la determinación *in situ* de

---

[424] S. Babichenko, E. Erme, T. Ivkina, L. Poryvkina, V. Sominsky. *A portable device and method for on-site detection and quantification of drugs*. PCT Int. Appl., (2005) WO 2005111586 A1 20051124

[425] T.J. Grundl, J.H. Aldstadt III, J.G.R.W. Harb, St. Germain, R.C. Schweitzer. *Demonstration of a Method for the Direct Determination of Polycyclic Aromatic Hydrocarbons in Submerged Sediments*. Environ. Sci. Technol., 37(6) (2003) 1189-1197

[426] Z. Jin, Y. Su, Y. Duan. *A low-power, atmospheric pressure, pulsed plasma source for molecular emission spectrometry*. Anal. Chem., 73(2) (2001) 360-365

[427] Z. Jin, Y. Duan. *Simple, sensitive nitrogen analyzer based on pulsed miniplasma source emission spectrometry*. Rev. Sci. Instrum., 74(12) (2003) 5156-5160

[428] R. Harmon, F.C. De Lucia, A.W. Miziolek, K.L. McNesby, R.A. Walters, P.D. French. *Laser-induced breakdown spectroscopy (LIBS) - An emerging field-portable sensor technology for real-time, in-situ geochemical and environmental analysis*. Geochem.: Explor. Environ., Anal., 5(1) (2005) 21-28

[429] A.J. Palma, A. Lapresta-Fernandez, J.M. Ortigosa-Moreno, M.D. Fernandez- Ramos, M.A. Carvajal, L.F. Capitan-Vallvey. *A simplified measurement procedure and portable electronic photometer for disposable sensors based on ionophore-chromoionophore chemistry for potassium determination*. Anal. Bioanal. Chem., 386(5) (2006) 1215-12241

[430] A.J. Palma, J.M. Ortigosa, A. Lapresta-Fernandez, M.D. Fernandez-Ramos, M.A. Carvajal, L.F. Capitan-Vallvey. *Portable light-emitting diode-based photometer with one-shot optochemical sensors for measurement in the field*. Rev. Sci. Instrum., 79(10, Pt.1) (2008) 103105/1-103105/8

constituyentes presentes en aguas naturales (nitrato y potasio) por medio de sensores desechables transparentes basados en química ionóforo-cromoionóforo. Otros casos están basados en medidas de reflectancia, así para metales pesados[432] o sulfatos[433] en agua.

Fernandez de Castro[434] patentó en 2003 un instrumento para medida simultánea de diferentes analitos en fluidos biológicos utilizando tiras reactivas. Zhou *et al.*[435] describieron un instrumento portátil para la determinación de hemoglobina y alanina aminotransferasa en muestras de sangre mediante reflectancia difusa y, posteriormente, lo mejoraron utilizando LEDs y fibra óptica para aumentar la estabilidad y la precisión[436]. Whitesides *et al.*[437] diseñaron un sistema basado en un material celulósico con áreas hidrofílicas separadas por líneas hidrofóbicas que conducían la muestra a las zonas de reacción conteniendo reactivos para glucosa y proteínas. Tras unas propuestas iniciales de uso de cámaras de teléfono móvil y escáneres portátiles para digitalizar el color de cada área con fines cuantitativos, plantearon el empleo de un colorímetro de transmisión diseñado específicamente en conjunción con la escala de grises[438]. Algunos ejemplos desarrollados para la determinación de gases se refieren a la

[431] M.D. Fernandez-Ramos, M. Greluk, A.J. Palma, E. Arroyo-Guerrero, J. Gomez- Sanchez, L.F. Capitan-Vallvey. *The use of one-shot sensors with a dedicated portable electronic radiometer for nitrate measurements in aqueous solutions*. Meas. Sci. Technol., 19(9) (2008) 095204/1-095204/7

[432] A. Ghauch, C. Turnar, C. Fachinger, J. Rima, A. Charef, J. Suptil, M. Martin-Bouyer. *Use of diffuse reflectance spectrometry in spot test reactions for quantitative determination of cations in water.* Chemosphere, 40(12) (2000) 1327-1333

[433] V.M. Ostrovskaya, Yu. Zolotov, L.K. Shpigun, P.M. Kamilova, Y.L. Shishkin. *Development of simple pocket test tools for fast determination of dissolved sulfate in waters*. Field Anal. Chem. Technol., 4(2-3) (2000) 147-153

[434] A.L. Fernandez Decastro. *Test strip for simultaneous detection of a plurality of analytes.* US patent 6,524,864 WO 2002063296 (2003)

[435] A. Zhou, W. Yue, B. He, C. Liu, Q. Yang, X. Cai. *A portable system for determination of hemoglobin based on optic biosensor.* Chuangan Jishu Xuebao, 19(5) (2006) 2092-2095

[436] W. Yue, A. Zhou, B. He, X. Cai. *A portable biochemical detection device based on fibre optic sensor*. Sens. Actuators B, B130(1) (2008) 21-24

[437] A.W. Martinez, S.T. Phillips, M.J. Butte, G.M. Whitesides. *Patterned paper as a platform for inexpensive, low-volume, portable bioassays*. Angew. Chem., Int. Ed., 46(8) (2007) 1318-1320

[438] A.K. Ellerbee, S.T. Phillips, A.C. Siegel, K.A. Mirica, A.W. Martinez, P. Striehl, N. Jain, M. Prentiss, G.M. Whitesides. *Quantifying Colorimetric Assays in Paper-Based Microfluidic Devices by Measuring the Transmission of Light through Paper*. Anal. Chem., 81(10) (2009) 8447-8452

determinación de tolueno[439] y formaldehído[440], medida de CO en emisiones de vehículos[441] y determinación de ozono[442].

En casos donde la respuesta química de un analito implica un cambio reversible de su color, la química puede ser incluida en el instrumento como una fina película por medio de una variedad de procedimientos de recubrimiento, con las ventajas de un tiempo de respuesta corto y escaso consumo de reactivos químicos. Se han empleado varias configuraciones ópticas basadas en transmitancia y reflectancia, con la película sensora ubicada bien en un soporte inerte[443-445], directamente sobre elementos electrónicos[446-448], fibras ópticas[449-451] o en guías de onda planas[452,453].

---

[439] K. Kawamura, M. Vestergaard, M. Ishiyama, N. Nagatani, T. Hashiba, E. Tamiya. *Development of a novel hand-held toluene gas sensor: Possible use in the prevention and control of sick building síndrome*. Measurement, 39(6) (2006) 490-496

[440] Y. Suzuki, N. Nakano, K. Suzuki. *Portable Sick House Syndrome Gas Monitoring System Based on Novel Colorimetric Reagents for the Highly Selective and Sensitive Detection of Formaldehyde*. Environ. Sci. Technol., 37(24) (2003) 5695-5700

[441] F.A.A. Matias, M. Tubino. *A portable fiber-optic chemical device for the quantitative determination of carbon monoxide from automobile exhaust emissions*. J. Air Waste Manage. Assoc., 51(7) (2001) 962-965

[442] Z-m. Qi, H-s.. Zhou, I. Honma, K. Itoh, H. Yanangi. *A disposable ozone sensor based on a grating-coupled glass waveguide coated with a tapered film of copper tetra-t-butylphthalocyanine*. Sens. Actuators B, B106(1) (2005) 278-283

[443] A. Pacquit, K.T. Lau, H. McLaughlin, J. Frisby, B. Quilty, D. Diamond. *Development of a volatile amine sensor for the monitoring of fish spoilage*. Talanta, 69(2) (2006) 515-520

[444] A. Pacquit, J. Frisby, D. Diamond, K.T. Lau, A. Farrell, B. Quilty, D. Diamond. *Development of a smart packaging for the monitoring of fish spoilage*. Food Chem., 102(2) (2007) 466-470

[445] P.R. Somani, A.K. Viswanath, R.C. Aiyer, S. Radhakrishnan. *Novel dye + solid polymer electrolyte material for optical humidity sensing*. Org. Electron., 2(2) (2001) 83-88

[446] R.L. Shepherd, W.S. Yerazunis, K.T. Lau, D. Diamond. *Low-cost surface-mount LED gas sensor*. IEEE Sens. J., 6(4) (2006) 861-866

[447] M. O'Toole, R. Shepherd, G.G. Wallace, D. Diamond. *Inkjet printed LED based pH chemical sensor for gas sensing*. Anal. Chim. Acta, 652(1-2) (2009) 308-314

[448] R. Shepherd, S. Beirne, K.T. Lau, B. Corcoran, D. Diamond. *Monitoring chemical plumes in an environmental sensing chamber with a wireless chemical sensor network*. Sens Actuators B, B121(1) (2007) 142-149

[449] X.M. Liu, W.L. Xing, G.R. Ou, J. Liang. *A new reagent immobilization method for a portable fiber optic probe for determination of ferrous ion*. Anal. Sci., 16(5) (2000) 473-476

[450] P. Suresh Kumar, S. Thomas Lee, C.P.G. Vallabhan, V.P.N. Nampoori, P. Radhakrishnan. *Design and development of an LED based fiber optic evanescent wave sensor for simultaneous detection of chromium and nitrite traces in water*. Opt. Commun., 214(1-6) (2002) 25-30

[451] V.G. Andreou, Y.D. Clonis. *A portable fiber-optic pesticide biosensor based on immobilized cholinesterase and sol-gel entrapped bromcresol purple for in-field use*. Biosens. Bioelectron., 17(1-2) (2002) 61-69

[452] C.S. Burke, L. Polerecky, B.D. MacCraith. *Design and fabrication of enhanced polymer waveguide platforms for absorption-based optical chemical sensors*. Meas. Sci. Technol., 15(6) (2004) 1140-1145

[453] L. Polerecky, C.S. Burke, B.D. MacCraith. *Optimization of absorption-based optical chemical sensors that employ a single-reflection configuration*. Appl. Opt., 41 (2002) 2879-2887

1.2.2. Sistemas basados en luminiscencia

El desarrollo de sensores ópticos portátiles luminiscentes se ha incrementado notablemente en los últimos años, principalmente en el campo de inmunoensayos de flujo lateral, debido a su simplicidad y rapidez en numerosas aplicaciones de diagnóstico[454-457]. Gutiérrez *et al.*[458] propusieron en 2008 un inmunoensayo competitivo indirecto basado en marcadores FITC y ELF97 para pesticidas organofosforados (LOD 0,5 mgL^{-1}) en aceite de oliva, mientras que para la detección de patógenos se ha utilizado un instrumento de cuatro canales denominado RAPTOR[459].

Estas medidas han sido ampliamente utilizadas para sensado de gases basados en interacciones reversibles que dan lugar a atenuación de la luminiscencia, destacando las propuestas para oxígeno de DeGraff y Demas[460], Trinkel[461], Lam[462], Costa-Fernández[463] y Xiao[464]. La mayoría de estos instrumentos portátiles están basados en el tiempo de vida de luminiscencia debido a sus ventajas (en lo que respecta a fotooxidación del colorante, fluorescencia intrínseca de la muestra, cambios en la intensidad de la fuente

---

[454] K K. Faulstich, R. Gruler, M. Eberhard, D. Lentzsch, K. Haberstroh, in: R.C. Wong, H.Y. Tse (Eds.). *Handheld and Portable Reader Devices for Lateral Flow Immunoassays* (Chapter 9). Lateral Flow Immunoassay, Humana Press, NewYork, 2009

[455] Z. Li, Y. Wang, J. Wang, Z. Tang, J.G. Pounds, Y. Lin. *Rapid and Sensitive Detection of Protein Biomarker Using a Portable Fluorescence Biosensor Based on Quantum Dots and a Lateral Flow Test Strip*. Anal. Chem., 82 (2010) 7008-7014

[456] X. Mao, Y. Ma, A. Zhang, L. Zhang, L. Zeng, G. Liu. *Disposable Nucleic Acid Biosensors Based on Gold Nanoparticle Probes and Lateral Flow Strip*. Anal. Chem., 81(4) (2009) 1660-1668

[457] G. Liu, X. Mao, J.A. Phillips, H. Xu, W. Tan, L. Zeng. *Aptamer-Nanoparticle Strip Biosensor for Sensitive Detection of Cancer Cells*. Anal. Chem., 81 (2009) 10013-10018

[458] A. Gutierrez, J.A. Burgos, E. Molto. *Development of an immunosensor based on the measurement of fluorescence*. Sens. Actuators B, B131(2) (2008) 621-626

[459] C.C. Jung, E.W. Saaski, D.A. McCrae, B.M. Lingerfelt, G.P. Anderson. *RAPTOR: a fluoroimmunoassay-based fiber optic sensor for detection of biological threats*. IEEE Sens. J., 3(4) (2003) 352-360

[460] B.A. DeGraff, J.N. Demas. *Luminescence-based oxygen sensors*. Rev. Fluoresc., 2 (2005) 125-151

[461] M. Trinkel, W. Trettnak, C. Kolle. *Oxygen trace analysis utilizing a miniaturized luminescence lifetime-based sensor instrumentation*. Quim. Anal., 19(Supl. 1) (2000) 112-117

[462] H. Lam, Y. Kostov. *Optical instrumentation for bioprocess monitoring*. Adv. Biochem. Eng./Biotechnol., 116 (2009) 1-28

[463] J.M. Costa-Fernandez, N. Bordel, J.C. Campo, F.J. Ferrero, M.A. Perez, A. Sanz-Medel. *Portable fibre optic oxygen sensor based on room-temperature phosphorescence lifetime*. Mikrochim. Acta, 134(3-4) (2000) 145-152

[464] D. Xiao, Y. Mo, M.M.F. Choi. *A hand-held optical sensor for dissolved oxygen measurement*. Meas. Sci. Technol., 14(6) (2003) 862-867

iluminante) frente a la medida de su intensidad. Capitán-Vallvey *et al.*[465] desarrollaron un instrumento portátil para la medida de oxígeno atmosférico mediante una membrana de poliestireno estabilizada que contenía el complejo octaetilporfirina de platino situado sobre un LED actuando como fuente de luz y un fotodiodo de silicio con salida digital como detector. El uso de fotodiodos recubiertos con películas sensoras favorece la miniaturización, además de las ventajas de respuesta rápida y bajo consumo de energía[466,467].

Por otra parte, se han descrito diversos instrumentos portátiles luminiscentes para medida de otros gases, tales como CO_2[468-470]. MacCraith *et al.*[471-474] presentaron diversas plataformas sensoras para medidas de oxígeno, dióxido de carbono e incluso humedad relativa para monitorización de la calidad del aire.

En la última década, han sido escasas las publicaciones sobre sistemas basados en quimioluminiscencia (CL) y electroquimioluminiscencia (ECL), y la mayoría requieren conexión a un ordenador para procesar los datos y los resultados. La medida ECL allana el camino a dispositivos de un solo uso, debido

---

[465] A.J. Palma, J. López-González, L.J. Asensio, M.D. Fernandez-Ramos, L.F. Capitan-Vallvey. *Microcontroller-based portable instrument for stabilized optical oxygen sensor*. Sens. Actuators B, B121(2) (2007) 629-638

[466] L.F. Capitan-Vallvey, L.J. Asensio, J. Lopez-Gonzalez, M.D. Fernandez-Ramos, A.J. Palma. *Oxygen-sensing film coated photodetectors for portable instrumentation*. Anal. Chim. Acta, 583(1) (2007) 166-173

[467] A.J. Palma, J. Lopez-Gonzalez, L.J. Asensio, M.D. Fernandez-Ramos, L.F. Capitan-Vallvey. *Open Air Calibration with Temperature Compensation of a Luminescence Quenching-Based Oxygen Sensor for Portable Instrumentation*. Anal. Chem., 79(8) (2007) 3173-3179

[468] I.M. Perez de Vargas-Sansalvador, M.A. Carvajal, O.M. Roldan-Munoz, J. Banqueri, M.D. Fernandez-Ramos, L.F. Capitan-Vallvey. *Phosphorescent sensing of carbon dioxide based on secondary inner-filter quenching*. Anal. Chim. Acta, 655(1-2) (2009) 66-74

[469] I.M. Perez de Vargas-Sansalvador, A. Martinez-Olmos, A.J. Palma, M.D. Fernandez-Ramos, L.F. Capitan-Vallvey. *Compact optical instrument for simultaneous determination of oxygen and carbon dioxide*. Microchim. Acta, 172(3-4) (2011) 455-464

[470] E. Kraker, A. Haase, B. Lamprecht, G. Jakopic, C. Konrad, S. Koestler. *Integrated organic electronic based optochemical sensors using polarization filters*. Appl. Phys. Lett., 92(3) (2008), 033302/1- 033302/3

[471] C. Malins, M. Niggemann, B.D. MacCraith. *Multi-analyte optical chemical sensor employing a plastic substrate*. Meas. Sci. Technol., 11(8) (2000) 1105-1110

[472] O. McGaughey, R. Nooney, A.K. McEvoy, C. McDonagh, B.D. MacCraith. *Development of a multi-analyte integrated optical sensor platform for indoor air-quality monitoring*. Proc. SPIE Int. Soc. Opt. Eng., 5993 (2005) 59930R/1-59930R/12

[473] C.S. Burke, J.P. Moore, D. Wencel, A.K. McEvoy, B.D. MacCraith. *Breath-by-breath measurement of oxygen using a compact optical sensor*. J. Biomed. Opt., 13(1) (2008) 014027/1 -014027/7

[474] C.S. Burke, J.P. Moore, D. Wencel, B.D. MacCraith. *Development of a compact optical sensor for real-time, breath-by-breath detection of oxygen*. J. Breath Res., 2(3) (2008) 037012/1 -037012/7

a que es posible el control del tiempo en las reacciones. Capitán-Vallvey *et al.*[475] describieron un luminómetro basado en ECL para lactato en saliva. Sin embargo, la mayoría de los instrumentos portátiles CL y ECL propuestos, son sensores de flujo que utilizan los reactivos en disolución[476-479].

[475] A. Martinez-Olmos, J. Ballesta-Claver, A.J. Palma, M.C. Valencia-Miron, L.F. Capitan-Vallvey. *A portable luminometer with a disposable electrochemiluminescent biosensor for lactate determination*. Sensors, 9(10) (2009) 7694-7710

[476] P. Pittet, G.N. Lu, J.M. Galvan, R. Ferrigno, L.J. Blum, B.D. Leca-Bouvier. *PCB technology-based electrochemiluminescence microfluidic device for low-cost portable analytical systems*. IEEE Sens. J., 8(5) (2008) 565-571

[477] W.J. Ho, J.S. Chen, M.D. Ker, T.K. Wu, C.Y. Wu, Y.S. Yang, Y.K. Li, C.J. Yuan. *Fabrication of a miniature CMOS-based optical biosensor*. Biosens. Bioelectron., 22(12) (2007) 3008-3013

[478] S. Joo, R.B. Brown. *Chemical sensors with integrated electronics*. Chem. Rev., 108(2) (2008) 638-651

[479] A. Waseem, M. Yaqoob, A. Nabi, G.M. Greenway. *Determination of Thyroxine Using Tris(2,2'-Bipyridyl)Ruthenium(III)-NADH Enhanced Electrochemiluminescence Detection*. Anal. Lett., 40 (2007) 1071-1083

2. OBJETIVOS

Los objetivos principales de los trabajos realizados y presentados en este capítulo son:

- Tras optimizar y caracterizar la matriz sensora utilizando instrumentación de sobremesa como se ha descrito en los capítulos previos, se pretende desarrollar un instrumento portátil basado en dicha matriz para la medida de pH que sea de pequeño tamaño, fácil uso y electrónica simple.

- Implementación del sistema de cálculo necesario en la memoria del microcontrolador del instrumento portátil para su utilización *in situ* sin necesidad de conexión a un procesador de datos externo.

Los objetivos particulares en la primera etapa del estudio son los siguientes:

- Adquisición de la información del color de la matriz por medio de una fuente de luz programable y un conjunto de detectores de color sensibles a las diferentes regiones espectrales roja, verde y azul, permitiendo la medida simultánea de las coordenadas RGB correspondientes a cada elemento sensor y calculando a partir de éstas los valores de H.

- Caracterización óptica y electrónica del instrumento portátil tras la optimización de la configuración de la fuente de luz programable, del área activa y del tiempo de integración de los sensores de color digitales y de las condiciones de medida.

- Estudio del número mínimo de elementos sensores necesarios para realizar una determinación unívoca y precisa del pH a partir de la modelización y calibración del instrumento.

- Validación del sistema de medida y aplicación a muestras de agua de grifo y naturales.

A continuación se recogen los objetivos a llevar a cabo en la segunda etapa del estudio:

- Mejora y adaptación del instrumento portátil para su utilización en el lugar del análisis sin necesidad de conexión a un procesador de datos externo. Para ello se aplica un algoritmo multi-objetivo con el fin de obtener un conjunto de ANN que utilicen el mínimo número de elementos sensores durante el proceso de calibración sin pérdida de precisión en la predicción del pH, y así reducir el coste del prototipo final y ahorrar energía. Por otra parte, se pretende la selección de la red neuronal óptima y su implementación en la memoria del microcontrolador del instrumento portátil.

- Evaluación del uso del instrumento como pH-metro, comparando la respuesta de cada elemento sensor frente al pH medido con el dispositivo diseñado y con el escáner convencional previamente utilizado.

- Determinación del pH en un amplio conjunto de muestras alimentarias, biológicas y de productos de uso cotidiano sin necesidad de tratamiento previo. Comparación de los resultados con aquellos obtenidos a partir de un escáner convencional y, por otra parte, con el método potenciómetro de referencia.

PUBLICACIÓN V:

Sensors and Actuators B: Chemical, 156 (2011) 840–848
DOI: 10.1016/j.snb.2011.02.052

Sensor array-based optical portable instrument for determination of pH

A. Martinez-Olmos[a], S. Capel-Cuevas[b], N. López-Ruiz[a], A. J. Palma[a],
I. de Orbe-Payá[b], L.F. Capitán-Vallvey[b,*]

[a]*Department of Electronics and Computer Technology.*
[b]*Department of Analytical Chemistry.*
Campus Fuentenueva, University of Granada, E-18071 Granada, Spain

Abstract

A portable optical instrument is presented that makes it possible to determine pH with a colorimetric sensor array. The use of four membranes containing acid-base indicators makes it possible to cover the full range of pH using the H (hue) coordinate measurements of the HSV colour space. pH sensitive membranes were directly cast onto a plastic support to form a two-dimensional array, located between an OLED display as the programmable light source and a set of digital colour detectors. The resulting microcontroller-based system is immune to optical and electrical interferences. A complete optical and electrical characterization and optimization of the hand-held instrument was carried out. The instrument was used to determine pH using a simple algorithm to select the sensor output that was programmed in the microcontroller. The initial eleven candidate pH membranes were reduced to only four, which permit to obtain reliable pH values. The pH response of the selected four sensing elements was modelled, and calibration curves were applied to a validation set and real samples obtaining positive correlations between the real and predicted data.

Keywords: Full-range optical pH sensor array; OLED display; Digital colour detector; HSV colour space; Portable instrumentation.

* Corresponding author; e-mail: lcapitan@ugr.es

1. Introduction

Chemical imaging is an analytical technique that combines standard digital imaging techniques with a variety of spectroscopic techniques, typically based on absorption, transmission or scattering (Raman) or emission (fluorescence, chemiluminescence) to provide the spatial distribution of sample components. It is of general use in a variety of industries to characterize both chemical composition and morphology [1].

With sensors, chemical imaging must use a detector array to monitor the desired chemical species with a number of distributed selective chemical sensors providing spatial resolution as well [2]. One example is microarray technology, with which the simultaneous analysis of thousands of analytes is possible in a single experiment such as array-based gene expression analysis or protein microarrays based on antigen–antibody or ligand-receptor reactions [3].

Different macroarrays have been described for the simultaneous analysis of a small number of analytes by means of different types of imaging devices. Examples of positional or two-dimensional arrays include the device described for iron speciation and full-range pH determination by immobilizing reagents on cellulosic paper and RGB coordinates [4,5]; an electrochemiluminescent enzymatic biosensor screen-printed array for L-lactate and D-glucose [6]; an array of individually addressable sites on a micromachined silicon chip containing microspheres derivatized with dehydrogenases for the fluorescent determination of β-D-glucose and β-D-galactose [7] and fluorescent specific reagents for common ions in water arranged in microtiter plates and based on luminescence decay time imaging [8]. Some examples of encoded bead macroarrays can be found in the literature, such as an optical imaging fiber for pH, O_2 and CO_2 in solutions [9].

However, the disadvantages of these approaches based on specific receptors –difficulties in obtaining good selectivity against similar analytes and the number of sensors needed, which increases proportionally with the number of analytes – have led to an alternative paradigm based on general or differential

receptors [10]. This concept results in arrays of non-specific or low selective sensors (electronic tongues/noses) that produce analytical signals useful for the analysis of multi-component samples that are later treated through advanced mathematical procedures for signal processing by pattern recognition and/or multivariate analysis both for qualitative and quantitative analysis [11]. Different experimental approaches have been proposed based on non-selective arrays and imaging, such as: arrays of optical fibers, with the sensing phase located on the distal extreme [12] or incorporated into microspheres situated in microcavities etched into the end of the fiber [13]; arrays of polymeric microspheres with chemically modified surfaces that enable the covalent binding of receptors (conventional reagents, enzymes, and antibodies) and arranged in micromachined cavities in Si structures [14,15]; arrays of molecular printing polymers used to discriminate between aromatic amines based on absorbance variation and linear discriminant analysis [16]; arrangement of reagents in microplate wells imaged by means of a CCD camera based on quenching fluorescence [17]; and arrays of colorimetric membranes placed on hydrophobic silica base retrieving colour change using a scanner [18].

In this report, a disposable optical sensor array was used to determine pH in the full-range. pH in optical sensors is a function of the concentration of the acid and basic forms of the indicator [19]. Thus, calibration functions in pH sensors come from mass-action law relationships between the pH and the optical signal typically resulting in narrow sigmoid shape dependence according to the Henderson-Hasselbalch equation. The main drawbacks of optical pH sensors are a short dynamic working range (2-3 pH units) and non-linear response, which requires different sensing membranes to cover the whole pH range, although different strategies have been devised to extend the working range of optical pH sensors [20].

Previous work by our group was focused on the development of a disposable optical sensor array to predict the pH of a solution in the full-range (0–14). This pH determination was obtained from the hue (H) values of the HSV colour space using a scanner to image the optical array containing 11 sensing elements with immobilized pH indicators and using diverse mathematical modelling [20,21]. In the first case [20] three different approaches for pH prediction were studied: Linear model, Sigmoid competition model and Sigmoid

surface model, providing mean square errors (MSE) of 0.111, 0.075 and 0.266, respectively, for tap and river water samples. Then, neural networks were used as a prediction technique [21]. The best network structure obtained with the traditional trial-and-error procedure using the Levenberg-Marquardt training algorithm was made up of 11 input neurons, 10 hidden neurons and one output neuron for pH prediction, providing an MSE of 0.043.

Here, a handheld instrument is presented for the measurement of pH using a disposable optical sensor array with a more simple electronics than our previously designed photometers [22,23]. The acquisition of colour information from the array is obtained with a wide and programmable light source and a set of colour detectors that output the measured RGB coordinates coming from each membrane, in digital format, and used to calculate the H of the HSV colour space as the analytical parameter. In this paper, a complete optical and electrical characterization of the instrument is carried out and its application for the determination of pH in the whole range is detailed.

2. Experimental

2.1. Reagents

The chemicals used to prepare the pH sensitive films were potassium tetrakis (4-chlorophenyl)borate (TCPB, CAS No. 14680-77-4), tridodecylmethylammonium chloride (TDMAC, CAS No. 7173-54-8), aliquat 336 (CAS No. 5137-55-3), o-nitrophenyloctylether (NPOE, CAS No. 37682-29-4), dioctyl sebacate (DOS, CAS No. 122-62-3), bis(1-butylpentyl)adipate (BBPA, CAS No. 77916-77-9), tributyl phosphate (TBP, CAS No. 126-73-8), high molecular weight polyvinyl chloride (PVC, CAS No. 9002-86-2), cellulose acetate (CA, CAS No. 9004-35-7), ethylenglycol (EG, CAS No. 107-21-1) and tetrahydrofuran (THF, CAS No. 109-99-9) all purchased from Sigma (Sigma-Aldrich Química S.A., Madrid, Spain). Bromothymol blue (CAS No. 76-59-5), phenol red (CAS No. 143-74-8), thymol blue (CAS No. 76-61-9), m-cresol purple (CAS No. 2303-01-7) and PAN (CAS No. 85-85-8) from Sigma, liphophilized Nile blue (CAS No. 125829-24-5) and purpurin (CAS No. 81-54-9) from Fluka (Fluka, Madrid, Spain), cresol red (CAS No. 1733-12-6)

from Panreac (Panreac, Barcelona, Spain), alizarine (CAS No. 72-48-0) from TCI (TCI Europe, Belgium), and sicomet red P (CAS No. 5281-04-9) from BASF (BASF, Ludwigshafen, Germany) were used as acid-base indicators. As support sheets, Mylar-type polyester (Goodfellow, Cambridge, UK) was used. HCl and NaOH were supplied by Sigma. All reagents were of analytical reagent grade and were used without any further purification. All aqueous solutions were prepared in reverse-osmosis type quality water (Milli-RO 12 plus Milli-Q station from Millipore, conductivity 18.2 mS).

2.2. Instrumentation and software

The optical spectra were measured with a mini-spectrometer RC series C11007MA (Hamamatsu Photonics, Japan) with 256 pixels, spectral resolution at 9 nm half width and 16 bits of intensity resolution. For the electrical characterization of the prototype, the following instrumentation was used: a mixed signal oscilloscope (MSO4101, Tektronix, USA), a 6½ digit multimeter (34410A, Agilent Technologies, USA), a 15 MHz waveform generator (33120A, Agilent Technologies, USA) and a DC power supply (E3630A, Agilent Technologies, USA). For the image acquisitions and digitalization, a commercial scanner ScanMaker i900 (Microtek, Taiwan) was used, with a 6400 x 3200 dpi resolution, a maximum optical density of 4.2 and 24-48 bits of colour. The software to manage the scanner was Silver Fast Ai provided by Microteck. The images were processed with a set of scripts and functions developed by us in Matlab r2007b (The MathWorks, Inc., Natick, MA, USA). Statistical calculations were performed with the Statgraphics software package (Manugistics Inc. and Statistical Graphics Corporation, USA, 1992), and Microsoft Excel (Microsoft Corp., Redmond, WA, USA) was used for general calculations. A Crison pH-meter (Crison Instruments, Barcelona, Spain, model Basic 20) with a combined double junction glass electrode, calibrated against two standard buffer solutions (pH 4.0 and 7.0), was used for the pH measurements.

2.3. Sensor array preparation

The sensor array was prepared on a 5 cm x 4 cm transparent Mylar polyester support covered with an adhesive black film of PVC with 12 holes (3 columns and 4 rows), 5 mm diameter each. A black opaque film was used to reduce the light dispersion and prevent cross information between the sensing elements (figure 7.1). The sensing films were cast by carefully placing 8 µL of the corresponding cocktail in each hole, whose surface tension and quick evaporation make it possible to prepare the sensing membrane. The different cocktails for the pH membranes were prepared by dissolving the different chemicals needed in 1 mL of distilled THF according to the composition indicated in table 7.1.

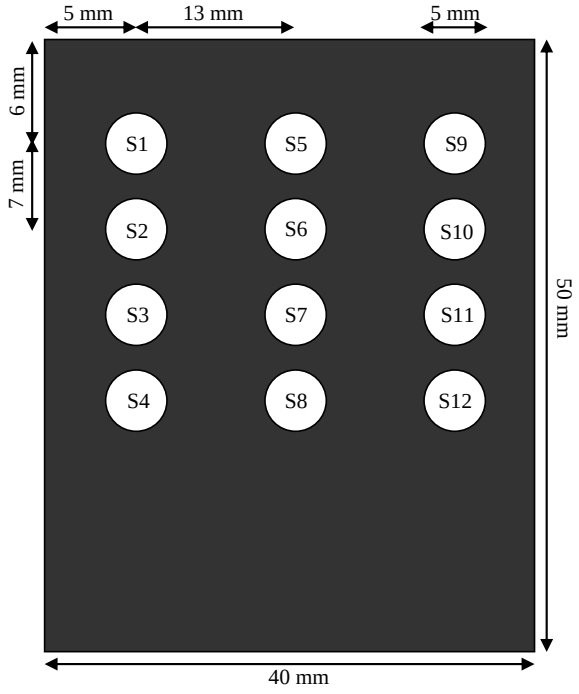

Figure 7.1. Design of the sensor array support indicating membrane positions and dimensions

The pH sensor arrays were prepared according to the conditions of: (a) no leaching; (b) a tonal colour coordinate change from the reaction; and (c) full coverage of the pH range by overlapping the responses of the different membranes. The selected sensing elements were prepared from different

cocktails containing different types and amounts of colorimetric acid-base indicators, polymers, plasticizers, lipophilic salts and, if necessary, humectant.

Table 7.1. Composition of the membranes (% w/w) used for the pH sensor array selection

Membrane	Indicator (%)	Lipophilic salt (%)	Plasticizer (%)	Membrane polymer (%)	Humectant (%)
S1	Sicomet red P (1.41)	Aliquat 336 (5.63)	NPOE (66.20)	PVC (26.76)	-
S2	m-Cresol purple (3.00)	TDMAC (13.47)	DOS (28.00)	CA (33.00)	EG (22.57)
S3	PAN (1.43)	TDMAC (10.00)	NPOE (65.00)	PVC (23.60)	-
S5	Purpurin (1.43)	TDMAC (8.29)	NPOE (67.00)	PVC (23.29)	-
S6	Cresol red (1.43)	Aliquat 336 (4.54)	NPOE (67.00)	PVC (27.00)	-
S7	Liphophilized Nile blue (1.43)	TCPB (3.63)	TBP (67.00)	PVC (27.91)	-
S8	Bromothymol blue (3.00)	TDMAC (4.00)	DOS (28.00)	CA (37.00)	EG (19.60)
S9	Alizarin (1.43)	TDMAC (10.29)	NPOE (67.00)	PVC (21.3)	-
S10	Thymol blue (3.14)	TDMAC (11.57)	DOS (28.00)	CA (37.00)	EG (20.43)
S11	Phenol red (1.43)	TDMAC (6.93)	BBPA (26.00)	CA (30.00)	EG (35.64)
S12	Thymol blue (5.00)	TDMAC (18.40)	DOS (28.00)	CA (33.00)	EG (15.60)

The composition of the different sensing elements was optimized considering leaching minimization (lipophilic salt, plasticizer, and membrane polymer), colour intensity (acid-base indicator) and response time (plasticizer, membrane polymer, humectant and cocktail volume). As a result, 11 different membranes, containing 10 different pH indicators, were prepared to cover the whole pH range.

Two different sensor arrays were prepared, both with the same structure. The first array contained the 11 different sensing elements studied and the second, the 4 pH membranes selected as the pH sensor array, with three replicates each. Additionally, one empty position of the support (S4) was used to test the illuminant of the instrument.

2.4. Description of the instrument

The block diagram of the portable instrument developed is presented in figure 7.2. This is a microcontroller-based system designed to measure the colour of an array of colorimetric sensing elements using their illumination with a programmable light source and collecting their transmitted light in an array of digital colour detectors. In this case, the measurement platform was used to measure the pH of a solution.

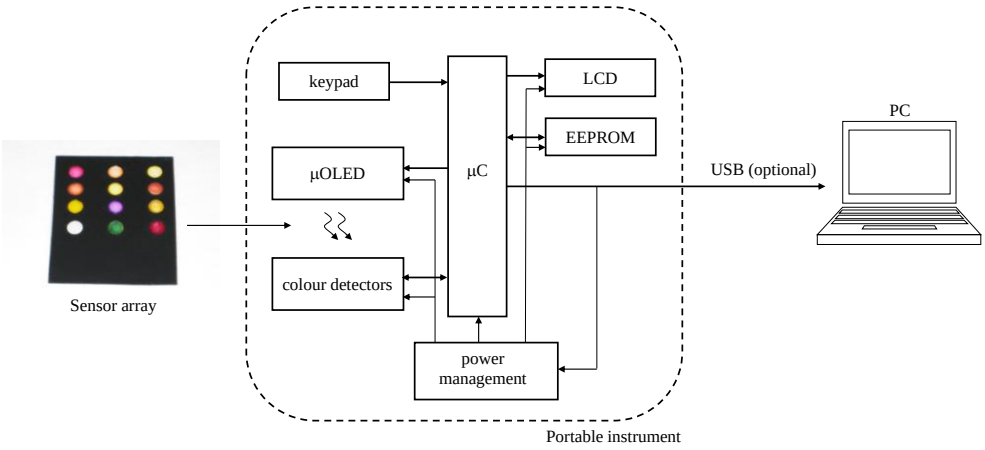

Figure 7.2. Block diagram of the developed instrument

The microcontroller in this prototype was model PIC18F4550 (Microchip Technology Inc., USA) which was selected because of the integration of a USB module that allows easy communication with the computer for design and calibration purposes, and the availability of five input-output ports to control all the other modules. The user interface of the portable instrument consists of a small keypad which lets the user select different measurement options through a menu which is presented on the LCD screen. The results of the measurements are also visible on this screen, although they can be also stored in an EEPROM memory for further processing.

2.4.1. Colour measuring module

This module is made up of an organic light-emitting diode display (OLED) working as a programmable light source [24,25] and twelve S9706 digital colour detectors (Hamamatsu Photonics, Japan) aligned with the sensor array. The light source is implemented by an OLED display, model 160-GMD1 (4D Systems, Australia), which communicates with the microcontroller via a two-wire serial bus. This is a compact, cost effective, all-in-one OLED display with an embedded graphics controller. The advantages of using this programmable light source against a light emitted diode (LED) lie on the possibility of the correction of the alignment with the detectors and the configuration of the light source by software. Due to these reasons the OLED was selected as light source despite its lower irradiance. The embedded commands not only control the background colour, but can produce text in a variety of sizes as well as draw shapes in 65 K colours while freeing up the host processor from screen control functions. Some of its main features are: 160 x 128 pixel resolution, 1.69" diagonal with an active area of 33.6 x 26.9 mm, only 5 pin interface to any host device, voltage supply from 3.6 V to 6.0 V and 40 mA nominal current when using a 5.0 V supply source, serial RS-232 (0-3.3 V), onboard micro-SD (µSD) memory card adaptor for storing illumination patterns and built-in graphics commands.

The colour measurement of the transmitted light through the sensor array is carried out with a set of 12 (3 x 4) colour detectors, model S9706 (Hamamatsu Photonics, Japan). This device is a digital colour sensor sensitive to red, green and blue spectral regions, which makes the simultaneous measurement of RGB colour coordinates possible. The chip integrates a set of photodiodes whose maximum sensitivity wavelength corresponds to the previous colours (λ_r=615 nm, λ_g=540 nm and λ_b=465 nm). The induced current of these photodiodes is on-chip processed to generate a digital output. This can be used to identify the colour of each element of the sensor array. The detected signals are serially output as 36-bit words, which make it possible to connect the sensors to the microcontroller without any need for additional signal processing. To enable measurement over a wide range of illuminants, the S9706 detector has two configuration parameters to select its active area and integration time. Internally, the active area of each detector (with dimensions of 1.2 x 1.2 mm) consists of 9 x 9 silicon photodiode elements in a mosaic, alternating red, blue and green sensitivity, and can be

configured in a high sensitivity mode, where the full area collects the incident light, or in a low sensitivity mode, where a 3 x 3 centre area is chosen to be active. In this work, a high sensitivity mode was always chosen to cover the entire membrane surface. The output of each detector was connected to a different input pin of the microcontroller. With this configuration, the measurement of all the membranes could be carried out at the same time, providing a fast response from the instrument.

2.5. Measurement procedure

The colour determination of the pH membranes was performed by measuring the transmitted light as follows: the sensor array was placed in the path of the light source from the programmable OLED display to the colour detector. In this design, the structure formed by the display and the colour detectors was shielded to prevent interferences due to external light; therefore, the instrument was enclosed in a black box with only one small opening to insert the sensor array board.

After the sensor array board was inserted into the instrument, the illumination pattern from the OLED display consists of a black background with the sequential illumination of circles (3 x 4), each aligned with an element of the sensor array and the corresponding colour detector. The pattern is not a static image, but a graphic sequence where the light source (circle) for each sensing element position only appears during the measurement of this element. Therefore, the illumination of each sensing element is done individually instead of simultaneously, in order to prevent stray light interference. The centre and the radii of these circles can be configured using software, which makes it possible to easily correct the alignment with the colour detectors. The photo in figure 7.3 shows the arrangement of the colour detectors and the light source pattern.

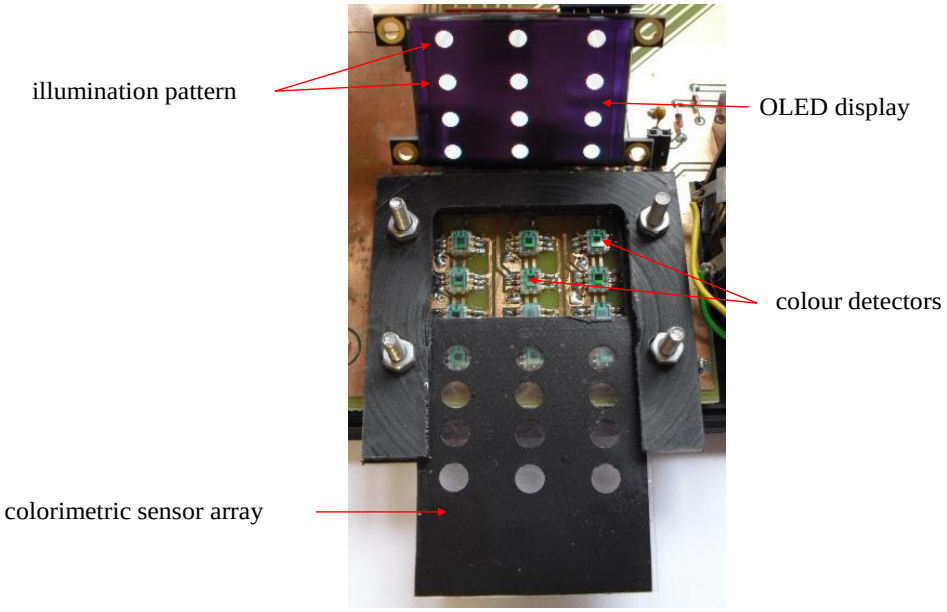

Figure 7.3. Photography of the sensing module showing the OLED display (with illumination circles), the colorimetric sensor array support and the digital colour detector array

The response of the measurement system was evaluated for each 0.1-0.2 pH unit from 0 to 14 by adding volumes of 1.0 M, 0.1 M or 0.01 M of HCl or of NaOH with a microburette to an aqueous solution containing the sensor array hanging from a support with a clamp. After each addition and magnetic stirring, the pH of the solution was measured using a potentiometric procedure. The array sensor was equilibrated for 5 min, and then was pulled out and inserted into the instrument to be measured.

3. Results and discussion

This section first discusses the results of the characterization and optimization of the measurement system, indicating the optimal configuration of the programmable light source, digital colour sensors and measurement conditions of the complete instrument. Later, a detailed discussion of its use as a pH-meter will be carried out, including a comparison with a laboratory colorimetric system, a study of the minimum number of sensing elements for univocal and precise determination of the pH with complete instrument modelling

and calibration. Finally, this calibration of the system will be validated and applied to real samples.

3.1 Characterization and optimization of measurement setup

3.1.1. OLED display

It is an advisable practice in colorimetric applications to use a light source as one of the standard illuminants. One of the most used illuminants is sunlight, such as the D65 illuminant [26]. As mentioned before, the light source used in the instrument is an OLED display which makes it possible to define up to 65,536 colours using the combination of three codes from 0 to 31 for the red and blue, and from 0 to 63 for green colour organic LEDs, all of which form the display. If the combination (31, 63, 31) is programmed in the display, its "white" colour is obtained. In figure 4, the spectrum of this white colour is displayed showing a notable excess of the blue component produced by the internal display configuration. Additionally, this figure shows the three separated spectral components, i.e., the (31, 0, 0), (0, 63, 0) and (0, 0, 31) colour codes corresponding to the separate activation of the red, green and blue organic LED of the display, respectively. Since the white colour has an excessive blue component – and in order to obtain an illuminant closest to the D65 standard – it was necessary to try other component combinations. The best result of this optimization process, reducing the blue component contribution, is shown in figure 7.4 and called "modified white", where the D65 spectrum is also shown with symbols for comparison. All the illuminant spectra depicted in figure 7.4 were tested as possible light source configurations. Best results were obtained with the "modified white"; therefore it was used as light source for the colour measurements. Given the spectral responses of the three RGB components of the display, some differences with the D65 spectrum can be observed, mainly below 450 nm and in the 525 to 600 nm spectral regions. Of course, these illuminant deficits will induce lower transmittance levels compared with those systems which have an illuminant closer to the D65 illuminant. Therefore, a priori, some differences may appear between this instrument and others.

In addition to the colour selection, the light intensity can be configured in this display. There are 16 levels of intensity from 0 (total darkness) to 15 (maximum brightness). The influence of this parameter was also analyzed, showing that an intermediate intensity range from 5 to 8 provides the best results for the sensing element array, showing a relative standard deviation (RSD) in the measured H value of 2.5%.

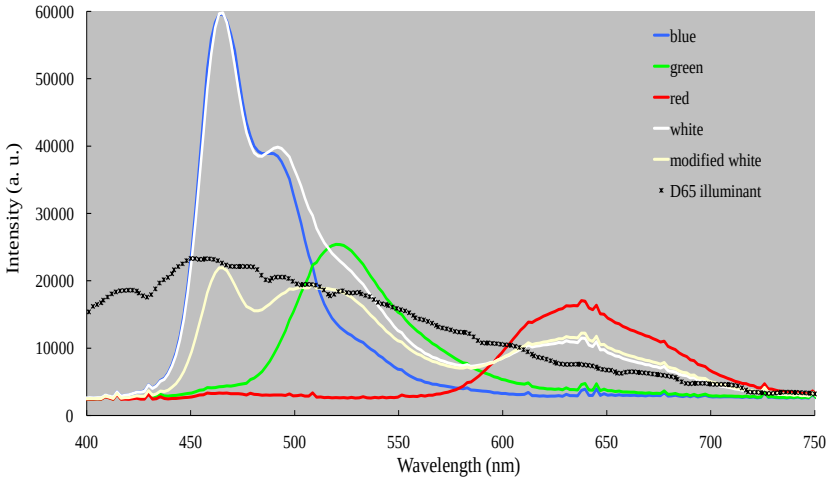

Figure 7.4. Spectra of the OLED display and D65 standard illuminant

After configuring an adequate illuminant spectrum and intensity, the lighting uniformity of the display was analyzed by sensing the emitted light with the digital colour sensor placed facing it in different positions. The results showed that the output signal presents no variation when the sensor is moved within the display area. Moreover, the stability of the display, as well as the velocity of the response, was tested measuring the light emitted when the display was switched on and off in alternate cycles from the modified white to black, as shown in figure 7.5. From this figure, it can be deduced that the light emission when the display is switched on is fast enough to prevent the need for time delays between the illumination and the measuring process. Moreover, figure 7.5 shows that the measured light is very stable and repetitive, with an RSD of 0.6% in H measurements.

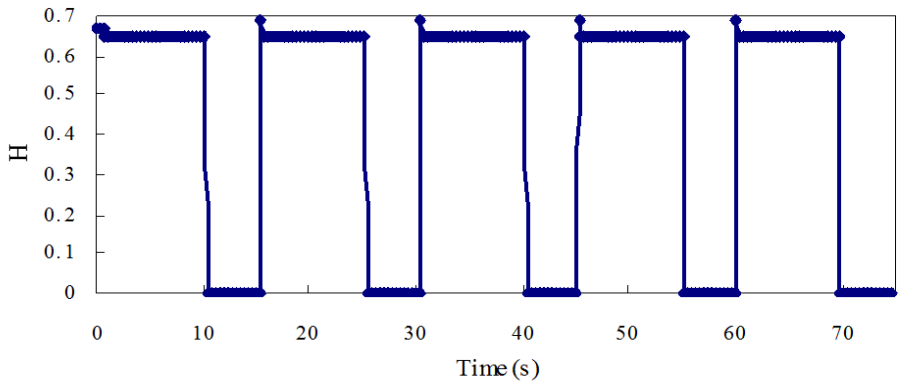

Figure 7.5. Stability and velocity test for illumination of the display with the modified white colour

As mentioned above, the light source for each sensing element is a circle with the modified white over a black background. The influence of the circle diameter on the system performance was also studied. It has been demonstrated that this does not produce any significant variation in the coordinate H calculation (less than 5% RSD) in the diameter range from 5.75 to 10.25 mm taking into account a sensor element diameter of 5 mm. Despite this, the error source does not affect the system because the circle diameter was fixed at 6.35 mm in this study.

3.1.2. Digital colour detectors

In addition to the sensitivity modes related to the selected active area, this sensor can externally configure the integration time, i.e., the time interval during the photodiode matrix generates a photocurrent for each optical radiation acquisition. This integration time can be easily changed from 10 μs to 100 s with a unique input pin. According to the device datasheet, under constant illumination conditions, the sensor output increases linearly with this time until reaching output saturation. A short integration time means fast acquisition, but with low intensity light collection, i.e., low sensitivity, whereas with a longer integration time, the sensitivity increases, but with a slower acquisition and the possibility of sensor output saturation. Therefore, there is a compromise in the choice of this configuration parameter. We checked the response of this sensor as a function of the integration time in the typical illumination conditions for this application and

concluded that the shortest time with optimal sensitivity and velocity of response was 200 ms. Moreover, our results show that there is no change in the H coordinate in the range from 150 ms to 500 ms, where the measured value presents an RSD of less than 0.8%.

Finally, the time stability of the S9706 detector response (integration time of 200 ms) was checked under continuous illumination. To reduce possible light source drifts, a white LED (NSPW300, Nichia, Japan), biased with a thermal stabilized current source, was used in this test, resulting in an output signal drift lower than 0.1%, acquiring a signal every 0.2 s during 90 minutes.

3.2. pH measurement

This section describes the procedure followed for the pH determination based on the colour measurements. First, the response of each sensing element in the full pH range was measured with the instrument. From these data, a minimization of the number of membranes needed for pH determination was carried out, reducing the initial array containing eleven elements to a four membrane array that covers the full pH range.

3.2.1. Characterization and minimization of the sensor array

The characterization of the sensor array was performed by measuring the H coordinate in the whole pH range using 12 replicate arrays. This was done by adding acid or base solutions to an aqueous solution containing the sensor array hanging from a support. As could be expected, the experimental curves for each membrane (figure 7.6) show the usual sigmoid shape, which in some cases was double.

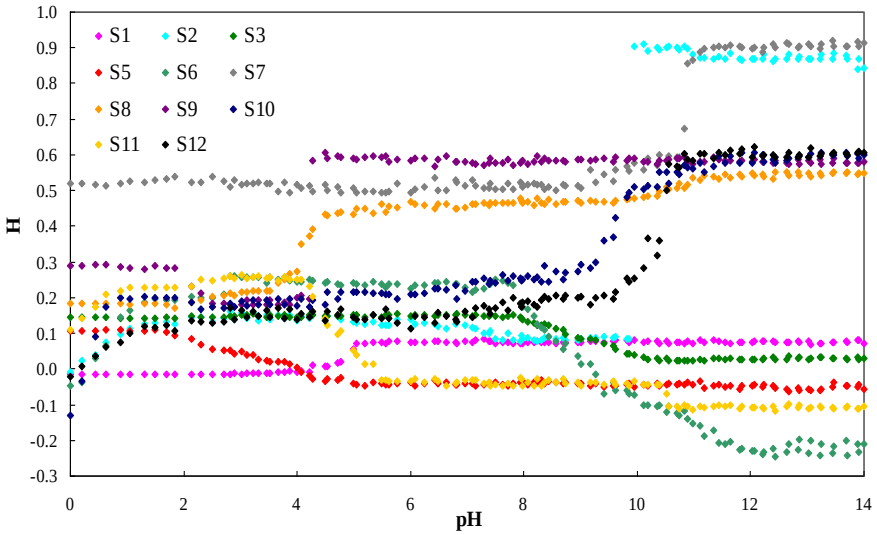

Figure 7.6. Sensor array response (in H coordinates) to pH.
Sensing element numbering was defined in figure 7.1

The immobilized acid-base indicators belong to neutral, cationic and anionic types, and the heterogeneous reaction with acid or base in the membrane phase involves either ion-exchange or co-extraction mechanisms characterized by an equilibrium constant K_e which includes the acidity constant, the distribution constant between aqueous and membrane phases of different species, and the dissociation constants for the different ion-pairs involved. Table 7.2 shows the corresponding K_e calculated for each membrane along with the transition pH range, the colour and the H values for the acid and basic forms. Comparing the K_e values obtained with the portable instrument and those provided by a scanner working in transmission mode, some differences can be observed, although for purpurin, bromothymol blue and phenol red, the differences were higher than one order of magnitude. The differences can be justified by differences in the illuminant and photodetectors used in each case.

Table 7.2. K_e values for sensing elements calculated from scanner and portable instrument H values

Membrane	Indicator	pH range	Scanner	Portable instrument	Membrane colours	
			K_e	K_e	Acid	Base
S1	Sicomet red P	5.18-6.60	$7.1 \cdot 10^{-5}$	$2.7 \cdot 10^{-5}$	Nadeshiko pink (0.976)	Navajo white (0.089)
S2	m-Cresol purple	0-1.90	$4.9 \cdot 10^{0}$	$1.4 \cdot 10^{0}$	Wild watermelon (0.992)	Canary yellow (0.150)
		8.65-10.77	$2.8 \cdot 10^{-9}$	$3.2 \cdot 10^{-9}$	Mustard (0.128)	Persian indigo (0.881)
S3	PAN	7.57-10.95	$3.4 \cdot 10^{-9}$	$4.3 \cdot 10^{-9}$	Lemon (0.159)	Scarlet (0.023)
S5	Purpurin	1.90-4.56	$2.0 \cdot 10^{-3}$	$7.0 \cdot 10^{-3}$	Chrome yellow (0.110)	Carnation pink (0.960)
		12.44-13.81	$9.4 \cdot 10^{-7}$	$2.9 \cdot 10^{-8}$	Mauvelous (0.970)	Pastel magenta (0.945)
		-	$7.3 \cdot 10^{-10}$	-	-	-
S6	Cresol red	7.35- 3.19	$4.3 \cdot 10^{-9}$	$4.5 \cdot 10^{-9}$	Canary yellow (0.167)	Violet (0.644)
S7	Liphophilized Nile blue	9.46–11.99	$1.3 \cdot 10^{-10}$	$3.2 \cdot 10^{-10}$	Deep sky blue (0.520)	Cerise pink (0.917)
S8	Bromothymol blue	2.82-7.15	$7.1 \cdot 10^{-6}$	$2.5 \cdot 10^{-4}$	Pear (0.185)	Cadet blue (0.541)
S9	Alizarin	4.56-6.35	$2.2 \cdot 10^{-5}$	$2.0 \cdot 10^{-4}$	Maize (0.290)	Dark pastel blue (0.580)
S10	Thymol blue	0-0.85	$3.7 \cdot 10^{0}$	$5.5 \cdot 10^{0}$	Hot magenta (0.875)	Lemon (0.182)
		8.87-10.36	$1.3 \cdot 10^{-8}$	$4.4 \cdot 10^{-9}$	Yellow (0.207)	Celestial blue (0.582)
S11	Phenol red	5.37-6.80	$1.2 \cdot 10^{-8}$	$4.4 \cdot 10^{-6}$	Old gold (0.137)	Amaranth (0.963)
		9.46-11.40		$3.3 \cdot 10^{-10}$	French rose (0.953)	Deep pink (0.905)
S12	Thymol blue	0-1.42	$1.5 \cdot 10^{0}$	$1.8 \cdot 10^{0}$	Deep cerise (0.979)	Golden yellow (0.127)
		9.04-11.56	$3.7 \cdot 10^{-9}$	$8.2 \cdot 10^{-10}$	Canary yellow (0.150)	Blue gray (0.609)

As an example, figure 7.7 presents the responses obtained for two membranes (S2 and S12) with the new prototype and a commercial scanner. The response curves are very similar, although they were obtained in very different ways: while the line was generated from digital images acquired with the scanner and processed in the computer to calculate the corresponding H value [27], the symbols were obtained from the output data of the S9706 colour detectors, with no further processing. This implies a considerable reduction in the complexity of the determination of the pH. Similar results were obtained in the comparison with

the rest of the sensing elements, showing only some minor discrepancies due to illuminant and detector differences.

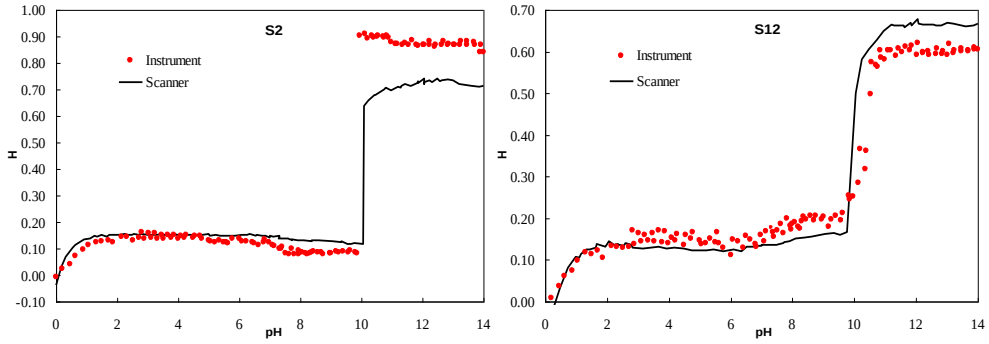

Figure 7.7. Comparison of the pH response of S2 (left) and S12 (right) sensing elements measured with the proposed system (symbols) and the commercial scanner (lines)

From the response curves (figure 7.6), it can be seen that the colour changes of the sensor array membranes cover the full pH range. Table 7.2 presents the pH ranges where the different membranes exhibit some colour variation. As can be seen, there are many membranes whose response covers the same pH range, which makes it possible to reduce the number of elements due to the fact that they generate redundant information. Taking into account the data from figure 7.6 and table 7.2, a minimization of the required membranes for full-range pH determination was done. The criteria followed for this minimization was selecting membranes with: (i) maximum H variation combined with maximum covered pH range and, (ii) minimum pH range overlapping. As a result, the sensing elements selected in this work were positions S2 (m-cresol purple membrane), S5 (purpurin membrane), S6 (cresol red membrane) and S8 (bromothymol blue membrane). The next section shows how to calculate a unique value of pH from the results of the colour measurements from only four sensing elements.

3.2.2. Response modelling and pH calculation

Figure 7.6 shows that the H value obtained for each sensing element can result in several values of pH in the full range, with only one of them being correct. Therefore, there is no univocal relationship between an H and a pH value

with the selected four sensing elements if they are individually analyzed. To solve this, a two-step procedure is proposed. First, the pH range which includes the correct value must be determined. To do this, all the possible pH values of the sensing elements corresponding to the measured H coordinates need to be calculated. With this objective, the responses of the selected membranes were modelled, splitting them into increasing or decreasing linear sections, as depicted in figure 7.8 for membranes S5 and S6.

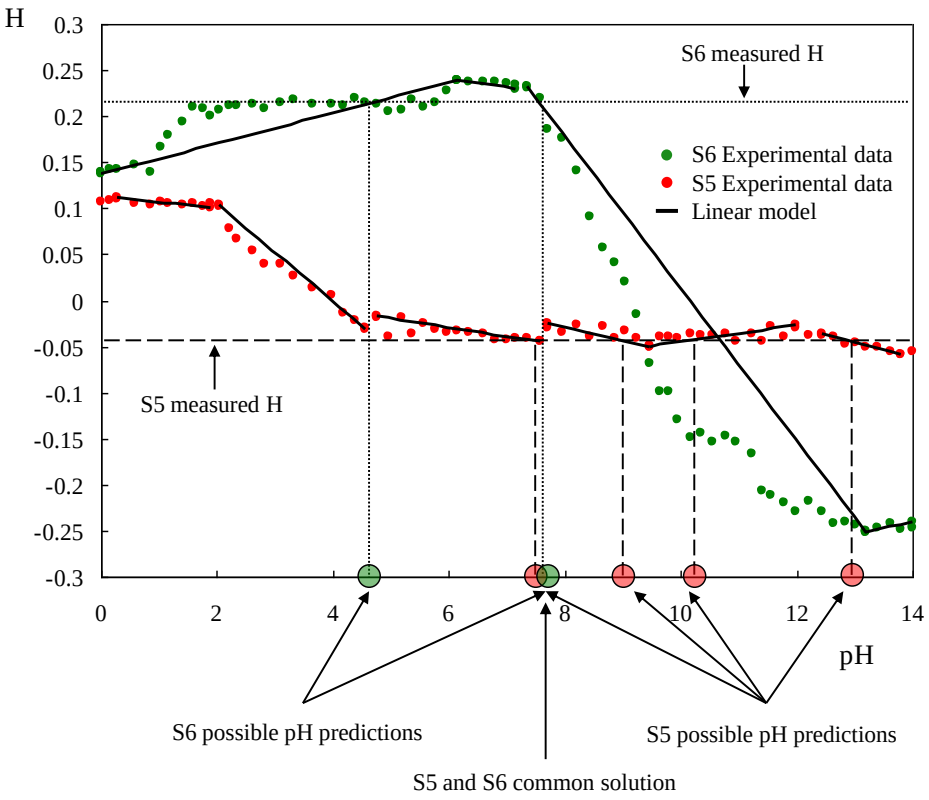

Figure 7.8. Linear modelling of the membrane S5 and S6 responses (linear sections). Dashed horizontal lines represent measured H values with possible pH ranges for each sensing element and common pH range on the abscise axis

This figure presents an example of the possible pH predictions for a given H measurement. As can be seen, there are several points of pH that provide the same value of H for each membrane. The microcontroller solves each linear equation resulting from the linear section applied to the experimental H and generates a list of possible pH predictions. In the example in figure 7.8, these

ranges correspond to Sections 2-5 in membrane S5, and Sections 1 and 3 in membrane S6. In this case, the only coincidence is found in Section 3 of each sensing element, indicating the approximate range where the final pH value will be. This process was repeated for the four selected membranes, obtaining four lists from which it is possible to determine the only range common to the four membranes as the correct solution. Since the linear model is not accurate, the pH ranges with the functioning corresponding sections are used as possible solutions, instead of the final pH values.

After this range was determined according to this method, a more precise pH value was calculated using a more accurate model of the corresponding sensing element response. Having to choose between the curve fit and the complex calculations needed for microcontroller programming, cubic polynomial modelling functions were selected. This made it possible to adjust the experimental data with high fidelity in the range of interest, i.e., the pH range where each sensing element changes its colour. These equations are simple enough to be able to calculate the pH with the microcontroller, which must provide a prediction of the pH within a short time after the colour measurements. Figure 7.9 shows the experimental H values measured for the selected four sensors presented as symbols and the polynomial fit of these curves in the appropriate pH range, shown as lines. Thus, the fine modelling is done with these functions:

$$H(pH) = A + B \cdot pH + C \cdot pH^2 + D \cdot pH^3 \qquad (7.1)$$

The coefficients of the fit functions, as well as the pH range where they are defined, are listed in table 7.3. It is must be noted that sensing element S5 was modelled in two different pH ranges. Finally, the pH calculation corresponding to a measured value of H was obtained by solving the third degree equation for the particular membrane modelled in the selected range.

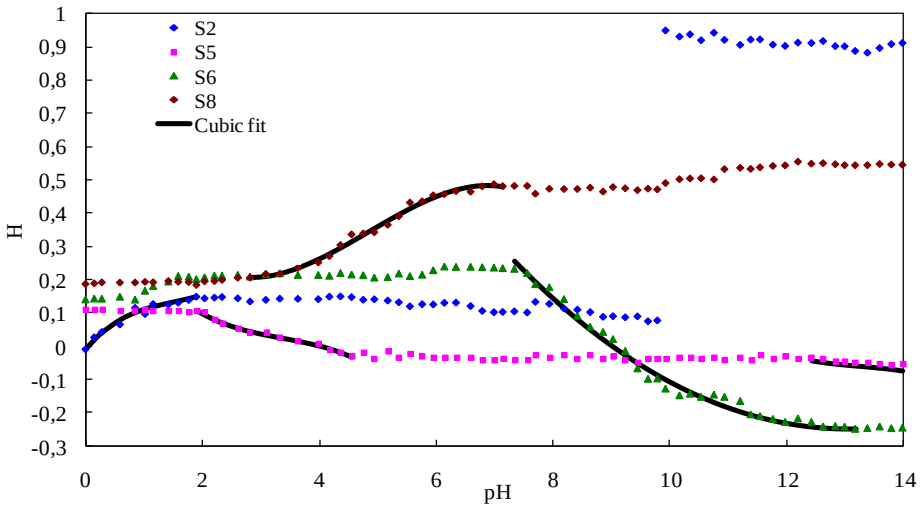

Figure 7.9. Experimental H values of the four selected sensing elements (symbols) and cubic modelling (solid lines) for the pH ranges of interest

Table 7.3. Cubic modelling coefficients, indicating valid pH ranges

Membrane	*A*	*B*	*C*	*D*	R^2	pH range
S2	-0.006	0.200	-0.109	0.024	0.973	0 - 1.90
S5	0.566	-0.416	0.113	-0.011	0.991	1.90 - 4.56
S8	0.794	-0.483	0.121	-0.008	0.991	2.82 - 7.15
S6	2.582	-0.459	0.020	-0.0002	0.988	7.35 - 13.19
S5	17.047	-3.840	0.288	-0.007	0.966	12.44 - 14.0

This reconstruction algorithm was applied to a set of 102 validation data, with twelve replicates, covering the full pH range. We applied a Kolmogorov-Smirnov test to check whether the validation data set and the model prediction may be assumed to be normal. The confidence level of the test was the standard 80%, providing the probability values of 0.476 (validation set) and 0.259 (prediction for the validation set). Therefore, all the data distributions passed the test since the p-values were higher than 0.2. In order to test the prediction performance of the method, we applied a Student's t-test with a confidence level of 95%, to check whether the data distributions resulting from the predicted values in the validation data set differ significantly from the real data (using a potentiometric method as reference). The probability value obtained was 0.6593

(higher than 0.05), so we may conclude that the model is able to predict pH suitably since there are no significant differences between the real and predicted pH data. To finish the analysis, we applied a Pearson's correlation test to measure the quality of the predicted versus the real values. The result of the test provided a probability value under 2.2×10^{-16} in the validation data set, and we therefore may conclude that there is a significant correlation between the real and predicted values. Figure 7.10A contains the regression line between the real and predicted data validation. The correlation coefficient R^2 was calculated and the test provided the value 0.997. Consequently, it may be assumed that the prediction model provides a suitable performance for the task of pH prediction. As can be seen, the pH predictions fit the original pH values with high fidelity in the range from 0 to 14, although the accuracy decreases for pH values higher than 13, due to the lower H variation of the sensor array in that range as is apparent in figures 7.6 and 7.7.

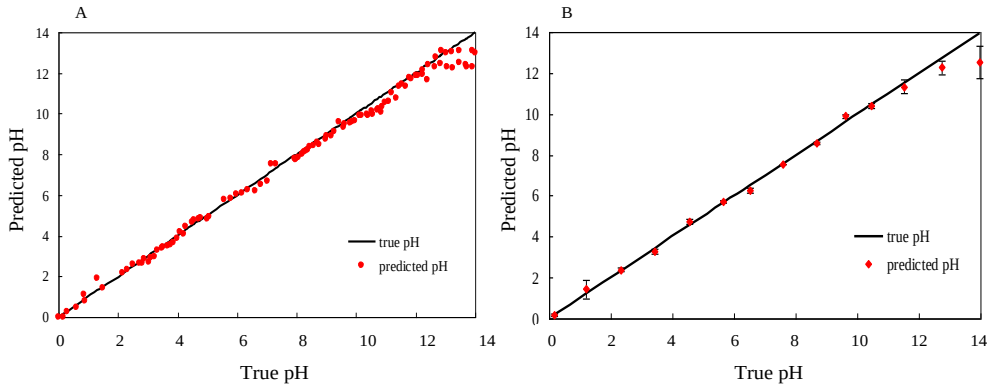

Figure 7.10. (A) Comparison between the modelling prediction of the four sensing elements (symbols) and validation experimental data (line) in the full pH range. (B) Comparison between pH values obtained from our system (symbols) and those measured by a reference method (line) for real samples. Error bars show three times the standard deviation of the values obtained with the proposed pH-meter

The main technical specifications of the developed instrument are listed in table 7.4. The resolution was calculated as follows: the coordinates RGB resulting from a colour measurement are coded as a 12-bit word each one. Therefore, the H parameter could be expressed as a 12-bit word since it is calculated as a linear combination of RGB coordinates. Assuming a worst case in

which only 10 bits are significative and a range of H from -0.3 to 1 (figure 7.9), the resolution of H is 0.0013. Taking into account that the corresponding pH range is 0 to 14, the resolution in units of pH is approximately 0.02. The accuracy is obtained from the validation data as the standard deviation. The value from this calculation is 0.2. The response time of the instrument was obtained as the sum of the response of each digital colour sensor which consists of the integration time (200 ms) and the processing of the RGB word (175 ms).

Table 4. Technical specifications

Number of sensors	12 max.
pH range	0-14
Resolution	0.02
Accuracy	0.2
Response time	1.5 s
Dimensions	15 cm × 17 cm × 5 cm
Weight	400 g
Connectivity	USB 2.0
Power	PP3 battery

3.2.3. Application to real samples

The proposed measurement system was applied to fourteen real water samples (tap and river water from Granada, Spain), with the pH adjusted with acid and base covering the full pH range from 0 to 14. After reaction with samples, the sensor arrays (6 replicates) were measured and the pH values calculated.

The MSE obtained for real water samples was 0.180. As in the case of the validation data set, different tests were applied to check the results. The Kolmogorov-Smirnov test, with a confidence level of 80%, provided the probability values of 0.001 for both test and prediction sets. Since these values are under 0.2, they cannot be assumed to be normal and the Student's t-test is not reliable. Thus, we applied the Kruskal-Wallis test, with a confidence level of 95%. The

probability value obtained was 0.9268 (higher than 0.05), so we can assume that there are no significant differences between the real (found by glass electrode potentiometry) and predicted pH values in the test data set. The Pearson correlation test provided a probability value under 2.07×10^{-14}, showing that there is a significant correlation between the reference and predicted values. The good correlation coefficient R^2 calculated (0.997) ensures a high positive correlation between the real and predicted data (figure 7.10B). These results confirm that the instrument is an efficient tool to automatically measure pH in solutions within a very wide range and with acceptable accuracy.

4. Conclusions

A portable optical multianalyte instrument with up to twelve sensing channels is presented and used for the determination of the full pH range. The analytical procedure is based on the colour determination of an array of four sensing membranes. This characteristic produces a very simple electronic design with an important reduction in the number of electronic components. The light source, an OLED programmable display, and an array of digital colour detectors were responsible for colour coordinate determination. A complete analytical and technical characterization was carried out, showing a good agreement with pH measurements from reference instruments. This resulted in a microcontrol-based easy-to-use measurement system with high optical and electrical interference immunity and extremely simple digital signal processing circuitry with commercially available electronic components. The MSE obtained for real water samples was 0.180, which is worse than those obtained in previous work using a Sigmoid competition approach (0.111) or neural networks (0.043), but it can be acceptable for a portable instrument [20,21].

Acknowledgements

We acknowledge financial support from the *Ministerio de Ciencia e Innovación, Dirección General de Investigación y Gestión del Plan Nacional de I+D+i* (Spain) (Projects CTQ2009-14428-C02-01 and CTQ2009-14428-C02-02);

and the *Junta de Andalucía* (*Proyecto de Excelencia* P08-FQM-3535). These projects were partially supported by European Regional Development Funds (ERDF).

References

[1] J. Workman, M. Koch, B. Lavine, R. Chrisman. *Process analytical chemistry*. Anal. Chem., 81(12) (2009) 4623-4643.

[2] W. Gopel. *Chemical imaging I, concepts and visions for electronic and bioelectronic noses*. Sens. Actuators B, 52 (1998) 125-142.

[3] A. Roda, M. Guardigli, P. Pasini, M. Mirasoli, E. Michelini, M. Musiani. *Bio- and chemiluminescence imaging in analytical chemistry*. Anal. Chim. Acta, 541(1-2) (2005) 25-35.

[4] A. Abbaspour, M.A. Mehrgardi, A. Noori, M.A. Kamyabi, A. Khalafi-Nezhad, M.N. Soltani Rad. *Speciation of iron(II), iron(III) and full-range pH monitoring using paptode: A simple colorimetric method as an appropriate alternative for optodes*. Sens. Actuators B, 113 (2006) 857-865.

[5] A. Safavi, N. Maleki, A. Rostamzadeh, S. Maesum. *CCD camera full range pH sensor array*. Talanta, 71 (2007) 498-501.

[6] B.P. Corgier, C.A. Marquette, L.J. Blum. *Screen-printed electrode microarray for electrochemiluminescent measurements*. Anal. Chim. Acta, 538(1-2) (2005) 1-7.

[7] T.E. Curey, A. Goodey, A. Tsao, J. Lavigne, Y. Sohn, J.T. McDevitt, E.V. Anslyn, D. Neikirk, J.B. Shear. *Characterization of multicomponent monosaccharide solutions using an enzyme-based sensor array*. Anal. Biochem., 293(2) (2001) 178-184.

[8] T. Mayr, G. Liebsch, I. Klimant, O.S. Wolfbeis. *Multi-ion imaging using fluorescent sensors in a microtiterplate array format*. Analyst, 127 (2002) 201-203.

[9] F.J. Steemers, D.R. Walt. *Multi-analyte sensing: from site-selective deposition to randomly-ordered addressable optical fiber sensors*. Mikrochim. Acta, 131(1-2) (1999) 99-105.

[10] J.J. Lavigne, E.V. Anslyn. *Sensing a paradigm shift in the field of molecular recognition: from selective to differential receptors*. Angew. Chem. Int. Ed., 40 (2001) 3118.

[11] Y. Vlasov, A. Legin, A. Rudnitskaya, C. Di Natale, A. D'Amico. *Nonspecific sensor arrays (electronic tongue) for chemical analysis of liquids: (IUPAC technical report)*. Pure Appl. Chem., 77(11) (2005) 1965-1983.

[12] K.L. Michael, L.C. Taylor, S.L. Schultz, F. Szurdoki, D.R. Walt. *Making sensors out of disarray: optical sensor microarrays*. Proc. SPIE, 3270 (1998) 34-41.

[13] D.R. Walt. *Techview: molecular biology. Bead-based fiber-optic arrays*. Science, 287 (2000) 451-452.

[14] A.P. Goodey, J.J. Lavigne, S.M. Savoy, M.D. Rodriguez, T. Curey, A. Tsao, G. Simmons, J. Wright, S.J. Yoo, Y. Sohn, E.V. Anslyn, J.B. Shear, D.P. Neikirk, J.T. McDevitt. *Development of multianalyte sensor arrays composed of chemically derivatized polymeric microspheres localized in micromachined cavities*. J. Am. Chem. Soc., 123(11) (2001) 2559-2570.

[15] J.J. Lavigne, S. Savoy, M.B. Clevenger, J.E. Ritchie, B. McDoniel, S.J. Yoo, E.V. Anslyn, J.T. McDevitt, J.B. Shear, D. Neikirk. *Solution-based analysis of multiple analytes by a sensor array: toward the development of an "electronic tongue"*. J. Am. Chem. Soc., 120 (1998) 6429-6430.

[16] N.T. Greene, S.L. Morgan, K.D. Shimizu. *Molecularly imprinted polymer sensor arrays*. Chem. Commun. (2004) 1172-1173.

[17] L. Baldini, A.J. Wilson, J. Hong, A.D. Hamilton. *Pattern-based detection of different proteins using an array of fluorescent protein surface receptors*. J. Am. Chem. Soc., 126(18) (2004) 5656-5657.

[18] C. Zhang, K.S. Suslick. *A colorimetric sensor array for organics in water*. J. Am. Chem. Soc., 127(33) (2005) 11548-11549.

[19] J. Janata. *Do Optical Sensors Really Measure pH?* Anal. Chem., 59 (1987) 1351-1356.

[20] S. Capel-Cuevas, M.P. Cuéllar, I. de Orbe Payá, M.C. Pegalajar, LF. Capitán-Vallvey. *Full-range optical pH sensor based on imaging techniques*. Anal. Chim. Acta, 681 (2010) 71-81.

[21] S. Capel-Cuevas, M.P. Cuéllar, I. de Orbe-Payá, M.C. Pegalajar, L.F. Capitán-Vallvey. *Full-range optical pH sensor array based on neural networks*. Microchem. J,. 97 (2011) 225-233.

[22] M.D. Fernández-Ramos, M. Greluk, A.J. Palma, E. Arroyo-Guerrero, J. Gómez-Sánchez, L.F. Capitán-Vallvey. *The use of one-shot sensors with a dedicated portable electronic radiometer for nitrate measurements in aqueous solutions*. Meas. Sci. Technol., 19(9) (2008) 095204/1-095204/7.

[23] A.J. Palma, A. Lapresta-Fernandez, J.M. Ortigosa-Moreno, M.D. Fernandez-Ramos, M.A. Carvajal, L.F. Capitan-Vallvey. *A simplified measurement procedure and portable electronic photometer for disposable sensors based on ionophore-chromoionophore chemistry for potassium determination*. Anal. Bioanal. Chem., 386(5) (2006) 1215-1224.

[24] D. Filippini, S.P.S. Svensson, I. Lundström. *Computer screen as a programmable light source for visible absorption characterization of (bio)chemical assays*. Chem. Commun., 2 (2003) 240-241.

[25] S. Macken, C. Di Natale, R. Paolesse, A. D'Amico, I. Lundstroem, D. Filippini. *Towards integrated devices for computer screen photo-assisted multi-parameter sensing*. Anal. Chim. Acta, 632(1) (2009) 143-147.

[26] G. Wyszecki, W. S. Stiles. *Color Science: Concepts and Methods, Quantitative Data and Formulae*. Wiley Classics Library, Denver, USA (2000).

[27] K. Cantrell, M.M. Erenas, I. de Orbe-Payá, L.F. Capitán-Vallvey. *Use of the Hue Parameter of the Hue, Saturation, Value Color Space As a Quantitative Analytical Parameter for Bitonal Optical Sensors*. Anal. Chem., 82 (2010) 531-542.

PUBLICACIÓN VI:

Sensors, 12 (2012) 6746-6763
DOI: 10.3390/s120506746

A Compact Optical Instrument with Artificial Neural Network for pH Determination

Sonia Capel-Cuevas[a], Nuria López-Ruiz[b], Antonio Martinez-Olmos[b], Manuel P. Cuéllar[c], Maria del Carmen Pegalajar[c], Alberto José Palma[b], Ignacio de Orbe-Payá[a], Luis Fermin Capitán-Vallvey[a,*]

[a]*Department of Analytical Chemistry, Campus Fuentenueva, Faculty of Sciences.*
[b]*Department of Electronics and Computer Technology, Campus Fuentenueva, Faculty of Sciences.*
[c]*Department of Computer Science and Artificial Intelligence.*
E.T.S. Ingenierías Informática y de Telecomunicación.
University of Granada, E-18071 Granada, Spain

Abstract

The aim of this work was the determination of pH with a sensor array-based optical portable instrument. This sensor array consists of eleven membranes with selective colour changes at different pH intervals. The method for the pH calculation is based on the implementation of artificial neural networks that use the responses of the membranes to generate a final pH value. A multi-objective algorithm was used to select the minimum number of sensing elements required to achieve an accurate pH determination from the neural network, and also to minimise the network size. This helps to minimise instrument and array development costs and save on microprocessor energy consumption. A set of artificial neural networks that fulfils these requirements is proposed using different combinations of the membranes in the sensor array, and is evaluated in terms of accuracy and reliability. In the end, the network including the response of the eleven membranes in the sensor was selected for validation in the instrument prototype because of its high accuracy. The performance of the instrument was

evaluated by measuring the pH of a large set of real samples, showing that high precision can be obtained in the full range.

Keywords: portable instrument; H coordinate; HSV colour space; pH sensor array; neural networks

* Corresponding author; e-mail: lcapitan@ugr.es

1. Introduction

In general, optical pH sensors are based on reversible changes induced by pH in the structure of an acid-base indicator and translated into changes in spectroscopic phenomena such as absorption, reflectance, luminescence, and energy transfer. Nevertheless, some optical sensors are not based on acid—base indicators, such as those based on changes in the ionisation of unclad silica optic fibre by pH traced by methylene blue adsorption via evanescent field [1] and the pH-dependent polymer swelling of functionalised polymer microspheres dispersed in a hydrogel membrane that change the membrane turbidity [2].

According to the Henderson–Hasselbalch equation, the change in the measured signal with pH results is described by a narrow sigmoidal shape. Thus, the dynamic working range for pH optical sensors is limited to a few pH units (2–3) [3] and even shorter if the linear relationship in the middle of the sigmoidal response is used. This short range is one of the main drawbacks of these optical sensors for pH, along with their nonlinear response, which requires different sensing membranes to cover the whole pH range.

A common strategy to extend the working range of pH optical sensors consists of the preparation of arrays of sensing membranes containing complementary pH indicators that acquire the analytical information by imaging techniques. In this way, commercial multi-colour pH paper strips have been measured with a conventional scanner [4,5]; alternatively, arrays of five pH membranes in a triacetylcellulose support measured with a CCD colour camera have been described [6]. In both cases, the average RGB values of each sensing area image are used for calibration with multi-linear mathematical models.

Suzuki *et al.* [7] developed a micro-well array chip system for parallel monitoring of single cell function, considering pH and oxygen concentrations as good indicators for cell activity. Fluorescein isothiocyanate (FITC) was used as a pH sensing indicator and the fluorescence intensity of each well was measured by using a high resolution microarray scanner.

One drawback of this calibration process is the non-linear dynamics of the functions to approximate the pH with respect to the colour parameters. Neural networks [8] have also been proposed to solve this problem, although the limitations of their classic training methods, becoming trapped in local optima solutions, may make the model calibration processes difficult [9]. Taib *et al.* [10] applied an artificial neural network for the analysis of the response of an optical fibre pH sensor (pH 2.51–9.76) based on a 3,4,5,6-tetrabromophenol sulphonephthalein indicator. The error produced during testing and application, using a network architecture of eight input neurons, 13 neurons in a single hidden layer and one output, was 0.08 and 0.07 pH, respectively. Other authors [11] have developed an optical pH sensor based on the immobilization of a mixture of two dyes on a triacetylcellulose membrane. The measuring range of the optode was extended by application of a back-propagation artificial neural network (ANN) to the whole pH range, providing mean square errors of 0.03 and 0.04 for test and control sets, respectively.

Previous work by our group has focused on the development of a disposable optical sensor array to predict the pH of a solution over the full-range (0–14). This pH determination was obtained from the hue (H) values of the HSV colour space using a scanner and custom developed portable instrumentation to image the optical array containing 11 sensing elements with immobilised pH indicators and using diverse mathematical modelling [12–14]. In the first case [12], three different approaches for pH prediction were studied: Linear models, Sigmoid competition models and Sigmoid surface models, providing mean square errors (MSE) of 0.111, 0.075 and 0.266, respectively, for tap and river water samples. Then, neural networks were used as a prediction technique [13]. The best network structure obtained with the traditional trial-and-error procedure and using the Levenberg–Marquardt training algorithm was made up of 11 input neurons, 10 hidden neurons and one output neuron for pH prediction, providing an MSE of 0.043. In the last case [14], a handheld instrument was presented for the

measurement of pH using a disposable optical sensor array with more simple electronics than our previously designed photometers [15,16]. The acquisition of colour information from the array is obtained with a wide and programmable light source and a set of colour detectors that output the measured RGB coordinates coming from each membrane, in digital format, and used to calculate the H of the HSV colour space as the analytical parameter.

In this paper, the previously characterised portable instrumentation, which was optical and electrical, has been improved and the neural network programming optimised for the prediction of the pH in the full range. In our approach, the hue colour feature, obtained by means of imaging techniques from a sensor array, is used as the input for a neural network that provides the pH of a sample. This network is implemented in the microcontroller of the portable instrument. In addition, we also provide a procedure to minimise the number of sensing elements during calibration that could be used to achieve a suitable pH prediction in test and validation, with the aim of minimising the final instrument prototype cost and saving energy. We explored this problem previously [16] for scanned images in the laboratory, obtaining very accurate results. In this work, the hue colour parameter from each sensing element is extracted by the colour detectors implemented in the portable instrument to build the calibration data set. Then, a multi-objective algorithm provides a set of neural networks with maximum accuracy and the optimal sensing elements to be included in the sensor array.

This calculation method for pH prediction has been included in the memory of the microcontroller of the instrument. The prototype was then used to measure pH in a large variety of real samples, with good performance and little error.

2. Experimental

2.1. Reagents and Materials

The chemicals used for preparing the pH sensitive films were high molecular weight polyvinyl chloride (PVC), o-nitrophenyloctylether (NPOE), dioctyl

sebacate (DOS), bis(1-butylpentyl)adipate (BBPA), tributyl phosphate (TBP), potassium tetrakis (4-chlorophenyl)borate (TCPB), tridodecyl-methylammonium chloride (TDMAC), Aliquat 336, cellulose acetate (CA), ethylene glycol and tetrahydrofuran (THF) all purchased from Sigma (Sigma-Aldrich Química S.A., Madrid, Spain). As acid-base indicators: 1-amino-4-hydroxyanthraquinone, sodium 3,3-[(1,1-biphenyl)-4,4-diyl(azo)] bis(4-aminonaphtalenesulfonate), N-[4-[bis[4-(dimethylamino)phenyl]methylene]-2,5-cyclohexadien-1-ylidene]-N-methylmethanaminium chloride (crystal violet), 2-(1,3-dihydro-3-oxo-2H-indol-2-ylidene)-1,2-dihydro-3H-indol-3-one (indigotin blue), 2-[2-[4-(dimethylamino)phenyl]diazenyl]-benzoic acid (methyl red), 4,4'-(1,1-dioxide-3H-2,1-benzoxathiol-3-ylidene)bis[2-bromo-3-methyl-6-(1-methylethyl)phenol (bromothymol blue), 4,4'-(1,1-dioxide-3H-2,1-benzoxathiol-3-ylidene)bis[2-bromo-6-methylphenol (bromcresol purple), N,N'-[(1,1-dioxide-3H-2,1-benzoxathiol-3-ylidene)bis[(6-hydroxy-5-methyl-3,1-phenylene)methylene]]bis[N-(carboxymethyl)-glycine (xylenol orange), 4,4'-(1,1-dioxide-3H-2,1-benzoxathiol-3-ylidene)bisphenol (phenol red), 4,4'-(1,1-dioxide-3H-2,1-benzoxa-thiol-3-ylidene)bis[5-methyl-2-(1-methylethyl)phenol] (thymol blue), 4,4'-(1,1-dioxide-3H-2,1-benzoxathiol-3-ylidene)bis[3-methylphenol] (m-cresol purple), N8,N8,3-trimethyl-2,8-phenazine-diamine hydrochloride (neutral red) and 1-phenylazo-2-naphthol (sudan I), 1-(2-pyridylazo)-2-naphthol (PAN) from Sigma, (1,2-benzo-7-(diethylamino)-3-(octadecanoylimino) phenoxazine (liphophilised Nile blue), 9-(diethylamino)-5H-benzo[a]phenoxazin-5-one (Nile red), 1,2,4-trihydroxy-9,10-anthracenedione (purpurin) and 4-(2-pyridylazo)resorcinol (PAR) from Fluka (Fluka, Madrid, Spain), 4,4'-(1,1-dioxide-3H-2,1-benzoxathiol-3-ylidene)bis[2-methylphenol] (cresol red) from Panreac (Panreac, Barcelona, Spain), 1,2-dihydroxy-9,10-anthracenedione (alizarine) from TCI (TCI Europe, Belgium), calcium 3-hydroxy-4-[2-(4-methyl-2-sulfophenyl)diazenyl]-2-naphthalene-carboxylate from BASF (BASF, Ludwigshafen, Germany), 1,4-dihydroxyanthraquinone and 1,5-dihydroxyanthraquinone from ICN (ICN K&K Laboratories, Plainview, NY, USA), 2,6-dihydroxy-anthraquinone from EGA (EGA Chemie, Steinheim, Germany) were used. Sheets of Mylar-type polyester (Goodfellow, Cambridge, UK) were used as support. HCl and NaOH were supplied by Sigma. All reagents were of analytical reagent grade and were used without any further purification. All solutions were prepared in reverse-osmosis type quality water (Milli-RO 12 plus Milli-Q station from Millipore, conductivity 18.2 Mohm/cm).

2.2. Instruments and Software

The optical spectra were measured with a mini-spectrometer RC series C11007MA (Hamamatsu Photonics, Hamamatsu, Japan) with 256 pixels, spectral resolution at 9 nm half width and 16 bits of intensity resolution. For the electrical characterisation of the prototype, the following instrumentation was used: a mixed signal oscilloscope (MSO4101, Tektronix, Beaverton, OR, USA), a 6½ digit multimeter (34410A, Agilent Technologies, Palo Alto, CA, USA), a 15 MHz waveform generator (33120A, Agilent Technologies) and a DC power supply (E3630A, Agilent Technologies). For the image acquisitions and digitalisation, a commercial scanner ScanMaker i900 (Microtek, Hsinchu, Taiwan) was used, with a 6,400 × 3,200 dpi resolution, a maximum optical density of 4.2 and 24 to 48 bits of colour. The software to manage the scanner was Silver Fast Ai provided by Microteck. The images were processed with a set of scripts and functions developed by us in Matlab r2007b (The MathWorks, Inc., Natick, MA, USA). Absorbance measurements of the membranes for comparative purposes were performed by a Hewlett Packard diode array spectrophotometer (model 8453; Nortwalk, CT, USA) equipped with a homemade membrane cell holder. Statistical calculations were performed with the Statgraphics software package (Manugistics Inc. and Statistical Graphics Corporation, Rockville, MD, USA, 1992), and Microsoft Excel (Microsoft Corp., Redmond, WA, USA) was used for general calculations. A Crison model Basic 20 pH-meter (Crison Instruments, Barcelona, Spain,) with a combined double junction glass electrode, calibrated against two standard buffer solutions (pH 4.0 and 7.0), was used for the pH measurements.

2.3. pH Sensor Array Preparation

The sensor array was prepared on a 5 cm × 4 cm transparent Mylar polyester support covered with an adhesive black film of PVC with 12 holes (3 columns and 4 rows), 5 mm in diameter each. A black opaque film was used to reduce the light dispersion and prevent cross information between the sensing elements, and one empty position of the support (S4) was used to test the illuminant of the instrument. The sensing films were cast by carefully placing 8 µL of the corresponding cocktail in each hole, whose surface tension and quick

evaporation make it possible to prepare the sensing membrane. The different cocktails for the pH membranes were prepared by dissolving the different chemicals needed in 1 mL of distilled THF according to the following composition. 1: 1.00 mg of sicomet red P, 4.00 mg of Aliquat 336, 47.00 mg of NPOE and 19.00 mg of PVC; 2: 2.10 mg of *m*-cresol purple, 9.40 mg of TDMAC, 19.60 mg of DOS, 23.10 mg of CA and 15.80 mg of ethylene glycol; 3: 1.00 mg of PAN, 7.00 mg of TDMAC, 45.50 mg of NPOE and 16.52 mg of PVC; 4: 0.50 mg of purpurin, 2.90 mg of TDMAC, 23.45 mg of NPOE and 8.15 mg of PVC; 5: 0.50 mg of cresol red, 1.59 mg of Aliquat 336, 23.45 mg of NPOE and 9.46 mg of PVC; 6: 0.50 mg of liphophilised Nile blue, 1.27 mg of TCPB, 23.45 mg of TBP and 9.77 mg of PVC; 7: 2.10 mg of bromothymol blue, 2.80 mg of TDMAC, 19.60 mg of DOS, 25.90 mg of CA and 19.60 mg of ethylene glycol; 8: 0.50 mg of alizarin, 3.60 mg of TDMAC, 23.45 mg of NPOE and 7.45 mg of PVC; 9: 1.10 mg of thymol blue, 4.05 mg of TDMAC, 9.80 mg of DOS, 12.95 mg of CA and 7.15 mg of ethylene glycol; 10: 1.00 mg of phenol red, 4.85 mg of TDMAC, 18.20 mg of BBPA, 21.00 mg of CA and 24.95 mg of ethylene glycol; 11: 3.50 mg of thymol blue, 12.88 mg of TDMAC, 19.60 mg of DOS, 23.10 mg of CA and 10.92 mg of ethylene glycol.

The pH sensing elements containing colorimetric acid-base indicators were selected according to the conditions of: (a) no leaching; (b) a tonal colour coordinate change by reaction; and (c) full coverage of the pH range by overlapping the responses of the different membranes. The selected sensing elements were prepared from different cocktails containing different types and amounts of colorimetric acid-base indicators, polymers, plasticisers, lipophilic salts and, if necessary, humectant.

The selection criteria for the pH membranes used were both high variation in H coordinate by reaction and non-redundant information from different sensing elements, so that the entire pH range was covered. At times, to displace the pH response of a membrane, we used the same acid-base indicator but changed the plasticiser, membrane polymer, lipophilic salt and/or lipophilic salt/indicator ratio. As a result, 11 different membranes, containing 10 different pH indicators were prepared to cover the whole pH range. The composition of the different sensing elements was optimised considering leaching minimisation (lipophilic salt, plasticiser, and membrane polymer), colour intensity (acid-base

indicator) and response time (plasticiser, membrane polymer, humectant and cocktail volume).

2.4. Description of the Instrument

The portable instrument used in this work is a microcontroller-based system designed to measure the pH of a solution using a neural network. The neural network implemented relates the H component from the HSV colour space of a set of colorimetric sensing elements to the pH. A diagram of the sensing module in the instrument is presented in figure 7.11. An organic light-emitting diode (OLED) display works as light source by illuminating the sensing elements of the array. The wavelengths transmitted by the sensor array being illuminated are captured by digital colour detectors which provide RGB measurement to the microcontroller. This device obtains the corresponding H coordinates in order to determine the pH value. A keypad and a Liquid Crystal Display (LCD) screen allow the user to interact with the prototype, working as user interface.

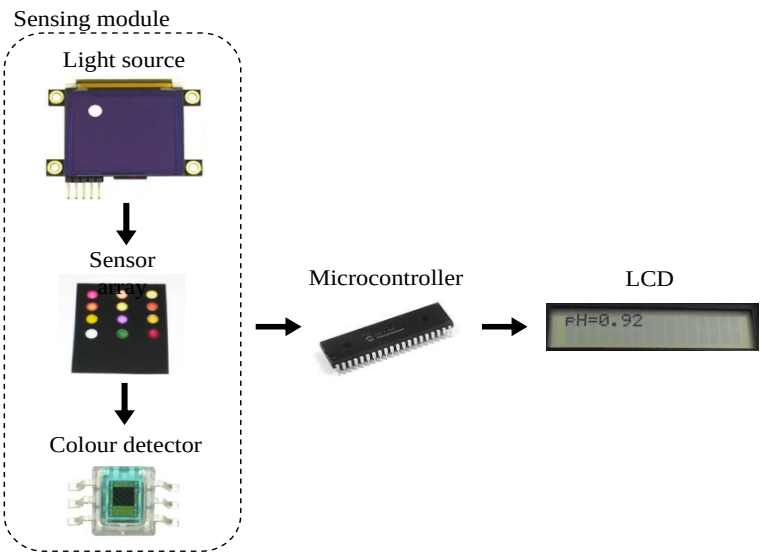

Figure 7.11. Instrument sensing design

Due to the different modules present in the design and the resources needed by the neural network, a PIC18F4550 model (Microchip Technology Inc., Chandler, AZ, USA) was selected since it has five input-output ports, 24 KB of flash memory and 2 KB of SRAM. The OLED display used as light source, model 160-GMD1 (4DSystems, Sydney, Australia), illuminates each element of the sensor array in a sequential way by displaying the circles with the illuminant for each position, as shown in figure 7.11. The main reason for using a display as the illuminant is the possibility of programming different configurations for the RGB components in order to obtain an illuminant similar to D65, which is widely used in colorimetric applications.

The transmitted wavelengths by the illuminated sensing elements are captured with a set of S9706 digital colour detectors (Hamamatsu Photonics, Hamamatsu City, Japan) which provide RGB information by means of a 36-bit word output which are serially sent to the microcontroller for further processing. The main configuration parameter of the detectors is the integration time that determines the interval during the photodiode matrix generates a photocurrent. A trade-off between sensitivity and response time determines this parameter and, in this case, a 200 ms time was programmed. The total measurement time is about 2.5 seconds, including the acquisition and processing times.

In figure 7.12, a photograph of the described prototype is presented. The keypad allows the user to change different parameters like integration time, illuminant or measurement mode for calibration purposes. An LCD is included in the design to show the different selectable options and the results of the pH obtained for each measurement. At the bottom of the instrument there is a slot to insert the sensor array. The prototype is integrated in a closed box to avoid interference with the ambient light. The device power consumption has been evaluated in two situations: while measuring, it is 450 mW; in a stand-by mode, the consumption is 5 mW.

Figure 7.12. Photograph of the prototype

2.5. pH Determination Model

Different approaches were considered in previous works as pH determination models. Imaging techniques and multivariate sensor response modelling developed in [12] have high computer memory and processor speed requirements, which are important limitations for the implementation on portable devices. On the other hand, neural networks were tested to overcome these problems in [13], obtaining higher accuracy with lower requirements in computer resources. In addition, neural networks and specifically Perceptron and recurrent models can be optimized and minimized using multi-objective optimization techniques [16], which allow us to reduce the number of sensing elements in the sensor array. For this, reason, in this work neural networks are used as prediction models for pH determination from colour features of the sensing elements in the array. A Multilayer Perceptron [8] with one hidden layer was designed for this purpose, where the hue (H) colour component from each sensing element is a candidate input for the network, and the output is the predicted pH value. The activation function for all hidden neurons was set to the sigmoid function, and the output neuron response is computed as the weighted linear aggregation of the output value provided by intermediate hidden neurons. Considering our aims of saving energy, minimising the array and final instrument prototype, and resource

management, we were also interested in discovering the minimum number of sensing elements in the array needed to provide a fine pH prediction. To achieve this, the neural network to be implemented in the instrument prototype was obtained using a multi-objective procedure with three criteria to be minimised (equation 7.2): (a) criterion $f_1(x)$ (equation 7.3) to minimise the number of sensing elements used for pH prediction, (b) criterion $f_2(x)$ (equation 7.4) to minimise the network prediction error, and (c) criterion $f_3(x)$ (equation 7.5) to minimise the number of hidden neurons. The first and second objectives attempt to obtain the sensing elements required to provide accurate pH approximation with minimum error. The error measure to be minimised is the maximum absolute error between the network response and all the calibration data. This error measurement does not depend on the number of training data, and is suitable to prevent overtraining when the data are unbalanced [16], *i.e.*, some pH ranges are better approximated than others. Finally, the third objective is used to reduce the microchip memory and processing consumption, and it also helps to avoid overtraining of networks with an excessive number of hidden neurons. These criteria are formulated in equations 7.2 to 7.5, where x stands for the neural network parameters to be optimised, x^* is the set of optimal solutions, pH_p is the real pH measured for the p-th sample in the calibration data, pH'_p is the pH approximation provided by the neural network, and $N^0(x)$ and $N^1(x)$ are the number of network neurons at input and hidden layers, respectively:

$$x^* = \min_x\{(f_1(x), f_2(x), f_3(x)\} \tag{7.2}$$

$$f_1(x) = N^0(x) \tag{7.3}$$

$$f_2(x) = \max_p\{|\ pH'_p - pH_p\ |\}\forall p \tag{7.4}$$

$$f_3(x) = N^1(x) \tag{7.5}$$

A hybrid version of the NSGA-II multi-objective algorithm has been designed in combination with the Levenberg-Marquardt non-linear optimisation method using the Baldwinian hybridation strategy [16]. The resulting method is able to provide a set of optimal neural networks according to the Pareto optimality criterion. In brief, the objective is to find a neural network or set of neural networks with optimal (minimum) values in all criteria [$f_1(x)$, $f_2(x)$, $f_3(x)$]. To

achieve this, the *dominance* over solutions of the multi-objective algorithm is defined in equation 7.6. In this work, a neural network *x* dominates the neural network *y*, and it reads *x* < *y*, if the solution *y* is not better than *x* in any of the criteria to be optimised, and also *x* is better than *y* in at least one of the three criteria. If a solution *x* does not dominate *y* and also *y* does not dominate *x*, both are *non-dominated solutions*. The *Pareto front* is composed of the set of solutions that are not dominated by any other solution. For the purpose of this work, the developed method in [16] is able to provide a Pareto front containing a set of networks that are optimal under this optimality criterion.

$$x < y \leftrightarrow \forall i \in \{1,2,...,n\}\ f_i(x) \leq f_i(y) \wedge \exists j \in \{1,2,...,n\} : f_j(x) < f_j(y) \qquad (7.6)$$

Additionally, we define the neural network parameters x to be optimised in this work regarding the pursued objectives. It is necessary to optimise the network weights and biases to achieve a suitable pH determination, the number of sensing elements in the array for minimisation of array and instrument prototype development cost and size, and the number of hidden neurons for processor energy consumption savings, processing speed and overtraining prevention. These parameters are represented in the proposed computer optimisation algorithm as follows: (a) a matrix *W* containing the network connection weights as real numbers, (b) a vector *B* with the bias values of the neurons as real numbers, (c) a vector *I* with binary values to indicate which sensing elements in the array are used for pH determination in the network, and (d) a vector *H* with binary values to indicate the network hidden neurons. This neural network representation is supported by a widely-used proposal in the literature for the multi-objective optimisation of neural networks [17], and has the advantage of being flexible enough to be used for the optimisation of more complex neural network models such as recurrent neural networks. Our contribution to this representation is the possibility of optimising the number of network inputs and was validated in [16]. For the sake of clarity, equations 7.7 to 7.10 describe a possible representation of a neural network with a maximum of five inputs (equation 7.9) and four hidden neurons (equation 7.10) as an example. Inputs 1, 2, 4 are active and would represent the sensing elements used in the array for pH determination in our work. The network contains two hidden neurons

called 2 and 4. The network weights and biases are represented in equations 7.7 and 7.8, respectively. Figure 7.13 draws the resulting network from this example:

$$W = \begin{pmatrix} w^1_{1,1} & w^1_{1,2} & w^1_{1,3} & w^1_{1,4} & w^1_{1,5} & 0 & 0 & 0 & 0 \\ w^1_{2,1} & w^1_{2,2} & w^1_{2,3} & w^1_{2,4} & w^1_{2,5} & 0 & 0 & 0 & 0 \\ w^1_{3,1} & w^1_{3,2} & w^1_{3,3} & w^1_{3,4} & w^1_{3,5} & 0 & 0 & 0 & 0 \\ w^1_{4,1} & w^1_{4,2} & w^1_{4,3} & w^1_{4,4} & w^1_{4,5} & 0 & 0 & 0 & 0 \\ 0 & 0 & 0 & 0 & 0 & w^2_{1,1} & w^2_{1,2} & w^2_{1,3} & w^2_{1,4} \end{pmatrix} \quad (7.7)$$

$$B = \begin{pmatrix} b^1_1 & b^1_2 & b^1_3 & b^1_4 & b^2_1 \end{pmatrix} \quad (7.8)$$

$$I = \begin{pmatrix} 1 & 1 & 0 & 1 & 0 \end{pmatrix} \quad (7.9)$$

$$H = \begin{pmatrix} 0 & 1 & 0 & 1 \end{pmatrix} \quad (7.10)$$

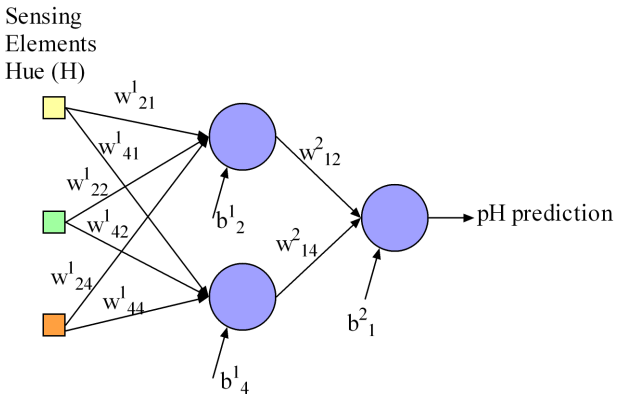

Figure 7.13. Example of the neural network described in equations 7.7-7.10

2.6. Measurement Procedure

The colour determination of the pH membranes was performed by measuring the transmitted light following the path indicated in figure 7.11: once the sensor array board is inserted into the instrument (see figure 7.12), the light is generated in the programmable OLED that acts as a white light source and illuminates the colour sensors in the array. This illumination is carried out in a sequential way by placing a white circle drawn on a black background facing the corresponding colour sensor. Each sensing element of the array works as a light filter and only transmits the wavelengths corresponding to its own colour. This

transmitted light reaches the surface of the colour detectors and they generate a digital output with the values of the RGB decomposition of the incident light, which is used to characterise the colour of the sensing elements.

The response of the measurement system was evaluated for each 0.1–0.2 pH unit from 0 to 14 by adding volumes of 1.0 M, 0.1 M or 0.01 M of HCl or of NaOH with a microburette to an aqueous solution containing the sensor array hanging from a support with a clamp. After each addition and magnetic stirring, the pH of the solution was measured using a potentiometric procedure. The array sensor was equilibrated for 5 min, and then was pulled out and inserted into the instrument to be measured. All measurements were made in an air-conditioned laboratory at room temperature (24±1 °C).

3. Results and Discussion

The RGB space is an additive representation of colour in which all the colours can be represented as a combination of red, green and blue primaries. The colour space used here, HSV, is an alternate representation of colour derived from the red, green, and blue intensity values of the RGB space. A pixel in this colour space is defined by its hue (H), saturation (S), and value (V) coordinates. In broad terms, H is a numerical representation of the colour, S gives the degree to which a single channel dominates, and V represents the brightness. We have demonstrated previously that the H value is stable, simple to calculate, and easily obtained from commercial devices, maintaining a superior precision with variations in indicator concentration, membrane thickness, detector spectral responsivity, and illumination [18]. Thus, the main reason to use H, which only considers hue variations of sensing elements and not intensity variations connected to S and V coordinates, is to prevent problems such as dye leaching or lot-to-lot variations. The evolution of S and V components with pH for different membranes was studied, observing small variations except in some cases, and in general they do not improve the results. Furthermore, the use of the S and V parameters involves a more complex treatment and a high consumption of computational time.

In a previous work, the same sensor array was individually characterised by means of spectrophotometry and scannometry, where imaging techniques were used to acquire the tonal information (H coordinate) of the HSV colour space [9]. As a first step, the H values obtained with our portable instrument were compared to the aforementioned laboratory techniques. The results obtained with the portable instrument are very similar to those obtained using imaging techniques to acquire the tonal information or absorbance measurements as shown in figure 7.14 for three colorimetric sensing elements of the array.

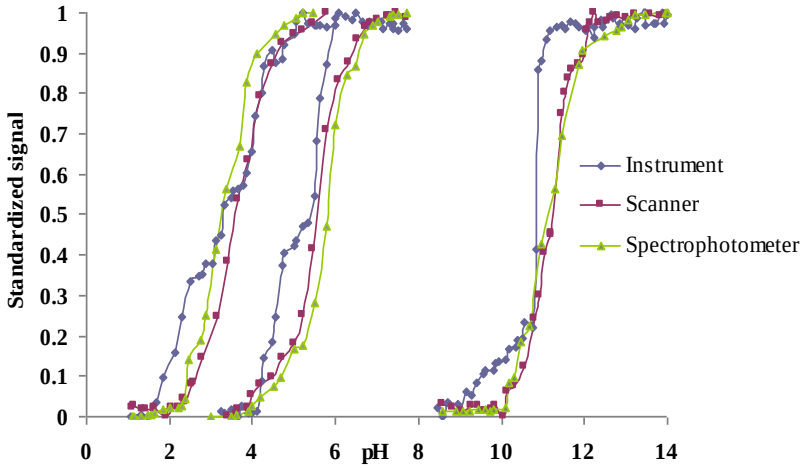

Figure 7.14. Comparison between the responses to pH of different sensing elements using different devices for three array sensors

3.1. Calibration and Neural Network Selection

The experiment was designed so that the pH range from 0 to 14 was uniformly sampled with 121 solutions to build the calibration data set. A sensor array was immersed in each solution and we made 12 replicates to prevent any outliers. Then, the hue (H) value of the 11 sensing elements in the sampled arrays was measured with the portable instrument and saved in the computer for neural network calibration. The multi-objective hybrid NSGA-II algorithm [16] was executed 30 times with these calibration data as input for better exploration of solution space and Pareto front acquisition, using the following parameters:

- Bounds for the number of hidden neurons: 2 (minimum) and 11 (maximum).
- Bounds for the number of sensing membranes considered: 1 (minimum) and 11 (maximum).
- Bounds for network biases and weights: [−10, 10].
- Number of layers of the neural networks: 1 (input), 1 (hidden), 1 (output).
- Crossover probability: 0.7.
- Mutation probability: 0.2 (number of sensing membranes used), 0.2 (number of hidden neurons), 0.2 (network weights), 0.1 (mutation per gene).
- Population size: 100.
- Number of algorithm generations: 700.
- Number of local search iterations with Levenberg-Marquardt: 10.

The hybrid NSGA-II procedure returned 21 non-dominated solutions in the Pareto frontier among the 30 executions, meeting the three objectives: number of sensing elements, hidden neurons, and pH prediction error minimisation. The performance of these solutions is summarised in table 7.5, which also includes the Mean Square Error (MSE) obtained in the calibration data set for comparison purposes with other techniques in the literature. For reading clarity, we describe in depth the sensing elements of the array used for pH prediction by each resulting network in column 5. We remark that the maximum absolute error of the networks obtained is high in the calibration data, but this is justified because all the replicates of the measurements in this data set were used for neural network training. We made the decision to improve the network noise tolerance that could be produced during the physical hue acquisition in the portable instrument, and such measurements could be interpreted as outliers. Nevertheless, the error in validation and testing is lower because we removed the outliers.

As shown in table 7.5, the solutions obtained cover a wide set of neural networks ranging from networks with low complexity, a low number of sensing elements and low accuracy to networks with high accuracy but also higher requirements of sensing elements necessary for the pH prediction. Some relevant results are networks 1, 10, 12, and 18. In the case of network 1, this network is able to obtain an MSE of 0.048 using seven sensing elements and a very low

complexity of four hidden neurons. Networks 10 and 12 make use of all the sensing elements in the array and provide a similar MSE of 0.031 and 0.028, respectively, but network 10 has a lower complexity of six neurons in contrast to network 12, which has a 9-neuron complexity. Finally, network 18 is able to obtain an MSE of 0.065 using four sensing elements only, and a medium complexity of five neurons. The main advantage of this multi-objective procedure used to calibrate the pH prediction method is that all the networks provided in Table 1 are optimal under the Pareto optimality criterion. Thus, the designer of the final portable instrument prototype could choose from a wide set of solutions to be implemented in the instrument and s/he could decide which to use, using different selection criteria such as instrument size, array development cost, computing time and accuracy.

To validate the portable instrument developed in this work, we selected network number 12 in the Pareto front to be included in the hardware, since it provides both the lowest MSE and maximum absolute error in pH determination. This selection is discussed in table 7.5. The network was implemented in C language and compiled using the PIC programming toolkit from Microchip for validation and testing. The code needed to implement this neural network in the program of the microcontroller was optimised to require only 10% of the available microcontroller's program memory. Therefore, the microcontroller selected here was able to perform all the signal processing necessary to generate the pH value prediction with no need for additional resources such as external memories.

Table 7.5. Performance of resulting networks from hybrid NSGA-II in calibration

Solution Number	Maximum Absolute Error (pH units)	Number of Hidden Neurons	Number of Network Inputs	Sensing Elements Used for pH Prediction	MSE (Calibration Data)
1	0.873	4	7	3 4 5 6 8 9 11	0.048
2	1.098	3	3	4 5 10	0.114
3	0.864	5	7	3 4 5 6 8 9 11	0.048
4	1.656	2	2	7 9	0.508
5	1.014	3	4	4 5 10 11	0.080
6	1.279	2	3	4 5 10	0.141
7	1.079	2	5	1 4 5 10 11	0.113
8	1.099	2	4	4 5 10 11	0.118
9	0.910	8	6	4 5 6 8 9 11	0.047
10	0.766	6	11	1 2 3 4 5 6 7 8 9 10 11	0.031
11	0.883	3	7	3 4 5 6 8 9 11	0.057
12	**0.734**	**9**	**11**	**1 2 3 4 5 6 7 8 9 10 11**	**0.028**
13	0.917	5	5	1 4 5 8 9	0.064
14	0.959	3	6	1 4 5 6 9 11	0.071
15	0.757	7	9	1 2 3 4 5 6 7 9 11	0.037
16	1.428	3	2	5 7	0.116
17	3.058	2	1	7	1.026
18	0.978	5	4	4 5 9 10	0.065
19	0.980	3	5	3 4 5 9 10	0.073
20	0.924	4	6	1 2 4 5 9 10	0.061
21	0.945	4	5	1 4 5 9 10	0.066

3.2. Validation and Test

A set of 50 equally spaced solutions covering the full pH range was used to validate the portable instrument, making measurements with five replicates of the array sensor in each case. In order to test the prediction performance of the method, we applied a Student's t-test with a confidence level of 95% to check whether the data distributions resulting from the predicted values in the validation data set differ significantly from the real data (using a potentiometric method as reference). The probability value obtained was 0.984 (higher than 0.05), so we may conclude that the model is able to predict pH suitably since

there are no significant differences between the real and predicted pH data. We also applied a Pearson correlation test to measure the quality of the predicted versus the real values. The result of the test provided a probability value under 2.2×10^{-16} in the validation data set, and we may therefore conclude that there is a significant correlation between the real and predicted values. The correlation coefficient R^2 was calculated and the test provided the value 0.999. Consequently, it may be assumed that the prediction model provides a suitable performance for the task of pH prediction in the validation data. The pH predictions fit the original pH values with high fidelity in the range from 0 to 14, although the accuracy decreases for pH values higher than 13, due to the lower H variation of the sensor array in that range. The MSE obtained in the validation data is 0.014 and the maximum absolute error in pH units is 0.296, which is produced in the pH range 13–14, as described previously. To finish the analysis of the portable instrument validation, we separated the validation data into two sets to distinguish the acid and basic pH range. The samples in acid range 0–7 contained 27 measurements with five replicates for each one, and the samples in basic range 7–14 contained the remaining 23, also with five replicates for each sample. We calculated the absolute error between the pH prediction and the reference pH for each sample, and compared the error data distributions with a Student's t-test with 95% of confidence level, to discover whether the pH prediction is uniform across the full pH range or if the portable instrument performs better in a specific pH range. We obtained a probability value of 0.227 (over 0.05), so that we may conclude that there are no significant differences in the error committed by the portable instrument either in acid or basic pH ranges, and the method provides a uniform error in the full pH range.

Additionally, the procedure was applied to 10 aqueous solutions to test the prediction model (test set), with five replicates again, with the pH adjusted with acid and base, sampling the full pH range from 0 to 14 uniformly. The MSE obtained in this case is 0.015, and the maximum absolute error in pH units is 0.229. Compared to laboratory experiments carried out in previous works [16], the results for pH determination are similar using the device developed in this work, which suggests that the proposed portable instrument and the methodology followed can be used for pH prediction. Again, we applied a Student's t-test with a confidence level of 95% to test whether the pH prediction differs significantly

from the pH measured with the reference method. The probability value obtained was 0.997, which indicates that there are no significant differences between pH prediction and reference pH data. The Pearson correlation test was applied to check if the predicted data match the real pH measurements, obtaining a probability value under 2.2×10^{-16}. Thus, this test concludes that there is a significant correlation between the real and predicted values, with a correlation coefficient R^2 of 0.999.

The correlation graph of pH predicted values against reference pH data for both validation and test data sets is presented in figure 7.15, where they have been fitted to straight lines that correspond to the reference pH. Measured and reference values of pH match with high accuracy, as it can be deduced from the correlation factor R^2 that is higher than 0.999 in both cases.

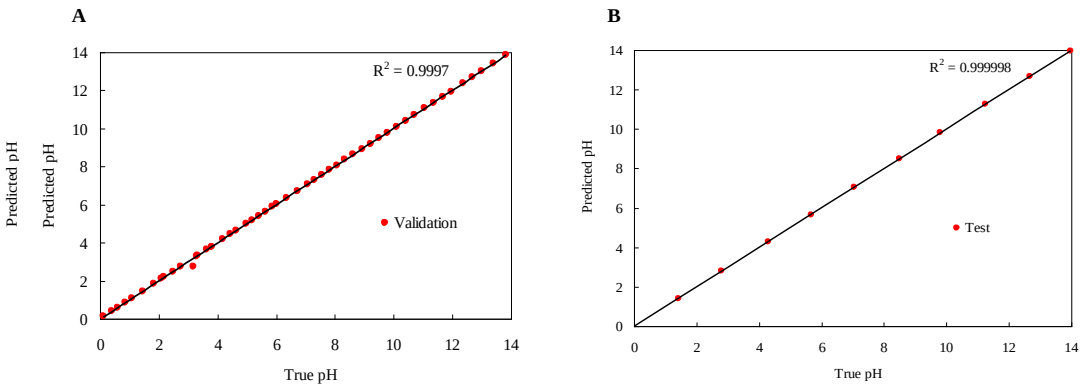

Figure 7.15. (a) Validation and (b) test measurements

3.3. Application to Real Samples

The pH of beverages, personal care products and cleaning samples such as orange, tangerine, tomato, peach, grape and pineapple juices; orange, lemon and cola soft drinks; milk; tap, river, mineral and carbonated waters; vinegar; lemon; alcohol-free and draught beers; ammonia solution; washing-up liquid; toothpaste solution; mouthwash, *etc.* was determined, validating the results against a pH-meter (table 7.6).

Table 7.6. Comparison between the pH of different samples measured with different devices

Sample	Potentiometer	Scanner	Error	Portable instrument	Error	P-value
Lemon dressing	**2.35**	**2.19**	**0.16**	**2.31**	**0.04**	**0.016**
Tonic	**2.49**	**2.59**	**0.10**	**2.39**	**0.10**	**0.027**
Orange soft drink	**2.75**	**2.83**	**0.08**	**2.67**	**0.08**	**0.044**
Orange fizzy drink	**2.91**	**2.98**	**0.07**	**2.92**	**0.01**	**0.035**
Blackberry liqueur	2.91	3.08	0.17	2.95	0.04	0.107
Lemon fizzy drink	**3.30**	**3.43**	**0.13**	**3.34**	**0.04**	**0.021**
Cola fizzy drink 1	2.85	2.78	0.07	2.89	0.04	0.055
Cola fizzy drink 2	**2.75**	**2.84**	**0.09**	**2.71**	**0.04**	**0.024**
Vinegar	3.03	2.99	0.05	3.09	0.06	0.616
White wine	3.35	3.29	0.05	3.36	0.02	0.117
Mandarin juice	3.57	2.44	0.13	3.52	0.04	0.228
Pineapple juice	3.68	2.69	0.01	3.67	0.02	0.633
Tomato juice	4.17	4.23	0.06	4.11	0.05	0.354
Orange juice	3.49	3.45	0.04	3.56	0.07	0.869
Apple juice	3.20	3.10	0.10	3.16	0.04	0.191
Peach juice	4.01	4.12	0.12	4.06	0.05	0.208
Grape juice	3.78	3.70	0.08	3.68	0.10	0.660
Tinned gherkins	**2.89**	**2.72**	**0.17**	**2.91**	**0.02**	**0.033**
Tinned artichokes	**3.80**	**3.78**	**0.02**	**3.72**	**0.08**	**0.021**
Tinned mushrooms	4.96	4.86	0.10	5.02	0.06	0.296
Tinned soya	3.97	4.07	0.10	4.05	0.08	0.558
Tinned olives	4.07	4.14	0.07	4.09	0.02	0.183
Tinned carrots	3.76	3.72	0.04	3.78	0.02	0.265
Beer	4.16	4.30	0.14	4.24	0.08	0.176
Alcohol-free beer	4.50	4.25	0.25	4.38	0.12	0.116
Black tea	4.93	5.08	0.15	5.21	0.28	0.068
Decaffeinated coffee solution	5.67	5.33	0.34	5.42	0.25	0.311
Skimmed milk	6.70	6.59	0.11	6.61	0.09	0.822

Table 2. *Cont.*

Sample	Potentiometer	Scanner	Error	Portable instrument	Error	P-value
Sparkling mineral water	5.30	5.29	0.01	5.36	0.06	0.292
Mineral water 1	7.17	7.19	0.02	7.14	0.03	0.149
Mineral water 2	7.29	7.66	0.36	7.35	0.06	0.217
Mineral water 3	7.59	7.58	0.01	7.62	0.03	0.892
Tap water	7.85	7.97	0.12	7.96	0.11	0.294
Toothpaste solution (1:3)	7.22	7.31	0.09	7.36	0.14	0.297
Mouthwash	7.30	7.53	0.23	7.43	0.13	0.178
Diluted washing-up liquid	7.30	6.87	0.42	7.02	0.28	0.299
Contact lens saline solution	7.54	7.35	0.20	7.40	0.14	0.442
Bleach solution (1:5)	**8.99**	**2.52**	**6.47**	**3.42**	**5.57**	**0.030**
Sodium bicarbonate saturated solution	8.44	8.37	0.07	8.30	0.14	0.527
Ammonia solution (1:10)	11.04	11.46	0.42	11.58	0.54	0.312
		Average error:	0.13	Average error:	0.09	

These products were used to validate the pH prediction capability of our portable instrument. An array was introduced into these products to measure their pH, and we used a pH-meter to validate the portable instrument response. In addition, we scanned the arrays and applied the method developed in [16] to calculate the pH using imaging techniques. We compared the results of pH prediction using both techniques (portable instrument and imaging) to validate the electronic performance of the proposed device in contrast to previous work. Table 7.6 shows the results obtained with the pH-meter and both imaging and

portable instrument techniques for all samples described in column 1. Column 2 describes the pH of the solution measured with the pH-meter, columns 3–4 show the average pH prediction and absolute error regarding the pH-meter with imaging techniques, columns 5–6 the average pH prediction and absolute error with our portable instrument. In almost all cases, the pH prediction using the portable instrument is an improvement over the imaging procedure using the scanner. We found only one sample in which we obtained an absolute error over 1 pH unity, the bleach solution (1:5). This occurred because the same sensing elements in the array react with the solution and become spoiled, and the hues measured by both scanner and portable instrument do not fit the real solution pH.

To validate our assumption, a statistical t-test with a 95% confidence level was applied to the error distributions in the overall results. The data from the bleach solution (1:5) were removed to prevent any outliers. A probability value of 0.006 was obtained, meaning that there are significant differences between the results from the scanner imaging and portable instrument. In this case, the portable instrument provides better results than scanner imaging since its average error is 0.09 and the average error of scanner imaging is 0.13, as shown in table 2. In addition, we studied the performance of the portable instrument for each solution class separately. We applied a means test with a 95% confidence level to compare the error distributions of pH prediction between scanner imaging and the portable instrument for the 40 samples separately. Column 7 in table 2 describes the resulting probability value for each case. We have highlighted those rows to distinguish the classes where we found significant differences in pH prediction. The pH prediction results in 31 of 40 samples have no statistical difference, whether we use scanner imaging techniques or our portable instrument. Regarding the remaining solutions, the portable instrument provided better results in 6 cases of the remaining 9 samples. These analyses show that the portable instrument is able to predict the pH of real samples accurately and at times it can provide even better results than other non-portable pH prediction techniques.

4. Conclusions

In this work, we have proposed a programmable portable instrument for full range pH determination using colorimetric acid-base indicators. A prototype of the device was developed that can acquire the hue (H) component of the HSV colour space from an array containing a maximum number of up to 12 sensing elements. An array with 11 sensing elements was designed in order to obtain colorimetric responses in the full pH range from 0 to 14. The response of some of these sensing elements overlaps, making it possible to calibrate an accurate pH prediction model. Regarding the calibration methodology, neural networks were used as the pH prediction technique, and we designed a multi-objective neural network calibration procedure with the aim of minimising prediction model complexity, maximising accuracy and minimising the number of sensing elements. The method returns a set of optimal solutions, in the sense of Pareto optimality, to provide the designer of the final instrument prototype with a large set of solutions to be implemented in the portable instrument. Thus, the designer can implement an optimal solution considering further industrial development decisions such as energy saving, computing time response, array development costs and instrument minimisation, among others. The portable instrument was validated with a neural network that uses an input array with 11 sensing elements and provides the best accuracy, and we obtained a Mean Square Error of 0.028 in calibration data, 0.014 in validation data, and 0.015 in test data. In addition, a maximum absolute error of 0.229 in pH units was obtained with the test data. Statistical tests concluded that our method does not provide pH prediction that differs significantly from pH measurements using potentiometric techniques. Finally, we applied our method to test pH prediction capabilities in real samples such as orange juice, vinegar, cola drink, lemon dressing, tea and beer, among others. The results obtained are promising, since most of samples obtained an absolute error of 10^{-2} order units in comparison with the potentiometric method. In addition, we compared these results with previously developed imaging techniques in the literature using a scanner and computer software to make the pH prediction. Statistical tests concluded that there are no significant differences between the method using imaging techniques and our portable instrumentation. Thus, the portable device developed has been validated

with previous works and it has been shown that it is able to provide a fine and accurate pH prediction.

Acknowledgments

We acknowledge financial support from the Ministerio de Ciencia e Innovación, Dirección General de Investigación y Gestión del Plan Nacional de I+D+i (Spain) (Projects CTQ2009-14428-C02-01 and CTQ2009-14428-C02-02); and the Junta de Andalucía (Proyecto de Excelencia P08-FQM-3535). These projects were partially supported by European Regional Development Funds (ERDF).

References

[1] B.J. Deboux, E. Lewis, P.J. Scully, R. Edwards. *A novel technique for optical fiber pH sensing based on methylene blue adsorption*. J. Lightwave Technol., 13 (1995) 1407-1414.

[2] Z.M. Shakhsher, I. Odeh, S. Jabr, W. Rudolf Seitz. *An Optical Chemical Sensor Based on Swellable Dicarboxylate Functionalized Polymer Microspheres for pH Copper and Calcium Determination*. Microchim. Acta, 144 (2004) 147-153.

[3] L.Y. Heng, T.H. Fang, L.H. Chern, M. Ahmad. *Influence of Methacrylic-Acrylic Copolymer Composition on Plasticiser-free Optode Films for pH Sensors*. Sensors, 3 (2003) 83-90.

[4] A. Abbaspour, M.A. Mehrgardi, A. Noori, M.A. Kamyabi, A. Khalafi-Nezhad, M.N. Soltani Rad. *Speciation of iron(II), iron(III) and full-range pH monitoring using paptode: A simple colorimetric method as an appropriate alternative for optodes*. Sens. Actuators B, 113 (2006) 857-865.

[5] A. Lapresta-Fernández, L.F. Capitán-Vallvey. *Environmental monitoring using a conventional photographic digital camera for multianalyte disposable optical sensors*. Anal. Chim. Acta, 706 (2011) 328-337.

[6] A. Safavi, N. Maleki, A. Rostamzadeh, S. Maesum. *CCD camera full range pH sensor array*. Talanta, 71 (2007) 498-501.

[7] M. Suzuki, H. Nakabayashi, M. Honda, Y. Iribe. *Micro-arrayed optical chemical sensor chips*. Chemical Sensors, 20 (2004) 76-78.

[8] S. Haykin. *Neural Networks: A Comprehensive Foundation*. Prentice Hall: Upper Saddle River, NJ, USA (1999).

[9] Y. Bengio, P. Simard, P. Frasconi. *Learning long-term dependencies with gradient descent is difficult*. IEEE T. Neural Networ., 5 (1994) 157-166.

[10] M.N. Taib, R. Andres, R. Narayanaswamy. *Extending the response range of an optical fibre pH sensor using an artificial neural network*. Anal. Chim. Acta, 330 (1996) 31-40.

[11] A. Safavi, M. Bagheri. *Novel optical pH sensor for high and low pH values*. Sens. Actuators B, 90 (2003) 143-150.

[12] S. Capel-Cuevas, M.P. Cuéllar, I. de Orbe-Payá, M.C. Pegalajar, L.F. Capitán-Vallvey. *Full-range optical pH sensor based on imaging techniques*. Anal. Chim. Acta, 681 (2010) 71–81.

[13] S. Capel-Cuevas, M.P. Cuéllar, I. de Orbe-Payá, M.C. Pegalajar, L.F. Capitán-Vallvey. *Full-range optical pH sensor array based on neural networks*. Microchem. J,. 97 (2011) 225-233.

[14] A. Martinez-Olmos, S. Capel-Cuevas, N. López-Ruiz, A.J. Palma, I. de Orbe, L.F. Capitán-Vallvey. *Sensor array-based optical portable instrument for determination of pH*. Sens. Actuators B, 156 (2011) 840-848.

[15] M.D. Fernández-Ramos, M. Greluk, A.J. Palma, E. Arroyo-Guerrero, J. Gómez-Sánchez, L.F. Capitán-Vallvey. *The use of one-shot sensors with a dedicated portable electronic radiometer for nitrate measurements in aqueous solutions*. Meas. Sci. Technol., 19 (2008) 095204-1-095204/7.

[16] M.P. Cuéllar, S. Capel-Cuevas, M.C. Pegalajar, I. de Orbe-Payá, L.F. Capitán-Vallvey. *Minimization of sensing elements for full-range optical pH device formulation*. New J. Chem. 35 (2011) 1042-1053.

[17] H.A. Abbass. *A memetic Pareto evolutionary approach to artificial neural networks*. Lect. Note. Artif. Intell., 2256 (2001) 1-12.

[18] K. Cantrell, M.M. Erenas, I. de Orbe-Payá, L.F. Capitán-Vallvey. *Use of the Hue Parameter of the Hue, Saturation, Value Color Space As a Quantitative*

Analytical Parameter for Bitonal Optical Sensors. Anal. Chem., 82 (2010) 531-542.

3. CONCLUSIONES

El objetivo de este capítulo ha sido el desarrollo de un instrumento portátil de bajo coste y fácil uso para la medida de pH en rango completo, basado en la matriz sensora óptica previamente estudiada.

El trabajo realizado se ha divido en dos partes. Como principales conclusiones de la primera parte del estudio cabe destacar:

- Se ha preparado la matriz sensora de pH sobre un soporte negro con micropocillos transparentes conteniendo los once elementos sensores previamente estudiados.

- Se ha diseñado un instrumento portátil, incluido en una caja negra con tan sólo una pequeña abertura para insertar la matriz sensora. La determinación del color de los elementos sensores se ha llevado a cabo mediante la medida de la luz transmitida a través de éstos con un conjunto de doce fotodetectores con salida RGB.

- La fuente de iluminación consiste en un pantalla OLED programable de fondo negro, la cual emite secuencialmente círculos de luz blanca en disposición 3 x 4, alineando cada círculo con un elemento de la matriz sensora y su correspondiente detector. Estos círculos se iluminan de forma secuencial para la medida de cada elemento sensor, que se hace de forma individual y no simultánea, al objeto de evitar interferencias de luz reflejada. La posición y el tamaño de los círculos han sido configurados para su correcta alineación. Se ha optimizado la fuente de luz para que fuera similar al iluminante estándar D65, el llamado “blanco modificado”.

- Los detectores de color son sensibles a las regiones espectrales roja, verde y azul, lo que ha permitido la medida simultánea de las coordenadas RGB y, a partir de éstas, se han calculado las coordenadas H. Tanto el área activa como el tiempo de integración de éstos han sido

optimizados.

- A partir de los datos de variación de H frente al pH, ha sido posible, gracias al sistema de modelización desarrollado, reducir el número de elementos sensores necesarios desde los once iniciales a cuatro finales.

- Se han calculado las constantes de equilibrio correspondientes a la respuesta de cada elemento sensor medida con el instrumento portátil y han sido comparadas con las constantes previamente obtenidas empleando un escáner convencional trabajando en modo transmisión.

- Se ha validado su funcionamiento y testeado mediante análisis de muestras de agua de grifo y de río procedentes de Granada. El MSE correspondiente fue 0,180, ligeramente superior a los obtenidos en estudios previos realizados (0,111 en el caso del ajuste mediante un modelo de competición de membranas y 0,043 usando ANN), aunque lo consideramos aceptable tratándose de un instrumento portátil.

Las principales conclusiones de la segunda parte del estudio son las siguientes:

- Se ha modificado el instrumento portátil para su uso *in situ* sin necesidad de conexión a un procesador de datos externo. Para ello se ha aplicado un algoritmo multi-objetivo que ha obtenido un conjunto de ANN. De entre éstas, se ha seleccionado la red neuronal óptima para la predicción del pH de acuerdo con los criterios establecidos, y posteriormente se ha implementado en la memoria del microcontrolador del instrumento portátil.

- La ANN implementada, basada en la respuesta de los once elementos sensores, ha arrojado los siguientes MSE (en unidades de pH): 0,028 en los datos de calibración; 0,014 en los datos de validación y 0,015 en las muestras de test. Los test estadísticos han corroborado los resultados obtenidos en este trabajo, concluyéndose que no hay diferencias estadísticamente significativas entre los valores de pH medidos

potenciométricamente y los predichos por el modelo.

- Finalmente se ha determinado el pH de un amplio conjunto de muestras alimentarias, biológicas y de productos de uso doméstico, comparando los resultados con los obtenidos utilizando el escáner convencional empleado anteriormente y un sistema potenciométrico de referencia. Para la aplicación de los test estadísticos, previamente se han eliminado los valores predichos de pH correspondientes a la disolución de lejía, ya que en ese caso, diversos elementos de la matriz experimentan reacciones de tipo redox que interfieren en el proceso de predicción y el error absoluto asociado es superior a la unidad. Los test estadísticos han permitido demostrar la validez del sistema.

CAPÍTULO 8

Sensores ópticos para calcio basados en éteres corona

"The important thing is not to stop questioning. Curiosity has its own reason for existing. One cannot help but be in awe when he contemplates the mysteries of eternity, of life, of the marvelous structure of reality. It is enough if one tries merely to comprehend a little of this mystery every day. Never lose a holy curiosity".

Albert Einstein

1. INTRODUCCIÓN

Actualmente, una de las tendencias en Química Analítica es el desarrollo de metodología analítica que pueda ser utilizada por el usuario donde se desee, como es el caso de los métodos rápidos de análisis que se realizan *in situ*. De las diversas formas de llevar a cabo este tipo de métodos, una de las más interesantes es la utilización de ensayos rápidos, que permiten realizar los análisis químicos de forma rápida, simple, económica y sin necesidad de personal especializado, evitando a su vez, en mayor o menor medida, las etapas de toma, tratamiento, conservación y transporte de muestras hasta los laboratorios convencionales de análisis, e incluso, el uso de instrumentación de laboratorio más o menos compleja[480].

La información que aportan estos procedimientos puede emplearse tanto para la obtención rápida de información cualitativa y/o cuantitativa como para discriminar la presencia de un constituyente en una muestra por encima de una determinada concentración, de modo que permita seleccionar sólo las muestras de interés y se reduzca de manera considerable el número de ellas a tomar y enviar al laboratorio.

Por otra parte, también presentan interés en el control de procesos donde el problema no sea la precisión, sino la monitorización de valores límite. Igualmente, pueden ser una buena solución en muestras con componentes muy lábiles, pues se obvia todo el proceso de conservación de muestra. Incluso pueden servir para una primera estimación de niveles en el establecimiento de estrategias de análisis en un problema dado. Además, pueden ser utilizados de forma particular para controlar el nivel de glucosa personal, decidir si es necesario añadir cloro o sal de amonio cuaternario a una piscina o conocer la dureza del agua.

De forma general, con este tipo de sistemas rápidos no se evita el análisis en laboratorios que emplean metodología certificada, sino que se establece un primer escalón en la obtención de información química, racionalizando de esta forma el trabajo en el laboratorio. Si a esto se le suma la

[480] M. Unger-Heumann. *Strategy of Analitical Tesk Kits.* Fresenius J. Anal. Chem., 354(7-8) (1996) 803-806

reducción del coste, de tiempo necesario y de personal especializado, se trata de una alternativa analítica interesante.

Estos ensayos rápidos, también llamados test kits[481], se basan habitualmente en reacciones (químicas, bioquímicas o inmunológicas) y procesos que dan lugar a un efecto observable visualmente (color desarrollado, extensión de una zona coloreada, número de elementos que reaccionan) o fácilmente medible (colorimetría, fotometría, reflectometría, fluorimetría, volumetría, etc.).

Los análisis mediante pruebas rápidas pueden llevarse a cabo de dos maneras: en disolución o en fase sólida. Los sistemas de fase sólida, también llamados tiras reactivas o sensores de gota plana, se pueden considerar como dispositivos analíticos autocontenidos. De una manera más precisa, se pueden describir como elementos analíticos integrales que habitualmente toman la forma de películas o delgadas almohadillas y que contienen, en estado sólido (seco al toque), todos los reactivos necesarios para un ensayo dentro de la almohadilla o film[482]. Estas zonas reactivas o matrices se encuentran adheridas a pequeñas tiras de material plástico que permiten su manipulación. Los ensayos en fase sólida deben estar basados en reacciones de suficiente selectividad, en conjunción con diversas operaciones analíticas, para lograr obtener resultados sobre problemas reales, sin necesidad de tratamiento previo de muestra ni adición de reactivos. Por otra parte, deben estar diseñados de forma que su manipulación sea fácil, sean robustos en su uso y estables durante el almacenamiento y se pueda realizar la medida con seguridad, generalmente mediante el uso de instrumentos dedicados.

La presencia de altas concentraciones de iones alcalinotérreos en aguas, especialmente calcio y magnesio, crea problemas graves tanto en el hogar como en la industria debido, entre otros aspectos, a la formación de depósitos de sus carbonatos. Además, desde el punto de vista fisiológico, estos iones, junto con los alcalinos, son el factor más importante en enfermedades cardiovasculares y pueden potencialmente afectar a la salud tanto de personas como de animales.

---

[481] Y. Zolotov. *Analytical tools for everybody: express test method.* Ann. Chim., 87 (1997) 285-295

[482] J.Y. Wang. *Reagent test device containing hydrophobic barriers*. US Patent 4,618,475 (1986)

La forma clásica de determinar la denominada dureza total, suma de calcio y magnesio, en agua, es mediante complexometría empleando el ácido etilendiaminotetraacético (AEDT) como agente valorante[483]. El procedimiento es barato, aunque requiere alguna destreza, consume tiempo y está sujeto a errores operacionales.

Para la determinación de estos iones alcalinotérreos, tanto individualmente como combinados en la denominada dureza total, se han empleado diversas aproximaciones instrumentales, como espectrofotometría UV-Vis[484], fluorescencia[485], fotometría de llama, espectrofotometría de absorción atómica o espectrometría de emisión atómica con plasma acoplado inductivamente[486].

El empleo de métodos potenciométricos basados en el empleo de electrodos selectivos de iones[487,488] suscitó especial interés, dando lugar a la publicación de diversos artículos relativos al diseño de ionóforos y a la optimización de la composición de la membrana para diferentes aplicaciones[489-492]. Existen diversos ionóforos para calcio[493] disponibles comercialmente, dentro de los cuales los más empleados son el dietil N,N'-[(4R, 5R)-4,5-dimetil-1,8-dioxo-

[483] W. Fresenius, K.E. Quentin, W. Schneider. *Water Analysis*. Springer-Verlag, Berlin (1988) 294-298

[484] H.M. Ma. *Direct Spectrophotometric Determination of Calcium in Human Serum and Cerebrospinal Fluids with Amino G Acid Chlorophosphonazo.* Anal. Lett., 32(4) (1999) 799-809

[485] B. Kepner, D. Hercules. *Fluorometric Determination of Calcium in Blood Serum.* Anal. Chem., 35(9) (1963) 1238-1240

[486] M.A.H. Franson. *Standard Methods for the Examination of Water and Wastewater*. 18th ed., American Public Health Association and Water Pollution Control Federation, Washington, DC, (1992)

[487] F.T. Fischbach. *Laboratory and Diagnostic Test*. 4th ed. Lippincott, Philadelphia USA (1992)

[488] D. Diamond, F.J. Sáez de Viteri. *Ion Selective Electrodes and Optrodes.* Principles of Chemical and Biological Sensors, Wiley and Sons Inc., New York, (1998)

[489] P. Anker, E. Wieland, D. Ammann, R.E. Dohner, R. Asper, W. Simon. *Neutral carrier based ion-selective electrode for the determination of total calcium in blood serum.* Anal. Chem., 53 (1981) 1970-1974

[490] P. Anker, D. Ammann, P.C. Meier, W. Simon. *Neutral carrier electrode for continuous measurement of blood Ca^{2+} in the extracorporeal circulation.* Clin. Chem., 30(3) (1984) 454-456

[491] U. Schefer, D. Ammenn, E. Pretsch, U. Oesch, W. Simon. *Neutral carrier based Ca^{2+}-selective electrode with detection limit in the sub-nanomolar range.* Anal. Chem., 58(11) (1986) 2282-2285

[492] K. Suzuki, K. Watanabe, Y. Matsumoto, M. Kobayashi, S. Sato, D. Siswanta, H. Hisamoto. *Design and Synthesis of Calcium and Magnesium Ionophores Based on Double-Armed Diazacrown Ether Compounds and Their Application to an Ion Sensing Component for an Ion-Selective Electrode.* Anal. Chem., 67(2) (1995) 324-334

[493] Fluka Química, Selectophore® Ionophores Membranes Mini-ISE (1996)

3,6-dioxaoctametleno)bis(12-metilamino-dodecanoato) (ETH 1001)[493,494] y el N,N,N',N'-tetraciclo-3-oxapentanodiamida (ETH 129)[12].

También se han desarrollado ISFETs selectivos para calcio[495,496], aunque no está completamente resuelta la preparación del electrodo de referencia miniaturizado para sensores de iones potenciométricos.

Por otra parte, también se ha propuesto un microsensor conductimétrico para la determinación de calcio[497]. La detección se realiza mediante la medida de la conductividad, empleando electrodos integrados de platino y una delgada membrana polimérica conteniendo un ionóforo comercial[493], de forma que la conductividad se puede relacionar con el contenido en ion primario de la disolución analizada. Esta forma de determinación de calcio ofrece la ventaja de presentar un diseño completo en estado sólido, lo que hace potencialmente posible su miniaturización e inclusión en verdaderos circuitos integrados dentro de la tecnología de microsistemas, aunque presenta el inconveniente de emplear ionóforos de elevado precio.

Existen numerosos ionóforos para calcio[498-500], tales como éteres corona[501,502] o agentes quelantes[503,504], entre ellos algunos derivados del ácido

---

494 W.E. Morf, K. Seiler, B. Rusterholz, W. Simon. *Design of a novel calcium-selective optode membrane based on neutral ionophores.* Anal. Chem., 62(7) (1990) 738-742

495 S.I. Wakida, M. Yamane, K. Higashi, K. Hiro, Y. Ujida. *Urushi matrix sodium, potassium, calcium and chloride-selective field-effect transistors*. Sens. Actuators B, B1(1-6) (1990) 412-415

496 P.D. Van der Wal, A. Van den Berg, N.F. de Rooij. *Universal approach for the fabrication of Ca^{2+}-, K^{+}- and NO^{3-}- sensitive membrane ISFETs.* Sens. Actuators B, 18(1-3) (1994) 200-207

497 U. Trebbe, M. Niggemann, K. Cammann, G.C. Fiaccabrino, M. Koudelka-Hep, S. Dzyadevich, O. Shulga. *A new calcium-sensor based on ion-selective conductometric microsensors–membranes and features.* J. Fresenius, Anal. Chem., 371(6) (2001) 734-739

498 P. Bühlmann, E. Pretsch, E. Bakker. *Carrier-based ion-selective electrodes and bulk optodes. 2. Ionophores for potentiometric and optical sensors.* Chem. Rev., 98(4) (1998) 1593-1688

499 U.E. Spichiger-Keller. *Chemical Sensors and Biosensors for Medical and Biomedical Applications*. Wiley-VCH, Weinheim (1998) pp. 425

500 Y. Qin, S. Peper, A. Radu, A. Ceresa, E. Bakker. *Plasticizer-free polymer containing a covalently immobilized Ca^{2+}-selective ionophore for potentiometric and optical sensors.* Anal. Chem., 75 (2003) 3038-3045

501 D.C. Ashworth, H.P. Huang, R. Narayanaswamy. *An optical calcium ion sensor.* Anal. Chim. Acta, 213 (1988) 251-257

502 D. Citterio, M. Omagari, T. Kawada, S. Sasaki, Y. Suzuki, K. Suzuki, *Chromogenic betaine lariates for highly selective calcium ion sensing in aqueous environment.* Anal. Chim. Acta, 504(2) (2004) 227-234

503 L.K. Chau, M.D. Porter. *Optical sensor for calcium: performance, structure, and reactivity of calcichrome immobilized at an anionic polymer film.* Anal. Chem., 62(18) (1990) 1964-1971

504 Y. Kawabata, R. Tahara, T. Imasaka, N. Ishibashi. *Fiber-optic calcium(II) sensor with reversible response.* Anal. Chim. Acta, 212(1-2) (1988) 267-271

etilendiaminotetraacético[505] y calixarenos[506,507]. Kürner *et al.*[508] presentaron un sensor para calcio basado en medida de absorbancia. La membrana de hidrogel utiliza un derivado del 1,3-bis(indoanilina)-2,4-bis-[(etilcarbonil)metoxil]-calix[4]areno como receptor, que una vez entrapado en el gel, no lixivia con facilidad, aunque no es muy estable. La complejación con calcio produce un efecto batocrómico de 70 nm y un incremento de absorbancia.

Otra alternativa es el empleo de diferentes sensores con transducción óptica[494,509-512], que ofrecen buena reproducibilidad y selectividad. Chau[513] usó un sensor óptico para la determinación selectiva de calcio preparado mediante inmovilización electrostática de calciocromo (ácido 2,8,8'-trihidroxi-1,1'-azonaftaleno-3,6,3',6'-tetrasulfónico) sobre una película polimérica de intercambio aniónico. Los cambios en las propiedades ópticas del reactivo inmovilizado son registrados mediante reflectancia difusa en el visible, destacando su corto tiempo de equilibración, gran selectividad y fácil construcción, aunque el proceso de inmovilización modifica el carácter ácido y la capacidad de complejación del indicador.

Para monitorizar el analito en tiempo real empleando sensores químicos, se ha recurrido al uso de sensores de tipo fluorescente, los cuales presentan las ventajas de ser muy sensibles, versátiles, de bajo coste y fáciles de realizar. Para

---

[505] A. Minta, J.P.Y. Kao, R.Y. Tsien. *Fluorescent indicators for cytosolic based on rhodamine and fluorescein chromophores.* J. Biol. Chem., 264 (1989) 8171-8178

[506] M. Ogata, K. Fujimoto, S.J. Shinkai. *Molecular design of calix[4]arene-based extractants which show high Ca2+ selectivity.* Am. Chem. Soc., 116(10) (1994) 4505-4506

[507] Y. Kubo, S. Tokita, Y. Kojima, Y.T. Osano, T.J. Matsuzaki. *A new family of indoaniline-derived calix[4]arenes: synthesis and optical recognition properties as a chromogenic receptor.* Org. Chem., 61(11) (1996) 3758-3765

[508] J.M. Kürner, T.J. Werner. *A calix[4]arene based calcium-selective optode membrane: measuring the absorbance maximum wavelength shift.* Fresenius J. Anal. Chem., 368 (2000) 759-762

[509] H. Hisamoto, K. Watanabe, E. Nakagawa, D. Siswanta, Y. Shichi, K. Suzuki. *Flow-through type calcium ion selective optodes based on novel neutral ionophores and a lipophilic anionic dye.* Anal. Chim. Acta, 299(2) (1994) 179-187

[510] K. Suzuki, K. Tohda, Y. Tanda, H. Ohzora, S. Nishihama, H. Inoue, T. Shirai. *Fiber-optic magnesium and calcium ion sensor based on a natural carboxylic polyether antibiotic.* Anal. Chem., 61(4) (1989) 382-384

[511] U.E. Spichiger, D. Freiner, E. Bakker, T. Rosatzin, W. Simon. *Optodes in clinical chemistry: potential and limitations.* Sens. Actuators B, 11 (1993) 263-271

[512] E. Werner, K. Séller, B. Rusterholz, W. Simon. *Design of a novel calcium-selective optode membrane based on neutral ionophores*. Anal. Chem., 62(7) (1990) 738-742

[513] L. Chau, M.D. Porter. *Optical sensor for calcium: performance, structure, and reactivity of calcichrome immobilized at an anionic polymer film.* Anal. Chem., 62(18) (1990) 1964-1971

la medida de calcio se han desarrollado múltiples indicadores fluorescentes[514-517].

Potyrailo propuso en 2006 un nuevo método de detección y cuantificación de Ca^{2+} en agua, basado en los cambios ópticos de películas sensoras sensibles a calcio depositadas sobre CDs y DVDs convencionales[518].

La necesidad de realizar un gran número de determinaciones conjuntas de calcio y magnesio, como dureza total, en aguas tanto públicas como privadas, así como en el control de depuradoras, ha fomentado el desarrollo de diferentes estrategias analíticas para su determinación mediante sistemas automáticos y sistemas rápidos. Se han adaptado varias técnicas a sistemas en flujo continuo, tales como espectrofotometría UV-Vis[519-523], FAAS[524] y electrodos selectivos de iones[525-528].

---

[514] A.P. de Silva, H.O.N. Gunaratne, T. Gunnlaugsson, A.J.M. Huxley, C.P. McCoy, J.T. Rademacher, T.E. Rice. *Signaling recognition events with fluorescent sensors and switches.* Chem. Rev., 97(5) (1997) 1515-1566

[515] C. Henquin, T. Tamagawa, M. Nenquin, M. Cogneau. *Glucose modulates magnesium(2+) fluxes in pancreatic islet cells.* Nature, 301(5895) (1983) 73-74

[516] G. Grynkiewicz, M. Poenie, R.Y.J. Tsien. *A new generation of Ca2+ indicators with greatly improved fluorescence properties.* Biol. Chem., 260(6) (1985) 3440-3450

[517] H. He, K. Jenkins, C. Lin. *A fluorescent chemosensor for calcium with excellent storage stability in water.* Anal. Chim. Acta, 611(2) (2008) 197-204

[518] R.A. Potyrailo, W.G. Morris, A.M. Leach, T.M. Sivavec, M.B. Wisnudel, S. Boyette. *Analog signal acquisition from computer optical disk drives for quantitative chemical sensing.* Anal. Chem., 78 (2006) 5893-5899

[519] E. Gómez, C. Tomás, A. Cladera, J.M. Estela, V. Cerdá. *Multicomponent techniques in sequential injection*. Analyst, 120 (1995) 1181-1184

[520] E. Gómez, J.M. Estela, V. Cerdá. *Simultaneous spectrophotometric determination of calcium and magnesium in water.* Anal. Chim. Acta, 249(2) (1991) 513-518

[521] M. Blanco, J. Coello, J. Gené, H. Iturriaga, S. Maspoch. *Use of diode-array detectors for the simultaneous spectrophotometric determination of calcium and magnesium by flow injection.* Anal. Chim. Acta, 224(1) (1989) 23-30

[522] O. Hernández, F. Jiménez, A.I. Jiménez, J.J. Arias, J. Havel. *Multicomponent flow injection based analysis with diode array detection and partial least squares multivariate calibration evaluation. Rapid determination of Ca(II) and Mg(II) in waters and dialysis liquids.* Anal. Chim. Acta, 320(2-3) (1996) 177-183

[523] F. Blasco, M.J. Medina-Hernández, S. Sagrado, F.M. Fernández. *Simultaneous spectrophotometric determination of calcium and magnesium in mineral waters by means of multivariate partial least-squares regression*. Analyst, 122(7) (1997) 639-643

[524] W.D. Basson, J.F. Van Staden. *Simultaneous determination of sodium, potassium, magnesium and calcium in surface, ground and domestic water by flow-injection analysis.* Fresenius Z. Anal. Chem., 302(5) (1980) 370-374

[525] R.J. Foster, D. Diamond. *Nonlinear calibration of ion-selective electrode arrays for flow injection analysis*. Anal. Chem., 64(15) (1992) 1721-1728

[526] J.W. Ross. *Calcium-selective electrode with liquid ion exchanger*. Science, 156(3780) (1967) 1378-1379

[527] *Handbook of Electrode Technology*. Orion Research Inc. Cambridge (1982) pp. 45

[528] M. Maj-Zurawska, M. Rouilly, W.E. Morf, W. Simon. *Determination of magnesium and calcium in water with ion-selective electrodes.* Anal. Chim. Acta, 218(1) (1989) 47-59

Por otra parte, se han adaptado diferentes métodos espectrofotométricos UV/Vis a metodologías de flujo que presentan ventajas de simplicidad y bajo coste, aunque con el inconveniente de baja selectividad. En algunos casos, un cambio en las condiciones químicas debido a, por ejemplo, pH[529] o uso de agentes enmascarantes[530], hace posible la determinación secuencial de ambos analitos. En otros casos, el tratamiento de los datos obtenidos mediante análisis multivariante, permite la determinación simultánea[531-536].

Otra alternativa propuesta para la determinación de calcio y magnesio consiste en un sensor de fibra óptica fluorescente basado en un antibiótico natural, el poliéster carboxílico A23187, que presenta un buen límite de detección y selectividad, pero tiene un tiempo de respuesta largo y un corto tiempo de vida[537]. Otro sensor de fibra óptica desarrollado permite medir la dureza del agua a partir de la variación de absorbancia de un agente metalocrómico, el negro de eriocromo T, que es inmovilizado en el extremo de la fibra empleando una membrana termoplástica de poliuretano (Tecoflex)[538].

La dureza del agua también se puede determinar directamente usando electrodos selectivos de iones divalentes basados en transportadores neutros,

---

[529] J. Marcos, A. Rios, M. Valcárcel. *Automated simultaneous determination of metal ions by use of variable flow rates in unsegmented systems.* Analyst, 117(10) (1992) 1629-1633

[530] T. Yamane, E. Goto. *Simultaneous determination of calcium and magnesium by using a flow-injection system with simultaneous injection of two sample plugs and a masking agent plug.* Talanta, 38(2) (1991) 139-143

[531] E. Gómez, C. Tomás, A. Cladera, J.M. Estela, V. Cerdá. *Multicomponent techniques in sequential injection.* Analyst, 120(4) (1995) 1181-1184

[532] E. Gómez, J.M. Estela, V. Cerdá. *Simultaneous spectrophotometric determination of calcium and magnesium in water.* Anal. Chim. Acta, 249(2) (1991) 513-518

[533] M. Blanco, J. Coello, J. Gené, H. Iturriaga, S. Maspoch. *Use of diode-array detectors for the simultaneous spectrophotometric determination of calcium and magnesium by flow injection.* Anal. Chim. Acta, 224(1) (1989) 23-30

[534] F. Blasco, M.J. Medina-Hernández, S. Sagrado, F.M. Fernández. *Simultaneous spectrophotometric determination of calcium and magnesium in mineral waters by means of multivariate partial least-squares regression.* Analyst, 122(7) (1997) 639-643

[535] I. Ruisánchez, A. Rius, M.S. Larrechi, M.P. Callao, F.X. Rius. *Automatic simultaneous determination of Ca and Mg in natural waters with no interference separation.* Chem. Intell. Lab. Syst., 24(1) (1994) 55-63

[536] J. Saurina, E. López-Aviles, A. Le Moal, S. Hernández-Cassou. *Determination of calcium and total hardness in natural waters using a potentiometric sensor array.* Anal. Chim. Acta, 464(1) (2002) 89-98

[537] K. Suzuki, K. Tohda, Y. Tanda, H. Ohzora, S. Nishihama, H. Inoue, T. Shirai. *Fiber-optic magnesium and calcium ion sensor based on a natural carboxylic polyether antibiotic.* Anal. Chem., 61(4) (1989) 382-384

[538] M. Achaerando, J. Alzueta, F. Arregui, J. Fernandez-Sanchez, A. Segura-Carretero, I. Matias. *Fiber-optic water hardness sensor based on eriochrome black T.* Chem. Sensors, 2020(Suppl. B) (2004) 796-797

cuyas membranas presentan igual selectividad para calcio y magnesio y discrimina al resto de iones alcalinos[527,539-541].

Por otra parte, se han empleado diferentes procedimientos tipo ensayo rápido para determinar la dureza total, los cuales pueden llevarse a cabo tanto en disolución como en fase sólida. Algunos tests han sido comercializados por diversas compañías, entre las que se pueden citar Serim™ Water Hardness Test Strips (Serim Research Co.), EM Quant® Total Hardness Test (Merck) o Aquadur® Total Hardness (Macherey-Nagel). Todos ellos se basan en la reacción entre un indicador químico depositado en la tira reactiva y los iones calcio y/o magnesio de una disolución acuosa que se ponen en contacto con ella, dando lugar a un cambio de color que se compara con una escala de colores, obteniéndose un resultado semicuantitativo.

Otra variante empleada son los test basados en multicapas para la determinación de iones alcalinotérreos individuales en fluidos biológicos basados en ionóforos neutros, normalmente coronanos, criptanos o podanos, medidos mediante reflectancia difusa[542,543].

1.1. Modelo teórico

En este capítulo se propone un método para la determinación de alcalinotérreos mediante la medida de la variación de la absorbancia de sensores ópticos de un solo uso. Estos sensores ópticos responden a actividad del analito y no a concentración, es decir, responden a la cantidad de analito disponible para interactuar con otras especies, no a la cantidad total de analito en disolución.

---

[539] J.W. Ross. *Calcium-Selective Electrode with Liquid Ion Exchanger.* Science, 156(3780) (1967) 1378-1379

[540] M. Maj-Zurawska, M. Rouilly, W.E. Morf, W. Simon. *Determination of magnesium and calcium in water with ion-selective electrodes.* Anal. Chim. Acta, 218(1) (1989) 47-59

[541] K. Toth, E. Lindner, M. Horváth, J. Jeney, E. Pungor, I. Bitter, B. Ágai, L. Töke. *Analytical performances of lipophilic diamides based alkaline earth ion-selective electrodes.* Electroanalysis, 5(9-10) (1993) 781-790

[542] M.L. Gantzer, P.R. Hemmes, R. Paul, D. Wong. US Patent 4, 670 (1987) 218

[543] P. Vogel, D. Thym, M. Fritz, D. Mosoiu. US Patent 5, 302 (1994) 346

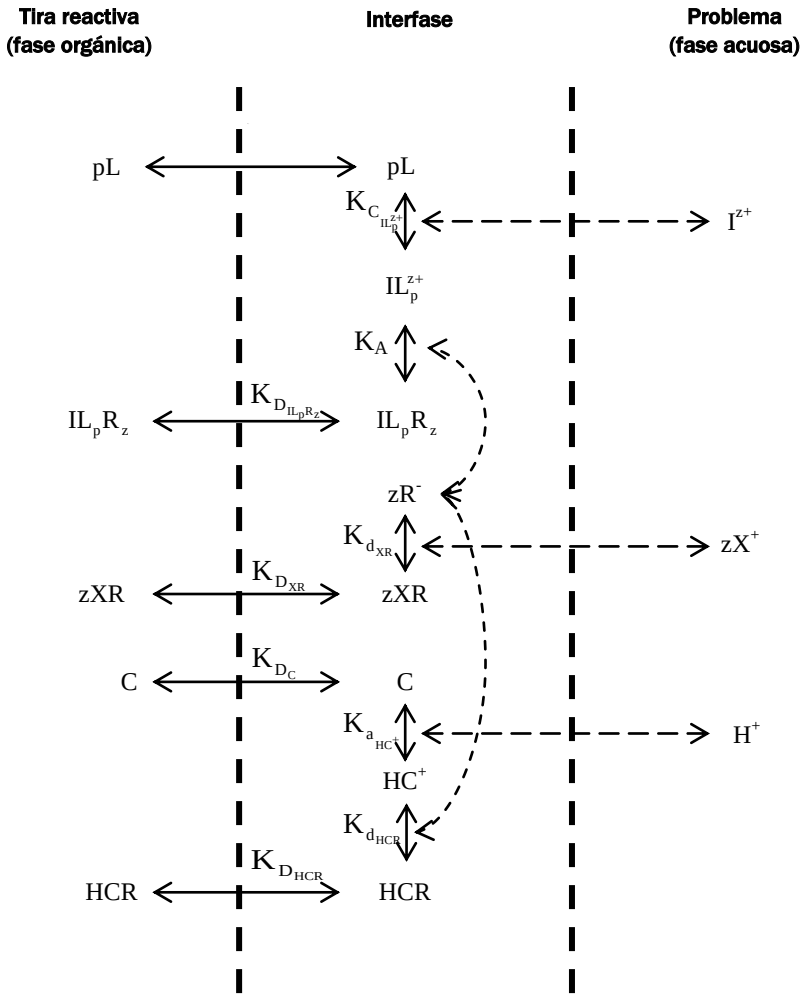

Figura VIII.1. Modelo de sensor basado en un ionóforo y un cromoionóforo básico

Como caso general, puede considerarse que el analito es un ion I^{z+} que reacciona con un ionóforo neutro L de carácter lipofílico para originar el complejo $IL_{p^{z+}}$ que se retendrá en la fase orgánica como par iónico IL_pR_z con el anión lipofílico R^-. En la figura VIII.1 se muestra el modelo de sensor basado en el uso conjunto de un ionóforo y un cromoionóforo básico en presencia de una sal de anión lipofílico, necesaria para que se pueda producir el equilibrio de cambio iónico.

La extracción del analito desde la disolución problema al sensor se puede describir mediante un esquema de tres etapas: a) difusión del analito a través de la interfase de la muestra; b) transferencia de fase y proceso de complejación/descomplejación; y c) difusión de las especies a través de la membrana[544].

Al introducir el sensor en una disolución que contiene el analito I^{z+} y para mantener la electroneutralidad en la membrana, se produce un intercambio de cationes, de modo que por cada carga positiva que entre en forma de analito para complejar al ionóforo y originar $\overline{IL}_{p^{z+}}$, debe salir otra carga positiva, y la única disponible es la ligada al cromoionóforo. Así como la entrada de analito no es perceptible, la salida de cargas positivas sí es susceptible de transducción óptica mediante la variación de la absorbancia al desprotonarse el cromoionóforo.

El equilibrio global de cambio iónico que tiene lugar entre la muestra y la tira reactiva viene dado por:

$$I^{z+} + p\overline{L} + z\overline{HC^+} \leftrightarrow \overline{IL}_p^{z+} + z\overline{C} + zH^+$$

en el que no se han incluido los aniones lipofílicos, ya que no intervienen en el intercambio de cargas, sólo lo permiten. Este equilibrio viene gobernado por la constante $K_{exch}^{IL_p}$:

$$K_{exch}^{IL_p} = \frac{a_{H^+}^z [C]^z [\overline{IL}_p^{z+}]}{a_{I^{z+}} [\overline{HC^+}] [L]^p} \qquad \text{(VIII.1)}$$

Las concentraciones en fase orgánica vienen dadas en molalidades (moles/kg) y sus coeficientes de actividad se denotan por "γ". En fase acuosa, las actividades se denotan por "a".

[544] K. Seiler, W. Simon. *Theoretical aspects of bulk optode membranes.* Anal. Chim. Acta, 266(1) (1992) 73-81

Esta constante $K_{exch}^{IL_p}$ será función de la constante de estabilidad del complejo, de la constante de acidez del cromoionóforo y de las lipofilias relativas del analito $K_{I^{z+}}$ y del protón K_{H^+}.

La constante de complejación se refiere al equilibrio:

$$I^{z+} + p\bar{L} \leftrightarrow IL_p^{z+}$$

y viene dada por

$$\beta_{IL_p^{z+}} = \frac{a_{IL_p^{z+}}}{a_{I^{z+}} a_L^p}$$

Esta constante simplifica el modelo formal presentado en la Figura VIII.1, aunque se relaciona con él de acuerdo con:

$$\beta_{IL_p^{z+}} = \frac{K_{D_{IL_pR_z}} K_{AS} K_{C_{IL_p^{z+}}} K_{d_{XR}}^z}{K_{D_L}^p K_{D_{XR}}^z} \qquad \text{(VIII.2)}$$

La constante de acidez del cromoionóforo, por su parte, responde al equilibrio:

$$\overline{HC^+} \leftrightarrow H^+ + \bar{C}$$

y viene dada por H

$$K_a = \frac{a_{H^+} a_C}{a_{HC^+}}$$

Como en el caso anterior, también se relaciona con el modelo según:

$$K_a = \frac{K_{D_C} K_{a_{HC^+}} K_{d_{HCR}} K_{D_{XR}}}{K_{d_{XR}}} \qquad \text{(VIII.3)}$$

Las lipofilias relativas del analito $K_{I^{z+}}$ y del protón K_{H^+} se pueden describir mediante los equilibrios:

$$H^+ \leftrightarrow \overline{H^+} \qquad K_{H^+} = \frac{\gamma_{\overline{H^+}}}{a_{H^+}} \qquad \text{(VIII.4)}$$

$$I^{z+} \leftrightarrow \overline{I^{z+}} \qquad K_{I^{z+}} = \frac{\gamma_{\overline{I^{z+}}}}{a_{I^{z+}}} \qquad \text{(VIII.5)}$$

Si se sustituyen las actividades por las correspondientes concentraciones y coeficientes de actividad en las cuatro constantes que se acaban de definir y, a su vez, se opera en la $K_{exch}^{IL_p}$ (ec. VIII.1), resulta que la constante de intercambio se relaciona con las constantes de formación del complejo, de acidez del cromoionóforo y las lipofilias de los iones principal y de referencia, así como con los coeficientes de actividad en fase membrana, según:

$$K_{exch}^{IL_p} = \frac{K_{I^{z+}} \beta_{IL_p^{z+}} K_a^z}{K_{H^+}^z} \left(\frac{\gamma_{HC^+}}{\gamma_C} \right)^z \frac{(\gamma_L)}{\gamma_{IL_p^{z+}}} \qquad \text{(VIII.6)}$$

Como puede verse, las actividades de todas las especies involucradas controlan el equilibrio, pero sólo la concentración del cromoionóforo será accesible a través de medidas ópticas. En consecuencia, es esencial que los coeficientes de actividad permanezcan constantes en todo el rango de medida. Para una membrana dada del tipo considerado, la fuerza iónica dentro de ella se debe mantener virtualmente constante, pues está definida por la concentración de sal lipofílica, lo que, de acuerdo con la teoría de Debye-Hückel, debe originar un coeficiente de actividad medio constante en la fase membrana. En una primera aproximación, los coeficientes de actividad de las especies cargadas serán despreciables y el cambio en los coeficientes de actividad de las especies neutras deberá ser relativamente pequeño dentro del rango de calibración, si su concentración total se mantiene baja. Cuando la cantidad de alguno se incrementa, como puede ser la de ionóforo por razones de selectividad, se observa un cambio en el coeficiente de actividad y, por tanto, en la constante de

equilibrio $K_{exch}^{IL_p}$ [545]. Esto significa que las concentraciones en la fase orgánica son proporcionales a las actividades. En resumen, la expresión anterior queda reducida a:

$$K_{exch}^{IL_p} = \frac{K_{I^{z+}} \beta_{IL_p^{z+}} K_a^z}{K_{H^+}^z} \qquad \text{(VIII.7)}$$

Para expresar la constante de equilibrio $K_{exch}^{IL_p}$ en función de parámetros experimentales, se realiza un balance de cargas en la membrana, llamando C_R a la concentración analítica de anión lipofílico:

$$C_R = [HC^+] + z[IL_p^{z+}] \qquad \text{(VIII.8)}$$

y los correspondientes balances de masas respecto a ionóforo (C_L concentración analítica de ionóforo) y cromoionóforo (C_C concentración analítica de cromoionóforo):

$$C_L = [L] + p[IL_p^{z+}] \qquad \text{(VIII.9)}$$

$$C_C = [C] + [HC^+] \qquad \text{(VIII.10)}$$

Asimismo, se define la fracción de cromoionóforo α como el cociente de forma no protonada a total:

$$[C] = \alpha[C_0] \qquad \text{(VIII.11)}$$

luego

$$[HC^+] = (1 - \alpha)[C_0] \qquad \text{(VIII.12)}$$

Como el cromoionóforo es la única especie detectable en la membrana, si se mide a una longitud de onda característica de la especie desprotonada, se puede definir una absorbancia normalizada como parámetro analítico, que será

[545] K. Seiler, K. Wang, E. Bakker, W.E. Morf, B. Rusterholz, U.E. Spichiger-Keller, W. Simon, *Characterization of sodium-selective optode membranes based on neutral ionophores and assay of sodium in plasma.* Clin. Chem., 37(8) (1991) 1350-1355

la misma fracción α anterior. Consecuentemente, si α = 1 no habrá cromoionóforo protonado y le corresponderá una absorbancia A_1 y si α = 0, todo el cromoionóforo estará protonado y su absorbancia correspondiente será A_o. La forma habitual de establecer A_1 consiste en tratar la membrana con una disolución 0,01 M de NaOH, lo que obliga a que todo el cromoionóforo esté en forma básica. En el caso de A_o se trata con HCl 0,01 M, con lo que el cromoionóforo se encontrará en forma ácida.

Sustituyendo, resulta:

$$\alpha = \frac{[C]}{[C_0]} \frac{A_0 - A}{A_0 - A_1} \qquad \text{(VIII.13)}$$

En consecuencia, el parámetro analítico que se usará será 1 - α:

$$1 - \alpha = \frac{A - A_1}{A_0 - A_1} \qquad \text{(VIII.14)}$$

Si se combinan las ecuaciones VIII.7, VIII.8, VIII.9, VIII.10 y VIII.13 se obtiene la función respuesta de la membrana sensora para el ion I^{z+}:

$$K_{exch}^{IL_p} = \frac{1}{a_{I^{z+}}} \left(\frac{a_{H^+}\alpha}{1-\alpha} \right)^z \frac{C_R - (1-\alpha)C_C}{z(C_L - \frac{p}{z}(C_R - (1-\alpha)C_C))^p} \qquad \text{(VIII.15)}$$

$$a_{I^{z+}} = \frac{1}{K_{exch}^{IL_p}} \left(\frac{a_{H^+}\alpha}{1-\alpha} \right)^z \frac{C_R - (1-\alpha)C_C}{z(C_L - \frac{p}{z}(C_R - (1-\alpha)C_C))^p} \qquad \text{(VIII.16)}$$

Dado que la membrana sensora está en equilibrio químico con la muestra conteniendo analito, lo que se mide no será concentraciones, sino el cociente de actividades entre el ion de referencia y el analito. Si se mantiene constante la actividad del ion de referencia, se puede despejar la actividad del analito.

Si se toman logaritmos en la ecuación anterior y se establece como variable independiente $\log a_{I^{z+}}$ y como variable dependiente $1 - \alpha$ y se renombran como X e Y, respectivamente, se llega a la ecuación VIII.17, cuya inversa Y=f(X) se puede observar en la figura VIII.3.

$$X = \log \left\{ \frac{1}{K_{exch}^{IL_p}} \left(\frac{a_{H^+}\ (1-Y)}{Y} \right)^z \frac{C_R - Y\ C_C}{z(C_L - \frac{p}{z}(C_R - YC_C))^p} \right\} \qquad \text{(VIII.17)}$$

Si se representa la actividad del analito frente al grado de protonación según la ecuación VIII.15, se obtiene la curva representada en la figura VIII.2, la cual no ofrece información interesante por el gran número de órdenes de magnitud que implica. Por ello, se usa la representación frente al logaritmo decimal de la actividad. Al representar la variación de $1 - \alpha$ en función de $\log a_{I^{z+}}$ tal como se muestra en la figura VIII.3, resulta un modelo de tipo sigmoidal. Este modelo no tiene la sencillez de
fácil, la determinación experime

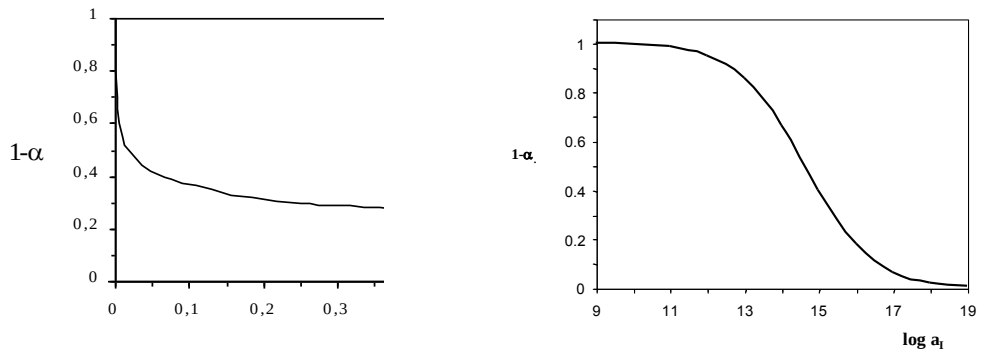

Figura VIII.2. Actividad del analito frente al grado de protonación

Si se tiene en cuenta en
2) z y p toman valores discretos
el comportamiento del cromoi

calcularse, bien teóricamente si se conocen las constantes de distribución y de formación de las especies implicadas, o bien empíricamente mediante el establecimiento del modelo sigmoidal comentado anteriormente; y 4) se conoce la actividad del catión de referencia en la disolución problema, entonces queda que:

$$a_{I^{z+}} = f(1-\alpha) \equiv f(A)$$

La actividad del ion está directamente relacionada con su concentración por medio del coeficiente de actividad γ según las ecuaciones:

$$a = [z_+]_{\gamma^+} \qquad \text{(VIII.18)}$$

$$a = [z_-]_{\gamma^-} \qquad \text{(VIII.19)}$$

donde z_+ y z_- son las cargas de cada ion.

Para calcular γ se utilizan las expresiones:

$$\log \gamma_+ = [z_+][z_-] \log \gamma_\pm \qquad \text{(VIII.20)}$$

$$\log \gamma_- = [z_+][z_-] \log \gamma_\pm \qquad \text{(VIII.21)}$$

En un principio se usó la aproximación de Debye-Hückel (ec. VIII.22) para el cálculo de $\gamma_\pm$, la cual supone al disolvente como un medio continuo, en lugar de un sistema de moléculas. Es bien sabido que los iones en disolución se encuentran solvatados, tanto más cuanto más polar sea el disolvente. Esto hace que la estructura del agua unida al ion sea diferente que la del agua pura, pero esta interacción entre ion y disolvente es un fenómeno muy complejo, que sólo se puede describir aproximadamente suponiendo el medio continuo.

$$\log \gamma_{\pm} = \frac{A|z_+ z_-|\sqrt{I}}{1 + B\sqrt{I}} \qquad \text{(VIII.22)}$$

Para poder calcular con mayor aproximación los coeficientes de actividad a altas concentraciones, que es donde tienen mayor importancia las interacciones electrostáticas que conducen a la formación de pares iónicos[546], se modifica la ecuación anterior de forma:

$$\log \gamma_{\pm} = \frac{A|z_+ z_-|\sqrt{I}}{1 + B\sqrt{I}} + C \cdot I \qquad \text{(VIII.23)}$$

donde A, B y C son parámetros experimentales tabulados para disoluciones acuosas a 25 ºC para los diferentes iones[547]. La tabla VIII.1 recoge los valores de estos parámetros para diferentes sales. Por su parte, I es el valor de la fuerza iónica que está relacionado con la concentración de iones disueltos en el medio, mediante la conocida expresión:

$$I = \frac{1}{2} \sum_i c_i z_i^2 \qquad \text{(VIII.24)}$$

Tabla VIII.1. Valores de los parámetros experimentales tabulados para diferentes sales

Parámetros	$MgCl_2$	$CaCl_2$	$SrCl_2$	$BaCl_2$	LiCl	NaCl	KCl
A	0,5108	0,5108	0,5108	0,5108	0,5108	0,5108	0,5108
B	1,7309	1,5800	1,4874	1,3712	1,4982	1,4255	1,2796
C	0,05195	0,04570	0,04283	0,3953	0,11115	0,02626	0,00393

Se debe tener en cuenta que en el medio se encuentran tanto la disolución reguladora como el analito, por lo que la fuerza iónica será:

[546] A. Eucken. *Química Física*. Marin Editor, Barcelona, (1941) pp. 688

[547] P.C. Meier. *Two-parameter Debye-Hueckel approximation for the evaluation of mean activity coefficients of 109 electrolyt*. Anal. Chim. Acta, 136 (1982) 363-368

$$I = I_{tampón} + I_{analito} \quad \text{(VIII.25)}$$

En algunas ocasiones el cromoionóforo presente no se puede protonar de forma completa, lo que se puede deber a diversas causas, como que la concentración de cromoionóforo sea mayor que la de sal lipofílica por razones de selectividad o bien a que el pH de trabajo no lo permita. Esto hace que no se pueda determinar A_o y, por tanto, tampoco α como indica la ecuación VIII.13. Para resolver el problema se utiliza un valor de α efectivo, α_{ef}, que señalará el grado de protonación en esas condiciones concretas de concentración de sal lipofílica o de pH. En este caso se ha utilizado α_{ef}, ya que permite conocer el grado de protonación con respecto a disoluciones reguladoras dadas. En consecuencia, el parámetro analítico considerado será:

$$1 - \alpha_{ef} = \frac{A - A_1}{A_{tampón} - A_1} \quad \text{(VIII.26)}$$

1.2. Selectividad

Se denomina selectividad a la capacidad de una membrana sensora para extraer información relacionada exclusivamente con el analito o con una clase de analitos, y para discriminar especies interferentes que respondan originando el mismo tipo de señal. Se define mediante el coeficiente de selectividad k_{IJ}^{Osel}. Así, un coeficiente de selectividad de 0,01 significa que la especie interferente es discriminada en un factor de 100 y que esta especie contribuye en un 1% a la señal del analito si ambos, analito e interferente, están presentes con la misma actividad[499].

Suponiendo que junto con el analito, el ion I^{z+}, se encuentra presente el ion interferente J^{v+} que reacciona con el ionóforo L originando el complejo JL_q^{v+}, de manera análoga a lo ocurrido con el analito puede definirse una constante de intercambio $K_{exch}^{JL_q}$:

$$K_{exch}^{JL_q} = \frac{a_{H^+}^{v}[c]^{v}[JL_q^{v+}]}{a_{I^{v+}}[HC^+][L]^q} \qquad \text{(VIII.27)}$$

Si sólo ocurriera intercambio entre J^{v+} y H^+, la actividad en J^{v+} vendría dada por una función respuesta para un solo ion, análoga a la ecuación VIII.16:

$$a_{J^{v+}} = \frac{1}{K_{exch}^{JL_q}}\left(\frac{a_{H^+}\alpha}{1-\alpha}\right)^{v}\frac{C_R-(1-\alpha)C_C}{v\left(C_L-\frac{q}{v}(C_R-(1-\alpha)C_C)\right)^{p}} \qquad \text{(VIII.28)}$$

Si, por el contrario, se encontraran presentes I^{z+} y J^{v+} en la disolución problema y compitieran por el mismo ionóforo presente en la membrana sensora para originar los complejos IL_p^{z+} y JL_q^{v+}, los balances de carga y masa quedarían como sigue:

$$C_R = [HC^+] + z[IL_p^{z+}] + v[JL_q^{v+}] \qquad \text{(VIII.29)}$$

$$C_L = [L] + p[IL_p^{z+}] + q[JL_q^{v+}] \qquad \text{(VIII.30)}$$

Suponiendo que las estequiometrías de ambos complejos son 1:1, esto es IL^{z+} y JL^{v+}, se pueden deducir expresiones para la distribución de ionóforo libre [L] y complejado IL^{z+} dentro de la membrana, al objeto de obtener la función respuesta para el ion primario I^{z+} en presencia del ion interferente J^{v+} [548].

Si a partir de la ecuación VIII.27 se define la fracción de complejo con el ion interferente χ como:

$$\chi = \frac{v}{z}K_{exch}^{JL_p}\left(\frac{[IL^{z+}]}{[C]a_{H^+}}\right)^{v}a_{J^{v+}} \qquad \text{(VIII.31)}$$

[548] E. Bakker, W. Simon. *Selectivity of ion-sensitive bulk optodes.* Anal. Chem., 64 (1992) 1805-1812

y si se combina con las ecuaciones VIII.26 y VIII.28, resulta:

$$[IL^{z+}] = \frac{1}{z}\left(C_R - [HC^+]\right) - \frac{v}{z}\chi[L] \qquad \text{(VIII.32)}$$

Por otra parte, usando las ecuaciones VIII.27 y VIII.32 para resolver la ecuación VIII.30, obtenemos:

$$[L] = \frac{C_L - \frac{1}{z}\left(C_R - [HC^+]\right)}{1 + \left(1 - \frac{v}{z}\right)\chi} \qquad \text{(VIII.33)}$$

Operando a partir de las ecuaciones VIII.27, VIII.32 y VIII.33, resulta la función respuesta para el ion primario I^{z+} en presencia del ion interferente J^{v+}:

$$a_{I^{z+}} + k_{IJ}^{Osel}\, a_{J^{v+}} = \frac{1}{K_{exch}^{IL_p}}\left(\frac{a_{H^+}\alpha}{1-\alpha}\right)^z \frac{C_R - (1-\alpha)C_C}{z\left(C_L - \frac{p}{z}(C_R - (1-\alpha)C_C)\right)} \qquad \text{(VIII.34)}$$

siendo el factor de selectividad k_{IJ}^{Osel}:

$$k_{IJ}^{Osel} = \frac{v}{z}\frac{K_{exch}^{JL_q}}{K_{exch}^{IL_p}}\left(\frac{a_{H^+}\alpha}{1-\alpha}\right)^{z-v} \frac{C_L - \frac{1}{v}C_R - (1-\alpha)C_C}{C_L - \frac{1}{z}C_R - (1-\alpha)C_C} \qquad \text{(VIII.35)}$$

Teniendo en cuenta las ecuaciones VIII.16 y VIII.28, se puede simplificar la ecuación VIII.35 como:

$$k_{IJ}^{Osel} = \frac{a_{I^{z+}}}{a_{J^{v+}}} \qquad \text{(VIII.36)}$$

La anterior ecuación VIII.34 es exacta cuando hay exceso de ionóforo y la estequiometría de los complejos es 1:1, pero, en el caso de que las

estequiometrías sean superiores y/o diferentes, esta aproximación se puede generalizar de la forma:

$$a_{I^{z+}} + \sum_j k_{IJ}^{Osel}\ a_{J^{v+}} = f\left(a_{I^{z+}}\right) = \frac{1}{K_e^{IL_p}} \left(\frac{a_{H^+}\alpha}{1-\alpha}\right)^z \frac{C_R - (1-\alpha)C_C}{z\left(C_L - \frac{p}{z}(C_R - (1-\alpha)C_C)\right)^p} \quad \text{(VIII.37)}$$

donde:

$$k_{IJ}^{Osel} = \frac{a_{I^{z+}}}{a_{J^{v+}}} = \frac{v}{z}\frac{K_e^{JL_q}}{K_e^{IL_p}} \left(\frac{a_{H^+}\alpha}{1-\alpha}\right)^{z-v} \frac{\left(C_L - \frac{q}{v}C_R - (1-\alpha)C_C\right)^q}{\left(C_L - \frac{p}{z}C_R - (1-\alpha)C_C\right)^p} \quad \text{(VIII.38)}$$

Tal como indica la ecuación VIII.36 en forma logarítmica:

$$\log k_{IJ}^{Osel} = \left(\log a_{I^{z+}}\right) - \left(\log a_{J^{v+}}\right) \quad \text{(VIII.39)}$$

el coeficiente de selectividad se puede estimar gráficamente[549,550] representando las funciones respuesta obtenidas para cada ión I^{z+} y J^{v+} por separado, esto es, $1 - \alpha$ (o $1 - \alpha_{ef}$) *vs* $\log a_M$ (M = i,j). Si el pH se mantiene constante, el coeficiente de selectividad viene dado por la distancia horizontal entre la dos curvas para un grado de protonación considerado, tal como lo muestran las Figuras VIII.4 y VIII.5 (distancia d). Este procedimiento de cálculo de los coeficientes de selectividad es el denominado método de las disoluciones separadas.

Al observar la ecuación VIII.39, se comprueba que el coeficiente de selectividad es función del grado de protonación ($1 - \alpha$). Por lo tanto, para poder comparar coeficientes de selectividad de diferentes interferentes, debe normalizarse ese parámetro refiriéndolo siempre al mismo valor. Para ello, se toma como valor fijo $1 - \alpha = 0{,}5$, ya que para ese valor no influye la carga del ion interferente, aunque sí influye la estequiometría.

---

[549] M. Lerchi, E. Bakker, B. Rusterholz, W. Simon. *Lead-selective bulk optodes based on neutral ionophores with subnanomolar detection limits.* Anal. Chem., 64 (1992) 1534-1540

[550] M. Lerchi, E. Reitter, W. Simon, E. Pretsch, A. Chowdhury, S. Kamata. *Bulk Optodes Based on Neutral Dithiocarbamate Ionophores with High Selectivity and Sensitivity for Silver and Mercury Cations.* Anal. Chem., 66(10) (1994) 1713-1717

En el caso de que el ion interferente tenga la misma carga que el analito

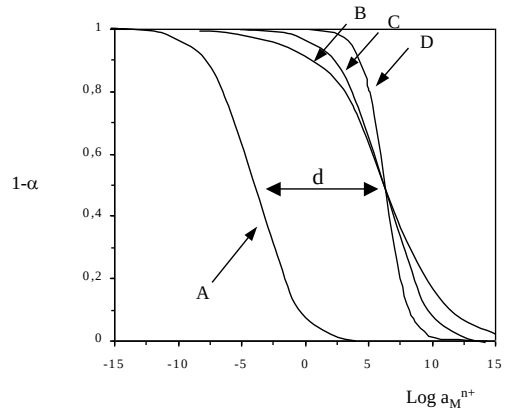

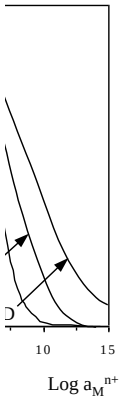

coeficientes de selectividad

[551] E. Bakker, P. Buhlmann, E. Pretsch. *Carrier-Based Ion-Selective Electrodes and Bulk Optodes. 1. General Characteristics.* Chem. Rev., 97(8) (1997) 3083-3132

$$K_{IJ}^{opt} = (k_{IJ}^{Osel})^{v/z}\, a_{i^{z+}}(I)^{1-(v/z)} \qquad \text{(VIII.41)}$$

donde $a_{i^{z+}}(I)$ es la actividad del ion primario en la muestra sin interferencia de otros iones de la muestra. Sustituyendo en la ecuación VIII.41 las ecuaciones VIII.26 y VIII.39, resulta:

$$K_{IJ}^{Opt} = \frac{\left\{ v\, K_e^{JL_q} \left(C_L - \frac{q}{v} C_R - (1-\alpha)C_C \right)^q \right\}^{z/v}}{\left\{ z\, K_e^{IL_p} \left(C_L - \frac{p}{z} C_R - (1-\alpha)C_C \right)^p \right\}^{p}} \left\{ C_L - (1-\alpha)C_C \right\}^{1-(z/v)} \qquad \text{(VIII.42)}$$

Este coeficiente, de tipo Nicolskii, se puede determinar experimentalmente mediante el método de las disoluciones separadas, midiendo independientemente la actividad del ion primario y del ion interferente que inducen un valor de α determinado. Esas dos actividades, junto con sus respectivos valores de pH, denotados con (I) y (J) si son diferentes, se introducen en la ecuación, quedando:

$$K_{IJ}^{opt} = \frac{a_I(I)}{a_J(J)^{z/v}} \left(\frac{a_H(J)}{a_H(I)} \right)^z \qquad \text{(VIII.43)}$$

Este coeficiente coincide, si el pH es igual para ambos iones, con el coeficiente de Nikolskii definido para electrodos selectivos de iones:

$$K_{IJ}^{opt} = \frac{a_I(I)}{a_J(J)^{z/v}} \qquad \text{(VIII.44)}$$

Sin embargo, y a diferencia de lo que ocurre en electrodos selectivos de iones, el coeficiente de selectividad depende de la señal medida (α), debido a que los cambios en absorbancia o fluorescencia medidos están acoplados a cambios en la concentración de la especie activa dentro de la membrana sensora, tal como se ve en las figuras VIII.39 y VIII.40. Como solución se suele definir el valor de K_{IJ}^{opt} para un valor de 1 - α determinado, generalmente 0,5. Por esta razón, es

habitual que las selectividades en sensores ópticos se expresen como k_{IJ}^{Osel} junto con los valores de K_{exch} determinados, pues son suficientes para una completa caracterización de la selectividad de un sensor dado.

2. OBJETIVOS

El objetivo general del trabajo que se presenta en este capítulo es:

- Desarrollar sensores ópticos para medida de calcio en disolución acuosa basados en una química de reconocimiento tipo ionóforo-cromoionóforo.

Los objetivos particulares a alcanzar son:

- Modificar las características electrodonoras y los efectos estéricos de ionóforos previamente descritos en bibliografía para incrementar la selectividad de los sensores preparados a partir de éstos. Para ello se recurre a la síntesis de nuevos éteres corona del tipo 18-corona-6 incluyendo sustituyentes en un par de átomos enlazantes (O ó N), y se caracterizan utilizando datos espectroscópicos procedentes de IR, ^{1}H-RMN, ^{13}C-RMN, HRMS MALDI y FAB^{+}.

- Preparación de las membranas sensoras ópticas mediante la técnica de recubrimiento por giro y evaporación sobre membranas transparentes de Mylar. Los cócteles utilizados contienen, además de alguno de los ionóforos tipo 18-corona-6 sintetizados, Azul Nilo lipofilizado como indicador ácido-base.

- Caracterización de las membranas sensoras fabricadas mediante un sistema de flujo de diseño propio y monitorización espectrofotométrica del cambio de color de la membrana debido a la complejación del alcalinotérreo. Representación, a partir de las medidas de absorbancia, de las variaciones de $1 - \alpha_{ef}$ frente al logaritmo de las actividades de los iones, obteniéndose las curvas sigmoidales correspondientes. Cálculo de las constantes de intercambio de los cuatro cationes estudiados.

- Cálculo de los coeficientes de selectividad de las membranas sensoras preparadas frente a alcalinos y alcalinotérreos utilizando el método de las disoluciones separadas, con objeto de seleccionar el ionóforo más adecuado para el sensor de flujo.

PUBLICACIÓN VII:

Talanta, 78 (2009) 1484–1488
DOI: 10.1016/j.talanta.2009.01.046

Double-armed crown ethers for calcium optical sensors

S. Capel-Cuevas[a], I. de Orbe-Payá[a], F. Santoyo-González[b], L.F. Capitán-Vallvey[a,*]

[a]*Solid Phase Spectrometry Research Group, Department of Analytical Chemistry.*
[b]*Department of Organic Chemistry.*
Faculty of Sciences, Campus Fuentenueva, University of Granada, E-18071 Granada, Spain

Abstract

This paper presents the characterization of optical sensing membranes for calcium based on ionophore–chromoionophore chemistry. Six different ionophores, 18-membered crown ether derivatives, were studied, coming from 18-crown-6 ether and 4,13-diaza-18-crown-6 ether to a series of double-armed crown ethers with different type of terminal groups. The study of optical membranes containing the same transducer and plasticizer allow drawing some conclusions on the influence of lipophilicity and size of the terminal group of the side chain on calcium selectivity. We have calculated the exchange constant $K^{IL_p}_{exch}$ for each equilibrium with alkaline and alkaline-earth ions and the selectivity coefficient $k^{Osel}_{I,J}$ for each ion against calcium as a way for a full characterization of sensing membranes. In all cases the ion:ionophore stability constants for calcium were the highest and the ionophore V containing an (N-adamantylcarbamoyl) acetyl moiety originated the most selective membrane for calcium. Analytical parameters for calcium determination using prepared membranes were calculated.

Keywords: Double-armed diazacrown ethers; Optical sensor; Ionophore–chromoionophore chemistry; Selectivity

* Corresponding author; e-mail: lcapitan@ugr.es

1. Introduction

Since Pedersen introduced them in 1967 [1], a wide variety of crown ethers have been synthesized and reported, especially during the last two decades [2-4]. The research interest focuses on their ability to form very stable molecular ensembles or complexes with alkaline, alkaline-earth metals and organic cations. Their affinity for a given cation, based on cooperative weak non-covalent interactions, depends on many factors, including the relative sizes of the cation and the macrocyclic cavity.

Double-armed crown ethers characterized by a parent macrocyclic ligand and a cation ligating sidearm [5] are suitable reagents for use as specific ionophores in areas as metal-sensing and separation processes. They form encapsulated and lipophilic complexes with stabilities intermediate between crown ethers and cryptands. Since these armed macrocycles are stronger cation binders than the crown ethers and more flexible than the cryptands, they offer great possibilities as analytical reagents.

This type of crown ethers is composed of two flexible cation-binding arms and a parent crown ring. The selectivity on the complexation is determined by the size of the crown ring and the nature and position of flexible side arms, which present a donor group that provides further coordination of a guest cation bonded in the crown ring. Consequently, it is possible to design a metal-selective reagent by choosing a combination of parent crown ring structure and functionalized side arms [6].

In this work we study the reactivity of a series of double-armed crown ethers based on an 18 atoms ring against alkaline and alkaline-earth ions. The ionophores are incorporated in optical membranes working on ion exchange. The use of the same cromoionophore as transducer permit to extract conclusions on the influence of lipophilicity and size of the terminal group of the side chain on calcium selectivity.

2. Experimental

2.1. Reagents and materials

Calcium, magnesium, sodium and potassium stock solutions (1.000 $mol \cdot L^{-1}$) were prepared in water from analytical reagent grade calcium, magnesium, sodium and potassium chlorides (Panreac, Barcelona, Spain) and standardized by atomic absorption spectrometry. Solutions of lower concentration were prepared by dilution with water. pH 8.5 and 9.0 buffer solutions 0.2 M were made from diethanolamine (Probus, Barcelona, Spain), Tris (Sigma-Aldrich Química S.A., Madrid, Spain) and HCl (Panreac). All chemicals used for the ionophore synthesis were of synthesis grade and reverse-osmosis type quality water (Milli-RO 12 plus Milli-Q station from Millipore) was used throughout (conductivity 18.2 mS).

The chromoionophore 1,2-benzo-7-(diethylamino)-3-(octadecanoylimino)phenoxazine (lipophilized Nile Blue) was synthesized, purified and identified by us according to [7] and the ionophores 18-crown-6 ether (ionophore I) and 4,13-diaza-18-crown-6 (ionophore II) were received from Fluka (Fluka, Madrid, Spain) and Sigma-Aldrich Chemie (Aldrich, Steinheim, Germany), respectively. The rest of the ionophores were synthesized by us. Other chemical used for preparing the sensitive films, high molecular weight poly (vinyl chloride) (PVC), tributylphosphate (TBP), potassium tetrakis (4-chlorophenyl)borate (TCPB), and tetrahydrofuran (THF) as solvent, were purchased from Sigma-Aldrich. Sheets of polyester type Mylar (Goodfellow, Cambridge, UK) were used as support (figure 8.1).

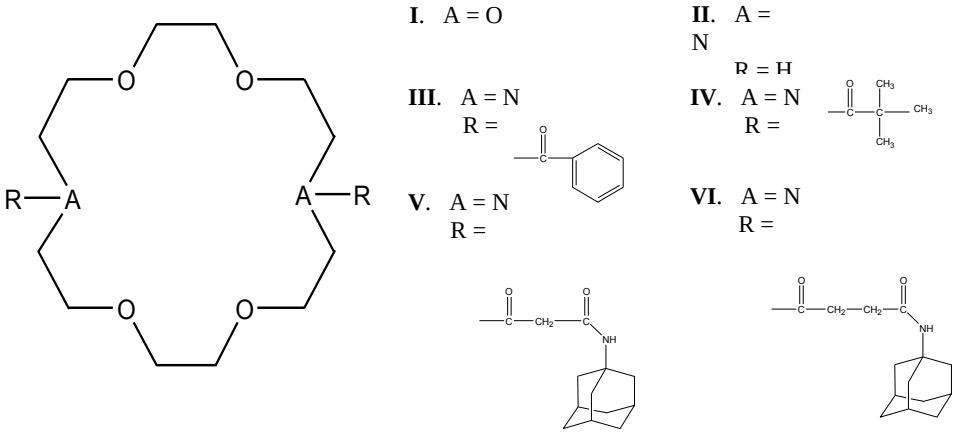

Figure 8.1. Structure of ionophores studied

2.2. Ionophore synthesis

The ionophore 7,16-[bis(N-adamantylcarbamoyl)acetyl]-1,4,10,13-tetraoxa-7,16-diazacyclooctadecane (ionophore V) was prepared according to Suzuki et al.[7]. Here, we present the synthesis of the new ionophores III, IV and VI. Characterization of the intermediate and the synthesized ionophores were made by ^{1}H-, ^{13}C-NMR, IR and HRMS (FAB^{+}).

2.2.1. Synthesis of 7,16-dibenzoyl-1,4,10,13-tetraoxa-7,16-diazacyclooctadecane (III)

To a solution of 4,13-diaza-18-crown-6 (200 mg; 0.8 mmol) in ethyl acetate (25 mL) was added drop by drop a solution of benzoyl chloride (266 µL; 2.3 mmol) and triethylamine (638 µL; 4.6 mmol) in ethyl acetate (2 mL). The reaction mixture was stirred at room temperature for 10 min. Then, ethyl acetate (25 mL) was added and washed the solution with H_2O (2 x 30 mL) and saturated aqueous $NaHCO_3$ (2 x 30 mL), and then dried (Na_2SO_4) and concentrated. The crude product was purified by column chromatography (10:1 ethyl acetate–methanol) giving the title compound (268 mg, 74%) isolated as a solid, mp 97–99 ºC. IR (KBr): 1628, 1572, 1428, 1134 and 1079 cm^{-1}. ^{1}H-NMR ($CDCl_3$, 400 MHz): δ (in ppm) 7.37 (s, 10H, Ph), 3.80 (s br, 8H, CH_2N) and 3.57 (s br, 8H, CH_2O). ^{13}C-NMR ($CDCl_3$, 300 MHz): δ (in ppm) 172.2 (CO), 136.8, 129.3, 128.5, 126.6

(aromatics C, CH), 70.6, 69.8 (CH_2O), 49.9 and 46.2 (CH_2N). HRMS (MALDI) calc. for $C_{26}H_{34}N_2O_6Na$ $[M+Na]^+$ 493.2314. Found 493.2305.

2.2.2. Synthesis of 7,16-dipivaloyl-1,4,10,13-tetraoxa-7,16-diazacyclooctadecane (IV)

A solution of pivaloyl chloride (72 µL; 0.6 mmol) and triethylamine (160 µL; 1.2 mmol) in ethyl acetate (2 mL) was added to a solution of 4,13-diaza-18-crown-6 (50 mg; 0.2 mmol) in ethyl acetate (10 mL). The reaction mixture was stirred at room temperature for 20 min. Next, ethyl acetate (50 mL) was added and washed the solution with H_2O (2 x 25 mL) and saturated aqueous $NaHCO_3$ (2 x 25 mL), and then dried (Na_2SO_4) and concentrated. The crude product was purified by column chromatography (10:1 ethyl acetate–methanol) giving the title compound (63 mg, 76%) isolated as a solid, mp 95–96 ºC. IR (KBr): 1614, 1102 and 1137 cm^{-1}. ^{1}H-NMR ($CDCl_3$, 400 MHz): δ (in ppm) 3.67 (s, 8H, CH_2N), 3.60 (s, 8H, CH_2O) and 1.28 (s, 18H, CH_3). ^{13}C-NMR ($CDCl_3$, 300 MHz): δ (in ppm) 177.8 (CO), 70.8, 70.2 (CH_2O), 48.5, 45.8 (CH_2N), 39.1 (CH_3) and 28.7 (C). HRMS (MALDI) calc. for $C_{22}H_{42}N_2O_6Na$ $[M+Na]^+$ 453.2940. Found 453.2938.

2.2.3. Synthesis of 7,16-[bis(N-adamantylcarbamoyl)propionyl]-1,4,10,13-tetraoxa-7,16-diazacyclooctadecane (VI)

The synthesis of ionophore VI was made using two steps with a 37% overall yield.

2.2.3.1. Synthesis of (N-adamantylcarbamoyl)propionic acid

To a solution of succinic anhydride (0.8 g; 8 mmol) in ethyl acetate (50 mL) was added a solution of 1-adamantylamine (1.2 g; 8 mmol) and triethylamine (1,110 µL; 8.8 mmol). The reaction mixture was stirred at room temperature for 30 min. After this time, the solid was separated, dissolved in water (25 mL) and acidified by addition of HCl 25 wt% (25 mL) until pH~2. The aqueous solution was extracted with CH_2Cl_2 (3×100 mL) and the combined organic phases were dried (Na_2SO_4) and concentrated giving a solid product that corresponding to the acid (957 mg, 49.5%), mp 183-185 ºC.

2.2.3.2. Synthesis of 7,16-[bis(N-adamantylcarbamoyl)propionyl]-1,4,10,13-tetraoxa-7,16-diazacyclooctadecane

0.32 g (1.26 mmol) of (N-adamantylcarbamoyl)propionic acid was dissolved in 15 mL of thionyl chloride. The reaction mixture was stirred at room temperature for 3.5 h. To remove the excess of thionyl chloride was added, and eliminated by evaporation, anhydrous toluene. To a solution of the reaction product in ethyl acetate (30 mL) was added a solution of 4,13-diaza-18-crown-6 (100 mg; 0.42 mmol) and triethylamine (351 µL; 2.52 mmol) in ethyl acetate (20 mL). After this time, the solution was washed with H_2O (2 x 35 mL), 5 wt% HCl (2 x 35 mL), saturated aqueous $NaHCO_3$ (2 x 35 mL) and next with H_2O (1 x 35 mL). The organic layer was dried (Na_2SO_4), filtered and concentrated to give a crude product that was purified by silica–gel column chromatography (10:1 methylene chloride–methanol) yielding ionophore VI (226 mg, 74%), isolated as a solid, mp 158–160 ºC. IR (KBr): 3489, 1636 and 1544 cm^{-1}. ^{1}H-NMR ($CDCl_3$, 400 MHz): δ (in ppm) 3.70-3.58 (m, 24H, CH_2O and CH_2N), 2.70-2.58 (m, 8H, CH_2), 2.06 (s, 6H, CH), 2.00 (s, 12H, CH_2) and 1.68 (s, 12H, CH_2). ^{13}C-NMR ($CDCl_3$, 300 MHz): δ (in ppm) 70.9-69.8 (CH_2O), 49.5, 48.1 (CH_2N), 29.5 and 29.1 (CH). HRMS (FAB^+) calc. for $C_{40}H_{64}N_4O_8Na$ $[M+Na]^+$ 751.4610. Found 751.4622.

2.3. Optosensing manifold

The single-line flow-injection system used consist of a peristaltic pump (Gilson Minipuls-2, France) and a self-constructed flow-through cell, of 700 µL volume and 9.9 mm ø quartz windows, containing the sensing membrane, mounted inside the sample compartment of a DAD spectrophotometer (HP-8453, Nortwalk, CT, USA) coupled to a computer-controlled data acquisition unit. Sample solutions were transferred to the flow system by continuous aspiration.

2.4. Preparation of sensing membranes and measurement set-up

The membranes were produced on a polyester substrate using a spin-coating technique. Mixtures for the preparation of sensing membranes were made from a batch containing ionophore, chromoionophore and lipophilic salt in 1:1:1 molar ratio (2.2 x 10^{-3} mmol each), next to 64.25 mg (68 wt%) of TBP and the adequate amount of PVC was added to complete the 100 wt%, all dissolved in 1 mL of freshly distilled THF. The membranes were cast by placing 20 µL of the cocktail on a 24 mm ø circular polyester sheet using a spin-coater and dried slowly in a dryer with saturated THF atmosphere at room temperature. The sensing area of the sensor is a transparent and red 10 mm ø circular film with a calculated thickness of about 25 µm.

The response of the sensors was evaluated by using standard solutions of alkaline and alkaline-earth ions under study ranging from 1 x 10^{-7} to 9 x 10^{-1} M in concentrations (50 mL volumetric flask) in pH 8.5 or pH 9.0 Tris buffer solution 2 x 10^{-2} M or pH 8.5 diethanolamine buffer solution 2 x 10^{-2} M. The membrane previously introduced in the flow-through cell was measured successively for the absorbance at 660 nm after equilibration with 10^{-2} M HCl (A_{HC^+}); 2 x 10^{-2} M buffer solution; buffered standard solutions to be measured (A), and 10^{-2} M NaOH solution (A_c). The membranes were not conditioned before use. All absorbance measurements were carried out at room temperature (22.0±0.5 ºC).

The exchange constants $K_{exch}^{IL_p}$ were calculated according to a least-squares approximation method [9] using 1 - α experimental values in the maximum slope zone of the response function obtained working at 8 different concentration levels and 3 replicates of each one. Activities were calculated according to the Debye Hückel formalism [10].

The selectivity of these sensing membranes against Ca(II) was measured by using the selectivity coefficients $k_{i,J}^{Osel}$ [11] that were determined using the separate solutions method (SSM) by plotting the single-ion response functions (1 1 - α) *vs* $\log a_{i^{z+}}$ according to eq. 8.4 for all cations studied. Since the pH was constant (pH 8.5), the selectivity coefficients were given by the horizontal distance

between curves of primary and interfering ions for a protonation degree 1 - α = 0.5 [12].

3. Results and Discussion

The sensing system is based on cation-exchange between a complete organic phase of plasticized PVC membrane and an aqueous problem containing the analyte, as was described by Bakker *et al.* [13]. The sensing membranes contain an ionophore L and a chromoionophore C selective for hydrogen ions, giving both the positively charged species in membrane phase, $\overline{IL_p^{z+}}$ and $\overline{HC^+}$, where p is the stoichiometry of the complexes formed. To permit the ion-exchange equilibrium was also incorporated an alkaline salt of a highly lipophilic anion R^- to the membrane.

In contact with the aqueous solution containing alkaline or alkaline-earth ions next equilibrium occurs in sensing membrane:

$$I^{z+} + p\bar{L} + z\overline{HC^+} \leftrightarrow \overline{IL_p^{z+}} + z\bar{C} + zH^+ \qquad (8.1)$$

where the ionophore is assumed to form 1:p (M:L) complexes. Species in the organic sensing phase are barred, while all others are in the aqueous phase. This equilibrium is characterized by the exchange constant $K_{exch}^{IL_p}$ defined as:

$$K_{exch}^{IL_p} = \frac{a_{H^+}^z [C]^z \left[\overline{IL_p^{z+}}\right]}{a_{I^{z+}} \left[\overline{HC^+}\right] [L]^p} \qquad (8.2)$$

where concentration in membrane phase are given in molalities and in aqueous solution in activities.

The change between the protonated and deprotonated forms of the chromoionophore (equation 8.1) depends on the activity of the ion I^{z+} in the aqueous phase. In a buffered solution, the analyte activity is determined by the degree of protonation of the chromoionophore (1 - α); which is optically calculated

using the absorbance for the fully protonated (A_{HC^+}), obtained in 10^{-2} M HCl, and deprotonated forms (A_C), obtained in 10^{-2} M NaOH, of the chromoionophore and the absorbance A for the buffered standard solution [14]:

$$1 - \alpha = \frac{HC^+}{C_0} = \frac{A - A_C}{A_{HC^+} - A_C} \tag{8.3}$$

The ion activities ratio in aqueous phase is related to the exchange constant $K_{exch}^{IL_p}$ and the degree of protonation $1 - \alpha$ through the sigmoidal response function:

$$a_{I^{z+}} = \frac{1}{K_{exch}^{IL_p}} \left(\frac{a_{H^+}\alpha}{1 - \alpha} \right)^z \frac{C_R - (1 - \alpha)C_C}{z(C_L - \frac{p}{z}(C_R - (1 - \alpha)C_C))^p} \tag{8.4}$$

where C_L, C_C and C_R are the analytical concentrations of ionophore, chromoionophore and lipophilic salt, respectively.

In this paper we are interested in the study of calcium ionophores for environmental sensors that could discriminate from concomitant alkaline and alkaline-earth ions. In this way, we have studied some ionophores crown ether type coming from 18-crown-6 ether to 4,13-diaza-18-crown-6 ether and then introducing N-substituent in the diaza parent crown ring to prepare a series of double-armed crown ethers. The donor group on the functionalized flexible sidearm, that provides further coordination with the guest alkaline or alkaline-earth cation complexed in the hydrophilic crown ring, is a carbonyl group in all cases coming from an amide bonding.

We have modified the lipophilicity of ionophore molecule using different terminal units varying in lipophilicity and size at the terminal of the side chains; namely benzoyl (III), pivaloyl (IV), and N-adamantylcarbamoyl with two different size chain: acetyl (V) and propionyl (VI). With the goal to know the complexing behaviour of these ionophores and their discrimination ability of Ca(II) against Mg(II), Na(I) and K(I), we have prepared optical membranes based on ionophore-chromoionophore chemistry. Thus, plasticized PVC membranes contained

lipophilized Nile Blue as chromoionophore in all cases and the corresponding ionophore were studied at pH 8.5 adjusted with Tris buffer 2 x 10^{-2} M. The answer of sensing membranes against alkaline and alkaline-earth ions under study was tested between 1 x 10^{-7} to 9 x 10^{-1} M using a flow-through cell according to the Experimental section. In each case, the experimental 1 - α values were calculated from spectroscopic data at 660 nm and were fitted to theoretical equation (equation 8.4) in logarithm of activities. The exchange constants $K_{exch}^{IL_p}$ for all ionophores and metallic ions studied were calculated (table 8.1) assuming a 1:1 stoichiometry (p = 1) in all the cases, except for K(I) complexes with ionophores IV, V and VI and all Na (I) complexes, with a 1:0.5 stoichiometry (p = 0.5).

Table 8.1. Exchange constants ($K_{exch}^{IL_p}$) of the sensing membranes based on the different ionophores studied for alkaline and alkaline-earth ions

Ionophore	$K_{exch}^{KL_p}$	$K_{exch}^{NaL_p}$	$K_{exch}^{MgL_p}$	$K_{exch}^{CaL_p}$
I	$(1.37\pm0.06)\cdot10^{-7}$	$(1.1\pm0.1)\cdot10^{-8}$	$(2.63\pm0.04)\cdot10^{-15}$	$(2.11\pm0.01)\cdot10^{-15}$
II	$(8.7\pm0.4)\cdot10^{-8}$	$(1.3\pm0.1)\cdot10^{-8}$	$(1.6\pm0.1)\cdot10^{-15}$	$(2.3\pm0.4)\cdot10^{-15}$
III	$(1.22\pm0.04)\cdot10^{-7}$	$(1.42\pm0.08)\cdot10^{-8}$	$(1.6\pm0.1)\cdot10^{-15}$	$(2.63\pm0.06)\cdot10^{-15}$
IV	$(7.7\pm0.4)\cdot10^{-9}$	$(1.25\pm0.01)\cdot10^{-8}$	$(1.50\pm0.01)\cdot10^{-15}$	$(2.48\pm0.01)\cdot10^{-15}$
V	$(5.65\pm0.01)\cdot10^{-9}$	$(1.18\pm0.06)\cdot10^{-8}$	$(3.7\pm0.3)\cdot10^{-15}$	$(4.27\pm0.06)\cdot10^{-15}$
VI	$(4.5\pm0.2)\cdot10^{-9}$	$(1.12\pm0.03)\cdot10^{-8}$	$(1.50\pm0.07)\cdot10^{-15}$	$(2.3\pm0.2)\cdot10^{-15}$

Potassium shows the biggest changes in exchange constant $K_{exch}^{IL_p}$ with the ionophore used, coming from 1.37 x 10^{-7} for ionophore I to 4.5 x 10^{-9} for ionophore VI. The effect of the reemplacement of two atoms of oxygen in crown ether (ionophore I) by two atoms of nitrogen (ionophore II) is clearly demonstrated and the $K_{exch}^{IL_p}$ correspondent to ionophore I is half an order of magnitude greater than that of the unsubstituted 4,13-diaza-18-crown ether; that suppose that the complex with ionophore II is more stable. This data contrast with the less stability reported for diazacrown ether complexes with alkaline ions in water respect to the parent crown ether [15].

The attachment of benzoyl-functionalized arms to the diaza-crown ring (ionophore III) significantly increases the $K_{exch}^{IL_p}$ value, decreasing thus the stability constant of K(I) complex. However, the change of this group for pivaloyl (ionophore IV) or adamantyl units (ionophores V and VI) supposes a considerable increase in complex stability due to the increase in length of side chain and lipophilicity next to the new carbonyl group.

On the other hand, Na(I) shows a nearly constant behaviour, with the greatest exchange constant $K_{exch}^{IL_p}$ value for ionophore III, due probably to their smaller ionic radius. In the case of Mg(II) the influence of side arms is very small with the only exception of ionophores V and I that originate less stable complexes. The behaviour of Ca(II) is very similar to Mg(II), being the exchange constant higher than that of Mg(II). All values are very similar with the exception of the less stable complex with ionophore V. These values calculated for $K_{exch}^{IL_p}$ are similar to values previously reported by us for Ca(II) and Mg(II) complexes of ionophores V [16] and VI [17].

Selectivity, expressed as logarithmic selectivity coefficients, $\log k_{Ca,J}^{Osel}$, respect to K(I) increases with the size and the lipophilicity of the terminal group of the side chains, being the highest for ionophore VI (table 8.2). The selectivity pattern is similar for Na(I), although selectivity is lower than for K(I). General speaking, the selectivity respect to Mg(II) is not very high, but there are some interesting differences. Ionophore I, 18-crown-6 ether, is more selective for Mg(II) than Ca(II), but substitution of O by N in the crown ring increases selectivity for Ca(II) and the introduction of double side arms do not suppose any variation in selectivity except for ionophores V and VI. The introduction of the N-adamantylcarbamoyl units in the diazacrown ether increases selectivity for Ca(II) respect to Mg(II). These results are surprising comparing to results given by Suzuki et al. that find ionophore V as a very selective ionophore for Mg(II) in potentiometric sensors [8] and also in optical sensors but using both a different plasticizer, NPOE, and chromoionophore [18]. Additionally, the selectivity coefficients obtained here for ionophore VI are lower than that calculated by us [17] probably due to the different composition of sensing membrane.

Table 8.2. Selectivity coefficients ($k^{Osel}_{Ca,J}$, I = primmary ion (Ca^{2+}), J = interfering ion) for sensing membranes studied

Selectivity coefficients, $\log k^{Osel}_{Ca,J}$			
Ionophore	K(I)	Na(I)	Mg(II)
I	-1.15	-1.20	0.10
II	-1.40	-1.18	-0.16
III	-1.31	-1.19	-0.23
IV	-1.43	-1.23	-0.22
V	-1.80	-1.49	-0.07
VI	-1.78	-1.38	-0.33

Figure 8.2 shows the complexing behaviour of these ionophores and their discrimination ability of Ca(II) against Mg(II), Na(I) and K(I). As a conclusion, the optical membrane based on the double-armed diazacrown ether possessing a malonic diamide in their side chains (ionophore V) exhibits the best Ca(II) selectivity. Additionally, it presents the highest selectivity respect to the alkaline ions K(I) and Na(I); however, it responds equally to Ca(II) and Mg(II). Consequently, the ionophore with the best Ca(II) selectivity over the rest of the cations studied is VI, since its answer to K(I) and Na(I) is similar to the corresponding to V and their differentiation from Mg(II) is the best.

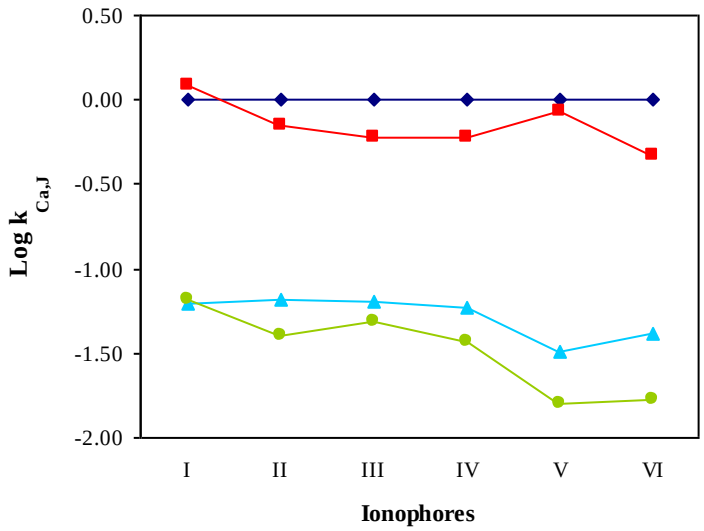

Figure 8.2. Selectivity (SSM method) variation of the membranes as function of ionophore used

In order to compare the $k_{I,J}^{Osel}$ values previously reported by us for alkaline and alkaline-earth ions for optical membranes using ionophore I [8], membranes with the same composition that the above-mentioned were prepared but the response of the sensor was evaluated using solutions buffered with pH 8.5 diethanolamine buffer solution 2 x 10^{-2} M instead of Tris buffer. The $k_{I,J}^{Osel}$ values obtained in these new conditions were -0.57 Mg(II); -0.63 Na(I) and -2.49 K(I) that compares favourably with selectivity coefficients values previously reported (-0.66 Mg(II); -1.58 Na(I) and -2.08 K(I)). Comparing results obtained using Tris buffer solution, the selectivity respect to Mg(II) and K(I) increases considerably, whereas it decreases respect to Na(I), which shows the significant role played by the buffer composition.

We have used ionophore V for hardness determination based on the equal response to calcium and magnesium of sensing membrane at pH 9.0 [16]. By this reason we have studied again the selectivity against alkaline and alkaline-earth ions using the same ionophore but at pH 9.0 adjusted with Tris buffer $2{\cdot}10^{-2}$ M. The resulting $k_{I,J}^{Osel}$ values in these conditions were -0.07 Mg(II); -1.47 Na(I) and -1.76 K(I), which means that is slightly more selective for Na(I) and K(I) than the method previously reported. It is important to emphasize that the selectivity coefficients obtained at pH 8.5 (table 8.2) and 9.0 were practically the same.

To compare the analytical characteristics of the different sensing membranes for Ca(II) we studied their range, detection limit and precision (table 8.3). As measuring range we use the linear relationship in the middle of the sigmoidal response function defined by means a *lack-of-fit* test and as the detection limit the intersection of the linear calibration function defined above and a linear function adjusted in the minimal slope zone. As upper range we consider the highest value tested in all the cases (231 mM).

Table 8.3. Analytical parameters for Ca(II) sensing membranes studied

Ionophore	I	II	III	IV	V	VI
Intercept	-0.0049	-0.0207	-0.0276	-0.0354	-0.0208	-0.0354
Slope	-0.1741	-0.1902	-0.1867	-0.1921	-0.1603	-0.1921
Probability level (%) (lack-of-fit test)	53.7	69.2	50.1	87.4	49.3	87.5
Linear range (activities)	$2.0 \cdot 10^{-4}$- 0.23 M	$2.3 \cdot 10^{-4}$- 0.23 M	$1.6 \cdot 10^{-4}$- 0.23 M	$1.7 \cdot 10^{-4}$- 0.23 M	$8.1 \cdot 10^{-5}$- 0.23 M	$5.9 \cdot 10^{-5}$- 0.23 M
Detection limit (activities)	$2.0 \cdot 10^{-4}$ M	$2.3 \cdot 10^{-4}$ M	$1.6 \cdot 10^{-4}$ M	$1.7 \cdot 10^{-4}$ M	$8.1 \cdot 10^{-5}$ M	$5.9 \cdot 10^{-5}$ M
Intermembrane precision RSD (%)						
0.8 mM[a]	2.47	3.70	0.93	0.97	1.10	1.03
48 mM[a]	1.52	0.92	0.54	0.67	0.91	0.41
231 mM[a]	3.16	0.65	0.21	0.37	1.31	0.12

[a] Activities tested in $mmol \cdot L^{-1}$

The detection limit decreases with the size and the lipophilicity of the terminal group of the side chains coming from 2.3×10^{-4} M for ionophore II to $5.9 \cdot 10^{-5}$ M for ionophore VI according to the exchange constant values $K_{exch}^{IL_p}$ for each ionophore.

Acknowledgements

We acknowledge financial support from *Ministerio de Educación y Ciencia, Dirección General de Enseñanza Superior* (Spain) (Projects CTQ2005-09060-C02-01 and CTQ2005-09060-C02-02); and *Junta de Andalucia* (Proyecto de Excelencia P06-FQM-01467).

References

[1] C.J. Pedersen. *Cyclic polyethers and their complexes with metal salts*. J. Am. Chem. Soc., 89(26) (1967) 7017-7036.

[2] G.W. *Gokel. Crown ether and cryptands*. 1st ed., The Royal Society of Chemistry, London (1991).

[3] J.W. Steed. *First- and second-sphere coordination chemistry of alkali metal crown ether complexes*. Coord. Chem. Rev., 215 (2001) 171-221.

[4] P.A. Gale. *Supramolecular chemistry: from complexes to complexity*. Philos. T. Roy. Soc. A, 358(1766) (2000) 431-453.

[5] H. Tsukube. *Double armed crown ethers and armed macrocycles as a new series of metal-selective reagents: A review*. Talanta, 40(9) (1993) 1313-1324.

[6] M. Hiraoka. *Crown Ethers and Analogous Compounds*. Elsevier: Amsterdam (1992).

[7] W.E. Morf, K. Seiler, B. Rusterholz, W. Simon. *Design of a novel calcium-selective optode membrane based on neutral ionophores*. Anal. Chem., 62(7) (1990) 738-742.

[8] K. Suzuki, K. Watanabe, Y. Matsumoto, M. Kobayashi, S. Sato, D. Siswanta, H. Hisamoto. *Design and Synthesis of Calcium and Magnesium Ionophores Based on Double-Armed Diazacrown Ether Compounds and Their Application to an Ion-Sensing Component for an Ion-Selective Electro*de. Anal. Chem., 67 (1995) 324-334.

[9] L.F. Capitán-Vallvey, M.D. Fernández-Ramos, P. Alvarez de Cienfuegos-Gálvez. *Optical test strip for calcium determination based on a neutral ionophore*. Anal. Chim. Acta, 451(2) (2002) 231-241.

[10] P.C. Meier. *Two-parameter Debye-Hückel approximation for the evaluation of mean acitivity coefficients of 109 electrolytes*. Anal. Chim. Acta, 136 (1982) 363-368.

[11] E. Bakker. *Selectivity comparison of neutral carrier-based ion-selective optical and potentiometric sensing schemes*. Anal. Chim. Acta, 350 (1997) 329-340.

[12] E. Bakker, W. Simon. *Selectivity of ion-sensitive bulk optodes*. Anal. Chem., 64(17) (1992) 1805-1812.

[13] E. Bakker, P. Bühlmann, E. Pretsch. *Carrier-Based Ion-Selective Electrodes and Bulk Optodes. 1. General Characteristics*. Chemical Rev., 97 (1997) 3083-3132.

[14] I. Tsagkatakis, S. Peper, E. Bakker. *Spatial and Spectral Imaging of Single Micrometer-Sized Solvent Cast Fluorescent Plasticized Poly(vinyl chloride) Sensing Particles*. Anal. Chem., 73(2) (2001) 315-320.

[15] B.G. Cox, P. Firman, H. Horst, H. Schneider. *Stability constants of diaza-crown-ether complexes of univalent metal ions and free energies of transfer of ligand and complexes from acetonitrile to several solvents*. Polyhedron, 2(5) (1983) 343-347.

[16] L.F. Capitán-Vallvey, M.D. Fernández-Ramos, P. Alvarez de Cienfuegos Gálvez, F. Santoyo-González. *Characterisation of a transparent optical test strip for quantification of water hardness*. Anal. Chim. Acta, 481 (2003) 139-148.

[17] L.F. Capitán-Vallvey, M.D. Fernández-Ramos, P. Álvarez de Cienfuegos Gálvez, F. Santoyo-González. *Calcium selective test strip for water and milk*. Analyst, 129 (2004) 783-788.

[18] D. Siswanta, H. Hisamoto, S. Sato, Y. Matsumoto, Y. Koike, S. Yamamori, K. Suzuki. *Magnesium ion-selective optodes based on a neutral ionophore and a lipophilic cationic dye*. Anal. Sci., 13(3) (1997) 429-435.

3. CONCLUSIONES

Como resultado del trabajo realizado podemos señalar que:

- Se han sintetizado y caracterizado estructuralmente, mediante datos espectroscópicos procedentes de IR, ^{1}H-RMN, ^{13}C-RMN, HRMS MALDI y FAB^{+}, los ionóforos siguientes:
  - 7,16-dibenzoil-1,4,10,13-tetraoxa-7,16-diazaciclooctadecano (III)
  - 7,16-dipivaloil-1,4,10,13-tetraoxa-7,16-diazaciclooctadecano (IV)
  - 7,16-[bis(N-adamantilcarbamoil)acetil]-1,4,10,13-tetraoxa-7,16-diazaciclooctadecano (V)
  - 7,16-[bis(N-adamantilcarbamoil)propionil]-1,4,10,13-tetraoxa-7,16-diazaciclooctadecano (VI)

- Se han preparado membranas sensoras ópticas a partir de los seis ionóforos anteriores, Azul Nilo lipofilizado, TCFB, TBP y PVC:

- Se ha estudiado la respuesta de las membranas sensoras frente a Ca^{2+}, Mg^{2+}, Na^{+} y K^{+} utilizando un sistema de flujo y monitorizando la absorbancia.

- A partir de las medidas de absorbancia se han calculado, para cada caso, los valores de $1 - \alpha_{ef}$ frente al logaritmo de las actividades de los iones, obteniéndose las curvas sigmoidales correspondientes, así como las constantes de intercambio de los cuatro cationes estudiados; en el caso del calcio, valores que oscilan entre $1{,}1 \cdot 10^{-16}$ y $5{,}6 \cdot 10^{-16}$.

- Los coeficientes de selectividad de las membranas se han calculado mediante el método de las disoluciones separadas, tomando como referencia el cóctel más selectivo para calcio, el V. De los resultados obtenidos se deduce que:
  - El ionóforo V es el más selectivo para Ca^{2+}, mientras que el I es el

menos selectivo.

- El ionóforo IV es menos selectivo para Ca^{2+} que el V, pero discrimina mejor a este catión respecto a Mg^{2+}.
- Los ionóforos II, III, IV y V discriminan de forma similar a los iones Na^{+} y K^{+} respecto a Ca^{2+}.
- Puede recurrirse a la preparación de sensores con los ionóforos II y III, cuya síntesis es notablemente menos compleja que la del ionóforo IV, pese a que sean algo menos selectivos para Ca^{2+}, ya que los coeficientes de selectividad asociados a estos tres ionóforos son similares.
- Los derivados del diazacorona con brazos laterales voluminosos son más selectivos para Ca^{2+}.

INFORMACIÓN COMPLEMENTARIA

1. 7,16-dibenzoil-1,4,10,13-tetraoxa-7,16-diazaciclooctadecano (III)

1.1. IR

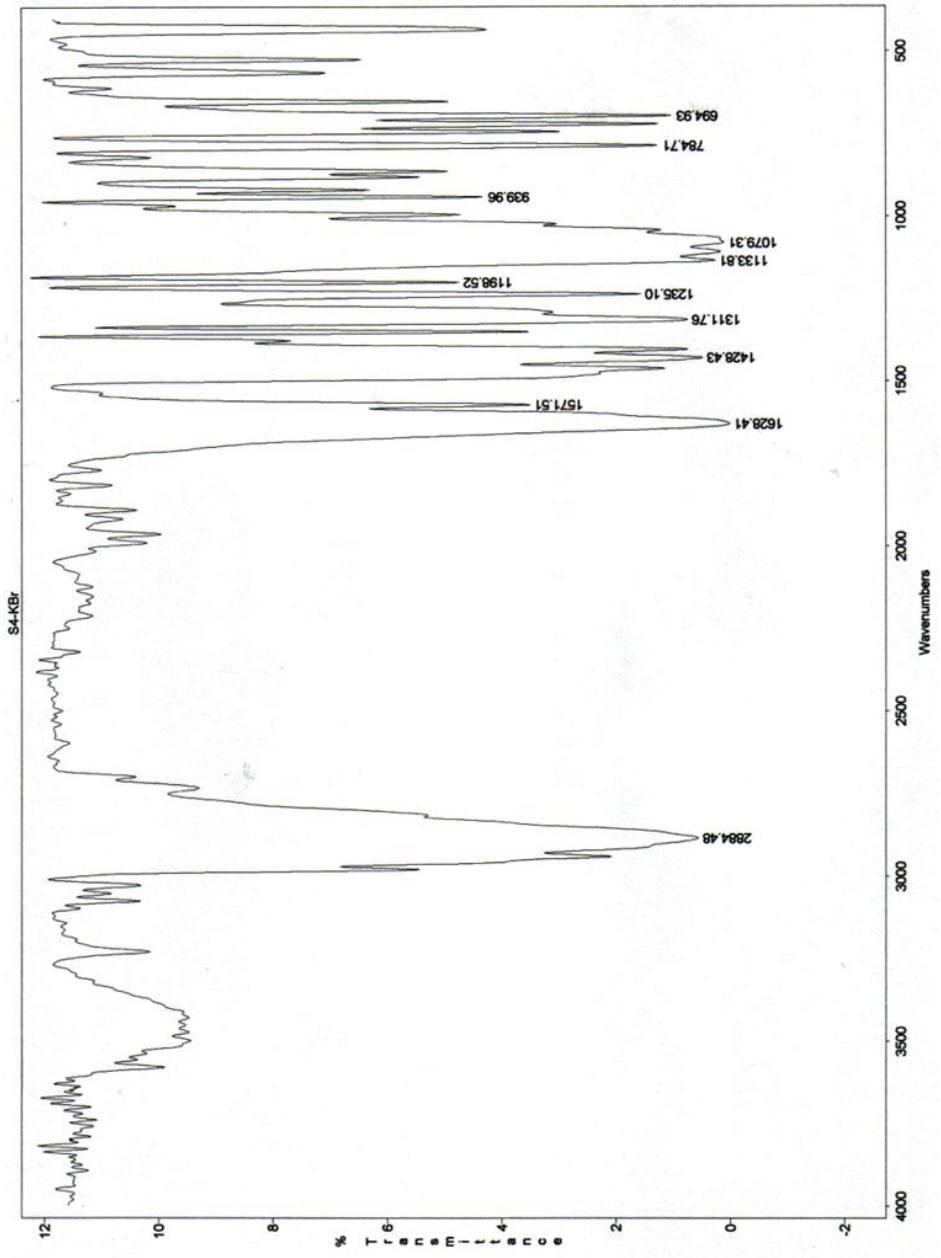

1.2. ^{1}H-NMR

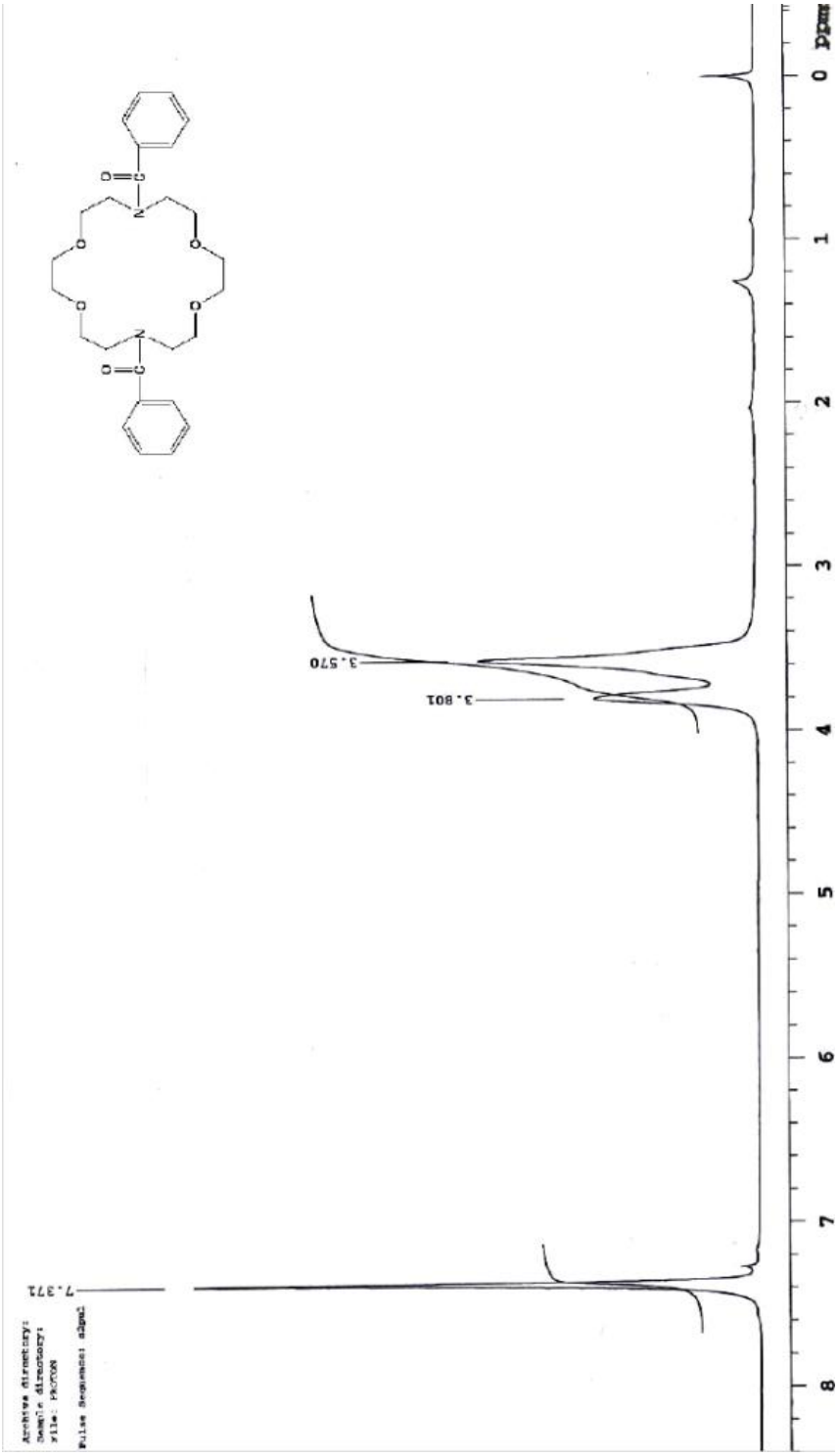

1.3. ^{13}C-RMN

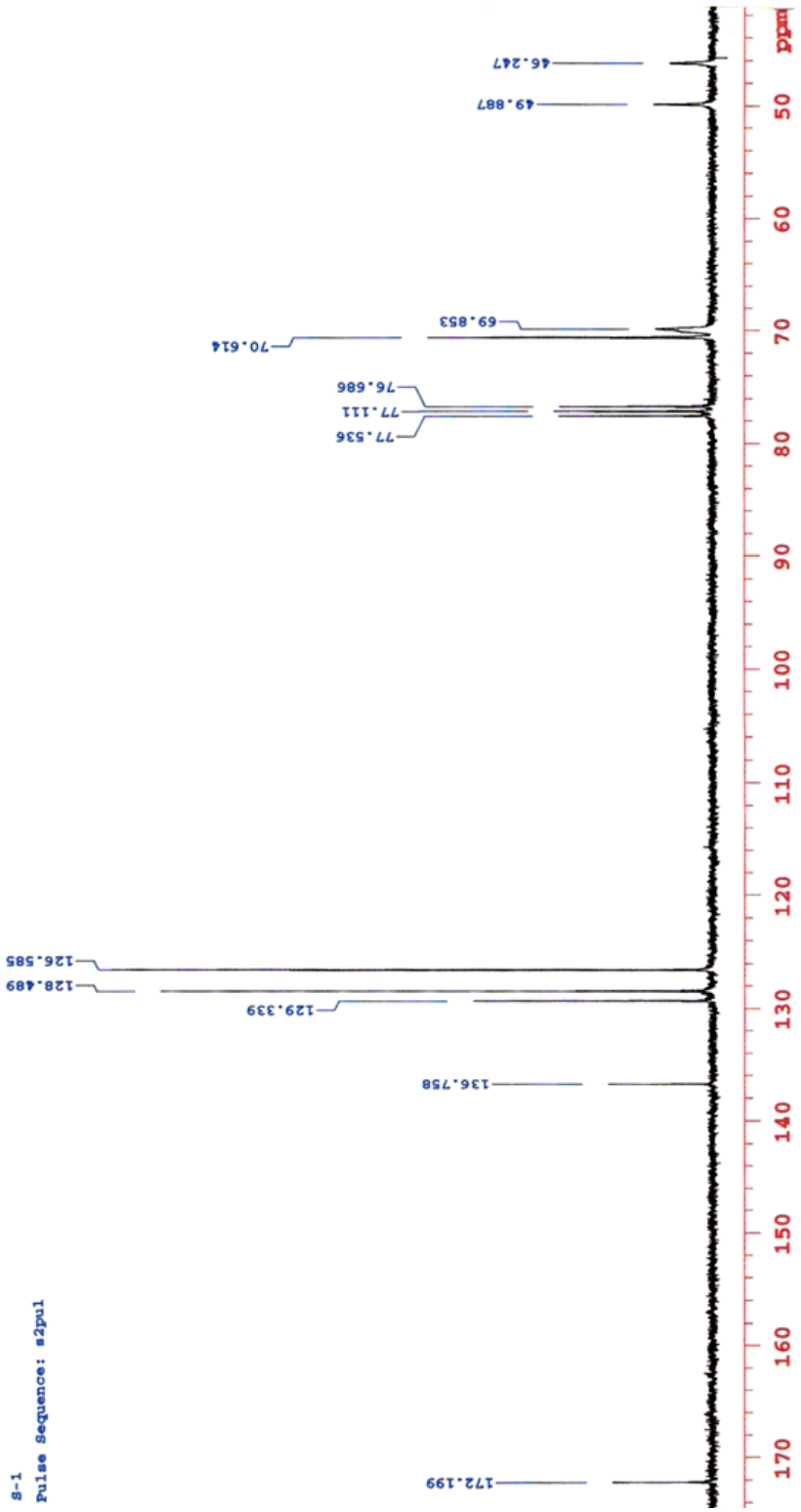
46.247
49.887
69.853
70.614
76.686
77.111
77.536
126.585
128.489
129.339
136.758
172.199
ppm
50
60
70
80
90
100
110
120
130
140
150
160
170
s-1
Pulse Sequence: s2pul

1.4. HRMS (MALDI)

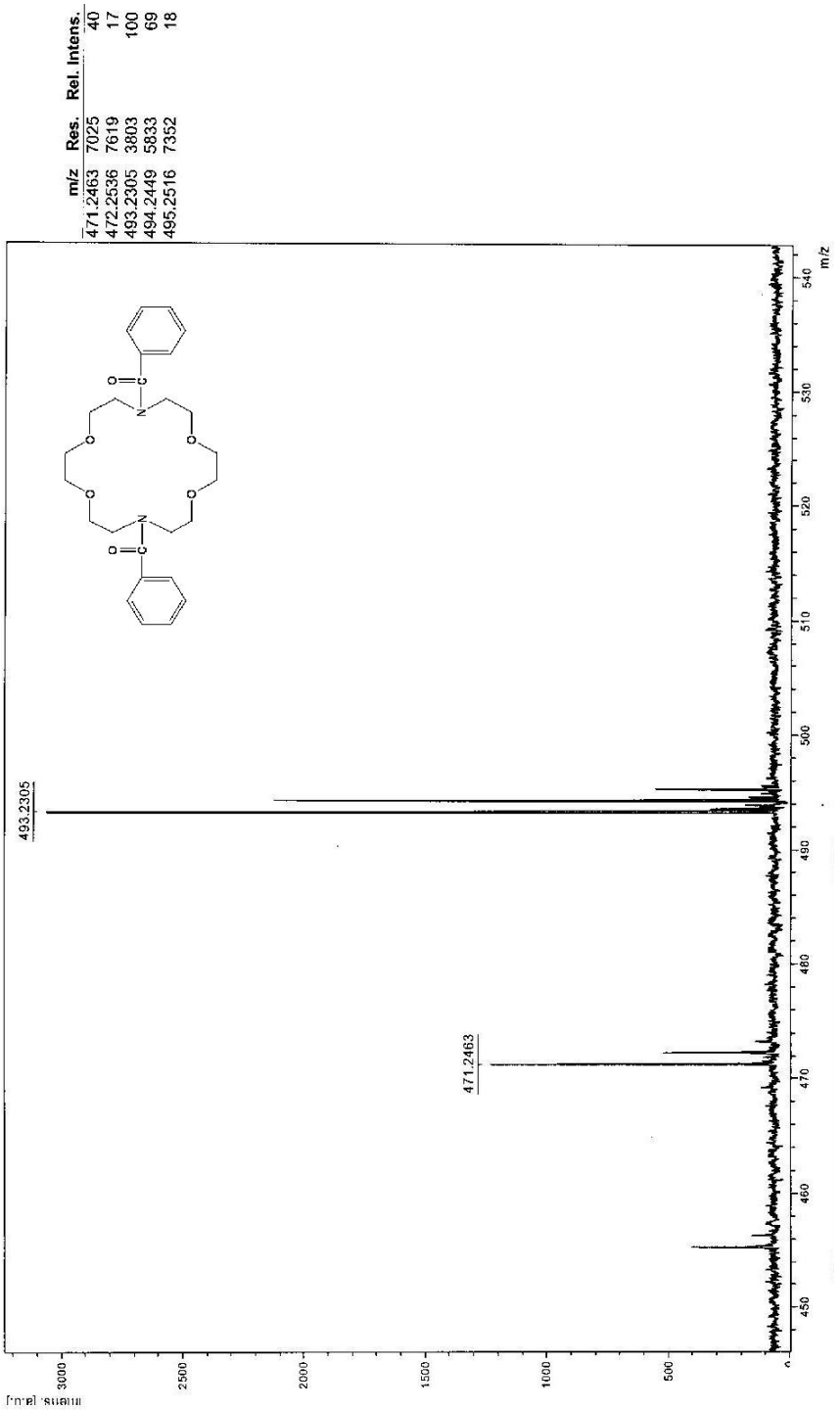

2. 7,16-dipivaloyl-1,4,10,13-tetraoxa-7,16-diazacyclooctadecane(IV)

2.1. IR

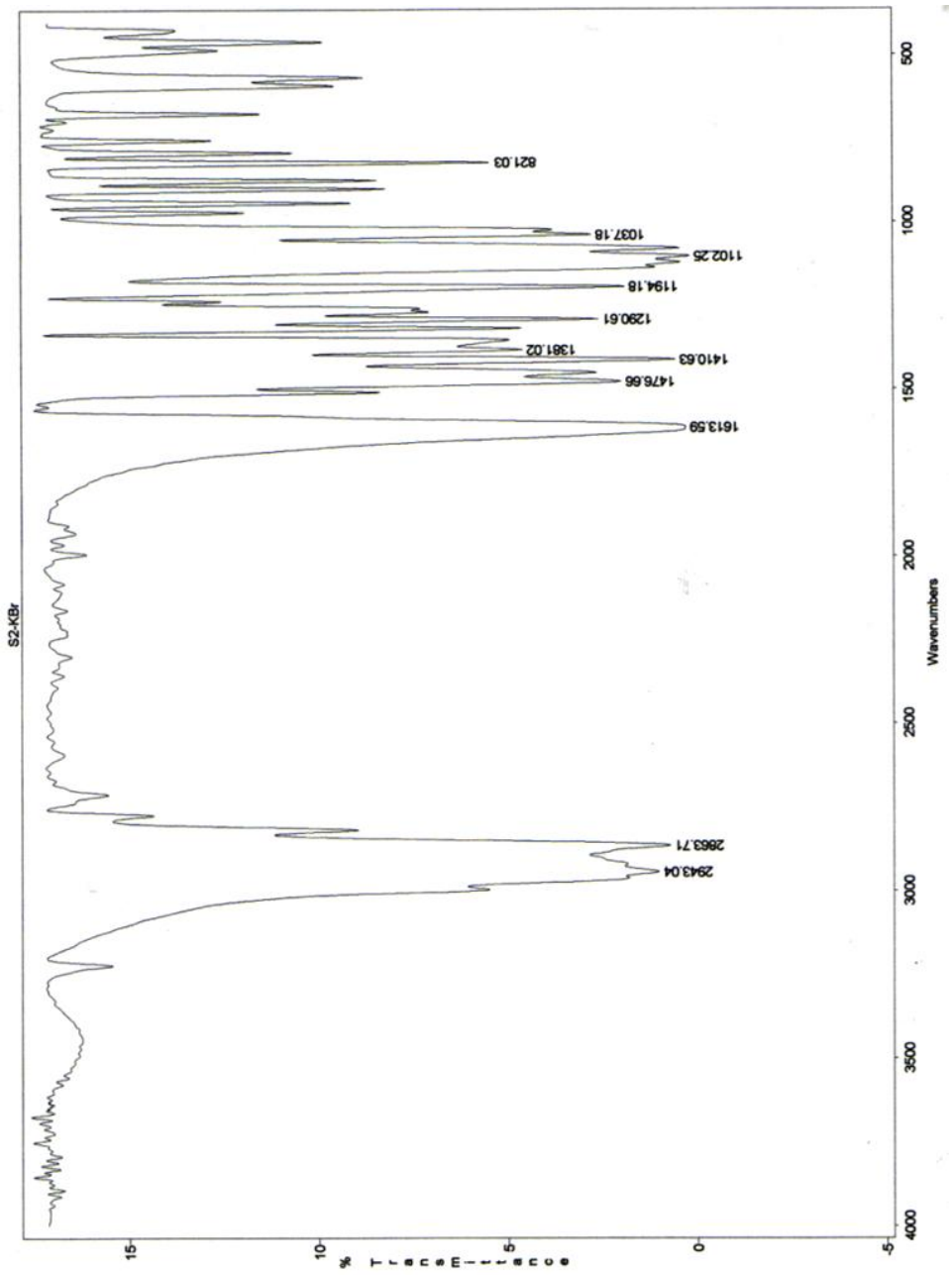

2.2. ^{1}H-RMN

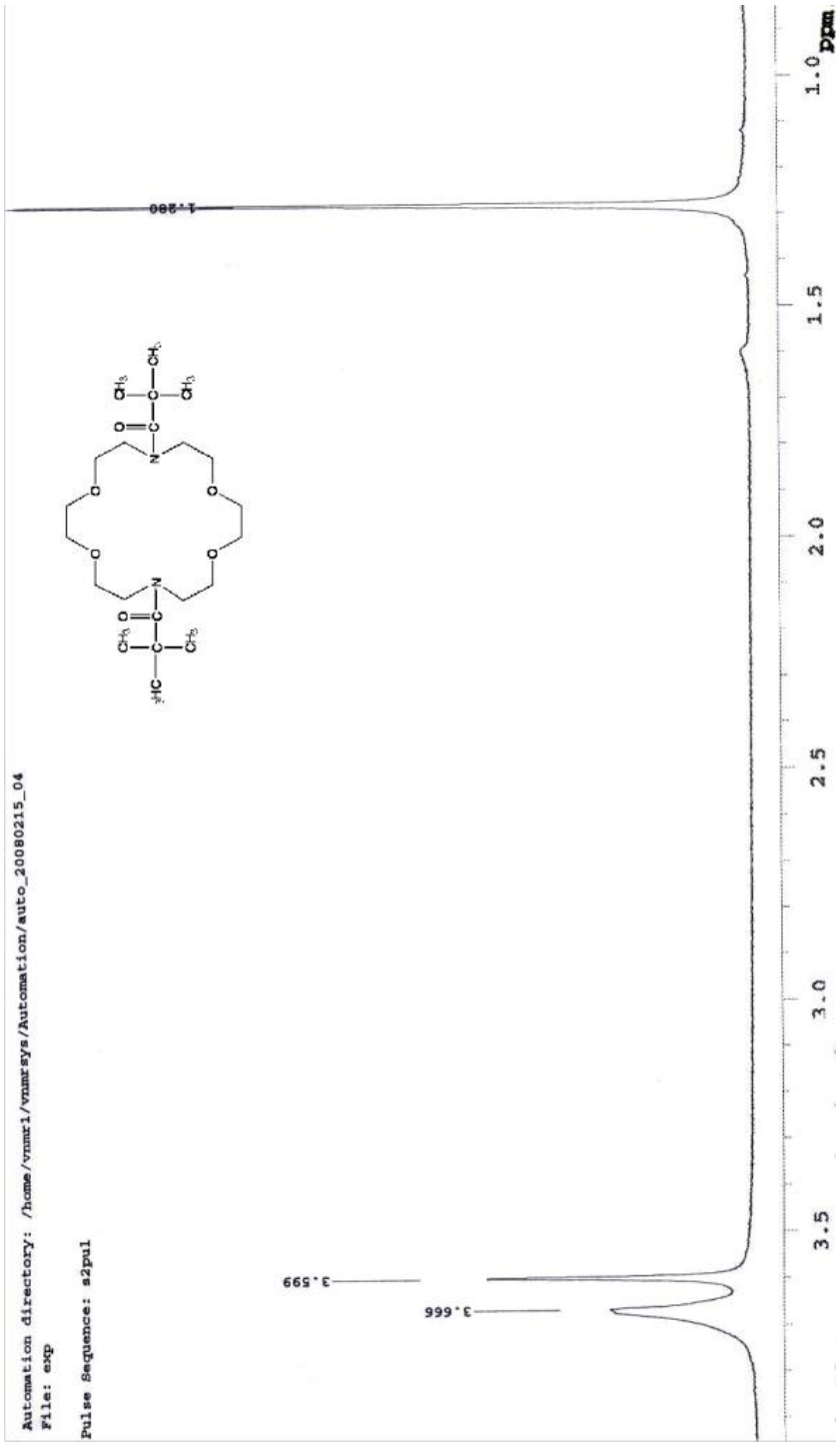
1.280
3.599
3.666
3.5
3.0
2.5
2.0
1.5
1.0
ppm
Automation directory: /home/vnmr1/vnmrsys/Automation/auto_20080215_04
File: exp
Pulse Sequence: s2pul

2.3. ^{13}C-RMN

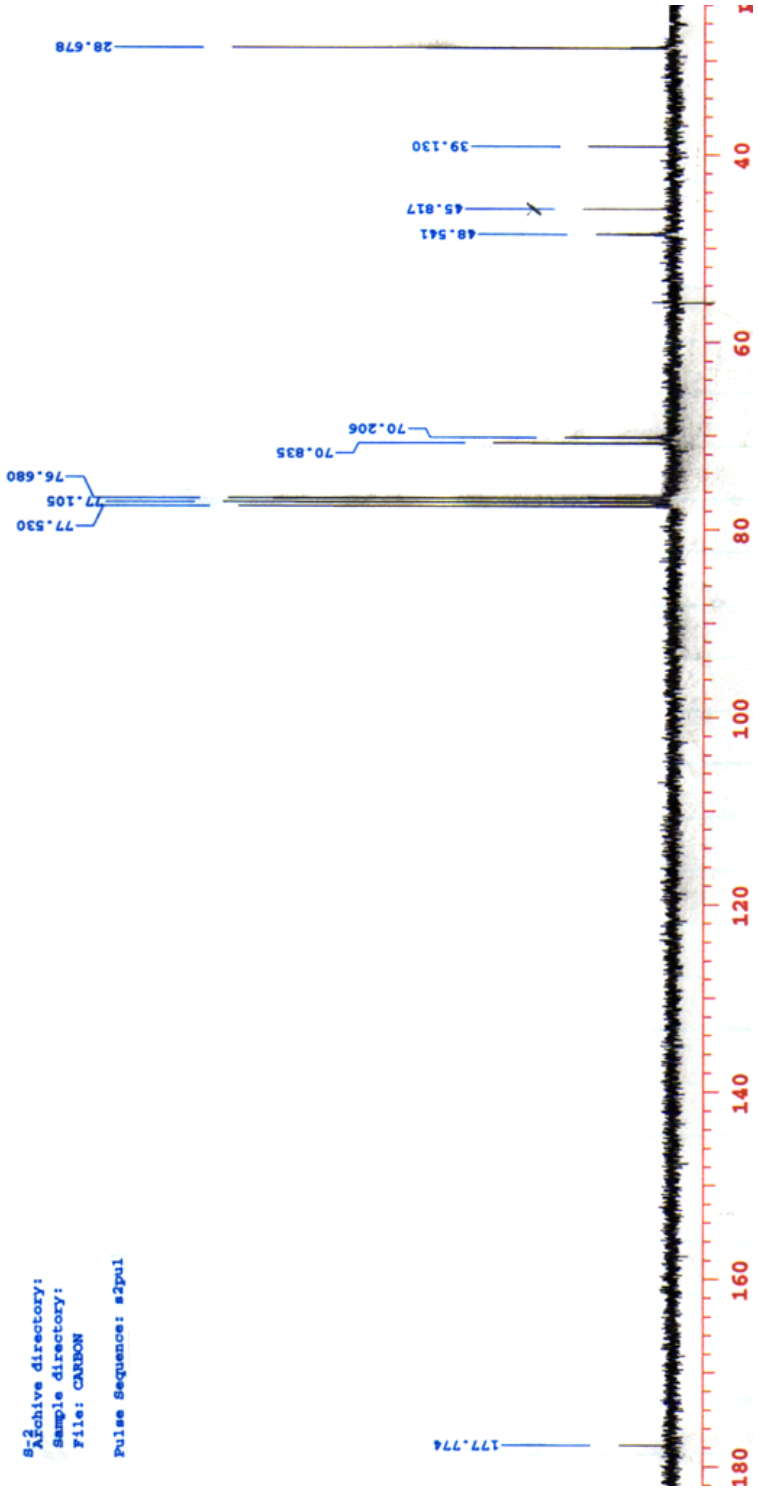
28.678
39.130
45.817
48.541
70.206
70.835
76.680
77.105
77.530
177.774
40
60
80
100
120
140
160
180
8-2
Archive directory:
Sample directory:
File: CARBON
Pulse Sequence: s2pul

2.4. HRMS (MALDI)

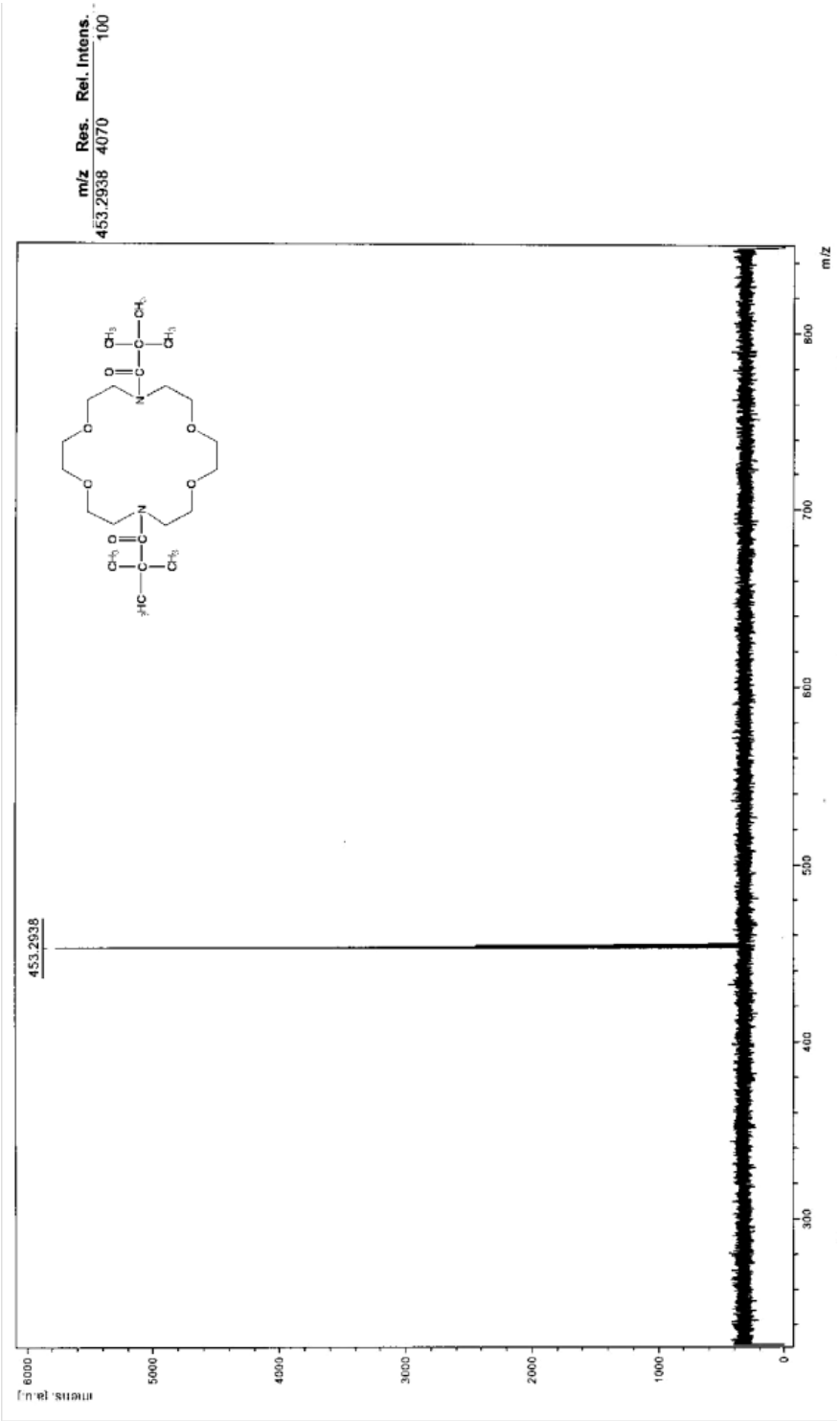

3. Synthesis of 7,16-[bis(N-adamantylcarbamoyl)propionyl]-1,4,10,13-tetraoxa-7,16-diazacyclooctadecane(VI)

3.1. Ácido 4-(N-adamantilcarbamoil)propanoico

3.1.1. IR

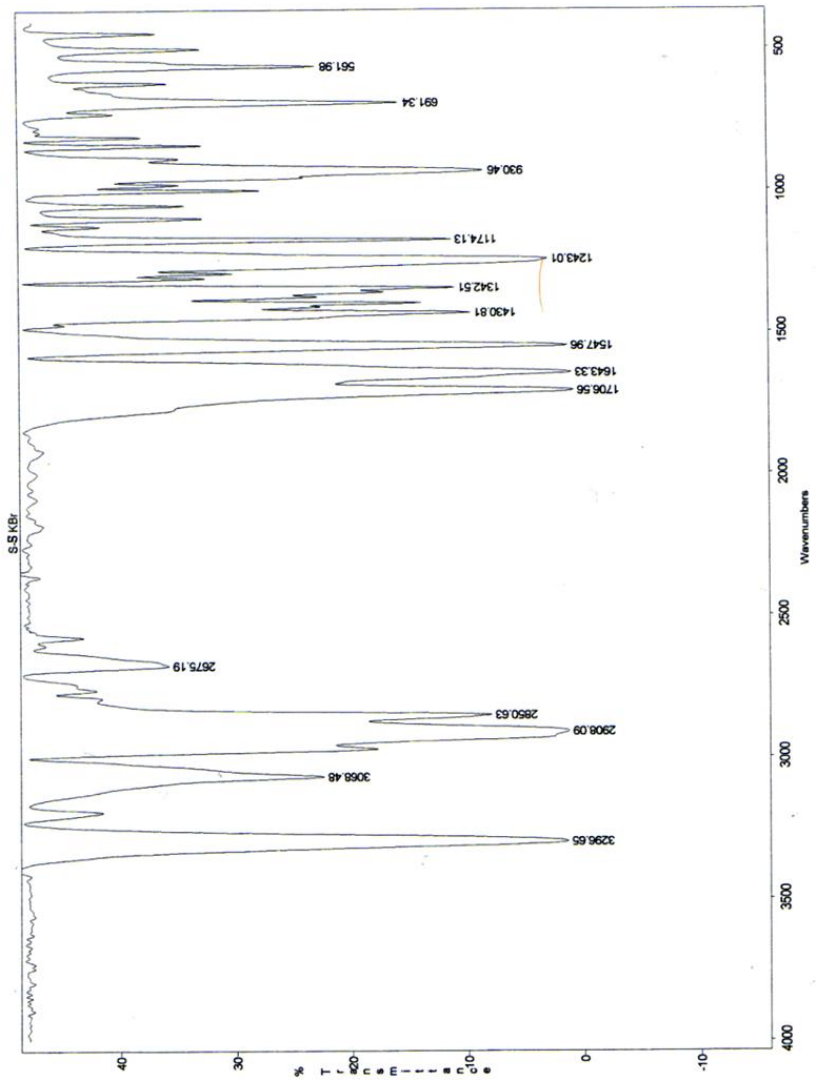

3.1.2. HRMS (FAB$^+$)

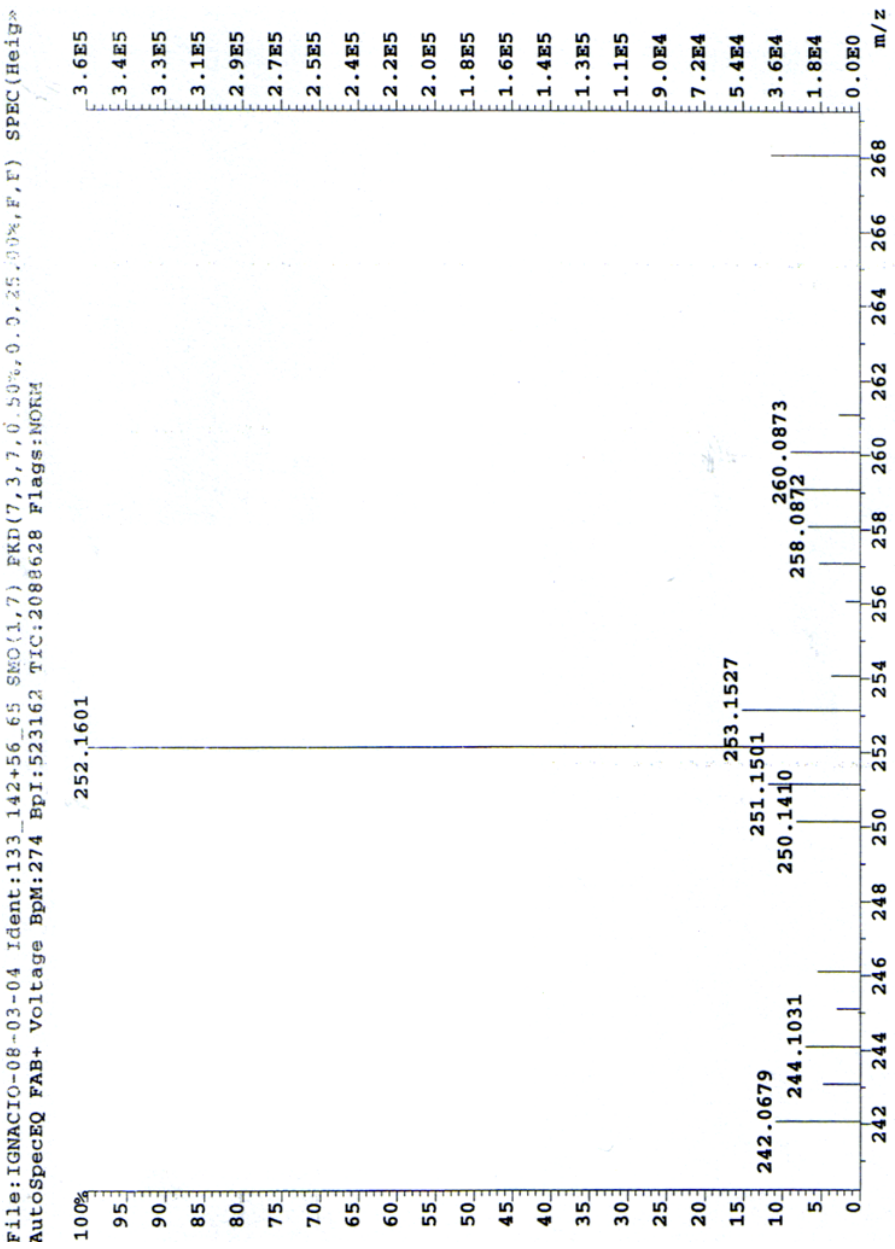
File:IGNACIO-08-03-04 Ident:133_142+56_65 SMO(1,7) EKD(7,3,7,0.50%,0.0,25.00%,F,F) SPEC(Heig
AutoSpecEQ FAB+ Voltage BpM:274 BpI:523162 TIC:2088628 Flags:NORM
252.1601
253.1527
251.1501
250.1410
242.0679
244.1031
258.0872
260.0873
m/z

3.2. 7,16-[bis(N-adamantilcarbamoil)propionil]-1,4,10,13-tetraoxa-7,16-diazaciclooctadecano

3.2.1. IR

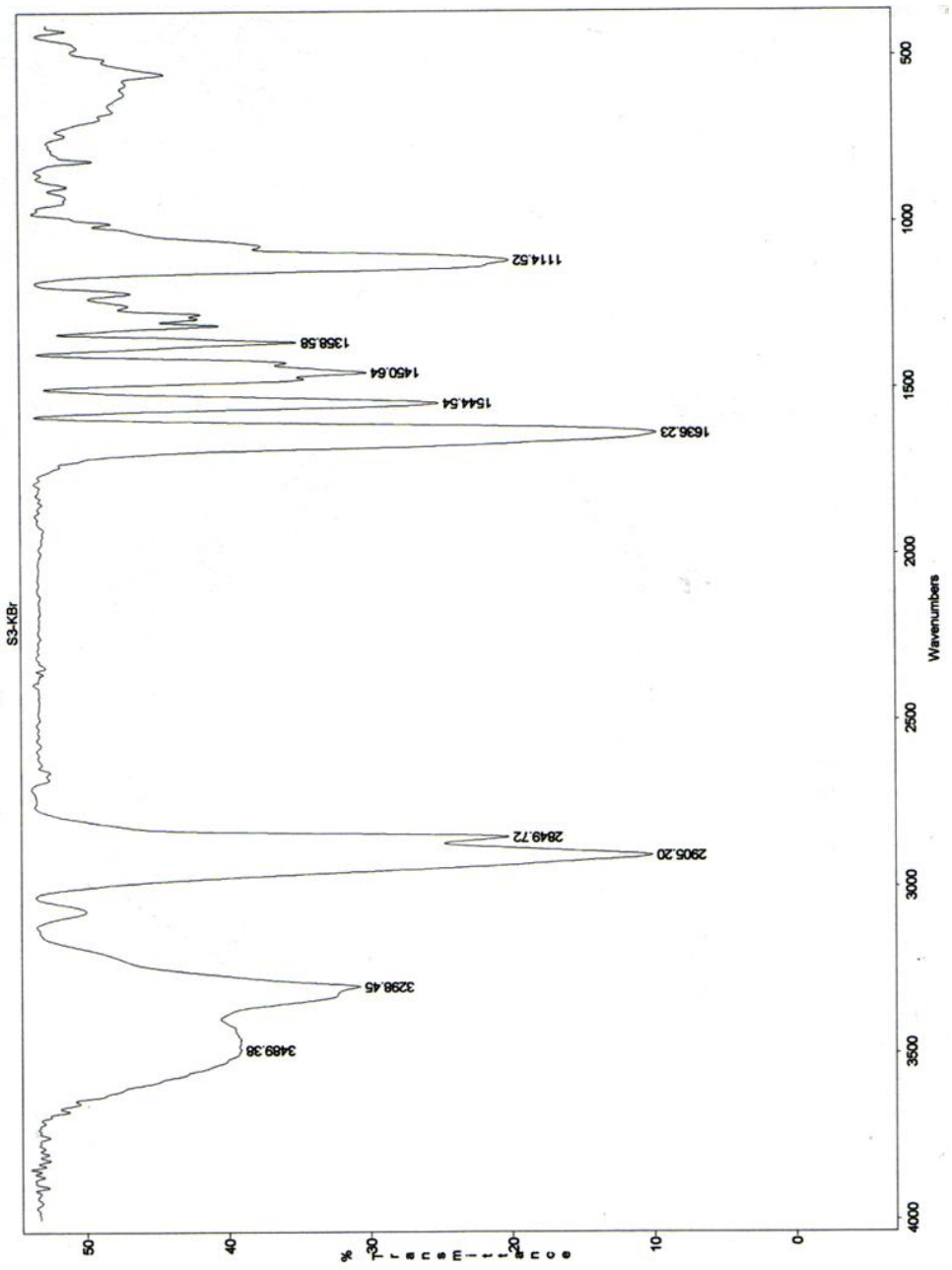

3.2.2. ^{1}H-RMN

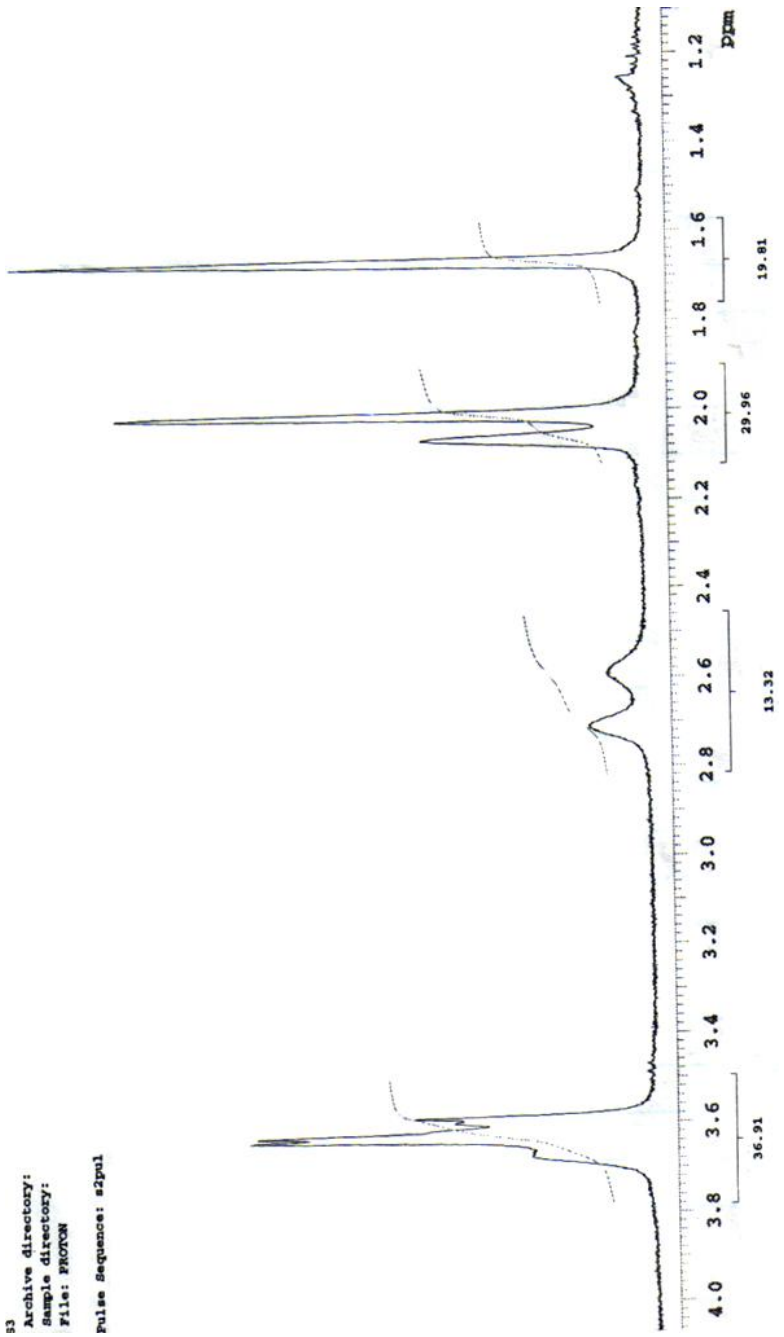
53
Archive directory:
Sample directory:
File: PROTON
Pulse Sequence: s2pul
4.0
3.8
3.6
3.4
3.2
3.0
2.8
2.6
2.4
2.2
2.0
1.8
1.6
1.4
1.2
ppm
36.91
13.32
29.96
19.81

3.2.3. ^{13}C-RMN

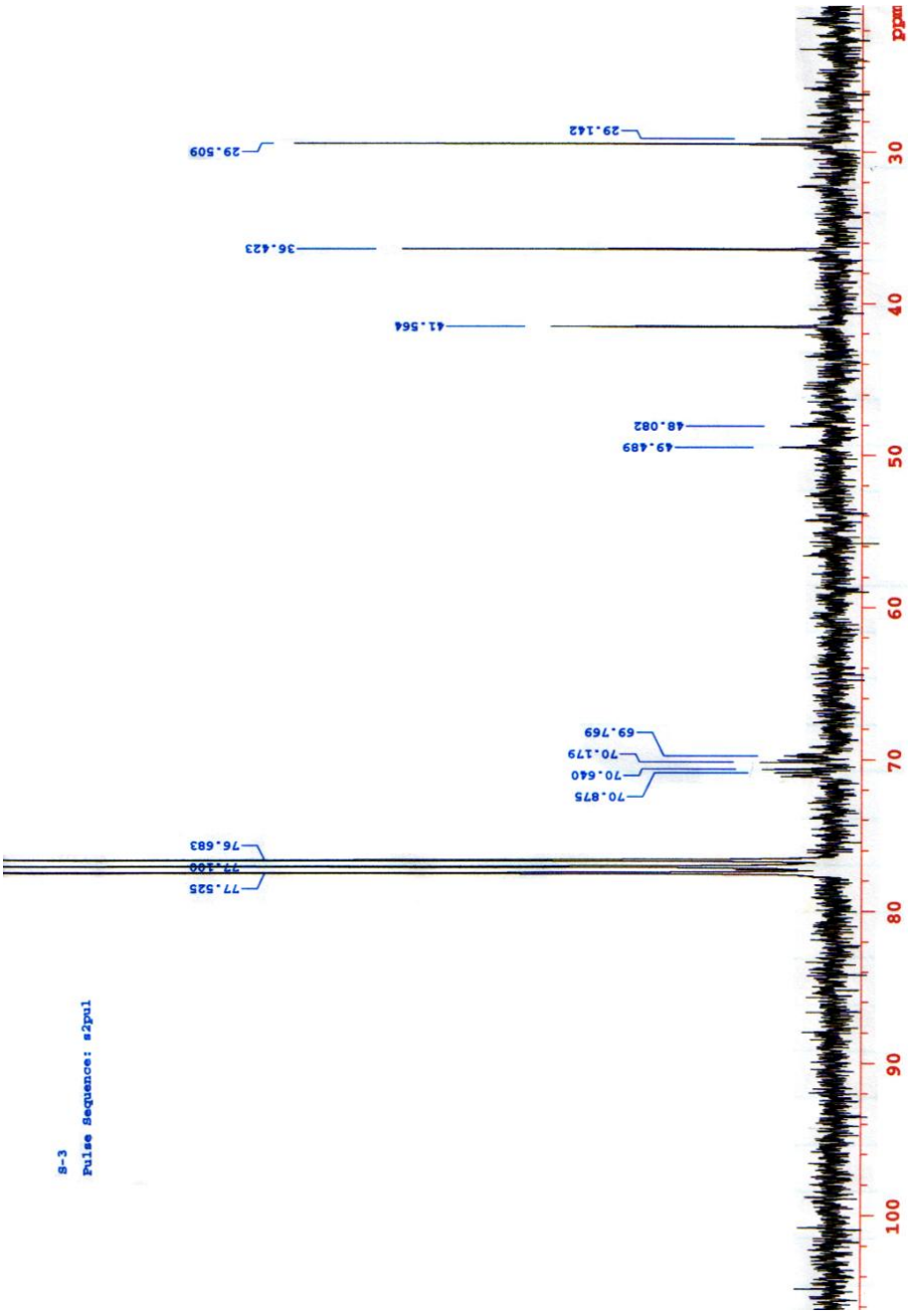
29.142
29.509
36.423
41.564
48.082
49.489
69.769
70.179
70.640
70.875
76.683
77.300
77.525
S-3
Pulse Sequence: s2pul
ppm
30
40
50
60
70
80
90
100

3.2.4. HRMS (FAB$^+$)

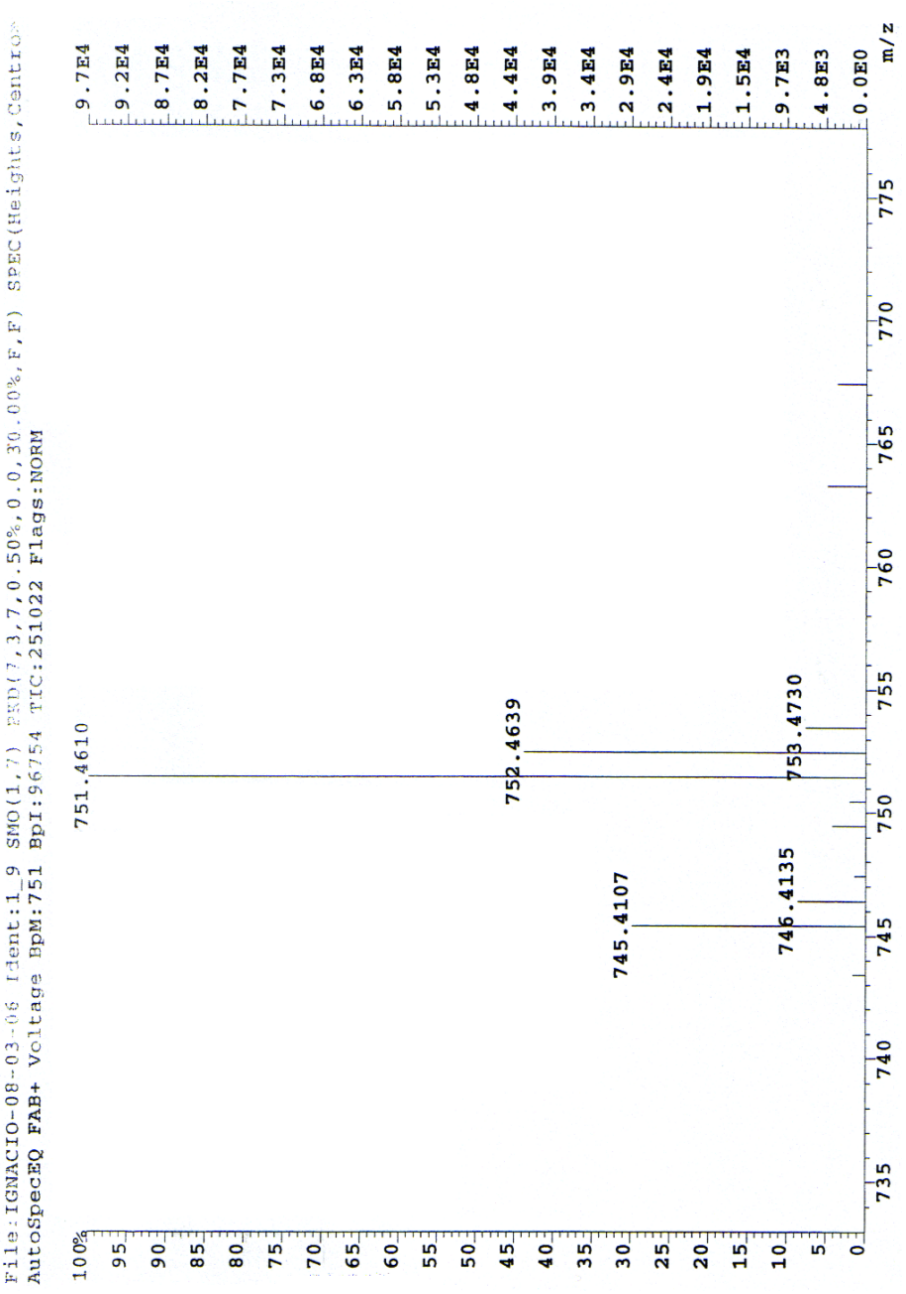
File:IGNACIO-08-03-06 Ident:1_9 SMO(1,7) BRD(7,3,7,0.50%,0.0,30.00%,F,F) SPEC(Heights,Centro
AutoSpecEQ FAB+ Voltage BpM:751 BpI:96754 TIC:251022 Flags:NORM
751.4610
752.4639
753.4730
745.4107
746.4135
m/z

CAPÍTULO 9

Hacia una lengua para la discriminación de sabores basada en una matriz ortogonal óptico-potenciométrica

"Misura ciò che è misurabile e rendi misurabile ciò che non lo è".

Galileo Galilei

1. INTRODUCCIÓN

Las porfirinas constituyen una amplia familia de compuestos químicos utilizada, entre otras aplicaciones, en sensores químicos. La química de la síntesis de porfirinas se ha desarrollado extensamente y es posible seleccionar de entre una gran biblioteca de sustituyentes para preparar el macrociclo seleccionado para una aplicación en particular[552]. Todas estas características son insuficientes para justificar el interés por las porfirinas si no se considera la riqueza de las propiedades que presentan estos macrociclos. Las características fotofísicas y de coordinación son un ejemplo de su potencialidad. Recientemente, los sensores basados en porfirinas han experimentado un crecimiento significativo.

1.1. Aspectos generales de las porfirinas

Las porfirinas son macrociclos tetrapirrólicos con un esqueleto base que consiste en cuatro unidades pirrol conectadas a través de cuatro puentes metino, y con hibridación sp^2 de los carbonos en la posición α de los anillos de pirrol[553]. El esqueleto molecular corresponde a la fórmula $C_{20}H_{14}N_4$. El macrociclo porfirínico es un sistema aromático que contiene 22 electrones π, de los cuales 18 están involucrados en la deslocalización electrónica. Una metaloporfirina se forma cuando un átomo de un metal se coordina reemplazando los dos átomos de hidrógeno del núcleo central. Las porfirinas que se pueden modificar con muy diversos grupos sustituyentes en sus posiciones periféricas se coordinan con gran número de metales de la tabla periódica (figura IX.1). Sus particulares propiedades químicas y físicas las convierten en candidatas muy atractivas para un gran número de aplicaciones. Su estructura básica puede sufrir numerosas modificaciones que influyen profundamente en las propiedades de coordinación y de sensado de estos compuestos.

---

[552] S. Horn, K. Dahms, M.O. Senge. *Synthetic transformations of porphyrins-advances 2004-2007*. J. Porphyrins and Phthalocyanines, 12(10) (2008) 1053-1077

[553] K.M. Smith. *Porphyrins and Metalloporphyrins,* Elsevier Science Ltd, Amsterdam (1975) pp. 934

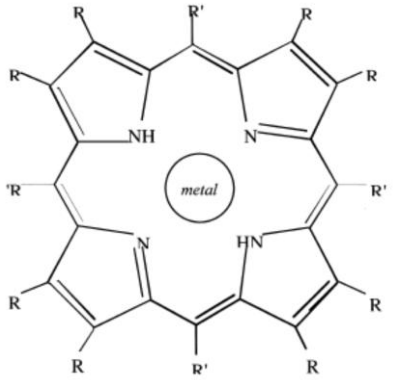

Figura IX.1. Estructura básica de la porfirina, que incluye un metal coordinado central y diversos posibles grupos sustituyentes

Las porfirinas se encuentran abundantemente en la naturaleza y desempeñan un papel muy importante en diversos procesos biológicos. Por ejemplo, el complejo formado por hierro (II) y protoporfirina IX es el grupo prostético de la hemoglobina y la mioglobina, responsable del transporte de oxígeno en los glóbulos rojos y del almacenamiento de este en los tejidos vivos. En las plantas, las porfirinas permiten la transferencia electrónica (citocromo c, citocromo oxidasa) y la conversión de energía (clorofila)[554].

El anillo de la porfirina ofrece distintas posibilidades de sustitución en su periferia, por lo que el control sintético permite el diseño de porfirinas para aplicaciones específicas. Se distinguen dos tipos de posiciones potencialmente funcionales: las posiciones β-pirrólicas y las posiciones puente o meso (figura IX.2).

[554] K.M. Kadish, K.M. Smith, R. Guilard. *The Porphyrin Handbook*, vol. 1, 1st edition Academic Press, San Diego, Calif, USA, (1999) pp. 405

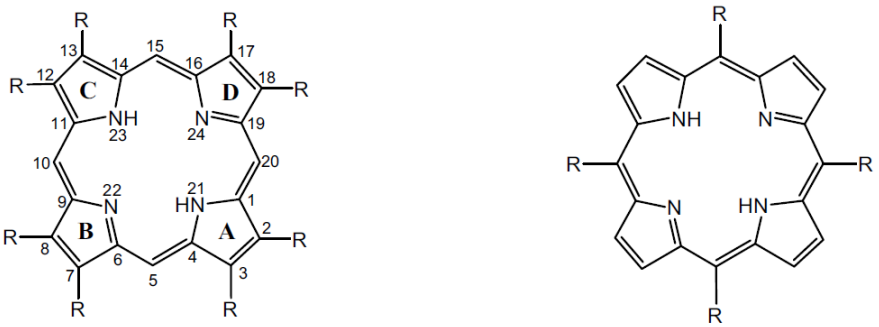

Figura IX.2. Tipos de porfirinas

Las porfirinas β-sustituidas presentan similitud estructural con las porfirinas de origen biológico. Las porfirinas *meso*-sustituidas, que han sido las utilizadas en este capítulo, no tienen análogos biológicos, pero su síntesis es fácilmente accesible y se utilizan como modelos biomiméticos y en química de materiales.

1.2. Síntesis de porfirinas y porfirinas *meso*-sustituidas

La porfirina, pese a su simple estructura, presenta una síntesis con serias dificultades. Su síntesis fue descrita por primera vez por Rothemund[555] y por Fischer y Gleim[556] en 1936. Rothemund hizo reaccionar una disolución de pirrol (0,42 M) y formaldehído (0,58 M) en MeOH/Py a 45 ºC durante 30 h, en atmósfera de argón y en un tubo cerrado, obteniendo la porfirina con un rendimiento de 0,09% (figura IX.3).

[555] P. Rothemund. *New porphyrin synthesis. Synthesis of porphin*. J. Am. Chem. Soc., 58 (1936) 625-627

[556] H. Fisher, W. Gleim. *Synthese des Porphins*. Liebigs Ann. Chem., 521(1) (1936) 157-160

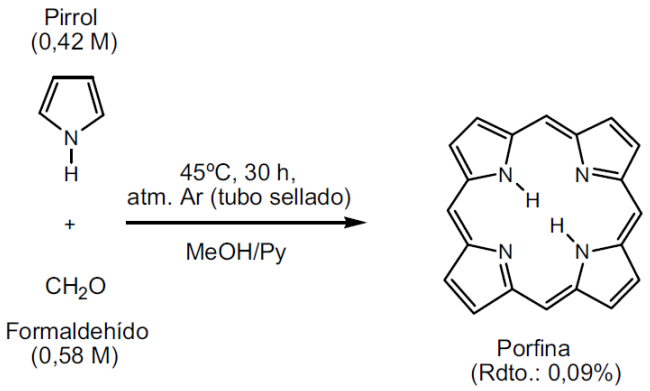

Figura IX.3. Método de obtención de porfirina descrito por Rothemund

En la síntesis propuesta por Fischer y Gleim se hizo reaccionar el pirrol-2-carbaldehído con ácido fórmico a ebullición, obteniéndose un rendimiento de porfirina inferior al 0,1%. Tras continuos esfuerzos para mejorar esta síntesis[557,558], en 1975, Longo *et al.* describieron una síntesis más eficiente. Calentando a 100 ºC 2 mL de 2-hidroximetilprirrol en 3 mL de etilbenceno durante dos semanas se obtuvo la porfirina con un rendimiento de 8-10%[559]. No obstante, el procedimiento de Rothemund seguía siendo el más utilizado debido a la mayor disponibilidad de los reactivos. En 1993, Neya[560] presentó una mejora de la síntesis de Rothemund haciendo reaccionar formaldehido y pirrol en una mezcla de ácido propiónico/piridina a 90 ºC durante 3 h 30 min. Los últimos 5 min se burbujeó aire dentro de la disolución caliente y, tras la purificación del crudo obtenido, aunque el rendimiento fue de 0,9%, se pudieron obtener 100 mg de porfirina en una reacción de un solo paso. En 1999, Taniguchi *et al.*[561] describieron una síntesis con un 31% de rendimiento a partir del acoplamiento de tripirrano y 2,5-bis(hidroximetil)pirrol, pero a pesar de la mejora, la difícil

[557] U. Eisner, R.P. Linstead. *Chlorophyll and related substances. I. The synthesis of chlorine*. J. Chem. Soc., (1955) 3742-3749

[558] S. Krol. *A new synthesis of porphine*. J. Org. Chem., 24 (1959) 2065-2067

[559] F.R. Longo, E.J. Thorne, A.D. Adler, S. Dym. *Notes on the synthesis of porphine*. J. Heterocyclic Chem., 12(6) (1975) 1305-1309

[560] S. Neya, H. Yodo, N. Funasaki. *Convenient synthesis of porphine*. J. Heterocyclic Chem., 30(2) (1993) 549-550

[561] S. Taniguchi, H. Hasegawa, M. Nishimura, M. Takahashi. *A facile route to tripyrrane from 2,5-bis(hydroxymethyl)pyrrole and the improved synthesis of porphine by the "3+1" approach* Synlett, 1 (1999) 73-74

obtención de los precursores lo convierte en un método de síntesis poco adecuado.

Finalmente, en 2002, Neya *et al.*[562] propusieron una nueva ruta sintética para la obtención de porfirina a partir de la desalquilación de las posiciones *meso* de la 5,10,15,20-tetraquis(*tert*-butil)porfirina (TTBP), la cual presenta un fácil acceso sintético. Calentando la TTBP a 90 ºC durante 15 min en una mezcla de H_2SO_4 conc,/1-butanol 1:1, el resultado fue un 74% de rendimiento de porfirina. En 2004, estos mismos investigadores consiguieron un rendimiento del 64%[563] mediante la desalquilación de la β-tetra(*tert*-butil)porfirina y en 2006 describieron otra vía alternativa basada en la descarboxilación de la meso-tetra(n-hexiloxicarbonil)porfirina. El rendimiento fue del 77%[564] calentándola a 180 ºC durante 30 min en una disolución acuosa de H_2SO_4 bajo atmósfera inerte.

La química de las porfirinas *meso*-sustituidas se inició con el trabajo de Rothemund[565] en 1935 acerca de la síntesis de *meso*-tetrametilporfirina (TMP) por reacción de pirrol y acetaldehído en metanol en tubo cerrado. Posteriormente, este mismo autor realizó síntesis similares de otras porfirinas *meso*-sustituidas[566].

La 5,10,15,20-tetrafenilporfirina (TPP) fue obtenida por primera vez por Rothemund[567] en 1941, con un rendimiento de 7,5-9%, mediante reacción de pirrol con benzoaldehído en piridina a 220 ºC durante 48 horas y en un tubo cerrado. En esta síntesis se detectó un subproducto presente en un 10-20%, una clorina[568,569] (2,3-dihidroporfirina), la cual podía ser convertida mediante oxidación a la correspondiente porfirina. Calvin *et al.* observaron, al estudiar esta

---

[562] S. Neya, N. Funasaki. *meso-Tetra(tert-butyl)porphyrin as a precursor of porphine*. Tetrahedron Lett., 43(6) (2002) 1057-1058

[563] S. Neya, J. Quan, T. Hoshino, M, Hata, N. Funasaki. *Convenient synthesis of porphine from β-tetra(tert-butyl)porphyrin*. Tetrahedron Lett., 45(47) (2004) 8629-8630

[564] S. Neya, J. Quan, T. Hoshino, M, Hata, N. Funasaki. *A novel and efficient synthesis of porphine*, Tetrahedron Lett., 47(49) (2006) 8731-8732

[565] P. Rothemund. *Formation of porphyrins from pyrrole and aldehydes*, J. Am. Chem. Soc., 57 (1935) 2010-2011

[566] P. Rothemund. *Porphyrin studies. III. The structure of the porphine ring system*. J. Am. Chem. Soc., 61 (1939) 2912-2915

[567] P. Rothemund, A.R. Menotti. *Porphyrin studies. IV. The synthesis of α,β,γ,δ-tetraphenylporphine*. J. Am. Chem. Soc., 63 (1941) 267-270

[568] S. Aronoff, M. Calvin. *The porphyrinlike products of the reaction of pyrrole with benzaldehyde*. J. Org. Chem., 8 (1943) 205-223

clorina formada, que al añadir acetato de zinc a la mezcla de reacción se duplicaba el rendimiento de la porfirina, de un 4-5% para la TPP a un 10-11% para la metaloporfirina de zinc (ZnTPP)[570]. Este fue uno de los primeros estudios del efecto plantilla que ejercen los iones metálicos en la síntesis de las porfirinas.

En 1964, Adler y Longo[571] propusieron un nuevo método sintético que permitió ampliar el abanico de benzaldehídos sustituidos aptos para la síntesis de porfirinas *meso*-sustituidas. El método consistía en calentar pirrol y benzaldehído a reflujo durante 30 min e ácido acético, ácido propiónico o benceno con ácido cloroacético o trifluoroacético. Usando ácido propiónico a reflujo, el rendimiento de tetrafenilporfirina (TPP) fueron del 20% (figura IX.4)[572]. El producto normalmente se obtiene contaminado con un 2-10% de cloro, pero ésta (tanto en forma de base libre como de quelato metálico) se transforma fácilmente a su respectiva porfirina por oxidación con 2,3-dicloro-5,6-diciano-1,4-benzoquinona (DDQ) en tolueno a reflujo[573,574]. En ácido acético, el rendimiento de TPP puede alcanzar un 35-40%, pero la reacción es mucho más rápida y la purificación más fácil cuando se utiliza ácido propiónico como disolvente.

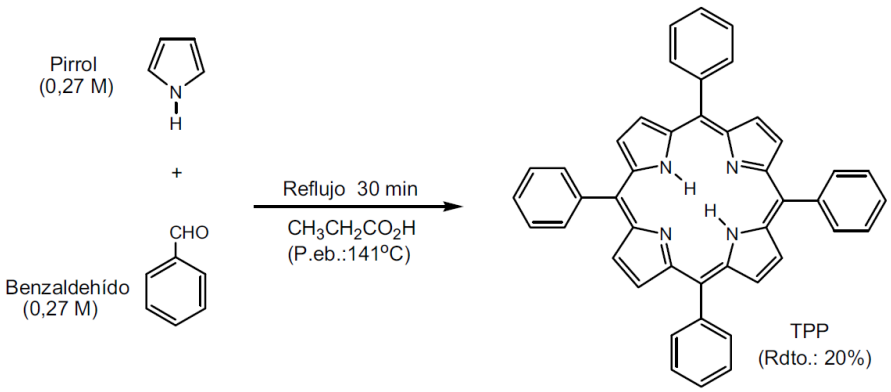

Figura IX.4. Síntesis de TPP según el método de Adler

[569] M. Calvin, R.H. Ball, S. Aronoff. *α,β,γ,δ-Tetraphenylchlorine*. J. Am. Chem. Soc., 65 (1943) 2259

[570] R.H. Ball, G.D. Dorough, M. Calvin. *Further study of the porphine-like products of the reaction of benzaldehyde and pyrrole*. J. Am. Chem. Soc., 68(11) (1946) 2278-2281

[571] A.D. Adler, F.R. Longo, W. Shergalis. *Mechanistic investigation of porphyrin synthesis. I. Preliminary studies on ms-tetraphenylporphin*. J. Am. Chem. Soc., 86(15) (1964) 3145-3149

[572] A.D. Adler, F.R. Longo, J.D. Firanelli, J. Goldmacher, J. Assour, L. Korsakoff. *A simplified synthesis for meso-tetraphenylporphine*. J. Org. Chem., 32(2) (1967) 476

[573] G.H. Barnett, M.F. Hudosn, K.M. Smith. *meso-Tetraphenylporphyrin purification*. Tetrahedron Lett., (30) (1973) 2887-2888

Posteriores estudios llevados a cabo por Adler[575,576], Dolphin[577] y Evans[578] demostraron que el porfirinógeno es el intermedio clave formado en la condensación de pirrol y benzaldehído y que su oxidación conduce a la formación de la porfirina.

A mediados de la década de los 80, Lindsey[579] propuso una nueva estrategia en la síntesis de porfirinas basada en dos etapas, que posteriormente ha sido optimizada para casos concretos[580-585]. En una primera etapa de condensación, pirrol y benzaldehído reaccionan reversiblemente a temperatura ambiente y con un catalizador ácido (ácido trifluoroacético o trifluoruro de boro en dietil éter) para formar el tetrafenilporfirinógeno (forma cíclica). Posteriormente, se añade un oxidante (DDQ o *p*-cloranilo) en cantidades estequiométricas que convierte de forma irreversible el porfirinógeno en porfirina, minimizando la presencia de aldehídos en el medio durante la oxidación. El

---

[574] K. Rousseau, D. Dolphin. *Purification of meso-tetraphenylporphyrin*. Tetrahedron Lett., (48) (1974) 4251-4254

[575] A.D. Adler, L. Sklar, F.R. Longo, J.D. Firanelli, M.G. Firanelli. *Mechanistic study of the synthesis of meso-tetraphenylporphin*. J. Heterocyclic Chem., 5(5) (1968) 669-678

[576] J.B. Kim, J.J. Leonard, F.R. Longo. *Mechanistic study of the synthesis and spectral properties of meso-tetraarylporphyrins*. J. Am. Chem. Soc., 94(11) (1972) 3986-3992

[577] D. Dolphin. *Porphyrinogens and porphodimethenes, intermediates in the synthesis of m-tetraphenylporphins from pyrroles and benzaldehyde*. J. Heterocyclic Chem., 7(2) (1970) 275-283

[578] B. Evans, K.M. Smith, J.H. Fuhrhop. *Sterically crowded porphyrins: meso-tetraphenyl-octaethylporphyrin*. Tetrahedron Lett., 5 (1977) 443-446

[579] J.S. Lindsey, I.C. Schreiman, H.C. Hsu, P.C. Kearney, A.M. Marguerettaz. *Rothemund and Adler-Longo reactions revisited: synthesis of tetraphenylporphyrins under equilibrium conditions*. J. Org. Chem., 52(5) (1987) 827-836

[580] J.S. Lindsey, R.W. Wagner. *Investigation of the synthesis of ortho-substituted tetraphenylporphyrins*. J. Org. Chem., 54(4) (1989) 828-836

[581] J.S. Lindsey, K.A. MacCrum, J.S. Tyhonas, Y. Chuang. *Investigation of a Synthesis of meso-Porphyrins Employing High Concentration Conditions and an Electron Transport Chain for Aerobic Oxidation*. J. Org. Chem., 59(3) (1994) 579-587

[582] F. Li, J.S. Tyhonas, K.A. MacCrum, J.S. Lindsey. *Beneficial effects of salts on an acid-catalyzed condensation leading to porphyrin formation*. Tetrahedron, 53(37) (1997) 12339-12360

[583] G.R. Geiger, Y Ciringh, F. Li, D.M. Haynes, J.S. Lindsey. *A survey of acid catalysts for use in two-step, one-flask syntheses of meso-substituted porphyrinic macrocycles*. Org. Lett., 2(12) (2000) 1745-1748

[584] G.R. Geiger, B.J. Littler, J.S. Lindsey. *Investigation of porphyrin-forming reactions. Part 3. The origin of scrambling in dipyrromethane + aldehyde condensations yielding trans-A2B2-tetraarylporphyrins*. J. Am. Chem. Soc., Perkin Trans, 2(5) (2001) 701-711

[585] G.R. Geiger, B.J. Littler, J.S. Lindsey. *Investigation of porphyrin-forming reactions. Part 4. Examination of the reaction course in syntheses of porphyrins via dipyrromethanecarbinols*. J. Am. Chem. Soc., Perkin Trans, 2(5) (2001) 712-718

método general de Lindsey[586] permitió ampliar el número de aldehídos para la síntesis de porfirinas *meso*-sustituidas.

En 1994, los grupos de Furuta[587] y Latos-Grazinsky[588] estudiaron el aislamiento, como subproducto de estas síntesis, de un isómero de la meso-tetrafenilporfirina que posee un anillo de pirrol invertido como consecuencia de un ataque electrófilo en la posición β del pirrol, el 2-aza-21-carba-5,10,15,20-tetrafenilporfirina (porfirina N-invertida, NC-TPP).

Para la obtención de la 5,10,15,20-tetraquis(*tert*-butil)porfirina (TTBP), Smith[589] optimizó el método general de Lindsey.

1.3. Características espectrales

Todas las porfirinas presentan un color intenso, que se debe a los procesos de absorción que implican la excitación de los electrones desde π a π* en los orbitales del anillo porfirínico. Los espectros de absorción del rango visible de las porfirinas muestran una intensa absorción hacia el segundo estado de excitación ($S_0 \rightarrow S_2$), normalmente entre 380 y 420 nm, correspondiente a la banda Soret o banda B. Esta banda es característica de un macrociclo altamente conjugado y desaparece cuando la deslocalización aromática es interrumpida. Además, aparecen cuatro bandas de absorción de baja intensidad entre 500 y 700 nm, que son atribuidas a transiciones débiles hacia el primer estado excitado ($S_0 \rightarrow S_1$). Estas son llamadas bandas Q o, en ocasiones, bandas satélites, y se identifican mediante números romanos I-IV en orden inverso de magnitud. La figura IX.5 muestra un espectro de absorción en el visible típico, donde se indican la banda Soret y las bandas Q.

---

[586] J.S. Lindsey. *The Porphyrin Handbook*. Academic Press, San Diego, CA. 1 (2000) 45-118

[587] H. Furuta, T. Asano, T. Ogawa. *"N-Confused Porphyrin": A New Isomer of Tetraphenylporphyrin*. J. Am. Chem. Soc., 116(2) (1994) 767-768

[588] P.J. Chmielewski, L. Latos-Grazynski, K. Rachlewicz, T. Glowiak. *Monoinverted tetra-p-tolylporphyrin: a novel porphyrin isomer*. Angew. Chem. Int. Ed. Engl., 33(7) (1994) 779-781

[589] M.O. Senge, I. Bischoff, N.Y. Nelson, K. Smith. *Synthesis, reactivity and structural chemistry of 5,10,15,20-tetraalkylporphyrins*. J. Porphyrins Phthalocyanines, 3(2) (1999) 99-116

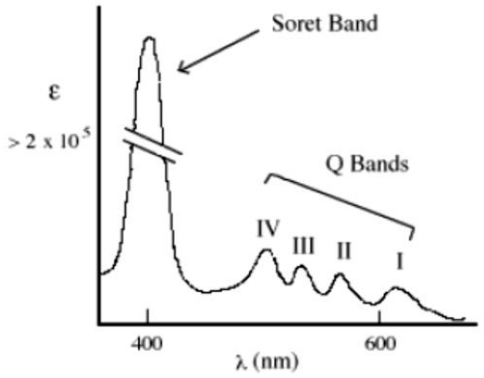

Figura IX.5. Espectro de absorbancia típico de una porfirina

Mientras que las variaciones de sustituyentes periféricos en el anillo porfirínico con frecuencia provocan pequeños cambios en la intensidad y en la longitud de onda de absorción, la protonación de los átomos de nitrógeno interno o la inserción de átomos metálicos en el macrociclo, habitualmente provocan fuertes cambios en el espectro de absorción visible. Los espectros típicos de los complejos metálicos de las porfirinas se describen en la siguiente sección.

1.3.1. Espectros de metaloporfirinas

Existen tres clases de espectros electrónicos metaloporfirínicos: *normal*, *hipso* e *hiper*, dividiéndose los espectros *hiper* en tipo-p y tipo-d.

Se observan espectros *normales* de metaloporfirinas con metales de los grupos 1 a 5 con estados de oxidación de I a V, respectivamente, y para otros metales d^0 o d^{10}. Como característica, los espectros *normales* presentan una intensa banda Soret de absorbancia entre 320 y 450 nm y una o dos bandas Q entre 450 y 700 nm en lugar de cuatro como en el caso de los espectros de porfirinas libres de metal. La diferencia del número de bandas es atribuida a la disminución de simetría desde D_{4h}, correspondiente a la metaloporfirina, hasta D_{2h}, mediante la protonación de los dos nitrógenos pirrólicos de la porfirina libre de metal.

El modelos de cuatro orbitales de Gouterman permitió explicar los espectros *normales*. En este modelo, los orbitales cuatro son orbitales porfirina π y π*; los dos orbitales moleculares más altos ocupados (HOMOs) de simetría a_{1u} y

a_{2u}, y los dos orbitales moleculares más bajos desocupados (LUMOs) de simetría e_g. Las dos absorciones principales son consecuencia del acoplamiento de las dos transiciones entre HOMOs y LUMOs (π - π*) (figura IX.6).

Las bandas Q son el resultado de dipolos de transición que prácticamente se cancelan mutuamente, lo que da lugar a una débil absorbancia. La elevada intensidad de absorbancia Soret es consecuencia de una combinación lineal de dos transiciones con dipolos de transición que se refuerzan.

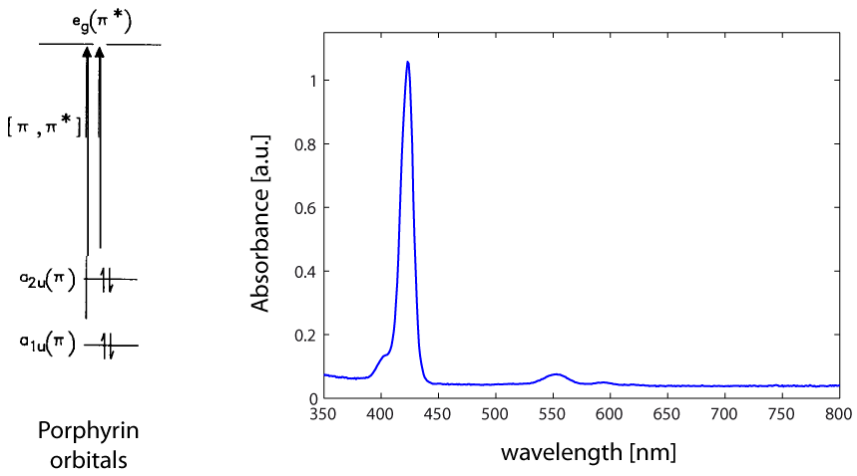

Figura IX.6. a) Diagrama de orbitales moleculares para la absorbancia de metaloporfirinas *normales* del modelo de cuatro orbitales. b) Ejemplo de un espectro *normal* (ZnTPP)

Los espectros *hipso* se parecen mucho a los normales, con la excepción de que la banda Q se desplaza hacia el azul, es decir, hacia longitudes de onda inferiores a 570 nm. Los espectros *hipso* corresponden a metales de transición de tipo entre d^6 y d^9 y, como consecuencia, sus electrones se ubican en orbitales $e_g(d_\pi)$. Ejemplos típicos son Pd^{2+}, Pt^{2+}, Rh^{2+} y Ni^{2+}. El desplazamiento al azul de la banda Q se explica a partir de la combinación de los orbitales e_g LUMO del anillo porfirínico con los orbitales del metal ocupados $e_g(d_\pi)$. Esta interacción desplaza el orbital LUMO de la porfirina hacia mayor energía, como muestra la figura IX.7, lo que incrementa la distancia energética π-π* de la porfirina.

El solapamiento es elevado para metales de tipo *4d* y *5d*, los cuales muestran los mayores desplazamientos hacia el azul. Dentro de una determinada fila de metales de transición, la energía de los electrones d_π decrece conforme

aumenta el número de electrones, ya que la distancia energética entre el LUMO de la porfirina y los metales se amplía y la mezcla de orbitales disminuye.

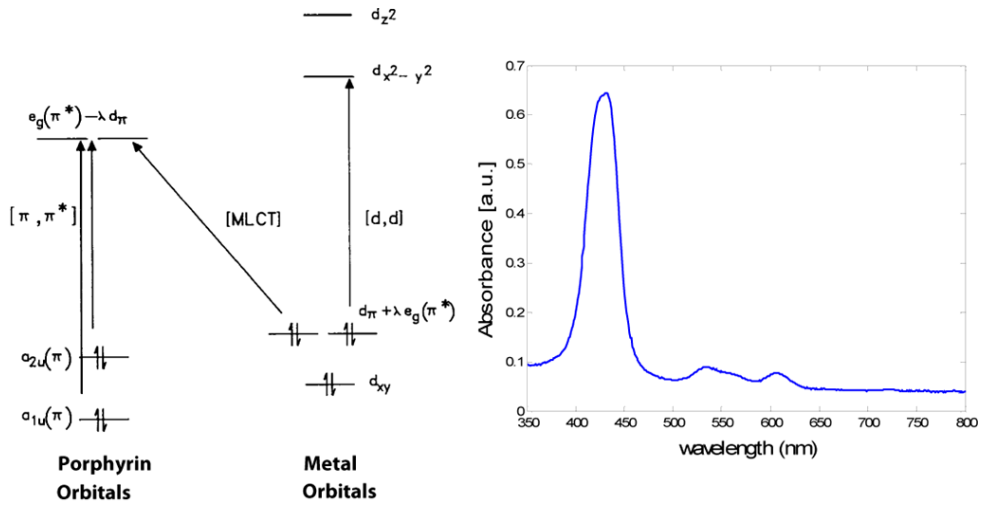

Figura IX.7. a) Diagrama de orbitales moleculares para metaloporfirinas *hipso*.
b) Ejemplo de un espectro *hipso* (NITPP)

El espectro *hiper* muestra una absorbancia adicional comparado con otras variedades. Estas bandas adicionales se deben generalmente al desplazamiento hacia el azul de las bandas Q y son de intensidad moderada. Los principales elementos de grupos con bajo estado de oxidación (por ejemplo, Sn^{2+}, Pb^{2+}, P^{3+}, As^{3+}) originan espectros *hiper* de tipo *p*. En este caso, las bandas extra se deben a la transferencia de carga metal-ligando. Como muestra la figura IX.8, la transferencia de carga se inicia en el orbital p_z del metal y consiste en $a_{2u}(np_z)$ (metal) → $e_g(\pi^*)$ (anillo).

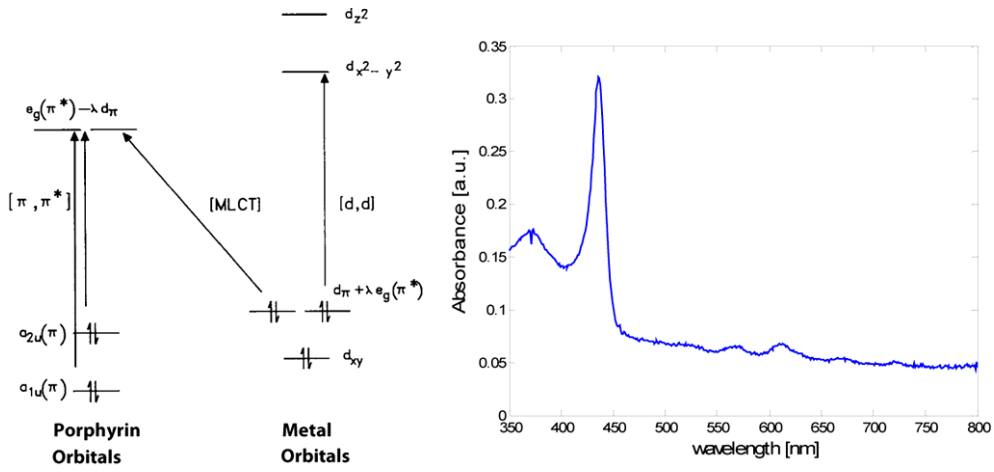

Figura IX.8. a) Diagrama de orbitales moleculares para metaloporfirinas *hiper* de tipo p. b) Ejemplo de un espectro *hiper* de tipo p (SnTPP)

Los espectros *hiper* de tipo d corresponden a metales de tipo d^1 a d^6, que presentan vacancias en los orbitales $e_g(d_\pi)$. Estas vacancias hacen posible una transferencia de carga del ligando porfirínico al metal, como muestra la figura IX.9. Debido a que la transferencia de carga da lugar a un cambio del estado de oxidación del metal, son deseables metales de potencial redox relativamente bajo para que el producto final sea más estable. Además, debe considerarse también que se produce la combinación de los orbitales d_π del metal con el LUMO de la porfirina, ya que presentan la misma simetría e_g. Esta intensa combinación explica los complejos espectros que frecuentemente se observan en porfirinas *hiper* de tipo d. Esta mezcla tiene lugar de forma más fácil cuando el LUMO porfirínico está próximo en energía a los orbitales del metal. Los cálculos han permitido demostrar que los orbitales de los metales Cr^{3+}, Mn^{3+} y Fe^{3+} son los únicos con una energía adecuada para que se produzca una combinación considerable[590].

[590] K.S. Suslick, R.A. Watson. *The Photochemistry of Chromium, Manganese, and Iron Porphyrin Complexes.* New. J. Chem., 16 (1992) 633-642

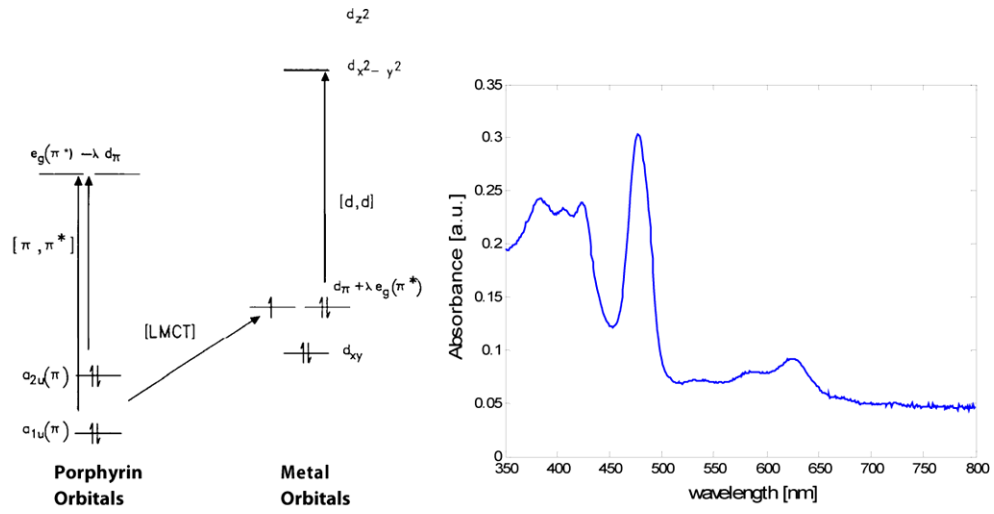

Figura IX.9. a) Diagrama de orbitales moleculares para metaloporfirinas *hiper* de tipo d. b) Ejemplo de un espectro *hiper* de tipo d (MnTPP)

Es importante destacar que las características espectroscópicas mostradas por las porfirinas en estado sólido son diferentes a las que presentan en disolución. Estas diferencias frecuentemente son descritas como interacciones electrónicas entre los cromóforos en el entorno de la membrana. Los espectros de las muestras monocapa se caracterizan normalmente por una banda Soret doble, con un componente de absorción desplazado hacia la región roja y otro hacia la región azul (≈ 400 nm) comparado con la absorción de la disolución del estado B (≈ 420 nm). Por el contrario, las características espectrales de la banda Q son bastante similares tanto para la muestra pelicular como en disolución. En estado sólido, debe tenerse en cuenta otra importante característica de las porfirinas: la presencia de interacciones π–π* entre los macrociclos; la consecuencia de este fenómeno de agregación en los espectros de absorción es el ensanchamiento, la división y el desplazamiento de las bandas con respecto a los espectros en disolución[591].

[591] G.A. Schick, I.C. Schreiman, R.W. Wagner, J.S. Lindsey, D.F. Bocian. *Spectroscopic Characterization of Porphyrin Monolayer Assemblies*. J. Am. Chem. Soc., 111 (1989) 1344-1350

1.4. Aplicaciones en sensores químicos

Las porfirinas y las metaloporfirinas son unos de los materiales más interesantes para la preparación de sensores químicos, debido a su estabilidad y a la variabilidad de sus propiedades, ya que además dejan margen para una amplia modulación de éstas mediante modificaciones o cambios de la coordinación del metal. Consecuentemente, las metaloporfirinas no se comportan habitualmente como receptores para el reconocimiento de moléculas objetivo específicas, sino como sensores selectivos globalmente, cuyo comportamiento es muy similar el encontrado en receptores olfativos. De hecho, se ha discutido el hecho de que los receptores olfativos localizados en el epitelio contienen complejos de coordinación con iones metálicos[592]. Por esta razón, la función del ion metálico coordinado en una metaloporfirina se considera de vital importancia para la determinación de la sensibilidad y la selectividad cuando son utilizados para identificar olores complejos en sistemas olfativos artificiales.

Una metaloporfirina ofrece una gran variedad de mecanismos de interacción que pueden ser explotados para el sensado químico, tales como enlaces de hidrógeno, polarización e interacciones polares entre moléculas volátiles y porfirinas. El papel del metal es de vital importancia para determinar las características de sensibilidad y selectividad de la molécula mediante unión axial de la molécula volátil, ya que las interacciones de coordinación tienen lugar en el centro metálico en complejos metaloporfirínicos[593]. Desde este punto de vista, dado que casi todos los metales pueden ser coordinados para formar complejos metaloporfirínicos, las propiedades de los ligandos metaloporfirínicos presentan una gran versatilidad. Los mecanismos de interacción de baja energía, tales como el enlace con hidrógeno, la polarización o las interacciones polares pueden producirse simultáneamente y contribuir en el enlace molecular del receptor total[594]. Por otra parte, se puede diseñar una disposición molecular

---

[592] J. Wang, Z. A. Luthey-Schulten, K.S. Suslick. *Is the olfactory receptor a metalloprotein?* PNAS, 100(6) (2003) 3035-3039

[593] R. Paolesse, F. Mandoj, A. Marini, C. Di Natale. *Porphyrin-based chemical sensors, in: H.S. Nalwa*. Encyclopedia of Nanosciences and Nanotechnology. American Scientific Publ., 2003

[594] T. Ohshiro, T. Ito, P. Bühlmann, Y. Umezawa. *Scanning Tunneling Microscopy with Chemically Modified Tips: Discrimination of Porphyrin Centers Based on Metal Coordination and Hydrogen Bond Interactions*. Anal. Chem., 73 (2001) 878-83

particular al objeto de obtener metaloporfirinas que mejoren notablemente la selectividad[595,596].

Para explotar las porfirinas como materiales sensores es fundamental acoplar la capa sensora con un transductor adecuado capaz de transducir la interacción con las moléculas objetivo en una señal medible, normalmente de naturaleza eléctrica. La elección está determinada por el parámetro físico que cambia como consecuencia de la formación del enlace. Una aproximación simple y sencilla consiste en la medida de la variación de masa tras la adsorción de volátiles sobre una película porfirínica. Se han utilizado microbalanzas de cristal de cuarzo[597] (QMB) y dispositivos de onda acústica[598] para medir cantidades inferiores a las ppm de varias clases de compuestos. Los dispositivos de efecto de campo[599] y las matrices de sensores capacitivos[600] han sido funcionalizados con diversos tipos de porfirinas para sensar compuestos volátiles. Sin embargo, nuestro principal interés radica en la modificación de las propiedades de absorción y luminiscencia desencadenada por las interacciones, que pueden ser detectadas con dispositivos ópticos. La siguiente sección recoge una visión general de las aplicaciones más representativas de los sensores químicos basados en porfirinas.

1.4.1. Sensores ópticos basados en porfirinas

Los sensores ópticos están basados en la variación de una propiedad óptica, tal como la absorción o la luminiscencia, del material sensor como consecuencia de la interacción con los analitos objetivo. Se ha demostrado que las porfirinas y compuestos relacionados muestran efectos solvatocrómicos

---

[595] C. Di Natale, R. Paolesse, A. D'Amico. *Metalloporphyrins based artificial olfactory receptors*. Sens. Actuators B, 121 (2007) 238-246

[596] A. D'Amico, C. Di Natale, R. Paolesse, A. Macagnano, A. Mantini. *Metalloporphyrins as basic material for volatile sensitive sensors*. Sens. Actuators B, 65 (2000) 209-215

[597] C. Di Natale, R. Paolesse, A. Macagnano, A. Mantini, P. Mari, A. D'Amico. *Qualitative structure-sensitivity relationship in porphyrins based QMB chemical sensors*. Sens. Actuators B, 68 (2000) 319-323

[598] M. Benetti, D. Cannatà, F. Di Pietrantonio, V. Foglietti, E. Verona. *Microbalance chemical sensor based on thin-film bulk acoustic wave resonators*. Appl. Phys. Lett., 87 (2005) 173504-173506

[599] M. Andersson, M. Holmberg, I. Lundstrom, A. Lloyd-Spetz, P. Martensson, R. Paolesse, C. Falconi, E. Proietti, C. Di Natale, A. D'Amico. *Development of a ChemFET sensor with molecular films of porphyrins as sensitive layer*. Sens. Actuators B, 77 (2001) 567-571

[600] E. Martinelli, M. Stabile, A. Catini, R. Paolesse, A. D'Amico, C. Di Natale. *An array of capacitive sensors based on a commercial fingerprint detectors*. Sens. Actuators B, 130 (2008) 264-268

significativos con un amplio rango de vapores (por ejemplo alcoholes, aminas, fosfinas, arenos y cetonas), lo cual provoca efectos colorimétricos distinguibles. Consecuentemente, metaloftalocianinas y metaloporfirinas son compuestos adecuados para ello debido a su fácil síntesis, alta estabilidad y a la presencia de una intensa transición π- π* en el rango visible.

Una de las primeras aplicaciones publicada de porfirinas basada en sensores ópticos, data de finales de la década de los ochenta y está relacionada con la detección de oxígeno[601]. Estos dispositivos están basados en complejos metálicos de varias porfirinas sustituidas que experimentan atenuación de la fosforescencia tras la interacción con oxígeno molecular, atenuación que es linealmente dependiente de la concentración de oxígeno según la relación de Stern-Volmer. Las metaloporfirinas más extensamente utilizadas para estas aplicaciones son derivados de platino y paladio, debido a sus altos rendimientos cuánticos de fosforescencia y a sus altos tiempos de vida. Desde entonces, se ha publicado un gran número de aplicaciones con diferentes configuraciones[602]. Dependiendo de la disposición, la intensidad de la atenuación puede ser incluso detectada, tanto visualmente como, de forma evidentemente más precisa, con una cámara CCD[603] u otros muchos dispositivos.

La coordinación de los ligandos en las posiciones axiales puede influir notablemente en la estructura electrónica y, consecuentemente, en los espectros electrónicos. En películas sólidas, la unión con compuestos orgánicos volátiles (VOCs) puede alterar las interacciones π-π entre macrociclos, conduciendo a modificaciones adicionales de los espectros. Se ha demostrado que todos estos cambios espectrales son interesantes y útiles para aplicaciones de sensores ópticos basadas en cambios de absorbancia. Una de las primeras aplicaciones presentadas de una nariz óptico-electrónica fue el uso de un LED operando en la región azul como fuente de luz, acoplado con fotodetectores, para medir la modificación espectral de una delgada película de metaloporfirinas tras la

---

[601] J. R. Bacon, J.N. Demas. *Determination of Oxygen Concentrations by Luminescence Quenching of a Polymer- Immobilized Transition-Metal Complex*. Anal. Chem., 59 (1987) 2780-2785

[602] S. M. Borisov, I. Klimant. *Luminescent nanobeads for optical sensing and imaging of dissolved oxygen*. Microchim. Acta, 164 (2009) 7-15

[603] X. Wang, X. Chen, Z. Xie, X. Wang. *Reversible Optical Sensor Strip for Oxygen*. Angew. Chem., 47 (2008) 7450-7453

exposición a VOCs[604]. En otras aplicaciones, la plataforma de transducción está basada en un espectrofotómetro. En este caso, es práctica común utilizar diferentes regiones espectrales dentro del rango UV-Vis correspondiente a las bandas típicas de absorción de porfirinas. Las películas de metaloporfirinas se preparan normalmente mediante métodos químicos o físicos, tales como las técnicas de deposición por vapor, *spin coating* y deposición Langmuir–Blodgett (LB). La exposición de una capa sensora de ZnTPP a los vapores orgánicos en una atmósfera controlada induce variaciones en las bandas de absorción[605]. Para ello, se ha propuesto utilizar la diferencia $I_n - I_{0n}$, donde I es la integral de la banda medida en presencia de vapores VOC y I_{0n} es la integral de la banda medida en atmósfera de referencia. El hecho de calcular así las respuestas se debe a que cada banda de absorción es proporcional al número de macromoléculas activas en el proceso de sensado. Consecuentemente, la diferencia en la integral proporciona un mejor sensado. De esta forma, se evaluó la respuesta óptica de la película frente a diversos analitos (por ejemplo isopropanol, etanol, metanol y acetona)[606].

1.4.1.1. Análisis mediante CSPT

El objetivo de la CSPT no es reproducir medidas espectroscópicas, sino detectar y clasificar sustancias. Consecuentemente, el hecho de conservar características de reconstrucción espectrales sin necesidad de una reconstrucción espectral completa es suficiente para este propósito. Bajo esta visión, se ha utilizado el sistema CSPT en numerosas aplicaciones para investigar características espectrales, tanto para evaluar reflectancia[607] como transmitancia. Mediante el empleo de membranas semitransparentes de porfirinas o compuestos relacionados se ha demostrado que es posible detectar respuestas correspondientes a moléculas tales como aminas, alcoholes, CO y

---

[604] C. Di Natale, D. Salimbeni, R. Paolesse, A. Macagnano, A. D'Amico. *Porphyrins-based opto-electronic nose for volatile compounds detection*. Sens. Actuators B, 65 (2000) 220-226

[605] J. Spadavecchia, R. Rella, P. Siciliano, M. G. Manera, A. Alimelli, R. Paolesse, C. Di Natale, A. D'Amico. *Optochemical vapour detection using spin coated thin film of ZnTPP*. Sens. Actuators B, 115 (2006) 12-16

[606] J. Spadavecchia, G. Ciccarella, P. Siciliano, S. Capone, R. Rella. *Spin-coated thin films of metal porphyrin-phthalocyanine blend for an optochemical sensor of alcohol vapours*. Sens. Actuators B, 100 (2004) 88-93

[607] D. Filippini, G. Comina, I. Lundström. *Computer screen photo-assisted reflectance fingerprinting*. Sens. Actuators B, 107 (2005) 580-586

NOx[608]. Se ha utilizado una matriz sensora basada en una plataforma de transducción CSPT para investigar la calidad del pescado monitorizando mediante espacio en cabeza la evolución de productos desde frescos a estropeados[609]. La técnica CSPT también puede ser usada como una especie de espectrofotómetro para caracterizar sustancias de acuerdo con sus propiedades de absorción y emisión de luz. Igualmente, en el caso de muestras complejas, tales como vino, ha sido posible la cuantificación de parámetros integrales (indicadores de color) y de compuestos específicos (antocianinas y polifenoles) con la ayuda de análisis multivariante de las huellas dactilares espectrales[610]. Se ha diseñado una plataforma óptico-potenciométrica basada en porfirinoides dispersos en membranas en PVC, usando los elementos sensores tanto como electrodos como membranas cromóforas. La matriz sensora permitió la evaluación y discriminación entre muestras de aceituna y semillas[611]. En aplicaciones basadas en medida de fluorescencia, la CSPT ha sido utilizada para la detección de la unión de cadenas complementarias de ADN mediante la interacción no covalente del ADN con un derivado fluorescente del politiofeno. La señal combinada de absorción-emisión puede llegar a detectar mediante esta plataforma hasta 15 μM de ADN[612].

Una característica interesante de la plataforma CSPT es que evalúa simultáneamente las propiedades tanto de absorción como de emisión. El componente de emisión puede ser obtenido a partir de la luz transmitida, convirtiéndolo en un sistema fácil para la adquisición de huellas dactilares de

---

608 D. Filippini, C. Di Natale, R. Paolesse, A. D'Amico, I. Lundström. *Computer screen photo-assisted techniques for global monitoring of environmental and sanitary parameters*. Sens. Actuators B, 121 (2007) 93-102

609 A. Alimelli, G. Pennazza, M. Santonico, R. Paolesse, D. Filippini, A D'Amico, I. Lundström, C. Di Natale. *Fish freshness detection by a computer screen photoassisted based gas sensor array*. Anal. Chim. Acta, 582 (2007) 320-328

610 A. Alimelli, D. Filippini, R. Paolesse, S. Moretti, G. Ciolfi, A. D'Amico, I. Lundström, C. Di Natale. *Direct quantitative evaluation of complex substances using computer screen photo-assisted technology: The case of red wine*. Anal. Chim. Acta, 597 (2007) 103-112

611 L. Tortora, M. Stefanelli, M. Mastroianni, L. Lvova, C. Di Natale, A. D'Amico, D. Filippini, I. Lundström, R. Paolesse. *The hyphenated CSPT-potentiometric analytical system: An application for vegetable oil quality control*. Sens. Actuators B, 142 (2009) 457-463

612 D. Filippini, P. Åsberg, P. Nilsson, O. Inganäs, I. Lundström. *Computer screen photo-assisted detection of complementary DNA strands using a luminescent zwitterionic polythiophene derivative*. Sens. Actuators B, 113 (2006) 410-418

sustancias fluorescentes[613]. La CSPT visualiza las diferentes contribuciones de la muestra, tanto de emisión como de absorción, dependiendo de la posición espectral relativa con respecto a los filtros de la cámara, capturando la firma espectral de la muestra cuando se excitó mediante una secuencia de color controlada[614].

Cabe mencionar que, tras analizar las características espectroscópicas de diversas clases de muestras, se han desarrollado otras técnicas usando pantallas de ordenador añadidas. En 2002, Lundström y Filippini desarrollaron una técnica basada en la *Scanning Light Pulse Technique* (SLPT) para generar imágenes químicas que son respuestas espacialmente resueltas de dispositivos de efecto de campo a los estímulos químicos[615]. Recientemente, se ha comprobado el funcionamiento del mismo simple dispositivo, fabricado a partir de una pantalla de ordenador y una cámara digital, para la resolución de ángulos y espectros de imágenes obtenidas mediante la técnica de Resonancia de Plasmón Superficial (SPR) de finas capas de oro y plata sobre las que estaban inmovilizadas proteínas[616]. Eventualmente, es también posible la medida elipsométrica del espesor con resolución en el rango de nanómetros[617].

---

[613] J.W.P. Bakker, D. Filippini, I. Lundström. *Enhancing classification capabilities of computer screen photo-assisted fluorescence fingerprinting*. Sens. Actuators B, 110 (2005) 190-194

[614] D. Filippini, J. Bakker, I. Lundström. *Fingerprinting of fluorescent substances for diagnostic purposes using computer screen illumination*. Sens. Actuators B, 106 (2005) 302-310

[615] D. Filippini, I. Lundström. *Chemical imaging by a computer screen aided scanning light pulse technique*. Applied Physics Lett., 81(20) (2002) 3891-3893

[616] D. Filippini, F. Winquist, I. Lundström, *Computer screen photo-excited surface plasmon resonance imaging*. Anal. Chim. Acta, 625 (2008) 207-214

[617] J.W.P. Bakker, H. Arwin, I. Lundström, D. Filippini. *Computer screen photoassist photoassisted off-null ellipsometry*. Applied Optics, 45 (2006) 7795-7799

2. OBJETIVOS

El objetivo general del trabajo que se presenta en este capítulo es:

- Poner las bases para el desarrollo de una lengua electrónica basada en una matriz ortogonal óptico-potenciométrica para discriminación de sabores en disolución.

Los objetivos particulares a alcanzar son:

- Preparación de membranas basadas en metaloporfirinas mediante deposición y evaporación directa sobre soportes conductores y transparentes de disoluciones conteniendo las porfirinas.

- Utilización del espacio de color RGB y la coordenada tonal H del espacio de color HSV como parámetros analíticos.

- Caracterización de las diferentes membranas utilizando los dos sistemas de transducción, óptico y potenciométrico, por separado sobre un conjunto de analitos modelo representativos de los cinco sabores humanos.

REPORT

Toward an optical-potentiometric porphyrin-based array for taste sensation discrimination in aqueous solution

S. Capel-Cuevas[a], F. Dini[b], C. Di Natale[b], P. Medaglia[c], I. Lundström[d], I. de Orbe-Payá[a], L.F. Capitán-Vallvey[a]

[a]*ECSens. Department of Analytical Chemistry. University of Granada, E-18071 Granada, Spain*

[b]*Department of Electronic Engineering. University of Rome "Tor Vergata", 00133 Rome, Italy*

[c]*Department of Mechanical Engineering. University of Rome "Tor Vergata", 00133 Rome, Italy*

[d]*Department of Physics, Chemistry and Biology. University of Linköping, SE-58183 Linköping, Sweden*

Abstract

Aluminium-doped zinc oxide (AZO) and indium-doped tin oxide (ITO) layers were used as transparent and conductive substrates for the preparation of an electronic tongue based on simultaneous optical and potentiometric transductions. The membranes were prepared using a casting technique from different THF solutions containing different metalloporphyrins, high molecular weight polyvinyl chloride (PVC) and dioctyl sebacate (DOS) as plasticizer. AZO and ITO glass slides were employed as transparent supports to prepare electrodes for potentiometric measurements, and chromophore spots for the CSPT technique.

The membranes measured separately with the two transduction setups were characterized in terms of stability, sensitivity and reproducibility towards the detection of model analytes, such as acetic acid, ethanol and ammonia, in the concentration range of 10^{-4} to 3 M. The sensing array was then tested to verify its response to five compounds selected as representative of human tastes: salty (NaCl), sweet (glucose), sour (HCl), bitter (quinine) and umami (monosodium glutamate). The results obtained were sufficiently different, both in potentiometric

and optical terms, for the five chemical models. This paves the way to the development of a hyphenated electronic tongue based on optical and potentiometric transductions that could represent a significant improvement in electronic tongues.

1. Introduction

Since the 1980s, the integration of chemical sensors in arrays has shown to be an advantageous solution in the measurement of environments characterized by the simultaneous presence of several compounds [1]. In this configuration, in fact, sensors do not necessarily have to be specific for a target analyte, but they can rather be broadly selective or even not selective at all, with the only necessary requisite being that they behave differently from each other, i.e. they provide partially correlated responses. In an analogy between this approach and the working mechanism of mammalian "chemical" senses, olfaction and taste, these sensor arrays are generally called either electronic noses (vapour phase sensors) or electronic tongues (liquid phase sensors). After the first approach by Persaud and Dodd [2], the development of electronic noses has become a well-consolidated field of research, several examples of these arrays have been widely reported in the literature and different instruments are also commercially available on the market [3].

In 1985 [4], multivariate analysis with arrays of ion-selective electrodes were proposed, and the first electronic tongue, based on ion-selective electrodes functionalised with lipid membranes, was proposed in 1990 by Toko et al. [5]. Electronic tongues based on ion-selective electrodes were then elaborated using a set of chalcogenide glasses-based electrodes, for both quantitative [6] and qualitative [7] analysis. Since then, different sensing principles have been employed in electronic tongues, the most prevalent being electrochemical [8-10] (potentiometric, voltammetric and amperometric), piezoelectric and optical [11],[12] techniques.

The development of sensing systems where two different transduction principles are simultaneously used could represent a viable approach to achieving high performance sensing systems. Porphyrins have been widely used as

ionophores in potentiometric electronic tongues based on ion-selective electrodes [13]. Additionally, porphyrins are dyes that are able to change colour when exposed to chemicals. These classes of molecules are fundamental in many natural processes, and their functions as complexing ligands or redox catalysts are essential for all living beings [14]. A large number of modified tetrapyrroles is present in nature or has been synthesized in laboratories. The properties of these macrocycles can be tuned by simple modifications to the basic molecular framework and these skeletal variations are used by nature to optimise the biological activities of different tetrapyrroles. Arrays of porphyrins have been used to detect different volatile compounds with an arrangement known as a Computer Screen Photoassisted Technique (CSPT), consisting of a computer camera that acquires subsequent images of the layer under the illumination of an LCD screen [15].

AZO is a highly conductive and transparent material that can be grown either on sapphire or glass. It thus represents a suitable substrate to develop a system that merges both optical and potentiometric transductions [16]. The aim of this study was the development of an optical-potentiometric artificial tongue based on a porphyrinoid material dispersed in a PVC membrane deposited on an AZO or ITO substrate to discriminate between the five fundamental tastes. Moreover patterning the layers could make it possible to develop a miniaturized and integrated sensor array where both principles are employed on the same substrate.

2. Experimental

2.1. Reagents and materials

The metallotetraporphyrins complexes used for preparing the pH-sensitive membranes were zinc (II) tetraphenylporphyrin (ZnTPP), zinc (II) 5,10,15,20-tetrakis(4-tert-butylphenyl)-porphyrin (ZnTBPP), tin (IV) tetraphenylporphyrin (SnTPP), tin (IV) 5,10,15,20-tetrakis(4-tert-butylphenyl)-porphyrin (SnTBPP), manganese (III) tetraphenylporphyrin (MnTPP), molybdenum(V) tetraphenylporphyrin (MoTPP), molybdenum (V) tetraphenylporphyrin bromide

(Mo(TPP)Br), chrome (III) tetraphenylporphyrin (CrTPP) and chrome (III) 5,10,15,20-tetrakis(4-tert-butylphenyl)-porphyrin (CrTBPP). Other chemical used to prepare the sensitive films were high molecular weight poly(vinyl chloride) (PVC), dioctyl sebacate (DOS), 5-amino-9-(diethylamino)benzo[a]phenoxazin-7-ium chloride (Nile blue), 4,4'-(1,1-dioxido-3H-2,1-benzoxathiol-3-ylidene)bis(2-bromo-6-methyl-phenol) (bromocresol purple), all purchased from Fluka, while tetrahydrofuran (THF) was received from Carlo Erba Reagents. Ammonium, acetic acid, ethanol, hydrochloric acid, sodium chloride, glucose, quinine and monosodium glutamate were supplied by Sigma-Aldrich. All chemicals were of analytical grade and used without further purification, while the THF was freshly distilled prior to use. Aluminium-doped zinc oxide (AZO) and indium-doped tin oxide (ITO) layers were used as transparent and conductive substrates. All solutions were prepared in reverse-osmosis type quality water (Milli-RO 12 plus Milli-Q station from Millipore, conductivity 18.2 Mohm/cm).

2.2 Instruments and Software

A TSP-based model 2602A dual-channel System Sourcemeter (Keithley, Peschiera Borromeo, Italy) (figure 9.1a) and a UV lamp model VL-4L 4 W: 365 nm (Vilber Lourmat, Marne-la-Vallée, France) were used for potentiometric measurements. The CSPT platform includes a regular LCD screen (Philips 170S4) used as a light source and a Philips webcam SPC900NC (figure 9.1b) operating at a resolution of 640 x 480 pixels and a 8x digital zoom as the image detector. For the results comparison, a conventional 10 Mpixels camera with a 28 mm wide-angle lens and a 5x optical zoom was used, illuminating with two white miniLED 12V lamps. For the measurement of pH and electrical conductivity, a 3-channel Multimeter 44 / 44 P (Crison, Lainate, Italy) was used.

a b

Figure 9.1. Instruments used for potentiometric and optical measurements. a: sourcemeter; b: webcam

The images were processed with a set of scripts and functions developed in Matlab® (v.7.6, MathWorks, 2008, Inc., Natick, MA, USA). Microsoft Excel (Microsoft Corp., Redmond, WA, USA) was used for general calculations.

2.3. Preparation of sensing membranes

The different cocktails were prepared by dissolution in 1mL of freshly distilled THF according to the following composition: 100 mg weight consisted of 1% (w/w) metalloporphyrin, PVC/DOS (1:2) and varying amounts of NB or BCP. The mixture was cast on transparent aluminium zinc oxide (AZO, surface resistivity 150-250 Ω/sq) or indium tin oxide (ITO, Sigma–Aldrich, conductive layer 300 Å, surface resistivity 30-60 Ω/sq) modified 1x1 cm glass slides. The AZO layer was grown on a sapphire substrate by the pulsed laser deposition (PLD) technique. The solvent was allowed to evaporate overnight. Potentiometric and optical properties of the sensor array were evaluated one day after preparation.

The sensor arrays composed of 9 potentiometric polymeric membranes were deposited on AZO or ITO modified glass slides. Separate electrical channels were made by cutting the conductive layers and they were connected to a dual-channel system sourcemeter. Electrodes were assembled in an array configuration and immersed simultaneously in the measured samples. The

potential changes in the sensors arrays were measured versus a saturated calomel reference electrode (SCE, AMEL, Italy), immersed in the outlet chamber. All measurements were performed at room temperature (≈25 ◦C), carried out with the following potentiometric cell: SCE; KCl sat/sample solution//membrane//AZO (or ITO) WE. A combined double junction glass electrode with Ag/AgCl as the reference electrode, calibrated against two standard buffer solutions (pH 4.0 and 7.0), was used for pH measurements.

2.4. Response evaluation

In the first arrangement, the membranes were measured separately with the two transduction setups and characterized in terms of stability, sensitivity and reproducibility towards the detection of model analytes such as ammonia, glutamate, ethanol and acetic acid in the concentration range from 10^{-4} to 3 M.

In the case of the experimental set-up used to carry out the potentiometric study, the response of each membrane deposited on AZO or ITO supports was evaluated by adding different volumes of the analytes under study to an aqueous solution containing the membrane hanging from a support with an alligator clip. Variations in pH and electrical conductivity of solutions were controlled with a 3-channel multimeter.

For CSPT measurement, the functionalized AZO or ITO slides were inserted in a Petri dish where the analyte solutions were introduced with a syringe. Colour changes in the sensing spots were transduced through a setup consisting of a computer screen that illuminates the sample and a webcam that acquires images of the layers (figure 9.2). The system was covered to prevent interference from external light.

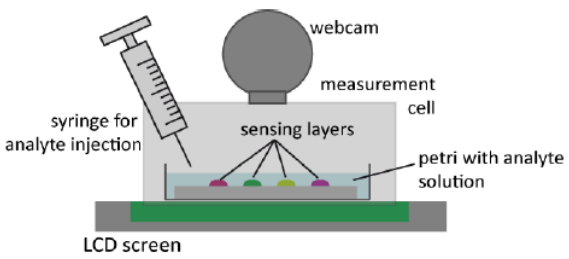

Figure 9.2. Scheme of the arrangement for CSPT measurement

2.5. CSPT measurements

During a CSPT measurement, the web camera captures the image of the array under two illuminating sequences provided by the screen (one rainbow of 50 colours and another of red [255 0 0], green [0 255 0] and blue [0 0 255] colours).

The light emerging from the assay is simultaneously acquired by the camera operating at a maximum capture rate of 90 frames/s. The result of this measurement is a digital video file (.avi format) of the array under different illuminating colours that is then decomposed into individual frames. From this video stream, a 5 mm diameter centred region of interest (ROI) for each sensing layer was selected (figure II.26) and the information extracted. The RGB values of the pixel enclosed by a ROI were averaged and a fingerprint for each sensitive layer of each substance was then calculated, subtracting the RGB sequence of the background. This subtraction is necessary to take into account the non-homogeneity of the computer screen illuminated camera images.

Red, green and blue channel signals are concatenated in this order and a fingerprint vector for each sensing layer is formed. This is a vector containing 50 (illumination colours)*3 (camera channels) elements. Eventually, the fingerprints of all the spots are composed into a single fingerprint of the array. Fingerprints were smoothed with a Savitzy–Golay filter [17] in order to remove the fluctuations mostly due to the instability of the computer screen. Software written in Matlab® controlled the illuminating sequence, the video acquisition, and extracted the information (CSPT fingerprints) from manually selected ROIs (defining the position and the radius). Fingerprints were then treated as spectral data and analyzed using multivariate techniques.

3. Results and discussion

First we studied the potentiometric behaviour of the prepared PVC membranes containing metalloporphyrins and DOS as plasticizer on AZO and ITO supports. The variation in the potential in the presence of different chemicals used as a model (ammonia, monosodium glutamate, ethanol and acetic acid) was measured. To do this, the supports containing the membrane were immersed

in purified water and different volumes of model analytes were tested, measuring both in dark conditions and illuminating with a LED or a UV lamp. As an example, figure 9.3 shows the evolution of the measured potential with the logarithm of aqueous ammonia concentration for different membranes containing ZnTPP prepared on the two supports tested.

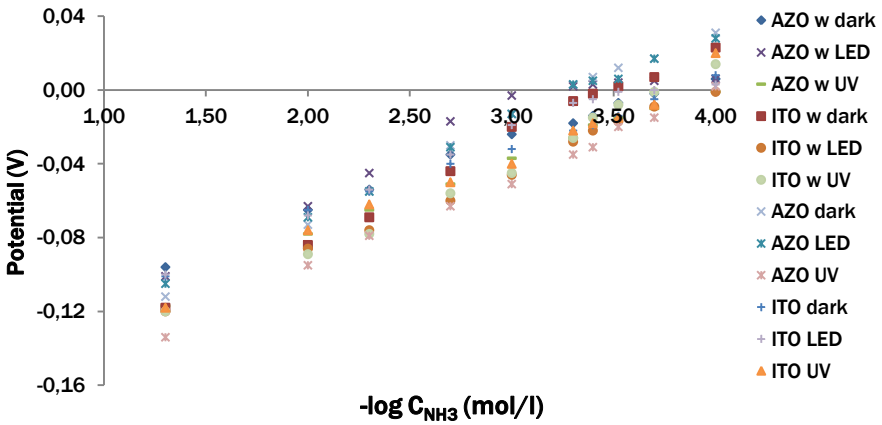

Figure 9.3. Evolution of the potential with ammonia concentration for ZnTPP-based membrane on AZO and ITO supports. w: support without membrane

Later, a similar study was carried out, but only using the AZO support with or without the membrane and measuring in dark conditions or with a UV lamp illuminating the support. It was observed that the illumination of the membrane with a white LED does not modify the signal, while in the case of UV illumination, the potentiometric signal strength decreases when the lamp is connected, recovering the signal when it is turned off (figure 9.4).

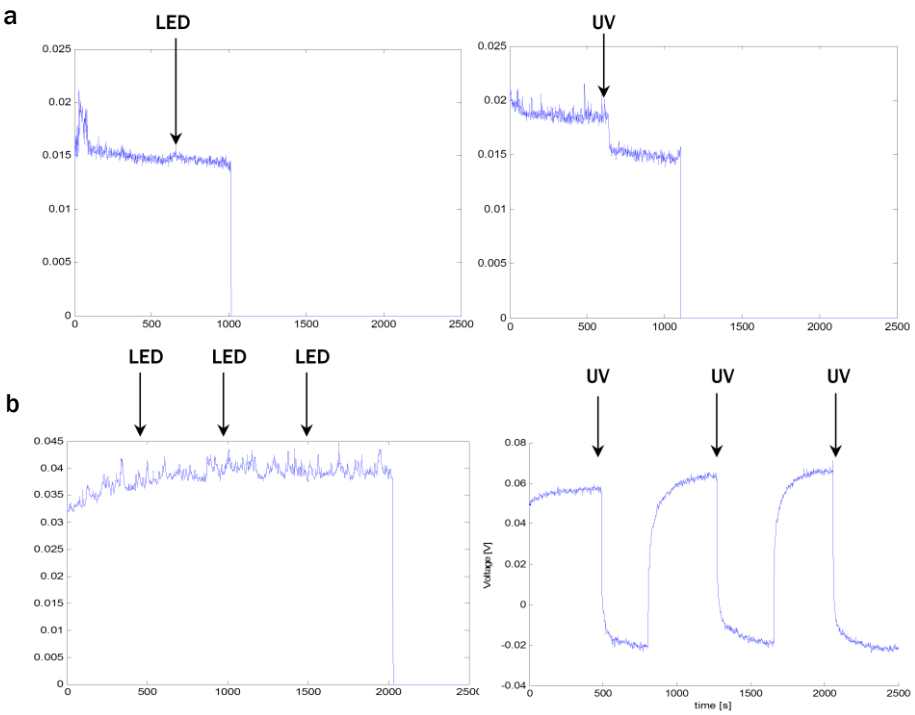

Figure 9.4. Influence of illumination (LED and UV lamp) on the potentiometric signal. a: AZO support without membrane; b: AZO support with membrane

Figure 9.5 shows the variation in the potential of the prepared electrodes on AZO support with or without ZnTPP when different concentrations of ammonia, monosodium glutamate, ethanol and acetic acid were tested.

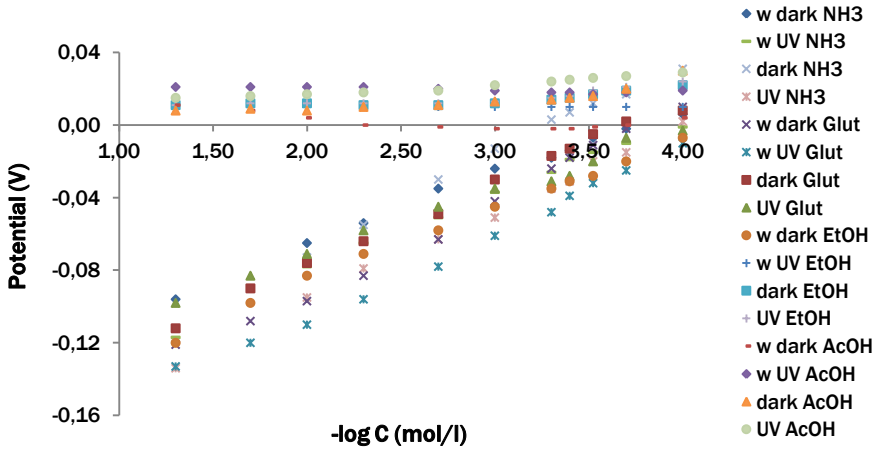

Figure 9.5. Evolution of the potential for electrodes prepared on AZO support with and without ZnTPP membrane. w: without, NH_3: ammonia, Glut: monosodium glutamate, EtOH: ethanol, AcOH: acetic acid

While measuring the evolution of the potential with the analyte concentration, the variations in pH and the electrical conductivity of the solutions were controlled with a 3-channel multimeter. Figures 9.6-9.9 show examples of the pH and electrical conductivity variations of the solutions during the measurements.

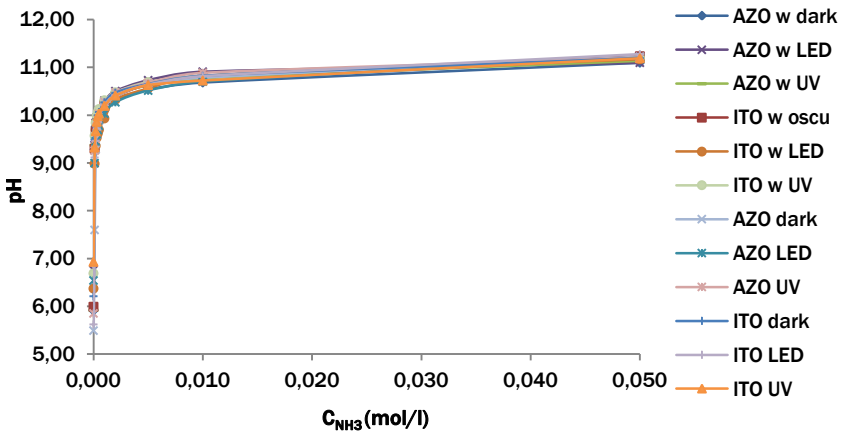

Figure 9.6. pH solution variations with the increasing of ammonia concentration. w: without membrane

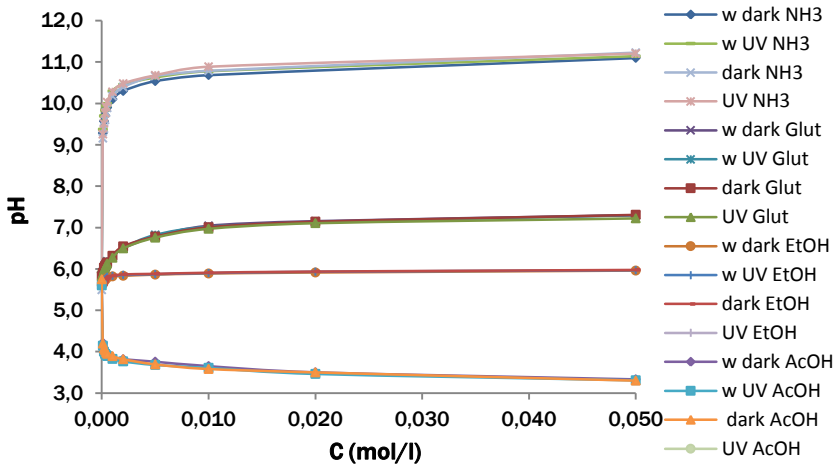

Figure 9.7. pH solution variations with the increasing of analyte concentrations. w: without membrane, NH3: ammonia, Glut: monosodium glutamate, EtOH: ethanol, AcOH: acetic acid

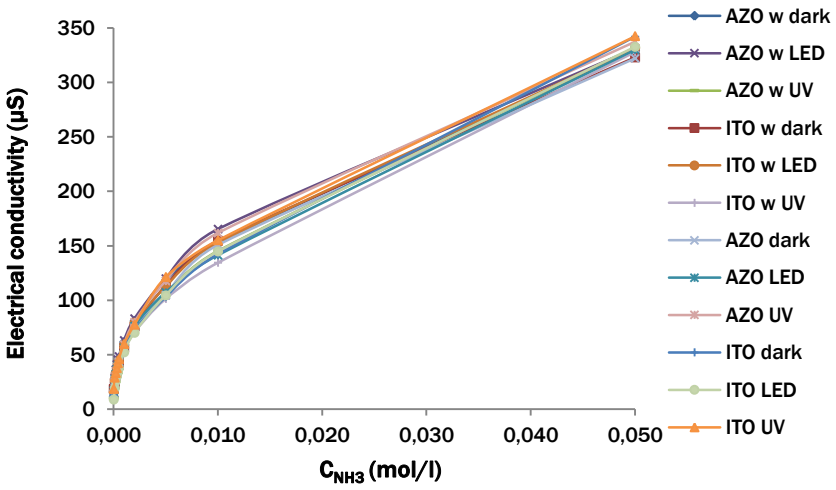

Figure 9.8. Electrical conductivity variations with the increasing of ammonia concentration. w: without membrane

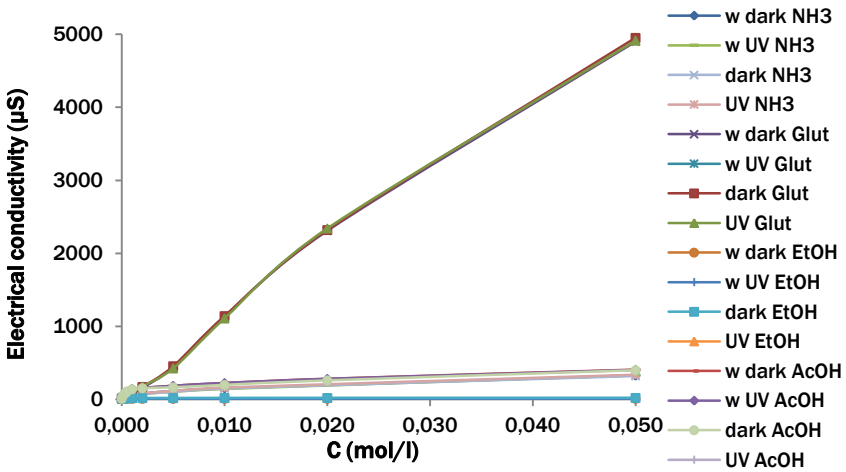

Figure 9.9. pH solution variations with the increasing of analyte concentrations. w: without membrane, NH3: ammonia, Glut: monosodium glutamate, EtOH: ethanol, AcOH: acetic acid

From the figures, it can be observed that the presence of the membranes does not modify, as expected, the pH and electrical conductivity values. These parameters only depend on the analyte concentration.

After studying the evolution of the potential of the prepared electrodes on

transparent support with the concentration of the selected analytes, the CSPT platform was used to study the evolution of the optical properties of the same membranes. First of all, the absorption spectra of the supports with and without membrane deposited were carried out to verify the absorption properties of the different membranes containing metallic tetraphenylporphirins. As an example, figure 9.10 shows the absorption spectra of the supports with and without the ZnTPP-based membrane deposited. The membrane was also deposited on a glass support for comparison purposes.

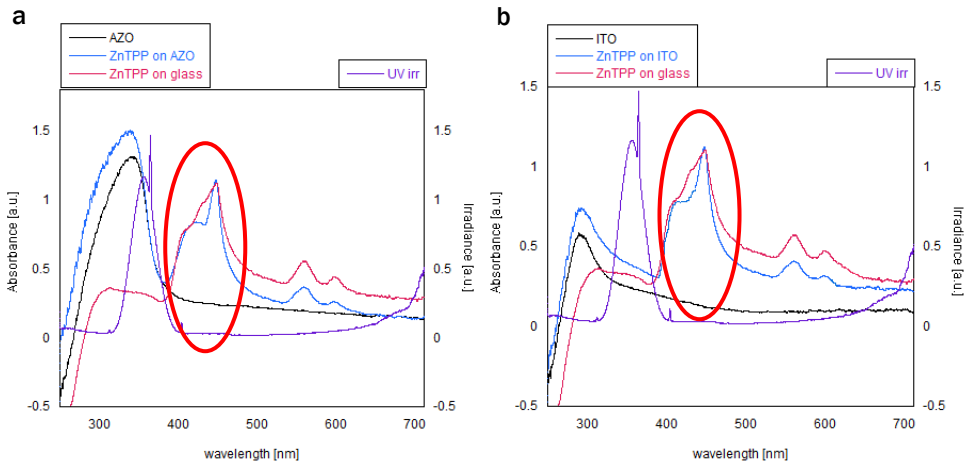

Figure 9.10. Absorption spectra of the supports with or without ZnTPP-based membrane deposited. a: AZO; b: ITO

Figure 9.11 shows an example of an image of the sensor array taken with the webcam of the CSPT system, illuminating the sample from below with the computer screen.

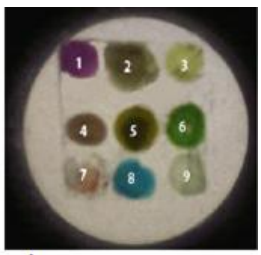

Figure 9.11. Image of the sensor array taken with the CSPT system

Colour measurements were carried out with a white screen light and a 50 colour sequence ranging from red to blue, and as analytical parameters, the RGB colour space and the hue coordinate H of the HSV colour space were selected [18]. RGB measurements were analyzed calculating the average intensity of the spot for every illuminating colour, while the mode of the set of H data obtained from all pixels of the membrane was used as the representative value. To compare results, the membrane was also measured using an arrangement consisting of a conventional 10 Mpixel camera with a 28 mm wide-angle lens and a 5x optical zoom, illuminating with two white miniLED 12V lamps working in continuous shot mode.

The spectral variations of metalloporphyrins were plotted in a colour scale ranging from dark red to yellow for increases in the analyte concentration. Figure 9.12 shows, as an example, the spectra of two membranes containing ZnTBPP in the first case, and MoTPP and BCP in the second one, when the ammonia concentration changes, measured with the 50 colour sequence.

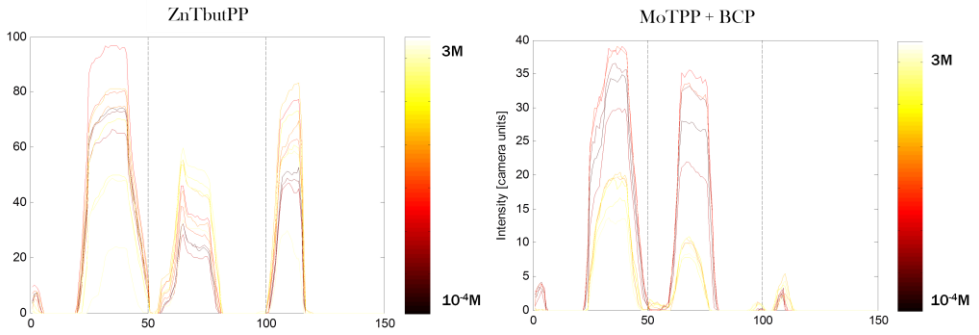

Figure 9.12. Spectral variations of ZnTBPP and MoTPP+BCP membranes against variations of ammonia concentration obtained with a sequence of 50 colours with the CSPT platform

Below are some examples of the optical results obtained (figure 9.13). The first three graphs correspond to the H, S and V variations of one membrane included in one of the sensor arrays. The rest of the graphs show the H, S and V variations for three different membranes when the concentration of the different analytes changes.

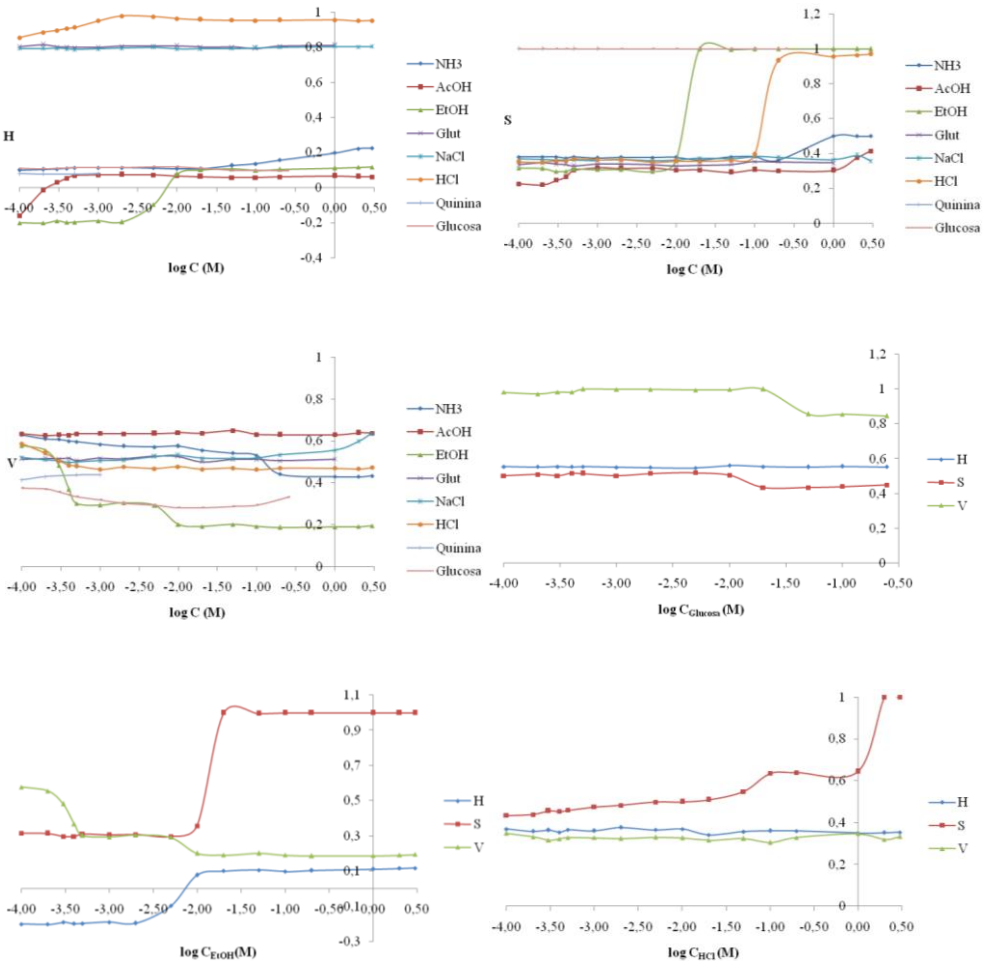

Figure 9.13. Examples of H, S and V variations for some membranes when the concentration of the different analytes changes

The data obtained measuring potential, colour coordinates and CSPT system for the different chemicals selected as models show interesting changes in the different analytical parameters. These results open the door to the use of a hyphenated CSPT/potentiometry system, as the design in figure 9.14 indicates, in which the use of a transparent, conductive support allows for the simultaneous measurement of optical and potentiometric responses of porphyrin-based arrays to the analyte model, with the final aim of developing an electronic tongue for taste sensation discrimination.

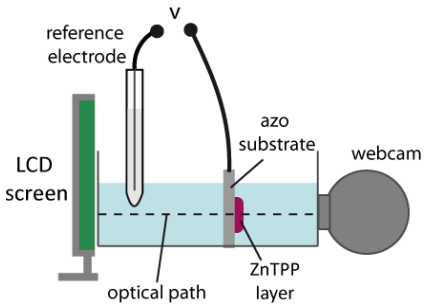

Figure 9.14. Scheme of the preliminary arrangement for the development of the hyphenated optical and potentiometric platform

4. Conclusions

The results obtained demonstrated that the combined use of potentiometric and CSPT techniques in a platform can provide a significant improvement in information and the classification of human tastes with respect to individual methods. Considering the simplicity of the integrated experimental apparatus, the hyphenated CSPT-potentiometric analytical system could provide a promising sensing platform for electronic tongues with great potential. Further exploration of the system is currently ongoing in our laboratories.

Finally, the discrimination of compounds, each belonging to one of the five fundamental tastes, has been shown to be a basic step in the development of porphyrin-based taste sensor systems for a variety of applications.

References

[1] S. Zaromb, J.R. Stetter. *Theoretical basis for identification and measurement of air contaminants using an array of sensors having partly overlapping selectivities*. Sens. Actuators, 6 (1984) 225-244.

[2] K.C. Persaud, G. Dodd. *Analysis of discrimination mechanisms in the mammalian olfactory using model nose*. Nature, 299 (1982) 352-355.

[3] J. Gardner, T. Pearce, T. Nagle, S.S. Schiffmann (Eds.). *Handbook of Machine Olfaction*. Wiley/VCH, New York/Weinheim (2002).

[4] M. Otto, J.D.R. Thomas. *Model studies in multiple chemical of free magnesium, sodium, and potassium at physiological concentration levels with ion-selective electrodes*. Anal. Chem., 57(13) (1985) 2647-2651.

[5] H. Hayashi, M. Yamanaka, K. Toko, K. Yamafuji. *Multichannel taste sensor using lipid membranes*. Sens. Actuators B, 2 (1990) 205-213.

[6] C. Di Natale, F. Davide, J. Brunink, A. D'Amico, Yu. Vlasov, A. Legin, A. Rudnitskaya. *Multicomponent analysis of heavy metal cations and inorganic anions in liquids by a non-selective chalcogenide glass sensor array*. Sens. Actuators B, 34 (1996) 539-542.

[7] A. Legin, A. Rudnitskaya, Yu. Vlasov, C. Di Natale, F. Davide, A. D'Amico. *Tasting of beverages using an electronic tongue*. Sens. Actuators B, 44 (1997) 291-296.

[8] F. Winquist, P. Wide, I. Lundström. *An electronic tongue based on voltammetry*. Anal. Chim. Acta, 357 (1997) 21-31.

[9] P. Ciosek, W. Wroblewski. *Sensor arrays for liquid sensing – electronic tongue Systems*. Analyst, 132(10) (2007) 963-976.

[10] A.K. Deisingh, D.C. Stone, M. Thompson. *Applications of electronic noses and tongues in food analysis*. Int. J. Food Sci. Technol., 39(6) (2004) 587-604.

[11] Y. Vlasov, A. Legin, A. Rudnitskaya. *Electronic tongues and their analytical application*. Anal. Bioanal. Chem., 373(3) (2002) 136-146.

[12] J.J. Lavigne, S. Savoy, M.B. Clevenger, J.E. Ritchie, B. McDoniel, S.J. Yoo, E.V. Anslyn, J.T. McDevitt, J.B. Shear, D. Neikirk. *Solution based analysis of multiple analytes by a sensor array: toward the development of an electronic tongue*. J. Am. Chem. Soc., 120 (1998) 6429-6430.

[13] L. Lvova, R. Paolesse, C. Di Natale, A. D'Amico. *Detection of alcohols in beverages: An application of porphyrin-based Electronic tongue*. Sens. Actuators B, B118 (1-2) (2006) 439-447.

[14] D. Dolphin (Ed.). *The Porphyrins*. Vols. VI (Part A) and VII (Part B), Academic Press, New York (1978).

[15] D. Filippini, A. Alimelli, C. Di Natale, R. Paolesse, A. D'Amico, I. Lundström. *Chemical sensing with familiar devices*. Angew. Chem. Int. Ed., 45(23) (2006) 3800-3803.

[16] M. Zhou, D.G. Yi, Z.M. Yu, L.R. Xiao, J. Li. *Preparation of aluminum doped zinc oxide films and the study of their microstructure, electrical and optical properties*. Thin Solid Films, 515(17) (2007) 6909-6914.

[17] S. Capel-Cuevas, M.P. Cuéllar, I. de Orbe-Payá, M.C. Pegalajar, L.F. Capitán-Vallvey. *Full-range optical pH sensor based on imaging techniques*. Anal. Chim. Acta, 681 (2010) 71-81.

[18] A. Savitsky, M. Golay. *Smoothing and differentiation of data by simplified least squares procedures*. Anal. Chem., 36 (1964) 1627–1639.

3. CONCLUSIONES

El objetivo de este capítulo ha sido explorar las posibilidades de uso de medidas simultáneas de potencial y color usando la técnica CSTP para el desarrollo de una lengua para discriminación de sabores.

Como principales conclusiones podemos resaltar las siguientes:

- Se han preparado membranas basadas en metaloporfirinas mediante deposición y evaporación directa sobre los soportes transparentes AZO e ITO de disoluciones en THF conteniendo las porfirinas.

- Se han caracterizado las diferentes membranas utilizando los dos sistemas de transducción por separado y se han analizado usando como analitos modelo amoníaco, etanol, ácido acético y glutamato monosódico en el rango de concentraciones 10^{-4} a 3 M y, posteriormente, se han medido disoluciones de diversa concentración de analitos representativos de los cinco sabores humanos diferentes.

- Los resultados obtenidos para los diferentes analitos modelo estudiados, tanto en potencial como en coordenadas cromáticas a partir del sistema CSPT, muestran unos cambios considerables. Esto plantea interesantes perspectivas sobre el uso de un sistema que utilice informacion óptica y potenciométrica integrada en una lengua electronica.

.

CONCLUSIONS

As a result of the research done for this PhD dissertation to achieve the ultimate goal of designing a sensing system for the pH measurement of aqueous solutions in the full range (0-14) by means of colour acquisition, we obtained the following conclusions:

1. A novel colour-based disposable sensor array for full pH range (0-14) measurement was developed. The pH sensing elements were prepared from a set of different acid-base indicators immobilized in plasticized polymeric membranes working by an ion-exchange or co-extraction mechanism. The colour changes of the 11 selected sensing elements were obtained from a commercial scanner using the H coordinate of the hue, saturation, value (HSV) colour space as the analytical parameter.

2. Three different approaches for pH prediction from the H of the sensing elements were studied: linear surface, sigmoid surface and sigmoid competition models, providing an MSE of 0.111, 0.075 and 0.266, respectively. Considering not only the performance of the approach but also the background aspects regarding the hardware, where it would be implemented, the sigmoid function competition approach might be a good choice if the electronic device has some memory limitations. However, for real-time processing requirements, the other two approaches could be used.

3. Different artificial intelligence techniques (artificial neural networks, genetic algorithms and expert systems) were applied to the model data. The neural network was trained with the calibration data set using the Levenberg-Marquardt training method. The network structure, comprising 11 input neurons (each matching the hue of each single element in the sensor array), 1 output (the pH approximation value) and 1 hidden layer with 10 hidden neurons, provided an MSE of 0.010 in the training data, 0.018 in the validation data and 0.043 in the test data coming from a set of real water samples.

   Then, as the initial array made up of 11 sensing elements involved complex treatment and a high consumption of computational time, which could complicate implementation in portable devices with low processing capacity, the number of elements was reduced. The aim was not only to

find the optimal minimum elements necessary to achieve a high prediction performance, but also to design a prediction model with optimal network performance. To achieve these goals, a multi-objective hybrid genetic algorithm based on NSGA-II and the Levenberg-Marquardt non-linear optimization technique was developed. A solution from the Pareto front was selected, concluding that the use of an array made up of 4 sensing elements offers a good pH prediction (MSE of 0.052) working with 4 hidden neurons.

Neural networks are black boxes whose operation cannot be easily modelled and explained for industrial development validation. To overcome these limitations, an expert system was applied. The rules can be easily understood by a user and may be modified without the need for recalibration for later developments or changes in the system, obtaining an MSE of 0.080 in real water samples.

4. A portable optical multianalyte instrument with an OLED programmable display as light source and an array of twelve digital colour detectors was developed and used for pH determination in the full range. A complete analytical and technical characterization was carried out, showing good agreement with pH measurements from reference instruments. This resulted in a microcontrol-based easy-to-use measurement system with high optical and electrical interference immunity, and extremely simple digital signal processing circuitry with commercially available electronic components. The pH response of the four selected sensing elements was modelled, and calibration curves –acquired using a computer– were applied to water samples obtaining an MSE of 0.180, which is worse than those obtained in previous studies using a sigmoid competition approach or neural networks, but acceptable for a portable instrument.

5. Then, a multi-objective neural network calibration procedure was designed, with the aim of minimising prediction model complexity and the number of sensing elements and maximising accuracy. The method returned a set of optimal solutions that could be implemented in the portable instrument. Thus, an optimal solution considering further industrial development decisions such as energy saving, computing time

response, array development costs and instrument minimisation was selected. The portable instrument was validated with a neural network that uses an input array with 11 sensing elements, obtaining an MSE of 0.028 in calibration data, 0.014 in validation data and 0.015 in test data. Finally, the method was applied to test pH prediction capabilities in beverages, personal care products and cleaning samples.

6. Different ionophores coming from 18-crown-6 ether and 4,13-diaza-18-crown-6 ether with different types of terminal groups were synthesized and characterized for sensing purposes. The exchange constant $K_{exch}^{IL_P}$ for each equilibrium with alkaline and alkaline-earth ions and membranes containing ionophores was calculated. Taking into account the selectivity, measured using the selectivity coefficients k_{IJ}^{Osel}, the ionophore containing (N-adamantylcarbamoyl) acetyl moiety generated the most selective membrane for calcium.

7. Aluminium-doped zinc oxide (AZO) and indium-doped tin oxide (ITO) layers were used as transparent and conductive substrates for the preparation of metalloporphyrin-based optical and potentiometric sensing membranes. The membranes were characterized using the two transduction setups in terms of stability, sensitivity and reproducibility towards the detection of model analytes, such as acetic acid, ethanol and ammonia, in the concentration range of 10^{-4} to 3 M, and then against five compounds selected as representative of the five fundamental human tastes: salty (NaCl), sweet (glucose), sour (HCl), bitter (quinine) and umami (monosodium glutamate). The results suggest that a hyphenated CSPT-potentiometric analytical system could provide a promising sensing platform for electronic tongues with great potential. Further exploration of the system is currently ongoing in our laboratories.

ANEXO

Publicaciones

Analytica Chimica Acta 681 (2010) 71–81

Contents lists available at ScienceDirect

Analytica Chimica Acta

journal homepage: www.elsevier.com/locate/aca

Full-range optical pH sensor based on imaging techniques

S. Capel-Cuevas[a], M.P. Cuéllar[b], I. de Orbe-Payá[a], M.C. Pegalajar[b], L.F. Capitán-Vallvey[a,*]

[a] Department of Analytical Chemistry, University of Granada, Faculty of Sciences, Avda. Fuentenueva s/n, E-18071, Granada, Spain
[b] Department of Computer Science and Artificial Intelligence, E.T.S. Ingenierías Informática y de Telecomunicación, University of Granada, C/ Periodista Daniel Saucedo Aranda s/n, E-18071, Granada, Spain

ARTICLE INFO

Article history:
Received 1 July 2010
Received in revised form
15 September 2010
Accepted 18 September 2010
Available online 25 September 2010

Keywords:
Full-range optical pH sensor
H coordinate
HSV colour space

ABSTRACT

A new colour-based disposable sensor array for a full pH range (0–14) is described. The pH sensing elements are a set of different pH indicators immobilized in plasticized polymeric membranes working by ion-exchange or co-extraction. The colour changes of the 11 elements of the optical array are obtained from a commercial scanner using the hue or *H* component of the hue, saturation, value (*HSV*) colour space, which provides a robust and precise parameter, as the analytical parameter. Three different approaches for pH prediction from the hue *H* of the array of sensing elements previously equilibrated with an unknown solution were studied: Linear model, Sigmoid competition model and Sigmoid surface model providing mean square errors (MSE) of 0.1115, 0.0751 and 0.2663, respectively, in the full-range studied (0–14). The performance of the optical disposable sensor was tested for pH measurement, validating the results against a potentiometric reference procedure. The proposed method is quick, inexpensive, selective and sensitive and produces results similar to other more complex optical approaches for broad pH sensing.

1. Introduction

pH measurement by potentiometry is the standard technique because of its simplicity, speed, precision, reversibility and inexpensiveness, but in some applications, optical sensors offer some advantages, mainly insensitivity to electrical interferences, electrical safety, lack of the need for a reference element, presentation as low-cost disposable, autoclavable, precalibrated sensor patches and better characteristics when measuring extreme pH values, low ionic strength solutions or in the presence of organic matter.

Optical pH sensors are mainly based on reversible changes in the indicator's structure induced by pH and translated into changes in spectroscopic phenomena such as absorption, reflectance, luminescence, and energy transfer. Notwithstanding, some optical sensors not based on acid–base indicators exist, such as that based on changes in the ionization of uncladded silica optic fibre by pH traced by methylene blue adsorption via evanescent field [1] and the pH-dependent polymer swelling of functionalized polymer microspheres dispersed in a hydrogel membrane that change the membrane turbidity [2].

Unlike potentiometric pH determination, in which the pH depends linearly on the activity of hydrogen ions, pH in optical sensors is a function of the concentration of the acid and basic forms of the indicator [3]. Thus, calibration functions in pH sensors come from mass-action law relationships between pH and radiation intensity, referring here only to absorption-based sensors, or experimental functions obtained by complete calibration in the case of pH-dependent interactions between indicator and matrix [4], and using in all cases: (a) single-intensity measurements both absolute [5], relative [6] or normalized signals [7] or (b) multiple intensity measurements as the intensity ratio at two or more wavelengths [8].

The immobilization of the indicating molecule is a key issue in determining the analytical and operational characteristics of pH sensors in any of the dispositions used: probe (optic fibre), flow or disposable format. Different types of immobilization techniques for pH indicating dyes have been used [9], including (a) dye entrapment in different materials such as cellulose acetate [10,11], sol–gel [12], PVC [7], methacrylic–acrylic copolymers [13] and different composites like SiO_2/ZrO_2-organic polymer (styrene/methyl methacrylate copolymer or Nafion) [14], (b) retention of dye by ion-exchange materials such as Amberlite XAD-2 resin [15] or Dowex I-X10 resin [16], in some instances including the ion-exchanger containing dyes in polymeric encapsulated membranes using PVC [17], (c) adsorption of the dye on materials such as non-ionic styrene/divinylbenzene copolymer [18], polyester/lycra blends textile [19], cellulose [20], cellulose acetate [21], or polymer track membranes combining retention in surface and bulk [22], (d) covalent binding of dye by different synthetic strategies to form microparticles or membranes, in some cases formed on glass fibre,

* Corresponding author at: Department of Analytical Chemistry, University of Granada, Faculty of Sciences, Avda. Fuentenueva s/n, E-18071 Granada, Spain. Tel.: +34 958248436; fax: +34 958 243 328.
E-mail address: lcapitan@ugr.es (L.F. Capitán-Vallvey).

0003-2670/$ – see front matter © 2010 Elsevier B.V. All rights reserved.
doi:10.1016/j.aca.2010.09.033

[21] T.P. Jones, M.D. Porter, Anal. Chem. 60 (1988) 404.
[22] A. Dybko, W. Wroblewski, J. Maciejewski, R. Romaniuk, Z. Brzózka, Sens. Actuators B 39 (1997) 207.
[23] C. Munkholm, D.R. Walt, F.P. Milanovich, S.M. Klainer, Anal. Chem. 58 (1986) 1427.
[24] A. Safavi, M. Pakniat, Anal. Chim. Acta 335 (1996) 227.
[25] Y. Kostov, G. Rao, Rev. Sci. Instrum. 74 (2003) 4129.
[26] A. Holobar, B.H. Weigl, W. Trettnak, R. Benes, H. Lehmann, N.V. Rodriguez, A. Wollschlager, P. O'Leary, P. Raspor, O.S. Wolfbeis, Sens. Actuators B B11 (1993) 425.
[27] P. Hashemi, R.A. Zarjani, Sens. Actuators B 135 (2008) 112.
[28] T. Seung, C. Yang, Pol. Bull. 42 (1999) 655.
[29] S. De Marcos, C. Asensio, I. Urunuela, F. Gallarta, J. Galban, J.R. Castillo, Quim. Anal. 19 (2000) 99.
[30] S. De Marcos, O.S. Wolfbeis, Anal. Chim. Acta 334 (1996) 149.
[31] P. Hashemi, R.A. Zarjani, M.M. Abolghasemi, A. Olin, Sens. Actuators B 121 (2007) 396.
[32] M. Bacci, F. Baldini, A.M. Scheggi, Anal. Chim. Acta 207 (1988) 343.
[33] F.B.M. Suah, M. Ahmad, M.N. Taib, Sens. Actuators B 90 (2003) 175.
[34] A. Safavi, A. Rostamzadeh, S. Maesum, Talanta 68 (2006) 1469.
[35] U.W. Grummt, A. Pron, M. Zagorska, S. Lefrant, Anal. Chim. Acta 357 (1997) 253.
[36] Z. Ge, C.W. Brown, L. Sun, S.C. Yang, Anal. Chem. 65 (1993) 2335.
[37] E. Primgsheim, E. Terpetchnig, O.S. Wolfbeis, Anal. Chim. Acta 357 (1997) 247.
[38] M.D.T. Sotomayor, M.A. Depaoli, W.A. Deoliveira, Anal. Chim. Acta 353 (1997) 275.
[39] J.Z. Tao, G.R. Xu, S.W. Yao, P. Liu, Y.P. Zhang, Guangpu Shiyanshi 25 (2008) 1053.
[40] A. Safavi, M. Bagheri, Sens. Actuators B 90 (2003) 143.
[41] M. Shamsipur, F. Abbasitabar, V. Zare-Shahabadi, M. Akhond, Anal. Lett. 41 (2008) 3113.
[42] G. Vishnoi, T.C. Goel, P.K.C. Pillai, Proc. SPIE-Int. Soc. Opt. Eng. 3538 (1999) 319.
[43] B.D. Gupta, S. Sharma, Opt. Commun. 154 (1998) 282.
[44] J. Lin, D. Liu, Anal. Chim. Acta 408 (2000) 49.
[45] F.J. Arregui, M. Otano, C. Fernandez-Valdivielso, I.R. Matias, Sens. Actuators B 87 (2002) 289.
[46] A. Safavi, N. Maleki, A. Rostamzadeh, S. Maesum, Talanta 71 (2007) 408.
[47] K. Cantrell, M.M. Erenas, I. Orbe-Paya, L.F. Capitan-Vallvey, Anal. Chem. 82 (2010) 531.
[48] A.R. Smith, Proceedings of the 5th Annual Conference on Computer Graphics and Interactive Techniques, Association for Computing Machinery Press, 1978, pp. 12–19.
[49] A. Lapresta-Fernandez, L.F. Capitan-Vallvey, Sens. Actuators B 134 (2008) 694.
[50] D. Michie, D.J. Spiegelhalter, C.C. Taylor, Machine Learning, Neural and Statistical Classification, Ellis Horwood, Chichester, UK, 1994.
[51] E. Bakker, P. Bühlmann, E. Pretsch, Chem. Rev. 97 (1997) 3083.
[52] A. Ceresa, Y. Qain, S. Peper, E. Bakker, Anal. Chem. 75 (2003) 133.
[53] R.H. Ng, K.M. Sparks, B.E. Statland, Clin. Chem. 38 (1992) 1371.
[54] I.d. Orbe-Paya, M. Erenas, L.F. Capitan-Vallvey, Sens. Actuators B 127 (2007) 586.
[55] D. Freiner, R.E. Kunz, D. Citterio, U.E. Spichiger, M.T. Gale, Sens. Actuators B 29 (1995) 277.

Microchemical Journal 97 (2011) 225–233

Contents lists available at ScienceDirect

Microchemical Journal

journal homepage: www.elsevier.com/locate/microc

Full-range optical pH sensor array based on neural networks

S. Capel-Cuevas [a], M.P. Cuéllar [b], I. de Orbe-Payá [a], M.C. Pegalajar [b], L.F. Capitán-Vallvey [a,*]

[a] Department of Analytical Chemistry, University of Granada, E-18071 Granada, Spain
[b] Department of Computer Science and Artificial Intelligence, University of Granada, E-18071 Granada, Spain

ARTICLE INFO

Article history:
Received 17 August 2010
Received in revised form 10 September 2010
Accepted 10 September 2010
Available online 17 September 2010

Keywords:
Full-range optical pH sensor array
Neural network
H coordinate
HSV colour space

ABSTRACT

A neural network multivariate calibration is used to predict the pH of a solution in the full-range (0–14) from hue (H) values coming from imaging an optical pH sensor array based on 11 sensing elements with immobilized pH indicators. Different colorimetric acid-base indicators were tested for membrane preparation fulfilling the following conditions: 1) no leaching; 2) change in tonal coordinate by reaction and 3) covering the full pH range with overlapping between their pH responses. The sensor array was imaged after equilibration with a solution using a scanner working in transmission mode. Using software developed by us, the H coordinate of the colour space HSV was calculated from the RGB coordinates of each element.
The neural network was trained with the calibration data set using the Levenberg–Marquardt training method. The network structure has 11 input neurons (each one matching the hue of a single element in the sensor array), 1 output (the pH approximation value) and 1 hidden layer with 10 hidden neurons. The network provides an MSE = 0.0098 in the training data, MSE = 0.0183 in the validation data and MSE = 0.0426 in the test data coming from a set of real water samples. The resulting correlation coefficient R obtained in the Pearson correlation test is R = 0.999.

1. Introduction

Optical pH sensors are principally based on reversible changes in the structure of an acid-base indicator induced by pH and translated into changes in spectroscopic phenomena such as absorption, reflectance, luminescence, and energy transfer.

The immobilization of the indicator molecule is a key issue in determining the analytical and operational characteristics of pH sensors in any of the usual dispositions, such as probe (optic fibre), flow or disposable format. Different types of immobilization techniques for pH indicating dyes have been used [1], including: a) dye entrapment in different materials such as cellulose acetate [2], sol–gel [3], PVC [4], methacrylic-acrylic copolymers [5] and different composites like SiO_2/ZrO_2-organic polymer [6]; b) retention of dye by ion-exchange materials such as Amberlite XAD-2 resin [7] or Dowex I-X10 resin [8], in some instances including the ion-exchanger containing dyes in polymeric encapsulated membranes using PVC [9]; c) adsorption of the dye on materials such as non-ionic styrene/divinylbenzene copolymer [10], polyester/lycra blends textile [11], cellulose [12], cellulose acetate [13], or polymer track membranes combining retention in surface and bulk [14]; d) covalent binding of dye by different synthetic strategies to form microparticles or membranes, in some cases formed on glass fibre, using different polymers such as polyacrylamide [15,16], triacetylcellulose [17,18], cellulose acetate [19,20], agarose [21] or polyamide [22], among others; e) polymerization of monomers to prepare both membrane and dye, as with aniline [23] or pyrrole [24].

Unlike potentiometric pH determination, in which the pH depends linearly on the activity of hydrogen ions, pH in optical sensors is a function of the concentration of the acid and basic forms of the indicator [25]. The change in the measured signal with pH results in a narrow sigmoidal shape dependence according to the Henderson–Hasselbalch equation. The main drawbacks of optical pH sensors are accordingly, short dynamic working range (2–3 pH units) and non-linear response, which require different sensing membranes to cover the whole pH range.

Different strategies have been devised to stretch the working range of optical pH sensors. The working range of membranes containing only one indicator can be broadened using polyprotic acids as indicators; for instance, when using neutral red the working pH ranges from 2.0 to 8.5 [26]. Additionally, in some instances the adsorption [27] or chemical immobilization [18] of indicators leads to broader ranges than in solution. In other cases, the whole reflectance spectra of the immobilised indicator along with multivariate techniques were used to model the pH in a broad range [28]. An interesting approach includes the dynamic optical response of a flow sensor as the analytical signal, increasing the range up to 10 pH units with only one indicator [29].

Some conductive polymers change their visible and near-IR absorption properties as a function of pH, as is the case with polyaniline

* Corresponding author.
E-mail address: lcapitan@ugr.es (L.F. Capitán-Vallvey).

0026-265X/$ – see front matter © 2010 Elsevier B.V. All rights reserved.
doi:10.1016/j.microc.2010.09.008

works that make use of the RGB colour space from three to one. In contrast to methods that use the absorbance spectra to make the prediction, our approach requires lower data pre-processing since the hue is automatically extracted from the sensing elements and does not require any specific apparatus to acquire the sensor signal.

Regarding the prediction accuracy, neural networks have shown a suitable performance obtaining an MSE of 0.042 in real water samples for the full pH range. Statistical tests helped to corroborate the results obtained in this work, and they concluded that there are no significant differences between the real pH values and the ones predicted by the approach, which corroborates its good prediction performance.

At this time, the development of small, hand-held, battery-operated instruments that will include developed algorithms to work with captured imaging data is being researched.

Acknowledgements

We acknowledge the financial support from the Ministerio de Educación y Ciencia, Dirección General de Enseñanza Superior (Spain) (Projects CTQ2009-14428-C02-01 and CTQ2009-14428-C02-02); and the Junta de Andalucia (Proyecto de Excelencia P06-FQM-01467 and P08-FQM-3535).

References

[1] J. Lin, Recent development and applications of optical and fiber-optic pH sensors, TrAC, Trends Anal. Chem. 19 (2000) 541–552.
[2] T.J. Cardwell, R.W. Cattrall, L.W. Deady, M. Dorkos, G.R. O'Connell, A fast-response membrane-based pH indicator optode, Talanta 40 (1993) 765–768.
[3] M. Garcia-Heras, C. Gil, N. Carmona, J. Faber, K. Kromka, M.A. Villegas, Optical behaviour of pH detectors based on sol–gel technology, Anal. Chim. Acta 540 (2005) 147–152.
[4] M. Puyol, S. Miltsov, I. Salinas, J. Alonso, Ketocyanine dyes: H+-selective ionophores for use in integrated waveguides absorbance optodes, Anal. Chem. 74 (2002) 570–576.
[5] L.Y. Heng, T.H. Fang, L.H. Chern, M. Ahmad, Influence of methacrylic-acrylic copolymer composition on plasticiser-free optode films for pH sensors, Sensors 3 (2003) 83–90.
[6] L.R. Allain, Z. Xue, Optical sensors for the determination of concentrated hydroxide, Anal. Chem. 72 (2000) 1078–1083.
[7] R. Narayanaswamy, F. Sevilla III, Reflectometric study of thre acid-base equilibria of indicators immobilised on a styrene/divinylbenzene copolymer, Anal. Chim. Acta 189 (1986) 365–369.
[8] M.C. Moreno-Bondi, M. Jiménez, C. Perez, C. Camara, Analytical performance of an optical pH sensor for acid–base titration, Anal. Chim. Acta 230 (1990) 35–40.
[9] B. Kuswandi, R. Narayanaswamy, Polymeric encapsulated membrane for optrodes, Fresenius J. Anal. Chem. 364 (1999) 605–607.
[10] G.F. Kirkbright, R. Narayanaswamy, N.A. Welti, Fibre-optic pH probe based on the use of an immobilised colorimetric indicator, Analyst 109 (1984) 1025–1028.
[11] D. Morris, S. Coyle, Y. Wu, K.T. Lau, G. Wallace, D. Diamond, Bio-sensing textile based patch with integrated optical detection system for sweat monitoring, Sens. Actuators B 139 (2009) 231–236.
[12] A. Abbaspour, M.A. Mehrgardi, A. Noori, M.A. Kamyabi, A. Khalafi-Nezhad, M.N. Soltani Rad, Speciation of iron(II), iron(III) and full-range pH monitoring using paptode: a simple colorimetric method as an appropriate alternative for optodes, Sens. Actuators B 113 (2006) 857–865.
[13] T.P. Jones, M.D. Porter, Optical pH sensor based on the chemical modification of a porous polymer film, Anal. Chem. 60 (1988) 404–406.
[14] A. Dybko, W. Wroblewski, J. Maciejewski, R. Romaniuk, Z. Brzózka, Efficient reagent immobilization procedure for ion-sensitive optomembranes, Sens. Actuators B 39 (1997) 207–211.
[15] J.I. Peterson, S.R. Goldstein, R.V. Fitzgerald, D.K. Buckhold, Fiber optic pH probe for physiological use, Anal. Chem. 52 (1980) 864–869.
[16] C. Munkholm, D.R. Walt, F.P. Milanovich, S.M. Klainer, Polymer modification of fiber optic chemical sensors as a method of enhancing fluorescence signal for pH measurement, Anal. Chem. 58 (1986) 1427–1430.
[17] A. Safavi, M. Pakniat, Dipicrylamine-modified triacetylcellulose membrane for optical pH and potassium ion measurement, Anal. Chim. Acta 335 (1996) 227–233.
[18] A.A. Ensafi, A. Kazemzadeh, Optical pH sensor based on chemical modification of polymer film, Microchem. J. 63 (1999) 381–388.
[19] Y. Kostov, G. Rao, Low-cost gated system for monitoring phosphorescence lifetimes, Rev. Sci. Instrum. 74 (2003) 4129–4133.
[20] A. Holobar, B.H. Weigl, W. Trettnak, R. Benes, H. Lehmann, N.V. Rodriguez, A. Wollschlager, P. O'Leary, P. Raspor, O.S. Wolfbeis, Experimental results on an optical pH measurement system for bioreactors, Sens. Actuators B B11 (1993) 425–430.
[21] P. Hashemi, R.A. Zarjani, A wide range pH optical sensor with mixture of Neutral Red and thionin immobilized on an agarose film coated glass slide, Sens. Actuators B 135 (2008) 112–115.
[22] T. Seung, C. Yang, Synthesis of Congo Red linked with alkyl amide polymer and its optical ion-sensing property, Pol. Bull. 42 (1999) 655–660.
[23] S. De Marcos, C. Asensio, I. Urunuela, F. Gallarta, J. Galban, J.R. Castillo, New approaches to polyaniline optical sensors: pH, acetic acid and ammonia determination, Quim. Anal. 19 (2000) 99–104.
[24] S. De Marcos, O.S. Wolfbeis, Optical Sensing of pH Based on Polypyrrole Films, Anal. Chim. Acta 334 (1996) 149–153.
[25] J. Janata, Do optical sensors really measure pH? Anal. Chem. 59 (1987) 1351–1356.
[26] P. Hashemi, R.A. Zarjani, M.M. Abolghasemi, A. Olin, Agarose film coated glass slides for preparation of pH optical sensors, Sens. Actuators B 121 (2007) 396–400.
[27] M. Bacci, F. Baldini, A.M. Scheggi, Spectrophotometric investigations on immobilized acid-base indicators, Anal. Chim. Acta 207 (1988) 343–348.
[28] F.B.M. Suah, M. Ahmad, M.N. Taib, Optimization of the range of an optical fiber pH sensor using feed-forward artificial neural network, Sens. Actuators B 90 (2003) 175–181.
[29] A. Safavi, A. Rostamzadeh, S. Maesum, Wide range pH measurements using a single H+-selective chromoionophore and a time-based flow method, Talanta 68 (2006) 1469–1473.
[30] U.W. Grummt, A. Pron, M. Zagorska, S. Lefrant, Polyaniline based optical pH sensor, Anal. Chim. Acta 357 (1997) 253–259.
[31] Z. Ge, C.W. Brown, L. Sun, S.C. Yang, Fiber-optic pH sensor based on evanescent wave absorption spectroscopy, Anal. Chem. 65 (1993) 2335–2338.
[32] E. Primgsheim, E. Terpetchnig, O.S. Wolfbeis, Optical sensing pH of using thin films of subtituted polyanilines, Anal. Chim. Acta 357 (1997) 247–252.
[33] M.D.T. Sotomayor, M.A. Depaoli, W.A. Deoliveira, Fiber optic pH sensor based on poly(o-methoxyaniline), Anal. Chim. Acta 353 (1997) 275–280.
[34] J.Z. Tao, G.R. Xu, S.W. Yao, P. Liu, Y.P. Zhang, Optical response of copolymer of 3-aminophenylboronic acid with aniline film against pH, Guangpu Shiyanshi 25 (2008) 1053–1056.
[35] A. Safavi, M. Bagheri, Novel optical pH sensor for high and low pH values, Sens. Actuators B 90 (2003) 143–150.
[36] M. Shamsipur, F. Abbasitabar, V. Zare-Shahabadi, M. Akhond, Broad-range optical ph sensor based on binary mixed-indicator doped sol–gel film and application of artificial neural network, Anal. Lett. 41 (2008) 3113–3123.
[37] G. Vishnoi, T.C. Goel, P.K.C. Pillai, A pH-optrode for the complete working range, Proc. SPIE Int. Soc. Opt. Eng. 3538 (1999) 319–325.
[38] B.D. Gupta, S. Sharma, A long-range fiber optic pH sensor prepared by dye doped sol–gel immobilization technique, Opt. Commun. 154 (1998) 282–284.
[39] J. Lin, D. Liu, An optical pH sensor with a linear response over a broad range, Anal. Chim. Acta 408 (2000) 49–55.
[40] F.J. Arregui, M. Otano, C. Fernandez-Valdivielso, I.R. Matias, An experimental study about the utilization of Liquicoat solutions for the fabrication of pH optical fiber sensors, Sens. Actuators B 87 (2002) 289–295.
[41] A. Safavi, N. Maleki, A. Rostamzadeh, S. Maesum, CCD camera full range pH sensor array, Talanta 71 (2007) 498–501.
[42] M.P. Cuellar, M.M. Erenas, M.C. Pegalajar, I. Orbe-Paya, L.F. Capitan-Vallvey, Automatic colour feature extraction from disposable optical sensors, International Workshop on Multivariate Image Analysis, 2009, p. 45.
[43] D.A. Forsyth, J. Ponce, Computer Vision: A Modern Approach, Prentice Hall, Upper Saddle River, NJ, US, 2002.
[44] Smith, A.R. Color gamut transform pairs 1978; Proceedings of the 5th Annual Conference on Computer Graphics and Interactive Techniques; 12-19.
[45] S. Haykin, Neural Networks: A comprehensive foundation, Prentice Hall, Upper Saddle River, NJ, USA, 1999.
[46] Cuellar, M. P.; Delgado, M.; Pegalajar, M. C. An application of non-linear programming to train recurrent neural networks in time series prediction problems 2005; Proc.International Conference on Enterprise and Information Systems; 35–42.
[47] K. Cantrell, M.M. Erenas, I. Orbe-Paya, L.F. Capitan-Vallvey, Use of the Hue Parameter of the Hue, Saturation, Value Color Space As a Quantitative Analytical Parameter for Bitonal Optical Sensors, Anal. Chem. 82 (2010) 531–542.
[48] E. Bakker, P. Bühlmann, E. Pretsch, Carrier-Based Ion-Selective Electrodes and Bulk Optodes. 1. General Characteristics, Chem. Rev. 97 (1997) 3083–3132.
[49] A. Ceresa, Y. Quin, S. Peper, E. Bakker, Mechanistic insights into the development of optical chloride sensor based on the mercuracarborand-3 ionophore, Anal. Chem. 75 (2003) 133–140.
[50] R.H. Ng, K.M. Sparks, B.E. Statland, Colorimetric determination of potassium in plasma and serum by reflectance photometry with a dry-chemistry reagent, Clin. Chem. 38 (1992) 1371–1372.
[51] I.D. Orbe-Paya, M. Erenas, L.F. Capitan-Vallvey, Potassium disposable optical sensor based on transflectance measurements, Sens. Actuators B 127 (2007) 586–592.
[52] D. Freiner, R.E. Kunz, D. Citterio, U.E. Spichiger, M.T. Gale, Integrated optical sensors based on refractometry of ion-selective membranes, Sens. Actuators B 29 (1995) 277–285.
[53] A. Lapresta-Fernandez, L.F. Capitan-Vallvey, Scanometric potassium determination with ionophore-based disposable sensors, Sens. Actuators B 134 (2008) 694–701.
[54] Capel-Cuevas, S.; Orbe-Paya, I.; Cuellar, M. P.; Pegalajar, M. C.; Capitan-Vallvey, L. F. Full-range optical pH sensor based on imaging techniques 2010; Proc. Europtrode X; 110.

NJC

Dynamic Article Links

Cite this: *New J. Chem.*, 2011, **35**, 1042–1053

www.rsc.org/njc

PAPER

Minimization of sensing elements for full-range optical pH device formulation

M. P. Cuéllar,[a] S. Capel-Cuevas,[b] M. C. Pegalajar,[a] I. de Orbe-Payá[b] and L. F. Capitán-Vallvey*[b]

Received (in Montpellier, France) 1st December 2010, Accepted 14th February 2011
DOI: 10.1039/c0nj00951b

The goal of this work is to find the minimum number of sensing elements that can be used to build a sensor array suitable for pH prediction for a full-range (0–14) optical pH sensor array based on hue (H) data from the HSV color space. The hue of each element coming from the pH sensor array imaging is used as input data for a neural network that provides the pH prediction approximation as the output response. This problem may be considered a multicriteria optimization task with the dual objectives of error minimization between the network pH prediction and the reference pH in the calibration data, and of minimizing the network complexity and the number of network inputs. To that end, this work proposes a multi-objective optimization method applied to a collection of 11 sensing elements that returns a set of optimal networks considering the Pareto optimality criterion. A solution from the Pareto front was selected to achieve a minimum pH prediction error with the minimum number of sensing elements. After this analysis, it can be concluded that the use of a sensor array made up of 4 sensing elements offers a good pH prediction (Mean Square Error of 0.052) over the full-range working with 4 hidden neurons.

Introduction

Unlike potentiometric pH determination, in which the pH depends linearly on the activity of hydrogen ions, pH in optical sensors is a function of the concentration of the acid and basic forms of the indicator.[1] Optical sensors for pH are mainly based on reversible changes in the structure of chemicals induced by pH and translated into changes in spectroscopic phenomena such as absorption, reflectance, luminescence, and energy transfer (acid–base indicator) chemically or physically immobilized in or on a solid support, and placed as a thin layer or coating. The change in the measured signal with the pH typically results in narrow sigmoidal shape dependence according to the Henderson–Hasselbalch equation. This leads to the main drawbacks of optical pH sensors—their short dynamic working range (2–3 pH units) and non-linear response[2]—which require different sensing membranes to cover the whole pH range.

Different strategies have been devised to extend the working range of optical pH sensors. The working range of membranes containing only one indicator can be broadened using polyprotic acids as indicators,[3] although in some instances the adsorption[4] or chemical immobilization[5] of the indicators leads to broader ranges than in solution. In other cases, the use of the whole reflectance spectra of an immobilized indicator[6] or the dynamic optical response of a flow sensor as an analytical signal[7] increases the range with only one indicator. Alternatively, some conductive polymers change their visible and near-IR absorption properties as a function of pH in a broad range, as is the case with polyaniline[8] and polypyrrole.[9] Another approach to broaden the pH range is to co-immobilize multiple pH indicators (two,[10,11] three[12] and even five indicators).[13]

A final strategy consists of using arrays of membranes containing complementary pH indicators acquiring the analytical information by imaging techniques. In this way, commercial multi-color pH paper strips have been measured with a conventional scanner;[14] alternatively, arrays of five pH membranes in a triacetylcellulose support measured with a CCD color camera have been described.[15] In both cases, the average RGB values of each sensing area image are used for calibration with multivariate mathematical models. One drawback of this calibration process is the non-linear dynamics of the functions to approximate the pH with respect to the color parameters. Here, neural networks[16] have been proposed to solve this problem, although the limitations of their classic

[a] *Department of Computer Science and Artificial Intelligence, E.T.S. Ingenierías Informática y de Telecomunicación, University of Granada, C/Periodista Daniel Saucedo Aranda s/n, E-18071, Granada, Spain. E-mail: manupc@decsai.ugr.es, mcarmen@decsai.ugr.es*
[b] *Department of Analytical Chemistry, University of Granada, Faculty of Sciences, Avda. Fuentenueva s/n, E-18071, Granada, Spain. E-mail: scapel@ugr.es, idorbe@ugr.es, lcapitan@ugr.es; Fax: +34 958 243328; Tel: +34 958 248436*

40 D. A. Forsyth and J. Ponce, *Computer Vision: A Modern Approach*, Prentice Hall, Upper Saddle River, NJ, USA, 2002.
41 A. R. Smith, *Proceedings of the 5th Annual Conference on Computer Graphics and Interactive Techniques*, 1978, 12–19.
42 K. Deb, A. Pratap, A. Agarwaland and T. Meyarivan, *IEEE Transactions on Evolutionary Computation*, 2002, **6**, 182–197.
43 R. Prudencio and T. Ludemir, *Proc. 26th Annu. Conf. Gesellschaft for Classifikation*, 2003, 617–621.
44 H. A. Abbass, *Australian Joint Conference on Artificial Intelligence*. Lecture Notes in Artificial Intelligence. Springer, 2001, vol. 2256, 1–12.
45 S. Capel-Cuevas, M. P. Cuellar, I. de Orbe-Paya, M. C. Pegalajar and L. F. Capitan-Vallvey, *Microchem. J.*, 2011, **97**, 225–233.

IEEE SENSORS JOURNAL, VOL. 12, NO. 5, MAY 2012 1197

An Expert System for Full pH Range Prediction Using a Disposable Optical Sensor Array

Sonia Capel-Cuevas, Manuel P. Cuéllar, María del Carmen Pegalajar, Ignacio de Orbe-Payá, and Luis Fermín Capitán-Vallvey

***Abstract*—The design of optical sensor arrays encompasses tasks such as the acquisition of sensor optical parameters, as for example color features, and the calibration of a multivariate method to model the array global behavior. Different techniques have been used to model the sensor array responses, such as multivariate regression or neural networks, although they show certain limitations. The former methods require either high amount of computer memory or speed so therefore they are not suitable for implementation in portable electronic devices with low resources, while the later is a black box whose operation cannot be easily modeled and explained for industrial development validation. This work addresses these problems and proposes an expert system to overcome the previous drawbacks. The approach makes an accurate pH prediction, and it comprises a balance between memory and microprocessor speed for its integration within embedded systems with low memory and chip resources. In addition, it is also able to provide a high expressive explanation of why such prediction was made, so that the industrial validation is easier than using other proposals such as neural networks.**

***Index Terms*—Expert systems, full pH range determination, H coordinate, optical sensor array.**

I. Introduction

CHEMICAL imaging combines standard digital imaging with spectroscopic techniques to provide the spatial distribution of sample components [1]. Chemical imaging with sensors use sensor arrays to monitor chemical species with a number of distributed selective chemical sensors providing spatial resolution [2]. Focusing on optical pH detection, the literature offers different solutions using sensor arrays [3]–[9], fluorescent excitation-ratiometric pH sensing dyes [10], and further fluorescent and fiber-optic pH sensors [11].

Multivariate calibration techniques have been used in previous works to solve the problem of the sensor array response modeling. Focusing on pH determination by means of optical sensors, on one hand we find linear and nonlinear regressions [4], [9]. If the number of sensing elements in the array is small, some researchers offer simple regression formulae to model the sensor response [4]. However, as the number of sensors increases, more complex techniques such as multidimensional surface fit approaches are required [9]. In these cases, the approaches have the drawback of high computer memory or processor speed requirements, which makes difficult their implementation in small hand-held devices with low processor resources. On the other hand, other approaches such as neural networks are used when the sensor response functions are difficult to approximate, due to non-linearities in the sensor array outputs or high dimensionality of the problem [12]. However, their validation for industrial developments is often hard since the interpretation and modeling of the network behavior cannot be easily explained and correctly justified.

In this work, we propose an alternative approach to solve the previous limitations, which is also statistically equivalent to previous calibration techniques in terms of approximation accuracy. We develop an expert system [13], [14] architecture to model the sensor array responses. The system operation is described in two stages: first, the model calibration comprises the approximation of a set of candidate pH prediction functions that depends on the input optical parameters acquired from the sensing elements in the array, and the generation of a knowledge base to select the best candidate functions to achieve an accurate pH prediction. To be more precise, the knowledge base contains production rules of the form

> If «Optical parameters have some value» Then «Use the pH prediction function X»

with a reliability degree of each rule. On the other hand, during the system use, the optical parameter values are fetched from the array and a reasoner module uses these values to infer the best pH prediction functions with a reliability degree that can be used to obtain an accurate pH approximation value. Finally, a predictor module coordinates the output of each pH prediction function selected by the reasoner to provide the pH prediction value.

In contrast to previous approaches in the literature, our proposal has the advantages of smaller computer memory and speed

Manuscript received August 30, 2011; accepted September 09, 2011. Date of publication September 19, 2011; date of current version April 11, 2012. This work was supported in part by the Ministerio de Ciencia e Innovación, Dirección General de Investigación y Gestión del Plan Nacional de I+D+i (Spain) under Projects CTQ2009-14428-C02-01 and CTQ2009-14428-C02-02 and in part by the Junta de Andalucía under Proyecto de Excelencia P08-FQM-3535. These projects were partially supported by European Regional Development Funds (ERDF). The associate editor coordinating the review of this paper and approving it for publication was Dr. S. Mukhopadhyay.

S. Capel-Cuevas is with the Department of Analytical Chemistry, University of Granada, Faculty of Sciences, Avda. Fuentenueva s/n, Granada 18071 Spain (e-mail: scapel@ugr.es).

M. P. Cuéllar is with the Department of Computer Science and Artificial Intelligence, E.T.S. Ingenierías Informática y de Telecomunicación, University of Granada, C/ Periodista Daniel Saucedo Aranda s/n, Granada 18071 Spain (e-mail: manupc@decsai.ugr.es).

M. C. Pegalajar is with the Department of Computer Science and Artificial Intelligence, E.T.S. Ingenierías Informática y de Telecomunicación, University of Granada, C/ Periodista Daniel Saucedo Aranda s/n, Granada 18071 Spain (e-mail: mcarmen@decsai.ugr.es).

I. de Orbe-Payá is with the Department of Analytical Chemistry, University of Granada, Faculty of Sciences, Avda. Fuentenueva s/n, Granada 18071 Spain (e-mail: idorbe@ugr.es).

L. F. Capitán-Vallvey is with the Department of Analytical Chemistry, University of Granada, Faculty of Sciences, Avda. Fuentenueva s/n, Granada 18071 Spain (e-mail: lcapitan@ugr.es).

Color versions of one or more of the figures in this paper are available online at http://ieeexplore.ieee.org.

Digital Object Identifier 10.1109/JSEN.2011.2168815

Sonia Capel Cuevas received the B.Sc. degree in chemistry from the University of Granada, Granada, Spain, in 2007, and she is currently working towards the Ph.D. degree in the Department of Analytical Chemistry at the University of Granada.

Her current research interests include the preparation and characterization of colorimetric optical arrays for their use in the analysis of solutions, including low-cost portable electronic instruments.

Manuel P. Cuéllar graduated in Computer Engineering in 2003. He finished the Ph.D. degree on time series prediction, parameter identification, and neural networks in 2006.

He is currently a full-time Teacher with the Department of Computer Science and Artificial Intelligence, University of Granada, Granada, Spain. His main interests are neural and social networks, evolutionary optimization, and fuzzy systems. He has also worked in multivariate image analysis and real-time control tasks.

María del Carmen Pegalajar received the M.Sc. and Ph.D. degrees in computer science from the University of Granada, Granada, Spain, in 1993 and 1997, respectively.

Since 2001, she has been an Associate Professor with the Department of Computer Science and Artificial Intelligence, University of Granada. Her current main research interests are in the fields of neural networks, fuzzy automata, grammatical inference, pattern recognition, time series prediction, evolutionary algorithms, mobile systems, and optical tongue.

Ignacio de Orbe-Payá is Associate Professor with the Department of Analytical Chemistry at the University of Granada, Granada, Spain.

His main areas of research are the development of the sensing phases for their use as chemical sensors in the determination of inorganic ions in several matrices, multivariate calibration methods for the quality control of pharmaceutical products, and development of analytical methodology using solid-phase spectrometry.

Luis Fermín Capitán-Vallvey received the B.Sc. and Ph.D. degrees in chemistry from the Faculty of Sciences, University of Granada, Granada, Spain, in 1973 and 1986, respectively.

He is Full Professor of Analytical Chemistry at the University of Granada, In 1983, he founded the Solid Phase Spectrometry group (GSB) and in 2000, together with Prof. P. López, the interdisciplinary group ECsens, which includes chemists, physicists and electrical and computer engineers at the University of Granada. His current research interests are the design, development and fabrication of sensors and portable instrumentation for environmental, health, and food analysis and monitoring. His work has produced nearly 270 peer-reviewed scientific papers, 15 book chapters and 6 patents.

Sensors and Actuators B 156 (2011) 840–848

Contents lists available at ScienceDirect

Sensors and Actuators B: Chemical

journal homepage: www.elsevier.com/locate/snb

Sensor array-based optical portable instrument for determination of pH

A. Martinez-Olmos[a], S. Capel-Cuevas[b], N. López-Ruiz[a], A.J. Palma[a], I. de Orbe[b], L.F. Capitán-Vallvey[b,*]

[a] Department of Electronics and Computer Technology, Campus Fuentenueva, Faculty of Sciences, University of Granada, E-18071 Granada, Spain
[b] Department of Analytical Chemistry, Campus Fuentenueva, Faculty of Sciences, University of Granada, E-18071 Granada, Spain

ARTICLE INFO

Article history:
Received 24 November 2010
Received in revised form 21 February 2011
Accepted 23 February 2011
Available online 3 March 2011

Keywords:
Full-range optical pH sensor array
OLED display
Digital colour detector
HSV colour space
Portable instrumentation

ABSTRACT

A portable optical instrument is presented that makes it possible to determine pH with a colorimetric sensor array. The use of four membranes containing acid–base indicators makes it possible to cover the full range of pH using the *H* (hue) coordinate measurements of the HSV colour space. pH sensitive membranes were directly cast onto a plastic support to form a two-dimensional array, located between an OLED display as the programmable light source and a set of digital colour detectors. The resulting microcontroller-based system is immune to optical and electrical interferences. A complete optical and electrical characterization and optimization of the hand-held instrument was carried out. The instrument was used to determine pH using a simple algorithm to select the sensor output that was programmed in the microcontroller. The initial eleven candidate pH membranes were reduced to only four, which permit to obtain reliable pH values. The pH response of the selected four sensing elements was modelled, and calibration curves were applied to a validation set and real samples obtaining positive correlations between the real and predicted data.

1. Introduction

Chemical imaging is an analytical technique that combines standard digital imaging techniques with a variety of spectroscopic techniques, typically based on absorption, transmission or scattering (Raman) or emission (fluorescence, chemiluminescence) to provide the spatial distribution of sample components. It is of general use in a variety of industries to characterize both chemical composition and morphology [1].

With sensors, chemical imaging must use a detector array to monitor the desired chemical species with a number of distributed selective chemical sensors providing spatial resolution as well [2]. One example is microarray technology, with which the simultaneous analysis of thousands of analytes is possible in a single experiment such as array-based gene expression analysis or protein microarrays based on antigen–antibody or ligand–receptor reactions [3].

Different macroarrays have been described for the simultaneous analysis of a small number of analytes by means of different types of imaging devices. Examples of positional or two-dimensional arrays include the device described for iron speciation and full-range pH determination by immobilizing reagents on cellulosic paper and RGB coordinates [4,5]; an electrochemiluminescent enzymatic biosensor screen-printed array for L-lactate and D-glucose [6]; an array of individually addressable sites on a micromachined silicon chip containing microspheres derivatized with dehydrogenases for the fluorescent determination of β-D-glucose and β-D-galactose [7] and fluorescent specific reagents for common ions in water arranged in microtiter plates and based on luminescence decay time imaging [8]. Some examples of encoded bead macroarrays can be found in the literature, such as an optical imaging fiber for pH, O_2 and CO_2 in solutions [9].

However, the disadvantages of these approaches based on specific receptors – difficulties in obtaining good selectivity against similar analytes and the number of sensors needed, which increases proportionally with the number of analytes – have led to an alternative paradigm based on general or differential receptors [10]. This concept results in arrays of non-specific or low selective sensors (electronic tongues/noses) that produce analytical signals useful for the analysis of multi-component samples that are later treated through advanced mathematical procedures for signal processing by pattern recognition and/or multivariate analysis both for qualitative and quantitative analysis [11]. Different experimental approaches have been proposed based on non-selective arrays and imaging, such as: arrays of optical fibers, with the sensing phase located on the distal extreme [12] or incorporated into microspheres situated in microcavities etched into the end of the fiber [13]; arrays of polymeric microspheres with chemically modified surfaces that enable the covalent binding of receptors (conventional reagents, enzymes, and antibodies) and arranged in

* Corresponding author.
E-mail address: lcapitan@ugr.es (L.F. Capitán-Vallvey).

0925-4005/$ – see front matter © 2011 Elsevier B.V. All rights reserved.
doi:10.1016/j.snb.2011.02.052

ing using paptode: a simple colorimetric method as an appropriate alternative for optodes, Sens.Actuators B 113 (2006) 857.
[5] A Safavi, N. Maleki, A. Rostamzadeh, S. Maesum, CCD camera full range pH sensor array, Talanta 71 (2007) 498.
[6] B.P. Corgier, C.A. Marquette, L.J. Blum, Screen-printed electrode microarray for electrochemiluminescent measurements, Anal. Chim. Acta 538 (2005) 1.
[7] T.E. Curey, A. Goodey, A. Tsao, J. Lavigne, Y. Sohn, J.T. McDevitt, E.V. Anslyn, D. Neikirk, J.B. Shear, Characterization of multicomponent monosaccharide solutions using an enzyme-based sensor array, Anal. Biochem. 293 (2001) 178.
[8] T. Mayr, G. Liebsch, I. Klimant, O.S. Wolfbeis, Multi-ion imaging using fluorescent sensors in a microtiterplate array format, Analyst 127 (2002) 201.
[9] F.J. Steemers, D.R. Walt, Multi-analyte sensing: from site-selective deposition to randomly-ordered addressable optical fiber sensors, Mikrochim. Acta 131 (1999) 99.
[10] J.J. Lavigne, E.V. Anslyn, Sensing a paradigm shift in the field of molecular recognition: from selective to differential receptors, Angew. Chem. Int. Ed. 40 (2001) 3118.
[11] Y. Vlasov, A. Legin, A. Rudnitskaya, C. Di Natale, A. D'Amico, Nonspecific sensor arrays (electronic tongue) for chemical analysis of liquids: (IUPAC technical report), Pure Appl. Chem. 77 (2005) 1965.
[12] K.L. Michael, L.C. Taylor, S.L. Schultz, F. Szurdoki, D.R. Walt, Making sensors out of disarray: optical sensor microarrays, Proc. SPIE 3270 (1998) 34.
[13] D.R. Walt, Techview: molecular biology. Bead-based fiber-optic arrays, Science 287 (2000) 451.
[14] A.P. Goodey, J.J. Lavigne, S.M. Savoy, M.D. Rodriguez, T. Curey, A. Tsao, G. Simmons, J. Wright, S.J. Yoo, Y. Sohn, E.V. Anslyn, J.B. Shear, D.P. Neikirk, J.T. McDevitt, Development of multianalyte sensor arrays composed of chemically derivatized polymeric microspheres localized in micromachined cavities, J. Am. Chem. Soc. 123 (2001) 2559.
[15] J.J. Lavigne, S. Savoy, M.B. Clevenger, J.E. Ritchie, B. McDoniel, S.J. Yoo, E.V. Anslyn, J.T. McDevitt, J.B. Shear, D. Neikirk, Solution-based analysis of multiple analytes by a sensor array: toward the development of an "electronic tongue", J. Am. Chem. Soc. 120 (1998) 6429.
[16] N.T. Greene, S.L. Morgan, K.D. Shimizu, Molecularly imprinted polymer sensor arrays, Chem. Commun. (2004) 1172.
[17] L. Baldini, A.J. Wilson, J. Hong, A.D. Hamilton, Pattern-based detection of different proteins using an array of fluorescent protein surface receptors, J. Am. Chem. Soc. 126 (2004) 5656.
[18] C. Zhang, K.S. Suslick, A colorimetric sensor array for organics in water, J. Am. Chem. Soc. 127 (2005) 11548.
[19] J. Janata, Do optical sensors really measure pH? Anal. Chem. 59 (1987) 1351.
[20] S. Capel-Cuevas, M.P. Cuellar, I. De Orbé Payá, M.C. Pegalajar, L.F. Capitan-Vallvey, Full-range optical pH sensor based on imaging techniques, Anal. Chim. Acta 681 (2010) 71.
[21] S. Capel-Cuevas, M.P. Cuellar, I. de Orbe-Paya, M.C. Pegalajar, L.F. Capitan-Vallvey, Full-range optical pH sensor array based on neural networks, Microchem. J. 97 (2011) 225.
[22] M.D. Fernandez-Ramos, M. Greluk, A.J. Palma, E. Arroyo-Guerrero, J. Gomez-Sanchez, L.F. Capitan-Vallvey, The use of one-shot sensors with a dedicated portable electronic radiometer for nitrate measurements in aqueous solutions, Meas. Sci. Technol. 19 (2008), 095204/1.
[23] A.J. Palma, A. Lapresta-Fernandez, J.M. Ortigosa-Moreno, M.D. Fernandez-Ramos, M.A. Carvajal, L.F. Capitan-Vallvey, A simplified measurement procedure and portable electronic photometer for disposable sensors based on ionophore-chromoionophore chemistry for potassium determination, Anal. Bioanal. Chem. 386 (2006) 1215.
[24] D. Filippini, S.P.S. Svensson, I. Lundström, Computer screen as a programmable light source for visible absorption characterization of (bio)chemical assays, Chem. Commun. (2003) 240.
[25] S. Macken, C. Di Natale, R. Paolesse, A. D'Amico, I. Lundstroem, D. Filippini, Towards integrated devices for computer screen photo-assisted multi-parameter sensing, Anal. Chim. Acta 632 (2009) 143.
[26] G. Wyszecki, W.S. Stiles, Color Science: Concepts and Methods, Quantitative Data and Formulae, Wiley Classics Library, Denver, USA, 2000.
[27] K. Cantrell, M.M. Erenas, I. Orbe-Paya, L.F. Capitan-Vallvey, Use of the hue parameter of the hue, saturation, value color space as a quantitative analytical parameter for bitonal optical sensors, Anal. Chem. 82 (2010) 531.

Biographies

Antonio Martínez Olmos was born in 1980 in Granada (Spain). He received the MSc degree and the PhD degree in Electronic Engineering from the University of Granada (Granada, Spain) in 2003 and 2009, respectively. Currently he works as Assistant Professor at the University of Granada. His current research includes the design of tomography sensors and the study of optical sensors for different biological measurements.

Sonia Capel Cuevas graduated in chemistry at the University of Granada (Spain) in July 2007. Since 2008 she is a PhD student at the Department of Analytical Chemistry in the University of Granada. Present research interests include the preparation and characterization of colorimetric optical arrays for their use in the analysis of solutions, including them in low-cost portable electronic instruments.

Nuria López Ruiz was born in 1985 in Barcelona (Spain). She received the BS and MSc degree in Telecommunications Engineering in 2003 and 2005, respectively, and the B.S. degree in Electronic Engineering in 2004 from University of Granada (Granada, Spain). Currently she works as research intern at the University of Granada. Her current research interests include the study of different colorimetric and optical sensors and the electronic instrumentation design.

Alberto J. Palma was born in 1968 in Granada (Spain). He received the BS and MSc degrees in physics (Electronics) in 1991 and the PhD degree in 1995 from the University of Granada, Granada, Spain. He is currently an associate professor at the University of Granada. Since 1992, he has been working on trapping of carriers in different electronic devices (diodes and MOS transistors) including characterization and simulation of capture cross sections, random telegraph noise, and generation-recombination noise in devices. From 2000, his current research interest is the study of the application of MOS devices as radiation sensors and the electronic instrumentation design directed to portable, low cost electronic systems in the fields of chemical and physical sensors.

Ignacio de Orbe-Payá is Associate Professor of the Department of Analytical Chemistry at the University of Granada (Spain). His main areas of research are the development of the sensing phases for their use as chemical sensors in the determination of inorganic ions in several matrices; multivariate calibration methods for the quality control of pharmaceutical products and development of analytical methodology using solid-phase spectrometry.

Luis Fermín Capitan-Vallvey, Full Professor of Analytical Chemistry at the University of Granada, received his BSc in Chemistry (1973) and PhD in Chemistry (1986) from the Faculty of Sciences, University of Granada (Spain). In 1983, he founded the Solid Phase Spectrometry group (GSB) and in 2000, together with Prof. Palma López, the interdisciplinary group ECsens, which includes Chemists, Physicists and Electrical and Computer Engineers at the University of Granada. His current research interests are the design, development and fabrication of sensors and portable instrumentation for environmental, health and food analysis and monitoring.

Sensors **2012**, *12*, 6746-6763; doi:10.3390/s120506746

OPEN ACCESS

sensors

ISSN 1424-8220

www.mdpi.com/journal/sensors

Article

A Compact Optical Instrument with Artificial Neural Network for pH Determination

Sonia Capel-Cuevas [1], Nuria López-Ruiz [2], Antonio Martinez-Olmos [2], Manuel P. Cuéllar [3], Maria del Carmen Pegalajar[3], Alberto José Palma [2], Ignacio de Orbe-Payá [1] and Luis Fermin Capitán-Vallvey [1,*]

[1] Department of Analytical Chemistry, Campus Fuentenueva, Faculty of Sciences, University of Granada, E-18071 Granada, Spain; E-Mails: scapel@ugr.es (S.C.-C.); idorbe@ugr.es (I.O.-P.); lcapitan@ugr.es (L.F.C.-V.)

[2] Department of Electronics and Computer Technology, Campus Fuentenueva, Faculty of Sciences, University of Granada, E-18071 Granada, Spain; E-Mails: nurilr@ugr.es (N.L.-R.); amartinez@ugr.es (A.M.-O.); ajpalma@ugr.es (A.J.P.)

[3] Department of Computer Science and Artificial Intelligence, E.T.S. Ingenierías Informática y de Telecomunicación, University of Granada, E-18071 Granada, Spain; E-Mails: manupc@decsai.ugr.es (M.P.C.); mcarmen@decsai.ugr.es (M.C.P.)

* Author to whom correspondence should be addressed; E-Mail: lcapitan@ugr.es; Tel.: +34-958-248-436; Fax: +34-958-243-328.

Received: 15 April 2012; in revised form: 15 May 2012 / Accepted: 21 May 2012 / Published: 22 May 2012

Abstract: The aim of this work was the determination of pH with a sensor array-based optical portable instrument. This sensor array consists of eleven membranes with selective colour changes at different pH intervals. The method for the pH calculation is based on the implementation of artificial neural networks that use the responses of the membranes to generate a final pH value. A multi-objective algorithm was used to select the minimum number of sensing elements required to achieve an accurate pH determination from the neural network, and also to minimise the network size. This helps to minimise instrument and array development costs and save on microprocessor energy consumption. A set of artificial neural networks that fulfils these requirements is proposed using different combinations of the membranes in the sensor array, and is evaluated in terms of accuracy and reliability. In the end, the network including the response of the eleven membranes in the sensor was selected for validation in the instrument prototype because of its high

8. Haykin, S. *Neural Networks: A Comprehensive Foundation*; Prentice Hall: Upper Saddle River, NJ, USA, 1999.
9. Bengio, Y.; Simard, P.; Frasconi, P. Learning long-term dependencies with gradient descent is difficult. *IEEE Trans. Neural Networks* **1994**, *5*, 157-166.
10. Taib, M.N.; Andres, R.; Narayanaswamy, R. Extending the response range of an optical fibre pH sensor using an artificial neural network. *Anal. Chim. Acta* **1996**, *330*, 31-40.
11. Safavi, A.; Bagheri, M. Novel optical pH sensor for high and low pH values. *Sens. Actuat. B* **2003**, *90*, 143-150.
12. Capel-Cuevas, S.; Cuéllar, M.P.; de Orbe-Payá, I.; Pegalajar, M.C.; Capitán-Vallvey, L.F. Full-range optical pH sensor based on imaging techniques. *Anal. Chim. Acta* **2010**, *681*, 71-81.
13. Capel-Cuevas, S.; Cuéllar, M.P.; de Orbe-Payá, I.; Pegalajar, M.C.; Capitán-Vallvey, L.F. Full-range optical pH sensor array based on neural networks. *Microchem. J.* **2011**, *97*, 225-233.
14. Martinez-Olmos, A.; Capel-Cuevas, S.; López-Ruiz, N.; Palma, A.J.; de Orbe, I.; Capitán-Vallvey, L.F. Sensor array-based optical portable instrument for determination of pH. *Sens. Actuat. B* **2011**, *156*, 840-848.
15. Fernandez-Ramos, M.D.; Greluk, M.; Palma, A.J.; Arroyo-Guerrero, E.; Gomez-Sanchez, J.; Capitan-Vallvey, L.F. The use of one-shot sensors with a dedicated portable electronic radiometer for nitrate measurements in aqueous solutions. *Meas. Sci. Technol.* **2008**, *19*, 095204-1-095204/7.
16. Cuéllar, M.P.; Capel-Cuevas, S.; Pegalajar, M.C.; de Orbe-Payá, I.; Capitán-Vallvey, L.F. Minimization of sensing elements for full-range optical pH device formulation. *New J. Chem.* **2011**, *35*, 1042-1053.
17. Abbass, H.A. A memetic Pareto evolutionary approach to artificial neural networks. *Lect. Note. Artif. Intell.* **2001**, *2256*, 1-12.
18. Cantrell, K.; Erenas, M.M.; Orbe-Payá, I.; Capitán-Vallvey, L.F. Use of the hue parameter of the hue, saturation, value color space as a quantitative analytical parameter for bitonal optical sensors. *Anal. Chem.* **2010**, *82*, 531-542.

Talanta 78 (2009) 1484–1488

Contents lists available at ScienceDirect

Talanta

journal homepage: www.elsevier.com/locate/talanta

Short communication

Double-armed crown ethers for calcium optical sensors

S. Capel-Cuevas[a], I. de Orbe-Payá[a], F. Santoyo-González[b], L.F. Capitán-Vallvey[a,*]

[a] Solid Phase Spectrometry Research Group, Department of Analytical Chemistry, Campus Fuentenueva, University of Granada, E-18071 Granada, Spain
[b] Department of Organic Chemistry, Faculty of Sciences, Campus Fuentenueva, University of Granada, E-18071 Granada, Spain

ARTICLE INFO

Article history:
Received 26 October 2008
Received in revised form 19 January 2009
Accepted 23 January 2009
Available online 4 February 2009

Keywords:
Double-armed diazacrown ethers
Optical sensor
Ionophore–chromoionophore chemistry
Selectivity

ABSTRACT

This paper presents the characterization of optical sensing membranes for calcium based on ionophore–chromoionophore chemistry. Six different ionophores, 18-membered crown ether derivatives, were studied, coming from 18-crown-6 ether and 4,13-diaza-18-crown-6 ether to a series of double-armed crown ethers with different type of terminal groups. The study of optical membranes containing the same transducer and plasticizer allow drawing some conclusions on the influence of lipophilicity and size of the terminal group of the side chain on calcium selectivity. We have calculated the exchange constant K^{ij}_{exch} for each equilibrium with alkaline and alkaline-earth ions and the selectivity coefficient $k^{Osel}_{i,j}$ for each ion against calcium as a way for a full characterization of sensing membranes. In all cases the ion:ionophore stability constants for calcium were the highest and the ionophore V containing an (N-adamantylcarbamoyl) acetyl moiety originated the most selective membrane for calcium. Analytical parameters for calcium determination using prepared membranes were calculated.

1. Introduction

Since Pedersen introduced them in 1967 [1], a wide variety of crown ethers have been synthesized and reported, especially during the last two decades [2–4]. The research interest focuses on their ability to form very stable molecular ensembles or complexes with alkaline, alkaline-earth metals and organic cations. Their affinity for a given cation, based on cooperative weak non-covalent interactions, depends on many factors, including the relative sizes of the cation and the macrocyclic cavity.

Double-armed crown ethers characterized by a parent macrocyclic ligand and a cation ligating sidearm [5] are suitable reagents for use as specific ionophores in areas as metal-sensing and separation processes. They form encapsulated and lipophilic complexes with stabilities intermediate between crown ethers and cryptands. Since these armed macrocycles are stronger cation binders than the crown ethers and more flexible than the cryptands, they offer great possibilities as analytical reagents.

This type of crown ethers is composed of two flexible cation-binding arms and a parent crown ring. The selectivity on the complexation is determined by the size of the crown ring and the nature and position of flexible side arms, which present a donor group that provides further coordination of a guest cation bonded in the crown ring. Consequently, it is possible to design a metal-selective reagent by choosing a combination of parent crown ring structure and functionalized side arms [6].

In this work we study the reactivity of a series of double-armed crown ethers based on an 18 atoms ring against alkaline and alkaline-earth ions. The ionophores are incorporated in optical membranes working on ion-exchange. The use of the same chromoionophore as transducer permit to extract conclusions on the influence of lipophilicity and size of the terminal group of the side chain on calcium selectivity.

2. Experimental

2.1. Reagents and materials

Calcium, magnesium, sodium and potassium stock solutions (1.000 mol L^{-1}) were prepared in water from analytical reagent grade calcium, magnesium, sodium and potassium chlorides (Panreac, Barcelona, Spain) and standardized by atomic absorption spectrometry. Solutions of lower concentration were prepared by dilution with water. pH 8.5 and 9.0 buffer solutions 0.2 M were made from diethanolamine (Probus, Barcelona, Spain), Tris (Sigma–Aldrich Química S.A., Madrid, Spain) and HCl (Panreac). All chemicals used for the ionophore synthesis were of synthesis grade and reverse-osmosis type quality water (Milli-RO 12 plus Milli-Q station from Millipore) was used throughout (conductivity 18.2 mS).

The chromoionophore 1,2-benzo-7-(diethylamino)-3-(octadecanoylimino)phenoxazine (lipophilized Nile Blue) was synthesized, purified and identified by us according to [7] and the

* Corresponding author.
E-mail address: lcapitan@ugr.es (L.F. Capitán-Vallvey).

0039-9140/$ – see front matter © 2009 Published by Elsevier B.V.
doi:10.1016/j.talanta.2009.01.046

Table 3
Analytical parameters for Ca(II) sensing membranes studied.

Ionophore	I	II	III	IV	V	VI
Intercept	−0.0049	−0.0207	−0.0276	−0.0354	−0.0208	−0.0354
Slope	−0.1741	−0.1902	−0.1867	−0.1921	−0.1603	−0.1921
Probability level (%) (lack-of-fit test)	53.7	69.2	50.1	87.4	49.3	87.5
Linear range (activities)	2.0×10^{-4}–0.23 M	2.3×10^{-4}–0.23 M	1.6×10^{-4}–0.23 M	1.7×10^{-4}–0.23 M	8.1×10^{-5}–0.23 M	5.9×10^{-5}–0.23 M
Detection limit (activities)	2.0×10^{-4} M	2.3×10^{-4} M	1.6×10^{-4} M	1.7×10^{-4} M	8.1×10^{-5} M	5.9×10^{-5} M
Intermembrane precision RSD (%)						
0.8 mM[a]	2.47	3.70	0.93	0.97	1.10	1.03
48 mM[a]	1.52	0.92	0.54	0.67	0.91	0.41
231 mM[a]	3.16	0.65	0.21	0.37	1.31	0.12

[a] Activities tested in mmol L^{-1}.

relationship in the middle of the sigmoidal response function defined by means a *lack-of-fit* test and as the detection limit the intersection of the linear calibration function defined above and a linear function adjusted in the minimal slope zone. As upper range we consider the highest value tested in all the cases (231 mM).

The detection limit decreases with the size and the lipophilicity of the terminal group of the side chains coming from 2.3×10^{-4} M for ionophore II to 5.9×10^{-5} M for ionophore VI according to the exchange constant values $K^{II_{Pb}}_{exch}$ for each ionophore.

Acknowledgements

We acknowledge financial support from *Ministerio de Educación y Ciencia, Dirección General de Enseñanza Superior* (Spain) (Projects CTQ2005-09060-CO2-01 and CTQ2005-09060-CO2-02); and *Junta de Andalucia* (Proyecto de Excelencia P06-FQM-01467).

Appendix A. Supplementary data

Supplementary data associated with this article can be found, in the online version, at doi:10.1016/j.talanta.2009.01.046.

References

[1] C.J. Pedersen, J. Am. Chem. Soc. 89 (1967) 7017.
[2] G.W. Gokel, Crown ether and cryptands, 1st ed., The Royal Society of Chemistry, London, 1991.
[3] J.W. Steed, Coord. Chem. Rev. 215 (2001) 171.
[4] P.A. Gale, Philos. Trans. R. Soc. Lond. Ser. A: Math. Phys. Eng. Sci. 358 (2000) 431.
[5] H. Tsukube, Talanta 40 (1993) 1313.
[6] M. Hiraoka, Crown Ethers and Analogous Compounds, Elsevier, Amsterdam, 1992.
[7] W.E. Morf, K. Seiler, B. Rusterholz, W. Simon, Anal. Chem. 62 (1990) 738.
[8] K. Suzuki, K. Watanabe, Y. Matsumoto, M. Kobayashi, S. Sato, D. Siswanta, H. Hisamoto, Anal. Chem. 67 (1995) 324.
[9] L.F. Capitán-Vallvey, M.D. Fernandez-Ramos, P. Alvarez de Cienfuegos, Anal. Chim. Acta 451 (2002) 231.
[10] P.C. Meier, Anal. Chim. Acta 136 (1982) 363.
[11] E. Bakker, Anal. Chim. Acta 350 (1997) 329.
[12] E. Bakker, W. Simon, Anal. Chem. 64 (1992) 1805.
[13] E. Bakker, P. Bühlmann, E. Pretsch, Chem. Rev. 97 (1997) 3083.
[14] I. Tsagkatakis, S. Peper, E. Bakker, Anal. Chem. 73 (2001) 315.
[15] B.G. Cox, P. Firman, H. Horst, H. Schneider, Polyhedron 2 (1983) 343.
[16] L.F. Capitán-Vallvey, M.D. Fernandez-Ramos, P. Alvarez de Cienfuegos, F. Santoyo-Gonzalez, Anal. Chim. Acta 481 (2003) 139.
[17] L.F. Capitán-Vallvey, M.D. Fernandez-Ramos, P. Alvarez de Cienfuegos, F. Santoyo-Gonzalez, Analyst 129 (2004) 783.
[18] D. Siswanta, H. Hisamoto, S. Sato, Y. Matsumoto, Y. Koike, S. Yamamori, K. Suzuki, Anal. Sci. 13 (1997) 429.

Publicaciones

1.- Double-armed crown ethers for calcium optical sensors. Talanta, 78 (2009) 1484-1488; doi:10.1016/j.talanta.2009.01.046

2.- Full-range optical pH sensor based on imaging techniques. Analytica Chimica Acta, 681 (2010) 71-81; doi:10.1016/j.aca.2010.09.033

3.- Full-range optical pH sensor array based on neural networks. Microchemical Journal, 97 (2011) 225-233; doi:10.1016/j.microc.2010.09.008

4.- Minimization of sensing elements for full-range optical pH device formulation. New Journal of Chemistry, 35 (2011) 1042-1053; doi:10.1039/c0nj00951b

5.- Sensor array-based optical portable instrument for determination of pH. Sensors and Actuators B, 156 (2011) 840-848; doi:10.1016/j.snb.2011.02.052

6.- Stability of Hydroxytyrosol in Aqueous Solutions at Different Concentration, Temperature and with Different Ionic Content: A Study Using UPLC-MS. Food Nutrition Science, 2 (2011) 1114-1120; doi:10.4236/fns.2011.210149

7.- An Expert System for full pH range prediction using a disposable optical sensor array. IEEE Sensors Journal, 12 (2012) 1197-1206; doi:10.1109/JSEN.2011.2168815

8.- A compact optical instrument with artificial neural network for pH determination. Sensors, 12 (2012) 6746-6763; doi:10.3390/s120506746

Capítulos de libro

Título libro: Isoflavones: Chemistry, Analysis, Function and Effects
Título del capítulo: The determination of isoflavones in supplemented foods. An overview
Editor: V. R. Preddy
Año: 2012
ISBN 10: 1849734194 / 1-84973-419-4. ISBN 13: 9781849734196

Contribuciones a Congresos

1.- Autores: S. Capel-Cuevas, I. de Orbe-Payá, L.F. Capitán-Vallvey
Título: Nuevos ionóforos para sensores ópticos de iones alcalinotérreos
Tipo de participación: Póster
Congreso: XI Reunión GRASEQA 2008
Publicación: ISBN: 978-84-96826-64-9
Lugar celebración: Huelva Fecha: 12-13 Junio 2008

2.- Autores: M.P. Cuellar, M.M. Erenas, M.C. Pegalajar, S. Capel-Cuevas, K. Cantrell, I. de Orbe-Payá, L.F. Capitan-Vallvey
Título: Automatic color feature extraction from disposable optical sensors
Tipo de participación: Póster. P15
Congreso: International Workshop on Multivariate Image Analysis
Lugar celebración: Valencia Fecha: 28-29 Septiembre 2009

3.- Autores: S. Capel-Cuevas, I. de Orbe-Payá, M.P. Cuellar, M.C. Pegalajar, L.F. Capitán-Vallvey
Título: Full-range optical pH sensor based on imaging techniques
Tipo de participación: Comunicación Oral. C.O.03
Congreso: VI Simposio de Investigadores Jóvenes RSEQ Sigma-Aldrich
Lugar celebración: Granada Fecha: 22-25 Noviembre 2009

4.- Autores: S. Capel-Cuevas, I. de Orbe-Payá, M.P. Cuellar, M.C. Pegalajar, L.F. Capitán-Vallvey
Título: Full-range optical pH sensor based on imaging techniques
Tipo de participación: Póster. P52
Congreso: X European Conference On Optical Chemical Sensors And Biosensors (EUROPTRODE)
Publicación: ISBN: 978-80-86269-20-7
Lugar celebración: Praga (República Checa) Fecha: 28-31 Marzo 2010

5.- Autores: S. Capel-Cuevas, I. de Orbe-Payá, M.P. Cuellar, M.C. Pegalajar, L.F. Capitán-Vallvey
Título: Sensor óptico de amplio rango para pH basado en redes neuronales
Tipo de participación: Póster. SC-91
Congreso: XII Reunión del Grupo Andaluz de la Sociedad Española de Química Analítica (GRASEQA) (BECADA)
Lugar celebración: Córdoba Fecha: 10-11 Junio 2010

6.- Autores: S. Capel-Cuevas, I. de Orbe-Payá, M.P. Cuellar, M.C. Pegalajar, L.F. Capitán-Vallvey
Título: Minimización del número de elementos sensores de un dispositivo óptico de amplio rango para pH
Tipo de participación: Póster. SC-90

Congreso: XII Reunión del Grupo Andaluz de la Sociedad Española de Química Analítica (GRASEQA) (BECADA)
Lugar celebración: Córdoba Fecha: 10-11 Junio 2010

7.- Autores: S. Capel-Cuevas, I. de Orbe-Payá, M.P. Cuellar, M.C. Pegalajar, L.F. Capitán-Vallvey
Título: Broad-range optical pH sensor based on neural networks
Tipo de participación: Extended abstract y póster. PO2-29
Congreso: VII Colloquium Chemiometricum Mediterraneum (BECADA)
Publicación: ISBN: 978-84-937483-4-0
Lugar celebración: Granada Fecha: 21-24 Junio 2010

8.- Autores: S. Capel-Cuevas, I. de Orbe-Payá, M.P. Cuellar, M.C. Pegalajar, L.F. Capitán-Vallvey
Título: Minimization of sensing elements for broad-range optical pH device formulation
Tipo de participación: Extended abstract y póster. PO2-30
Congreso: VII Colloquium Chemiometricum Mediterraneum (BECADA)
Publicación: ISBN: 978-84-937483-4-0
Lugar celebración: Granada Fecha: 21-24 Junio 2010

9.- Autores: M.P. Cuellar, S. Capel-Cuevas, M.C. Pegalajar, I. de Orbe-Payá, L.F. Capitán-Vallvey
Título: An Expert System for wide range pH prediction using disposable optical sensors
Tipo de participación: Artículo corto y comunicación oral
Congreso: III Simposio de Inteligencia Computacional (SICO'2010)
Publicación: ISBN: 978-84-92812-62-2
Lugar celebración: Valencia Fecha: 07-10 Septiembre 2010

10.- Autores: S. Capel-Cuevas, I. de Orbe-Payá, M.P. Cuellar, M.C. Pegalajar, L.F. Capitán-Vallvey
Título: Sensor array-based portable optical instrument for pH determination
Tipo de participación: Comunicación Oral. O12
Congreso: VII Simposio de Investigadores Jóvenes RSEQ Sigma-Aldrich
Lugar celebración: Valencia Fecha: 10-12 Noviembre 2010

11.- Autores: S. Capel-Cuevas, A. Martínez Olmos, I. de Orbe-Payá, A.J. Palma, L.F. Capitán-Vallvey
Título: Determinación del pH en muestras alimentarias, biológicas y de uso cotidiano mediante un instrumento portátil basado en un array sensor colorimétrico
Tipo de participación: Comunicación Oral. SJM4
Congreso: I Simposio de Jóvenes Investigadores en Espectroscopia Aplicada
Lugar celebración: Madrid Fecha: 6-9 Julio 2011

12.- Autores: S. Capel-Cuevas, M. Ariza Avidad, A. Martínez Olmos, N. López Ruiz, I. de Orbe-Payá, A.J. Palma, L.F. Capitán-Vallvey
Título: Sensor array-based colorimetric portable instrument for pH determination in different matrices
Tipo de participación: Póster.
Congreso: Euroanalysis
Lugar celebración: Belgrado (Serbia) Fecha: 11-15 Septiembre 2011

13.- Autores: S. Capel-Cuevas, A. Martínez Olmos, N. López Ruiz, M.P. Cuéllar, M.C. Pegalajar, I. de Orbe-Payá, A.J. Palma, L.F. Capitán-Vallvey
Título: pH determination of different matrices using a sensor array-based colorimetric portable instrument
Tipo de participación: Póster. CSA-P23
Congreso: 13as Jornadas de Análisis Instrumental (JAI) (BECADA)
Lugar celebración: Barcelona Fecha: 13-16 Noviembre 2011

14.- Autores: S. Capel-Cuevas, F. Dini, C. Di Natale, P. Medaglia, I. Lundström, I. de Orbe-Payá, L.F. Capitán-Vallvey
Título: CSPT-potentiometric analytical porphyrin-based array for analysis of liquid samples
Tipo de participación: Póster. P-175
Congreso: XI European Conference On Optical Chemical Sensors And Biosensors (EUROPTRODE)
Lugar celebración: Barcelona Fecha: 1-4 Abril 2012

15.- Autores: S. Capel-Cuevas, F. Dini, C. Di Natale, P. Medaglia, I. Lundström, I. de Orbe-Payá, L.F. Capitán-Vallvey
Título: Array CSPT-potenciométrico basado en porfirinas para el análisis de muestras líquidas
Tipo de participación: Comunicación Oral. CO-2
Congreso: XIII Reunión del Grupo Andaluz de la Sociedad Española de Química Analítica (GRASEQA) (BECADA)
Lugar celebración: Málaga Fecha: 10-11 Junio 2012

Organización de Congresos

Título: I Reunión sobre Innovación Docente en Química (INDOQUIM)

Ámbito: Miembro del Comité Organizador

Lugar celebración: Granada Fecha: 26-28 Septiembre 2006

Universidad de Granada
2012

Facultad de Ciencias
Departamento de Química Analítica
Universidad de Granada